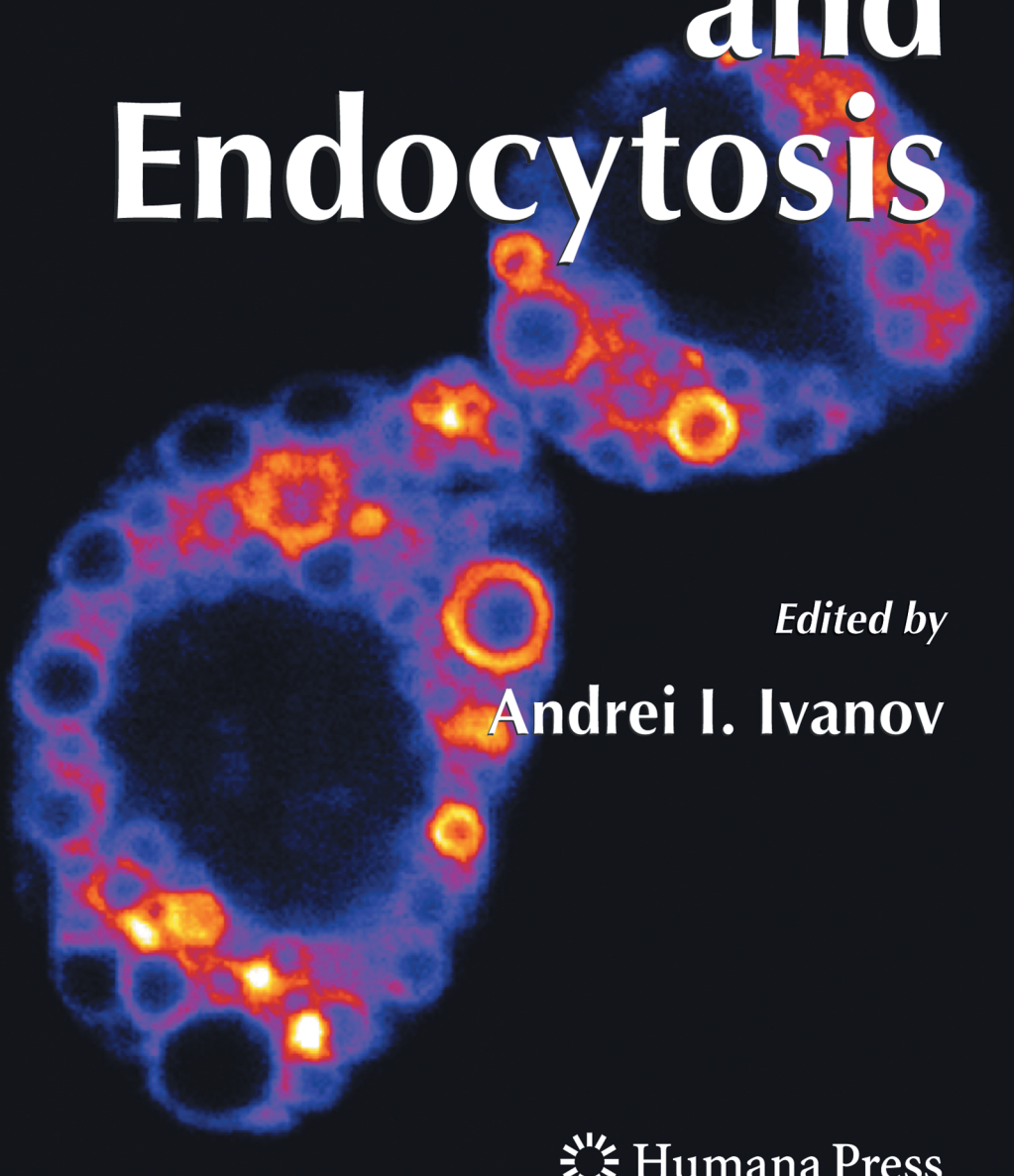


Exocytosis and Endocytosis

A fluorescence microscopy image showing two cells. The cells are stained with a blue dye, likely DAPI, to highlight the nuclei. Several bright orange and red spots are visible within the cells, representing specific organelles or processes such as exocytosis and endocytosis. The background is black, making the blue and orange colors stand out.

Edited by

Andrei I. Ivanov

Exocytosis and Endocytosis

METHODS IN MOLECULAR BIOLOGY

John M. Walker, Series Editor

457. Membrane Trafficking, edited by Ales Vancura, 2008
456. Adipose Tissue Protocols, Second Edition, edited by Kaiping Yang, 2008
455. Osteoporosis, edited by Jennifer J. Westendorf, 2008
454. SARS- and Other Coronaviruses: Laboratory Protocols, edited by Dave Cavanagh, 2008
453. Bioinformatics, Volume 2: Structure, Function, and Applications, edited by Jonathan M. Keith, 2008
452. Bioinformatics, Volume 1: Data, Sequence Analysis, and Evolution, edited by Jonathan M. Keith, 2008
451. Plant Virology Protocols: From Viral Sequence to Protein Function, edited by Gary Foster, Elisabeth Johansen, Yiguo Hong, and Peter Nagy, 2008.
450. Germline Stem Cells, edited by Steven X. Hou and Shree Ram Singh, 2008.
449. Mesenchymal Stem Cells: Methods and Protocols, edited by Darwin J. Prockop, Douglas G. Phinney, and Bruce A. Brunnell, 2008.
448. Pharmacogenomics in Drug Discovery and Development, edited by Qing Yan, 2008.
447. Alcohol: Methods and Protocols, edited by Laura E. Nagy, 2008.
446. Post-translational Modification of Proteins: Tools for Functional Proteomics, Second Edition, edited by Christoph Kannicht, 2008.
445. Autophagosome and Phagosome, edited by Vojo Deretic, 2008.
444. Prenatal Diagnosis, edited by Sinhue Hahn and Laird G. Jackson, 2008.
443. Molecular Modeling of Proteins, edited by Andreas Kukol, 2008.
442. RNAi: Design and Application, edited by Sailen Barik, 2008.
441. Tissue Proteomics: Pathways, Biomarkers, and Drug Discovery, edited by Brian Liu, 2008.
440. Exocytosis and Endocytosis, edited by Andrei I. Ivanov, 2008.
439. Genomics Protocols, Second Edition, edited by Mike Starkey and Ramnanth Elasarapu, 2008
438. Neural Stem Cells: Methods and Protocols, Second Edition, edited by Leslie P. Weiner, 2008
437. Drug Delivery Systems, edited by Kewal K. Jain, 2008
436. Avian Influenza Virus, edited by Erica Spackman, 2008
435. Chromosomal Mutagenesis, edited by Greg Davis and Kevin J. Kayser, 2008
434. Gene Therapy Protocols: Volume 2: Design and Characterization of Gene Transfer Vectors, edited by Joseph M. LeDoux, 2008
433. Gene Therapy Protocols: Volume 1: Production and In Vivo Applications of Gene Transfer Vectors, edited by Joseph M. LeDoux, 2008
432. Organelle Proteomics, edited by Delphine Pflieger and Jean Rossier, 2008
431. Bacterial Pathogenesis: Methods and Protocols, edited by Frank DeLeo and Michael Otto, 2008
430. Hematopoietic Stem Cell Protocols, edited by Kevin D. Bunting, 2008
429. Molecular Beacons: Signalling Nucleic Acid Probes, Methods and Protocols, edited by Andreas Marx and Oliver Seitz, 2008
428. Clinical Proteomics: Methods and Protocols, edited by Antonia Vlahou, 2008
427. Plant Embryogenesis, edited by Maria Fernanda Suarez and Peter Bozhkov, 2008
426. Structural Proteomics: High-Throughput Methods, edited by Bostjan Kobe, Mitchell Guss, and Huber Thomas, 2008
425. 2D PAGE: Sample Preparation and Fractionation, Volume 2, edited by Anton Posch, 2008
424. 2D PAGE: Sample Preparation and Fractionation, Volume 1, edited by Anton Posch, 2008
423. Electroporation Protocols: Preclinical and Clinical Gene Medicine, edited by Shulin Li, 2008
422. Phylogenomics, edited by William J. Murphy, 2008
421. Affinity Chromatography: Methods and Protocols, Second Edition, edited by Michael Zachariou, 2008
420. Drosophila: Methods and Protocols, edited by Christian Dahmann, 2008
419. Post-Transcriptional Gene Regulation, edited by Jeffrey Wilusz, 2008

Exocytosis and Endocytosis

Andrei I. Ivanov

*Department of Medicine, Gastroenterology and Hepatology Division,
University of Rochester School of Medicine and Dentistry, Rochester, NY*

 Humana Press

Volume Editor

Andrei I. Ivanov
Department of Medicine
Gastroenterology and Hepatology Division
University of Rochester School of Medicine
and Dentistry, Rochester, NY

Series Editor

John M. Walker, Professor Emeritus
School of Life Sciences
University of Hertfordshire
Hatfield
Hertfordshire AL10 9AB, UK

ISBN: 978-1-58829-865-2

e-ISBN: 978-1-59745-178-9

Library of Congress Control Number: 2007933723

© 2008 Humana Press, a part of Springer Science+Business Media, LLC

All rights reserved. This work may not be translated or copied in whole or in part without the written permission of the publisher (Humana Press, 999 Riverview Drive, Suite 208, Totowa, NJ 07512 USA), except for brief excerpts in connection with reviews or scholarly analysis. Use in connection with any form of information storage and retrieval, electronic adaptation, computer software, or by similar or dissimilar methodology now known or hereafter developed is forbidden.

The use in this publication of trade names, trademarks, service marks, and similar terms, even if they are not identified as such, is not to be taken as an expression of opinion as to whether or not they are subject to proprietary rights.

While the advice and information in this book are believed to be true and accurate at the date of going to press, neither the authors nor the editors nor the publisher can accept any legal responsibility for any errors or omissions that may be made. The publisher makes no warranty, express or implied, with respect to the material contained herein.

Cover illustration: A live image of a transgenic *Caenorhabditis elegans* in which GFP-tagged Rab-7 is visualized on membranes of late endosomes in a pair of worm's coelomocytes. (Courtesy of Drs. Dmitry Poteryaev and Anne Spang.)

Printed on acid-free paper

9 8 7 6 5 4 3 2 1

springer.com

Preface

The plasma membrane of eukaryotic cells serves not only as a protective barrier that preserves the unique chemical composition and architecture of the cell interior, but also as a front line of the communications between the cell and its environment. Such communications are largely mediated by different membrane-coated vesicles that constantly bud off the plasma membrane and enter the cytoplasm or arrive from the cytoplasm and fuse with the plasma membrane. The former process is known as *endocytosis*, whereas the latter represents *exocytosis*. At the cellular level, endocytosis and exocytosis mediate crucial housekeeping and specialized functions, including nutrient uptake, termination of receptor signaling, vesicle and granule release, cytokinesis, and cell migration. At the tissue and organ levels, exocytosis and endocytosis underlie fundamental physiological processes such as embryonic and reparative morphogenesis, neuronal synaptic transmission, innate and adaptive immune responses, secretion of hormones and mediators, and more. Altogether, this makes studying intracellular vesicle trafficking one of the most important and exciting topics of cellular and integrative physiology.

The aim of *Exocytosis and Endocytosis* is to provide a comprehensive step-by-step guide to a variety of techniques for examining exocytosis and endocytosis *in vitro* and *in vivo*. The book targets not only cell biologists studying the mechanisms of intracellular vesicle trafficking and fusion but also a large cohort of physiologists, developmental biologists, immunologists, and neurobiologists whose research interests focus on cellular processes mediated by exocytosis and endocytosis. *Exocytosis and Endocytosis* should be helpful for newcomers as well as for researchers actively working in this field. The volume begins with two reviews summarizing experimental strategies commonly used to manipulate endocytic and exocytic pathways. Part II (Chapters 3–9) describes cell-free assays of exo- and endocytosis as well as some biochemical protocols to analyze the vesicle trafficking machinery. Part III (Chapters 10–24) presents assays of exocytosis and endocytosis in cultured cells. It describes a large variety of methods ranging from amperometry to modern microscopic techniques such as total internal reflection fluorescence and atomic force microscopy. Part IV (Chapters 25–28) provides examples of how to examine endocytosis and exocytosis in model organisms. These chapters were selected to demonstrate the power of molecular

biology and imaging strategies for investigating vesicle trafficking in multicellular organisms with different levels of complexity.

I would like to thank all the contributors for sharing their expertise and carefully guiding readers through all the hidden details of their techniques. I am very grateful to the series editor, Dr. John Walker, for his enormous help during the editing process. I would also like to acknowledge Moshe Bachar for his valuable assistance in proofreading and organizing this volume.

Andrei I. Ivanov

Contents

Preface	v
Contributors	xi
Part I An Overview of Methods for Analyzing Vesicular Trafficking	
1 Vesicular Trafficking: Molecular Tools and Targets	3
Elena V. Vassilieva and Asma Nusrat	
2 Pharmacological Inhibition of Endocytic Pathways: Is It Specific Enough to Be Useful?	15
Andrei I. Ivanov	
Part II Cell-Free and Biochemical Assays of Exocytosis and Endocytosis	
3 In Vitro Assays to Measure SNARE-Mediated Vesicle Fusion	37
Susanne Kreye, Jörg Malsam, and Thomas H. Söllner	
4 Imaging Ca²⁺-Triggered Exocytosis of Single Secretory Granules on Plasma Membrane Lawns from Neuroendocrine Cells	51
Thorsten Lang	
5 FRAP Analysis of Secretory Granule Lipids and Proteins in the Sea Urchin Egg	61
Julian L. Wong and Gary M. Wessel	
6 A Cell-Free Assay for Endocytosis of E-Cadherin	77
Toshiaki Sakisaka and Yoshimi Takai	
7 Cell-Surface Biotinylation to Study Endocytosis and Recycling of Occludin	89
Noriyuki Nishimura and Takuya Sasaki	

8	Fractionation of Subcellular Membrane Vesicles of Epithelial and Nonepithelial Cells by OptiPrep™ Density Gradient Ultracentrifugation	97
	Xuhang Li and Mark Donowitz	
9	Identification and Characterization of Interacting Partners of Rab GTPases by Yeast Two-Hybrid Analyses.	111
	Mark Kail and Angelika Barnekow	
Part III Analysis of Endocytosis and Exocytosis in Different Cell Systems		
10	High-Throughput Analysis of the Dynamics of Recycling Cell Surface Proteins	129
	Roland Govers, David E. James, and Adelle C.F. Coster	
11	Studying Phagocytosis by Live-Cell Scintillation Proximity Assay	147
	Walter Stockinger and Axel Nohturfft	
12	Transcytosis of Polymeric Immunoglobulin A in Polarized Madin–Darby Canine Kidney Cells	157
	Asli Oztan, Christine Rondanino, and Gerard Apodaca	
13	The Use of Syntaxin Chimeras to Study Polarized Protein Trafficking in Epithelial Cells	171
	Martin B.A. ter Beest	
14	Targeting the Epithelial SNARE Machinery by Bacterial Neurotoxins.	187
	Véronique Proux-Gillardeaux and Thierry Galli	
15	Exocytosis of Endothelial Cells Is Regulated by <i>N</i>-Ethylmaleimide-Sensitive Factor	203
	Munekazu Yamakuchi, Marcella Ferlito, Craig N. Morrell, Kenji Matsushita, Craig A. Fletcher, Wangsen Cao, and Charles J. Lowenstein	
16	Molecular Dissection of HCl Secretion in Gastric Parietal Cells Using Streptolysin O Permeabilization.	217
	Xia Ding, Fang Wu, Zhen Guo, and Xuebiao Yao	
17	Addressing Membrane Protein Topology Using the Fluorescence Protease Protection (FPP) Assay	227
	Holger Lorenz, Dale W. Hailey, and Jennifer Lippincott-Schwartz	

18 Visualizing Clathrin-Mediated IgE Receptor Internalization by Electron and Atomic Force Microscopy	235
Alan R. Burns, Janet M. Oliver, Janet R. Pfeiffer, and Bridget S. Wilson	
19 Analyzing Endosomes in Nonsectioned Cells by Transmission Electron Microscopy	247
Willem Stoorvogel	
20 Imaging Exocytosis of Single Insulin Secretory Granules With TIRF Microscopy	259
Shinya Nagamatsu and Mica Ohara-Imaizumi	
21 Reconstitution of Depolarization and Ca²⁺-Evoked Secretion in <i>Xenopus</i> Oocytes Monitored by Membrane Capacitance	269
Roy Cohen, Bernhard M. Schmitt, and Daphne Atlas	
22 Low-Noise Recording of Single-Vesicle Capacitance Steps in Cell-Attached Patches	283
Vitaly Klyachko, Zhenjie Zhang, and Meyer Jackson	
23 Good Practices in Single-Cell Amperometry.	297
David J. Machado, Mónica S. Montesinos, and Ricardo Borges	
24 Analysis of Single-Vesicle Exocytotic Events Recorded by Amperometry	315
Eugene V. Mosharov	
Part IV Analysis of Exocytosis and Endocytosis in Model Organisms	
25 Application of RNAi Technology and Fluorescent Protein Markers to Study Membrane Traffic in <i>Caenorhabditis elegans</i>.	331
Dmitry Poteryaev and Anne Spang	
26 FM 1-43 Labeling of Synaptic Vesicle Pools at the <i>Drosophila</i> Neuromuscular Junction.	349
Patrik Verstreken, Tomoko Ohyama, and Hugo J. Bellen	
27 Probing E-Cadherin Endocytosis by Morpholino-Mediated Rab5 Knockdown in Zebrafish.	371
Florian Ulrich and Carl-Philipp Heisenberg	
28 Quantifying Endocytosis In Vivo Using Intravital Two-Photon Microscopy	389
Ruben M. Sandoval and Bruce A. Molitoris	
Index	403

Contributors

Gerard Apodaca

Department of Medicine, University of Pittsburgh, Pittsburgh, PA

Daphne Atlas

Department of Biological Chemistry, The Hebrew University of Jerusalem,
Jerusalem, Israel

Angelika Barnekow

Department of Experimental Tumor Biology, University of Muenster, Muenster,
Germany

Hugo J. Bellen

Department of Molecular and Human Genetics, Baylor College of Medicine,
Houston, TX

Ricardo Borges

Pharmacology Unit, Faculty of Medicine, University of La Laguna, Tenerife, Spain

Alan R. Burns

Biomolecular Interfaces and Systems Department, Sandia National Laboratories,
Albuquerque, NM

Wangsen Cao

Department of Medicine, The Johns Hopkins University School of Medicine,
Baltimore, MD

Roy Cohen

Department of Biological Chemistry, The Hebrew University of Jerusalem,
Jerusalem, Israel

Adelle C. F. Coster

School of Mathematics and Statistics, University of New South Wales, Sydney,
Australia

Xia Ding

Department of Physiology, Morehouse School of Medicine, Atlanta, GA

Mark Donowitz

GI Division, Department of Medicine, The Johns Hopkins University School of Medicine, Baltimore, MD

Marcella Ferlito

Department of Medicine, The Johns Hopkins University School of Medicine, Baltimore, MD

Craig A. Fletcher

Department of Molecular and Comparative Pathobiology, The Johns Hopkins University School of Medicine, Baltimore, MD

Thierry Galli

Jacques Monod Institute, University of Paris, Paris, France

Roland Govers

Faculty of Medicine, Institut national de la santé et de la recherche médicale Avenir Team, Nice, France

Zhen Guo

Department of Physiology, Morehouse School of Medicine, Atlanta, GA

Dale W. Hailey

Cell Biology and Metabolism Branch, NICHD, National Institutes of Health, Bethesda, MD

Carl-Philipp Heisenberg

Max Planck Institute for Molecular Cell Biology and Genetics, Dresden, Germany

Andrei I. Ivanov

Department of Medicine, Gastroenterology and Hepatology Division, University of Rochester School of Medicine and Dentistry, Rochester, NY

Meyer Jackson

Department of Physiology, University of Wisconsin, Madison, WI

David E. James

Diabetes and Obesity Program, Garvan Institute of Medical Research, Sydney, Australia

Mark Kail

Department of Experimental Tumor Biology, University of Muenster, Muenster, Germany

Vitaly Klyachko

Howard Hughes Medical Institute and Molecular Neurobiology Laboratory, The Salk Institute, La Jolla, CA

Susanne Kreye

Biochemistry Center (BZH), University of Heidelberg, Heidelberg, Germany

Thorsten Lang

Department of Neurobiology, Max Planck Institute for Biophysical Chemistry,
Göttingen, Germany

Xuhang Li

GI Division, Department of Medicine, The Johns Hopkins University School
of Medicine, Baltimore, MD

Jennifer Lippincott-Schwartz

Cell Biology and Metabolism Branch, NICHD, National Institutes of Health,
Bethesda, MD

Holger Lorenz

Cell Biology and Metabolism Branch, NICHD, National Institutes of Health,
Bethesda, MD

Charles J. Lowenstein

Department of Medicine, The Johns Hopkins University School of Medicine,
Baltimore, MD

David J. Machado

Pharmacology Unit, Faculty of Medicine, University of La Laguna, Tenerife, Spain

Jörg Malsam

Biochemistry Center (BZH), University of Heidelberg, Heidelberg, Germany

Kenji Matsushita

Department of Medicine, The Johns Hopkins University School of Medicine,
Baltimore, MD

Bruce A. Molitoris

Department of Medicine, Indiana University School of Medicine, Indianapolis, IN

Mónica S. Montesinos

Pharmacology Unit, Faculty of Medicine, University of La Laguna, Tenerife, Spain

Craig N. Morrell

Department of Molecular and Comparative Pathobiology, The Johns Hopkins
University School of Medicine, Baltimore, MD

Eugene V. Mosharov

Department of Neurology, Columbia University, New York, NY

Shinya Nagamatsu

Department of Biochemistry, Kyorin University School of Medicine, Tokyo, Japan

Noriyuki Nishimura

Department of Biochemistry, Institute of Health Biosciences, The University
of Tokushima Graduate School, Tokushima, Japan

Axel Nohturfft

Department of Molecular and Cellular Biology, Harvard University, Cambridge, MA

Asma Nusrat

Department of Pathology and Laboratory Medicine, Emory University School of Medicine, Atlanta, GA

Mica Ohara-Imaizumi

Department of Biochemistry, Kyorin University School of Medicine, Tokyo, Japan

Tomoko Ohyama

Department of Molecular and Human Genetics, Baylor College of Medicine, Houston, TX

Janet M. Oliver

Department of Pathology and Cancer Center, University of New Mexico School of Medicine, Albuquerque, NM

Asli Oztan

Department of Medicine, University of Pittsburgh, Pittsburgh, PA

Janet R. Pfeiffer

Department of Pathology and Cancer Center, University of New Mexico School of Medicine, Albuquerque, NM

Dmitry Poteryaev

Division of Biochemistry, Biozentrum, University of Basel, Basel, Switzerland

Véronique Proux-Gillardeaux

Jacques Monod Institute, University of Paris, Paris, France

Christine Rondanino

Department of Medicine, University of Pittsburgh, Pittsburgh, PA

Toshiaki Sakisaka

Department of Molecular Biology and Biochemistry, Osaka University Graduate School of Medicine, Suita, Japan

Ruben M. Sandoval

Department of Medicine, Indiana University School of Medicine, Indianapolis, IN

Takuya Sasaki

Department of Biochemistry, Institute of Health Biosciences, The University of Tokushima Graduate School, Tokushima, Japan

Bernhard M. Schmitt

Department of Physiology, University of Otago, New Zealand

Thomas H. Söllner

Biochemistry Center (BZH), University of Heidelberg, Heidelberg, Germany

Anne Spang

Division of Biochemistry, Biozentrum, University of Basel, Basel, Switzerland

Walter Stockinger

Max F. Perutz Laboratories, Vienna, Austria

Willem Stoorvogel

Department of Biochemistry and Cell Biology, University of Utrecht, Utrecht,
The Netherlands

Yoshimi Takai

Department of Molecular Biology and Biochemistry, Osaka University Graduate
School of Medicine, Suita, Japan

Martin B.A. ter Beest

Department of Surgery, The University of Chicago, IL

Florian Ulrich

Max Planck Institute for Molecular Cell Biology and Genetics, Dresden, Germany

Elena V. Vassilieva

Department of Pathology and Laboratory Medicine, Emory University School
of Medicine, Atlanta, GA

Patrik Verstreken

VIB, Department of Molecular and Developmental Genetics and K.U. Leuven,
Center for Human Genetics, Leuven, Belgium

Gary M. Wessel

Department of Molecular Biology, Cellular Biology and Biochemistry, Brown
University, Providence, RI

Bridget S. Wilson

Department of Pathology and Cancer Center, University of New Mexico School
of Medicine, Albuquerque, NM

Julian L. Wong

Department of Molecular Biology, Cellular Biology and Biochemistry, Brown
University, Providence, RI

Fang Wu

Laboratory of Cell Dynamics, University of Science and Technology of China,
Hefei, China

Munekazu Yamakuchi

Department of Medicine, The Johns Hopkins University School of Medicine,
Baltimore, MD

Xuebiao Yao

Department of Physiology, Morehouse School of Medicine, Atlanta, GA

Zhenjie Zhang

Department of Physiology, University of Wisconsin, Madison, WI

Part I
An Overview of Methods
for Analyzing Vesicular Trafficking

1

Vesicular Trafficking: Molecular Tools and Targets

Elena V. Vassilieva and Asma Nusrat

1	Introduction.....	3
2	Endocytosis	5
3	Manipulation of Vesicular Trafficking During Exocytosis	7
4	Dissecting the Role of Small GTPases and Their Effectors in Vesicular Trafficking.....	9
5	Endocytosis Research In Vivo: Phenotypic and Developmental Effects	10
6	Conclusions.....	11
	References.....	11

Summary Intracellular trafficking of membrane-coated vesicles represents a fundamental process that controls the architecture of different intracellular compartments and communication between the cell and its environment. Major trafficking pathways consist of an inward flux of endocytic vesicles from the plasma membrane and an outward flux of exocytic vesicles to the plasma membrane. This overview describes a number of molecular biology tools commonly used to analyze endocytic and exocytic pathways. The overall emphasis is on major proteins responsible for vesicle formation, recognition, and fusion. These include components of vesicle coats, adaptor complexes, SNARE (soluble *N*-ethylmaleimide-sensitive factor attachment protein receptor) proteins, and Rab guanosine 5'-triphosphatases (GTPases), which represent attractive targets for genetic manipulation aimed at unraveling mechanisms of endocytosis and exocytosis.

Keywords Endocytosis; exocytosis coat complexes; molecular tools; vesicular transport.

1 Introduction

Vesicle trafficking plays a central role in the formation and maintenance of different intracellular compartments as well as in the communications between the cells and the environment. Since its initial discovery in the late 19th century by Ilya Mechnikov, the study of membrane trafficking has become a front line of cell

biology and has had an impact on the understanding of normal and pathologic events in cells. A simplified view of vesicle trafficking shows two major intracellular routes, referred to as endocytosis and exocytosis. *Endocytosis* represents the formation and inward movement of plasma membrane vesicles; *exocytosis* refers to delivery of proteins in the opposite direction to the plasma membrane. Both endo- and exocytosis require intermediate steps that involve vesicle fusion with different compartments of the cell. Formation of membrane vesicles is a complex process that is dependent on the nature of the vesicle protein coat and the cargo.

The endocytic pathways can be categorized as clathrin-dependent or clathrin-independent. Clathrin-dependent endocytosis involves the formation of vesicles coated with clathrin. Similarly, the vesicles of the early exocytic pathway can be formed with participation of coat protein complex I and II (COPI and COPII, respectively). Specific coat proteins function to recruit different cargo as well as determine different intracellular destinations of the endocytic and exocytic vesicles.

Molecular biology/genetic tools have significantly advanced our understanding of exo- and endocytosis of proteins. The best-known examples are data obtained with phenotype selection of *sec* mutants in yeast and *shibire* mutants in *Drosophila*. Early experiments with temperature-sensitive secretion-defective *Saccharomyces cerevisiae sec* mutants led to the identification of key players of the protein secretion pathway (1,2) and provided a foundation for our modern concepts of exocytosis (3), whereas the temperature-sensitive single-gene *shibire* mutant of *Drosophila melanogaster* that lacked the ability to pinch off clathrin-coated vesicles yielded information about dynamin (4).

The most widely used molecular biology tools for manipulating intracellular vesicular trafficking include recombinant deoxyribonucleic acid (DNA) encoding wild type, dominant-negative point mutations and truncated protein constructs, etc. and ribonucleic acid interference (RNAi) machinery to downregulate protein expression. Investigators have shown a preference for RNAi, given that it downregulates protein expression without introducing side effects of protein overproduction (5). However, the choice of particular investigative tools is a balancing act and has its pros and cons. The RNAi-mediated knockdown of a specific protein in cell culture is rapid, and it often provides a clear phenotype; at the same time, complete knockout of some proteins through targeted gene disruption in an animal may be lethal, as exemplified by the embryonic lethality of clathrin adaptor protein complex 2 (AP2) knockout mice (6). As in other biological studies, model organisms and transfected cell lines have been commonly used to study the function of candidate proteins in vesicular transport. In addition, naturally occurring mutations in proteins that participate in vesicle formation/trafficking and are responsible for disease have further advanced our understanding of mechanisms of vesicular trafficking.

In this review, we discuss molecular tools that have been utilized to probe intracellular trafficking of proteins and address examples of commonly used tools that have been used to analyze vesicular trafficking in the endocytic and exocytic pathways.

2 Endocytosis

2.1 Clathrin-Mediated Endocytosis

Clathrin-mediated endocytosis is characterized by formation of morphologically distinct clathrin-coated vesicles (CCVs) on the cytoplasmic side of the plasma membrane. This pathway commonly mediates internalization of plasma membrane receptors such as receptors for transferrin, epidermal growth factor (EGFR), and low-density lipoproteins (LDLR).

The polyhedral clathrin coat is formed by the assembly of a clathrin lattice consisting of three heavy and three light chains. Adaptor proteins regulate the formation of CCVs by linking membrane components and cargo proteins with clathrin. Two types of adaptor proteins in endocytosis include the multimeric adaptor AP2, which is involved in the formation of CCVs, and the monomeric clathrin-associated sorting proteins (CLASPs). AP2 consists of two large subunits (α and β 2) and two small subunits (μ 2 and σ 2). CLASPs include Epsin-1, AP180/clathrin assembly lymphoid myeloid leukemia protein (CALM), Disabled-2 (Dab2), Numb, autosomal recessive hypercholesterolemia protein (ARH), β -arrestins 1 and 2, EGFR pathway substrate clone 15 (Eps15), and Stonin2 (7).

Interference with the clathrin coat assembly has been utilized to inhibit clathrin-mediated endocytosis. Two major techniques have been used to modulate clathrin function in cells. The first method consists of overexpression of the C-terminal third of the clathrin heavy chain, which is also referred to as the clathrin hub domain (8). Increased expression of the hub domain has a dominant negative effect on the assembly of the clathrin coat, thereby influencing its endocytic function. Using this approach, clathrin-mediated endocytosis was effectively disrupted in HeLa cells (9).

The second method involves downregulation of the clathrin heavy chain expression by small interfering RNA (siRNA). It should be noted that interfering with clathrin function may not only affect endocytosis at the plasma membrane, but also influence the vesicle transport between Golgi and ER that has also been reported to require clathrin. Thus, for example, siRNA-mediated clathrin knockdown in HeLa cells resulted in the formation of large intracellular vacuoles and swelling of the *trans*-Golgi network (TGN) (5).

Clathrin-mediated endocytosis can also be inhibited by interfering with the function of adaptor proteins involved in clathrin-mediated endocytosis. Lakadamyali and coworkers inhibited the function of the AP2 complex by RNAi-mediated downregulation of its μ 2 subunit (10). As expected, such disruption of AP2 inhibited the uptake of transferrin. However, internalization of LDL and EGF was not affected, which suggests alternative adaptor function in this pathway (5,10).

Several studies have used RNAi to downregulate expression of monomeric adaptors in the arrestin family (11). Arrestins play a critical role in clathrin-mediated endocytosis of G protein-coupled receptors by interacting with the phosphorylated (activated) receptor and linking the activated receptor to the AP2 adaptor complex.

Table 1 Manipulation of the Clathrin Endocytic Pathway

Target	Tool	Effect	Reference
Clathrin	Overexpression of D/N mutant (Hub fragment) in HeLa cells	Inhibits clathrin lattice formation and transferrin internalization	(9)
Eps15	Mutant lacking second and third EH domain	Clathrin pits not formed; transferrin endocytosis inhibited in HeLa	(12)
AP180	Overexpression of wild-type or C-terminus of AP180 (residues 530–915)	Inhibited uptake of epidermal growth factor (EGF) and transferrin	(13)
Epsin-1	Overexpression of R63H73 mutant deficient in phosphatidylinositol-4,5-bisphosphate and inositol-1,4,5-triphosphate binding in COS-7 cells	Inhibited clathrin lattice formation and transferrin internalization due to interference with the membrane curvature	(14)

Several other examples of inhibition of clathrin-mediated endocytosis are summarized in [Table 1](#).

2.2 Clathrin-Independent Endocytosis

Clathrin-independent endocytosis includes several internalization pathways that use an alternative protein coat or do not require a protein coat for the formation of endocytic vesicles. The most intensively characterized internalization pathway in this category is the caveolar endocytic pathway. Caveolae are plasma membrane invaginations that are enriched in cholesterol and sphingolipids. In addition, these invaginations also accumulate special cholesterol-binding proteins, termed caveolins, on the cytosolic face of vesicles (reviewed in 15–18). Ligands such as the SV40 virus, which are internalized via caveolae, are likely to be delivered to a special endosomal compartment referred to as a caveosome (19). Caveosomes containing caveolins do not accumulate transferrin, lack EEA1 and other early endosomal markers, have normal pH, and can act as a sorting stations (15).

Caveolar-mediated endocytosis can be modulated by influencing expression of caveolin. Overexpression of caveolin-1 and -3 but not of caveolin-2 resulted in a significant increase in the amount of caveolae at the plasma membrane of different cultured cells (15,17,20). Accordingly, RNAi-mediated knockdown of caveolin-1 was associated with the disappearance of caveolae in kidney epithelial cells (21). Similarly, in vivo RNAi-mediated caveolin-1 downregulation induced a loss of caveolae from the lung vascular endothelium (22). Consistent with such morphological effects on caveolae, RNAi-mediated downregulation of caveolin-1 inhibited fibronectin internalization in myofibroblasts (23) and impaired albumin uptake in bovine aortic endothelial (BAEK) cells (24). Furthermore, caveolin is necessary for internalization of LRP6 and activation of the Wnt/ β -catenin signaling pathway in cervical epithelial cells (25). In addition, overexpression of caveolin-1 increased

endocytosis of the growth hormone receptor in fibroblasts (26) and accelerated the uptake of synthetic cationic polymers in cell lines (27).

Interestingly, overexpression of caveolin-1 can also have a negative effect on caveolae-mediated endocytosis due to the stabilization of caveolae association with the plasma membrane (28). Thus, modulation of caveolin expression can both accelerate and inhibit the rate of protein internalization (28,29).

2.3 Dynamin-Dependent Endocytosis

Dynamin is a critical regulator of both clathrin-dependent and -independent endocytosis. This large guanosine triphosphatase (GTPase) has a unique ability to activate itself through oligomerization. Dynamin self-assembly around liposomes in cell-free systems drives dispersion of liposomes into small vesicles (30). More importantly, dynamin activity regulates fission of plasma membrane vesicles in living cells. Since the role of dynamin in both clathrin-mediated and caveolae-dependent endocytosis is well characterized, genetic manipulations of this protein do not distinguish between these protein internalization pathways. A detailed review on dynamin domain mutations and their influence on vesicular trafficking has been published (30).

Mutation of lysine 44 in the guanosine 5'-triphosphate (GTP)-binding domain of dynamin (K44A) inhibited clathrin-mediated internalization of transferrin and the EGFR (31,32). An elegant method to regulate dynamin function in cells and study its effect on endocytosis is by expressing this mutant under the control of a tetracycline-regulated promoter using an adenoviral system for transfection. This technique was used to inhibit carbachol-induced endocytosis of M1 muscarinic acetylcholine receptor (M1 mAChR) in Madin-Darby canine kidney (MDCK) cells (33). Dramatic inhibition of clathrin-mediated endocytosis was also achieved by overexpression of the S45N mutant of the GTP-binding domain of dynamin as well as by a mutant with deletion of the entire GTP-binding domain (34).

3 Manipulation of Vesicular Trafficking During Exocytosis

3.1 Coat Protein Complexes I and II

Similar to early endocytic events, trafficking of proteins between the Golgi compartments and ER involves formation of coated vesicles. Two types of coats have been extensively characterized, with COPII involved in the trafficking of newly synthesized proteins from the ER to the Golgi and COPI involved in the trafficking of proteins within the Golgi compartments and retrograde trafficking back to the ER.

The major exocytic COPII coat has been extensively studied in yeast, as recently reviewed (35). Formation of COPII vesicles on the ER is initiated by activation of the small GTPase, SAR1, by membrane-bound Sec12. GTP-Sar1 becomes membrane associated and recruits the Sec23–Sec24 complex. The trans-membrane ER cargo is captured by the cargo adaptor protein Sec24. Further assembly of the transport vesicles requires the scaffolding Sec13–Sec31 cage complex (35). All human components of COPII have been identified, some of them with multiple isoforms, as summarized by Stankewich and coworkers (36), who have proposed a possible role of Sec31A and Sec31B in determining cargo specificity in different tissues.

The COPI coatomer consists of seven subunits: α , β , β' , γ , σ , ϵ , and ζ -COP. This vesicle coat is formed in the cytoplasm and, with the Arf1-GTPase and its membrane-bound GTPase activating protein (GAP) polymerizes into a lattice on the membrane, thereby generating a coated bud. During vesicle formation, the coat concentrates cargo and bends the membrane, while all the components of the coat repeatedly cycle on and off the membrane (*see Ref. 37* for review). A temperature-sensitive mutation in the ϵ -subunit of COPI in Chinese hamster ovary (CHO) cells resulted in disruption of ER the Golgi through and trafficking protein section in rapid degradation of the LDLR. In addition, introduction of normal ϵ -subunit DNA into these cells was sufficient in correcting this trafficking defect (38).

3.2 Clathrin Adaptors in the trans-Golgi Network

Adaptor protein complexes AP1, AP3, and AP4 have been identified in the TGN/endosomal membranes. However, only AP1 participates in the clathrin coat formation (reviewed in *Ref. 39*). A role of AP1 in sorting of proteins to the epithelial basolateral membrane of LLC-PK1 renal epithelial cell line has been reported. Interestingly, LLC-PK1 cells missort basolateral proteins to the apical pole. These cells do not express the μ 1B subunit of AP1. Expression of the μ 1B subunit of AP1 in these cells was sufficient in correcting the targeting of the LDLR and transferrin receptor to the basolateral membrane (40). GGA (Golgi-localized γ -year-containing Arf-binding proteins) is another set of specific monomeric adaptors in the Golgi that are capable of promoting clathrin assembly *in vivo* and *in vitro*. Expression of human GGA1 in HeLa cells caused an increased association of clathrin with the TGN (41).

3.3 Vesicle Recognition and Fusion Machinery

The final stage of vesicular trafficking involves fusion of secretory vesicles to the target membrane. Vesicular fusion events are controlled by so-called soluble *N*-ethylmaleimide-sensitive factor attachment protein receptors (SNAREs). The

classical SNARE hypothesis states that the pairing of compartment-specific SNARE in the transport vesicle, v-SNARE, with a complimentary t-SNAREs on the target compartment provides specificity of membrane fusion (42,43). Formation of the extremely stable SNARE core complex apparently drives membrane fusion (44).

The core of the neuronal SNARE complex is made of four parallel α -helices provided by the v-SNARE (synaptobrevin or VAMP) and t-SNAREs syntaxin and synaptosome associated protein of 25kDa (SNAP 25) on the plasma membrane. A critical role of SNAP-25 in action potential-driven neurotransmitter release was demonstrated in embryonically lethal SNAP-25 knockout mice. Action potential-dependent transmitter release was abolished in neuromuscular junctions of the homozygote embryos, while heterozygous mice were defective in neuronal dopamine signaling (45). SNAP-25 was not required for stimulus-independent neurotransmitter release, but was essential for evoked synaptic transmission (45). Syntaxin-6 (Syn6) is a SNARE protein in endosomes and in the Golgi. Expression of Syn6 that lacks the membrane anchor induce, a defect in the delivery of endosomal cargo to lysosomes (46).

It was recently shown that inhibition of the SNARE complex disassembly by dominant negative α -SNAP L294A results in inhibition of vesicle tethering, thereby implying an upstream role of this SNARE complex in vesicle fusion (47).

4 Dissecting the Role of Small GTPases and Their Effectors in Vesicular Trafficking

The assembly of coats and vesicle formation, budding, tethering, and fusion are regulated by members of the Arf and Rab GTPases and their effectors (48–51). Expression of Arf and Rab dominant-negative guanosine 5'-diphosphate (GDP)-bound mutations and constitutively active GTP hydrolysis-resistant mutations has been used to investigate the role of these proteins in vesicular trafficking. Rab proteins have been differentially localized in specific endosomal compartments (48). For example, Rab5 is involved in clathrin-mediated endocytosis and early endosomal fusion. Overexpression of Rab5-GTP mutant Rab5Q79L in BHK and HeLa cells resulted in increased internalization of transferrin and in the enlargement of early endosomes. Furthermore, overexpression of S34N Rab5 mutant which preferentially binds GDP, inhibited transferrin endocytosis and induced endosomal fragmentation.

Rab GTPase function is regulated by guanidine nucleotide exchange factors (GEFs) and GTPase-activating proteins (GAPs). Activated Rab proteins associate with membranes; in the cytosol, inactive Rab proteins bind to a GDP-dissociation inhibitor (GDI) that prevents their membrane association (49). Furthermore, GDI-displacement factors (GDFs) are needed to effectively dissociate Rab proteins from GDI. Thus, Rab activity can be modified by manipulating these proteins. Human PRA1 protein (homolog of yeast Yip3) is a GDF for endosomal Rab proteins. Indeed, membranes

purified from HEK293 cells overexpressing Yip3 demonstrated an increased ability in recruitment of Rab9 from inactive Rab9-GDI complexes. In addition, siRNA-mediated knockdown of Yip3 in HeLa S-3 cells decreased the membrane-associated pool of endosomal Rab9 (50).

Arf GTPases are another family of GTPases important in vesicular trafficking. Arf1 is involved in membrane recruitment of coat proteins such as COPI, AP1 AP3, and AP4 (reviewed in *Ref. 37,51*). In HeLa cells and in normal rat kidney (NRK) cells expression of dominant-active Q71L Arf-1 enhanced the association of COPI with the Golgi and an intermediate compartment between the ER and Golgi. Overexpression of dominant-negative T31N Arf1 resulted in disassembly of coat proteins and Golgi collapse (52–54).

5 Endocytosis Research In Vivo: Phenotypic and Developmental Effects

Numerous studies to elucidate endocytic mechanisms have been undertaken in model systems that include yeast, fruit flies, and worms. Although there are some common features, differences in the endocytic machinery have been observed in these model organisms and mammals. In *Drosophila*, both clathrin-dependent and clathrin-independent endocytosis have been observed, even though caveolin is not present (55). While the K44A dynamin mutant prevents fluid-phase endocytosis in *Drosophila* cells, it does not do so in mammalian HeLa cells.

Interestingly, zebrafish models have yielded important data pertaining to the function of two caveolin isoforms (caveolin-1 α and caveolin-1 β). Morpholino oligomer downregulation of the caveolin isoforms resulted in a tissue-specific decrease in the number of caveolae (56). Pronounced abnormalities were evident by 12h after fertilization, which led to embryonic lethality. Importantly, caveolin-1 α and caveolin-1 β were not able to substitute for each other, and mutant caveolin-1 α isoform (mutated at Y14 Src phosphorylation site [Y14F]) could not rescue caveolin-1 α deficiency.

In contrast to the dramatic effects in zebrafish, caveolin-1 knockout mice were viable while lacking caveolae in tissues (57), and caveolin-3 (muscle-specific isoform) knockout mice lacked caveolae in the plasma membrane of muscle cells (17, 58). Such differences in caveolin knockdown in zebrafish vs. mammals can be explained by redundant compensatory mechanisms in the latter. Thus, the zebrafish model has served as a valuable investigative tool in dissecting the function of caveolin-1 (59).

Physiological outcomes of clathrin adaptor complex disruption have been reviewed (6). AP2- and AP1-deficient mice were embryonically lethal; AP3-deficient mice had a specific phenotype that was not lethal. In humans, almost complete absence of the β 3A subunit of AP3 complex due to natural mutation was identified in a subtype 2 of Hermansky–Pudlak syndrome that is characterized by pigmentation defects and bleeding disorder caused by mistargeting of lysosomal proteins such as LAMP proteins to

the plasma membrane. Pigmentation and bleeding disorders were characteristic of AP3 natural mutations in mice, while knockout of neuron-specific AP3B in mice led to impaired neurotransmission (6).

6 Conclusions

Molecular tools to study cellular endocytic functions have played an important role in advancing our understanding of this field. While the key principles of endo- and exocytic pathways have been defined in simple models such as yeast, we are still far from understanding these processes in complex mammalian systems. The development of new protein targets, transfection protocols, and assays will greatly advance our understanding of intracellular protein transport.

Acknowledgments This work was supported by the Crohn's and Colitis Foundation of America and National Institutes of Health DK53202 and DK59888 (A.N.).

References

1. Novick, P., Field, C., and Schekman, R. (1980) Identification of 23 complementation groups required for post-translational events in the yeast secretory pathway. *Cell* **21**, 205–215.
2. Schekman, R., and Novick, P. (2004) 23 genes, 23 years later. *Cell* **116**, S13–S15, 11 pp. following S19.
3. Bonifacino, J.S., and Glick, B.S. (2004) The mechanisms of vesicle budding and fusion. *Cell* **116**, 153–166.
4. Kosaka, T., and Ikeda, K. (1983) Reversible blockage of membrane retrieval and endocytosis in the garland cell of the temperature-sensitive mutant of *Drosophila melanogaster*, shibirets1. *J. Cell Biol.* **97**, 499–507.
5. Motley, A., Bright, N.A., Seaman, M.N., and Robinson, M.S. (2003) Clathrin-mediated endocytosis in AP-2-depleted cells. *J. Cell Biol.* **162**, 909–918.
6. Ohno, H. (2006) Physiological roles of clathrin adaptor AP complexes: lessons from mutant animals. *J. Biochem. (Tokyo)* **139**, 943–948.
7. Maldonado-Baez, L., and Wendland, B. (2006) Endocytic adaptors: recruiters, coordinators and regulators. *Trends Cell Biol.* **16**, 505–513.
8. Liu, S.H., Wong, M.L., Craik, C.S., and Brodsky, F.M. (1995) Regulation of clathrin assembly and trimerization defined using recombinant triskelion hubs. *Cell* **83**, 257–267.
9. Liu, S.H., Marks, M.S., and Brodsky, F.M. (1998) A dominant-negative clathrin mutant differentially affects trafficking of molecules with distinct sorting motifs in the class II major histocompatibility complex (MHC) pathway. *J. Cell Biol.* **140**, 1023–1037.
10. Lakadamyali, M., Rust, M.J., and Zhuang, X. (2006) Ligands for clathrin-mediated endocytosis are differentially sorted into distinct populations of early endosomes. *Cell* **124**, 997–1009.
11. Moore, C.A., Milano, S.K., and Benovic, J.L. (2007) Regulation of receptor trafficking by GRKs and arrestins. *Annu. Rev. Physiol.* **69**, 451–482.
12. Benmerah, A., Bayrou, M., Cerf-Bensussan, N., and Dautry-Varsat, A. (1999) Inhibition of clathrin-coated pit assembly by an Eps15 mutant. *J. Cell Sci.* **112**(Pt. 9), 1303–1311.

13. Ford, M.G., Pearse, B.M., Higgins, M.K., et al. (2001) Simultaneous binding of PtdIns(4,5)P₂ and clathrin by AP180 in the nucleation of clathrin lattices on membranes. *Science* **291**, 1051–1055.
14. Ford, M.G., Mills, I.G., Peter, B.J., et al. (2002) Curvature of clathrin-coated pits driven by epsin. *Nature* **419**, 361–366.
15. Parton, R.G., and Simons, K. (2007) The multiple faces of caveolae. *Nat. Rev. Mol. Cell Biol.* **8**, 185–194.
16. Parton, R.G. (2003) Caveolae—from ultrastructure to molecular mechanisms. *Nat. Rev. Mol. Cell Biol.* **4**, 162–167.
17. Cohen, A.W., Hnasko, R., Schubert, W., and Lisanti, M.P. (2004) Role of caveolae and caveolins in health and disease. *Physiol. Rev.* **84**, 1341–1379.
18. Hommelgaard, A.M., Roepstorff, K., Vilhardt, F., et al. (2005) Caveolae: stable membrane domains with a potential for internalization. *Traffic* **6**, 720–724.
19. Pelkmans, L., Kartenbeck, J., and Helenius, A. (2001) Caveolar endocytosis of simian virus 40 reveals a new two-step vesicular-transport pathway to the ER. *Nat. Cell Biol.* **3**, 473–483.
20. Stan, R.V. (2005) Structure of caveolae. *Biochim. Biophys. Acta* **1746**, 334–348.
21. Manninen, A., Verkade, P., Le Lay, S., et al. (2005) Caveolin-1 is not essential for biosynthetic apical membrane transport. *Mol. Cell Biol.* **25**, 10087–10096.
22. Miyawaki-Shimizu, K., Predescu, D., Shimizu, J., Broman, M., Predescu, S., and Malik, A.B. (2006) siRNA-induced caveolin-1 knockdown in mice increases lung vascular permeability via the junctional pathway. *Am. J. Physiol. Lung Cell Mol. Physiol.* **290**, L405–L413.
23. Sottile, J., and Chandler, J. (2005) Fibronectin matrix turnover occurs through a caveolin-1-dependent process. *Mol. Biol. Cell* **16**, 757–768.
24. Gonzalez, E., Nagiel, A., Lin, A.J., et al. (2004) Small interfering RNA-mediated down-regulation of caveolin-1 differentially modulates signaling pathways in endothelial cells. *J. Biol. Chem.* **279**, 40659–40669.
25. Yamamoto, H., Komekado, H., and Kikuchi, A. (2006) Caveolin is necessary for Wnt-3a-dependent internalization of LRP6 and accumulation of beta-catenin. *Dev. Cell* **11**, 213–223.
26. Lobie, P.E., Sadir, R., Graichen, R., et al. (1999) Caveolar internalization of growth hormone. *Exp. Cell Res.* **246**, 47–55.
27. Manunta, M., Nichols, B.J., Tan, P.H., et al (2006) Gene delivery by dendrimers operates via different pathways in different cells, but is enhanced by the presence of caveolin. *J. Immunol. Methods* **314**, 134–146.
28. Le, P.U., Guay, G., Altschuler, Y., and Nabi, I.R. (2002) Caveolin-1 is a negative regulator of caveolae-mediated endocytosis to the endoplasmic reticulum. *J. Biol. Chem.* **277**, 371–3379.
29. Pelkmans, L., and Helenius, A. (2002) Endocytosis via caveolae. *Traffic* **3**, 311–320.
30. Hinshaw, J.E. (2000) Dynamin and its role in membrane fission. *Annu. Rev. Cell Dev. Biol.* **16**, 483–519.
31. van der Blik, A.M., Redelmeier, T.E., Damke, H., et al. (1993) Mutations in human dynamin block an intermediate stage in coated vesicle formation. *J. Cell Biol.* **122**, 553–563.
32. Damke, H., Baba, T., Warnock, D.E., and Schmid, S.L. (1994) Induction of mutant dynamin specifically blocks endocytic coated vesicle formation. *J. Cell Biol.* **127**, 915–934.
33. Shmuel, M., Nodel-Berner, E., Hyman, T., et al. (2007) Caveolin 2 regulates endocytosis and trafficking of the M1 muscarinic receptor in MDCK epithelial cells. *Mol. Biol. Cell.* **18**, 1570–1585.
34. Herskovits, J.S., Burgess, C.C., Obar, R.A., and Vallee, R.B. (1993) Effects of mutant rat dynamin on endocytosis. *J. Cell Biol.* **122**, 565–578.
35. Gurkan, C., Stagg, S.M., Lapointe, P., and Balch, W.E. (2006) The COPII cage: unifying principles of vesicle coat assembly. *Nat. Rev. Mol. Cell Biol.* **7**, 727–738.

36. Stankewich, M.C., Stabach, P.R., and Morrow, J.S. (2006) Human Sec31B: a family of new mammalian orthologues of yeast Sec31p that associate with the COPII coat. *J. Cell Sci.* **119**, 958–969.
37. Lippincott-Schwartz, J., and Liu, W. (2006) Insights into COPI coat assembly and function in living cells. *Trends Cell Biol.* **16**, e1–e4.
38. Guo, Q., Vasile, E., and Krieger, M. (1994) Disruptions in Golgi structure and membrane traffic in a conditional lethal mammalian cell mutant are corrected by epsilon-COP. *J. Cell Biol.* **125**, 1213–1224.
39. Robinson, M.S. (2004) Adaptable adaptors for coated vesicles. *Trends Cell Biol.* **14**, 167–174.
40. Folsch, H., Ohno, H., Bonifacino, J.S., and Mellman, I. (1999) A novel clathrin adaptor complex mediates basolateral targeting in polarized epithelial cells. *Cell* **99**, 189–198.
41. Puertollano, R., Randazzo, P.A., Presley, J.F., et al. (2001) The GGAs promote ARF-dependent recruitment of clathrin to the TGN. *Cell* **105**, 93–102.
42. Sollner, T., Whiteheart, S.W., Brunner, M., et al. (1993) SNAP receptors implicated in vesicle targeting and fusion. *Nature* **362**, 318–324.
43. Duman, J.G., and Forte, J.G. (2003) What is the role of SNARE proteins in membrane fusion? *Am. J. Physiol. Cell Physiol.* **285**, C237–C249.
44. Chen, Y.A., and Scheller, R.H. (2001) SNARE-mediated membrane fusion. *Nat. Rev. Mol. Cell Biol.* **2**, 98–106.
45. Washbourne, P., Thompson, P.M., Carta, M., et al. (2002) Genetic ablation of the t-SNARE SNAP-25 distinguishes mechanisms of neuroexocytosis. *Nat. Neurosci.* **5**, 19–26.
46. Kuliawat, R., Kalinina, E., Bock, J., et al. (2004) Syntaxin-6 SNARE involvement in secretory and endocytic pathways of cultured pancreatic beta-cells. *Mol. Biol. Cell* **15**, 1690–1701.
47. Bentley, M., Liang, Y., Mullen, K., Xu, D., Sztul, E., and Hay, J.C. (2006) SNARE status regulates tether recruitment and function in homotypic COPII vesicle fusion. *J. Biol. Chem.* **281**, 38825–38833.
48. Zerial, M., and McBride, H. (2001) Rab proteins as membrane organizers. *Nat. Rev. Mol. Cell Biol.* **2**, 107–117.
49. Pfeffer, S., and Aivazian, D. (2004) Targeting Rab GTPases to distinct membrane compartments. *Nat. Rev. Mol. Cell Biol.* **5**, 886–896.
50. Sivars, U., Aivazian, D., and Pfeffer, S.R. (2003) Yip3 catalyses the dissociation of endosomal Rab-GDI complexes. *Nature* **425**, 856–859.
51. McNiven, M.A., and Thompson, H.M. (2006) Vesicle formation at the plasma membrane and trans-Golgi network: the same but different. *Science* **313**, 1591–1594.
52. Dascher, C., and Balch, W.E. (1994) Dominant inhibitory mutants of ARF1 block endoplasmic reticulum to Golgi transport and trigger disassembly of the Golgi apparatus. *J. Biol. Chem.* **269**, 1437–1448.
53. Zhang, C.J., Rosenwald, A.G., Willingham, M.C., Skuntz, S., Clark, J., and Kahn, R.A. (1994) Expression of a dominant allele of human ARF1 inhibits membrane traffic in vivo. *J. Cell Biol.* **124**, 289–300.
54. Volpicelli-Daley, L.A., Li, Y., Zhang, C.J., and Kahn, R.A. (2005) Isoform-selective effects of the depletion of ADP-ribosylation factors 1–5 on membrane traffic. *Mol. Biol. Cell* **16**, 4495–4508.
55. Fischer, J.A., Eun, S.H., and Doolan, B.T. (2006) Endocytosis, endosome trafficking, and the regulation of *Drosophila* development. *Annu. Rev. Cell Dev. Biol.* **22**, 181–206.
56. Fang, P.K., Solomon, K.R., Zhuang, L., et al. (2006) Caveolin-1alpha and -1beta perform nonredundant roles in early vertebrate development. *Am. J. Pathol.* **169**, 2209–2222.
57. Drab, M., Verkade, P., Elger, M., et al. (2001) Loss of caveolae, vascular dysfunction, and pulmonary defects in caveolin-1 gene-disrupted mice. *Science* **293**, 2449–2452.

58. Galbiati, F., Engelman, J.A., Volonte, D., et al. (2001) Caveolin-3 null mice show a loss of caveolae, changes in the microdomain distribution of the dystrophin-glycoprotein complex, and t-tubule abnormalities. *J. Biol. Chem.* **276**, 21425–21433.
59. Frank, P.G., and Lisanti, M.P. (2006) Zebrafish as a novel model system to study the function of caveolae and caveolin-1 in organismal biology. *Am. J. Pathol.* **169**, 1910–1912.

2

Pharmacological Inhibition of Endocytic Pathways: Is It Specific Enough to Be Useful?

Andrei I. Ivanov

1	Introduction.....	15
2	Inhibitors of Clathrin-Mediated Endocytosis.....	17
3	Inhibitors of Lipid Raft/Caveolae-Mediated Endocytosis	21
4	Inhibitors of Macropinocytosis and Phagocytosis	25
5	Conclusion and Perspectives.....	27
	References.....	28

Summary Eukaryotic cells constantly form and internalize plasma membrane vesicles in a process known as endocytosis. Endocytosis serves a variety of housekeeping and specialized cellular functions, and it can be mediated by distinct molecular pathways. Among them, internalization via clathrin-coated pits, lipid raft/caveolae-mediated endocytosis and macropinocytosis/phagocytosis are the most extensively characterized. The major endocytic pathways are usually distinguished on the basis of their differential sensitivity to pharmacological/chemical inhibitors, although the possibility of nonspecific effects of such inhibitors is frequently overlooked. This review provides a critical evaluation of the selectivity of the most widely used pharmacological inhibitors of clathrin-mediated, lipid raft/caveolae-mediated endocytosis and macropinocytosis/phagocytosis. The mechanisms of actions of these agents are described with special emphasis on their reported side effects on the alternative internalization modes and the actin cytoskeleton. The most and the least-selective inhibitors of each major endocytic pathway are highlighted.

Keywords Caveolae; clathrin; lipid rafts; macropinocytosis; phagocytosis; selectivity.

1 Introduction

The plasma membrane of eukaryotic cells represents a crucial interface that mediates communication between the cell interior and its environment. One of the central communication processes involves bidirectional fluxes of membrane-coated

vesicles in and out of the cell surface. Formation and inward cytosolic movement of plasma membrane vesicles is termed *endocytosis*. Endocytosis is a fundamental feature of living cells that serves a variety of housekeeping and specialized functions. The former includes nutrient uptake, termination of receptor signaling, and regulation of cell shape and volume, and the latter encompasses neuronal synaptic transmission, transcellular transport, regulation of cell migration, and immune defense functions.

Three major endocytic pathways have been extensively investigated (1). The first pathway involves the assembly of a specific coat protein, clathrin, on the intracellular face of the plasma membrane, resulting in the formation of a clathrin-coated pit. This pathway is characteristic of receptor-mediated endocytosis; in addition to clathrin, it requires a number of adaptor and accessory molecules for controlling different steps in the assembly and maturation of the coated pits. Among these proteins, a so-called adaptor protein (AP)2 complex is critical for the initial linkages between cargo molecules and clathrin, whereas amphiphysin and dynamin guanosine triphosphatase (GTPase) regulate later conversion of membrane invagination into a vesicle (1,2).

The second pathway involves invagination of cholesterol-enriched microdomains within the plasma membrane that may contain a coat protein known as caveolin. These structures are referred to as *lipid rafts* or *caveolae* (3). Lipid raft/caveolae-mediated endocytosis participates in the internalization of glycosylphosphatidylinositol (GPI)-anchored proteins, cholera toxin entry, and intracellular cholesterol trafficking (1,3). The molecular mechanisms of this pathway involve dynamin activity and tyrosine kinase signaling.

The third major internalization pathway involves the formation of large F-actin-coated vacuoles that serve to uptake either solid particles (phagosomes) or liquid (macropinosomes) from the extracellular space (4–6). Phagocytosis is a characteristic of specialized cells such as leukocytes, whereas macropinocytosis can be induced in many cell types on stimulation with mitogens and growth factors. Phagocytosis and macropinocytosis are initiated by the changes in the dynamics of cortical actin and are regulated by intracellular protein machinery that controls actin polymerization (4–6).

Studies of different internalization pathways attract attention not only from classical cell biologists but also from researchers working in different fields of neurobiology, immunology, and pathophysiology. For such a diverse community, it is critical to have simple, reliable, and affordable tools that can be used to analyze endocytosis *in vitro* and *in vivo*. Direct probing of endocytosis in living cells is commonly achieved using pharmacological (chemical) inhibitors. Several advances of these inhibitors over more sophisticated molecular biological tools, targeting particular endocytic proteins, can be envisioned.

First, pharmacological inhibitors equally affect all cells in a population, and these effects can be easily titrated and quantified. Second, cells are usually exposed to inhibitors over a short period of time, which precludes the development of delayed side effects or compensatory mechanisms. Third, pharmacological

inhibitors still represent the tools of choice for *in vivo* studies. Last but not least, approaches that use chemical inhibitors remain the most time and labor efficient as well as the most affordable.

One major problem that may undermine the use of pharmacological inhibitors of endocytosis is their potential for poor specificity. However, this problem is frequently overlooked because a particular inhibitor might demonstrate high pathway specificity in one experimental condition but cause side effects in different experimental setups. Since pharmacological inhibitors of endocytosis remain extensively used, it is important to have an unbiased view of their specificity and possible side effects.

This review examines the specificity of pharmacological/chemical inhibitors most frequently used to probe different endocytic pathways. An inhibitor's specificity is evaluated based on two criteria. The first criterion implies that the particular agent affects only an endocytic pathway of interest without interfering with alternative internalization modes. The second criterion requires that the inhibitor does not affect actin cytoskeleton. It is particularly important because reorganization of cortical actin filaments may induce nonselective endocytosis-dependent and -independent changes in distribution, biochemical properties, and functions of various plasma membrane proteins. Using these simple criteria, I examine the literature on inhibition of three major endocytic pathways to determine which pharmacological tools can be considered the most selective and cause the fewest side effects on the living cells.

2 Inhibitors of Clathrin-Mediated Endocytosis

The history of chemical inhibition of clathrin-dependent internalization began in the early 1980s when monodansylcadaverine (MDC) (7), potassium depletion (8), and hypertonic sucrose (9) were introduced to block receptor-mediated endocytosis. Now, these early tools along with several other drugs and chemical maneuvers are widely used to probe internalization via clathrin-coated pits.

2.1 Hypertonic Sucrose

Hypertonic (0.4–0.5 *M*) sucrose represents probably the most popular chemical inhibitor of clathrin-mediated endocytosis. The underlying mechanism of such inhibition reportedly involves the dispersion of clathrin lattices on the plasma membrane (10). Although blockage of protein internalization by hypertonic sucrose is considered as strong evidence for clathrin-mediated endocytosis (11–13), this treatment may also affect non-clathrin-mediated internalization pathways. Indeed, an early ultrastructural study by Carpentier et al. (14) observed that hypertonic sucrose not only reduced the number of clathrin-coated pits on

fibroblast plasma membrane but also caused the disappearance of noncoated invaginations. Furthermore, this treatment inhibited internalization of a classical lipid raft ligand, cholera toxin, along with a fluid-phase (macropinocytosis) marker, horseradish peroxidase. It is noteworthy that the decreased uptake of fluid-phase markers in cells incubated with hypertonic sucrose was confirmed by several subsequent reports (15,16). Furthermore, a study in cardiac myocytes showed abnormal swelling of caveolae and disappearance of their resident proteins after an exposure to even moderately hypertonic (150 mM) sucrose (17). Overall, these data suggest that hypertonic sucrose may interfere with all three major internalization pathways.

Moreover, it is well known that extracellular hypertonicity induces cell shrinkage, which in its turn causes compensatory activation of a number of plasma membrane ion transporters, pumps, and channels (18). Stimulation of the ion transport activates a variety of intracellular kinases that may lead to the remodeling of the cortical actin cytoskeleton. Indeed, hypertonic medium was shown to trigger the assembly of polygonal F-actin network in aortic endothelial cells (18) and to cause redistribution of F-actin from the perijunctional belt into disorganized bundles in kidney epithelial cells (19). Such a dramatic effect on the F-actin architecture adds yet another level of nonspecificity to the intracellular actions of hypertonic sucrose.

2.2 Potassium Depletion

Potassium depletion represents another classical (8), but still useful (20,21), chemical procedure to block internalization via clathrin-coated pits. Technically, this procedure consists of two steps, an initial hypotonic shock followed by an incubation in isotonic potassium-free medium (8). Similar to hypertonic sucrose, potassium depletion is thought to block clathrin-mediated endocytosis by removing plasma membrane-associated clathrin lattices (10). However, potassium depletion appears to be a more selective inhibitor of clathrin-dependent internalization when compared to hypertonic media. To the best of my knowledge, no inhibitory effects of potassium depletion on lipid raft/caveolae-mediated endocytosis have been reported. Although a decreased uptake of fluid-phase markers in potassium-depleted cells has been observed (22,23), this effect may be caused by an increase in the regurgitation of the markers rather than the inhibition of macropinocytosis per se (22).

Nevertheless, two studies have reported that potassium depletion affects the actin cytoskeleton. One study observed that potassium depletion blocked reorganization of F-actin filaments from circumferential bundles into linear stress fibers in fibroblasts, which resulted in the inhibition of cell spreading (24). Another study showed that this treatment blocked the activation of Rho GTPase and attenuated the formation of basal stress fibers in renal epithelial cells acquiring the apico-basal cell polarity (25). These data suggest that potassium depletion might cause some

side effects because of its interference with reorganization of the cortical actin cytoskeleton.

2.3 Cytosolic Acidification

Internalization through clathrin-coated pits can be blocked by decreasing the cytosolic pH of the cell (13,26–28). Two major procedures for cytosolic acidification have been described. The first procedure involves preincubation of cells with 10–30 mM NH_4Cl to load them with NH_4^+ ion, followed by transferring cells into an ammonium-free medium (28). Intracellular NH_4^+ dissociates into membrane-permeable NH_3 and a proton, which cannot cross the plasma membrane. Therefore, after the removal of NH_4Cl , NH_3 rapidly diffuses out of the cell, whereas the protons temporarily remain inside and lower the cytosolic pH. The second procedure involves incubating the cells with millimolar concentrations of weak acids, such as acetic or succinic acids (27,28). In the protonated form, these acids rapidly cross the plasma membrane and enter the cells. Once inside the cell, the acids dissociate and lower the cytosolic pH.

In contrast to hypertonic sucrose and potassium depletion, cytosolic acidification does not prevent the formation of clathrin lattices but rather inhibits the budding off of clathrin-coated pits from the membrane (10). Despite these different mechanisms, cytosolic acidification is associated with the same side effects as the two other inhibitors of clathrin-dependent internalization. Examples of these side effects include inhibited uptake of macropinocytosis markers in fibroblasts (26) and attenuation of apical endocytosis of nonclathrin ligand ricin in polarized epithelial cells (29). Furthermore, cytosolic acidification has noticeable effects on the actin cytoskeleton, which include triggering global depolymerization of F-actin in neutrophils (30) and inducing translocation of actin microfilaments from the lateral plasma membrane to cytoplasmic aggregates in polarized epithelial cells (31). Overall, these data reveal pleiotropic effects of cytosolic acidification on intracellular trafficking and the cytoskeleton that may complicate the interpretation of the actions of this treatment.

2.4 Chlorpromazine

Chlorpromazine is a cationic amphipathic drug that, when used in a micromolar range (50–100 μM) inhibits clathrin-mediated endocytosis of various plasma membrane proteins (11–13,20). Such inhibition likely involves a loss of clathrin and the AP2 adaptor complex from the cell surface and their artificial assembly on endosomal membranes (13,32). There is no evidence in the literature that chlorpromazine affects lipid raft/caveolae-mediated endocytosis. Furthermore, several studies have demonstrated that receptor-mediated endocytosis, which can be inhibited

by chlorpromazine, is insensitive to the agents that block internalization via lipid rafts and vice versa (11,12). However, chlorpromazine was shown to block phagocytosis in immune cells such as neutrophils and macrophages (33,34) and inhibit neutrophil degranulation (33).

These data suggest that, in addition to affecting clathrin-coated pits, chlorpromazine may interfere with the biogenesis of large intracellular vesicles such as phagosomes, macropinosomes, and granules. Two possible mechanisms may underline this interference. First, since chlorpromazine is an amphipathic molecule, it can easily incorporate into the lipid bilayers and can increase lipid fluidity within the plasma membrane (35). This alteration in the physical state of the plasma membrane lipids may block the formation of large membrane invaginations similar to the known inhibitory actions of other membrane fluidizers on macropinocytosis (36). The second possible mechanism may involve a reported inhibitory effect of chlorpromazine on phospholipase C (PLC) (37), which is an important regulator of actin dynamics (38) and macropinocytosis (39,40). Such multiple interactions of chlorpromazine with intracellular lipids and cytoskeletal regulators should be considered as potential sources for the side effects of this inhibitor.

2.5 *Monodansylcadaverine*

Since 1980, monodansylcadaverine (MDC) has been extensively used to block clathrin-mediated endocytosis in different mammalian cells (7,15,41,42). The inhibitory activity of MDC is attributed to the stabilization of clathrin-coated pits by the drug (42). However, the evidence for this mechanism has been obtained only in cell-free systems using purified clathrin and very high (0.7–10 mM) concentrations of MDC (43). It remains to be investigated if similar stabilization of clathrin-coated pits can be achieved at lower (100–300 μ M) concentrations of MDC that attenuate endocytosis in living cells.

Monodansylcadaverine appears to be a relatively specific blocker of clathrin-mediated internalization. No studies have reported inhibitory actions of this drug on the lipid raft/caveolae-dependent pathway. Furthermore, its effects on macropinocytosis and phagocytosis remain controversial, with some studies demonstrating inhibition (44,45) and others reporting no observable blockage (15,46) of these pathways.

Some possible side effects of MDC treatment may originate from its known inhibitory activity toward the enzymes of the transglutaminase family (47). These enzymes are involved in posttranscriptional transamidation of various proteins. Particularly, transglutaminases have been shown to be important for the activation of Rho GTPases (48), which are the key regulators of actin assembly and dynamics. Furthermore, transglutaminase activity is required for the self-association of the major F-actin motor, myosin II (49). Therefore, inhibition of transglutaminase by MDC may result in global changes in the organization and dynamics of the actin cytoskeleton (48,49).

2.6 *Phenylarsine Oxide*

Phenylarsine oxide (PAO) is another chemical compound that, at low micromolar (1–20 μM) concentrations, blocks clathrin-dependent endocytosis (23,27,50,51). The exact mechanism of such inhibition remains unknown since no ultrastructural studies examining the effects of PAO on the formation of clathrin-coated pits have been reported. Furthermore, PAO is not selective to the clathrin pathways and has also been shown to inhibit macropinocytosis in adipocytes (52) and phagocytosis in mast cells (53).

Phenylarsine oxide is a trivalent arsenite that is known to crosslink vicinal sulfhydryl groups (54). Therefore, it is not surprising that it can inhibit multiple intracellular targets, including major cytoskeletal regulators such as protein tyrosine phosphatases (55) and Rho GTPase (56). Such effects together with the reported PAO-dependent depletion of intracellular adenosine triphosphate (ATP) (50) may explain the dramatic disorganization of actin cytoskeleton observed in PAO-treated cells (55,56). Overall, these serious side effects outweigh the usefulness of PAO as a selective inhibitor of clathrin-mediated endocytosis.

2.7 *Summary of Inhibitors of the Clathrin-Mediated Pathway*

Despite the common belief that the above pharmacological agents or chemical maneuvers selectively inhibit internalization via clathrin-coated pits, none of the inhibitors possesses absolute selectivity. In particular, all these inhibitors have been shown to block uptake of fluid-phase markers and therefore cannot be used to distinguish between clathrin-mediated endocytosis and macropinocytosis. In addition, all pharmacological blockers of the clathrin pathway may cause the reorganization of the cortical actin cytoskeleton and therefore grossly affect biochemical and functional properties of plasma membrane proteins via endocytosis-independent mechanisms. However, some of these inhibitors, such as potassium depletion, chlorpromazine, and MDC, can still be used for the initial discrimination between clathrin-mediated internalization and other endocytic pathways. On the other hand, hypertonic sucrose and PAO appear to be a poor choice to probe clathrin-mediated endocytosis because of their abundant side effects.

3 **Inhibitors of Lipid Raft/Caveolae-Mediated Endocytosis**

A vast majority of pharmacological inhibitors of caveolae/lipid-raft mediated endocytosis target cholesterol, a critical lipid constituent of membrane rafts and caveolae (3,57). Four different strategies have been used to modify the content or chemical properties of membrane cholesterol (57). The first strategy

involves general inhibition of cholesterol biosynthesis by statins. The second approach utilizes the extraction of cholesterol from the plasma membrane using cyclodextrins. The third strategy involves cholesterol sequestration within the membrane by polyene antibiotics such as filipin and nystatin. The fourth commonly used method utilizes the enzymatic modification of plasma membrane cholesterol by cholesterol oxidase. Detailed protocols for alterations of the plasma membrane cholesterol by these approaches have been described (57).

3.1 *Statins*

One of the most effective ways to deplete intracellular cholesterol involves inhibition of cholesterol synthesis by a group of low molecular weight substances termed statins. Statins such as lovastatin, simvastatin, and pravastatin are reversible inhibitors of the 3-hydroxy-3-methylglutaryl coenzyme A (HMG-CoA) reductase, which is a rate-limiting enzyme in cholesterol biosynthesis (58,59). Incubation of cells with 10–100 μM of statins for 3–4 h has been shown to result in almost 100% blockage of cholesterol synthesis (60). However, such a dramatic cholesterol depletion appears to have a general and nonspecific inhibitory effect on endocytosis. Indeed, treatment with statins reportedly blocked clathrin-dependent receptor-mediated internalization in lymphocytes and epithelial cells (60,61), inhibited internalization of the fluid-phase marker in epitheliocytes (60), and blocked phagocytosis in macrophages (62).

The inhibitory effects of statins on different internalization pathways have a simple mechanistic explanation. Statins block the synthesis of L-mevalonic acid, which is a common precursor not only for cholesterol but also for other isoprenoids such as farnesylpyrophosphate and geranylgeranylpyrophosphate (58). These last two intermediates serve as important lipid moieties for post-translational modification (isoprenylation) of various intracellular proteins, including members of Ras, Rho, and Rab families of small GTPases (58,63). A lack of the isoprenylation has been shown to prevent targeting of small GTPases to the cell membranes where they subsequently become activated. Hence, the incubation with statins causes the accumulation of inactive cytosolic forms of Rho and Rab (58,63,64), thus leading to a profound and nonspecific disruption of intracellular vesicle trafficking and the actin cytoskeleton.

3.2 *Methyl- β -cyclodextrin*

Methyl- β -cyclodextrin (M β CD) is a widely used inhibitor that alters the structure of cholesterol-rich domains in the cell membranes (57). M β CD is a cyclic

heptasaccharide containing a hydrophobic core that has a high affinity for cholesterol (65). When added to cells at 5–10 mM concentrations, M β CD rapidly (within 1 h) forms soluble inclusion complexes with cholesterol, thereby depleting this lipid from the cell membranes (66). This treatment was shown to cause the flattening of caveolae and mislocalization of caveolin-1 in mouse fibroblasts (67). Furthermore, M β CD reportedly inhibits internalization of several marker ligands of lipid rafts and caveolae, including cholera toxin (68), glucose transporter (69), and nitric oxide synthase (70).

In addition to its effects on lipid raft/caveolae-mediated endocytosis, acute cholesterol depletion by M β CD was shown to block internalization of a classical ligand of clathrin-mediated pathway, transferrin (69,71). This side effect can be explained by the blockage of invagination of clathrin-coated pits in the M β CD-treated cells (71). In addition, M β CD was shown to block fluid-phase endocytosis in epithelial and endothelial cells (72,73). Such a nonspecific inhibition of several internalization pathways by acute cholesterol depletion is not surprising when considering the dramatic effects of M β CD treatment on cellular cytoskeleton and signaling. These effects include the dispersion of a cortical F-actin in adipocytes (74), inhibition of phosphatidylinositol turnover in A431 carcinoma cells (75), and activation of Ras GTPase in Cos-7 epithelial cells (76).

3.3 *Filipin and Nystatin*

Polyene antibiotics such as filipin and nystatin readily interact with cholesterol in model and biological membranes and are able to change properties of cholesterol-rich membrane domains. Both antibiotics create large aggregates in the membrane that are visible by freeze-fracture electron microscopy (77). The aggregates accumulate cholesterol, thereby sequestering this lipid from the membrane structures. As a result, filipin (~1 μ M) and nystatin (20–50 μ M) induce a profound distortion of the structure and functions of the cholesterol-rich membrane domain, including aberrations in the caveolar shape (78), dispersion of GPI-anchored proteins from these structures (79), as well as the inhibition of lipid raft ligands internalization (78,80,81).

Polyene antibiotics appear to be quite selective inhibitors of the lipid raft/caveolae pathway. In contrast to M β CD, nystatin and filipin do not inhibit the internalization of transferrin (57,78), which suggests that these drugs have little effect on the clathrin-mediated endocytosis. Furthermore, one recent study demonstrated that although M β CD blocked macropinocytosis in rat fibroblasts, filipin treatment did not affect this pathway (82). However, two possible side effects of filipin treatment should be considered. The first involves permeabilization of the plasma membrane that occurs because of filipin's interactions not only with cholesterol but also with membrane phospholipids (83). Fortunately, membrane permeabilization occurs at relatively high (above 10 μ M) levels of filipin, and this side effect can be minimized by lowering the drug concentration. Another reported side effect of filipin involves

disruptions of the linkage between cortical F-actin and the plasma membrane (84). The mechanisms behind this cytoskeletal effect of filipin and its impact on inhibition of endocytosis remain to be investigated.

3.4 Cholesterol Oxidase

Cholesterol oxidase converts cholesterol into 4-cholesten-3-one (85). The oxysterol remains enriched in caveolae and dramatically changes their properties (86). These changes include translocation of caveolin from the plasma membrane to the Golgi complex in fibroblasts (86) and a decrease in the number of caveolae in smooth muscle cells (87). Only a few studies used cholesterol oxidase to block caveolae-mediated endocytosis, but they showed that this treatment attenuates internalization of caveolae ligands as efficiently as the more popular procedures of cholesterol depletion (27,69). In comparison to the related techniques, the treatment with cholesterol oxidase appears to be a more selective method of cholesterol depletion. This superior selectivity is based on the high substrate specificity of the enzyme as well as on its non-permeability thorough the plasma membrane. In addition, this treatment appears to be well tolerated by cells and does not induce significant leakage of the plasma membrane (88).

Nevertheless, two possible problems of using cholesterol oxidase as an inhibitor of lipid raft/caveolae-mediated endocytosis should be considered. The first is inefficient oxidation of cholesterol in living cells. Indeed, the action of cholesterol oxidase depends on a variety of factors, including phospholipid composition, surface pressure of the plasma membrane, presence of divalent cations, and ionic strength of the media (89). The second possible problem of using cholesterol oxidase arises from its enigmatic ability to switch protein internalization from caveolae to clathrin-coated pits (90). Both problems may lead to a false-negative conclusion on the involvement of lipid raft/caveolae-mediated endocytosis.

3.5 Summary of Inhibitors of Lipid Raft/ Caveolae-Mediated Endocytosis

A body of literature suggests that lipid raft/caveolae-mediated endocytosis can be selectively inhibited by an acute depletion of the plasma membrane cholesterol. Among different protocols of cholesterol depletion, the incubation with filipin and nystatin and cholesterol oxidase treatment produce the fewest side effects. However, appropriate controls should be included while performing both procedures, such as a control for plasma membrane integrity during filipin exposure and a control for the efficiency of cholesterol oxidase treatment. It should be stressed that chronic inhibition of cholesterol synthesis by statins or acute cholesterol depletion by M β CD nonspecifically disrupts intracellular vesicle trafficking and the actin

cytoskeleton and should not be used to probe lipid raft/caveolae-mediated endocytosis.

4 Inhibitors of Macropinocytosis and Phagocytosis

Despite the fact that macropinocytosis and phagocytosis are the oldest known types of endocytosis, only a few pharmacological tools have been developed to study these internalization pathways in living cells. This has two explanations. First, unlike clathrin-coated pits and caveolae that possess a specific protein or lipid coat, no unique protein or lipid targets for pharmacological inhibition have been identified in macropinosomes or phagosomes. Furthermore, it is generally believed that macropinosomes and phagosomes can be easily distinguished from other types of plasma membrane-derived vesicles because of their large size (above 0.2 μm diameter; 6). However, this criterion does not always work since recent studies have demonstrated the clathrin-dependent formation of large intercellular vesicles during internalization of bacteria and epithelial junctions (91,92).

Three major types of pharmacological inhibitors have been used to disrupt macropinocytosis and phagocytosis. They include inhibitors of sodium–proton exchange, F-actin-depolymerizing agents, and drugs that target phosphoinositide metabolism.

4.1 Inhibitors of Sodium–Proton Exchange

An early serendipitous observation that epidermal growth factor simultaneously stimulates pinocytosis and amiloride-sensitive sodium–proton exchange in A431 carcinoma cells prompted researchers to use amiloride for the inhibition of macropinocytosis (93). Subsequently, amiloride and its derivatives 5-(*N*-ethyl-*N*-isopropyl) amiloride (EIPA) and dimethyl amiloride (DMA) were shown to block constitutive and stimulated macropinocytosis and phagocytosis in a variety of mammalian cells (40,94–96). Amiloride blocks macropinocytosis when used at millimolar concentrations (93), whereas EIPA and DMA are effective in the range of 50–100 μM (94,95,97). These differences in potency suggest that the blockage of the activity of the Na^+/H^+ exchanger isoform 1 underlies the inhibitory actions of amiloride and its derivatives.

Although the original study found no effect of amiloride on internalization of the classical clathrin pathway ligand transferrin (93), subsequent publications demonstrated that this group of inhibitors may also block clathrin-mediated endocytosis (27,98). In addition, amiloride was shown to attenuate internalization through lipid rafts (99), whereas EIPA reportedly altered morphology and the intracellular distribution of early and late endosomes (97). Furthermore, EIPA was shown to induce reorganization of the F-actin in epithelial cells, which included the disassembly of

stress fibers, pseudopod retraction, and loss of cell–matrix adhesions (100). These data clearly show multiple side effects of amiloride and its derivatives on intracellular vesicle trafficking and the cytoskeleton.

4.2 *F-Actin-Depolymerizing Drugs*

Since macropinosomes and phagosomes represent large F-actin-coated vesicles (4–6), disruption of their F-actin coat should prevent the formation of these structures. Submicromolar concentrations of two pharmacological agents, cytochalasin D and latrunculins, have been commonly used to disassemble the actin cytoskeleton in living cells (101). Cytochalasin D blocks actin polymerization by occupying a faster-growing “barbed” end of actin filaments, whereas latrunculins bind to monomeric actin, thus preventing its incorporation into filaments (101). Both types of F-actin-depolymerizing drugs have reportedly blocked membrane ruffling and inhibited macropinocytosis and phagocytosis under various experimental conditions (102–104).

It is noteworthy that recent studies have implicated the actin cytoskeleton in the regulation of different endocytic pathways (*see, for review, Refs. 105 and 106*). Indeed, confocal microscopy imaging of living cells revealed that the formation and internalization of both clathrin-coated pits and caveolae are accompanied by the recruitment of actin to these structures. Furthermore, pharmacological inhibition of actin polymerization has been shown to block endocytosis via clathrin-coated pits and caveolae (105,106). These data strongly suggest that cytochalasin D and latrunculins should be considered as global and nonselective inhibitors of all internalization pathways rather than specific blockers of macropinocytosis and phagocytosis.

4.3 *Inhibitors of Phosphoinositide Metabolism*

Macropinocytosis and phagocytosis have also been targeted by inhibiting either phosphoinositide 3-kinase (PI3K) or phosphoinositide-specific PLC, which are the key enzymes involved in phosphoinositide metabolism (4,39). PI3K is known to phosphorylate the hydroxyl group at the third carbon in the inositol ring of phosphoinositides, generating the so-called D3 products (107), whereas PLC hydrolyzes one of the D3 phosphoinositides to produce a diacylglycerol and inositol 1,4,5-triphosphate (38). Two PI3K inhibitors, wortmannin (100–200 nM) and LY290042 (~20 μM) were used to block constitutive and stimulated macropinocytosis and phagocytosis in macrophages, fibroblasts, and epithelial cells (102–104,108). Likewise, these internalization pathways appear to be sensitive to PLC inhibitors nitrocarboxyphenyl-*N*, *N*-diphenylcarbamate (50–100 μM) and U73122 (1 μM)(39,40,103). The relationship between PI3K and PLC signaling during macropinocytosis remains poorly understood, although one recent study suggested their sequential activation and placed PLC downstream of PI3K in the signaling cascade (39).

Two major mechanisms are likely to underlie the role of phosphatidylinositide-metabolizing enzymes in endocytosis. The first involves the assembly of multiprotein complexes critical for the formation and fusion of intracellular vesicles (38,107,109). This mechanism is determined by the ability of phosphatidylinositides to bind scaffolding and signaling proteins and link them to phospholipid membranes. Proteins possessing phosphatidylinositide-binding domains include several clathrin adaptors, dynamin GTPase, as well as an early endosomal protein EEA1 (107,109). The second mechanism involves reorganization of the actin cytoskeleton since PI3K- and PLC-generated lipid mediators are known to regulate several important steps (nucleation, elongation, and bundling) in the assembly of actin filaments (38,107). The ability of phosphoinositides to modulate different steps in intracellular vesicle trafficking and cytoskeletal reorganizations is inconsistent with their selective involvement in macropinocytosis and phagocytosis. Indeed, PI3K and PLC inhibitors have pleiotropic effects on endocytosis as they are able to block the internalization of known ligands of the clathrin- and caveolae-mediated pathways (110).

4.4 Summary of Inhibitors of Macropinocytosis and Phagocytosis

A wealth of published data casts doubts on the specificity of all pharmacological tools used to block macropinocytosis and phagocytosis. It is obvious that F-actin-depolymerizing drugs and inhibitors of phosphoinositide metabolisms may interrupt different internalization pathways and affect the architecture and dynamics of a cortical F-actin. As a result, their inhibitory effects on endocytosis are difficult to interpret unambiguously. Of all drugs discussed in this section, selective inhibitors of the Na⁺/H⁺ exchanger such as EIPA and DMA may have the fewest side effects and should be considered as a first choice for the pharmacological probing of macropinocytosis and phagocytosis. However, possible endocytosis-unrelated effects of these drugs on ion transport and cytoskeleton should be considered.

5 Conclusion and Perspectives

One simple conclusion of this review is that none of the popular inhibitors of different endocytic pathways possesses an absolute specificity to the pathway of interest. This lack of absolute specificity does not mean that pharmacological inhibitors should be excluded from probing different endocytic pathways. Some of them remain useful tools, especially when used in combination with modern molecular and cell biology approaches. Furthermore, a renewal of interest in using small molecular inhibitors to probe intracellular vesicle trafficking can be predicted based on the rising popularity of the chemical compound library screenings and on the

increased numbers of successful structural studies of the critical proteins involved in different endocytic pathways. Relevant examples of fruitful chemical library screens include two different inhibitors of dynamin GTPase (*111,112*), whereas structural studies have already led to the development of a peptide that selectively inhibits clathrin-mediated endocytosis by disrupting the interaction between the clathrin adaptor, amphiphysin, and dynamin (*2*). We can expect therefore that future work will discover more highly selective pharmacological inhibitors of endocytosis that can be used for experimental and clinical applications.

Acknowledgments I thank Moshe Bachar for his excellent editorial assistance and Drs. Alex Mongin and Andrew Kowalczyk for their valuable comments on the manuscript. This work was supported by a Career Development Award from the Crohn's and Colitis Foundation of America.

References

1. Conner, S.D., and Schmid, S.L. (2003) Regulated portals of entry into the cell. *Nature* **422**, 37–44.
2. Marsh, M., and McMahon, H.T. (1999) The structural era of endocytosis. *Science* **285**, 215–220.
3. Parton, R.G., and Richards, A.A. (2003) Lipid rafts and caveolae as portals for endocytosis: new insights and common mechanisms. *Traffic* **4**, 724–738.
4. Amyere, M., Mettlen, M., Van Der Smissen, P., et al. (2002) Origin, originality, functions, subversions and molecular signalling of macropinocytosis. *Int. J. Med. Microbiol.* **291**, 487–494.
5. Niedergang, F., and Chavrier, P. (2004) Signaling and membrane dynamics during phagocytosis: many roads lead to the phagos(R)ome. *Curr. Opin. Cell Biol.* **16**, 422–428.
6. Swanson, J.A., and Watts, C. (1995) Macropinocytosis. *Trends Cell Biol.* **5**, 424–428.
7. Davies, P.J., Davies, D.R., Levitzki, A., et al. (1980) Transglutaminase is essential in receptor-mediated endocytosis of alpha 2-macroglobulin and polypeptide hormones. *Nature* **283**, 162–167.
8. Larkin, J.M., Brown, M.S., Goldstein, J.L., and Anderson, R.G. (1983) Depletion of intracellular potassium arrests coated pit formation and receptor-mediated endocytosis in fibroblasts. *Cell* **33**, 273–285.
9. Daukas, G., and Zigmond, S.H. (1985) Inhibition of receptor-mediated but not fluid-phase endocytosis in polymorphonuclear leukocytes. *J. Cell Biol.* **101**, 1673–1679.
10. Hansen, S.H., Sandvig, K., and van Deurs, B. (1993) Clathrin and HA2 adaptors: effects of potassium depletion, hypertonic medium, and cytosol acidification. *J. Cell Biol.* **121**, 61–72.
11. Inal, J., Miot, S., and Schifferli, J.A. (2005) The complement inhibitor, CRIT, undergoes clathrin-dependent endocytosis. *Exp. Cell Res.* **310**, 54–65.
12. Tulapurkar, M.E., Schafer, R., Hanck, T., et al. (2005) Endocytosis mechanism of P2Y2 nucleotide receptor tagged with green fluorescent protein: clathrin and actin cytoskeleton dependence. *Cell. Mol. Life Sci.* **62**, 1388–1399.
13. Yao, D., Ehrlich, M., Henis, Y.I., and Leof, E.B. (2002) Transforming growth factor- β receptors interact with AP2 by direct binding to β 2 subunit. *Mol. Biol. Cell* **13**, 4001–4012.
14. Carpentier, J.L., Sawano, F., Geiger, D., et al. (1989) Potassium depletion and hypertonic medium reduce “non-coated” and clathrin-coated pit formation, as well as endocytosis through these two gates. *J. Cell Physiol.* **138**, 519–526.

15. Bradley, J.R., Johnson, D.R., and Pober, J.S. (1993) Four different classes of inhibitors of receptor-mediated endocytosis decrease tumor necrosis factor-induced gene expression in human endothelial cells. *J. Immunol.* **150**, 5544–5555.
16. Synnes, M., Prydz, K., Lovdal, T., Brech, A., and Berg, T. (1999) Fluid phase endocytosis and galactosyl receptor-mediated endocytosis employ different early endosomes. *Biochim. Biophys. Acta* **1421**, 317–328.
17. Page, E., Winterfield, J., Goings, G., Bastawrous, A., and Upshaw-Earley, J. (1998) Water channel proteins in rat cardiac myocyte caveolae: osmolarity-dependent reversible internalization. *Am. J. Physiol.* **274**, H1988–H2000.
18. Malek, A.M., Xu, C., Kim, E.S., and Alper, S.L. (2006) Hypertonicity triggers RhoA-dependent assembly of myosin-containing striated polygonal actin networks in endothelial cells. *Am. J. Physiol. Cell Physiol.* **292**, C1645–C1659.
19. Bustamante, M., Roger, F., Bochaton-Piallat, M.L., et al. (2003) Regulatory volume increase is associated with p38 kinase-dependent actin cytoskeleton remodeling in rat kidney MTAL. *Am. J. Physiol. Renal Physiol.* **285**, F336–F347.
20. Liu, J., Kesiry, R., Periyasamy, S.M., et al. (2004) Ouabain induces endocytosis of plasmalemmal Na/K-ATPase in LLC-PK1 cells by a clathrin-dependent mechanism. *Kidney Int.* **66**, 227–241.
21. Idkowiak-Baldys, J., Becker, K.P., Kitatani, K., and Hannun, Y.A. (2006) Dynamic sequestration of the recycling compartment by classical protein kinase C. *J. Biol. Chem.* **281**, 22321–22331.
22. Cupers, P., Veithen, A., Kiss, A., Baudhuin, P., and Courttoy, P.J. (1994) Clathrin polymerization is not required for bulk-phase endocytosis in rat fetal fibroblasts. *J. Cell Biol.* **127**, 725–735.
23. Yumoto, R., Nishikawa, H., Okamoto, M., et al. (2006) Clathrin-mediated endocytosis of FITC-albumin in alveolar type II epithelial cell line RLE-6TN. *Am. J. Physiol. Lung Cell Mol. Physiol.* **290**, L946–L955.
24. Altankov, G., and Grinnell, F. (1993) Depletion of intracellular potassium disrupts coated pits and reversibly inhibits cell polarization during fibroblast spreading. *J. Cell Biol.* **120**, 1449–1459.
25. Rajasekaran, S.A., Palmer, L.G., Moon, S.Y., et al. (2001) Na,K-ATPase activity is required for formation of tight junctions, desmosomes, and induction of polarity in epithelial cells. *Mol. Biol. Cell* **12**, 3717–3732.
26. Cosson, P., de Curtis, I., Pouyssegur, J., Griffiths, G., and Davoust, J. (1989) Low cytoplasmic pH inhibits endocytosis and transport from the *trans*-Golgi network to the cell surface. *J. Cell Biol.* **108**, 377–387.
27. Ivanov, A.I., Nusrat, A., and Parkos, C.A. (2004) Endocytosis of epithelial apical junctional proteins by a clathrin-mediated pathway into a unique storage compartment. *Mol. Biol. Cell* **15**, 176–188.
28. Sandvig, K., Olsnes, S., Petersen, O.W., and van Deurs, B. (1987) Acidification of the cytosol inhibits endocytosis from coated pits. *J. Cell Biol.* **105**, 679–689.
29. Eker, P., Holm, P.K., van Deurs, B., and Sandvig, K. (1994) Selective regulation of apical endocytosis in polarized Madin–Darby canine kidney cells by mastoparan and cAMP. *J. Biol. Chem.* **269**, 18607–18615.
30. Suzuki, K., and Namiki, H. (2007) Cytoplasmic pH-dependent spreading of polymorphonuclear leukocytes: regulation by pH of PKC subcellular distribution and F-actin assembly. *Cell Biol. Int.* **31**, 279–288.
31. Huotari, V., Vaaranemi, J., Lehto, V.P., and Eskelinen, S. (1996) Regulation of the disassembly/assembly of the membrane skeleton in Madin–Darby canine kidney cells. *J. Cell Physiol.* **167**, 121–130.
32. Wang, L.H., Rothberg, K.G., and Anderson, R.G. (1993) Mis-assembly of clathrin lattices on endosomes reveals a regulatory switch for coated pit formation. *J. Cell Biol.* **123**, 1107–1117.
33. Elferink, J.G. (1979) Chlorpromazine inhibits phagocytosis and exocytosis in rabbit polymorphonuclear leukocytes. *Biochem. Pharmacol.* **28**, 965–968.

34. Watanabe, S., Hirose, M., Miyazaki, A., et al. (1988) Calmodulin antagonists inhibit the phagocytic activity of cultured Kupffer cells. *Lab. Invest.* **59**, 214–218.
35. Ogiso, T., Iwaki, M., and Mori, K. (1981) Fluidity of human erythrocyte membrane and effect of chlorpromazine on fluidity and phase separation of membrane. *Biochim. Biophys. Acta* **649**, 325–335.
36. Giocondi, M.C., Mamdouh, Z., and Le Grimellec, C. (1995) Benzyl alcohol differently affects fluid phase endocytosis and exocytosis in renal epithelial cells. *Biochim. Biophys. Acta* **1234**, 197–202.
37. Walenga, R.W., Opas, E.E., and Feinstein, M.B. (1981) Differential effects of calmodulin antagonists on phospholipases A₂ and C in thrombin-stimulated platelets. *J. Biol. Chem.* **256**, 12523–12528.
38. Wells, A., Ware, M.F., Allen, F.D., and Lauffenburger, D.A. (1999) Shaping up for shipping out: PLC γ signaling of morphology changes in EGF-stimulated fibroblast migration. *Cell Motil. Cytoskeleton* **44**, 227–233.
39. Amyere, M., Payrastra, B., Krause, U., et al. (2000) Constitutive macropinocytosis in oncogene-transformed fibroblasts depends on sequential permanent activation of phosphoinositide 3-kinase and phospholipase C. *Mol. Biol. Cell* **11**, 3453–3467.
40. Veithen, A., Cupers, P., Baudhuin, P., and Courtoy, P.J. (1996) ν -Src induces constitutive macropinocytosis in rat fibroblasts. *J. Cell Sci.* **109**, 2005–2012.
41. Panicker, A.K., Buhusi, M., Erickson, A., and Maness, P.F. (2006) Endocytosis of β 1 integrins is an early event in migration promoted by the cell adhesion molecule L1. *Exp. Cell Res.* **312**, 299–307.
42. Wang, J., and Liu, X.J. (2003) A G protein-coupled receptor kinase induces *Xenopus* oocyte maturation. *J. Biol. Chem.* **278**, 15809–15814.
43. Nandi, P.K., Van Jaarsveld, P.P., Lippoldt, R.E., and Edelhoeh, H. (1981) Effect of basic compounds on the polymerization of clathrin. *Biochemistry* **20**, 6706–6710.
44. Leu, R.W., Herriott, M.J., Moore, P.E., et al. (1982) Enhanced transglutaminase activity associated with macrophage activation. Possible role in Fc-mediated phagocytosis. *Exp. Cell Res.* **141**, 191–199.
45. Thompson, K., Rogers, M.J., Coxon, F.P., and Crockett, J.C. (2006) Cytosolic entry of bisphosphonate drugs requires acidification of vesicles after fluid-phase endocytosis. *Mol. Pharmacol.* **69**, 1624–1632.
46. Schlegel, R., Dickson, R.B., Willingham, M.C., and Pastan, I.H. (1982) Amantadine and dansylcadaverine inhibit vesicular stomatitis virus uptake and receptor-mediated endocytosis of alpha 2-macroglobulin. *Proc. Natl. Acad. Sci. U. S. A.* **79**, 2291–2295.
47. Mishra, S., and Murphy, L.J. (2004) Tissue transglutaminase has intrinsic kinase activity: identification of transglutaminase 2 as an insulin-like growth factor-binding protein-3 kinase. *J. Biol. Chem.* **279**, 23863–23868.
48. Singh, U.S., Pan, J., Kao, Y.L., et al. (2003) Tissue transglutaminase mediates activation of RhoA and MAP kinase pathways during retinoic acid-induced neuronal differentiation of SH-SY5Y cells. *J. Biol. Chem.* **278**, 391–399.
49. Kang, S.J., Shin, K.S., Song, W.K., et al. (1995) Involvement of transglutaminase in myofibril assembly of chick embryonic myoblasts in culture. *J. Cell Biol.* **130**, 1127–1136.
50. Gibson, A.E., Noel, R.J., Herlihy, J.T., and Ward, W.F. (1989) Phenylarsine oxide inhibition of endocytosis: effects on asialofetuin internalization. *Am. J. Physiol.* **257**, C182–C184.
51. Sturrock, A., Alexander, J., Lamb, J., et al. (1990) Characterization of a transferrin-independent uptake system for iron in HeLa cells. *J. Biol. Chem.* **265**, 3139–3145.
52. Frost, S.C., Lane, M.D., and Gibbs, E.M. (1989) Effect of phenylarsine oxide on fluid phase endocytosis: further evidence for activation of the glucose transporter. *J. Physiol.* **141**, 467–474.
53. Massol, P., Montcourrier, P., Guillemot, J.C., and Chavrier, P. (1998) Fc receptor-mediated phagocytosis requires Cdc42 and Rac1. *EMBO J.* **17**, 6219–6229.
54. Frost, S.C., and Lane, M.D. (1985) Evidence for the involvement of vicinal sulfhydryl groups in insulin-activated hexose transport by 3T3-L1 adipocytes. *J. Biol. Chem.* **260**, 2646–2652.

55. Retta, S.F., Barry, S.T., Critchley, D.R., et al. (1996) Focal adhesion and stress fiber formation is regulated by tyrosine phosphatase activity. *Exp. Cell Res.* **229**, 307–317.
56. Gerhard, R., John, H., Aktories, K., and Just, I. (2003) Thiol-modifying phenylarsine oxide inhibits guanine nucleotide binding of Rho but not of Rac GTPases. *Mol. Pharmacol.* **63**, 1349–1355.
57. Smart, E.J., and Anderson, R.G. (2002) Alterations in membrane cholesterol that affect structure and function of caveolae. *Methods Enzymol.* **353**, 131–139.
58. Liao, J.K., and Laufs, U. (2005) Pleiotropic effects of statins. *Annu. Rev. Pharmacol. Toxicol.* **45**, 89–118.
59. Tobert, J.A. (2003) Lovastatin and beyond: the history of the HMG-CoA reductase inhibitors. *Nat. Rev. Drug Discov.* **2**, 517–526.
60. Sidaway, J.E., Davidson, R.G., McTaggart, F., et al. (2004) Inhibitors of 3-hydroxy-3-methylglutaryl-CoA reductase reduce receptor-mediated endocytosis in opossum kidney cells. *J. Am. Soc. Nephrol.* **15**, 2258–2265.
61. Chan, P.C., Lafreniere, R., and Parsons, H.G. (1997) Lovastatin increases surface low density lipoprotein receptor expression by retarding the receptor internalization rate in proliferating lymphocytes. *Biochem. Biophys. Res. Commun.* **235**, 117–122.
62. Loike, J.D., Shabtai, D.Y., Neuhut, R., et al. (2004) Statin inhibition of Fc receptor-mediated phagocytosis by macrophages is modulated by cell activation and cholesterol. *Arterioscler. Thromb. Vasc. Biol.* **24**, 2051–2056.
63. Desnoyers, L., Anant, J.S., and Seabra, M.C. (1996) Geranylgeranylation of Rab proteins. *Biochem. Soc. Trans.* **24**, 699–703.
64. Cordle, A., Koenigsknecht-Talboo, J., Wilkinson, B., et al. (2005) Mechanisms of statin-mediated inhibition of small G-protein function. *J. Biol. Chem.* **280**, 34202–34209.
65. Irie, T., Fukunaga, K., and Pitha, J. (1992) Hydroxypropylcyclodextrins in parenteral use. I: Lipid dissolution and effects on lipid transfers in vitro. *J. Pharm. Sci.* **81**, 521–523.
66. Kilsdonk, E.P., Yancey, P.G., Stoudt, G.W., et al. (1995) Cellular cholesterol efflux mediated by cyclodextrins. *J. Biol. Chem.* **270**, 17250–17256.
67. Westermann, M., Steiniger, F., and Richter, W. (2005) Belt-like localization of caveolin in deep caveolae and its re-distribution after cholesterol depletion. *Histochem. Cell Biol.* **123**, 613–620.
68. Lu, L., Khan, S., Lencer, W., and Walker, W.A. (2005) Endocytosis of cholera toxin by human enterocytes is developmentally regulated. *Am. J. Physiol. Gastrointest. Liver Physiol.* **289**, G332–G341.
69. Shigematsu, S., Watson, R.T., Khan, A.H., and Pessin, J.E. (2003) The adipocyte plasma membrane caveolin functional/structural organization is necessary for the efficient endocytosis of GLUT4. *J. Biol. Chem.* **278**, 10683–10690.
70. Maniatis, N.A., Brovkovich, V., Allen, S.E., et al. (2006) Novel mechanism of endothelial nitric oxide synthase activation mediated by caveolae internalization in endothelial cells. *Circ. Res.* **99**, 870–877.
71. Rodal, S.K., Skretting, G., Garred, O., et al. (1999) Extraction of cholesterol with methyl-beta-cyclodextrin perturbs formation of clathrin-coated endocytic vesicles. *Mol. Biol. Cell* **10**, 961–974.
72. Liu, N.Q., Lossinsky, A.S., Popik, et al. (2002) Human immunodeficiency virus type 1 enters brain microvascular endothelia by macropinocytosis dependent on lipid rafts and the mitogen-activated protein kinase signaling pathway. *J. Virol.* **76**, 6689–6700.
73. Lu, H., Sun, T.X., Bouley, R., et al. (2004) Inhibition of endocytosis causes phosphorylation (S256)-independent plasma membrane accumulation of AQP2. *Am. J. Physiol. Renal Physiol.* **286**, F233–F243.
74. Kanzaki, M., and Pessin, J.E. (2002) Caveolin-associated filamentous actin (Cav-actin) defines a novel F-actin structure in adipocytes. *J. Biol. Chem.* **277**, 25867–25869.
75. Pike, L.J., and Miller, J.M. (1998) Cholesterol depletion delocalizes phosphatidylinositol bisphosphate and inhibits hormone-stimulated phosphatidylinositol turnover. *J. Biol. Chem.* **273**, 22298–22304.

76. Kranenburg, O., Verlaan, I., and Moolenaar, W.H. (2001) Regulating c-Ras function. cholesterol depletion affects caveolin association, GTP loading, and signaling. *Curr. Biol.* **11**, 1880–1884.
77. Kitajima, Y., Sekiya, T., and Nozawa, Y. (1976) Freeze-fracture ultrastructural alterations induced by filipin, pimarinic, nystatin and amphotericin B in the plasma membranes of *Epidermophyton*, *Saccharomyces* and red complex-induced membrane lesions. *Biochim. Biophys. Acta* **455**, 452–465.
78. Ros-Baro, A., Lopez-Iglesias, C., Peiro, S., et al. (2001) Lipid rafts are required for GLUT4 internalization in adipose cells. *Proc. Natl. Acad. Sci. U. S. A.* **98**, 12050–12055.
79. Rothberg, K.G., Ying, Y.S., Kamen, B.A., and Anderson, R.G. (1990) Cholesterol controls the clustering of the glycosphospholipid-anchored membrane receptor for 5-methyltetrahydrofolate. *J. Cell Biol.* **111**, 2931–2938.
80. Orlandi, P.A., and Fishman, P.H. (1998) Filipin-dependent inhibition of cholera toxin: evidence for toxin internalization and activation through caveolae-like domains. *J. Cell Biol.* **141**, 905–915.
81. Singh, R.D., Puri, V., Valiyaveetil, J.T., et al. (2003) Selective caveolin-1-dependent endocytosis of glycosphingolipids. *Mol. Biol. Cell* **14**, 3254–3265.
82. Monis, G.F., Schultz, C., Ren, R., et al. (2006) Role of endocytic inhibitory drugs on internalization of amyloidogenic light chains by cardiac fibroblasts. *Am. J. Pathol.* **169**, 1939–1952.
83. Milhaud, J. (1992) Permeabilizing action of filipin III on model membranes through a filipin-phospholipid binding. *Biochim. Biophys. Acta* **1105**, 307–318.
84. Harder, T., Kellner, R., Parton, R.G., and Gruenberg, J. (1997) Specific release of membrane-bound annexin II and cortical cytoskeletal elements by sequestration of membrane cholesterol. *Mol. Biol. Cell* **8**, 533–545.
85. MacLachlan, J., Wotherspoon, A.T., Ansell, R.O., and Brooks, C.J. (2000) Cholesterol oxidase: sources, physical properties and analytical applications. *J. Steroid Biochem. Mol. Biol.* **72**, 169–195.
86. Smart, E.J., Ying, Y.S., Conrad, P.A., and Anderson, R.G. (1994) Caveolin moves from caveolae to the Golgi apparatus in response to cholesterol oxidation. *J. Cell Biol.* **127**, 1185–1197.
87. Thyberg, J. (2003) Cholesterol oxidase and the hydroxymethylglutaryl coenzyme A reductase inhibitor mevinolin perturb endocytic trafficking in cultured vascular smooth muscle cells. *J. Submicrosc. Cytol. Pathol.* **35**, 457–468.
88. Brasaemle, D.L., and Attie, A.D. (1990) Rapid intracellular transport of LDL-derived cholesterol to the plasma membrane in cultured fibroblasts. *J. Lipid Res.* **31**, 103–112.
89. Lange, Y. (1992) Tracking cell cholesterol with cholesterol oxidase. *J. Lipid Res.* **33**, 315–321.
90. Okamoto, Y., Ninomiya, H., Miwa, S., and Masaki, T. (2000) Cholesterol oxidation switches the internalization pathway of endothelin receptor type A from caveolae to clathrin-coated pits in Chinese hamster ovary cells. *J. Biol. Chem.* **275**, 6439–6446.
91. Piehl, M., Lehmann, C., Gumpert, A., et al. (2007) Internalization of large double-membrane intercellular vesicles by a clathrin-dependent endocytic process. *Mol. Biol. Cell* **18**, 337–347.
92. Veiga, E., and Cossart, P. (2006) The role of clathrin-dependent endocytosis in bacterial internalization. *Trends Cell Biol.* **16**, 499–504.
93. West, M.A., Bretscher, M.S., and Watts, C. 1989. Distinct endocytotic pathways in epidermal growth factor-stimulated human carcinoma A431 cells. *J. Cell Biol.* **109**, 2731–2739.
94. Marechal, V., Prevost, M.C., Petit, C., et al. (2001) Human immunodeficiency virus type 1 entry into macrophages mediated by macropinocytosis. *J. Virol.* **75**, 11166–11177.
95. Nakase, I., Niwa, M., Takeuchi, T., et al. (2004) Cellular uptake of arginine-rich peptides: roles for macropinocytosis and actin rearrangement. *Mol. Ther.* **10**, 1011–1022.
96. von Delwig, A., Bailey, E., Gibbs, D.M., and Robinson, J.H. (2002) The route of bacterial uptake by macrophages influences the repertoire of epitopes presented to CD4 T cells. *Eur. J. Immunol.* **32**, 3714–3719.
97. Fretz, M., Jin, J., Conibere, R., et al. (2006) Effects of Na⁺/H⁺ exchanger inhibitors on subcellular localisation of endocytic organelles and intracellular dynamics of protein transduction domains HIV-TAT peptide and octaarginine. *J. Control Release* **116**, 247–254.

98. Meier, O., Boucke, K., Hammer, S.V., et al. (2002) Adenovirus triggers macropinocytosis and endosomal leakage together with its clathrin-mediated uptake. *J. Cell Biol.* **158**, 1119–1131.
99. Wadia, J.S., Stan, R.V., and Dowdy, S.F. (2004) Transducible TAT-HA fusogenic peptide enhances escape of TAT-fusion proteins after lipid raft macropinocytosis. *Nat. Med.* **10**, 310–315.
100. Lagana, A., Vadnais, J., Le, P.U., et al. (2000) Regulation of the formation of tumor cell pseudopodia by the Na⁺/H⁺ exchanger NHE1. *J. Cell Sci.* **113**, 3649–3662.
101. Peterson, J.R., and Mitchison, T.J. (2002) Small molecules, big impact: a history of chemical inhibitors and the cytoskeleton. *Chem. Biol.* **9**, 1275–1285.
102. Dharmawardhane, S., Schurmann, A., Sells, M.A., et al. 2000. Regulation of macropinocytosis by p21-activated kinase-1. *Mol. Biol. Cell* **11**, 3341–3352.
103. Mettlen, M., Platek, A., Van Der Smissen, P., et al. (2006) Src triggers circular ruffling and macropinocytosis at the apical surface of polarized MDCK cells. *Traffic* **7**:589–603.
104. Montaner, L.J., da Silva, R.P., Sun, J., et al. (1999) Type 1 and type 2 cytokine regulation of macrophage endocytosis: differential activation by IL-4/IL-13 as opposed to IFN- γ or IL-10. *J. Immunol.* **162**, 4606–4613.
105. Kaksonen, M., Toret, C.P., and Drubin, D.G. (2006) Harnessing actin dynamics for clathrin-mediated endocytosis. *Nat. Rev. Mol. Cell Biol.* **7**, 404–414.
106. Merrifield, C.J. (2004) Seeing is believing: imaging actin dynamics at single sites of endocytosis. *Trends Cell Biol.* **14**, 352–358.
107. Takenawa, T., and Itoh, T. (2001) Phosphoinositides, key molecules for regulation of actin cytoskeletal organization and membrane traffic from the plasma membrane. *Biochim. Biophys. Acta* **1533**, 190–206.
108. Araki, N., Johnson, M.T., and Swanson, J.A. (1996) A role for phosphoinositide 3-kinase in the completion of macropinocytosis and phagocytosis by macrophages. *J. Cell Biol.* **135**, 1249–1260.
109. Roth, M.G. (2004) Phosphoinositides in constitutive membrane traffic. *Physiol. Rev.* **84**, 699–730.
110. Jess, T.J., Belham, C.M., Thomson, F.J., (1996) Phosphatidylinositol 3'-kinase, but not p70 ribosomal S6 kinase, is involved in membrane protein recycling: wortmannin inhibits glucose transport and downregulates cell-surface transferrin receptor numbers independently of any effect on fluid-phase endocytosis in fibroblasts. *Cell Signal.* **8**, 297–304.
111. Hill, T., Odell, L.R., Edwards, J.K., et al. (2005) Small molecule inhibitors of dynamin I GTPase activity: development of dimeric tyrphostins. *J. Med. Chem.* **48**, 7781–7788.
112. Macia, E., Ehrlich, M., Massol, R., et al. (2006) Dynasore, a cell-permeable inhibitor of dynamin. *Dev. Cell* **10**, 839–850.

Part II
Cell-Free and Biochemical
Assays of Exocytosis and Endocytosis

3

In Vitro Assays to Measure SNARE-Mediated Vesicle Fusion

Susanne Kreye, Jörg Malsam, and Thomas H. Söllner

1	Introduction.....	38
2	Materials	39
3	Methods.....	41
4	Notes	47
	References.....	49

Summary Membrane fusion is fundamental for a broad variety of physiological processes, such as synaptic transmission, fertilization, and viral entry. Intracellular fusion along the secretory and endocytic pathway is mediated by SNARE (soluble *N*-ethylmaleimide-sensitive factor attachment protein receptor) proteins. When recombinant v- and t-SNAREs are reconstituted into distinct liposome populations, membrane fusion can be monitored by either lipid or content mixing. The in vitro assays use fluorescence dequenching to measure vesicle fusion. The lipid-mixing assay is based on fluorescence resonance energy transfer between the fluorophores 7-nitro-2-1,3-benzoxadiazol-4-yl (NBD) and rhodamine, which are covalently coupled to lipids. Fusion of labeled v-SNARE liposomes with unlabeled t-SNARE liposomes increases the distance between NBD and rhodamine, increasing the NBD fluorescence. In the content-mixing assay, the water-soluble fluorophore 8-Hydroxypyrene-1,3,6-trisulfonic acid trisodium salt (HPTS) (pyranine) and its quencher *p*-Xylene-*bis*-pyridinium bromide (DPX) are incorporated into v-SNARE vesicles. The fusion of labeled v-SNARE vesicles with unlabeled t-SNARE vesicles dilutes the quencher and thus increases HPTS fluorescence. By controlling the lipid and protein composition, these assays provide important tools to detect fusion intermediates (e.g., hemifusion), and to elucidate the molecular mechanisms that regulate membrane fusion.

Keywords Content mixing; DPX; HPTS; lipid; lipid mixing; liposome; membrane fusion; NBD; rhodamine; SNAREs; vesicle.

1 Introduction

Intracellular membrane fusion involves the pairing of cognate v- and t-SNAREs (soluble *N*-ethylmaleimide-sensitive factor attachment protein receptor) on opposing membranes. SNAREs are compartment-specific proteins and can be classified as v-SNAREs, which usually function on transport vesicles, and t-SNAREs, which are located on target membranes (1). SNAREs contain so-called SNARE motifs (α -helical regions of 50–60 amino acids), which assemble into a four-helix bundle (2). A v-SNARE contributes one helix and the t-SNARE three helices to the bundle (3). Separate v- and t-SNAREs are largely unfolded, and thus protein folding—the assembly of the four-helix bundle—provides the driving force for membrane fusion. Indeed, when two liposome populations, containing reconstituted v- and t-SNAREs, respectively, are incubated together, the SNARE proteins spontaneously assemble into complexes fusing the vesicles (4). Therefore, SNAREs are the minimal machinery for membrane fusion, a model that is further supported by a cell–cell fusion assay (5). In vivo, t-SNARE and v-t-SNARE complex formation is tightly controlled by inhibitory and stimulatory components. Thus, reconstituted in vitro fusion assays are important tools for the study of SNARE-dependent vesicle fusion and its regulation.

A lipid-mixing assay that uses fluorescence dequenching is described (6). In this assay, the fluorophores NBD and rhodamine coupled to phosphatidylethanolamine are incorporated at the same molar amount into v-SNARE vesicles (4). The donor NBD and the acceptor rhodamine show efficient resonance energy transfer (6). Therefore, the donor fluorescence is efficiently quenched in the v-SNARE vesicles. During the fusion of labeled v-SNARE vesicles with unlabeled t-SNARE vesicles, the membrane lipids are mixed, and the distance between the donor and the acceptor fluorophores increases. As a result, the resonance energy transfer from NBD to rhodamine decreases, and the amount of emitted fluorescent light of the donor NBD increases. Please note that the energy transfer depends on the donor–acceptor distance with an inverse sixth-order law (7). Therefore, fusion can be visualized as an increase in NBD fluorescence. The fusion kinetics and the extent of the signal depend on the SNARE copy number per liposome and the liposome concentration. By using v-SNARE vesicles with high copy numbers (e.g., 300) of v-SNARE molecules and an excess (e.g., fivefold) of t-SNARE vesicles with low copy numbers of t-SNAREs (e.g., 70 copies), several rounds of fusion can occur during the incubation time, thus increasing the final signal (4,8). However, at the neuronal synapse, the copy number of the v-SNARE vesicle-associated membrane protein (VAMP2) on synaptic vesicles is approx 70 (9). The cognate t-SNARE consists of syntaxin1 and synaptosome-associated protein of 25 kDa (SNAP-25), but the surface density of t-SNAREs in the plasma membrane still needs to be determined. By changing the number of reconstituted SNAREs in the vesicle, the sensitivity for regulatory components can be altered (10).

Remarkably, neuronal SNAREs are the targets of botulinum neurotoxins, which cleave specific SNARE proteins at defined positions (11). Thus, these neurotoxins are tools to detect SNARE-independent fusion in in vitro assays. Here, we use botulinum

neurotoxin D (BoNT/D), which proteolytically cleaves VAMP2 between Lys59 and Leu60, in the center of the SNARE motif (12). After cleavage of VAMP2 by BoNT/D, stable v-/t-SNARE complexes cannot be formed, fusion is blocked, and the increase in NBD fluorescence is reduced to background levels.

During complete membrane fusion, lipids and aqueous contents of the two vesicle populations mix. Thus, in vitro fusion of v- and t-SNARE liposomes can also be measured by a content-mixing assay, which is again based on fluorescence dequenching. In this assay, the fluorophore HPTS (pyranine) and its quencher DPX (13,14) are both incorporated into v-SNARE vesicles. The optimal molar ratio of HPTS to DPX has been experimentally tested by reconstitution of vesicles in the presence of different ratios of HPTS to DPX. The experiments showed that a 1.5- to 2-fold molar excess of DPX to HPTS is the optimal ratio. Under these conditions, the HPTS fluorescence is efficiently quenched. The fusion of labeled v-SNARE vesicles with unlabeled t-SNARE vesicles increases the internal volume of the vesicles and dilutes both the fluorophore and its quencher. Therefore, fusion of vesicles is measured as an increase of HPTS fluorescence.

An increase of HPTS fluorescence during fusion could be caused not only by the fusion of v- and t-SNARE vesicles but also by HPTS leakage. To test for or eliminate signals derived from content leakage, the fusion reaction is performed in the presence of an excess of DPX in the medium. Under these conditions, an increase in HPTS fluorescence can only be caused by full membrane fusion because leaking HPTS is immediately quenched by DPX present in the medium. In turn, leaky fusion would also result in DPX influx into fusing vesicles, again abolishing the fluorescence signal.

In the fusion assays described here, we reconstituted recombinant neuronal SNAREs into vesicles. In general, SNAREs functioning at other intracellular transport steps can be reconstituted in a similar manner into vesicles (3,15,16).

By comparing the kinetics of the two different fusion assays described here it should be possible to detect distinct fusion intermediates such as hemifusion. During hemifusion, the NBD fluorescence should increase, and the HPTS fluorescence should remain constant. Apparently, regulatory components that arrest such intermediates can be identified by these assays.

2 Materials

2.1 Protein Expression and Purification

1. Luria-Bertani (LB) medium: 10 g/L tryptone, 5 g/L yeast extract, 5 g/L NaCl. Adjust to pH 7.2 with NaOH and autoclave.
2. Antibiotics: 100 µg/mL ampicillin, 50 µg/mL kanamycin, 34 µg/mL chloramphenicol dissolved in ethanol.

3. *t*-SNARE breaking buffer: 50mM HEPES-KOH (pH 7.4), 400mM KCl, 10% (w/v) glycerol, 2% (v/v) Triton X-100, 20mM imidazole, 3mM β -mercaptoethanol.
4. Buffer A: 25mM HEPES-KOH (pH 7.4), 200mM KCl, 10% (w/v) glycerol, 1% (w/v) octyl- β -D-glucopyranosid, 40mM imidazole, 3mM β -mercaptoethanol.
5. Buffer B: 25mM HEPES-KOH (pH 7.4), 200mM KCl, 10% (w/v) glycerol, 1% (w/v) octyl- β -D-glucopyranosid, 500mM imidazole, 3mM β -mercaptoethanol.
6. *v*-SNARE breaking buffer: 25mM HEPES-KOH (pH 7.4), 100mM KCl, 10% (w/v) glycerol, 2% Triton X-100, 2mM β -mercaptoethanol.
7. Buffer C: 25mM HEPES-KOH (pH 7.4), 400mM KCl, 10% (w/v) glycerol, 1% (v/v) Triton X-100, 20mM imidazole, 2mM β -mercaptoethanol.
8. Buffer D: 25mM HEPES-KOH (pH 7.4), 1M KCl, 10% (w/v) glycerol, 2% (v/v) Triton X-100, 20mM imidazole, 2mM β -mercaptoethanol.
9. Buffer E: 25mM HEPES-KOH (pH 7.4), 100mM KCl, 10% (w/v) glycerol, 2mM β -mercaptoethanol, 1% octyl- β -D-glucopyranosid, 20mM imidazole.
10. Buffer F: 25mM HEPES-KOH (pH 7.4), 100mM KCl, 10% (w/v) glycerol, 2mM β -mercaptoethanol, 1% octyl- β -D-glucopyranosid, 500mM imidazole.
11. *v*-SNARE dilution buffer: 25mM HEPES-KOH (pH 7.4), 10mM KCl, 10% (w/v) glycerol, 1% (w/v) octyl- β -D-glucopyranosid, 1mM dithiothreitol (DTT).
12. Low-salt buffer: 25mM HEPES-KOH (pH 7.4), 50mM KCl, 10% (w/v) glycerol, 1% (w/v) octyl- β -D-glucopyranosid, 1mM DTT.
13. High-salt buffer: 25mM HEPES-KOH (pH 7.4), 1M KCl, 10% (w/v) glycerol, 1% (w/v) octyl- β -D-glucopyranosid, 1mM DTT.
14. Protease inhibitor cocktail (1000 \times stock):

Aqueous: 1.5 mg/mL leupeptin, 2.5 mg/mL antipain, 25 mg/mL turkey trypsin inhibitor, 12.5 mg/mL benzamidine, 6.25 mg/mL pefabloc Sc, and 1.25 mg/mL aprotinin dissolved in water.
 Hydrophobic: 5 mg/mL chymostatin and 2.5 mg/mL pepstatin dissolved in dimethyl sulfoxide (DMSO).
15. Ni-NTA beads (Qiagen, Hilden, Germany).
16. Mono-S column (5/50 GL, GE Healthcare, Munich, Germany).

2.2 Reconstitution of *v*- and *t*-SNARE Liposomes

1. POPC: 1-Palmitoyl-2-oleyl-sn-glycero-3-phosphocholine (Avanti Polar Lipids, Alabaster, Alabama).
2. DOPS: 1,2-Dioleoyl-sn-glycero-3-phosphoserine (Avanti Polar Lipids, Alabaster, Alabama).
3. NBD-DPPE: 1,2-Dipalmitoyl-sn-glycero-3-phosphoethanolamine-*N*-(7-nitro-2-1,3-benzoxadiazol-4-yl) (Avanti Polar Lipids, Alabaster, Alabama).
4. Rhodamine-DPPE: 1,2-Dipalmitoyl-sn-glycero-3-phosphoethanolamine-*n*- (lissamine rhodamine B sulfonyl) (Avanti Polar Lipids, Alabaster, Alabama).

5. ^3H -DPPC: 1,2-Dipalmitoyl-sn-glycero-3-phosphocholine [N-methyl- ^3H], 37 MBq/mL, 1.5–3.33 TBq/mmol (GE Healthcare, Munich, Germany).
6. Reconstitution buffer: 25 mM HEPES-KOH (pH 7.4), 100 mM KCl, 10% (w/v) glycerol, 1 mM DTT.
7. HPTS: 8-Hydroxypyrene-1,3,6-trisulfonic acid trisodium salt (Sigma-Aldrich, Munich, Germany).
8. DPX: p-Xylene-*bis*-pyridinium bromide (Invitrogen, Karlsruhe, Germany).
9. HPTS/DPX buffer: 30 mM HPTS, 45 mM DPX in reconstitution buffer.

3 Methods

3.1 Protein Expression and Purification

3.1.1 Expression and Purification of t-SNARE

The t-SNARE components syntaxin1 and SNAP-25 are coexpressed in bacteria using a polycistronic plasmid, encoding full-length syntaxin1 without a tag and SNAP-25 with an carboxy-terminal His₆-tag. The his-tagged SNAP-25 and the associated syntaxin1 (preassembled t-SNARE) are purified on a Ni-NTA column. Since SNAP-25 lacks a membrane anchor, the molecule becomes incorporated into vesicles as part of the preassembled t-SNARE complex, whereas free SNAP-25 is removed during vesicle isolation. This procedure bypasses a requirement for regulatory components that control t-SNARE complex assembly. (When not otherwise noted, all procedures are performed on ice or at 4 °C, and all buffers should be stored on ice.)

1. Dilute an overnight culture of BL21(DE3) cells transformed with rat syntaxin1A and mouse SNAP-25B-His₆ (pTW34) (8) 20-fold into 12 L prewarmed LB medium containing 50 µg/mL kanamycin. Incubate at 37 °C with vigorous shaking until the cells reach an optical density of 0.6 (at 600 nm).
2. Induce protein expression by the addition of 1 mM IPTG.
3. After 4 h induction time, collect cells by centrifugation at 4000 g for 15 min (Rotor H-12000, RC12 BP centrifuge, Sorvall) and wash the cells with 200 mL ice-cold phosphate-buffered saline (PBS).
4. Resuspend cells in 100 mL 2X breaking buffer (without Triton X-100 and β-mercapthoethanol) and adjust the volume with water to 180 mL (*see Notes 1 and 2*).
5. Add 200 µL each of the aqueous and the hydrophobic protease inhibitor cocktail (1000X stock), 2 mM β-mercapthoethanol, and 20 mL (one-tenth volume) of 20% Triton X-100. Pass cells through a cell disrupter (Microfluidizer Processor M-110L) at 18,000 psi.
6. Remove insoluble material by centrifugation of the cell lysate at 125,000 g in a 45 Ti rotor (Beckman) for 1 h. Recover supernatant. Keep 50 mL and snap freeze the rest (*see Note 3*).

7. Equilibrate 6 mL settled Ni-NTA beads by washing four times with 40 mL breaking buffer (*see Note 4*).
8. Incubate 50 mL of the clarified cell lysate with 6 mL Ni-NTA beads for 2 h on a rotating wheel.
9. Wash beads once with 40 mL breaking buffer, resuspend in a final volume of 15 mL and incubate with 2500 U benzonase (Merck) in breaking buffer containing 1 mM MgCl₂ for 30 min.
10. Transfer beads into a column and wash with five column volumes breaking buffer at a flow rate of 1 mL/min using a chromatography system (e.g., Akta System, Amersham). Note that Triton X-100 absorbs at 280 nm.
11. Wash beads with ten column volumes of buffer A to completely exchange Triton X-100 against octyl- β -D-glucopyranosid (*see Note 5*).
12. Elute the protein with an imidazole gradient from 40 to 500 mM imidazole (buffer A and B) in five column volumes at a flow rate of 0.5 mL/min. Collect fractions of 1-mL volume and analyze by sodium dodecyl sulfate polyacrylamide gel electrophoresis (SDS-PAGE).
13. Pool peak fractions and determine the protein concentration. Snap freeze aliquots in liquid nitrogen and store at -80°C .

3.1.2 Expression and Purification of VAMP2

The v-SNARE protein VAMP2 is purified by affinity chromatography followed by ion exchange chromatography.

1. Dilute an overnight culture of BL21CodonPlus(DE3)-RIL cells transformed with mouse VAMP2-His₆ (pTW2) (4) 20-fold into 12 L prewarmed LB medium containing 100 $\mu\text{g}/\text{mL}$ ampicillin and 34 $\mu\text{g}/\text{mL}$ chloramphenicol. Incubate at 37°C with vigorous shaking until the cells reach an optical density of 0.6 (600 nm).
2. Add 0.5 mM IPTG and express protein for 2 h.
3. Isolate cells as described for t-SNARE.
4. Resuspend cells in 100 mL v-SNARE breaking buffer (without β -mercaptoethanol and without Triton X-100) (*see Note 1*).
5. Before disrupting the cells, add 2 mM β -mercaptoethanol, protease inhibitors, and Triton X-100 (2% v/v).
6. Lyse cells and remove insoluble material as described for t-SNAREs. Add 10 mM imidazole to the supernatant from a 1 M stock solution (adjust pH with HCl to 7.4).
7. Equilibrate Ni-NTA beads with breaking buffer (*see Note 4*).
8. Incubate the clarified cell lysate with 6 mL equilibrated Ni-NTA beads for 2 h on a rotating wheel. Under these conditions, the Ni-NTA beads are saturated with VAMP2 to reduce the binding of contaminating proteins to a minimum.
9. Wash beads once with 40 mL v-SNARE breaking buffer including 2% Triton X-100, resuspend in a final volume of 15 mL, and incubate with 2500 U benzonase in breaking buffer containing 2% Triton X-100 and 1 mM MgCl₂ for 30 min.

10. Transfer beads into a column and wash with five column volumes buffer C at a flow rate of 1 mL/min. Note that Triton X-100 absorbs at 280 nm.
11. Wash beads with five column volumes buffer D.
12. Wash beads with ten column volumes buffer E to completely exchange Triton X-100 against octyl- β -D-glucopyranosid (*see Note 5*).
13. Elute protein with 10 mL buffer F at 1 mL/min. Collect fractions of 1 mL.
14. Pool fractions with high protein concentrations and dilute with five volumes of dilution buffer.
15. Leave the diluted solution at 4 °C overnight to precipitate misfolded proteins or aggregates.
16. Clear the protein solution at 118,000 g for 1 h in a 70 Ti rotor and load supernatant at 0.5 mL/min onto an ion exchange Mono-S column (5/50 GL) equilibrated with low-salt buffer.
17. Wash the column with ten column volumes of low-salt buffer.
18. Elute protein with a gradient: 0–50% high-salt buffer in 20 column volumes at a flow rate of 0.5 mL/min. Collect 0.5-mL fractions.
19. Pool peak fractions and determine the protein concentration. Snap freeze aliquots in liquid nitrogen and store at –80 °C.

3.2 Reconstitution of SNARE Liposomes

3.2.1 Reconstitution of t-SNARE Liposomes

To obtain substantial fusion signals, the SNAREs used for the liposome reconstitution should have a protein concentration of at least 1 mg/mL. The procedure yields small unilamellar vesicles (SUVs) with a diameter of about 35–100 nm (4). Using a higher copy number of v-SNARE- than t-SNARE molecules on the respective vesicles allows the fusion of a single v-SNARE vesicle with several t-SNARE vesicles. After one round of fusion, free v-SNARE molecules are still available on the fused vesicle. Therefore, fusion of those vesicles can proceed with other t-SNARE vesicles until most of the v-SNARE molecules are consumed and assembled into v-/t-SNARE complexes.

1. Make a 15 mM lipid mixture (total concentration) containing POPC and DOPS in a molar ratio of 85:15 in chloroform (*see Note 6*).
2. Transfer 300 μ L of the lipid mixture into a glass tube and dry to a thin film with nitrogen gas for 10–20 min at room temperature. Dry the lipid film in a vacuum for 1 h at room temperature to remove any remaining traces of chloroform.
3. Add 1.5 mL purified t-SNARE protein solution (2–3 mg/mL) to the dried lipid film and overlay the solution with nitrogen gas.
4. Dissolve the lipids in the protein solution by gentle mixing for 15 min at room temperature on a vortex.

5. Dilute the protein–lipid mixture with 3 mL reconstitution buffer by adding droplets of the buffer to the mixture while vortexing. Vesicles are formed spontaneously by the dilution of the detergent octyl- β -D-glucopyranosid below the critical micellar concentration.
6. Remove the detergent by continuous flow dialysis of the vesicle suspension against 4L reconstitution buffer overnight.
7. Float up the vesicles in a Nycodenz density gradient to concentrate the vesicles and to remove proteins that are not incorporated. Mix 4.5 mL dialyzed vesicle suspension with 4.5 mL 80% Nycodenz. Transfer 3 mL of the solution into a 11 \times 60 mm ultracentrifuge tube (Beckman). Overlay the solution with 750 μ L of 30% Nycodenz followed by 250 μ L of reconstitution buffer (*see Note 7*).
8. Spin samples in a centrifuge at 310,000 g in a SW60 rotor (Beckman) for 3 h and 40 min at 4 °C.
9. Isolate vesicles from the 0/30% Nycodenz interface by harvesting 400 μ L from the top of each gradient (*see Notes 8 and 9*).

3.2.2 Reconstitution of v-SNARE Liposomes

1. Make a 3 mM lipid mixture containing POPC, DOPS, NBD-DPPE, and rhodamine–DPPE in a molar ratio of 83.4:15:0.8:0.8 in chloroform (*see Note 6*).
2. Add 100 μ L lipid mixture to a glass tube and dry to a thin film with nitrogen gas for approx 10 min at room temperature. Dry the lipids for 1 h at room temperature in a vacuum to remove any remaining traces of chloroform.
3. Add 100 μ L purified VAMP2–protein solution (2 mg/mL) to the dried lipid film and overlay the solution in the tube with nitrogen gas (*see Note 10*).
4. Dissolve the lipids in the protein solution by gentle mixing for 15 min at room temperature on a vortex.
5. Dilute the protein–lipid mixture with 200 μ L reconstitution buffer by slowly adding droplets of the buffer to the mixture while vortexing. Vesicles are formed spontaneously by dilution of the detergent octyl- β -D-glucopyranosid below the critical micellar concentration.
6. Remove the detergent by continuous flow dialysis of the vesicle suspension against 4L reconstitution buffer overnight.
7. Float up the vesicles in a Nycodenz density gradient to concentrate the vesicles and to remove proteins not incorporated. Mix 300 μ L dialyzed vesicle suspension with 300 μ L 80% Nycodenz. Transfer the solution into a 8 \times 35 mm Quick-Seal polyallomer ultracentrifuge tube (Beckman). Overlay the solution with 300 μ L 30% Nycodenz followed by 300 μ L reconstitution buffer to fill the tube completely (*see Note 7*).
8. Heat seal the tubes with a Tube Topper (Beckman).
9. Spin samples at 340,000 \times g in a TLN120 rotor (Beckman) for 45 min at 4 °C.
10. Isolate vesicles from the 0/30% Nycodenz interface with a syringe (~100 μ L per gradient) (*see Notes 8 and 9*).

3.2.3 Reconstitution of v-SNARE Liposomes Containing HPTS and DPX

Use the procedure for v-SNARE liposome reconstitution as described in the previous section with the following modifications:

1. Dilute the protein–lipid mixture with 200 μ L freshly prepared HPTS/DPX solution in reconstitution buffer and dialyze the solution over night (*see Note 11*).
2. Isolate reconstituted vesicles by centrifugation at 218,000 g in a SW55 rotor (Beckman) for 4 h at 4 $^{\circ}$ C. (*see Note 11*).
3. Isolate vesicles from the 0/30% Nycodenz interface by harvesting 75 μ L from the top of each gradient (*see Notes 8 and 9*).

3.3 Fusion Assay

3.3.1 Lipid-Mixing Assay

The fusion assays (*Fig. 1*) can be performed in a standard fluorescence photometer or in a fluorescence microtiter plate reader. The use of a microtiter plate reader allows the analyses of many samples in parallel. Small sample volumes such as 50 μ L are sufficient for each experiment. However, when small volumes are used, evaporation of the aqueous solution can increase the signal at prolonged measuring times.

1. Transfer 45 μ L unlabeled t-SNARE vesicles into a preheated 96-well plate (Nunc 96 microwell plates for fluorescence and luminescence, white), containing 20–30 μ L reconstitution buffer and incubate at 37 $^{\circ}$ C for approx 20 min.
2. Mix the t-SNARE vesicle solution with 5 μ L labeled v-SNARE vesicles preheated to 37 $^{\circ}$ C (*see Note 12*).
3. Control sample: To inhibit fusion, incubate v-SNARE vesicles with 0.15 μ g botulinum neurotoxin D light chain for 20 min at 37 $^{\circ}$ C before mixing with t-SNARE vesicles.
4. Immediately after mixing the v- and t-SNARE vesicles, start the measurement in a fluorimeter (Fluoroskan Ascent FL, Thermo). Measure the dequenching of the NBD fluorescence at an excitation of 460 nm (24-nm bandwidth) and at an emission of 538 nm (25-nm bandwidth).
5. After about 2 h, add 10 μ L 2.5% dodecyl- β -D-maltoside to each sample to terminate the reaction and to measure maximum NBD fluorescence.

3.3.2 Content-Mixing Assay

1. Transfer 45 μ L unlabeled t-SNARE vesicles into a preheated 96-well plate (Nunc) containing 20–30 μ L reconstitution buffer and incubate at 37 $^{\circ}$ C for approx 20 min (*Fig. 2*).

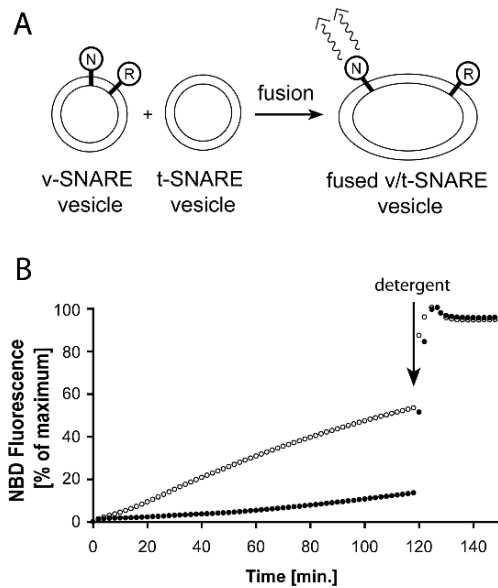


Fig. 1 Lipid-mixing assay. **(A)** Illustration of the lipid-mixing assay based on fluorescence resonance energy transfer. v-SNARE vesicles containing NBD (N) and rhodamine (R) are mixed with unlabeled t-SNARE vesicles. During the fusion of v- and t-SNARE vesicles, the distance between the two fluorophores increases, and the efficiency of energy transfer from NBD to rhodamine decreases. As a result, fusion can be monitored by an increase in NBD fluorescence. **(B)** Untreated (open circles) or BoNT/D-treated (closed circles) v-SNARE vesicles containing NBD and rhodamine were mixed with unlabeled t-SNARE vesicles. Fusion was monitored by measuring the NBD fluorescence at 37 °C. After 2 h, dodecyl- β -D-maltoside was added to measure the maximum NBD fluorescence. The experiment was normalized by setting the minimal fluorescence to 0% and the maximal fluorescence after lysis of the vesicles by detergent to 100% (see [Note 13](#)).

2. Mix the t-SNARE vesicles with 10 μ L preheated (37 °C) v-SNARE vesicles containing HPTS and DPX (see [Note 12](#)).
3. Control sample: To inhibit fusion incubate v-SNARE vesicles with 0.3 μ g botulinum neurotoxin D light chain for 20 min at 37 °C before mixing with t-SNARE vesicles.
4. Immediately after mixing the v- and t-SNARE vesicles, start the measurement in a fluorimeter. Measure the dequenching of the HPTS fluorescence by excitation at 460 nm (24-nm bandwidth) and emission at 520 nm (10-nm bandwidth).
5. Add 10 μ L 2.5% dodecyl- β -D-maltoside to each sample to terminate the reaction.

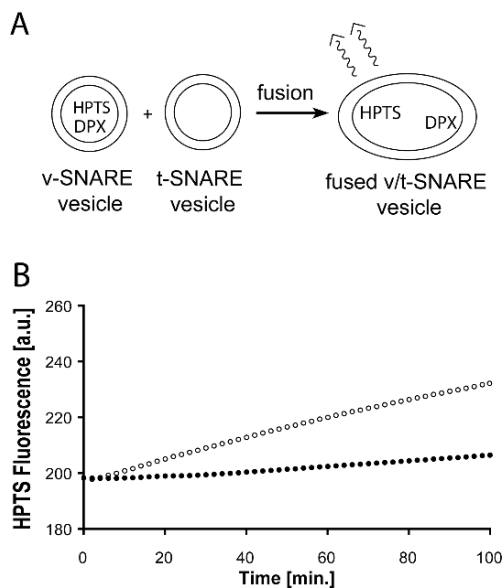


Fig. 2 Content-mixing assay. **(A)** Illustration of the content-mixing assay using the fluorophore HPTS and its quencher DPX. v-SNARE vesicles containing HPTS and DPX are incubated with unlabeled t-SNARE vesicles. Fusion is monitored by measuring the HPTS fluorescence, which increases during fusion because of an increase of the internal volume of the vesicles. **(B)** v-SNARE vesicles containing HPTS and DPX were mixed with unlabeled t-SNARE vesicles. Fusion was monitored by measuring the HPTS fluorescence at 37 °C for approx 2 h (open circles). One sample of v-SNARE vesicles was preincubated with botulinum neurotoxin D before mixing with t-SNARE vesicles (closed circles).

3.3.3 Content-Mixing Assay with DPX in the Medium

To check for content leakage during the measurement period, add 50 mM DPX into the incubation medium and perform fusion analysis as described above (*see Note 12*). Depending on the quality of the vesicles (storage period), the addition of DPX can lower the initial HPTS signal (*Fig. 3*).

4 Notes

1. Cells washed with PBS and resuspended in breaking buffer can be frozen in liquid nitrogen and stored at -20°C .
2. The pH value has to be adjusted to 7.4 because SNAP-25 precipitates at lower pH values.
3. The clarified lysate can be snap frozen in liquid nitrogen and stored at -80°C .

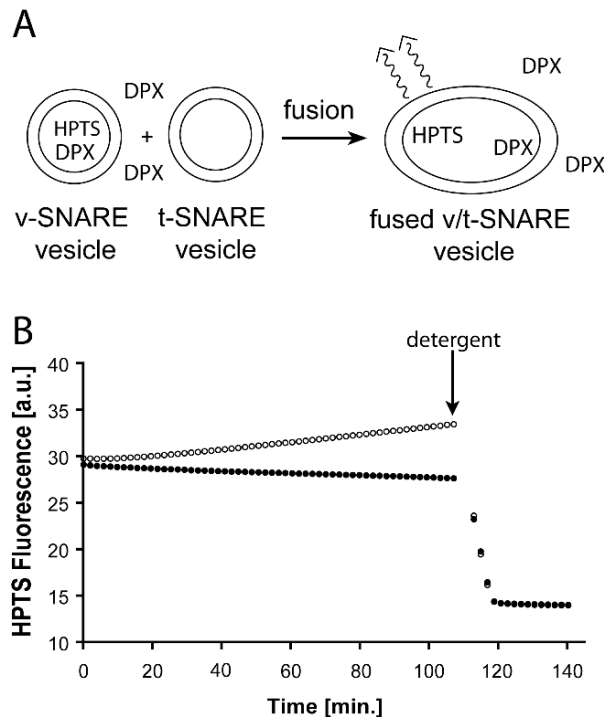


Fig. 3 Content-mixing assay with DPX present in the incubation medium. **(A)** Illustration of the content-mixing assay with DPX in the incubation medium. Labeled v-SNARE vesicles are mixed with unlabeled t-SNARE vesicles in the presence of DPX in the medium. Addition of DPX to the medium quenches the fluorescent signal caused by the leakage of HPTS from v-SNARE vesicles. **(B)** Untreated (open circles) or BoNT/D treated (closed circles) v-SNARE vesicles containing the fluorophore HPTS and its quencher DPX were mixed with unlabeled t-SNARE vesicles. Fusion was monitored by measuring the HPTS fluorescence at 37°C. After 2 h, the vesicles were lysed by the addition of dodecyl- β -D-maltoside.

4. Use Ni-NTA beads from Qiagen or beads with a similar binding capacity. When we used Ni-NTA beads with higher binding capacity, we observed protein aggregation in some instances.
5. It is important to remove the Triton X-100 completely because liposome formation is perturbed in the presence of Triton X-100.
6. Lipids dissolved in organic solvent should be overlaid with Ar or N₂ gas and stored in tightly sealed glass vials at -20°C protected from light. Otherwise, the lipids oxidize, and the organic solvent will evaporate. To transfer lipids dissolved in organic solvent between reaction vials, use glassware such as Hamilton syringes and glass capillaries.
7. Make 80% (w/v) Nycodenz in reconstitution buffer. Weigh 40 g Nycodenz into a 50-mL Falcon tube, add 10 mL 5X reconstitution buffer, mix, and fill the tube with distilled water to 50 mL. Incubate overnight on a rotating wheel at room temperature to completely dissolve the Nycodenz.

8. Reconstituted v-SNARE liposomes with fluorescently labeled lipids and unlabeled t-SNARE liposomes can be stored for a few days at 4 °C or at –80 °C for long-term storage. The reconstituted v-SNARE vesicles containing HPTS and DPX should be stored at 4 °C and should be used within a week. Content leakage occurs during freezing and thawing of the vesicles.
9. To quantify the reconstitution efficiency of VAMP2 and the t-SNARE, the protein amounts are determined by a suitable method, such as Amido Black staining (17). Lipid recovery is determined by adding trace amounts of ³H-DPPC to the lipid mixture (e.g., 1 μL per 100 μL lipid stock). A defined fraction (e.g., 2%) of the initial reconstitution sample and the harvested liposomes are removed, and the radioactivity is determined by scintillation counting. Based on the amount of protein and lipid recovered in the liposomes, the protein/lipid ratio can be calculated. A typical phospholipid covers a surface area of about 65 Å² (18). Thus, when the vesicle size is known the copy number of SNAREs per vesicle can be calculated.
10. To integrate lower copy numbers of VAMP2 into v-SNARE liposomes, the VAMP2 protein solution can be diluted with reconstitution buffer containing 1% octyl-β-D-glycopyranoside.
11. The dialysis of the vesicles does not quantitatively remove free HPTS and DPX. Furthermore, during the flotation of the vesicles, leakage of HPTS and the quencher DPX can occur.
12. For the in vitro fusion assay, the protein and buffer solutions should be preincubated at 37 °C. Otherwise, a drop of the fluorescent signal is observed during the first 10–15 min of the measuring time, which can obscure the analysis.
13. The measured fluorescence signal of NBD in the lipid-mixing assay was normalized by the following equation:

$$F_{norm} [\%] = \left(\frac{(F_{measured} - F_{min})}{(F_{max} - F_{min})} \right) * 100$$

with F_{norm} the normalized fluorescence in percent, $F_{measured}$ the measured fluorescence at a distinct point, F_{min} the minimal fluorescence of all measured values, and F_{max} the maximal fluorescence of all measured values.

Acknowledgments We would like to thank Jean Michel Krause for technical assistance. The work was supported by National Institutes of Health grant NS 43391 (to T.H. Söllner).

References

1. Söllner, T., Whiteheart, S.W., Brunner, M., et al. (1993) SNAP receptors implicated in vesicle targeting and fusion. *Nature* **362**, 318–324.
2. Sutton, R.B., Fasshauer, D., Jahn, R., and Brunger, A.T. (1998) Crystal structure of a SNARE complex involved in synaptic exocytosis at 2.4 Å resolution. *Nature* **395**, 347–353.

3. Parlati, F., McNew, J.A., Fukuda, R., Miller, R., Söllner, T.H., and Rothman, J.E. (2000) Topological restriction of SNARE-dependent membrane fusion. *Nature* **407**, 194–198.
4. Weber, T., Zemelman, B.V., McNew, J.A., et al. (1998) SNAREpins: minimal machinery for membrane fusion. *Cell* **92**, 759–772.
5. Hu, C., Ahmed, M., Melia, T.J., Sollner, T.H., Mayer, T., and Rothman, J.E. (2003) Fusion of cells by flipped SNAREs. *Science* **300**, 1745–1749.
6. Struck, D.K., Hoekstra, D., and Pagano, R.E. (1981) Use of resonance energy transfer to monitor membrane fusion. *Biochemistry* **20**, 4093–4099.
7. Stryer, L., and Haugland, R.P. (1967) Energy transfer: a spectroscopic ruler. *Proc. Natl. Acad. Sci. U. S. A.* **58**, 719–726.
8. Parlati, F., Weber, T., McNew, J.A., Westermann, B., Söllner, T.H., and Rothman, J.E. (1999) Rapid and efficient fusion of phospholipid vesicles by the alpha-helical core of a SNARE complex in the absence of an N-terminal regulatory domain. *Proc. Natl. Acad. Sci. U. S. A.* **96**, 12565–12570.
9. Takamori, S., Holt, M., Stenius, K., et al. (2006) Molecular anatomy of a trafficking organelle. *Cell* **127**, 831–846.
10. Tucker, W.C., Weber, T., and Chapman, E.R. (2004) Reconstitution of Ca²⁺-regulated membrane fusion by Synaptotagmin and SNAREs. *Science* **304**, 435–438.
11. Schiavo, G., Matteoli, M., and Montecucco, C. (2000) Neurotoxins affecting neuroexocytosis. *Physiol. Rev.* **80**, 717–766.
12. Yamasaki, S., Baumeister, A., Binz, T., et al. (1994) Cleavage of members of the Synaptobrevin/VAMP family by types D and F botulinum neurotoxins and tetanus toxin. *J. Biol. Chem.* **269**, 12764–12772.
13. Daleke, D. L., Hong, K., and Papahadjopoulos, D. (1990) Endocytosis of liposomes by macrophages: binding, acidification and leakage of liposomes monitored by a new fluorescence assay. *Biochim. Biophys. Acta* **1024**, 352–366.
14. Barreto, J., and Lichtenberger, L.M. (1992) Vesicle acidification driven by a millionfold proton gradient: a model for acid influx through gastric cell membranes. *Am. J. Physiol.* **262**, G30–G34.
15. Fukuda, R., McNew, J.A., Weber, T., et al. (2000) Functional architecture of an intracellular membrane t-SNARE. *Nature* **407**, 198–202.
16. McNew, J.A., Parlati, F., Fukuda, R., et al. (2000) Compartmental specificity of cellular membrane fusion encoded in SNARE proteins. *Nature* **407**, 153–159.
17. Schaffner, W., and Weissmann, C. (1973) A rapid, sensitive, and specific method for the determination of protein in dilute solution. *Anal. Biochem.* **56**, 502–514.
18. Nagle, J.F., and Tristram-Nagle, S. (2000) Structure of lipid bilayers. *Biochim. Biophys. Acta* **1469**, 159–195.

4

Imaging Ca²⁺-Triggered Exocytosis of Single Secretory Granules on Plasma Membrane Lawns from Neuroendocrine Cells

Thorsten Lang

1	Introduction.....	51
2	Materials	52
3	Methods.....	55
4	Notes	57
	References.....	59

Summary This cell-free assay for exocytosis is particularly useful when spatial information about exocytotic sites and biochemical access to the plasma membrane within less than a minute is required. It is based on the study of plasma membrane lawns from secretory cells exhibiting secretory granules filled with neuropeptide Y-green fluorescent protein (NPY-GFP). The sample is prepared by subjecting NPY-GFP-expressing cells to a brief ultrasound pulse, leaving behind a basal, flat plasma membrane with fluorescent attached secretory organelles. These sheets can then be incubated in defined solutions with the benefit that complete solution changes can be achieved in less than 1 min. Individual secretory granules are monitored in the docked state and during exocytosis by video microscopy.

Keywords Cell-free assay; dense core granules; fluorescence microscopy; GFP; peptide hormone; plasma membrane sheets; secretion.

1 Introduction

Neurotransmitter and hormone release is a highly regulated process, involving many factors that form membrane protein complexes, which facilitate the fusion of secretory organelles with the plasma membrane. The nature of these complexes implicates that they are difficult to characterize biochemically. Many methods have been developed to unravel the exocytotic cascade of biochemical reactions. These include biochemical cell-free assays, electrophysiological approaches such as amperometry and capacitance measurements, or optical detection of exocytosis. Each type of assay has its advantages and limitations

concerning the rate at which exocytosis is monitored, the ease by which the biological sample can be manipulated biochemically, and detection of secretory organelles not only during fusion but also when transported and docked to special sites of the plasma membrane.

The cell-free assay described here provides spatial information about exocytotic sites and quick biochemical access to the plasma membrane. Mechanically removing the upper part of the cell (for review, *see Ref. 1*), the inner leaflet of the basal plasma membrane is made biochemically accessible within seconds. To this end, cells are subjected to shearing forces that are generated by a brief ultrasound pulse, leaving behind a flat, cortical membrane lawn with attached secretory granules. Granules are labeled with green fluorescent protein (GFP) by expression of a corresponding GFP-based secretory granule marker (2). Such granules can be monitored by fluorescence microscopy before, during, and occasionally after exocytosis (3). The experimental time window and sampling frequency are limited by the brightness of the secretory granules and the sensitivity of the camera system. In practice, taking four images per minute at diffraction-limited resolution for 15 min is feasible, thus allowing temporal and spatial resolution of individual fusion events and monitoring of biological activity occurring during a stimulus. GFP fluorescence can be well separated from fluorophores emitting in the red or far-red range, allowing for simultaneous monitoring of exocytosis and a fluorescent-labeled membrane-associated protein present at the exocytotic site (4).

2 Materials

2.1 Cell Culture and Transfection

1. Cell culture: PC12 cells (clone 251; 5) are cultured at 37 °C in 10% CO₂ at 90% relative humidity in Dulbecco's modified Eagle's medium (DMEM with 4.5 g/L glucose) supplemented with 10% horse serum, 5% fetal calf serum, 4 mM L-glutamine, 60 U/mL penicillin and 60 U/mL streptomycin (*see Note 1*).
2. Poly-L-lysine solution: 100 µg/mL poly-L-lysine (molecular weight ~ 300,000 kDa) in sterile double-distilled (dd) water. For storage, prepare a 20X stock solution, sterilize the solution by filtering through a 0.2-µm filter, and keep 2-mL aliquots at -20 °C.
3. Glass coverslips: Use round, 100-µm thick glass coverslips with a 25-mm diameter (*see Note 2*).
4. Cytomix: 120 mM KCl, 10 mM KH₂PO₄, 10 mM K₂HPO₄, 0.15 mM CaCl₂, 2 mM ethylene glycol-bis(2-amino-ethylether)-N,N,N',N'-tetraacetic acid (EGTA), 5 mM MgCl₂, 2 mM adenosine triphosphate (ATP), 5 mM glutathione, and

25 mM HEPES-KOH, pH 7.6 (6), sterilized by filtering through a 0.2- μ m filter. Store 1.5-mL aliquots at -20°C .

5. NPY-GFP plasmid: The plasmid encodes a fusion protein of human neuropeptide Y (NPY) fused C-terminally to enhanced GFP (EGFP) in the mammalian expression vector pEGFP-N1 (Clontech) (4). The concentration of the plasmid should not be lower than 0.5 $\mu\text{g}/\mu\text{L}$.

2.2 Generation of Membrane Sheets

1. Sonication buffer: 120 mM potassium glutamate, 20 mM potassium acetate, 10 mM EGTA, 4 mM MgCl_2 , 2 mM ATP, 0.5 mM dithiothreitol, and 20 mM HEPES-KOH, pH 7.2. Store 50-mL aliquots at -20°C .
2. Sonifier: A Branson sonifier 450 (Branson Ultrasonics Corp., Danbury, CT) equipped with a 2.5-mm sonication tip can be used.
3. Sonication chamber: Use an approx 9-cm dish as the sonication chamber. The sonication tip of the sonifier is centered within the dish (Fig. 1) and its distance to the bottom of the dish is adjusted to 1 cm.

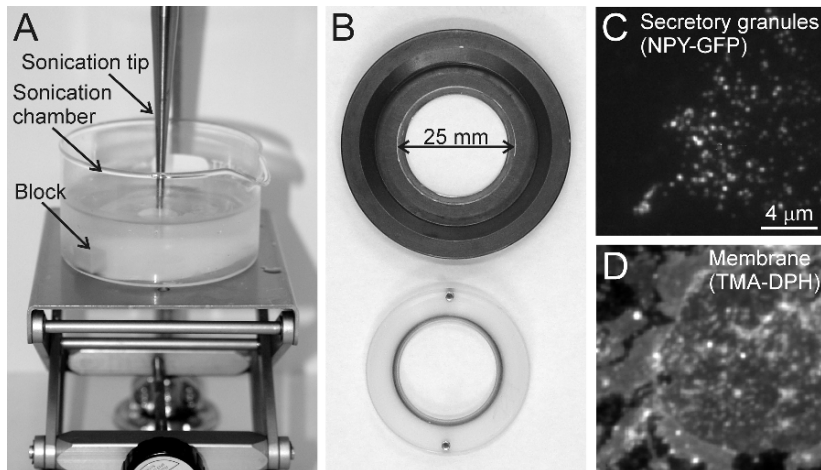


Fig. 1 Generation of membrane sheets with fluorescent docked secretory granules. **(A)** The sonication tip is centered in the sonication chamber at a distance of 1 cm between tip and bottom of the dish. To this end, a metal block 1 cm high can be put in the chamber and used as reference. Then, a glass cover slip is put below the tip (cell side up), and a sonication pulse is applied. The coverslip is taken out of the sonication chamber and mounted quickly in the microscopy chamber. **(B)** The microscopy chamber has to allow for quick mounting of the glass coverslip, for example, by sealing the chamber by screwing in an insert (we found a circular chamber to be easiest to handle, especially when the thread between chamber body and insert is large and the insert material is plastic). **(C)** Image of a membrane sheet in the green channel (visualizing NPY-GFP in secretory granules) and **(D)** the blue channel (visualizing phospholipid membranes stained by TMA-DPH).

2.3 Monitoring Exocytosis by Fluorescence Microscopy

1. Microscopy chamber: Use an open chamber that allows mounting of the glass coverslip within less than 1 min (Fig. 1).
2. Calcium-buffered solutions: For concentrations of free calcium in the range from 0 to 1.35 μM , use solutions containing 10 mM EGTA and 1–9 mM CaCl_2 (see Note 3). The $[\text{Ca}^{2+}]_{\text{free}}$ is calculated from the K_d of EGTA for Ca^{2+} , which is dependent on ionic strength, temperature, and pH (for dissociation constants in 0.1 M KCl, see Ref. 7). For higher $[\text{Ca}^{2+}]_{\text{free}}$, use diethylenetriaminepentaacetic acid (DPTA) instead of EGTA (assuming a Ca^{2+} dissociation constant of 81 μM ; 8).
3. TMA-DPH solution: For a saturated solution of TMA-DPH [1-(4-trimethylammonium)-6-phenyl-1,3,5-hexatriene-*p*-toluenesulfonate], add 10–20 mg TMA-DPH powder to 2 mL phosphate-buffered saline solution (137 mM NaCl, 2.7 mM KCl, and 8.1 mM Na_2HPO_4 , pH 7.3). After vortexing, undissolved TMA-DPH is spun down, and the supernatant is used for experiments. For membrane staining, add 25 μL saturated TMA-DPH solution to 0.5 mL chamber buffer.
4. Fluorescence microscopy: A standard epifluorescence microscope with an 100 \times magnifying objective lens is used (for an example, see Ref. 4). Use the following filters for detection of GFP and TMA-DPH: GFP, excitation BP 450–490, BS 510, emission BP 515–565; TMA-DPH, excitation G 365, BS 395, emission LP 420. It is highly recommended to control the focal position using a low-voltage piezo translator driver in combination with a linear variable transformer displacement sensor/controller (for an example, see Ref. 3). This device allows changing the focal plane in 100-nm steps, a prerequisite for focusing properly on secretory granules. In addition, it allows for more precise corrections of axial focal plane drifts that occur during the experiments.
5. Camera: A highly sensitive camera that records at diffraction-limited resolution is required for detection and resolution of individual secretory granules. When back-illuminated charge-coupled device (CCD) cameras with large pixels are used, additional magnifying lenses (e.g., see Ref. 4) are required to avoid spatial undersampling (to meet the Nyquist criterion). For instance, for camera pixels with a size of 24 \times 24 μm , an additional 2.5 \times magnifying lens is required to obtain 96-nm pixel sizes in the image.

2.4 Data Analysis

For image acquisition and data analysis, the Metamorph (Universal Imaging Corp., West Chester, PA) program can be used.

3 Methods

The optical readout of the assay requires fluorescent labeling of secretory organelles (*see Note 4*). For GFP labeling of secretory granules, we transfect a plasmid for expression of human NPY fused C-terminally to GFP (NPY-GFP) into PC12 cells via cell electroporation (*4*). In principle, other cell types or secretory organelle markers can also be used (*see Notes 1 and 5*). Transfected cells are plated onto poly-L-lysine-coated glass coverslips and are used 2 d after electroporation (*see Note 6*).

For generation of membrane sheets, coverslips are treated with an ultrasound pulse that removes the upper parts of the cells and leaves behind the flat, glass-adhered basal plasma membrane with docked secretory granules (*see Note 7*). During generation and screening for a suitable membrane sheet, the preparation is kept in calcium-free solution to avoid triggering of exocytosis.

Once a membrane sheet has been selected and if necessary treated with biochemical reagents, the initial distribution and status of secretory granules are documented by taking an image. For triggering exocytosis, the buffer is exchanged with a solution containing a micromolar concentration of free calcium, and the recording of an image sequence is subsequently started. Exocytosis of single secretory granules is documented in the resulting image sequence, in which changes of granule intensities indicate a fusion event (*see Note 8*). After the experiment, the phospholipids of the membrane sheet are visualized by staining with TMA-DPH to document the integrity of the plasma membrane. Data are analyzed, and exocytosis is presented as a percentage of granules that underwent exocytosis.

3.1 Cell Culture and Transfection

3.1.1 Coating of Glass Coverslips

1. Glass coverslips are cleaned by putting about 100 coverslips in a 500-mL glass beaker containing 100 mL ethanol. Shake the beaker gently for 1–2 h. Continue working under sterile conditions in the cell culture hood.
2. Take out coverslips one by one and flame them briefly (take precautions not to set fire to the ethanol in the glass beaker), allow the coverslips to cool, and place them into cell culture dishes with a diameter of 35 mm (use of six-well plates is recommended). The rim of the coverslips should have no contact with the wall of the dish; otherwise, plated poly-L-lysine solution or cell suspension will not remain on the coverslips.
3. Pipet about 500 μ L poly-L-lysine solution onto each coverslip. Make sure that the coverslip is evenly covered with the solution. After 20 min, suck off the poly-L-lysine solution and wash once briefly with about 2 mL sterile ddH₂O.
4. After 2 h of air drying, coverslips can be used for experiments or can be stored at 4 °C up to several weeks.

3.1.2 Cell Transfection

1. Grow PC12 cells in 75-cm² flasks. Passage them 1:2 when cells become almost confluent. Cells are detached from the substrate by trypsination, and the suspension is divided into two halves. Centrifuge the suspensions and use one pellet for the new passage and the other for transfection by electroporation. The cell pellet for passaging is resuspended and triturated in medium, and cells are transferred into a new flask.
2. The cell pellet for transfection is resuspended and triturated in 1.5 mL cytomix.
3. Transfer 350 μ L of the cytomix cell suspension (should contain approx 2×10^6 cells) into an electroporation cuvette (2-mm gap between electrodes; total volume about 0.5 mL) and add 20–50 μ g NPY-GFP plasmid deoxyribonucleic acid (DNA) (not more than 50 μ L). Gently resuspend the cells (as they settle) and apply a 1150-V, 50- μ F, and 50- Ω pulse using a cell electroporator. Transfer the cell suspension from the cuvette into a tube containing 3 mL medium.
4. Resuspend cells and plate 500 μ L per coverslip. Make sure that cells are evenly distributed. Wait for 20 min to allow cells to settle and then carefully add 2 mL medium to each coverslip, pipeting the solution at the wall of the dish. Cells are transferred into the incubator and are ready to use for experiments after 2–3 d.

3.2 Generation of Membrane Sheets

1. Fill the sonication chamber with 200 mL ice-cold sonication buffer and keep it on ice.
2. Place a coverslip on the bottom of the chamber and center it. Transfer the chamber to the sonication device and position the tip of the sonication device above the glass coverslip at a distance of 1 cm (Fig. 1). Apply one 100-ms pulse at low energy (see Note 9).
3. Mount the coverslip in a microscopy chamber and fill it with sonication buffer containing reagents for biochemical treatment (e.g., ATP derivatives, rat brain cytosol, or SNARE [soluble *N*-ethylmaleimide-sensitive factor attachment protein receptor] interacting proteins) of the plasma membrane if required (see Note 10). Start a timer (see Note 11).

3.3 Monitoring Exocytosis by Fluorescence Microscopy

1. Mount the microscopy chamber on the microscope and find a suitable membrane sheet for the experiment. Membrane sheets should be large with a high number of brightly fluorescent secretory granules (Fig. 1). This procedure takes between 5 and 10 min, setting a limitation between membrane sheet generation and stimulation of exocytosis. Use a fixed time window between membrane sheet generation and triggering of exocytosis (e.g., 10 min).
2. Once a membrane sheet has been found, wait for the chosen time window to elapse (see step 1) after mounting of the coverslip in the chamber. Image the

membrane sheet, add a buffer containing calcium-buffered solution, and start the image recording. For solution exchange, use a pipet. Using a back-illuminated CCD camera system, approx 100 images can be taken before GFP signals are lost because of bleaching. It is recommended to take not more than 50 images at a frequency that depends on the experimental time window (e.g., 2 images/min for 25 min, with exposure times of about 1 s).

3. After monitoring exocytosis, the studied membrane sheet should be visualized by a lipophilic dye to document the continuity of the plasma membrane. To this end, add TMA-DPH and image the preparation in the blue channel.

3.4 Data Analysis

1. For statistical reasons, analyze only membrane sheets with at least 15 secretory granules. Place circles on individual secretory granules visible in the first image (before buffer exchange).
2. Playing the image sequence, granules should show no lateral mobility. Regarding granule intensities, they might be stable, become dimmer, become brighter, or lose the signals. The last three types indicate exocytosis (*see Note 8*). For each granule, indicate the type of behavior, and if necessary the time-point when the exocytotic event occurred can be documented (*see Note 12*).
3. Express exocytotic activity as percentage of active secretory granules or plot events against time after normalizing to the total number of secretory granules on a membrane sheet (only applicable if a membrane sheet contains a sufficiently high number of granules and if time resolution of the experiment is low).
4. For each condition, approx 10 membrane sheets should be analyzed and averaged.

3.5 Two Channel Recordings

For recording exocytotic activity, only the green channel is required, and for documenting the integrity of the membrane sheets the blue channel is used. Using the red or far-red channels, simultaneous immunostainings (4), fluid phase uptake during exocytosis followed by direct retrieval of granules (3), or fluorescent-labeled bound protein can be monitored.

4 Notes

1. Other cell types can also be used; for example, pancreatic β -cell lines and bovine chromaffin cells have been tested. The only requirement is that cells attach firmly to the glass coverslip.

2. Shape and size of the coverslips do not matter as long as they are not thicker than 100 μm and larger than several square centimeters. This minimum area is recommended because the efficiency of membrane sheet generation is low, and screening a larger area for suitable membrane sheets is required. In general, round coverslips can be mounted quicker into a microscopy chamber than square coverslips.
3. Free-calcium concentrations in the range of 1–10 μM have been reported to be optimal for triggering exocytosis from PC12 cells in in vitro systems. When setting up the assay, a range of $[\text{Ca}^{2+}]_{\text{free}}$ should be tested to find out the best condition. Please note that higher $[\text{Ca}^{2+}]_{\text{free}}$ can become inhibitory for exocytosis.
4. This can be achieved by incubating cells with the fluorescent dye acridine orange, which accumulates in acidic compartments like secretory granules (9), or by overexpression of a GFP-labeled peptide hormone that is sorted into secretory granules (2). Although cell transfection is necessary as an additional step for GFP labeling, it is the method of choice compared to acridine orange because it causes less photodamage, is more resistant to bleaching, and labels secretory organelles more specifically.
5. The granule marker should be releasable. If an integral secretory organelle protein is used, detection of exocytosis is only possible if GFP is localized inside the granule lumen and the lumen is acidic. In this case, exocytosis causes lighting up of the pH-sensitive GFP (e.g., see Ref. 10).
6. Expression and sorting of the protein takes 2 d, with maximal expression within the first day. After more than 4 d, GFP fluorescence is lost because expression has stopped, and the NPY-GFP produced has a turnover rate of about 24 h.
7. Secretory granules only fluoresce when the original cell was expressing NPY-GFP (the rate of transfection is between 10% and 30%), and often membrane sheets without secretory granules are generated. For this reason, a suitable membrane sheet has to be found by screening large areas on the glass coverslip.
8. Fusion results in granules becoming brighter (dequenching of the pH-sensitive GFP), dimmer (partial release of GFP), or losing their signal (emptying of granules).
9. The right energy setting of the sonication device has to be found out by testing the range of available settings. First, the pulse length is adjusted as short as possible (usually 100 ms), and then one pulse at lowest energy is applied to a coverslip. The cells adsorbed to the glass create slight turbidity. If after sonication the turbidity still covers the entire coverslip, the pulse energy is too low. Take another coverslip and increase the energy stepwise until sonication generates a clearing. The stronger the pulse, the larger is the clearing, finally leading to removal of all cells. The best setting is obtained if a large, starlike clearing is formed.
10. The buffer should contain EGTA to avoid triggering of exocytosis by traces of calcium prior to stimulation. In the absence of Mg-ATP, a loss of exocytotic activity within minutes is observed.

11. Treatments should not take longer than 10 min as run down of SNARE activity, for example, is observed after about 20 min.
12. Manual counting of exocytosis is recommended if only a low number of experimental conditions are tested; otherwise, algorithms for detection of exocytotic activity can be developed.

Acknowledgments I would like to thank Dr. Philip Holroyd for critical comments on the manuscript and providing images of membrane sheets.

References

1. Heuser, J. (2000) The production of “cell cortices” for light and electron microscopy. *Traffic* **1**, 545–552.
2. Lang, T., Wacker, I., Steyer, S., et al. (1997) Ca²⁺-triggered peptide secretion in single cells imaged with green fluorescent protein and evanescent wave microscopy. *Neuron* **18**, 857–863.
3. Holroyd, P., Lang, T., Wenzel, D., De Camilli, P., and Jahn, R. (2002) Imaging direct, dynamin-dependent recapture of fusing secretory granules on plasma membrane lawns from PC12 cells. *Proc. Natl. Acad. Sci. U. S. A.* **99**, 16806–16811.
4. Lang, T., Bruns, D., Wenzel, D., et al. (2001) SNAREs are concentrated in cholesterol-dependent clusters that define docking and fusion sites for exocytosis. *EMBO J.* **20**, 2202–2213.
5. Heumann, R., Kachel, V., and Thoenen, H. (1983) Relationship between NGF-mediated volume increase and “priming effect” in fast and slow reacting clones of PC12 pheochromocytoma cells. Role of cAMP. *Exp. Cell Res.* **145**, 179–190.
6. van den Hoff, M.J., Moorman, A.F., and Lamers, W.H. (1992) Electroporation in “intracellular” buffer increases cell survival. *Nucleic Acids Res.* **20**, 2902.
7. Tsien, R., and Pozzan, T. (1989) Measurement of cytosolic free Ca²⁺ with quin 2. *Methods Enzymol.* **172**, 230–262.
8. Heinemann, C., Chow, R.H., Neher, E., and Zucker, R.S. (1994) Kinetics of the secretory response in bovine chromaffin cells following flash photolysis of caged Ca²⁺. *Biophys. J.* **67**, 2546–2557.
9. Avery, J., Ellis, D.J., Lang, T., et al. (2000) A cell-free system for regulated exocytosis in PC12 cells. *J. Cell Biol.* **148**, 317–324.
10. Taraska, J.W., Perrais, D., Ohara-Imaizumi, M., Nagamatsu, S., and Almers, W. (2003) Secretory granules are recaptured largely intact after stimulated exocytosis in cultured endocrine cells. *Proc. Natl. Acad. Sci. U. S. A.* **100**, 2070–2075.

5

FRAP Analysis of Secretory Granule Lipids and Proteins in the Sea Urchin Egg

Julian L. Wong and Gary M. Wessel

1 Introduction.....	61
2 Materials.....	63
3 Methods.....	66
4 Notes.....	72
References.....	74

Summary Cortical granules of the sea urchin are secreted at fertilization in response to sperm fusion. Approximately 15,000 of these vesicles are tightly tethered to the cytoplasmic face of the egg plasma membrane prior to insemination such that the vesicle–plasma membrane complex may be isolated and manipulated in vitro. Furthermore, this complex remains fusion competent and can thus be used for in vitro biochemical studies of secretion on a per-vesicle or a population scale. We document approaches to study the dynamics of membrane lipids and proteins in these secretory vesicles. Their large size (1.3- μm diameter), vast number, and ease of manipulation enable several unique approaches to study general secretion mechanisms.

Keywords Cortical granules; exocytosis; fertilization; fluorescence redistribution after photobleaching; FRAP; secretory vesicles.

1 Introduction

Eggs undergo major cell surface changes at fertilization that reflect its interaction with the successful sperm. Just before fertilization, the egg extracellular matrix and cell surface proteins activate and enhance fusion with sperm. Immediately after sperm–egg fusion, however, the egg cell surface is transformed by the contents of secretory vesicles found within the egg cortex (reviewed in *Refs. 1 and 2*). In animals such as sea urchins, this transformation may take as little as 30s, and the majority of the biochemical and molecular changes to an egg cell surface result from the contents of secretory granules, called *cortical granules* (Fig. 1). This cell surface transition process is called the “physical” or “slow” block to

polyspermy (3) and is strongly selected for in most animals since multiple sperm-derived centrioles cause aberrant cleavage in the early embryo, ultimately resulting in death (4).

The stimulus for exocytosis of cortical granules is calcium. Free cytoplasmic calcium originates from stores in the egg endoplasmic reticulum, where it is released via the inositol-1,4,5-trisphosphate (IP3) receptor, ryanodine receptor, and nicotinic acid adenine dinucleotide phosphate (NAADP) pathways (5–7). Calcium causes changes in the egg that are indicative of its reactivation, including calmodulin and protein kinase C (PKC) activity (8,9). Together, these protein-dependent signaling pathways result in cytoplasmic alkalination through ion transporters (10), initiation of protein synthesis (11), and cytoskeletal reorganization (12). All these changes facilitate mitotic progression of the zygote (13).

Sea urchin eggs each possess approx 15,000 cortical granules poised in preparation for exocytosis at its cell surface (Fig. 1b) (14). The vesicles are so tightly attached to the cytoplasmic face of the plasma membrane that they are not displaced upon centrifugation or even homogenization of the egg (Fig. 2 inset) (14–16). They may remain in this state for months without premature content release (17). Only on exposure to 1–2.5 μM free calcium (18) does the vesicle population completely and uniformly release its contents over the surface of the cell (3). Together, the high-affinity attachment to the plasma membrane, predictable response to calcium, and abundance and size (1.3 μm diameter) of these organelles contribute to their utility in examining mechanisms of stimulus-dependent exocytosis (14,19).

The proteins responsible for stimulus-dependent secretion are hypothesized to include members and regulators of the soluble *N*-ethylmaleimide-sensitive factor

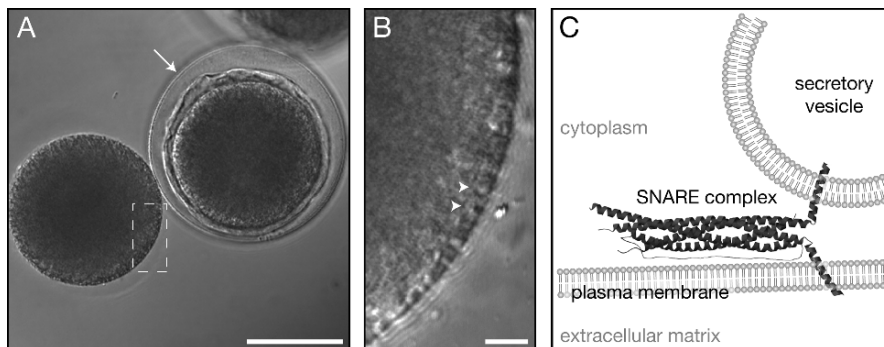


Fig. 1 *The model.* (A) DIC image of *Strongylocentrotus purpuratus* egg before (left) and after (right) fertilization. Contents of the cortical granule give rise to both the fertilization envelope (arrow) and the hyaline layer (wrinkled layer adjacent to the plasma membrane). Bar = 50 μm . (B) DIC image of the egg cortex showing cortical granules (arrowheads) adjacent to the plasma membrane. Bar = 5 μm . (C) Diagram of the relationship between cortical granules and the plasma membrane indicating the participation of SNARE proteins assembled in the fusion-catalyzing complex. (Crystal structures adapted with permission from Ref. 22.).

attachment protein receptor (SNARE) family (reviewed in *Refs. 20–22*). A SNARE protein is generally classified first by the membrane with which it mainly associates, specifically the vesicle membrane (v-SNARE) or the membrane targeted by the vesicle for fusion (t-SNARE). Assembly of select v- and t-SNAREs into a complex (Fig. 1c) contributes to the pairing of vesicles to their target membrane by means of limited intracellular distribution of specific members (20,21). This regulated trafficking is aided by small guanosine 5'-triphosphate (GTP)-binding proteins of the Rab family and the calcium-binding protein synaptotagmin, which both participate in vesicle targeting, attachment, and retention at the destination membrane (20,23,24). The mechanisms behind the role of each regulator during the process of exocytosis are not clear, but the presence of SNARE proteins and their putative regulators on the egg cortical granule (19,25,26) highlights their contributions to the formation of the physical block to polyspermy at fertilization.

In this chapter, we document methods for utilizing cortical granules from sea urchin eggs to study the secretion process. The uniformity across over 10 million eggs in the clutch of a single female allows for the rapid isolation of cell surface complex in abundance. A modification to the cell surface complex isolation protocol (14) generates lawns of egg cortex containing the same cortical granule–plasma membrane complex, but now spread on glass in an orientation that exposes the cytoplasmic surface to experimental manipulation. These preparations retain their fusion competency, thereby allowing a detailed analysis of the molecular mechanisms of egg exocytosis (14). Some of the treatments made possible by these lawn preparations include assessing the dynamics of the modified lawns during exogenous calcium exposure, labeling of the membrane with lipid dyes, or tagging the membrane-associated proteins with antibodies. Here, we detail how to use fluorescence redistribution after photobleaching (FRAP) to understand the dynamic nature of the secretory vesicle membrane and its association with the egg plasma membrane (27).

2 Materials

2.1 Handling of Eggs

1. 0.5 M KCl in distilled water. Stored at room temperature.
2. Artificial seawater (ASW): 0.5 M NaCl, 10 mM KCl, 30 mM MgCl₂, 20 mM MgSO₄, 8 mM CaCl₂, 2.4 mM NaHCO₃, pH 8.2; can be made from instant salts such as Instant Ocean (Aquarium Systems, Mentor, OH). The salinity should measure 34–36 parts per thousand (3.4–3.6%), and the pH should be adjusted to 8.2 using sodium bicarbonate (*see Note 1*).
3. Acidic seawater is made using hydrochloric acid to lower the pH of ASW to 5.2. The process of titrating is delicate since the buffering capacity of seawater near pH 5.0 is weak. If the pH drops below 5.2, use this seawater to fine-adjust a new batch of pH 8.2 ASW.

4. Calcium-free seawater (CFSW): 0.45 M NaCl, 9.4 mM KCl, 48.3 mM MgSO₄, 6 mM NaHCO₃, 10 mM ethylene glycol-bis(2-amino-ethylether)-N,N,N',N'-tetraacetic acid (EGTA), pH 8.2.

2.2 Preparation of Cortical Granule Lawns

1. Glass coverslips: The larger, rectangular glass (22 × 50 mm) coverslips are best to maximize the number of cortical lawns (*see Note 2*).
2. Poly-L-lysine is dissolved in distilled water to 10 mg/mL. This stock may be aliquoted and stored at -20°C. Alternatively, 1 mg/mL of protamine sulfate dissolved in water may be used.
3. Make a humid chamber from the box used for racking pipet tips, such as from TipOne® preracked filter tips (USA Scientific Incorporated, Ocala, FL, USA). The perforated surface is used as a shelf. Fill the bottom of the box with ice and then bury the entire chamber in ice to keep the samples cold. Carefully close and open the tip box lid so the coverslips incubating inside are not disturbed.
4. Calcium-free buffer (CFB): 0.5 M NaCl, 0.01 M KCl, 1.5 mM NaHCO₃, 60 mM NaOH, 20 mM EGTA, pH 8.0. It should be prechilled to 4°C and kept on ice until needed. Alternatively, isoosmotic (1000 milliosmoles) solutions containing at least 10 mM EGTA, pH 7.0–8.0 will also work. For example, use a solution of 1 M glycerol with 10 mM EGTA, 10 mM HEPES, pH 7.5 (*see also 28*).

2.3 Labeling Reagents

1. Various viable lipid dyes are commercially available (Invitrogen Corporation, Carlsbad, CA, USA). If provided as a solid, dissolve these in ethanol, methanol, or dimethylsulfoxide (DMSO) at a 1000X stock concentration. Otherwise, use according to instructions.
2. Isothiocyanate derivatives (Sigma-Aldrich Corporation, St. Louis, MO, USA) or AlexaFluor® fluorescent dyes (Invitrogen) for protein labeling. These may be the same dye provided in the immunoglobulin antigen binding fragment (Fab) labeling kit (*see Subheading 2.4.*, item 11). Dissolve solids in DMSO, CFB, or appropriate solvent based on manufacturer's instructions (*see Note 3*).

2.4 Generating Fluorophore-Conjugated Fabs Against Specific Membrane-Associated Proteins

1. Any immobilized protein A can be used to purify the immunoglobulin Gs (IgGs) from solution. Any resin that minimizes nonspecific protein purification should be favored, such as Sepharose 4B (Sigma-Aldrich).

2. 100 mM glycine in distilled water; pH 2.5 adjusted with hydrochloric acid.
3. Buffered saline solution: Any standard buffered solution may be used, including phosphate-buffered saline (140 mM NaCl, 3 mM KCl, 5 mM Na₂HPO₄, 1.4 mM KH₂PO₄, pH 8.0) or Tris-buffered saline (185 mM NaCl, 50 mM Tris base, pH 8.0). The main consideration will be how much free calcium such a buffer will encounter during the procedure since calcium phosphate readily precipitates out of solution. These solutions should be sterilized with a 0.22- μ m filter.
4. Disposable 12-mL capacity columns with sealing caps, such as sold by Bio-Rad (Bio-Rad Laboratories, Hercules, CA, USA). The caps should fit snugly to prevent leaking when the column is inverted. To ensure against leaks, wrap the vulnerable connections with wax film after capping.
5. Sample concentrators that hold at least 2 mL, with a molecular weight cutoff less than or equal to 30,000, such as Centricon or Amicon filters (Millipore Corporation, Billerica, MA, USA). Follow manufacturer's instructions when using, including equilibration of the filter itself with deionized water sterilized through a 0.22- μ m filter.
6. Sodium phosphate buffer: 8.9 mM Na₂HPO₄, 7.8 mM NaH₂PO₄, 10 mM ethylenediaminetetraacetic acid (EDTA), pH 7.0. This solution should be sterilized through a 0.22- μ m filter.
7. Bradford (Bio-Rad) and BCA assays (Pierce, Rockford, IL, USA). Either is suitable for this procedure; use the version adapted for microtiter plates to minimize the volume of sample sacrificed to make the measurements.
8. The ImmunoPure Fab preparation kit (Pierce) is a reliable system for making Fabs, but the amount of serum necessary may be high. Follow manufacturer's instructions to prepare fragments. If using antiserum with a high titer of activity, a scaled-down preparation protocol may be used and is described below in steps with an asterisk (*).
9. Microvolume spin columns for microcentrifuges, such as Handee columns (Pierce).
10. Bicarbonate buffer: Phosphate-buffered saline solution (*see* Subheading 2.4, item 3) plus 100 mM NaHCO₃, pH 8.0. This solution should be sterilized using a 0.22- μ m filter.
11. Fluorophore protein-labeling kit, such as the AlexaFluor Microscale protein-labeling kit (Invitrogen). These kits contain all equipment necessary for Fab conjugation and purification (*see* **Note 3**).

2.5 Labeling of Cortical Lawns

1. Vacuum grease: This is used to dam off a region of interest to retain additional buffer around the sample when it is finally mounted (*see* **Note 4**).
2. Glass slides should be slightly larger than the cover glass.
3. Quick-dry nail polish is used to seal the cover glass to the slide, limiting leakage of excess buffer onto the microscope. Any brand will work.

3 Methods

3.1 Handling of Eggs (see also 29)

1. Obtain sea urchin eggs by injecting 0.5 M potassium chloride into the coelomic cavity of females. A syringe ended with a 25-gage needle is used to pierce the tough membrane between the test (shell) and the mouth. Eggs will release from the gonadal pores found on the surface opposite the mouth. *Strongylocentrotus purpuratus* eggs are orange; sperm are a glistening white.
2. Collect eggs by inverting the female over a beaker filled with ASW. Eggs will settle to the bottom of the beaker. While the female sheds, keep the beaker on ice. Following shedding, decant or aspirate off excess ASW.
3. Dejelley about 0.5 mL eggs by pouring the cells into a beaker of chilled, acidic ASW and invert periodically for 10 min (Fig. 2). The rest of the eggs can be kept in ASW on ice—often for a few days—until needed. The wash is complete when the eggs have settled to the bottom of the beaker. Decant or aspirate off excess ASW.
4. Resuspend eggs in ice-cold CFSW. Allow the eggs to settle by gravity while on ice, remove buffer and resuspend in a volume of new buffer. This is a single wash; repeat for a total of three washes. Keep all media and eggs on ice.

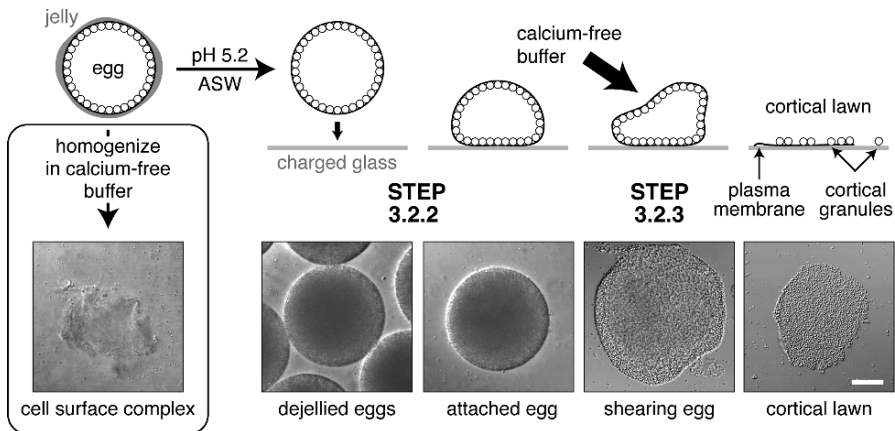


Fig. 2 Creation of egg cortex preparations. Sequence of steps illustrating the process of egg isolation through cortical lawn preparations on glass coverslips is shown. Corresponding DIC images of the eggs in various stages of the protocol are included. Inset shows the analogous preparation of cell surface complex using a similar calcium-free buffer (see Subheading 2.2., item 4). Bar = 25 μ m.

3.2 Preparation of Cortical Granule Lawns

1. Spread approx 100 μ L poly-L-lysine solution in a generous area of the cover glass, leaving an edge of at least 3 mm. Incubate this solution on the glass for 10 min and then wash off with deionized water. Thoroughly dry the slide by wicking the edge with a dust-free tissue and store in a dust-free space.
2. With a transfer pipet or wide-bore pipet tip, gently transfer up to 0.5 mL of a dense suspension of dejellied eggs in CFSW to the treated coverslip. Allow the eggs to settle onto the glass for 10 min, holding the cover glass in a level humid chamber (Fig. 2).
3. Fill a 10-mL syringe with chilled CFB. Spray CFB through a 25-gauge needle, directing the jet toward the eggs attached to the cover glass. The optimal angle of attack is 35°–45°. Use quick, side-to-side or circular motion to maximize egg removal without overshearing cells. Ideally, slides have an even gradient of shearing, from only broken eggs to a complete loss of all organelles (Fig. 2).
4. Return cover glass to the level humid chamber and gently overlay samples with up to 200 μ L CFB, filling in from the edge.

3.3 Labeling Reagents

1. Stocks of lipid dyes should be dissolved directly into chilled CFB just before use. The final concentration of lipid dye can range between 1 and 5 mM, depending on the length of the aliphatic chains (see Note 5).
2. To label all exposed proteins in the sample, the stock of reactive fluorophore dye is diluted into CFB. Centrifuge or filter the solutions just before adding to the sample to minimize contaminating the samples with undissolved dye particles (see Note 6).

3.4 Generating Fluorophore-Conjugated Fabs Against Specific Membrane-Associated Proteins

1. Generating Fabs from IgGs requires sera with a good titer. Start with at least 2 mL of serum for this protocol. Volumes can be scaled up as necessary.
2. Inactivate complement in the serum at 56 °C for 30 min (Fig. 3). Pellet insoluble protein at 18,000 g for 5 min at room temperature.
3. Pack up to 1 mL of immobilized protein A in the disposable column using gravity to settle the resin. Equilibrate immobilized protein A by first washing with 2 bed volumes of 100 mM glycine, pH 2.5. Then, wash with 10 bed volumes of buffered saline. For each wash, allow the fluid to pass through the resin at a rate determined by gravity. Cap and seal the bottom of the column to prevent drying out. This sealing process should be done as necessary throughout the protocol.

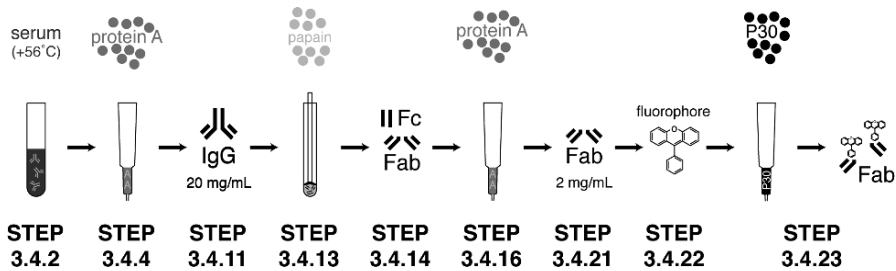


Fig. 3 Generation of fluorophore-conjugated Fabs. Chronology of major stages necessary to generate antibody Fabs from total serum is shown. Key steps are illustrated.

4. Combine the inactivated serum with the protein A resin in the bottom-capped, disposable column (**Fig. 3**). Cap the top of the column and seal with additional wax film. Allow the mixture to incubate for 30 min at room temperature, inverting constantly. This batch binding saturates the resin with immunoglobulins.
5. Return the column to its upright orientation. Remove the wax film and uncap the top. Allow the resin to settle before removing the lower cap. Capture the flowthrough in a separate tube and store at 4°C in case binding failed. If desired, sodium azide may be added to 0.001% (w/v) before storing.
6. Wash the resin with 5 bed volumes of buffered saline. Repeat for a total of five times. Washes may be saved for analysis if desired. Do not allow the bed resin to dry out.
7. Elute the IgGs with 0.5 bed volume of 100 mM glycine, pH 2.5. Capture each elution in fresh tubes containing 0.1 bed volume of 1 M Tris, pH 8.0 and invert or vortex immediately to neutralize the glycine. This minimizes the exposure of IgG to the acid wash. Repeat for a total of eight elutions.
8. Wash the immobilized protein A resin once with 10 mL buffered saline. Store the slurry at 4°C until needed again during the separation of the immunoglobulin constant fragments (Fc) from the Fab fragments (step 15).
9. Analyze the amount of IgG per elution in a spectrophotometer reading OD 280 or by sodium dodecyl sulfate polyacrylamide gel electrophoresis (SDS-PAGE). Stain the gel for total proteins with Coomassie blue. Use only those elutions enriched with IgG fragments (150 kDa under nonreducing conditions; 25 and 60 kDa under reducing conditions). Generally, the first four elutions are enriched in IgGs.
10. Pool and concentrate the chosen elutions using the sample concentrators. Exchange the elution buffer for sodium phosphate buffer using at least three washes of about 2 mL. This removes the buffering agent Tris, which will interfere with the alkalization of the solution by cysteine for optimal papain activity (step 13). The final volume of concentrated IgGs should be between 50 and 100 μL.

11. Determine the protein concentration of the IgG concentrate using up to 10 μL of the solution in the method of choice. If necessary, continue to concentrate solution or dilute the sample with sodium phosphate buffer to 20 mg/mL (Fig. 3).
12. Prepare fresh ImmunoPure digest buffer as per instructions. Use 4 mL digest buffer to wash 150 or 500 μL of the papain resin slurry in a 16 \times 100 mm round-bottom glass tube. Separate resin from the digest buffer with the ImmunoPure filter. Resuspend the papain resin in an equal volume of digest buffer. The 150- μL volume of resin is appropriate for the scaled-down protocol (*), whereas the 500- μL volume follows the manufacturer's instructions.
13. Add 0.5 mL equilibrated IgG (20 mg/mL) and 0.5 mL fresh ImmunoPure digest buffer to the resin resuspension in the glass tube. Press filter just to the top level of the solution to create a closed system in which the resin cannot be lost up the sides of the tube. Incubate this mixture at 37°C for about 16 h (Fig. 3). Keep the slurry in suspension using a shaker, similar to ones set up for bacterial culturing.
- *13. Combine 150 μL equilibrated IgGs (20 mg/mL), 150 μL fresh ImmunoPure digest buffer, and 150 μL resin resuspension in a sterile 500- μL capacity tube. Seal carefully to avoid losing fluid, then wrap the lid with wax film. Incubate this mixture at 37°C for about 16 h (Fig. 3). Keep the slurry in suspension by placing tubes in an Erlenmeyer flask secured to the shaking platform of a bacterial culturing incubator or by taping the tubes directly to the shaking platform.
14. Use the filter to separate the fluid containing the IgG fragments from the papain resin. Decant the fluid to a new tube. Wash the resin with 1.5 mL ImmunoPure IgG-binding buffer to capture extra IgG fragments, pooling the wash fluid with the reaction fluid. These contain the IgG fragments (Fig. 4).
- *14. Transfer the digest reaction and resin into a Handee column. Centrifuge columns at 2000 *g* for 30 s and save the resultant fluid. Wash the resin twice by applying 750 μL ImmunoPure IgG-binding buffer to the columns, followed by centrifugation under similar conditions. Collect and pool all fluids that flow through. These contain the IgG fragments (Fig. 3).
15. Wash the pre-packed column containing 1 mL used immobilized protein A resin (step 7) with 4 mL 100 mM glycine, pH 5.2, followed by 4 mL ImmunoPure elution buffer. Then, wash with 10 mL ImmunoPure IgG-binding buffer. Discard all equilibration washes appropriately. Cap and seal the bottom of the column.
16. Combine the solution of IgG fractions (step 14) with the equilibrated, used protein A resin (step 15). Cap the top of the column and seal with additional wax film. Allow the mixture to incubate for 60 min at room temperature, inverting constantly (Fig. 3). This batch binding saturates the resin with the Fc and uncut IgGs, thereby separating them from the desired Fab fragments.
17. Return the column to its upright orientation. Remove the wax film and uncap the top. Allow the resin to settle before removing the lower cap. Capture the flowthrough in a separate tube. This fluid is enriched for Fabs; the Fc and uncut IgGs are retained on the immobilized protein A.

18. Wash the resin once with 5 mL ImmunoPure IgG binding buffer and pool with the flowthrough to maximize Fab yields.
19. Elute the Fc portions with 5 mL ImmunoPure elution buffer. Save this elution for analysis.
20. Pool and concentrate the Fab and Fc slurries separately using the sample concentrators. Exchange the fluid for bicarbonate buffer to remove amines from the proprietary ImmunoPure buffers. Free amines will compete for the reactive fluorophore conjugates and thus should be removed for maximal labeling efficiency. The final volume of concentrated Fabs should be between 50 and 100 μ L; the Fcs solution volume may be higher.
21. Determine the protein concentration of the Fab and Fc concentrate using method of choice. If necessary, continue to concentrate solution or dilute it with bicarbonate buffer to 2 mg/mL (Fig. 3).
22. Conjugate chosen fluorophore to Fabs according to the manufacturer's protocol. Scale down the protocol appropriately to accommodate the lower total protein masses obtained from smaller starting serum volumes.
23. Separate the Fabs from free dye by passing through a long, narrow P30 size exclusion column provided in some kits (AlexaFluor Microscale labeling kit, Invitrogen). Elution volumes should not exceed 0.5 mL to maximize Fab concentration (Fig. 3). This step may require about 3 h.
- *23. Separate the Fabs from free dye by using 300- μ L P30 size exclusion resin packed in a Handee microfuge spin column. Equilibrate the resin to buffered saline and centrifuge the column at 2000 *g* for 30 s to remove the liquid. Transfer the column to a clean microfuge tube. Add the labeled Fab reaction mix to the resin, allowing it to enter by gravity. Save the flowthrough in the tube and transfer the column to a new tube. Centrifuge columns at 2000 *g* for 30 s and save the resultant fluid. Add 200 μ L buffered saline to the resin to wash the resin. Repeat collections steps, saving each elution in a new microfuge tube (Fig. 3).
24. Analyze the fractions enriched for labeled Fabs by SDS-PAGE. Visualize fluorescence in each fraction using a transilluminator or other flatbed fluorescence scanner. Stain the gel for total proteins with Coomassie blue to evaluate the purity of the fractions for Fabs (50–60 kDa under nonreducing conditions; 25 kDa under reducing conditions) vs Fcs and IgGs.
25. Test the Fabs for retention of activity under appropriate conditions (e.g., immunoblotting or immunolocalization). Labeled Fabs may be further enriched by affinity purification if necessary. See Ref. 30, for example, for such a protocol.

3.5 Labeling Cortical Lawns

1. Overlay cortical lawn preparations with diluted lipid dye, reactive fluorophore, or Fab solutions. Use between 75 and 100 μ L per rectangular cover glass.
2. Incubate the samples with probe in the humid chamber while still on ice. The times required for lipid dyes are 10 min for shorter aliphatic chains and more than

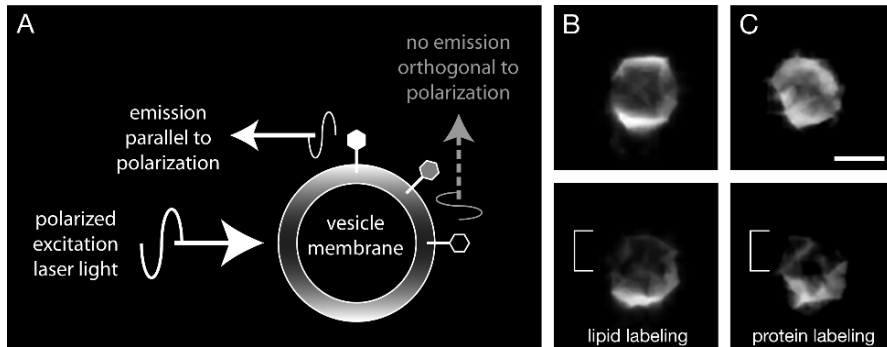


Fig. 4 Fluorescence bleaching experiments. (A) Schematic showing the effects of polarized laser light on the emission profile of fluorophores associated with vesicle lipid membrane. This phenomenon is a reflection of the fluorophore orientation within the lipid membrane relative to the polarized incident excitatory light and can be seen by confocal microscopy because of the small diameter of the vesicle. (B) Anisotropy of one cortical granule labeled with the lipid dye di-8-ANEPPS, a member of the aminonaphthylethylpyridinium (ANEP) dye family containing 8 unsaturated carbons in its aliphatic chain. (C) Single-granule labeling using AlexaFluor-488-conjugated antisynaptotagmin Fab. Images shown are pre- (top) and postbleach (bottom). The bleach area used is bracketed. Images were resampled to print resolution using Genuine Fractals (LizardTech, Seattle, WA, USA). Bar = 1 μm .

30 min for longer chains; for the reactive fluorophore, time is 10 min, and the Fabs require 30 min. While longer times may enhance lipid dye incorporation, extending times with other probes often results in higher background staining.

3. Following incubation, wash samples at least five times with CFB by gentle pipeting to exchange media.
4. Dry a border surrounding the samples on the coverslip with dust-free tissue. Apply a thin bead of vacuum grease, no thicker than 1 mm, to the cover glass. This will provide a wall to trap CFB and to prevent sample compression when the slide is imaged.
5. Add up to 50 μL CFB within the walled space. Carefully set a glass slide over the cover glass, allowing the slide to seat firmly on the vacuum grease walls. Avoid trapping air bubbles within the CFB volume, but do not move or remove the slide once it contacts the vacuum grease.
6. Seal the edges of the cover glass to the slide using nail polish.

3.6 Parameters for Imaging and FRAP Time Series (see Note 7)

1. Cortical granules are about 1.5 μm in diameter. On a Zeiss LSM510, the best resolution can be attained using an $\times 63/1.4$ NA PlanApochromat oil immersion objective. The digital zoom should be set to achieve a pixel size equal to the Nyquist sample distance for the specific microscope parameters (see Note 8).

2. Open the pinhole completely to ensure that each point in the image represents all of the fluorescence in the z-dimension. During data analysis (*see Note 13*), it is assumed that all of the fluorescence from the vesicle is collected in the image.
3. Do not use line or frame averaging. This ensures minimal time delay and accurate readings between individual frames.
4. Use the lowest laser power necessary to obtain a high signal-to-noise ratio to minimize photobleaching of the sample during the time series acquisition.
5. Photomultiplier tube gain should lie in the linear range of the detector, from 550 to 850 units on the Zeiss LSM510. Use of amplifier gain should be avoided to minimize the noise throughout the image.
6. The minimal pixel value of the background cover glass should be above 10 units (8 bit) or 200 units (12 bit), and maximal pixel value of specific emission should not exceed 240 units (8-bit image) or 3900 units (12-bit image) (*see Note 10*).
7. Time series are used to acquire data. At least 5 prebleach frames should be taken, followed by at least 55 postbleach time-points. The time delay between each image of the time series will depend on redistribution dynamics (*see Note 11*).
8. Laser settings for a bleach period should be set at 100% power for the optimal excitation wavelength. If this is not 488 nm, the corresponding argon laser line may also be used to enhance the bleaching process.
9. Bleaches in the specific region should fall between 30% and 50% prebleach fluorescence. The longest side of a bleach region should be parallel to the direction of laser movement to optimize the speed with which the bleaching is accomplished (*see Note 12*).
10. Remember to change the immersion oil regularly, even with the same sample (*see Note 13*).

4 Notes

1. Additional sources for seawater salt mixes as well as information on *Strongylocentrotus purpuratus* husbandry can be found in *Ref. 31*.
2. The thickness of the cover glass should be matched to the objective used on the confocal microscope, information that corresponds with the lens optical correction (in millimeter thicknesses). Generally, lens correction of 0.17 is used on objectives, so a coverslip thickness averaging 170 μm (no. 1.5) is recommended.
3. The choice of fluorophore should be matched to the excitation optimum of the most powerful laser available on the available confocal microscope. On the Zeiss LSM510, this is likely the 488-nm argon.
4. It is easiest to apply vacuum grease through the bore of a 10-mL syringe. Apply light but even pressure against the cover glass while sliding the syringe along the desired path. The final thickness should not exceed 1 mm.
5. The shorter chain lengths often label more efficiently than the longer lengths; thus, a general rule is to use higher concentrations for longer chains. For commercial

stains with proprietary concentrations, dilute the stock in CFB as recommended by the manufacturer.

6. Some examples of treatments with specific dyes are as follows:
 - Dissolve rhodamine B or fluorescein isothiocyanate in DMSO to make a stock of 1 mg per 20 μ L. Dilute this into 4 mL CFB and vortex to dissolve it further. Pass this working solution through a 0.22- μ m filter immediately before applying to the sample to remove undissolved particles that would otherwise contaminate the preparations.
 - Dissolve amine-reactive AlexaFluor conjugates directly in CFB at the concentration recommended by the manufacturer. Undissolved particles are separated by centrifugation at 18,000 g for 5 min. Volumes to be used are immediately removed from the top of the stock solution following centrifugation. This stock may be further diluted in CFB to optimize staining.
7. Some general hints for finding samples and staining variability are included below. More specific explanations related to the parameters listed in the Methods section are indicated.
 - The focal plane of each sample is often difficult to find by bright-field microscopy. Use of the epifluorescence feature is easier and more productive, especially to assess lawn preparation and staining quality. Ideal fields should have granules stained brightly, with vesicles separated from each other on the plasma membrane and some individual vesicles scattered on the glass.
 - Staining of individual vesicles will vary with the type of probe and the method of visualization. All lipid dyes will report cortical granules as rings by epifluorescence but appear as two mirrored crescents under the polarized laser light. This anisotropy is an effect of the orientation of the lipid dyes in the vesicle membrane. Conversely, total protein staining or Fab labeling shows up as a circle with a slightly brighter edge by both epifluorescent and confocal microscopy (Fig. 4). The presence of a brighter spot of fluorescence along the ring of a vesicle is likely a remnant of the plasma membrane attachment site and corresponds to an unattached cortical granule.
8. The choice of digital zoom depends on the Nyquist sample distance for the specific microscope setup. The Nyquist sampling distance is a parameter used to minimize undersampling the signal from a sample when it is converted to a digital image for quantitation. Its value is dependent on the point-spread function of the optical system, which is defined primarily by the numerical aperture of the lens and on the excitation wavelength. The Nyquist sampling distance is approx one-half of the actual resolution of the imaging system. For a detailed description of Nyquist criteria in the context of the point-spread function of light, *see* support.svi.nl/wiki/NyquistRate. To calculate the Nyquist sampling distance for your system, *see* support.svi.nl/wiki/NyquistCalculator.
9. Analysis techniques to calculate the diffusion rates of proteins and dyes may be found in *Ref. 32*.

10. The range of pixel values suggested falls within the linear range of most detectors. Following these guidelines ensures that the emission intensity does not extend beyond the measurable range (e.g., few if any pixels register a value of 0, or 255 for 8-bit images or 4095 for 12-bit images). Ideally, all values will fall within the middle 85% of the total range. Background values are arithmetically subtracted from each pixel during the analysis.
11. Region of interest should be centered about a single granule and should exceed the overall dimensions of the granule by at least 10 pixels. This provides leeway for granule movement during the acquisition. When optimizing the data collection for fluorophore redistribution, start with zero time delay (e.g., imaging occurs as fast as a single image can be scanned) to assess the amount of redistribution caused by rapidly diffusing species. If there is little redistribution in a short time period, the time delay should be increased. It is essential to have good data for (a) prebleach distribution, (b) immediate postbleach distribution to demonstrate the extent of asymmetry created by the bleach pulse, (c) the exponential redistribution time period, and (d) the plateau region of the curve to assess the mobile fraction. A useful breakdown is to have 5–10 images per phase within the redistribution period. Time intervals should be extended as necessary to accommodate the observed redistribution rates.
12. Bleached areas should extend beyond the granule edges to ensure completeness. Optimize the severity of the bleach by adjusting dwell time (the scan time of a laser per line of a field) or iterations of bleach. Excessive bleaching times inaccurately measure the redistribution rates since dyes will be photobleached before they are measured as a contributor to the redistribution. Conversely, insufficient photobleaching does not generate enough asymmetry in postbleach images to accurately calculate the redistribution rates.
13. As a slide moves over the lens, small air bubbles can be trapped in the immersion medium. These behave as refractory lenses that will dramatically distort both the excitation and emission light, greatly diminishing the signal and the resolution of the microscope. If on a particular field image quality or signal is weak or drops off, clean both the slide and lens with appropriate cleaner and lens paper. Then, carefully remount the sample with fresh immersion medium without moving the microscope stage. This should leave the sample in approx the same field as prior to the cleaning.

Acknowledgments We are grateful to Ann E. Cowan and Dennis E. Koppel at University of Connecticut Health Science Center for many productive conversations about FRAP techniques. Grants from the National Institutes of Health and National Science Foundation supported this work.

References

1. Wessel, G.M., Brooks, J.M., Green, E., et al. (2001) The biology of cortical granules. *Int. Rev. Cytol.* **209**, 117–206.
2. Wong, J.L., and Wessel, G.M. (2006) Defending the zygote: search for the ancestral animal block to polyspermy. *Curr. Top. Dev. Biol.* **72**, 1–151.

3. Just, E.E. (1919) The fertilization reaction in *Echinarachinus parma*. *Biol. Bull.* **36**, 1–10.
4. Rothschild, L. (1952) The fertilization reaction in the sea urchin. *J. Exp. Biol.* **30**, 57–67.
5. Patel, S. (2004) NAADP-induced Ca^{2+} release—a new signalling pathway. *Biol. Cell* **96**, 19–28.
6. Runft, L.L., Jaffe, L.A., and Mehlmann, L.M. (2002) Egg activation at fertilization: where it all begins. *Dev. Biol.* **245**, 237–254.
7. Santella, L., Lim, D., and Moccia, F. (2004) Calcium and fertilization: the beginning of life. *Trends Biochem. Sci.* **29**, 400–408.
8. Epel, D., Patton, C., Wallace, R.W., and Cheung, W.Y. (1981) Calmodulin activates nad kinase of sea urchin eggs: an early event of fertilization. *Cell* **23**, 543–549.
9. Shen, S.S., and Burgart, L.J. (1986) 1,2-Diacylglycerols mimic phorbol 12-myristate 13-acetate activation of the sea urchin egg. *J. Cell Physiol.* **127**, 330–340.
10. Dube, F., Schmidt, T., Johnson, C.H., and Epel, D. (1985) The hierarchy of requirements for an elevated intracellular pH during early development of sea urchin embryos. *Cell* **40**, 657–666.
11. Grainger, J.L., Winkler, M.M., Shen, S.S., and Steinhardt, R.A. (1979) Intracellular pH controls protein synthesis rate in the sea urchine egg and early embryo. *Dev. Biol.* **68**, 396–406.
12. Chandler, D.E. (1991) Multiple intracellular signals coordinate structural dynamics in the sea urchin egg cortex at fertilization. *J. Electron Microsc. Tech.* **17**, 266–293.
13. Whitaker, M., and Larman, M.G. (2001) Calcium and mitosis. *Semin. Cell Dev. Biol.* **12**, 53–58.
14. Vacquier, V.D. (1975) The isolation of intact cortical granules from sea urchin eggs: calcium ions trigger granule discharge. *Dev. Biol.* **43**, 62–74.
15. Detering, N.K., Decker, G.L., Schmell, E.D., and Lennarz, W.J. (1977) Isolation and characterization of plasma membrane-associated cortical granules from sea urchin eggs. *J. Cell Biol.* **75**, 899–914.
16. Wong, J.L., and Wessel, G.M. (2006) Rendezvin: an essential gene encoding independent, differentially-secreted egg proteins that organize the fertilization envelope proteome following self-association. *Mol. Biol. Cell* **17**, 5241–5252.
17. Walker, C.W., Harrington, L.M., Lesser, M.P., and Fagerberg, W.R. (2005) Nutritive phagocyte incubation chambers provide a structural and nutritive microenvironment for germ cells of *Strongylocentrotus droebachiensis*, the green sea urchin. *Biol. Bull.* **209**, 31–48.
18. Shen, S.S. (1995) Mechanisms of calcium regulation in sea urchin eggs and their activities during fertilization. *Curr. Top. Dev. Biol.* **30**, 63–101.
19. Tahara, M., Coorssen, J.R., Timmers, K., et al. (1998) Calcium can disrupt the snare protein complex on sea urchin egg secretory vesicles without irreversibly blocking fusion. *J. Biol. Chem.* **273**, 33667–33673.
20. Jahn, R., and Scheller, R.H. (2006) Snares—engines for membrane fusion. *Nat. Rev. Mol. Cell Biol.* **7**, 631–643.
21. Pelham, H.R. (2001) Snares and the specificity of membrane fusion. *Trends Cell Biol.* **11**, 99–101.
22. Bonifacino, J.S., and Glick, B.S. (2004) The mechanisms of vesicle budding and fusion. *Cell* **116**, 153–166.
23. Sudhof, T.C. (2004) The synaptic vesicle cycle. *Annu. Rev. Neurosci.* **27**, 509–547.
24. Zerial, M., and McBride, H. (2001) Rab proteins as membrane organizers. *Nat. Rev. Mol. Cell Biol.* **2**, 107–117.
25. Conner, S., Leaf, D., and Wessel, G. (1997) Members of the snare hypothesis are associated with cortical granule exocytosis in the sea urchin egg. *Mol. Reprod. Dev.* **48**, 106–118.
26. Leguia, M., Conner, S., Berg, L., and Wessel, G.M. (2006) Synaptotagmin i is involved in the regulation of cortical granule exocytosis in the sea urchin. *Mol. Reprod. Dev.* **73**, 895–905.
27. Wong, J.L., Koppel, D.E., Cowan, A.E., and Wessel, G.M. (2007) Membrane hemifusion is a stable intermediate of exocytosis. *Dev. Cell* **12**, 653–659.
28. Wessel, G.M., and Vacquier, V. (2004) Isolation of organelles and components from sea urchin eggs and embryos, in *Development of Sea Urchins, Ascidians and Other Non-vertebrate*

- Deuterostomes: Experimental Approaches* (C.A. Etnensohn, G.M. Wessel, and G.A. Wray, eds.), Elsevier Academic Press, San Diego, CA, pp. 491–522.
29. Foltz, K.R., Adams, N.L., and Runft, L.L. (2004) Echinoderm eggs and embryos: procurement and culture, in *Development of Sea Urchins, Ascidians and Other Non-vertebrate Deuterostomes: Experimental Approaches* (C.A. Etnensohn, G.M. Wessel, and G.A. Wray, eds.), Elsevier Academic Press, San Diego, CA, pp. 39–74.
 30. Harlow, E., and Lane, D. (1999) *Using Antibodies: A Laboratory Manual*. Cold Spring Harbor Laboratory Press, Cold Spring Harbor, NY.
 31. Boettger, S.A., Walker, C.W., and Unuma, T. (2004) Care and maintenance of adult echinoderms, in *Development of Sea Urchins, Ascidians and Other Non-vertebrate Deuterostomes: Experimental Approaches* (C.A. Etnensohn, G.M. Wessel, and G.A. Wray, eds.), Elsevier Academic Press, San Diego, CA, pp. 17–38.
 32. Cowan, A.E., Olivastro, E.M., Koppel, D.E., Loshon, C.A., Setlow, B., and Setlow, P. (2004) Lipids in the inner membrane of dormant spores of bacillus species are largely immobile. *Proc. Natl. Acad. Sci. U. S. A.* **101**, 7733–7738.

6

A Cell-Free Assay for Endocytosis of E-Cadherin

Toshiaki Sakisaka and Yoshimi Takai

1 Introduction.....	77
2 Materials	78
3 Methods.....	80
4 Notes	85
References.....	86

Summary E-Cadherin is a key cell–cell adhesion molecule at adherens junctions (AJs) and undergoes endocytosis when AJs are disrupted by the action of extracellular signals. To elucidate the mechanism of this endocytosis, we developed a new cell-free assay system for this reaction using the AJ-enriched fraction from rat liver. Non-*trans*-interacting E-cadherin, but not the *trans*-interacting one, underwent endocytosis in a clathrin-dependent manner. The endocytosis of *trans*-interacting E-cadherin was inhibited by Rac and Cdc42 small G proteins, which were activated by *trans*-interacting E-cadherin. Here, we describe the assay method for the endocytosis of E-cadherin from the AJ-enriched fraction prepared from rat liver.

Keywords Cell-free assay; E-cadherin; endocytosis; Rho family small G proteins.

1 Introduction

Adherens junctions (AJs) are the principal mediators of cell–cell adhesion in epithelial and nonepithelial cells and highly dynamic structures that turn over rapidly. This highly dynamic structure is especially important for epithelial tissue morphogenesis and tumor cell invasion. E-Cadherin is the major component of AJs responsible for homophilic cell–cell adhesion (1–4). E-Cadherin first forms *cis*-dimers on the cell surface of the same cells, followed by formation of *trans*-dimers on the cell surface of two neighboring cells, causing cell–cell adhesion. As migrating epithelial cells do not always exhibit changes in the protein expression of E-cadherin (5), it is probable that the cellular processes that regulate the assembly/disassembly of AJs contribute to the acquisition of migratory potential.

The endocytosis of E-cadherin represents one such cellular process that could regulate cellular migration (6–9). Various modes of the endocytosis for cellular control of cell surface events are known: Epidermal growth factor (EGF) receptor and nerve growth factor (NGF) receptor are internalized when their ligands bind, such as EGF for the EGF receptor and NGF for the NGF receptor (ligand-dependent endocytosis) (10,11). In contrast, the cell-matrix adhesion molecule integrin is constitutively internalized in the absence of binding partners, such as collagen for integrin (ligand-independent endocytosis) (12). In the case of E-cadherin, cell–cell contact-dependent regulation of endocytosis has potential implications for understanding the dynamics of the expression of E-cadherin at the cell surface. For example, cell–cell contact-dependent inhibition of endocytosis may contribute to the stabilization of E-cadherin at the cell surface that has been commonly documented to occur as cells grow to confluence (6). Although the importance of the endocytosis of E-cadherin has been well documented, little is known about the molecular mechanisms of how cell–cell contact regulates the endocytosis of E-cadherin. It is attractive to speculate that the formation of *trans*-dimers (the *trans*-interaction) of E-cadherin influences the cytoplasmic machinery responsible for the endocytosis of E-cadherin.

Recent cell-level studies using chemical inhibitors have shown that E-cadherin might be internalized by clathrin-dependent or caveolin-dependent endocytosis (6,13–17). However, the results obtained in this way are indirect and not substantial because the low-resolution indirect immunofluorescence staining could only follow the appearance of E-cadherin in large vesicular structures (early or late endosomes) as a morphological measure for the endocytosis of E-cadherin. Therefore, we attempted to develop a new biochemical assay that efficiently reconstitutes the endocytosis of E-cadherin using the AJ-enriched fraction. It can be used to directly characterize the function of components involved in the endocytosis of E-cadherin.

2 Materials

2.1 Isolation of AJ-Enriched Fraction

1. Four rats (Charles River, Yokohama, Japan; Sprague–Dawley [SD] rats, male, 7W, 210–240g).
2. Hypotonic buffer: 1 mM NaHCO₃/HCl (pH 7.5) and 2 µg/mL leupeptin.
3. NP-40 solution: 10 mM HEPES/KOH (pH 7.5), 100 mM KCl, 1 mM MgCl₂, 0.1% (v/v) NP-40.
4. Phenylmethylsulfonyl fluoride (PMSF) (Wako, Osaka, Japan, cat. no. 162-12182).
5. α-Phenylmethylsulfonyl fluoride (APMSF) (Wako, cat. no. 010-10393).
6. Leupeptin (Peptide Institute, Osaka, Japan, cat. no. 4041).
7. 50 mL loosely fitted Teflon-glass homogenizer (Ikemoto, Tokyo, Japan).
8. Himac CR 21 G centrifuge (Hitachi, Tokyo, Japan).
9. Himac CP 80α centrifuge (Hitachi).

10. R20A2 angle rotor (Hitachi).
11. 28 S swing rotor (Hitachi).
12. 50AT-2 angle rotor (Hitachi).

2.2 Preparation of the Rat Brain Cytosol

1. Twelve rats (Charles River; SD rats, male, 7W, 210–240 g).
2. Buffer A: 85 mM sucrose, 100 mM KOAc, 1 mM Mg(OAc)₂, 20 mM HEPES/KOH (pH 7.4), 10 μM APMSF, 10 μg/mL leupeptin, and 2 μg/mL aprotinin.
3. Buffer B: 25 mM HEPES/KOH (pH 7.4) and 100 mM KOAc.
4. Aprotinin (Sigma, St. Louis, MO, cat. no. A-6279).
5. 50-mL tight-fitted Teflon-glass homogenizer (Ikemoto).
6. Himac CS120 centrifuge (Hitachi).
7. 70AT2 angle rotor (Hitachi).
8. 100AT4 angle rotor (Hitachi).

2.3 Preparation of Cef (Cadherin Extracellular Fragment)

1. Sf-9 insect cells (Invitrogen, Carlsbad, CA).
2. High Five insect cells (Invitrogen).
3. EX-CELL 400 medium (JRH Biosciences, Lenexa, KS).
4. pFastBac1 vector (Gibco BRL, Bethesda, MD).
5. Complementary deoxyribonucleic acid (cDNA) for the honeybee melittin signal peptide (ATGAAATTCTTAGTCAACGTTGCCCTTGTTTTTATGGTC GTGTA CATTCTTACATCTATGCG).
6. cDNA for human immunoglobulin G (IgG) Fc (accession no. AAH53984; amino acids 239–470).
7. cDNA for the extracellular fragment of E-cadherin (accession no. X06115; amino acids 25–699).
8. Baculoviruses bearing the cDNAs encoding the E-cadherin extracellular domain fused to human IgG (Cef).
9. Buffer C: 0.1 M glycine/HCl (pH 2.5).
10. Buffer D: 25 mM HEPES/KOH (pH 7.4) and 100 mM KOAc.
11. Protein A-Sepharose CL-4B beads (Amersham Biosciences, Little Chalfont, UK, cat. no. 17-0780-01).

2.4 Cell-Free Assay for the Endocytosis of E-Cadherin

1. KOAc buffer: 20 mM HEPES/KOH (pH 7.4), 87.5 mM KOAc, 100 mM KOAc, 1 mM Mg(OAc)₂, 10 μM APMSF, 10 μg/mL leupeptin, and 2 μg/mL aprotinin.

2. Sorbitol buffer: 20 mM HEPES/KOH (pH 7.4) and 250 mM sorbitol.
3. TBS-T buffer: 50 mM Tris-HCl (pH 7.5), 200 mM NaCl, and 0.02% Tween-20.
4. Blocking buffer: 5% (w/v) nonfat dry milk in TBS-T.
5. CF15R refrigerated centrifuge (Hitachi).
6. Microtube mixer (Tomy, Tokyo, Japan, MT360).
7. Immobilon-P transfer membrane (Millipore, Bedford, MA, cat. no. IPVH00010).
8. A mouse anti-E-cadherin (cytoplasmic portion) monoclonal antibody (mAb) (BD Transduction Laboratories, Lexington, KY, cat. no. 610182).
9. Secondary antibody (Ab): Horseradish peroxidase-conjugated sheep antimouse IgG whole Ab (Amersham Biosciences, cat. no. NA931V).
10. ECL™ Western blotting detection reagents (Amersham Biosciences, cat. no. RPN2106).
11. Hyperfilm™ ECL (Amersham Biosciences, cat. no. RPN2114K).
12. Densitometer Fluorchem™ (Alpha Innotech, San Leandro, CA).

2.5 Regulation of Endocytosis of E-Cadherin by Its trans-Interaction

1. Cef.
2. CaCl₂-containing KOAc buffer: 2 mM CaCl₂ in KOAc buffer.

2.6 Activation of Rac and Cdc42 by trans-Interaction of E-Cadherin

1. Lipid-modified Rac and Cdc42.
2. Buffer E: 50 mM Tris-HCl (pH 8.0), 12 mM MgCl₂, 2 mM ethylenediamine-tetraacetic acid (EDTA), 0.4 mM dithiothreitol (DTT), 0.06% CHAPS 3-[(3-cholamidopropyl)dimethylammonio]-1-propanesulfonic acid, 100 μM adenosine triphosphate (ATP), and 12 μM [³⁵S]GTPγS (6 × 10³ cpm/pmol).
3. [³⁵S]GTPγS (Amersham Biosciences, cat. no. SJ1320).
4. Nitrocellulose filter (Schleicher and Schuell, Dassel, Germany, cat. no. BA-85).

3 Methods

3.1 Isolation of AJ-Enriched Fraction

The procedure described below for isolation of the AJ-enriched fraction is based on that described by Tsukita and Tsukita (18).

1. Dissect out livers from four fasting rats.
2. Mince on a dental paraffin sheet with a blade.
3. Immerse in about 250 mL hypotonic buffer.
4. Discard the supernatant with decantation.
5. Immerse in about 250 mL hypotonic buffer.
6. Discard the supernatant with decantation.
7. Immerse in about 250 mL hypotonic buffer and place on the bench for 20 min.
8. Discard the supernatant with decantation.
9. Bring to 150 mL with hypotonic buffer containing the proteinase inhibitor cocktails (1 mM PMSF, 20 μ g/mL leupeptin, and 1 μ g/mL pepstatin A).
10. Homogenize at maximum speed with four strokes in 50 mL loosely fitted Teflon-glass homogenizer.
11. Bring measure to 400 mL.
12. Filter twice with four layers of gauze.
13. Centrifuge at 1500g maximum for 10 min using R20A2 angle rotor (3540rpm) to produce a pellet (P1) and a supernatant (S1).
14. Recover the pellet (decantation) and bring to 7.8 mL with hypotonic buffer.
15. Resolve the pellet with pipeting.
16. Add 57.7 mL 55% sucrose to make the final sucrose concentration 48.45%.
17. Pour 11 mL of the sample in a centrifuge tube; overlay by 25 mL 42.9% sucrose.
18. Centrifuge at 100,000g maximum for 66 min using the 28S swing rotor (23,500rpm, Acc:Dec = 6:6).
19. Collect the BC fraction, which is recovered in the 42.9%:48.45% sucrose interface.
20. Dilute the fraction with 10 volumes hypotonic buffer.
21. Centrifuge at 4500g maximum for 30 min using the R20A2 angle rotor (5770rpm.)
22. Recover the pellet with decantation.
23. Suspend the pellet with 500 mL/tube of NP-40 solution, then collect and bring to 18 mL with the solution.
24. Place at 4 °C for 20 min.
25. Overlay 18 mL of the sample on the sucrose bed that is made of 8 mL of 50% and 8.5 mL of 20% sucrose.
26. Centrifuge at 100,000g maximum for 66 min using the 28S swing rotor (23,500rpm, Acc:Dec = 6:6).
27. Collect the AJ-enriched fraction, which is recovered in the 20%:50% interface.
28. Dilute the fraction with 10 volumes hypotonic buffer.
29. Centrifuge at 100,000g maximum for 30 min using 50AT-2 angle rotor (28,700rpm).
30. Recover the pellet.
31. Suspend with 500 mL hypotonic buffer.
32. Freeze in liquid N₂ and store at -80 °C.

3.2 Preparation of the Rat Brain Cytosol

1. Dissect out cerebra from 12 rats.
2. Mince on a dental paraffin sheet with a blade.
3. Add 7 mL buffer A containing the protease inhibitor cocktails (1 mM PMSF, 20 µg/mL leupeptin, and 1 µg/mL pepstatin A).
4. Homogenize at maximum speed with six strokes in 50-mL tight-fitted Teflon-glass homogenizer.
5. Centrifuge at 27,000 *g* maximum for 45 min using the 70AT2 angle rotor (17,400 rpm).
6. Recover the supernatant and centrifuge at 200,000 *g* maximum for 60 min using the 100AT4 angle rotor (61,000 rpm).
7. Recover the supernatant and dialyze with buffer B for 4 h (1 h and 20 min three times).
8. Centrifuge at 200,000 *g* maximum for 60 min using the 100AT4 angle rotor (61,000 rpm).
9. Freeze in liquid N₂ and store at –80 °C.

3.3 Preparation of Cef

1. Construct pFastBac1-Msp-Fc, a baculovirus transfer vector, by subcloning the inserts encoding the honeybee melittin signal peptide and human IgG Fc into pFastBac1.
2. Construct pFastBac1-Msp-Fc-E-cadherin-EX by subcloning the inserts encoding the extracellular fragment of E-cadherin in pFastBac1-Msp-Fc.
3. Prepare baculoviruses bearing the cDNAs encoding Cef with pFastBac1-Msp-Fc-E-cadherin-EX using Sf-9 cells according to the manufacturer's protocol.
4. Infect High Five insect cells grown in serum-free EX-CELL 400 medium with a baculovirus bearing the cDNA encoding Cef and cultured at 26 °C for 72 h.
5. Collect culture supernatants and subject them to protein A Sepharose beads.
6. Elute the bound Cef with buffer C.
7. Neutralize the eluted Cef to pH 7.5 with 1.5 M Tris-HCl at pH 8.8.
8. Dialyze the Cef against buffer D.
9. Freeze in liquid N₂ and store at –80 °C.

3.4 Cell-Free Assay for the Endocytosis of E-Cadherin

The procedure for cell-free assay for the endocytosis of E-cadherin is schematically shown in [Fig. 1](#).

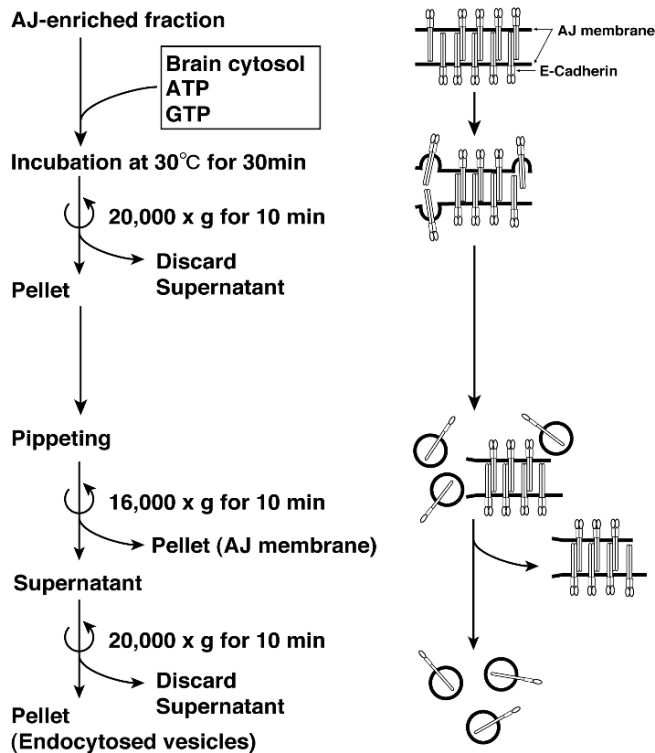


Fig. 1 A cell-free assay system for the endocytosis of E-cadherin. Flow diagram of the steps and schematic morphologies of the AJ-enriched fraction.

1. Set up 40- μ L transport reactions containing the components indicated in [Table 1](#) in 1.5-mL microfuge tubules (*see Note 1*). A reaction cocktail consisting of the salts, ATP-regenerating system, and waters is added first, followed by the cytosol and finally the AJ-enriched fraction. Mix by pipetting up and down four times using a P20 Gilson tip.
2. Transfer the reactions to a 30°C water bath and incubate for 15 min.
3. Terminate the reactions on ice, centrifuge at 20,000 g maximum for 10 min using the 100AT4 angle rotor (27,000 rpm), and harvest the membrane pellet (*see Note 2*).
4. Add 50 μ L sorbitol buffer and disperse the membrane pellet by pipetting up and down five times using a P200 Gilson tip.
5. Incubate the membranes for 10 min on ice.
6. Repeat the trituration procedure by pipetting up and down ten times using a P200 Gilson tip.
7. Add 10.6 mL KOAc buffer.
8. Centrifuge at 16,000 g maximum for 5 min using the CF15R refrigerated centrifuge (14,000 rpm) and harvest the membrane pellet.

Table 1 Reaction Cocktail for a Cell-Free Assay System for the Endocytosis of E-Cadherin

Solution	Volume (μL)	Final concentration
AJ-enriched fraction	5	~ 0.5 mg/mL protein [5 mM HEPES (pH 7.4), 31.25 mM sorbitol, 8.75 mM KOAc, and 0.125 mM $\text{Mg}(\text{OAc})_2$]
Cytosol	8	5 mg/mL protein [5 mM HEPES (pH 7.4) and 25 mM KOAc]
20X ATP-regenerating system	2	1 mM ATP, 5 mM creatine phosphate, and 0.2 IU creatine phosphate kinase
10X Ca^{2+} /EGTA buffer	4	5 mM EGTA, 1.8 mM CaCl_2 (100 nM free Ca^{2+})
0.1 M $\text{Mg}(\text{OAc})_2$	1	2.5 mM
1 M KOAc	1	40 mM
2.5 M sorbitol	3.5	218.75 mM
1 M HEPES (pH 7.4)	1.1	27.5 mM
H_2O	To 40	

9. Take the top 42.4- μL supernatant fraction from the side of the tube opposite the pellet.
10. Transfer to a 1.5-mL Eppendorf tube and harvest the vesicles by centrifugation at 100,000 g maximum for 20 min using the 100AT4 angle rotor (60,000 rpm).
11. Carefully aspirate the supernatant and add 20 μL sodium dodecyl sulfate (SDS) sample buffer (*see Note 3*).
12. Shake the tube on the microtube mixer for 30 min at room temperature (RT).
13. Subject the samples to SDS polyacrylamide gel electrophoresis (PAGE) and transfer to Immobilon-P transfer membrane electrophoretically.
14. Incubate the membrane in blocking buffer for 1 h at RT.
15. Discard the blocking buffer and incubate the membrane in blocking buffer containing a 1:1000 dilution of the anti-E-cadherin mAb.
16. Discard the anti-E-cadherin mAb and wash the membrane three times for 5 min with TBS-T buffer.
17. Incubate the membrane in blocking buffer containing a 1:2000 dilution of the secondary Ab.
18. Discard the secondary Ab and wash the membrane five times for 10 min with TBS-T buffer.
19. Incubate the membrane in the ECL reagent and place the membrane in an X-ray film cassette with a film for a suitable exposure time.
20. Measure the band intensity using a densitometer and determine the relative amount of E-cadherin in the MSP and HSP from each reaction.

3.5 Regulation of Endocytosis of E-Cadherin by Its trans-Interaction

1. Incubate the AJ-enriched fraction with Cef in the presence of CaCl₂-containing KOAc buffer on ice for 30 min.
2. Collect the membrane by centrifugation at 20,000 g maximum for 10 min using the 100AT4 angle rotor (6100 rpm) and harvest the membrane pellet. The membrane pellet was processed as described in Subheading 3.3.

3.6 Activation of Rac and Cdc42 by trans-Interaction of E-Cadherin

1. Purify lipid-modified Rac and Cdc42 from baculovirus-infected Sf9 cells.
2. Incubate the AJ-enriched fraction (25 μg protein) and the lipid-modified guanosine 5'-diphosphate (GDP)-bound form of Rac or Cdc42 with or without Cef in the presence of 2 mM CaCl₂-containing buffer E at 30 °C for 30 min (see [Notes 4–6](#)).
3. Apply the mixture to a nitrocellulose filter and measure the radioactivity.

4 Notes

1. The preparation of the ATP-regenerating system and Ca²⁺/EGTA buffer was described by Schwaninger et al. (19). Endocytosis inhibitors, such as Cef and the ENTH domain of epsin, are dialyzed against buffer D prior to addition to the assay, and the volumes of the salts in the reaction cocktail are adjusted to achieve the final concentrations described in [Table 1](#). The reaction can be preincubated on ice for up to 45 min with no loss of transport assay.
2. All of the membrane-bound E-cadherin is sedimented at 20,000 g following the 32 °C incubation. In the vesicle formation assay, membranes are resuspended in the sorbitol buffer prior to differential centrifugation.
3. Because the vesicles are small and translucent, care should be taken to avoid loss during aspiration of the high-speed supernatant.
4. The AJ-enriched fraction was used for the reconstitution of signaling events, such as hepatocyte growth factor (HGF)/scatter factor (SF) signaling. HGF-dependent activation of Ras and Rab5 can be measured as described in *Ref. 21*.
5. Removal of Rho family proteins by pretreatment of Rho-GDP dissociation inhibitor (RhoGDI) enhanced the endocytosis of E-cadherin (20). The effect of RhoGDI is inhibited by restoration of Rac-GTPγS and Cdc42-GTPγS. Removal of Rab family proteins by pretreatment of Rab-GDP dissociation inhibitor

(RabGDI) inhibited the endocytosis of E-cadherin (21). The inhibitory effect of RabGDI is rescued by restoration of Rab5-GTP γ S.

6. The *trans*-interacting nectin induces the activation of Rap1, which binds to afaadin, making it enhance the binding of p120^{cas} to E-cadherin (22). This binding prevents non-*trans*-interacting E-cadherin from endocytosis. Rac and Cdc42 activated by *trans*-interacting nectin and *trans*-interacting E-cadherin inhibit the endocytosis of E-cadherin through IQGAP-dependent reorganization of the actin cytoskeleton (20). Inactivation of Rap and Rac and activation of Rab5 are required for the endocytosis of E-cadherin. There is a signal crosstalk among Rap, Rac, and Rab5 during the endocytosis of E-cadherin. Molecular mechanisms for this signal crosstalk are important issues to be addressed in the future for our understanding of formation and destruction of cell–cell adhesion.

References

1. Takeichi, M. (1988) The cadherins: cell–cell adhesion molecules controlling animal morphogenesis. *Development* **102**, 639–655.
2. Yap, A.S., Brieher, W.M., and Gumbiner, B.M. (1997) Molecular and functional analysis of cadherin-based adherens junctions. *Annu. Rev. Cell Dev. Biol.* **13**, 119–146.
3. Adams, C.L., and Nelson, W.J. (1998) Cytomechanics of cadherin-mediated cell–cell adhesion. *Curr. Opin. Cell Biol.* **10**, 572–577.
4. Gumbiner, B.M. (2000) Regulation of cadherin adhesive activity. *J. Cell Biol.* **148**, 399–404.
5. Miller, J.R., and McClay, D.R. (1997) Characterization of the role of cadherin in regulating cell adhesion during sea urchin development. *Dev. Biol.* **192**, 323–339.
6. Le, T.L., Yap, A.S., and Stow, J.L. (1999) Recycling of E-cadherin: a potential mechanism for regulating cadherin dynamics. *J. Cell Biol.* **146**, 219–232.
7. Kamei, T., Matozaki, T., Sakisaka, T., et al. (1999) Coendocytosis of cadherin and c-Met coupled to disruption of cell–cell adhesion in MDCK cells—regulation by Rho, Rac and Rab small G proteins. *Oncogene* **18**, 6776–6784.
8. Fujita, Y., Krause, G., Scheffner, M., et al. (2002) Hakai, a c-Cbl-like protein, ubiquitinates and induces endocytosis of the E-cadherin complex. *Nature Cell Biol.* **4**, 222–231.
9. Palacios, F., Schweitzer, J.K., Boshans, R.L., and D'Souza-Schorey, C. (2002) Arf6-GTP recruits NM23-H1 to facilitate dynamin-mediated endocytosis during adherens junctions disassembly. *Nature Cell Biol.* **4**, 929–936.
10. Schmid, S.L. (1997) Clathrin-coated vesicle formation and protein sorting: an integrated process. *Annu. Rev. Biochem.* **66**, 511–548.
11. Brodsky, F.M., Chen, C.Y., Kneuhl, C., Towler, M.C., and Wakeham, D.E. (2001) Biological basket weaving: formation and function of clathrin-coated vesicles. *Annu. Rev. Cell Dev. Biol.* **17**, 517–568.
12. Lawson, M.A., and Maxfield, F.R. (1995) Ca²⁺- and calcineurin-dependent recycling of an integrin to the front of migrating neutrophils. *Nature* **377**, 75–79.
13. Akhtar, N., and Hotchin, N.A. (2001) RAC1 regulates adherens junctions through endocytosis of E-cadherin. *Mol. Biol. Cell.* **12**, 847–862.
14. Palacios, F., Schweitzer, J.K., Boshans, R.L., and D'Souza-Schorey, C. (2002) Arf6-GTP recruits NM23-H1 to facilitate dynamin-mediated endocytosis during adherens junctions disassembly. *Nature Cell Biol.* **4**, 929–936.

15. Thomsen, P., Roepstorff, K., Stahlhut, M., and van Deurs, B. (2002) Caveolae are highly immobile plasma membrane microdomains, which are not involved in constitutive endocytic trafficking. *Mol. Biol. Cell.* **13**, 238–250.
16. Paterson, A.D., Parton, R.G., Ferguson, C., Stow, J.L., and Yap, A.S. (2003) Characterization of E-cadherin endocytosis in isolated MCF-7 and Chinese hamster ovary cells: the initial fate of unbound E-cadherin. *J. Biol. Chem.* **278**, 21050–21057.
17. Ivanov, A.I., Nusrat, A., and Parkos, C.A. (2003) Endocytosis of epithelial apical junctional proteins by a clathrin-mediated pathway into a unique storage compartment. *Mol. Biol. Cell.* **15**, 176–188.
18. Tsukita, S., and Tsukita, S. (1989) Isolation of cell-to-cell adherens junctions from rat liver. *J. Cell Biol.* **108**, 31–41.
19. Schwaninger, R., Plutner, H., Davidson, H.W., Pind, S., and Balch, W.E. (1992) Transport of protein between endoplasmic reticulum and Golgi compartments in semiintact cells. *Methods Enzymol.* **219**, 110–124.
20. Izumi, G., Sakisaka, T., Baba, T., Tanaka, S., Morimoto, K., and Takai, Y. (2004) Endocytosis of E-cadherin regulated by Rac and Cdc42 small G proteins through IQGAP1 and actin filaments. *J. Cell Biol.* **166**, 237–248, 2004.
21. Kimura, T., Sakisaka, T., Baba, T., Yamada, T., and Takai, Y. (2006) Involvement of the Ras-Ras-activated Rab5 guanine nucleotide exchange factor RIN2-Rab5 pathway in the hepatocyte growth factor-induced endocytosis of E-cadherin. *J. Biol. Chem.* **281**, 10598–10609.
22. Hoshino, T., Sakisaka, T., Baba, T., Yamada, T., Kimura, T., and Takai, Y. (2005) Regulation of E-cadherin endocytosis by nectin through afadin, Rap1, and p120^{cas}. *J. Biol. Chem.* **280**, 24095–24103.

7

Cell-Surface Biotinylation to Study Endocytosis and Recycling of Occludin

Noriyuki Nishimura and Takuya Sasaki

1 Introduction.....	89
2 Materials	90
3 Methods.....	92
4 Notes	95
References.....	96

Summary The dynamic turnover of adherens junctions (AJs) and tight junctions (TJs) is essential for epithelial morphogenesis during normal development and differentiation. Although the endocytic recycling of E-cadherin is characterized and implicated in AJ turnover, the molecular basis for TJ turnover is poorly understood. Occludin and claudins are distinct transmembrane proteins localized to the TJs. Although claudins are an indispensable structural component of TJ strands, depletion of occludin in mice reveals well-developed TJ strands and complex histological abnormalities. To examine the intracellular transport of transmembrane proteins to and from the cell surface, cell-surface biotinylation is a proven powerful method. Using this method, we successfully demonstrated that occludin was endocytosed and recycled back to the cell surface in both fibroblastic baby hamster kidney (BHK) and epithelial MTD-1A cells. The endocytic recycling of occludin as well as the formation of functional TJs was dependent on Rab13 and a junctional Rab13-binding protein (JRAB)/molecule interacting with CasL-like 2 (MICAL-L2). We describe the method to study the intracellular transport of occludin to and from the cell surface in both fibroblastic and epithelial cells.

Keywords BHK cell; biotinylation; endocytosis; JRAB/MICAL-L2; MTD-1A cell; occludin; Rab13; recycling; tight junction.

1 Introduction

Adherens junctions (AJs) and tight junctions (TJ) are very plastic cellular structures that are subjected to dynamic remodeling during epithelial morphogenesis (1). Cadherins are the principal adhesion molecules within AJs supporting not only

stable cell–cell contacts but also dynamic morphogenetic events such as epithelial–mesenchymal transitions (EMTs) and mesenchymal–epithelial transitions (METs) (2). While E-cadherin is downregulated by the transcriptional silencing or protein degradation during EMT, the endocytic recycling of E-cadherin provides an alternative mechanism that allows cells to undergo rapid morphological changes in response to extracellular stimuli (3). Integral TJ proteins, including claudins and occludin, mediate cell–cell adhesion and create a physical intercellular barrier. Although the polymerization of claudins, which comprise a multigene family consisting of at least 24 members in mammals, is primarily responsible for the formation of TJ strands, the precise function of occludin has not yet been established (4–6). Like cadherin, both claudins and occludin are transcriptionally silenced during EMT (7).

Using the cell-surface biotinylation method, we have examined the intracellular transport of occludin to and from the cell surface. Occludin was endocytosed and recycled back to the cell surface in both fibroblastic baby hamster kidney (BHK) and epithelial MTD-1A cells (8). The endocytic recycling of occludin was controlled by Rab13 and junctional Rab13-binding protein (JRAB)/molecule interacting with casL-like 2 (MICAL-L2) (8,9). JRAB/MICAL-L2 specifically bound to the guanosine 5'-triphosphate (GTP)-bound form of Rab13 and localized at TJs. A JRAB/MICAL-L2 mutant lacking the Rab13-binding domain as well as Rab13 Q67L inhibited the plasma membrane recruitment of occludin and the development of functional TJs during the Ca²⁺ switch in MTD-1A cells. This chapter describes the method for analyzing the endocytosis and recycling of occludin in both fibroblastic and epithelial cells.

2 Materials

2.1 Cells and Antibodies

1. BHK cells (American Type Culture Collection, Manassas, VA).
2. MTD-1A cells (isolated from mouse mammary tumor and kindly supplied by Dr. S. Tsukita, Kyoto University, Kyoto, Japan).
3. Mouse anti-FLAG antibody (M2, Sigma, St. Louis, MO).
4. Rabbit anti-occludin antibody (Zymed, San Francisco, CA).
5. Rabbit anti-claudin-1 antibody (Zymed).
6. Mouse anti-transferrin receptor (TfR) antibody (H68.4, Zymed).
7. Horseradish peroxidase-coupled secondary antibody (Jackson ImmunoResearch Laboratories, West Grove, PA).

2.2 Expression Plasmids

Rab3B complementary deoxyribonucleic acid (cDNA) was kindly supplied by Dr. Y. Takai (Osaka University, Osaka, Japan) and described previously (10). Other

cDNAs were isolated by reverse transcriptase polymerase chain reaction (RT-PCR). Rab3B T36N, Rab3B Q81L, Rab13 T22N, and Rab13 Q67L were constructed using the Quick Change mutagenesis kit (Stratagene, La Jolla, CA) according to the manufacturer's instructions.

1. pBS-occludin-FLAG (mouse occludin cDNA).
2. pBS-claudin-1-FLAG (mouse claudin-1 cDNA).
3. pCR3.1-TfR (human TfR cDNA).
4. pCI-neo-HA-Rab3B (bovine Rab3B cDNA).
5. pCI-neo-HA-Rab3B T36N (dominant-negative mutant of Rab3B).
6. pCI-neo-HA-Rab3B Q81L (dominant-active mutant of Rab3B).
7. pCI-neo-HA-Rab13 (human Rab13 cDNA).
8. pCI-neo-HA-Rab13 T22N (dominant-negative mutant of Rab13).
9. pCI-neo-HA-Rab13 Q67L (dominant-active mutant of Rab13).
10. pCI-neo-Myc-JRAB/MICAL-L2-F (mouse JRAB/MICAL-L2 cDNA, amino acids 1–1009).
11. pCI-neo-Myc-JRAB/MICAL-L2-N (amino acids 1–805).
12. pCI-neo-Myc-JRAB/MICAL-L2-C (amino acids 806–1009).

2.3 Recombinant Virus

vTF7-3 was described previously (11). Recombinant adenovirus was constructed using Transpose-Ad Adenoviral Vector System kit (Qbiogene, Carlsbad, CA) according to the manufacturer's instructions.

1. vTF7-3 (recombinant vaccinia virus expressing T7 ribonucleic acid [RNA] polymerase).
2. Ad-EGFP (recombinant adenovirus expressing enhanced green fluorescent protein [EGFP]).
3. Ad-EGFP-Rab13 Q67L (recombinant adenovirus expressing EGFP-Rab13 Q67L).
4. Ad-Myc-JRAB/MICAL-L2-F (recombinant adenovirus expressing Myc-JRAB/MICAL-L2-F).
5. Ad-Myc-JRAB/MICAL-L2-N (recombinant adenovirus expressing Myc-JRAB/MICAL-L2-N).
6. Ad-Myc-JRAB/MICAL-L2-C (recombinant adenovirus expressing Myc-JRAB/MICAL-L2-C).

2.4 Buffers

1. Phosphate-buffered saline (PBS)/CM, pH7.2: 10 mM Na₂HPO₄, 2 mM KH₂PO₄, 137 mM NaCl, 2.7 mM KCl, 0.9 mM CaCl₂, 0.33 mM MgCl₂.
2. TBS/C: 50 mM Tris-HCl, pH 8.6, 100 mM NaCl, 2.5 mM CaCl₂.

3. Lysis buffer: 1.25% Triton X-100, 0.25% sodium dodecyl sulfate (SDS), 50 mM Tris-HCl, pH 8.0, 150 mM NaCl, 5 mM ethylenediaminetetraacetic acid (EDTA), 5 mg/mL iodoacetamide, 10 µg/mL (4-aminophenyl)-methanesulfonyl fluoride (APMSF).
4. Wash buffer: 0.5% Triton X-100, 0.1% SDS, 50 mM Tris-HCl, pH 8.0, 150 mM NaCl, 5 mM EDTA.
5. SDS polyacrylamide gel electrophoresis (PAGE) sample buffer: 50 mM Tris-HCl, pH 6.8, 2% SDS, 100 mM dithiothreitol (DTT), 10% glycerol, 0.02% bromophenol blue (BPB).
6. TBS-T: 20 mM Tris-HCl, pH 7.5, 150 mM NaCl, 0.1% Tween-20.

2.5 Other Reagents

1. Sulfo-NHS-SS-Biotin (Pierce, Rockford, IL).
2. NeutrAvidin beads (Pierce).
3. 2-Mercaptoethanesulfonic acid (MESNA) (Sigma).
4. Iodoacetamide (Wako Pure Chemicals, Osaka, Japan).
5. FuGENE6 (Roche, Basel, Switzerland).
6. Immobilon-P (0.45 µm, Millipore, Billerica, MA).
7. Block Ace (Dainippon Pharmaceutical, Osaka, Japan).
8. ECL-Plus kit (GE Healthcare, Piscataway, NJ).

3 Methods

3.1 Recombinant T7 Vaccinia Virus System

To express cargo and regulator proteins in fibroblastic BHK cells, the recombinant T7 vaccinia virus system, which relies on the synthesis of the bacteriophage T7 RNA polymerase in the cytoplasm, was used. Occludin, claudin-1, TfR, Rab3B, Rab13, and JRAB/MICAL-L2 cDNAs were placed under the control of T7 RNA polymerase promoter. Expression was achieved by transfecting the resulting expression plasmids into the cells infected with vTF7-3, a recombinant vaccinia virus encoding the bacteriophage T7 RNA polymerase (8,11).

1. Plate BHK cells at confluency in Dulbecco's modified Eagle's medium (DMEM)/10% fetal bovine serum (FBS).
2. Wash cells three times with PBS at 18–24 h after plating.
3. Prepare the vTF7-3 infection medium by diluting the partial purified stock of vTF7-3 in DMEM without FBS to give a multiplicity of infection (MOI) of 10–15 (see [Note 1](#)).

4. Incubate cells with the vTF7-3 infection medium at 37 °C for 30 min with rocking.
5. Wash cells three times with PBS.
6. Transfect cells with either pBS-occludin-FLAG, pBS-claudin-1-FLAG, or pCR3.1-TfR alone or in combination with pCI-neo-HA-Rab3B T36N, pCI-neo-HA-Rab3B Q81L, pCI-neo-HA-Rab13 T22N, pCI-neo-HA-Rab13 Q67L, pCI-neo-Myc-JRAB/MICAL-L2-F, pCI-neo-Myc-JRAB/MICAL-L2-N, or pCI-neo-Myc-JRAB/MICAL-L2-C using FuGENE6 transfection reagent (*see Note 2*).
7. Incubate cells at 37 °C for 6–8 h to achieve enough expression.

3.2 Recombinant Adenovirus Infection

To express regulator proteins in epithelial MTD-1A cells, the recombinant adenovirus expressing Rab13 Q67L, JRAB/MICAL-L2-F, JRAB/MICAL-L2-N, or JRAB/MICAL-L2-C was used (8,9).

1. Plate MTD-1A cells at confluency in DMEM/10% FBS.
2. Wash cells three times with PBS at 18–24 h after plating.
3. Prepare the adenovirus infection medium by diluting the partially purified stock of Ad-EGFP, Ad-EGFP-Rab13 Q67L, Ad-Myc-JRAB/MICAL-L2-F, Ad-Myc-JRAB/MICAL-L2-N, and Ad-Myc-JRAB/MICAL-L2-C in DMEM without FBS to give an MOI of 100 (*see Note 3*).
4. Incubate cells with the adenovirus infection medium at 37 °C for 2 h with rocking.
5. Wash cells three times with PBS.
6. Incubate cells in DMEM/10% FBS at 37 °C for 24–30 h to achieve enough expression.

3.3 Cell Surface Biotinylation

To achieve the selective labeling and removal of only the cell-surface proteins, the cleavable, water-soluble, and membrane-impermeable biotin analog sulfo-NHS-SS-biotin was used. Then, free sulfo-NHS-SS-biotin was quenched by NH_4Cl (8,9,12) (*see Note 4*).

1. Wash BHK cells expressing cargo and regulator proteins or MTD-1A cells expressing regulator proteins three times with PBS/CM.
2. Incubate cells with 0.5 mg/mL sulfo-NHS-SS-biotin in PBS/CM on ice for 30 min with rocking (*see Note 5*).
3. Incubate cells three times with 50 mM NH_4Cl in PBS/CM on ice for 5 min to quench free biotin.
4. Wash cells three times with PBS/CM.

3.4 *Endocytosis and Recycling*

Endocytosis was detected by the accumulation of the sulfo-NHS-SS-biotin-labeled cargo proteins within the cells, which were protected from reduction by MESNA. Recycling was detected by the disappearance of the endocytosed sulfo-NHS-SS-biotin-labeled cargo proteins on the cell surface, which were subjected to reduction by MESNA. Free SH groups were quenched by iodoacetamide (8,9,13–15) (*see Note 6*).

1. Incubate cells with DMEM/10% FBS (prewarmed at 37 °C) at 37 °C for 0–120 min to induce endocytosis.
2. Transfer cells on ice to stop endocytosis.
3. Wash cells three times with PBS/CM.
4. Incubate cells three times with 100 mM MESNA in TBS/C at 4 °C for 10 min to remove biotin from the sulfo-NHS-SS-biotin-labeled proteins on the cell surface (*see Note 5*).
5. Incubate cells three times with 5 mg/mL iodoacetamide in PBS/CM on ice for 5 min to quench free SH groups (*see Note 5*). (For endocytosis assay, proceed to Subheading 3.5.).
6. Incubate cells with DMEM/10% FBS (prewarmed at 37 °C) at 37 °C for 0–60 min to induce recycling.
7. Transfer cells on ice to stop recycling.
8. Incubate cells three times with 100 mM MESNA in TBS/C at 4 °C for 10 min to remove biotin from the sulfo-NHS-SS-biotin-labeled proteins on the cell surface.
9. Incubate cells three times with 5 mg/mL iodoacetamide in PBS/CM on ice for 5 min to quench free SH groups.

3.5 *Cell Lysis and Isolation of Biotinylated Proteins*

1. Lyse cells with lysis buffer on ice for 15 min.
2. Sonicate lysates for 1 min using a cup sonicator and centrifuge them at 15,000 *g* at 4 °C for 15 min.
3. Collect supernatant and take an aliquot to determine the amounts of total cargo proteins.
4. Add NeutrAvidin beads to the residual supernatant and incubate at 4 °C for more than 2 h with rotating.
5. Collect NeutrAvidin beads by centrifugation at 1,000 *g* at 4 °C for 3 min and wash them three times with ice-cold wash buffer.
6. Elute the sulfo-NHS-SS-biotin-labeled proteins from NeutrAvidin beads with SDS-PAGE sample buffer at 100 °C for 10 min (*see Note 7*).

3.6 Western Blot and Quantitation

1. Resolve total and biotinylated occludin, claudin-1, and TfR on an SDS-polyacrylamide gel and transfer them to an Immobilon-P membrane.
2. Incubate the blot with 100% Block Ace for 1 h and wash it twice with TBS-T for 10 min.
3. Incubate the blot with anti-FLAG, anti-occludin, anti-claudin-1, or anti-TfR antibody in 10% Block Ace for 1 h and wash it three times with TBS-T for 10 min.
4. Incubate the blot with horseradish peroxidase-coupled antibody in 10% Block Ace for 1 h and wash it three times with TBS-T for 10 min.
5. Develop the blot using an ECL-Plus kit.
6. Quantitate the scans of autoradiograph films with nonsaturated signals using the Image J program (<http://rsb.info.nih.gov/ij/>) (see **Note 8**).

4 Notes

1. Before use, the vTF7-3 partially purified stock was thawed on ice and sonicated twice for 10 s using a cup sonicator to disrupt aggregates.
2. To examine the effect of regulator proteins on the transport of cargo proteins, two- or threefold more regulator plasmids were cotransfected with cargo plasmids to minimize the number of cells expressing cargo proteins but not regulator proteins. We routinely used 3.0 μ g pBS-occludin-FLAG, pBS-claudin-1-FLAG, or pCR3.1-TfR alone or 1.0 μ g pBS-occludin-FLAG, pBS-claudin-1-FLAG, or pCR3.1-TfR in combination with 3.0 μ g pCI-neo-HA-Rab3B T36N, pCI-neo-HA-Rab3B Q81L, pCI-neo-HA-Rab13 T22N, pCI-neo-HA-Rab13 Q67L, pCI-neo-Myc-JRAB/MICAL-L2-F, pCI-neo-Myc-JRAB/MICAL-L2-N, or pCI-neo-Myc-JRAB/MICAL-L2-C to transfect BHK cells cultured in 60-mm tissue culture dishes.
3. To express enough proteins, an appropriate MOI needs to be determined for each recombinant adenovirus.
4. Control experiment without sulfo-NHS-SS-biotin should be performed to check the specificity and efficiency of the biotinylation reaction.
5. We dissolved sulfo-NHS-SS-biotin, MESNA, and iodoacetamide in PBS/CM, TBS/C, and PBS/CM, respectively, just before use.
6. To begin, cells without endocytosis should be reduced and quenched to confirm the complete reaction.
7. Elution volumes need to be adjusted to give autoradiograph films with nonsaturated signals. We routinely eluted with 100–200 μ L SDS sample buffer for BHK or MTD-1A cells cultured in 60-mm tissue culture dishes.
8. Biotinylated occludin, claudin-1, and TfR were normalized by total occludin, claudin-1, and TfR, respectively.

References

1. Schock, F., and Perrimon, N. (2002) Molecular mechanisms of epithelial morphogenesis. *Annu. Rev. Cell Dev. Biol.* **18**, 463–493.
2. Thiery, J.P. (2003) Epithelial–mesenchymal transitions in development and pathologies. *Curr. Opin. Cell Biol.* **15**, 740–746.
3. Bryant, D.M., and Stow, J.L. (2004) The ins and outs of E-cadherin trafficking. *Trends. Cell Biol.* **14**, 427–434.
4. Tsukita, S., Furuse, M., and Itoh, M. (2001) Multifunctional strands in tight junctions. *Nat. Rev. Mol. Cell Biol.* **2**, 285–293.
5. Schneeberger, E.E., and Lynch, R.D. (2004) The tight junction: a multifunctional complex. *Am. J. Physiol. Cell Physiol.* **286**, C1213–C1228.
6. Anderson, J.M., Van Itallie, C.M., and Fanning, A.S. (2004) Setting up a selective barrier at the apical junction complex. *Curr. Opin. Cell Biol.* **16**, 140–145.
7. Ikenouchi, J., Matsuda, M., Furuse, M., and Tsukita, S. (2003) Regulation of tight junctions during the epithelium–mesenchyme transition: direct repression of the gene expression of claudins/occludin by Snail. *J. Cell Sci.* **116**, 1959–1967.
8. Morimoto, S., Nishimura, N., Terai, T., et al. (2005) Rab13 mediates the continuous endocytic recycling of occludin to the cell surface. *J. Biol. Chem.* **280**, 2220–2228.
9. Terai, T., Nishimura, N., Kanda, I., Yasui, N., and Sasaki, T. (2006) JRAB/MICAL-L2 is a junctional Rab13-binding protein mediating the endocytic recycling of occludin. *Mol. Biol. Cell* **17**, 2465–2475.
10. Matsui, Y., Kikuchi, A., Kondo, J., Hishida, T., Teranishi, Y., and Takai, Y. (1988) Nucleotide and deduced amino acid sequences of a GTP-binding protein family with molecular weights of 25,000 from bovine brain. *J. Biol. Chem.* **263**, 11071–11074.
11. Fuerst, T.R., Niles, E.G., Studier, F.W., and Moss, B. (1986) Eukaryotic transient-expression system based on recombinant vaccinia virus that synthesizes bacteriophage T7 RNA polymerase. *Proc. Natl. Acad. Sci. U. S. A.* **83**, 8122–8126.
12. Nishimura, N., Plutner, H., Hahn, K., and Balch, W.E. (2002) The δ subunit of AP-3 is required for efficient transport of VSV-G from the *trans*-Golgi network to the cell surface. *Proc. Natl. Acad. Sci. U. S. A.* **99**, 6755–6760.
13. Graeve, L., Drickamer, K., and Rodriguez-Boulan, E. (1989) Polarized endocytosis by Madin–Darby canine kidney cells transfected with functional chicken liver glycoprotein receptor. *J. Cell Biol.* **109**, 2809–2816.
14. Matter, K., Whitney, J.A., Yamamoto, E.M., and Mellman, I. (1993) Common signals control low density lipoprotein receptor sorting in endosomes and the Golgi complex of MDCK cells. *Cell* **74**, 1053–1064.
15. Le, T.L., Yap, A.S., and Stow, J.L. (1999) Recycling of E-cadherin: a potential mechanism for regulating cadherin dynamics. *J. Cell Biol.* **146**, 219–232.

8

Fractionation of Subcellular Membrane Vesicles of Epithelial and Nonepithelial Cells by OptiPrep™ Density Gradient Ultracentrifugation

Xuhang Li and Mark Donowitz

1 Introduction.....	97
2 Materials.....	98
3 Methods.....	101
4 Notes.....	108
References.....	109

Summary Density gradient ultracentrifugation (DGUC) is widely used for physical isolation (enrichment rather than purification) of subcellular membrane vesicles. It has been a valuable tool to study specific subcellular localization and dynamic trafficking of proteins. While sucrose has been the main component of density gradients, a few years ago synthetic OptiPrep™ (iodixanol) began being used for separation of organelles because of its iso-osmotic property. Here, we describe a detailed protocol for density gradient fractionation of various mammalian subcellular vesicles, including endoplasmic reticulum (ER), Golgi apparatus, endosomes, and lipid rafts, as well as apical and basolateral membranes of polarized epithelial cells.

Keywords Density gradient ultracentrifugation; epithelia; lipid rafts; OptiPrep; organelles; subcellular membrane vesicles.

1 Introduction

Density gradient ultracentrifugation (DGUC) is a common separation technique that is used in separation of both protein complexes and subcellular membrane vesicles based on size and density. The principle of DGUC is based on the difference in terminal velocities V_t of different particles (proteins or vesicles in this case) as defined by Stoke's law: $V_t = 2R^2(P_s - P)a/(9\mu)$, where R is the radius of the particle, P_s is the density of the particle, P is the density of the medium, a is the centrifugal acceleration of the centrifuge, and μ is the viscosity of the medium. At a given centrifugal force

(a), V_i is essentially a function of radius (R) and density (P_s) of the particles for a particular separation medium of fixed density and viscosity. The other important variable in this equation is the density of the medium (P), which is the key to separate different particles when a gradual density gradient is present along the path of particle sedimentation. Typically, larger (in size) and heavier (in density) particles will travel through a gradient faster and settle further down the gradient. In the case of membrane vesicle separation by a density gradient, at equilibrium a particular vesicle species will remain in a specific fraction, with the density of this fraction equal to the density of the vesicles. At this stage, V_i is zero (no vesicle movement). (For more information on principles and applications of centrifugation methods, see *Ref. 1*.)

Sucrose has always been a major component of density gradient centrifugation for separation of both organelles or subcellular vesicles from various sources (1–4). A simple search of PubMed with key words “sucrose density gradient” yielded 8883 publications on March 3, 2007, indicating its extensive biological application. In 1994, Rickwood’s group (5,6) first introduced a new nonionic density gradient medium, iodixanol, which is a dimer of Nycodenz. Iodixanol has significant advantages over previously iodinated density gradient media (such as sucrose): Its aqueous solutions are iso-osmotic up to a density of 1.32 g/m (5).

Iodixanol has been marketed as OptiPrep™ by the Diagnostic Division of Nycomed Pharma (Norway), which was later acquired by Axis-Shield in 2000. We are among the earliest groups to use OptiPrep to separate apical, basolateral, and endosomal membrane vesicles of polarized epithelial cells (7,8). Primarily because of the attractive isoosmotic property of OptiPrep, the new medium has become widely used for separating cells and subcellular membrane vesicles in spite of a higher price than sucrose (see the Axis-Shield Web site for more information about OptiPrep and extensive references: <http://www.axis-shield.com/densityhome/density/optiHome.htm>)

In this chapter, we focus on the application of OptiPrep DGUC in separation of organelles or subcellular membrane vesicles, including lipid rafts (LRs).

2 Materials

2.1 Density Gradient Preparation

For density gradient preparation, use OptiPrep as 60% of iodixanol as the original package available from Axis-Shield (Oslo, Norway) or Sigma (St. Louis, MO).

2.2 Animals, Cell Culture, and Lysis Buffer

1. Animal: Male New Zealand white rabbits weighing 2.5–5 kg.

2. Cell lines: Caco-2 cell (human colon cancer cell) and PS120/E3V cell (an Na⁺/H⁺ exchanger-deficient derivative of the Chinese hamster lung fibroblast CCL39 cell line; E3V denotes that this PS120 cell line was stably transfected with VSV G-tagged NHE3 [rabbit Na⁺/H⁺ exchanger 3]).
3. Cell culture media and conditions: All cells were grown in 5% CO₂/95% O₂ at 37°C in the following media: For Caco-2 cells, Dulbecco's modified Eagle's medium (DMEM) supplemented with 10% fetal bovine serum (FBS) (v/v), 0.1 mM nonessential amino acids, 1 mM pyruvate, 100 U/mL penicillin, 100 μg/mL streptomycin; for PS120 cells, DMEM supplemented with 10% FBS, 100 U/mL penicillin, and 100 μg/mL streptomycin.
4. Cell lysis buffers: All buffers contain 1 mM Na₃VO₄, 1 mM phenylmethylsulfonyl fluoride (PMSF), and a protease inhibitor cocktail (Sigma, cat. P8340, 1:500 dilution).
 - a. HEPES buffer: 25 mM HEPES bis-Tris propane (HEPES-BTP) (pH 7.4) containing 150 mM NaCl, 1 mM dithiothreitol (DTT), 2 mM ethylene glycol-bis(2-amino-ethylether)-N,N,N',N'-tetraacetic acid (EGTA).
 - b. TNE buffer: 25 mM Tris-HCl, pH 7.4, 150 mM NaCl, 5 mM ethylenediaminetetraacetic acid (EDTA), 5 mM DTT.

2.3 Buffers for Ileal Mucosal Total Membranes and Brush Border Preparation

1. Brush border (BB) isolation buffers: All three BB isolation buffers contain the following protease inhibitors: 1 mM PMSF, a protease inhibitor cocktail (Sigma, cat. no. P8340), and phosphoramidon (10 μg/mL).

a. BB isolation buffer 1, pH 7.1:

Reagent/Final concentration	For 500 mL	For 250 mL
Mannitol/300 mM	27.33 g	13.67 g
Tris-HCl/12 mM	0.726 g	0.363 g
EGTA/5 mM	0.950 g	0.475 g
Na ₃ VO ₄ /10 mM	50 mL (100 mM stock)	25 mL
β-Glycerophosphate/5 mM	0.540 g	0.27 g
Phenylalanine/5 mM	0.4125 g	0.21 g

b. BB isolation buffer 2, pH 7.1:

Reagent/Final concentration	For 500 mL	For 250 mL
Mannitol/60 mM	5.468 g	2.734 g
EGTA/5 mM	0.950 g	0.475 g
β-Glycerophosphate/1 mM	0.108 g	0.05 g
Phenylalanine/1 mM	0.0825 g	0.041 g
Na ₃ VO ₄ /1 mM	5 mL (100 mM stock)	2.5 mL

Adjust pH with 1M Tris base.

c. BB isolation buffer 3, pH 7.1:

Reagent/Final concentration	For 500 mL	For 250 mL
Mannitol/300 mM	27.32 g	13.67 g
HEPES/20 mM	2.382 g	1.19 g
Mg-gluconate/5 mM	0.515 g	0.257 g
β -Glycerophosphate/1 mM	0.108 g	0.05 g
Phenylalanine/1 mM	0.0825 g	0.04 g
Na_3VO_4 /1 mM	5 mL (100 mM stock)	2.5 mL

Adjust pH with 1M Tris base.

2. Saline (0.9% NaCl): 36 g NaCl dissolved in 4000 mL DI (deionized) H_2O .

2.4 Sodium Dodecyl Sulfate Polyacrylamide Gel Electrophoresis (SDS-PAGE)

1. Polyacrylamide/bis solution (29%/1%) (Bio-Rad).
2. 5X sample buffer (prepare as a 5X stock [*see Note 1*]; use 1X as final concentration):

Reagent/Final concentration	For 50 mL at 1X after dilution	For 200 mL
Tris-HCl (1 M stock, pH 6.8)/44.0 mM	11 mL	22 mL
EDTA-2Na/4.33 mM	0.403 g	1.612 g
SDS/1.8%	4.5 g	18 g
Glycerol/10%	25 mL	100 mL
β -Mercaptoethanol/2%	5 mL	20 mL
Bromophenol blue/0.012%	24 mg	96 mg

3. 5X running buffer (prepare as a 5X stock; use 1X as final concentration):

Reagent/Final concentration at 1X after dilution	For 1 L	For 10 L
Tris base/24.8 mM	15 g	150 g
Glycine/192 mM	72 g	720 g
SDS (w/v)/0.1%	5 g	50 g

2.5 Western Blotting: 10X Transfer Buffer

Prepare as a 10X stock; use 1X as final concentration:

Reagent/Final concentration at 1X after dilution	For 1 L	For 10 L
Tris base/34.3 mM	41.53 g	415.3 g
Glycine/39 mM	39 g	390 g
SDS (w/v)/0.0357%	0.357 g	3.57 g

3 Methods

3.1 Preparation of Total Cellular Membranes (see Note 2)

3.1.1 Total Cellular Membrane Preparation from Caco-2 Cells for Isolation of Lipid Rafts

All procedures are performed at 4 °C except step 1.

1. Caco-2/E3V cells, which were transfected with NHE3 epitope tagged at the C-terminus with VSVG (9), are grown on 100 mm Costar Brand Transwell dish inserts (Corning, cat. no. 3419). After 1 or 2 wk postconfluence, the Caco-2 cells are incubated with serum-free medium overnight before use for experiments.
2. Rinse both sides of each Transwell three or four times with cold (4 °C) phosphate-buffered saline (PBS) buffer. Use 15–20 mL per rinse. Completely remove the HEPES buffer with aspiration after the last rinse.
3. Add 1 mL cold TNE buffer in the upper chamber of the Transwell and gently scrape cells in each Transwell into a 1.5-mL Eppendorf tube using a disposable plastic scraper. To avoid breaking the Transwell membranes, place the Transwell onto the lid of the housing Petri dish. Avoid bubbles trapped under the Transwell.
4. Remove the TNE buffer by centrifuging cells at 3000 g for 3 min.
5. Resuspend cells in TNE buffer (1.5–2 mL per 10-cm Transwell dish).
6. Sonicate at 4 °C for ten pulses and repeat two more times, using Sonicator with output and cycle set at 30%. Allow 10 s between each ten pulses. Note that all samples should be sonicated in exactly the same way. Otherwise, resulting membrane vesicles may be different.
7. Pass each sonicated cell lysate through a 23-gage (or 25-gage) syringe (3 mL maximum volume) ten times. This step helps break additional unbroken cells through shear forces generated by forced passages of cells through the needle.
8. Centrifuge homogenates at 3000 g for 15 min to remove unbroken cells, cell debris, and nuclei. Each resulting supernatant, which consists of total cellular membranes and cytosol, is referred to as total cell lysate.
9. Ultracentrifuge each cell lysate for 45 min at 200,000 g. Each resulting pellet is referred to as total membrane, and this supernatant is called cytosol.
10. Resuspend each membrane pellet with 1 mL TNE buffer. The membrane pellet is usually quite sticky and therefore hard to be resuspended. Pass each resuspension through a 23-gage syringe needle/syringe (1 mL maximum volume) five times until a milky solution is formed without any visible particulate matter. The total membrane suspension usually is used immediately for LR analysis by density gradient floatation (see Subheading 3.4.).

3.1.2 Total Cellular Membrane Preparation from PS120 Cells for Subcellular Fractionation of Organelles

All procedures are performed at 4 °C except step 1.

1. PS120/E3V cells grown to confluence are rinsed three or four times with cold (4 °C) PBS buffer. Use approx 15 mL per rinse. Completely remove the PBS buffer with aspiration after the last rinse.
2. Add 1 mL cold HEPES buffer over the cell layer and gently scrape cells in each dish into a 1.5-mL Eppendorf tube using a disposable plastic scraper.
3. Remove the HEPES buffer by centrifuging cells at 3000 *g* for 2–3 min.
4. Resuspend cells in HEPES buffer (1 mL per 10-cm dish).
5. Homogenize the cells by passing through a 23-gage syringe (3 mL maximum volume) 15 times.
6. The rest of the procedure is the same as described in Subheading 3.1.1., steps 8–10, except resuspension of the membrane pellets is done with HEPES buffer instead of TNE buffer.

3.1.3 Total Cellular Membrane Preparation from Rabbit Ileal Mucosa

1. Ileal mucosa (villous cells) are obtained from New Zealand White rabbits as described in detail in Subheading 3.2. (7,10).
2. Isolated mucosa is transferred directly into a 50-mL plastic tube containing 30 mL of BB isolation buffer 3.
3. The mucosa is homogenized with a Polytron (at a speed of 5) ten times, 10-s burst each time, followed by a 20-s interval in a cold room.
4. The rest of the procedure is the same as described in Subheading 3.1.1., steps 8–10, except that resuspension of the membrane pellets is done with BB isolation buffer 3 (see Subheading 2.3c) instead of TNE buffer.

3.2 Preparation of Rabbit Ileal Brush Border Membranes (BBMs) (see Note 2)

Male New Zealand White rabbits weighing 2.5–5 kg are sacrificed by overdose of intravenous nembutal (according to Johns Hopkins University School of Medicine (JHUSOM) approved animal protocol), and distal half of the small intestine, referred to as the ileum, is obtained. The rest of the procedure is as described below (all procedures are performed at 4 °C).

1. Dissect out ileum (~4 ft) and remove all the fat.
2. Cut the ileum into equal halves and flush out waste in the lumen with ice-cold saline twice (more times if necessary until no visible waste in the lumen) using a 100-mL syringe, then transfer the ileum to a beaker containing cold saline (4 °C).
3. In cold room (4 °C), blot the ileal segments on Kimwipe to remove excess saline, open the ileum along the mesenteric border with a pair of scissors, and

gently scrape ileal mucosa (predominantly villous cells) with two glass slides by using one slide to hold one end of the ileum and the other to scrape against a glass or plastic plate. Deposit mucosa into 60-mL BB isolation buffer 1 on ice. If necessary, pool all the scraped mucosa, blot quickly with filter paper to remove the excess saline, and weigh (~6–8 g are desired).

4. Homogenize the isolated ileal mucosa with a Polytron (at a speed of 5 out of 10) for ten times, with a 10-s burst each time followed by a 20-s interval on wet ice (a mix of equal volume of ice and water) in a cold room. Take 100 μ L homogenate into a Eppendorf tube for total protein estimate. This total protein fraction can be used for estimating the enrichment (purity) of BBM preparation when necessary.
5. Divide each homogenate equally into two centrifuge tubes (for Sorvall SS-34 rotor; ~ 35 mL per tube). Add 350 μ L of 1M $MgCl_2$ to each centrifuge tube (10mM final concentration of $MgCl_2$). Incubate on ice for 15 min. This is a magnesium precipitation step (also in step 10) that will remove cellular membranes other than BBM, particularly basolateral membranes.
6. Remove the foam at the top of the tube by suction. Centrifuge for 15 min at 3000 g at 4 °C.
7. Remove the lipids floating on the top of the centrifuge tube and transfer the supernatant into another centrifuge tube of the same kind. Discard the pellets.
8. Centrifuge for 30 min at 23,000 g at 4 °C. Discard the supernatant.
9. Resuspend the pellets in 25 mL (each tube) of BB isolation buffer 2. Homogenize in a glass-Teflon homogenizer on wet ice ten times (one complete up-and-down motion is counted as one time; set voltage at 100 V). Allow a 20-s interval after the first five times to avoid overheating.
10. Add 250 μ L 1M $MgCl_2$ to each tube and mix well. Incubate on ice for 15 min.
11. Pour each homogenate into a centrifuge tube and centrifuge for 15 min at 3000 g. Discard the pellets.
12. Centrifuge each supernatant at 23,000 g for 30 min. Discard the supernatant. Homogenize each pellet in 15 mL BB isolation buffer 3 in a glass-Teflon homogenizer on ice as stated in the step 9.
13. Centrifuge at 23,000 g for 40 min. Discard the supernatant.
14. Resuspend and homogenize each pellet in 300–500 μ L isolation buffer BB 3 with a 23-gage syringe (1 mL volume) to yield BBM.
15. Measure protein concentration and adjust the final protein concentration to approx 10 μ g/ μ L. The suspension should be milky. Store the BBM preparation in 100- μ L aliquots in –80 °C freezer or liquid nitrogen for long-term storage.

3.3 Preparation and Fractionation of OptiPrep Density Gradients for Membrane Vesicle Fractionation (see Notes 3 and 4)

3.3.1 Preparation of a Good Step Gradient

As a personal favorite, we use a rotor with swinging buckets rather than a fixed-angle rotor. The longer the centrifuge tubes, the better the expected separation will

be. An 11-step OptiPrep gradient of 10–30% (2.5% increments are described here and previously (8).

1. Make a thin cross cut (~1-mm thick) of a Oak cork from a wine or champagne bottle. The cork is sliced and soaked in DI water for a week with several changes of water (to remove the alcohol and sugar). Trim the cork slice round to make it fit well inside the centrifuge tube. The cork has to be able to float smoothly inside the centrifuge tube when each step of the gradient is overlaid.
2. Load the first step gradient with the highest density (30%) at the bottom of the centrifuge tube, then drop the cork into the tube. The cork should float flat on the top of the gradient.
3. Load the rest of the step gradients one by one slowly from the highest density to the lowest. Place the pipette tip ~2 mm above the cork slice and gently release each gradient. There should be at least 1.5 mL volume of space left at the top of the gradient for the loading of the total membrane preparation to be fractionated. Once the gradient is made, care must be taken to avoid disturbing it.
4. Load the sample (0.5–1 mL volume, 1 mg total protein) at the top of gradient (*see Note 5*).
5. Gently remove the cork before centrifugation. Note: Each centrifuge tube has to be at least 90% full to avoid collapse of the tube at the top.
6. Centrifuge at 100,000 *g* for 16 h at 4 °C.

3.3.2 Fractionation of a Gradient

The best way to collect fractions is to use a peristaltic pump that is connected with appropriate tubing (Fig. 1). A capillary tube (a 10- μ L capacity micropipet, VWR, cat. no. 53432-728), which is connected to one end of the tubing, is vertically inserted (slowly) to the bottom of the centrifuge tube so that the fractionation starts from the bottom of the gradient. Normally, 20 fractions are collected (for subcellular fractionation of membrane vesicles) from an ultracentrifuge tube that fits into an SW40 swinging bucket (Beckman, 0.6 mL each fraction). As many fractions as necessary can be collected. More fractions are done only if the vesicles to be separated are close in density. After fractionation, proteins of interest in each fraction (use 60–80 μ L) can be analyzed by SDS-PAGE using a Bio-Rad Protein IIxi gel system and Western blot (Figs. 2 and 3). Alternatively, vesicles in each fraction can be used directly for other assays.

3.4 Isolation of Lipid Rafts by Density Gradient Flootation

All procedures are performed at 4 °C unless described otherwise. To achieve the specificity of each signaling pathway, in addition to maintaining spatial separation of various molecules through specialized subcellular membranes/organelles, cells also employ a recently identified mechanism of compartmentation via Lipid rafts

Fig. 1 Flow chart illustrating the process of fractionation of membrane vesicles by density gradient fractionation. Total membranes were isolated from cells and then loaded onto an OptiPrep gradient. After centrifuging at 100,000 g for 16h, the gradient was fractionated using a peristaltic pump from the bottom of the tube. Proteins in each fraction were then analyzed by SDS-PAGE and Western blotting. Different gray scales indicate the gradual decrease of the OptiPrep density from the bottom to the top of the centrifuge tube.

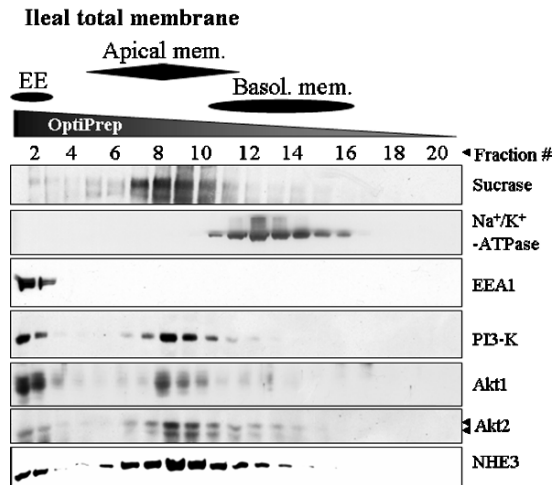
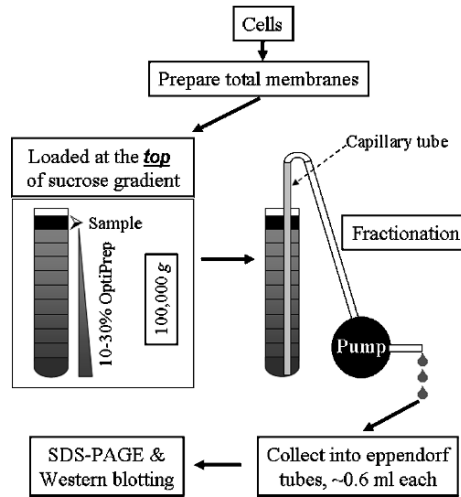


Fig. 2 A clear separation of early endosomes, apical and basolateral (basol.) membranes from rabbit ileal villus Na-absorptive cells was achieved by OptiPrep density gradient fractionation: NHE3 and membrane-associated PI3K and Akt are colocalized in the apical membrane and early endosomes of rabbit ileal villus cells. Total membranes (1.5 mg proteins) prepared from ileal villus cells were loaded on the top of the gradient and subjected to fractionation using OptiPrep gradients (10–30%) as illustrated in Fig. 1. Proteins in each fraction were analyzed by SDS-PAGE and Western blotted with antibodies against the proteins indicated. Established membrane markers used include the apical marker sucrase, early endosomal marker EEA1 (early endosomal antigen 1), and Na⁺/K⁺-ATPase, a marker of basolateral membranes. Both PI3K and Akt2 were mainly localized at the apical membrane of ileal villus cells (lanes 7–10). A portion of PI3K and Akt2 was also present in endosomes (lanes 1 and 2). In contrast, more than 50% of Akt1 was present in endosomal compartment. The double bands of Akt2 indicated by the double arrows are likely the representation of different states of Akt2 phosphorylation. (Adapted from *Ref. 8* with permission of Elsevier Inc.).

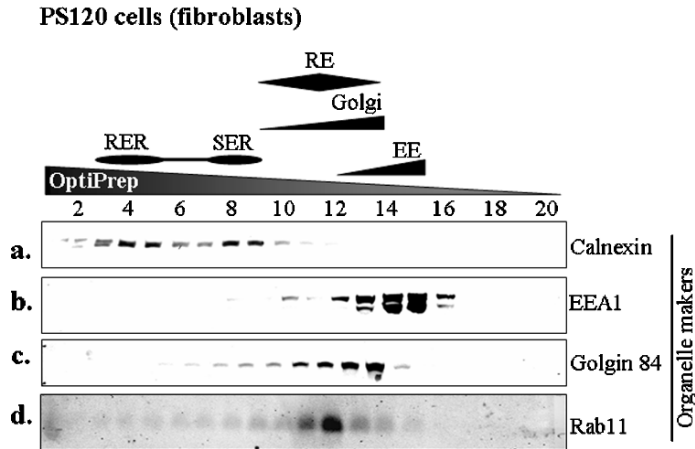


Fig. 3 Several intracellular organelles from PS120 cells were separated by OptiPrep density gradient fractionation. Residential marker proteins for different membrane vesicles, including calnexin for the ER (endoplasmic reticulum; RER and SER refer to rough and smooth ER, respectively) (a), EEA1 for early endosomes (b), Golgin 84 for Golgi (c), and Rab11 for recycling endosomes (RE) (d), were used to locate the migration of these membrane vesicles along the density gradients. The enrichment and location of each marker are indicated at the top. Total membranes (~1 mg proteins) were loaded on the top of the gradient and fractionated as illustrated in Fig. 1.

(LRs). LRs, also known as lipid microdomains and referred to as DRMs (detergent-resistant membranes), are defined as dynamic lipid membrane structures that are enriched in glycosphingolipids and cholesterol (11–13). LRs have been suggested as involved in many cellular processes, including signal transduction, apical membrane protein trafficking in epithelial cells, endocytosis, and exocytosis (11, 14–17). LRs also function as signaling platforms that cluster certain cell surface receptors, membrane proteins, and signaling molecules to confined regions while excluding others. LRs can be isolated to a high purity (or at least highly enriched) by density gradient floatation, which is based on the strategy that low-density membrane vesicles, including LRs, will float to low-density fractions during centrifugation when detergent-treated cell membranes are placed at the bottom of a density gradient. Here, we describe the use of OptiPrep density gradients for LR isolation. Sucrose density gradients are also widely used for this purpose.

1. Ileal BBM and the total membranes of Caco-2 cells are incubated or not (control) with 10 mM M β CD (methyl- β -cyclodextrin; Sigma) at 37 °C for 30 min (see Notes 5 and 6).
2. Untreated and M β CD-treated total membranes are solubilized with 0.5% Triton X-100 for 30 min on a rotary shaker at 4 °C.
3. Adjust each sample to 35% of OptiPrep with 60% original stock (1 mL final volume). Transfer each sample to the bottom of an ultracentrifuge tube (fits Beckman SW40 rotor).
4. Overlay each sample with 30%, 20%, 10%, and 5% OptiPrep. Each step gradient (~2.25 mL) contains 0.1% Triton X-100.

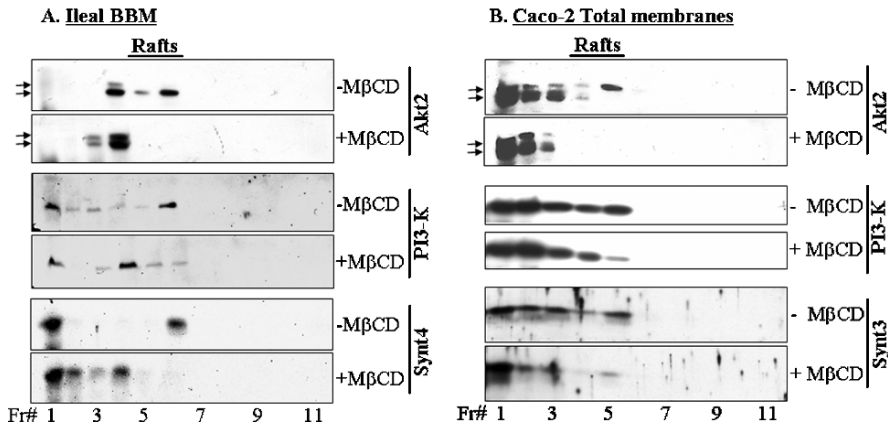


Fig. 4 Akt2 and PI3K are associated with LR in both rabbit ileal BBM and Caco-2 Cells. Ileal BBM (A) and the total membranes of Caco-2 cells (B) (~1 mg protein each) were solubilized with 1% Triton X-100 at 4°C with or without M β CD pretreatment at 37°C for 30 min. Samples were then subjected to OptiPrep density gradient flotation and fractionated into 11 fractions as illustrated in Fig. 1 (except that the sample was loaded at the bottom of the gradient instead of on the top). Proteins in each fraction were analyzed by SDS-PAGE and Western blotted with different antibodies as indicated. Fractions 1 through 11 were fractions from the highest (35%) (fraction 1) to the lowest density (5%) (fraction 11). Significant amounts of Akt2 and PI3K were in the LR fractions that were shifted from lighter fractions (A, fractions 5–6; B, lanes 4–5) to heavier fractions (A, fractions 3–4; B, fractions 1–3) after M β CD treatment. This was similar to syntaxin 4, a marker for LR of BBM (shifted from fraction 6 to fractions 1–4; A) and syntaxin 3, a marker for LR of Caco-2 cells (shifted from fractions 4 and 5 to fractions 1–3; B). Double arrows on the left indicate the doublet of Akt2 recognized by Akt antibodies. Representatives of three similar experiments are shown. (Adapted from Ref. 8 with permission of Elsevier Inc.).

5. Centrifuge in a Beckman SW40 rotor at 100,000 g at 4°C for 4 h.
6. Fractionate each sample into 11 fractions (~1 mL per fraction) from the bottom of each tube, as described in Fig. 1 and Subheading 3.3.2.
7. Analyze one-ninth of each fraction with SDS-PAGE and Western blotting for proteins of interest (as shown in Fig. 4 for Akt2 and PI-3 K).

3.5 SDS-PAGE and Western Blotting

Proteins in each density fraction are mixed with 5X SDS-PAGE sample buffer (*see* Subheading 2.4) to make a final sample buffer concentration of 1X, separated on 10% SDS polyacrylamide gels using Bio-Rad Protein IIxi Cell, and then electroblotted onto nitrocellulose membranes using a Bio-Rad gel transfer system (*see* running buffer and transfer buffer in Subheadings 2.4 and 2.5, respectively). Immunofluorescent detection of proteins of interest is performed at room temperature. Briefly, nitrocellulose membranes are incubated first in PBST-milk (PBS buffer containing 0.1% Tween-20 and 5% nonfat milk) for 1 h and then with primary antibodies diluted with

PBST-milk for another hour, with constant rocking on a shaker. At the end of incubation, the blots are washed three times for 10 min each with PBST and subsequently incubated with horseradish peroxidase (HRP)-conjugated secondary antibodies diluted in PBST-milk for 1 h. After three washes of 10 min each, the blots are incubated with Renaissance Enhanced Luminol Reagent (NEN™ Life Science Products) for 20 s and exposed to Hyperfilm™ MP film (Amersham).

4 Notes

1. Making 5X sample buffer stock for SDS-PAGE can be difficult because of the high concentration of each component, particularly SDS and glycerol. Here is a little trick: Dissolve EDTA-2Na first and then SDS in 1M Tris-HCl stock on a heated stir plate (heat but *not* boil). Add glycerol, stir, and let cool to room temperature. Add β -mercaptoethanol and adjust pH with HCl to 6.8. Add double deionized water to desired volume before bromophenol blue is added last. The entire preparation should be done in a fume hood because of the strong odor of β -mercaptoethanol. Store in 0.5- or 1-mL aliquots at -20°C . The stock is good for at least 6 mo.
2. When considering how to lyse cells for total membranes, different approaches may be applied according to which cell types are to be handled. To isolate total membranes, cells have to be broken mechanically in a detergent-free buffer. The PS120 cell, which is a fibroblast cell line, can be lysed much more easily than epithelial cells, particularly intestinal epithelial cells such as Caco-2 cells, of which fewer than 50% of cells can be lysed by “syringing” alone. Therefore, sonication is not necessary for PS120 cell lysis. To achieve a maximum yield, sonication may be used. However, sonication may significantly change the properties of membrane vesicles. Therefore, if cells of several experimental conditions are to be compared and sonication is to be used, sonication should be used for cells under all experimental conditions for consistency. If cell membranes are to be prepared from tissues or organs, a Polytron homogenizer and a glass-Teflon homogenizer are recommended.
3. Select a correct range of OptiPrep densities and appropriate number of fractions for purifying the vesicles of interest: If you have no idea what range to use for the best separation of your vesicles, an 11-step OptiPrep gradient of 10–30% (2.5% increments, as described previously in *Ref. 8* and here or 10–40% (3% increments) should be tried. We found these ranges are suitable for separation of several types of vesicles, including early endosomes, plasma membrane (apical membranes, basolateral membranes), and TGN. We tested preparations of membrane vesicles from several tissues (including kidney cortex and small intestine) and cell lines (including PS120 fibroblasts and the human colon cancer cell line Caco-2). If there is extensive overlapping between two types of vesicles you want to separately isolate, use smaller increments of densities that will cover the fractions in which the two types of vesicles equilibrate. The increments can be as small as 0.5% if using a simple device (a thin slice of wine cork) to make an

excellent gradient. Try to prepare each step gradient with the same buffer that is used for the membrane vesicle preparation. Furthermore, in general the more fractions that are collected, the better will be the separation between different membrane populations.

4. Accurate pipeting is very important to generate reproducible density gradients. The step density gradients prepared as described here are very simple and highly reproducible. Such reproducibility is almost impossible to achieve if continuous density gradients are to be manually prepared. To achieve reproducible density gradients, pipeting is most critical. Because the higher-density fractions contain OptiPrep up to 40%, pipet tips with low resistance or coated with silicone are recommended.
5. Regarding the amount of proteins loaded on the gradient, to achieve the best separation of different populations of cellular membranes/organelles, the amount of total membranes loaded on a gradient should be kept to a minimum (as long as enough of the membranes of interest can be obtained for subsequent analysis). The more proteins (total membranes) are used, the poorer the resolution (more overlaps) of different membrane vesicles will be. We prefer to use the term *enrichment* rather than *purification* of a particular subcellular membrane population/organelle when using the density gradient fractionation approach because generally there will probably always be a small degree of contamination of other unwanted membrane vesicles.
6. In all buffers described in this chapter, protease inhibitors, including PMSF (1 mM) and a protease inhibitor cocktail (Sigma; use as manufacturer suggested), must be added freshly (right before use). When treating cell membranes with M β CD described in LR isolation, to prevent proteins from degradation at 37 °C, those protease inhibitors (see above) should be added freshly again even though they are already present in buffers used in total cellular membrane preparation. For ileal total membrane and BBM isolation as well as subsequent use of these membranes in density gradient fractionation or LR isolation, phosphoramidon (10 μ g/mL) should always be added for inhibition of intestinal-specific proteases. Phosphoramidon is not required in membrane analysis of nonintestinal epithelial cells.

Acknowledgments This work was supported by in part by the National Institutes of Health, NIDDK grants KO1-DK62264, RO1-DK26523, RO1-DK61765, PO1-DK44484, PO1-DK72084, and R24-DK64388 (Hopkins Digestive Diseases Basic Research Development Core Center); Broad Medical Research Program grant (IBD-0119R2); and the Hopkins Center for Epithelial Disorders. We thank Elsevier Inc. for permission to reuse the figures originally published in its journal *Gastroenterology*.

References

1. Ngsee, J.K., Trimble, W.S., Elferink, L.A., et al. (1990) Molecular analysis of proteins associated with the synaptic vesicle membrane. *Cold Spring Harb. Symp. Quant. Biol.* **55**, 111–118.
2. Li, X., and Sze, H. (1999) A 100kDa polypeptide associates with the V0 membrane sector but not with the active oat vacuolar H(+)-ATPase, suggesting a role in assembly. *Plant J.* **17**, 19–30.

3. Huber, L.A., Pfaller, K., and Vietor, I. (2003) Organelle proteomics: implications for subcellular fractionation in proteomics. *Circ. Res.* **92**, 962–968.
4. Gutwein, P., Stoeck, A., Riedle, S., et al. (2005) Cleavage of L1 in exosomes and apoptotic membrane vesicles released from ovarian carcinoma cells. *Clin. Cancer Res.* **11**, 2492–2501.
5. Ford, T., Graham, J., and Rickwood, D. (1994) Iodixanol: a nonionic iso-osmotic centrifugation medium for the formation of self-generated gradients. *Anal. Biochem.* **220**, 360–366.
6. Graham, J., Ford, T., and Rickwood, D. (1994) The preparation of subcellular organelles from mouse liver in self-generated gradients of iodixanol. *Anal. Biochem.* **220**, 367–373.
7. Li, X., Galli, T., Leu, S., et al. (2001) Na⁺-H⁺ exchanger 3 (NHE3) is present in lipid rafts in the rabbit ileal brush border: a role for rafts in trafficking and rapid stimulation of NHE3. *J. Physiol.* **537**, 537–552.
8. Li, X., Leu, S., Cheong, A., et al. (2004) Akt2, phosphatidylinositol 3-kinase, and PTEN are in lipid rafts of intestinal cells: role in absorption and differentiation. *Gastroenterology* **126**, 122–135.
9. Janecki, A.J., Montrose, M.H., Tse, C.M., de Medina, F. S., Zweibaum, A., and Donowitz, M. (1999) Development of an endogenous epithelial Na⁽⁺⁾/H⁽⁺⁾ exchanger (NHE3) in three clones of caco-2 cells. *Am. J. Physiol.* **277**, G292–G305.
10. Cohen, M.E., Wesolek, J., McCullen, J., et al. (1991) Carbachol- and elevated Ca⁽²⁺⁾-induced translocation of functionally active protein kinase C to the brush border of rabbit ileal Na⁺ absorbing cells. *J. Clin. Invest.* **88**, 855–863.
11. Simons, K., and Toomre, D. (2000) Lipid rafts and signal transduction. *Nat. Rev. Mol. Cell Biol.* **1**, 31–39.
12. Simons, K., and Vaz, W.L. (2004) Model systems, lipid rafts, and cell membranes. *Annu. Rev. Biophys. Biomol. Struct.* **33**, 269–295.
13. Brown, D.A. (2006) Lipid rafts, detergent-resistant membranes, and raft targeting signals. *Physiol. (Bethesda)* **21**, 430–439.
14. Lusa, S., Blom, T.S., Eskelinen, E.L., et al. (2001) Depletion of rafts in late endocytic membranes is controlled by NPC1-dependent recycling of cholesterol to the plasma membrane. *J. Cell Sci.* **114**, 1893–1900.
15. Lafont, F., Verkade, P., Galli, T., Wimmer, C., Louvard, D., and Simons, K. (1999) Raft association of SNAP receptors acting in apical trafficking in Madin–Darby canine kidney cells. *Proc. Natl. Acad. Sci. U. S. A.* **96**, 3734–3738.
16. Bagnat, M., Keranen, S., Shevchenko, A., Shevchenko, A., and Simons, K. (2000) Lipid rafts function in biosynthetic delivery of proteins to the cell surface in yeast. *Proc. Natl. Acad. Sci. U. S. A.* **97**, 3254–3259.
17. Fullekrug, J., and Simons, K. (2004) Lipid rafts and apical membrane traffic. *Ann. N. Y. Acad. Sci.* **1014**, 164–169.

9

Identification and Characterization of Interacting Partners of Rab GTPases by Yeast Two-Hybrid Analyses

Mark Kail and Angelika Barnekow

1 Introduction.....	111
2 Materials.....	112
3 Methods.....	114
4 Notes.....	124
References.....	125

Summary Much of our knowledge of the mechanisms governing vesicular transport has come from the combination of genetic and biochemical approaches that have identified Ypt/Rab guanosine 5'-triphosphatases (GTPases) as key components of transport processes in both yeast and mammalian cells. More recently, research has focused on establishing the complex protein-protein interactions necessary for the regulation of vesicular transport by a variety of methods, including the yeast two-hybrid interaction assay. A central component of the signaling pathway regulated by Ypt/Rab proteins is the GTPase cycle, in which the proteins cycle between an active guanosine 5'-triphosphate (GTP)-bound form and an inactive guanosine 5'-diphosphate (GDP)-bound form. Alterations in the conformation of the Ypt/Rab proteins when either GTP or GDP is bound specify the interaction of effector proteins and influence membrane binding. Our work has focused on identifying interacting partners for the GTPases Rab1 and Rab6 and their isoforms, which regulate transport steps between the endoplasmic reticulum and Golgi in mammalian cells. We have employed both active (GTP-bound) and inactive (GDP-bound) Rab1 and Rab6 mutants to identify potential new interacting proteins using the yeast two-hybrid system and have verified these interactions using alternative methods.

Keywords Rab1; Rab6; small GTPases; vesicle transport; yeast two hybrid.

1 Introduction

The yeast two-hybrid system can be applied for identifying, characterizing, and confirming protein-protein interactions. One can screen complementary deoxyribonucleic acid (cDNA) libraries for novel proteins that interact with a known bait protein.

Positive interactions, once identified, can be verified and further characterized by a variety of other methods, including immunofluorescence, glutathione S-transferase (GST) pulldown or coimmunoprecipitation.

2 Materials

2.1 Culture Media

1. YPD (yeast extract, peptone, dextrose) medium/1 L agar: 10 g yeast extract, 20 g peptone, 20 g agar (for plates), 950 mL H₂O; adjust to pH 6.5 and autoclave. Allow medium to cool to approx 55 °C and add 50 mL 40% glucose, filter sterilized.
2. Synthetic dropout (SD) medium/1 L agar: 6.7 g yeast nitrogen base without amino acids, 20 g agar (for plates), 850 mL H₂O. Add 100 mL sterile 10X concentrated dropout (DO) supplements solution lacking the required amino acids for selection of the auxotrophic markers. For example, to prepare SD/-Trp/-Leu/-His use a 10X DO supplement lacking Trp, Leu, and His. Adjust the pH to 5.8, autoclave, and allow to cool about 55 °C before adding 3-amino-1,2,4-triazol (3-AT), 30 mM final concentration, for 3-AT selection plates (store at 4 °C for up to 2 months).
3. 10X DO supplements: 300 mg/L L-isoleucine, 1500 mg/L L-valine, 200 mg/L L-adenine hemisulfate salt, 200 mg/L L-arginine HCl, 300 mg/L L-lysine HCl, 200 mg/L L-methionine, 500 mg/L, L-phenylalanine, 2000 mg/L L-threonine, 300 mg/L L-tyrosine, 200 mg/L L-uracil (*see Note 1*). The DO supplements may be autoclaved and stored at 4 °C.
4. Additives: 100X L-histidine HCl monohydrate (2 g/L), 100X L-leucine (10 g/L), 100X L-tryptophan (2 g/L).
5. 2X YT medium, 1 L: 16 g tryptone, 10 g yeast extract, 5 g NaCl; adjust to pH 7.0 with 5N NaOH and make up to 1 L with water.

2.2 Buffers and Solutions

1. Cracking buffer stock solution: 8 M urea, 5% (w/v) sodium dodecyl sulfate (SDS), 40 mM Tris-HCl, pH6.8, 0.1 mM ethylenediaminetetraacetic acid (EDTA), 0.4 mg/mL bromophenol blue. Before use, add 10 µL β-mercaptoethanol, 50 µL phenylmethylsulfonyl fluoride (PMSF), and 70 µL protease inhibitor mix Complete™ (Roche Diagnostics, Mannheim, Germany) to 1 mL cracking buffer stock solution. Additional protease inhibitors may be added.
2. PMSF stock solution: 100 mM PMSF dissolved in isopropanol.

2.3 *Buffers and Solutions for Yeast Transformation and Reporter Assay*

1. Transformation master mix, for 10 transformations: 2.4 mL 50% polyethylene glycol (PEG) 3350, 360 μ L 1 M lithium acetate (LiAc), 50 μ L denatured herring testis carrier DNA, 690 μ L H₂O.
2. Library screen transformation master mix: 7.2 mL 50% PEG, 1.08 mL 1 M LiAc, 750–1000 μ g cDNA library, 0.3 mL denatured herring testis carrier DNA; make up to 11.6 mL with water.
3. Z buffer: 16.1 g/L Na₂HPO₄ 7H₂O, 5.5 g/L NaH₂PO₄ H₂O, 0.75 g/L KCl, 0.246 g/L MgSO₄ 7H₂O. Adjust to pH 7.0 and autoclave.
4. X-gal stock solution: 20 mg/ mL 5-bromo-4-chloro-3-indolyl- β -D-galactopyranoside (X-gal) dissolved in -dimethyl formamide (DMF).
5. β -Galactosidase substrate: 5 mL Z buffer, 85 μ L X-gal, 13.5 μ L β -mercaptoethanol.

2.4 *Polymerase Chain Reaction Conditions*

For polymerase chain reaction (PCR) reaction mix for one 50- μ L PCR reaction, bring 5 μ L PCR buffer (10 \times concentrated), 4 μ L dNTP mix (2.5 mM), 50 pmol primers 1 and 2, 0.5 μ L Taq polymerase 5 U/ μ L, and 3 μ L template cell suspension to 50 μ L total volume with water.

2.5 *Plasmids*

1. Bait plasmid: pAS2-1, an ADH1 promoter, expresses *TRP1* gene, allowing selection on SD plates lacking tryptophan.
2. Prey plasmids: pGADT7 and pACT2, an ADH1 promoter, expresses *LEU2* gene, allowing selection on SD plates lacking leucine.

2.6 *Yeast Strain*

Y190 yeast strain genotype (**I**): *MATa*, *ura3-52*, *his3-200*, *ade2-101*, *lys2-801*, *trp1-901*, *leu2-3*, *112*, *Gal4 Δ* , *Gal80 Δ* , *cyh^r2*, *LYS2::GAL1_{UAS}-HIS3_{TATA}-HIS3*, *MEL1*, *URA3::GAL1_{UAS}-GAL1_{TATA}-lacZ*

Reporters: *HIS3*, *lacZ*, *MEL1*

Transformation markers: *trp1*, *leu2*, *cyh^r2*

3 Methods

3.1 Principle of the Yeast Two-Hybrid Method

The Matchmaker GAL4-based two-hybrid system from Clontech makes use of the GAL4-responsive elements within the UAS (upstream activating sequences) of galactose-responsive genes along with the GAL4 transcription activator to drive the expression of reporter genes as a readout for the interaction of protein partners. Transcription activators such as GAL4 contain two distinct functional domains, the DNA-binding domain (BD) and the activating domain (AD), which are both necessary for transcription.

The modular nature of such proteins permits the expression of these as separate chimeric fusions of the proteins of interest from plasmids encoding either the BD or AD of GAL4. When a physical interaction occurs between the chimeric protein partners, a functional transcription factor is reproduced, which is able to induce reporter gene expression. In the host yeast strain Y190 provided, the reporter genes *lacZ* and *HIS3* are both under the control of the GAL1 UAS, producing high-level expression of the reporter genes as a result of a positive two-hybrid interaction. However, the host strain Y190 also possesses the minimal promoter for the *HIS3* reporter, consisting of two TATA boxes, one of which is constitutively regulated (*HIS3* TC). This, however, leads to significant constitutive (leaky) expression, which can result in high background growth on selective plates. The yeast host strain Y190 also carries deletions of *gal4* and *gal80* genes to circumvent interference by endogenous *GAL4* and *GAL80* transcription activators and lesions of *LEU2* and *TRP1*, which allows selection of the transformed yeast cells containing the appropriate plasmids.

The cloning vectors pGADT7 and pACT2 that we used in our interaction assays encode the GAL4 AD and the selection marker *LEU2* under the control of the constitutively activated *ADH1* promoter. The pGADT7 vector also expresses the HA tag, permitting detection of the fusion protein by Western blotting. Likewise, expression of the GAL4 BD fusion proteins from the pAS2-1 bait vector, which contains the selection marker *TRP1*, is also regulated by the *ADH1* promoter. The level of expression from this promoter is maximal during logarithmic growth and is repressed during late log phase by the buildup of ethanol in the medium as a result of yeast metabolism.

3.2 Application of the Yeast Two-Hybrid Methods

To obtain more information on the cellular function of the small guanosine triphosphatases (GTPases), we generated mutants, which present the inactive (guanosine diphosphate [GDP]-bound) and active (guanosine 5'-triphosphate [GTP]-bound) forms and used them in yeast two-hybrid screening experiments to identify interacting proteins.

The yeast reporter strain Y190 was transformed (e.g., with the bait plasmid pAS Rab1B Q67R or pAS Rab6A Q72R/L mutant fused to the GAL4 BD). The transformation protocol was based on the lithium acetate method (2). The bait containing yeast strain was grown in synthetic medium lacking tryptophan, and in our studies was transformed with a human placenta or brain cDNA library in pACT2 (Clontech-Takara Bio Europe, Saint-Germain-en-Laye, France). We screened up to 1×10^7 clones and detected several putative positive clones. The corresponding prey plasmids were isolated and retransformed, and the interaction was verified with bait vectors expressing, for example, just the GAL4 BD and with plasmids encoding GAL4 BD fusion proteins of Rab1B or Rab6A wild type (wt), Rab1B S22N or Rab6A T27N, and Rab1B Q67R or Rab6A Q72R, respectively.

For yeast cotransformation assays, Y190 yeast cells were simultaneously transformed with the corresponding bait and prey constructs. After growing for 5 to 8 d on selection medium, transformants were monitored for expression of β -galactosidase and *HIS3* reporter genes. For liquid β -galactosidase assays, yeast cells were incubated overnight in the corresponding selection medium. Subsequently, the cultures were diluted with synthetic medium lacking tryptophan and leucine and incubated until the cultures reached the log phase of cell growth (OD_{600} of 0.8–1.0). Liquid β -galactosidase and β -galactosidase colony filter-lift assays were performed according to the manufacturer's protocol (yeast protocols handbook, Clontech-Takara Bio Europe).

3.3 Cultivation of Yeast Cells

To recover host yeast strains from frozen stocks:

1. Streak a YPD plate using a sterile inoculation loop with an inoculum from a frozen stock. This can be obtained by scraping the surface of the frozen culture with the inoculation loop (see Note 2).
2. Incubate the plates at 30 °C for approx 3 d or until good-size (2-mm) colonies are visible.

The plates can be stored sealed with Parafilm at 4 °C up to 2 mo, so colonies from these plates can be used to inoculate liquid cultures. Fresh YPD plates should be restreaked to maintain the cultures (see Note 3).

3.4 Liquid Overnight Cultures

1. Inoculate 5 mL YPD in a sterile tube with a colony from the stock plate. If the colony does not disperse, vortex the medium to disperse the clumps (see Note 4).
2. Incubate at 30 °C for 16–18 h with shaking at 220 rpm. After this period, the culture should reach stationary phase with an OD_{600} above 1.5.

3.5 *Growth of Transformed Yeast Strains*

Yeast liquid cultures can be stored for up to 2 mo at 4 °C and can be used to inoculate fresh YPD medium to generate overnight cultures. Transformed yeast strains can be selected on appropriate SD medium lacking the specific amino acid (e.g., tryptophan in the case of pAS2-1, which carries the *TRP1* nutritional marker). If selecting for more than one plasmid, then the appropriate nutritional marker must also be excluded from the DO medium. Selection of two-hybrid interactions is carried out on medium also lacking the specific marker encoded by the activated reporter gene (e.g., *HIS3* in the GAL4 Matchmaker system). To inhibit basal expression of the *HIS3* gene the medium should be supplemented with 3-AT, which inactivates the *HIS3* gene product. We generally use a 30–50 mM concentration of 3-AT in selection media, depending on the bait construct.

3.6 *Preparation of Yeast Protein Extracts*

Initially, it is advisable to verify the expression of the fusion proteins by standard SDS polyacrylamide gel electrophoresis (PAGE) and Western blotting techniques. Monoclonal antibodies to either GAL4 AD or GAL4 BD are available from Clontech to detect the AD or BD fusions. Alternatively, GAL4 AD fusion proteins expressed from the pGADT7 plasmid can be detected using an anti-HA antibody directed against the HA fusion tag.

1. To prepare yeast protein extracts of the transformed yeast strain, inoculate 5 mL of the appropriate SD medium with a single colony from an SD plate. As a control, a transformed yeast strain expressing an unrelated protein may be used to run alongside the protein of interest on the Western blot. Alternatively, an untransformed yeast colony grown in YPD could be used as a negative control.
2. Vortex the overnight culture to disperse cell clumps and inoculate a 50-mL volume of YPD with the whole overnight culture.
3. Incubate on a shaker (220 rpm) at 30 °C until the culture reaches an OD_{600} of 0.4–0.6. This usually takes 4–5 h, depending on the fusion protein. The OD_{600} units can be calculated by multiplying the OD_{600} value by the culture volume. This will be used later to determine the amount of cracking buffer required to lyse the yeast pellets.
4. During the incubation period, fresh cracking buffer can be prepared (see sub-heading 2.2) and prewarmed to 60 °C.
5. At the end of the incubation period, the culture is poured into tubes half filled with ice and then centrifuged for 5 min at 1000 *g* in a precooled rotor at 4 °C.
6. The supernatant can be discarded and the pellet resuspended in 50 mL ice-cold H₂O and then centrifuged for 5 min at 1000 *g*.
7. Discard the supernatant and snap freeze the pellet in liquid nitrogen. The pellets can be stored at –70 °C until required.

8. Add 100 μL prewarmed cracking buffer per 7.5 OD_{600} units of cells to thaw the pellet quickly (*see Note 5*).
9. PMSF stock solution (1 μL per 100 μL cracking buffer) should be added at 15-min intervals to maintain protease inhibition.
10. Transfer the cell suspension units to a 1.5-mL microcentrifuge tube and add 80 μL of glass beads per 7.5 OD_{600} units.
11. Vortex for 1 min, centrifuge at full speed in a microfuge for 5 min, and transfer the supernatants to a fresh tube on ice.
12. Boil the pellets in a water bath at 100°C for 5 min.
13. Vortex for 1 min and centrifuge at full speed for 5 min at 4°C.
14. Combine both supernatants from steps 11 and 13 and boil for 5 min before loading onto an SDS-PAGE for analysis. Details of the analytical protein methods have been described previously (3,4).

3.7 *Small-Scale Transformation or Cotransformation of Yeast*

The small-scale transformation of yeast with single plasmids can be used to check for the expression of the protein of interest as described above or to prepare yeast cells for library screening by transformation with a bait plasmid such as pAS2-1 encoding the GAL4 BD. Alternatively, cotransformation experiments may be carried out by transforming the yeast simultaneously with two different plasmids encoding a potential interacting protein pair. The success of the transformation procedure depends critically on the viability and growth phase of the yeast culture. Typically, the transformation efficiency for transformation with a single plasmid is in the region of 10^4 CFU/ μg and 10^3 CFU/ μg for simultaneous transformations. Transformants can be selected on the appropriate DO medium.

1. Grow the yeast cells overnight in 5 mL YPD medium at 30°C with shaking at 220 rpm.
2. Transfer enough of the overnight culture to fresh YPD medium to give an OD_{600} of 0.1–0.2.

The final volume will depend on the number of transformations to be carried out; 50- to 200-mL volumes are sufficient for 10–40 transformations.

3. Shake the cultures at 30°C at 220 rpm as long as it takes for the cell population to double twice (*see Note 6*).
4. Centrifuge the culture for 5 min with 2000 g at room temperature and decant the supernatant. Resuspend the pellet in 25 mL H_2O and centrifuge as previously.
5. Decant the supernatant and resuspend the pellet in 3 mL 100 mM LiAc and incubate for 15 min at 30°C with shaking at 220 rpm.
6. Prepare the transformation master mix (see buffers and solutions).

7. Transfer the plasmid DNA required for transforming the yeast cells to microcentrifuge tubes (*see Note 7*).
8. Centrifuge the yeast suspension 5 min at 2000g and carefully resuspend the pellet in the transformation master mix.
9. Transfer 345 μL of the yeast cell suspension to the plasmid DNA in the tubes and incubate the suspension for 30 min at 30 °C with shaking at 200 rpm.
10. Heat shock the cells for 30 min at 42 °C in a heating block, centrifuge the cells for 10 s at full speed in a microfuge, and resuspend the pellet in 100–200 μL H_2O .
11. Plate 100 μL of the cell suspension onto the SD plates that will select for the desired transformants.

3.8 Controls

Before undertaking a cDNA library screen such as we have carried out using Rab1B or Rab6A active or inactive mutants as bait constructs, it is crucial to test whether the target protein is capable of inducing autoactivation of the reporter genes. This test can be performed by transforming the yeast cells with the single bait construct, for instance, in pAS2-1 and an empty prey plasmid such as pGADT7, and checking for reporter gene activity by assaying β -galactosidase activity of colonies growing on *HIS3* selection plates. In our hands, we have not found that the Rab bait constructs induce autoactivation in our system. However, should autoactivation arise, an alternative cloning strategy may have to be considered using alternative vectors carrying the GAL4 AD and BD fusions.

A further important control is to include a protein sequence that is a known interaction partner for the Rab protein so that a positive control is included in the interaction assay. We have identified a number of Rab6A interacting partners, including BICD1 and 2 (Bicaudal1/2), phosphomannomutase 1 (PMM1), dynein light chain 2A (DNLC2A), and Mint3, all of which induce reliable reporter expression with the Rab6A active mutant in the Matchmaker yeast two-hybrid system (3–5). For the Rab1B, we also found several interacting proteins, like GM130, the MICAL proteins, and Iporin (6–9).

3.9 Library Amplification

Before starting a library screen, the library must be amplified to obtain enough plasmid DNA to ensure that the highest repertoire of independent clones is represented. The following protocol uses 2YT medium and 47 \times 31 cm trays to obtain even growth over a large surface area.

1. Pipet 1–10 μL of the cDNA library into 500 μL 2YT medium, mix, and add 30 mL 2YT.

2. Spread 3 mL of the suspension onto $10 \times 47 \times 31$ cm trays, each containing 600 mL 2YT agar plus ampicillin, using a sterile glass spreading rod until all of the liquid has been absorbed to ensure even spreading of the inoculum.
3. Incubate the trays at 30 °C for 38–48 h (*see Note 8*).
4. After incubation, scrape the bacterial colonies and resuspend in 400 mL 2YT medium plus ampicillin (*see Note 9*).
5. Increase the volume of the suspension to 2 L, divide into four 1-L flasks, and shake at 190 rpm for 2–3 h at 30 °C. (This step can be omitted if the density of the colonies on the trays is high.)
6. Pellet the bacteria by centrifugation at 4000g for 20 min at 4 °C.
7. The pellets can be frozen at –20 °C, or plasmid DNA can be prepared immediately following the Qiagen Plasmid Giga kit according to the manufacturer's instructions.

3.10 Large-Scale Yeast Transformation

This method can be used to perform a yeast two-hybrid screen of a cDNA library with the protein of interest fused to the DNA BD of GAL4 (e.g., pAS2-1 vector). The affinity of the DNA BD for the UAS favors the construction of cDNA libraries in vectors expressing the GAL4 AD to avoid the generation of false positives because of the tendency of the AD alone to induce autoactivation of the reporter genes. For tissue-specific interactions such as for Rab6B, we used a cDNA library made from brain tissue. For screening a cDNA library, we use five 47×31 cm trays.

1. Transform yeast with the pAS2-1 vector expressing the GAL4 DNA BD fusion protein (bait) and select on SD T⁻ (lacking trp) plates.
2. Inoculate an overnight 5 mL SD T⁻ culture with a colony from the transformed yeast strain.
3. Transfer the overnight culture to 300 mL SD T⁻ to yield an OD₆₀₀ of 0.1–0.2.
4. Shake the culture at 30 °C at 200 rpm until the cell number has doubled twice.
5. Centrifuge for 5 min at 2000g and resuspend the pellet in 100 mL H₂O.
6. Repeat the centrifugation step and resuspend the pellet in 18 mL 100 mM lithium acetate and incubate for 15 min at 30 °C with shaking at 200 rpm.
7. Resuspend the yeast pellet in the transformation mix (*see library screen transformation mix*) and incubate for 30 min at 30 °C with shaking at 200 rpm.
8. Incubate the suspension for 40 min at 42 °C in a water bath and then centrifuge for 5 min at 2000g.
9. Resuspend the pellet in 24 mL H₂O and plate 5 mL onto trays containing SD T⁻ L⁻ H⁻ agar with 30–50 mM 3-AT. Incubate the trays at 30 °C for up to 14 d.
10. Once the size of the colonies is more than 2 mm \varnothing = diameter, transfer these to two 15-cm \varnothing master plates with SD T⁻ L⁻ H⁻ containing 30–50 mM 3-AT. Incubate the plates 3–4 d at 30 °C.

From one master plate, colony lifts can be made for the β -galactosidase reporter assay. The filter can be oriented by stabbing the filter with a syringe needle at three of four asymmetric points.

To calculate the number of clones screened, plate in duplicate 0.5-, 1-, and 5- μ L aliquots from the transformation in 100 μ L H₂O on SD T⁻ L⁻ 10-cm \emptyset agar plates and incubate at 30°C for 3–4 d. The number of clones screened should be at least 1×10^6 .

3.11 β -Galactosidase Reporter Assay

The colony-lift filter assay that we use to measure β -galactosidase activity is a relatively sensitive technique that can be used to screen a large number of cotransformants growing on the *HIS3* selection plates. The yeast cells are rapidly freeze/thawed in liquid nitrogen, which efficiently permeabilizes the yeast cell wall to allow quantification of the β -galactosidase activity.

1. Prepare the Z buffer/X-gal solution (see preparation of buffers).
2. Prepare a 10- to 15-cm \emptyset Petri dish with a round filter soaked in 5 mL Z buffer/X-gal solution.
3. Take lifts from the colonies growing on the SD plate by pressing the surface of the filter paper with the smooth end of the forceps handle to help attach the yeast cells to the filter paper.
4. Lift the filter paper with the forceps in one rapid motion and immerse in liquid nitrogen for 10 s. Remove the filter and allow to thaw.
5. Place the filter presoaked in the Z buffer/X-gal solution colony side up and avoid trapping bubbles underneath.
6. Cover the dish with a lid and incubate the filters at room temperature until the blue color develops. This may take 0.5–2 h for strong interactions or up to 8 h for weak interactions.

3.12 Analysis of Yeast Plasmid Inserts

After library screening has produced a set of potential interacting cloned sequences, the next step is to analyze the plasmid inserts by PCR to ascertain the insert size. Using primers, which flank the insert, and a nested set of primers in a second-round PCR, it is possible to verify the size of the cloned insert. The resulting products can be grouped according to size, and this will provide an indication of how many independent cloned sequences have been identified in the screen. Multiple copies of an abundant sequence will often be represented by a PCR product of the same size. A large screen may result in several hundred clones, so it is important to be able to screen these efficiently, such as we have done by performing the method described below.

1. Prepare 0.5-mL microcentrifuge tubes containing 30 μ L 20 mM NaOH. Using a sterile loop, transfer some of the yeast clone to the tubes and incubate for 15 min at room temperature.

2. For the PCR, prepare enough of the PCR master mix containing all of the components for the number of clones to be screened (see PCR reaction mix 2.4).
3. The PCR master mix can be aliquoted into PCR tubes and the template added.
4. Run the PCR using the following program; the annealing temperatures will need to be adjusted accordingly:

Step 1: 94°C	2 min	
Step 2: 94°C	1 min	
Step 3: 58°C	1 min	}
Step 4: 72°C	3 min	
Step 5: 72°C	5 min	
Step 6: 4°C	∞	

5. Use 3 μL of the PCR products generated in the first round as a template for the second-round PCR. Use the following PCR program:

Step 1: 94°C	5 min	
Step 2: 94°C	1 min	
Step 3: 58°C	1 min	}
Step 4: 72°C	2 min	
Step 5: 72°C	5 min	
Step 6: 4°C	∞	

The products can be visualized on a 1% agarose gel and clones grouped according to size.

3.13 Isolation of Yeast Plasmids

We have used the Qiaprep Spin miniprep kit for isolating plasmids from yeast following the manufacturer's protocol. To obtain sufficient DNA for restriction digest, *Escherichia coli* must be transformed with the purified plasmids from yeast and the plasmid DNA isolated from the bacterial cultures. Since the interacting clone from the cDNA library used in the screen is represented by the GAL4 AD (prey) clone, it is necessary to select this plasmid for further analysis by eliminating the GAL4 BD (bait) construct. This can be carried out by growing the yeast cotransformant strain for several generations in medium that maintains selection of the desired plasmid; for example, pACT2 can be selected by growing the yeast in SD–Leu medium. Plasmids, which are not selected (e.g., pAS2-1 in this case), are lost at a rate of 10–20% every generation. Subsequently, the clones can be sequenced.

3.14 Applications

Performing a yeast two-hybrid screen following the protocol described, we identified several interacting partners of the small GTPases Rab6 and Rab1 (3–9). Using the dominant-active mutant Rab6A Q72R, we first characterized the interaction with Bicaudal 1 and 2 (BICD1, BICD2), known as the mammalian homologs of the

Drosophila Bicaudal-D protein (10). BICD is an evolutionary conserved coiled-coil protein that is involved in cytoplasmic dynein-mediated motility. BICD1 and BICD2 colocalize with Rab6A on the trans-Golgi network and cytoplasmic vesicles and associate with Golgi membranes in an Rab6A-dependent manner (3). BICD1/2 interact with their carboxyterminal domains (BICD C) with Rab6A, Rab6A', and Rab6B, which are involved in the regulation of membrane traffic from the Golgi apparatus to the endoplasmic reticulum via a coat protein complex I (COPI)-independent pathway (Table 1). No interaction could be observed with Rab6C (Table 1).

In addition, we and others were able to show that the BICD2 C (third coiled-coil segment) also binds to p150^{Glued}, the subunit component of the dynactin complex (11,12; Fig. 1). Applying the yeast two-hybrid system to characterize the p150^{Glued} BDs, we demonstrated that Rab6A and BICD2C independently bind to different regions of the p150^{Glued} protein to form a tertiary complex (Fig. 1).

Besides BICD1/2 and p150^{Glued}, we detected dynein light-chain 2A (DLC2A) and PMM1 as interacting partners of the Rab6A GTPase (5,13–15). The yeast two-hybrid cotransformation system is also suitable for clarifying the interacting protein domain required for the interaction. In the case of PMM1, the cotransformation results revealed that the whole PMM1 molecule is needed for the interaction (Fig. 2). Further cotransformations also showed that the related PMM2 molecule is unable to bind to Rab6A (Table 2).

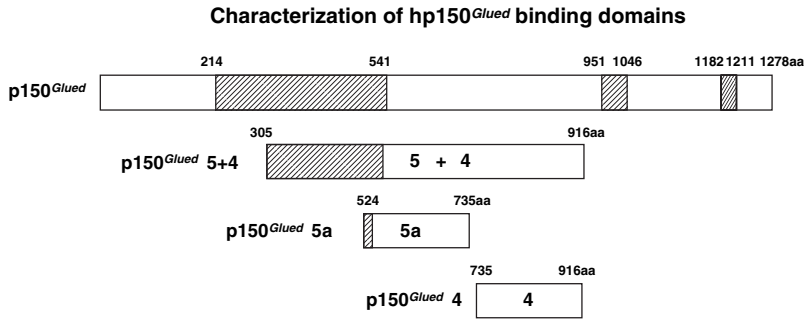
To characterize the role of Rab6A in Alzheimer precursor protein (APP) trafficking and to identify effector proteins of the active Rab6A protein, we isolated from a yeast two-hybrid screen an interacting cDNA clone encoding part of the adaptor protein Mint3 (4). Using the yeast two-hybrid cotransformation assay, we could demonstrate that the interaction of Rab6A and Mint3 is GTP dependent and requires the intact phosphotyrosine-binding (PTB) domain of the Mint protein, which also mediates its association with APP (4).

Table 1 BICD1 and BICD2 Interact with Rab6A, Rab6A', and Rab6B

Bait	Prey			
	BICD1 VK1		BICD2 C	
	Selection	β-gal assay	Selection	β-gal assay
Rab6A wt	+++	++	+++	++
Rab6A' wt	+++	++	+++	++
Rab6B wt	++	+	+++	++
Rab6C wt	+	–	+	–

For two-hybrid interactions, corresponding strains were cultivated on synthetic media lacking leucine, tryptophan, and histidine and supplemented with 30mM 3-AT. In addition, β-galactosidase reporter gene activity (lacZ) was determined on replica filters using X-gal as substrate.

–, no growth on selection media or no β-galactosidase activity; +, low growth or low β-galactosidase activity; ++, strong growth on selection media or strong β-galactosidase activity; +++, very strong growth on selection media or high β-galactosidase activity.



pAS 2-1	pGADT7	
	BICD2C	Rab6A Q72L
hp150 ^{Glued} - 4	-	++
hp150 ^{Glued} - 5a	+++	-
hp150 ^{Glued} - 5+4	+++	+++

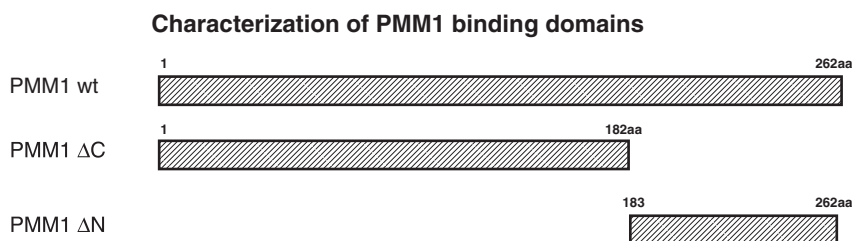
Fig. 1 For two-hybrid interactions corresponding strains were cultivated on synthetic media lacking leucine, tryptophan and histidine, supplemented with 30 mM 3-AT. In addition, β -galactosidase reporter gene activity (lacZ) was determined on replica filters using X-gal as substrate.

- = no growth on selection media or no β -galactosidase activity; ++ = strong growth on selection media or strong β -galactosidase activity; +++ = very strong growth on selection media or high β galactosidase activity. - = coiled coil domains; aa = amino acid.

The strategy of yeast two-hybrid screening also proved to be very helpful when investigating the function of another small GTPase, the Rab1 protein, an essential regulating component in vesicle transport between the endoplasmic reticulum and the Golgi apparatus. We isolated the *cis*-Golgi matrix protein GM130 as a direct Rab1 effector (6). We identified the MICAL proteins 1/2/3 as interacting partners of Rab1, which suggested a link between the Golgi apparatus-associated Rab1 and the intermediate filament cytoskeleton (7,8). Finally, we detected Iporin as a Rab1-interacting protein (9). By using the two-hybrid system and in vitro binding assays, we could show that the Rab1-Iporin2 interaction is GTP dependent and Rab1 specific. Furthermore, we mapped the putative Rab1-binding site to the C-terminus of Iporin and could show that Iporin displays some significant differences in comparison to the previously characterized Rab1 effector protein GM130 (9).

In summary, we have used the yeast two-hybrid system for the following approaches:

1. To identify Rab-interacting proteins
2. To characterize the specificity of the interaction using Rab mutants representing the inactive (GDP) or activated (GTP) state of the small GTPases (Figs. 1 and 2) or Rab6 isoforms (Table 1)
3. To identify and characterize specific BDs within the bait and prey proteins by constructing and using deletion mutants in the cotransformation assay (Figs. 1 and 2)



Cotransformation assays with Rab6 and PMM1

pACT2 (pray)	pAS 2-1 (bait)			
	Rab6A Q72L	Rab6A T27N	Rab6B Q72L	Rab6A' Q72L
PMM1 wt	+++	–	+++	+++
PMM1 ΔC	–	n.t.	n.t.	n.t.
PMM1 ΔN	–	n.t.	n.t.	n.t.
PMM2 wt	–	–	–	–

Fig. 2 For two-hybrid interactions corresponding strains were cultivated on synthetic media lacking leucine, tryptophan and histidine, supplemented with 30 mM 3-AT. In addition, β -galactosidase reporter gene activity (*lacZ*) was determined on replica filters using X-gal as substrate.

– = no growth on selection media or no β -galactosidase activity; +++ = very strong growth on selection media or high β galactosidase activity. n.t. = not tested; wt = wild type.

4 Notes

1. Serine, aspartic acid, and glutamic acid are not included in the DO supplements as these lower the pH of the medium and can be synthesized endogenously by the yeast.
2. In our hands, recovering yeast from frozen stocks has been problematic. We have found that using stocks stored at 4 °C as a starting point for generating fresh cultures is more reliable.
3. Should the yeast cells not grow from frozen stocks, thaw the vial, mix, and streak out a larger volume. The vial can be refrozen at –70 °C.
4. If the clumps are not dispersed, the cells inside the clumps will not have access to the medium and therefore will be unable to grow.
5. To increase the speed of thawing, the tubes may be incubated at 60 °C for 2 min.
6. If the doubling time is longer than 4 to 4.5 h, the viability of the yeast cells is suspect. Discard the cells and start again.
7. The actual amount of plasmid DNA required for good transformation efficiency can be determined but usually lies in the range of 0.1–0.5 μ g and in a

volume of 10–15 μ L. To reduce the risk of transformation of a single yeast cell with multiple library plasmids, low amounts of plasmid DNA should be used while at the same time maximizing the transformation efficiency.

8. Incubation at 30 °C ensures that slower-growing clones are not outcompeted by faster-growing colonies.
9. Use a cut 25-mL glass pipet for resuspension first, then a 5-mL pipet. Resuspension might take up to 2 h.

Acknowledgments We would like to thank Bruno Goud, Fumiko Nagano, Casper Hoogenraad, and Anna Akmanova for collaborating on Rab6A/mint, Rab6A/p150Glued, and Rab6A/BICD. We greatly acknowledge our coworkers K. Bilbilis, J. Boettcher, C. Holz, T. Matanis, and M. Rosing for contributing to the results summarized in this chapter. This work was supported by the DFG Deutsche Forschungsgemeinschaft and an FCI Fonds der Chemischen Industrie grant to A.B.

References

1. Harper, J.W., Adami, G.R., Wei, N., Keyomarsi, K., and Elledge, S.J. (1993) The p21 Cdk-interacting protein Cip1 is a potent inhibitor of G1 cyclin-dependent kinases. *Cell* **75**, 805–816.
2. Gietz, R.D., and Schiestl, R.H. (1995) Transforming yeast with DNA. *Methods Mol. Cell Biol.* **5**, 255–269.
3. Matanis, T., Akhmanova, A., Wulf, P., et al. (2002) Bicaudal-D regulates COPI-independent Golgi-ER transport by recruiting the dynein–dynactin motor complex. *Nat. Cell Biol.* **4**, 986–992.
4. Teber, I., Nagano, F., Kremerskothen, J., Bilbilis, K., Goud, B., and Barnekow, A. (2005) Rab6 interacts with the mint3 adaptor protein. *Biol. Chem.* **386**, 671–677.
5. Kaufmann, M., Kail, M., Bilbilis, K., and Barnekow, A. (2005) Dynein light chain 2A—A link between the small GTPase Rab6A and the motor protein Dynein. *Eur. J. Cell Biol.* **84**, 49.
6. Weide, T., Bayer, M., Koster, M., Siebrasse, J.P., Peters, R., and Barnekow, A. (2001) The Golgi matrix protein GM130: a specific interacting partner of the small GTPase Rab1b. *EMBO Rep.* **2**, 336–341.
7. Weide, T., Teuber, J., Bayer, M., and Barnekow, A. (2003) MICAL-1 isoforms, novel Rab1 interacting proteins. *Biochem. Biophys. Res. Commun.* **306**, 79–86.
8. Fischer, J., Weide, T., and Barnekow, A. (2005) The MICAL proteins and Rab1: a possible link to the cytoskeleton? *Biochem. Biophys. Res. Commun.* **328**, 415–423.
9. Bayer, M., Fischer, J., Kremerskothen, J., et al. (2005) Identification and characterization of Iporin as a novel interaction partner of Rab1. *BMC Cell Biol.* **6**, 1–15.
10. Hoogenraad, C.C., Akhmanova, A., Howell, S.A., et al. (2001) Mammalian Golgi-associated Bicaudal-D2 functions in the dynein–dynactin pathway by interacting with these complexes. *EMBO J.* **20**, 4041–4054.
11. Barr, F.A., and Short, B. (2003) Golgins in the structure and dynamics of the Golgi apparatus. *Curr. Opin. Cell Biol.* **15**, 405–413.
12. Short, B., Haas, A., and Barr, F.A. (2005) Golgins and GTPases, giving identity and structure to the Golgi apparatus. *Biochim. Biophys. Acta* **1774**, 383–395.
13. Jiang, J., Yu, L., Huang, X., et al. (2001) Identification of two novel human dynein light chain genes, DNLC2A and DNLC2B, and their expression changes in hepatocellular carcinoma tissues from 68 Chinese patients. *Gene* **281**, 103–113.
14. Schroer, T. (2004) Dynactin. *Annu. Rev. Cell Dev. Biol.* **20**, 759–779.
15. Matthijs G., Schollen, E., Pirard, M., Budarf, M. L., Van Schaftingen, E., and Cassiman, J.J. (1997) PMM (PMM1), the human homologue of SRC53 or yeast phosphomannomutase, is localized on chromosome 22q13. *Genomics* **40**, 41–47.

Part III
Analysis of Endocytosis and Exocytosis
in Different Cell Systems

10

High-Throughput Analysis of the Dynamics of Recycling Cell Surface Proteins

Roland Govers, David E. James, and Adelle C.F. Coster

1 Introduction.....	129
2 Materials	131
3 Methods.....	132
4 Notes	144
References.....	145

Summary Recycling via the plasma membrane is a key feature that is shared by many membrane proteins. Using a combination of indirect immunofluorescence labeling and fluorescence detection using a fluorescence multiwell plate reader, we exploited the possibilities of quantitatively measuring the trafficking kinetics of transmembrane proteins. Parameters that can be studied include dynamic appearance/presence at the cell surface, recycling via the cell surface, and internalization. For the insulin-responsive glucose transporter GLUT4 (glucose transporter number 4), details are presented on how to quantitatively measure insulin-induced GLUT4 translocation toward the plasma membrane (transition state) and to analyze cell surface recycling of GLUT4 in basal and insulin-stimulated cells (steady state).

Keywords Cell surface recycling; GLUT4; high throughput; immunofluorescence; intracellular trafficking.

1 Introduction

Many transmembrane proteins fulfill their normal function at the plasma membrane. This includes receptors, channels, or transporter proteins; each communicates with the external environment of the cell in some way to aid

the regulation of cell growth and maintenance. Such proteins are synthesized in the endoplasmic reticulum (ER) but are equipped with targeting signals to enable them to navigate throughout the biosynthetic track to the plasma membrane. Although some membrane proteins are virtually excluded from the plasma membrane (e.g., nuclear and ER proteins), others are resident plasma membrane proteins, continually recycle between the cell surface and intracellular membranes, or even appear at the plasma membrane in a highly regulated fashion so that their specific function can be called on only when required. An example of the last is the insulin-responsive glucose transporter GLUT4 (glucose transporter number 4); its cell surface appearance is regulated by insulin to aid in the absorption of nutrients after a meal (1).

Although it can be readily established via various methods whether a transmembrane protein trafficks via the cell surface, it remains a challenge to quantitatively analyze this feature. Cell surface iodination and biotinylation have been used as well as immunofluorescence microscopy in a qualitative or semiquantitative manner, but these techniques are laborious and not highly quantitative (*see Note 1*). In addition, the trafficking of cell surface proteins has been studied using labeled ligands, but obviously this method is limited to receptors only, while the binding of the ligand to its receptor may very well modify its trafficking, thereby only allowing the analysis of the activated receptor.

We have developed a novel, straightforward, high-throughput 96-well assay to measure cell surface recycling in a highly quantitative fashion based on indirect immunofluorescence labeling and detection using a multiwell fluorescence plate reader (2,3) (*see Note 2*). This assay is not limited to receptor studies but allows for the analysis of trafficking of all cell surface transmembrane proteins in both stimulated and nonstimulated cells. In the current report, using GLUT4 as an example, we describe in detail two different aspects of protein trafficking that can be analyzed with this technique.

First, in transition experiments it can be readily and quantitatively determined what percentage of the protein resides at the plasma membrane before and after stimulation, at what speed the transition takes place, and whether a quantal mechanism or a mechanism of constant turnover underlies this process. In the case of GLUT4, the last point addresses the question whether insulin dose dependently increases the trafficking speed of all GLUT4 molecules in the cell or whether insulin dose dependently recruits quantal amounts of GLUT4 toward the cell surface (3). Second, steady-state experiments determine the relative amount of the protein that participates in cell surface recycling (which does not necessarily need to be 100%, as is the case for GLUT4), the time that it takes for all participating molecules to reach the plasma membrane, and exocytosis and endocytosis rates. Taken together, the technique described here readily determines many variables of cell surface protein trafficking in a highly quantitative manner. As this is a high-throughput technique, it may also very well be useful for drug-screening studies.

2 Materials

2.1 Cell Culture of BOSC23 Cells and Production of Retroviral Particles

1. Dulbecco's modified Eagle's medium (DMEM) with 4.5 g/L glucose (Invitrogen, Paisley, UK), supplemented with 10% fetal bovine serum (FBS; Invitrogen), penicillin (200 units/L), and streptomycin (200 µg/L; Invitrogen).
2. DMEM with 4.5 g/L glucose (Invitrogen), supplemented with 10% FBS (Invitrogen) but without penicillin and streptomycin.
3. Dulbecco's phosphate-buffered saline (PBS) without CaCl₂ and MgCl₂ (Invitrogen).
4. Solution of trypsin (0.5 g/L) and ethylenediaminetetraacetic acid (EDTA; 0.2 g/L) in Hanks' balanced salt solution without CaCl₂ and MgCl₂ (Invitrogen).
5. 0.2% gelatin (Merck/VWR, Strasbourg, France) (*see Note 3*).
6. 0.5% glutaraldehyde (Sigma-Aldrich, Lyon, France).
7. 50 mM glycine (Sigma).
8. 25 µM chloroquine (Sigma) in DMEM, with 4.5 g/L glucose (Invitrogen), supplemented with 10% FBS (Invitrogen), without penicillin and streptomycin. The chloroquine solution should be prepared just before use.
9. HBS solution (2X): 50 mM HEPES, 10 mM KCl, 12 mM D-glucose, 280 mM NaCl, 1.5 mM Na₂HPO₄, pH 7.05.
10. CaCl₂ (2M).
11. Deoxyribonucleic acid (DNA): Complementary DNA (cDNA) encoding hemagglutinin (HA)-tagged GLUT4 in retroviral pBABE vector (4).

2.2 Cell Culture of 3T3-L1 Cells and Viral Infection

1. 3T3-L1 preadipocytes were obtained from the American Type Culture Collection (LGC Promochem, Molsheim, France).
2. 3T3-L1 preadipocyte propagation medium: DMEM with 4.5 g/L glucose (DMEM) (Invitrogen), supplemented with 10% newborn calf serum (NBS) (PAA, Pasching, Austria), penicillin (200 units/L), and streptomycin (200 µg/L; Invitrogen).
3. 700 µM human insulin (Lilly, Suresnes, France), stored at 4 °C.
4. 500 mM 3-isobutyl-1-methylxanthine (IBMX, Sigma) in dimethylsulfoxide (DMSO); aliquots are stored at -20 °C and are not refrozen after thawing. Final concentration in medium: 0.5 mM.
5. Biotin (Sigma), dissolved at a concentration of 0.1 mg/mL in water; aliquots are stored at 4 °C. Final concentration in medium: 0.1 µg/mL.

6. Dexamethasone (Sigma), dissolved at a concentration of 1 mg/mL in ethanol; aliquots are stored at -20°C . Final concentration in medium: 0.1 $\mu\text{g/mL}$.
7. 3T3-L1 preadipocyte differentiation medium A: DMEM with 4.5 g/L glucose (DMEM) (Invitrogen), supplemented with 10% FBS (PAA), penicillin (200 units/L), streptomycin (200 $\mu\text{g/L}$; Invitrogen), 860 nM insulin, 0.5 mM IBMX, 0.1 $\mu\text{g/mL}$ biotin, 0.1 $\mu\text{g/mL}$ dexamethasone.
8. 3T3-L1 preadipocyte differentiation medium B: DMEM with 4.5 g/L glucose (DMEM) (Invitrogen), supplemented with 10% FBS (PAA), penicillin (200 units/L), streptomycin (200 $\mu\text{g/L}$; Invitrogen), 350 nM insulin.
9. Polybrene hexadimethrine bromide (Sigma), at a concentration of 1 mg/mL in water. Aliquots are stored at -20°C and not refrozen on thawing.
10. Puromycin (Sigma), dissolved at a concentration of 10 mg/mL in water. Aliquots are stored at -20°C and not refrozen on thawing. For selection medium, 100 μL stock are added to 500 mL DMEM supplemented with 10% NBS, penicillin, and streptomycin (final concentration puromycin is 2 $\mu\text{g/mL}$).

2.3 Fluorescence Assays

1. Black clear-bottom 96-well plates (Greiner, Poitiers, France).
2. Electronic multichannel pipetor (Impact 2, Matrix, Cheshire, UK) (*see Note 4*).
3. 700 μM human insulin (Lilly), stored at 4°C .
4. Paraformaldehyde (Fischer Scientific, Illkirch, France), which is dissolved in sodium phosphate buffer at a concentration of 16% (w/v), final pH 7.4. Aliquots are stored at -20°C and not refrozen after thawing.
5. 50 mM glycine (Sigma).
6. Saponin (Sigma), 10% (w/v) in PBS containing 0.92 mM CaCl_2 and 0.50 mM MgCl_2 . Solution is filtered through a 0.22- μm filter and stored at room temperature.
7. Normal swine serum (Dako Corp., Trappes, France), stored at 4°C .
8. Murine anti-HA ascites (Covance, Berkeley, CA), stored at -20°C .
9. Mouse gamma globulin (Jackson ImmunoResearch, West Grove, PA), stored at -20°C .
10. Alexa 488-conjugated goat-antimouse antibody (Molecular Probes/Invitrogen).
11. Fluorescence multiwell plate reader (FLUOstar Optima, BMG Labtech, Offenburg, Germany).

3 Methods

For the ectopic expression of HA-GLUT4 in 3T3-L1 adipocytes, 3T3-L1 preadipocytes are infected with retrovirus that is generated using the packaging cell line BOSC23. After infection and selection of the 3T3-L1 preadipocytes, their differentiation into adipocytes is induced.

The described assays are based on indirect immunofluorescence detection. The principle of transition-state experiments is schematically represented in Fig. 1. The cells, expressing an HA epitope tag in an extracellular domain of GLUT4, are chemically fixed and either left untreated or permeabilized with saponin, after which the tag is immunolabeled. As can be seen from Fig. 2, the choice and concentration of the permeabilizing agent is important (see also Ref. 5). In

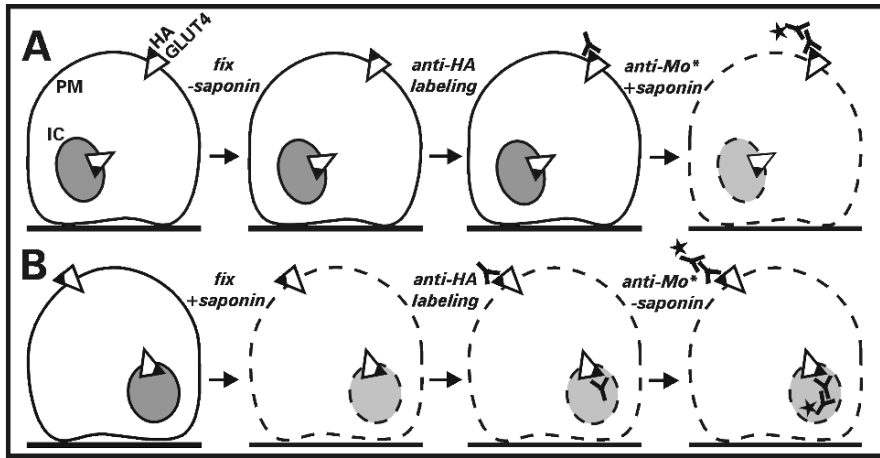


Fig. 1 Experimental setup of transition state assay. Cells are grown in 96-well plates, incubated with or without insulin, fixed, and left untreated (A) or permeabilized (B). Then, all cells are incubated with primary murine anti-HA antibody and fluorescent antimouse secondary antibody subsequently. Fluorescence is measured using a multiwell plate reader. Ratio A:B × 100 gives percentage HA-GLUT4 at the cell surface. HA, influenza hemagglutinin epitope tag; IC, intracellular compartment; PM, plasma membrane.

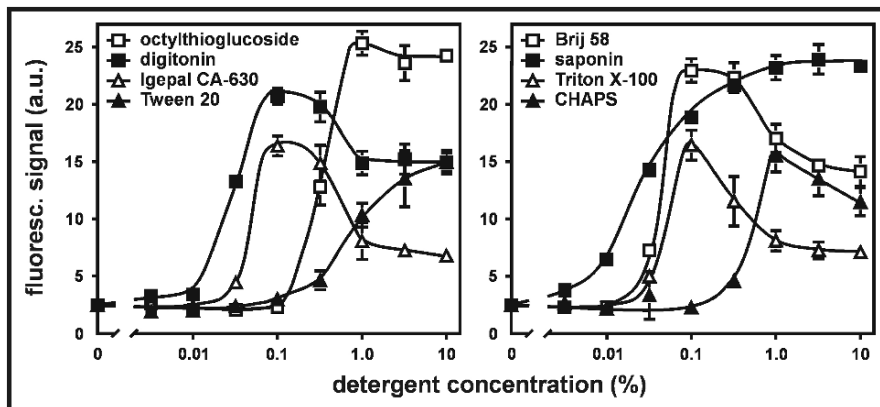


Fig. 2 Effect of detergents on the detection of total cellular HA-GLUT4. Cells are chemically fixed and treated for 20min with the indicated permeabilizing agents at various concentrations. Cells are labeled with murine anti-HA antibody and fluorescent antimouse antibody subsequently. Note that not all permeabilizing agents allow the detection of the same amount of HA-GLUT4.

addition, for quantitative analysis it is essential to establish the level of nonspecific binding of the antibodies and to correct for this background (Fig. 3).

For steady-state experiments, live cells are incubated with anti-tag antibody, followed by chemical fixation and immunofluorescent detection of the anti-tag antibody. The level of fluorescence when the cells are permeabilized with saponin and incubated with primary antibody after fixation provides the normalizing measure of the total cellular HA-GLUT4. The steady-state experiments determine the dynamics of cell surface GLUT4 recycling in basal and insulin-stimulated cells and the percentage of GLUT4 that is involved in this recycling pathway. Examples of transition and steady-state assays are shown in Fig. 4.

3.1 Propagation of BOSC23 Cells

1. BOSC23 cells are routinely grown in 6-cm Petri dishes at 37 °C and 5% CO₂.
2. The medium is replaced every 2 or 3 days with fresh medium (DMEM with 4.5 g/L glucose and FBS, penicillin, and streptomycin).
3. Once the cells are almost confluent, the medium is aspirated, 1.5 mL of trypsin/EDTA solution are added (see Note 5), and the cells are incubated for 1 min at 37 °C.
4. Using an inverted light microscope, the cells are examined to ensure that they are detached, and medium is added. The cells are then transferred to a tube and centrifuged for 5 min at 300 g in a tabletop centrifuge.
5. Medium/trypsin is aspirated, and the cells are resuspended in fresh medium and seeded in a 1:5 dilution (cells from one dish are seeded into five new dishes) (see Note 6).

3.2 Production of Retroviral Particles

1. One day before infection, 10-cm tissue culture Petri dishes are coated with 0.2% gelatin for 1 h.
2. Gelatin is discarded, and dishes are rinsed once with PBS.
3. The Petri dish is incubated for 10 min with 0.5% glutaraldehyde in PBS.
4. Glutaraldehyde is discarded, and the dish is rinsed once with PBS.
5. The remaining glutaraldehyde is quenched by incubating the Petri dish for 5 min with 50 mM glycine in PBS and two times for 5 min with DMEM/FBS (discarding medium in between).
6. The BOSC23 cells are trypsinized (as in Subheading 3.1., steps 3–5) and seeded into the gelatin-coated Petri dish in such a way that the next day the confluence will be 80% (in practice, this means that the cells from two nearly confluent 10-cm dishes are seeded into three gelatin-coated dishes).

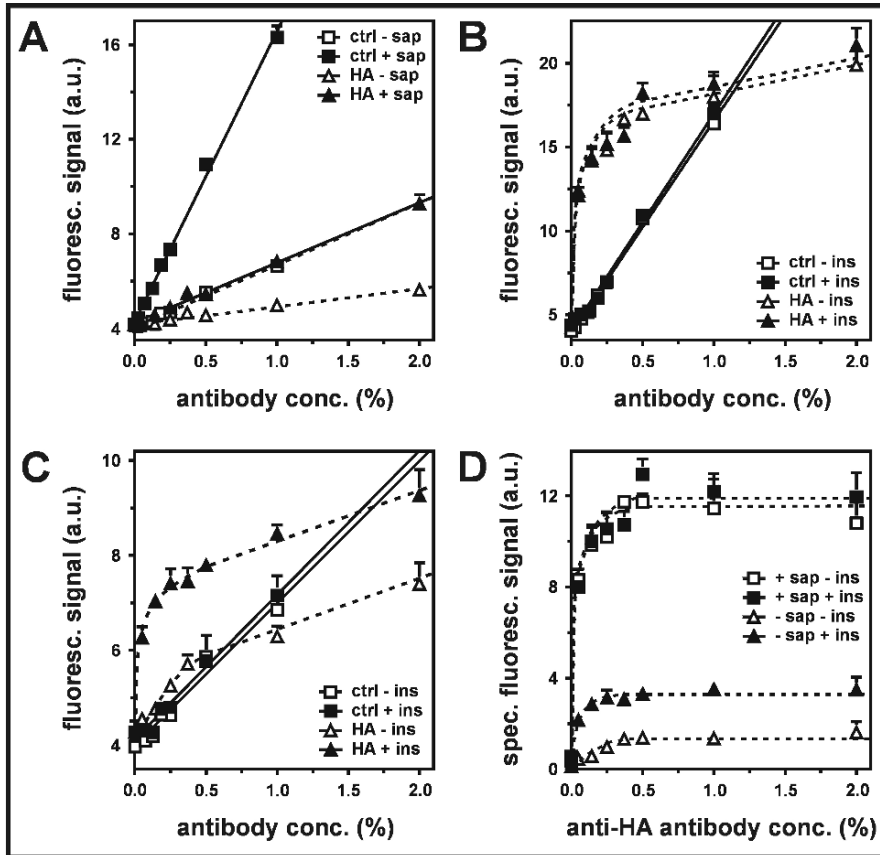


Fig. 3 Analysis of nonspecific background of anti-HA antibody and determination of the concentration to use in transition assay. **(A)** Noninfected cells were fixed and left untreated ($-sap$) or permeabilized using saponin ($+sap$). Then, the cells were incubated with various concentrations (v/v) of anti-HA tag antibody (HA) or nonspecific control antibody (ctrl) and subsequently with fluorescent secondary antibody. In this way, the relative concentration of the nonspecific antibody that needs to be used in the assay was determined in relation to the concentration of anti-HA antibody (giving similar background fluorescence). **(B)** Basal ($-ins$) and insulin-stimulated ($+ins$) HA-GLUT4-expressing cells were fixed and permeabilized, followed by labeling with nonspecific control (ctrl) or anti-HA antibody. Note that at concentrations of anti-HA higher than 0.5% (v/v) the increase in fluorescence signal is linear (representing nonspecific signal), indicating that from this concentration all HA epitopes are saturated with antibody. **(C)** Basal ($-ins$) and insulin-stimulated ($+ins$) HA-GLUT4-expressing cells were fixed without permeabilization, followed by labeling with nonspecific control (ctrl) or anti-HA antibody. Note that also, at concentrations of anti-HA higher than 0.5% (v/v), the increase in fluorescence signal is linear. **(D)** Basal ($-ins$) and insulin-stimulated ($+ins$) HA-GLUT4-expressing cells were fixed and left intact ($-sap$) or permeabilized ($+sap$), followed by labeling with nonspecific control (ctrl) or anti-HA antibody. At each concentration of anti-HA antibody, the background fluorescence was calculated (by means of nonspecific antibody, corrected for the difference in background fluorescence as determined in **(A)**), and subtracted. Note that concentrations of anti-HA antibody higher than 0.5% (v/v) did not result in more specific fluorescence, indicating that this concentration could be used for transition experiments.

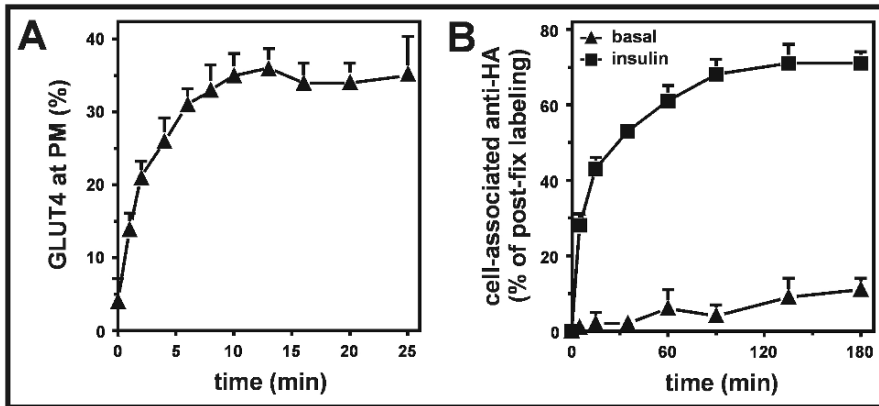


Fig. 4 Examples of transition-state and steady-state experiments. **(A)** Transition-state experiment: Insulin (200 nM) is added to the cells, and the increase in cell surface GLUT4 levels is measured **(B)** Steady-state experiment: Cells are incubated for 20 min in the absence or presence of 200 nM insulin (resulting in a steady-state GLUT4 distribution), followed by the addition of anti-HA antibody. Amounts of antibody taken up by the cell are determined and expressed as percentage of the total amount of antibody that can bind to fixed permeabilized cells. (Reproduced from *Ref. 4* with permission from the American Society for Microbiology.).

7. One day after seeding of the cells into the gelatin-coated dishes, just prior to transfection of the cells, the medium is replaced with 4 mL DMEM/FBS without penicillin/streptomycin, supplemented with 25 μ M chloroquine.
8. For each dish, 10 μ g DNA and H₂O are combined to a total volume of 438 μ L, and 62 μ L of 2 M CaCl₂ are added. The solution is vortexed, and dropwise 500 μ L of the 2X HBS solution is added while keeping the tube on the vortex.
9. The DNA/calcium phosphate solution is directly added to the chloroquine-containing medium that is covering the cells.
10. After 10 h, the medium is replaced with 5 mL DMEM/FBS without penicillin/streptomycin.
11. Virus-containing medium is collected at 48 h after transfection of the cells. In case the cells become fully confluent at 24 h after transfection, the virus is collected at this time-point.
12. The medium is centrifugated for 5 min at 300 g in a tabletop centrifuge.
13. The virus is aliquoted and stored at -80°C (or used directly) (*see Note 7*).

3.3 Propagation of 3T3-L1 Preadipocytes

1. The cells are cultured at 37 $^{\circ}\text{C}$ and 10% CO₂.
2. The medium is replaced every 2 or 3 d with fresh medium (DMEM with 4.5 g/L glucose, NBS, penicillin, and streptomycin).

3. Once the cells are 60–80% confluent, medium is aspirated, cells are washed once with PBS, and trypsin/EDTA solution is added (5 mL for a 175-cm² cell culture flask) (see **Note 8**).
4. After 5–15 s, trypsin/EDTA is aspirated, and cells are incubated for 3.5 to 4 min at 37 °C.
5. The cells are examined for detachment using an inverted light microscope, resuspended in propagation medium, and seeded onto new culture plastics (dilution 1:10 to 1:40).

3.4 *Retroviral Infection of 3T3-L1 Preadipocytes (see Note 9)*

1. One day before infection, the preadipocytes are trypsinized and seeded into 10-cm Petri dishes so that the next day they will be 30% confluent (in practice, this means diluting a 50% confluent cell culture 1:2.5).
2. The next day, 2 mL virus suspension is added to 2 mL DMEM/10% FBS without penicillin/streptomycin and 12 µL 1 mg/mL polybrene (final concentration 30 µg/mL).
3. The medium of the dish is replaced with the virus/polybrene solution.
4. The cells are incubated for 5 h at 37 °C.
5. The virus solution is replaced with DMEM/10% FBS without penicillin/streptomycin.
6. After 24 h, the cells should be 40–50% confluent; they are trypsinized and seeded into two new 10-cm Petri dishes in DMEM medium with 10% NBS, penicillin, streptomycin, and 2 µg/mL puromycin.
7. Over the next few days, the noninfected cells will start to die.
8. The cells are cultured similarly as before infection except that puromycin is included in predifferentiation (NBS) and postdifferentiation (FBS) medium.
9. To quantitatively measure cell surface appearance and recycling of GLUT4, the (retrovirally infected) 3T3-L1 preadipocytes are seeded into black clear-bottom 96-well plates that have a coating of glutaraldehyde-fixed gelatin (as in Subheading 3.2., steps 1–5).

3.5 *Differentiation of 3T3-L1 Preadipocytes into Adipocytes (see Note 10)*

1. Once the preadipocytes are 100% confluent, the culture medium is refreshed, and the cells are cultured for another 48 h.
2. The cells are cultured for 3 d in differentiation medium A (DMEM containing FBS, penicillin, streptomycin, insulin, IBMX, biotin, and dexamethasone) and

for another 3 d in differentiation medium B (DMEM containing FBS, penicillin, streptomycin, and 350 nM insulin) (*see Note 11*).

3. Differentiation medium B is replaced with DMEM containing 4.5 g/L glucose, FBS, penicillin, streptomycin, and puromycin.
4. The cells are used for experiments between 8 and 11 d after the addition of differentiation medium A (onset of differentiation).

3.6 Transition State Assay

1. The cells are cultured in black clear-bottom 96-well plates.
2. Cells are serum starved for 2 h in serum-free DMEM containing 0.2% bovine serum albumin (Sigma).
3. Medium is replaced with serum- and bicarbonate-free DMEM supplemented with 20 mM HEPES (pH 7.4) and 0.2% bovine serum albumin (100 μ L/well), and the plate is transferred to a 37 °C water bath. The cells are maintained in this medium throughout the experiments (*see Note 12*).
4. Insulin (200 nM final concentration; *see Note 13*) is added to the cells at different time-points.
5. The plate is transferred to ice and 300 μ L ice-cold PBS is added to each well.
6. PBS is replaced with 4% paraformaldehyde in PBS (100 μ L/well). Cells are fixed for 15 min on ice and 15 min at room temperature (*see Note 14*).
7. Cells are washed once with PBS, incubated for 5 min with 50 mM glycine, and washed once more with PBS.
8. Cells are incubated for 20 min with 5% normal swine serum (NSS) in the absence or presence of 0.5% saponin (to label cell surface GLUT4 or total cellular GLUT4, respectively) (*Fig. 1*).
9. Cells are incubated for a further 60 min with murine anti-HA antibody or non-specific murine antibody (total serum gamma globulin) in PBS containing 2% NSS, after which they are washed three times for 5 min with PBS.
10. Cells are incubated for 20 min with 5% normal swine serum in the absence or presence of 0.5% saponin to permeabilize all cells so that the background labeling of the secondary antibody is similar for all cells.
11. Cells are incubated for 60 min with a saturating concentration of Alexa 488-conjugated goat-anti-mouse antibody, followed by three washes of 5 min with PBS.
12. Fluorescence is measured using the bottom reading mode of a fluorescence microtiter plate reader (485-nm excitation wavelength; 520-nm emission wavelength) (*see Note 15*).
13. The percentage of GLUT4 at the plasma membrane is calculated by subtracting the fluorescence values of the nonspecific antibody from those of the anti-HA antibody and subsequently by dividing the resulting fluorescence of nonpermeabilized cells by that of permeabilized cells (*see Fig. 1 and Note 16*).

3.7 *Steady-State Assay*

1. Cells are cultured and serum starved as described in Subheading 3.6., steps 1–3.
2. For the insulin-stimulated state, the cells are incubated for 20 min with 200 nM insulin (*see Note 13*).
3. At certain time-points, medium is replaced by fresh BSA- and HEPES-supplemented DMEM containing murine anti-HA antibody or murine nonspecific antibody (total serum gamma globulin) with or without insulin. Cells are incubated with antibody for different time-periods (up to 3 h).
4. The plate is transferred to ice and 300 μ L ice-cold PBS are added to each well.
5. PBS is replaced with 4% paraformaldehyde in PBS (100 μ L/well). Cells are fixed for 15 min on ice and 15 min at room temperature (*see Note 14*).
6. The cells are washed once with PBS, incubated for 5 min with 50 mM glycine, and washed once more with PBS.
7. All cells are incubated for 20 min with 5% NSS in the presence of 0.5% saponin.
8. The wells that did not receive anti-HA before fixation and are used to measure the total cellular GLUT4 amount are incubated for 60 min with murine anti-HA antibody or nonspecific murine antibody (total serum gamma globulin) in PBS containing 2% NSS, after which they are washed three times for 5 min with PBS.
9. All cells are incubated for a further 60 min with a saturating concentration of Alexa 488-conjugated goat-antimouse antibody, followed by three washes of 5 min with PBS.
10. Fluorescence is measured using the bottom reading mode of a fluorescence microtiter plate reader.
11. Percentage of GLUT4 that recycles via the plasma membrane is calculated by subtracting the fluorescence values of the nonspecific antibody from those of the anti-HA antibody and subsequently by dividing the resulting fluorescence by the specific fluorescence of the cells that have been incubated with primary antibody after fixation.

3.8 *Interpreting the Data: Experimental Design, Modeling Pitfalls and Tricks*

Interpretation of data obtained from this experimental system requires consideration of a number of variables. For example, the protein under investigation will likely be moving between cellular compartments constantly. The conformation of the protein may change under certain conditions, or the expression of the protein may be modified either transcriptionally or at the level of protein turnover. Each of these variables must be carefully considered in formulating a model.

Changes in experimental variables could include changes in

- the amount of antibody binding
- the amount of antigen-binding sites

Changes in intrinsic cellular variables may include changes in

- the amount of the protein at a particular location like the plasma membrane
- the rate of exocytosis of the protein
- the rate of endocytosis of the protein
- the total amount of protein recycling

There may be changes in more than one of these variables at any given time.

Considering the two experimental data sets shown in Fig. 4A,B, both are well fitted by the exponential rise:

$$y = A - B \exp(-t/\tau),$$

as shown in Fig. 5A,B, respectively.

The parameters A , B , and τ represent the following: A is the long-term (as $t \rightarrow \infty$) level $y = y_\infty = A$. At $t = 0$, $y = y_0 = A - B$, or $B = y_\infty - y_0$, the difference in the initial and long-term levels. τ is the time range from the initial level to the long-term level. The smaller the τ is, the more rapid the rise.

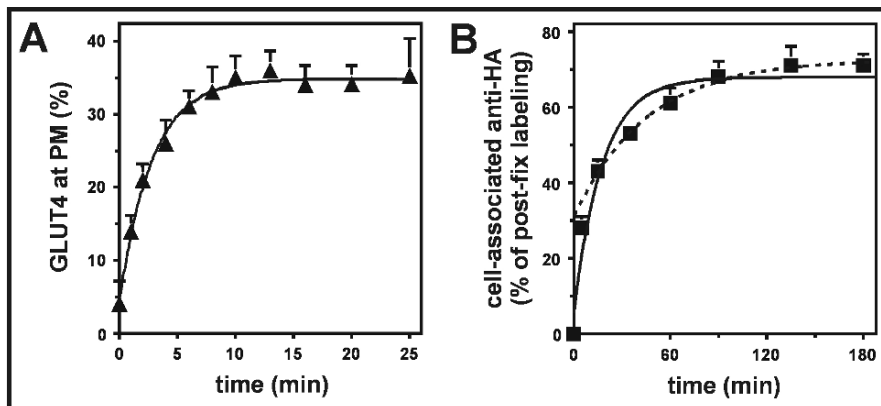


Fig. 5 Least-squares fits to the data for transition-state and steady-state experiments of Fig. 4 to $y = A - B \exp(-t/\tau)$. **(A)** Transition-state experiment in which 200 nM insulin is added at $t = 0$, with coefficients (with 95% confidence bounds) of $A = 34.88$ (33.78, 35.97), $B = 30.43$ (28.2, 32.66), and $\tau = 2.81$ (2.38, 3.43); the goodness of fit had SSE 8.338 R^2 0.9924; adjusted R^2 0.9904; and RMSE 1.021. **(B)** Steady-state experiment of cells preequilibrated in the presence of 200 nM insulin. Two fits are shown. The solid curve includes all data in the fit, with coefficients (with 95% confidence bounds) of $A = 67.72$ (59.77, 75.67), $B = 62.55$ (48.03, 77.06), and $\tau = 17.44$ (6.292, 28.58); the goodness of fit had SSE 166.4; R^2 0.9619; adjusted R^2 0.9466; and RMSE 5.769. The dashed curve excludes both the $t = 0$ and $t = 5$ data points, with coefficients (with 95% confidence bounds) of $A = 72.56$ (69.45, 75.66), $B = 41.7$ (35.89, 47.51), and $\tau = 44.87$ (29.88, 59.86); the goodness of fit had SSE 2.656; R^2 0.9958; adjusted R^2 0.9931; and RMSE 0.9408.

In the two experiments, however, the experimental interpretation of the parameters A , B , and τ is very different.

Figure 6 shows a model for the recycling of the protein. It undergoes exocytosis at a rate K_1 and endocytosis at a rate K_2 , so that there is an amount p at the plasma membrane and an amount r in the rest of the recycling pathway. Depending on the situation, any or all of these variables can change with time t .

It is important to emphasize that under a specific experimental condition the distribution of a particular protein within the cell will likely reach a steady state such that the total amount of that protein at various cellular locations will remain constant. However, this steady state is a function of the integrated equilibrium between multiple rate constants that govern the movement of that protein between each of its itinerant stopping points within the cell. In many cases, it is desirable to challenge the cell in some way, in the case of GLUT4 with insulin, in which case the cell will move to a new steady state. The challenge then is to be able to measure as many of the rate constants as possible that depict this dynamic process because this provides invaluable information about the process. For example, in the case of insulin-regulated GLUT4 trafficking it is important to determine if insulin stimulates exocytosis or decreases endocytosis.

To achieve this end point, there are two kinds of experiments that can be performed. The first is a transition kind of experiment in which one studies the system as it changes from one steady state to another. The second is the steady-state experiment in which one analyses the system only after it has reached a new equilibrium. Both of these experiments have their pros and cons as described below.

3.8.1 Transition Kinetics

In Fig. 5A, the data were derived from a transition assay. At $t = 0$, the cells, which were in the basal state, were exposed to 200 nM insulin. It has been suggested that this exposure changes the exocytosis and to some extent also the endocytosis rates,

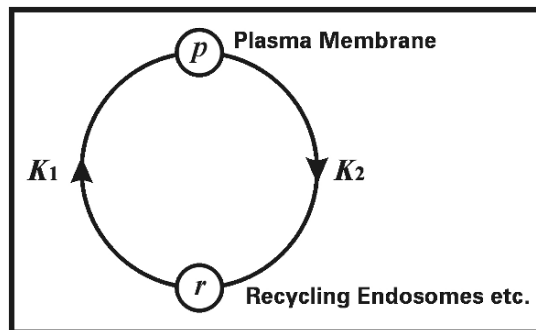


Fig. 6 Hypothesized model for the experiments in Fig. 4. K_1 is the exocytosis rate, and K_2 is the endocytosis rate. The amount of protein at the plasma membrane is p and in the rest of the recycling pathway is r . All these intrinsic variables can be functions of time t .

thereby increasing the amount of GLUT4 at the plasma membrane of the cells. Thus, in this scenario, intrinsic variables of our model are changing with time. The data y display the surface levels of HA-tagged GLUT4 at different stages during the exposure. It is assumed that the proportion of HA-GLUT4 remains constant and evenly distributed compared to endogenous GLUT4 during the process.

At time $t = 0$, we can evaluate the *surface level* of HA-GLUT4 as $y = y_0 = A - B$. This is the basal level at the plasma membrane, before the transition starts. The exocytosis and endocytosis rates may equilibrate very rapidly to new levels in response to the stimulation, but the amount of time taken to redistribute the protein, and the amount of the reporter shuttling between various locations throughout the cell according to these new rates (the new steady state determined by the insulin level) may take a very long time. If the experiment was left to proceed for a sufficient length of time, the system will eventually proceed to this new steady state, but naturally the experiment cannot be performed for an infinite time, and other considerations such as the stability of the cells need to be considered. The fit to the data, however, can be extrapolated to predict the long-term surface level of HA-GLUT4. Letting $t \rightarrow \infty$, we have $y = y_\infty = A$, the final *surface level* in the presence of insulin.

In the case of transport of HA-GLUT4 (both exocytosis and endocytosis) at constant rates, then the time constant τ is the inverse of the exocytosis rate, as is the case in the steady-state assay in Fig. 5B. However, we hypothesized that the change in the surface level was possibly caused by a change in the exocytosis rate. Thus, τ cannot be interpreted as a direct measure of the exocytosis rate but rather as a measure of the speed of the process of transition of the cell from the basal steady state to a steady state in the presence of insulin.

3.8.2 Steady-State Kinetics

In Fig. 5B, the data were derived from a steady-state assay. In this case, the cells are allowed to equilibrate in the presence of 200 nM insulin. Then, at $t = 0$, the anti-tag antibody is added to the extracellular medium, and the total amount of antibody taken up by the cells is measured as a function of time. This amount increases in time as HA-GLUT4 molecules arrive at the surface of the cell, where they are exposed to the anti-HA antibody.

In this experiment, the intrinsic cellular variables, like exocytosis and endocytosis rates, are constant, as are the *total* amounts of GLUT4 at the plasma membrane and the rest of the recycling pathway. The experimental variables, such as the amount of antibody-bound HA-GLUT4 (and thus fluorescing) are, however, changing. The variable y here is the total amount of fluorescence as a function of time t . Using the fit to the data and extrapolating the fit back to $t = 0$, $y = y_0 = A - B = p$ is a measure of the total amount of HA-GLUT4 at the *plasma membrane* in the presence of insulin.

Actually, the process of antibody binding takes a finite amount of time, so by excluding early data points from the fit a better estimate can be obtained for the surface level of HA-GLUT4 in the presence of insulin. A comparison of fits to the data excluding early data points is shown in Fig. 5B.

In this assay, the exo- and endocytosis rates are constant. In this case, the time constant τ reflects the rate at which new, unbound HA-GLUT4 is brought to the surface of the cell. This is, of course, the inverse of the exocytosis rate K_1 .

In addition, as the cell is in a steady state, the ratio of the amount at the plasma membrane, $p = (A - B)$ to that in the rest of the recycling pathway r is equal to the ratio of the endocytosis K_2 and exocytosis rates K_1 :

$$\frac{p}{r} = \frac{K_2}{K_1}$$

Extrapolating the fit to predict the long-term level of HA-GLUT4, we let $t \rightarrow \infty$, giving $y = y_\infty = A = r + p$, the total amount of HA-GLUT in the recycling pathway in the presence of insulin. Putting all these together gives a complete set of values for the intrinsic variables of the model shown in Fig. 6.

The assumptions one makes in a model also affect the results. For example, in these assays, the amounts of HA-GLUT4 are measured relative to the total cellular amount observed in a permeabilized cell. If it is assumed that after a sufficient length of time, *all* the cellular HA-GLUT4 has entered the recycling pathway at one point, then this would mean that A is set to 100%. Free parameter fits to the steady-state assay data, as in Fig. 5b, however, show that this level is better fit by a value of around 70% for a 200 nM insulin stimulation and less for lower insulin concentrations (3), meaning that not all cellular HA-GLUT4 enters the recycling pathway. Using a value of $A = 100$ may also produce fits that have reasonable statistical measures and fit with the hypothesis. However, this may not reflect the true underlying process.

3.8.3 Comparing the Experiments

Using different types of assays can also be a useful tool to provide independent estimates of the intrinsic variables. For instance, we can obtain an estimate for the long-term surface level of HA-GLUT4 in the presence of insulin p from both transition and steady-state experiments. For the transition assay, this was determined to be parameter A . The fit to the data found this value to be approx $35 \pm 1\%$. For the steady-state assay, the surface level was related to two of the fitted parameters, $p = A - B$.

Two different fits to the steady-state assay data are shown in Fig. 5b. At $t = 0$, the antibody was applied, so we could hypothesize that this will instantly bind with all HA-GLUT4 at the plasma membrane. In this case, the data point at $t = 0$ (and thus the fit at $t = 0$) should be the surface level of HA-GLUT4 in the presence of insulin. The fit to the steady-state assay data, including all the data points, is shown as a solid curve in Fig. 5b, which gives an estimate for this of approx $5 \pm 11\%$. The second fit, shown as a dashed curve in Fig. 5b, excludes the data at $t = 0$ and at $t = 5$. From this fit, we obtain an estimate of approx $31 \pm 5\%$.

So, we have good correlation between the transition assay result and that from the fit to the steady-state assay data that excluded the data at $t = 0$ and at $t = 5$. This would indicate that the time taken for the antibody to bind affects the data for up to 15 min (the next data point) after application. Of course, this example only

compares single experiments, and better statistical comparisons can be made if repeated trials are made of both assays.

By using models for the system, experimental investigations can be designed to best test the hypotheses and assumptions that are made. In this way, the data fitting and modeling is not just a final stage of the process but can guide and shortcut what can be a long and intensive experimental study.

4 Notes

1. The advantage of the technique described here over the most recently (and currently most frequently) used technique (6) is that the assays described here are high throughput (one does not need to analyze individual cells by microscopy), and this method establishes the exact relative amount of GLUT4 at the cell surface rather than a ratio between two fluorophores (fluorescent Cy5 label at the cell surface vs intensity of the green fluorescent protein [GFP] label that is attached to GLUT4) (6). The technique described here is obviously also more quantitative than the so-called GLUT4 rim assay, in which the relative amount of cells are scored (by microscopy) in which endogenous GLUT4 appears to be present at or nearby the plasma membrane (7).
2. A provisional patent has been filed for this technique (PCT/AU2004/001057; D.E. James and R. Govers).
3. The source of the gelatin is essential. The gelatin that is used for the production of retroviral particles and fluorescence assays is from Merck (cat. no. 1.04078.1000). Note that the gelatin works very well for some cells but not for others. For example, assays with HeLa cells work well without coating but not when the microtiter plates are coated with gelatin. Gelatin coating of the cell culture plastics can be done 1 d before seeding of the cells; in this case, the final DMEM wash remains in the wells just until the cells are seeded.
4. All handling of the 96-well plates (including gelatin coating) are performed using a cordless electronic multichannel pipetor in combination with extended 1250- μ L tips. This is quite essential for easy handling.
5. Note that while cells in culture usually require rinsing with PBS before trypsin/EDTA treatment, the BOSC23 are not washed before trypsin/EDTA is added. This is not required and only leads to cell loss as the BOSC23 cells do not adhere to culture plastics very strongly. It is also for this reason that they are grown on gelatin for the generation of retrovirus.
6. With passaging, the BOSC23 cells are not diluted more than five times; otherwise, these cells form clumps.
7. Once the retrovirus particles are generated, they are frozen at -80°C and thawed just before use but never refrozen. Refreezing strongly reduces infection efficiency.
8. When propagating 3T3-L1 preadipocytes, they are never allowed to grow to confluence as this negatively affects their subsequent differentiation into adipocytes.

9. The use of retrovirus as described here does not result in extreme overexpression as is the case when, for example, using electroporation-mediated transfer of cDNA. However, after 1 wk of puromycin selection nearly all cells (>95%) express HA-GLUT4.
10. The cell type used in the assays described here (3T3-L1 preadipocytes) do not always differentiate very efficiently. There are batches of these cells on the market that differ in their differentiation efficiency, and not all types and batches of FBS allow good differentiation.
11. Puromycin is not included in the medium during differentiation as this inhibits the differentiation process. It is added to the cells, however, when the differentiation process is completed.
12. In the assays described here, it is essential to use DMEM instead of, for example, Krebs–Ringer phosphate (KRP) solution because of the presence of amino acids in DMEM (8).
13. In the experiments shown in this chapter (Figs. 3 and 4), insulin is used at a concentration of 200 nM. At this concentration, insulin has its maximum effect in transition- and steady-state experiments. At lower doses, insulin displays submaximal effects (5).
14. Note that all wells are fixed at the same time. This means that the cells receive insulin (and antibody for the steady-state assays) at different time-points.
15. Choice of wavelength is important. For this technique, fluorescence can easily be measured for green (Alexa 488, FITC) or far-red fluorophores (Alexa 647, Cy5). However, this is much more difficult for red fluorophores (Alexa 594, TRITC, Cy3) as the cells display considerable fluorescence background in the spectra of these fluorophores.
16. For the determination of the binding of anti-HA or nonspecific antibody at least four wells are used for every trial of condition or time-point (quadruplicate).

Acknowledgments This work was supported by fellowships from the European Molecular Biology Organization (EMBO) and Institut national de la santé et de la recherche médicale (Inserm, France) and an Inserm Avenir grant (all to R.G.). DEJ is an Australian NHMRC Senior Principal Research Fellow. This work was funded in part by an Australian NHMRC project grant to DEJ and ACFC.

References

1. Bryant, N.J., Govers, R., and James, D.E. (2002) Regulated transport of the glucose transporter GLUT4. *Nat. Rev. Mol. Cell Biol.* **3**, 267–277.
2. Govers, R., Coster, A.C., and James, D.E. (2004) Insulin increases cell surface GLUT4 levels by dose dependently discharging GLUT4 into a cell surface recycling pathway. *Mol. Cell. Biol.* **24**, 6456–6466.
3. Coster, A.C., Govers, R., and James, D.E. (2004) Insulin stimulates the entry of GLUT4 into the endosomal recycling pathway by a quantal mechanism. *Traffic* **5**, 763–771.

4. Morgenstern, J.P., and Land, H. (1990) Advanced mammalian gene transfer: high titre retroviral vectors with multiple drug selection markers and a complementary helper-free packaging cell line. *Nucleic Acids Res.* **18**, 3587–3596.
5. Hannah, M.J., Weiss, U., and Huttner, W.B. (1998) Differential extraction of proteins from paraformaldehyde-fixed cells: lessons from synaptophysin and other membrane proteins. *Methods* **16**, 170–181.
6. Zeigerer, A., McBrayer, M.K., and McGraw, T.E. (2004) Insulin stimulation of GLUT4 exocytosis, but not its inhibition of endocytosis, is dependent on RabGAP AS160. *Mol. Biol. Cell* **15**, 4406–4415.
7. Yang, C., Watson, R.T., Elmendorf, J.S., Sacks, D.B., and Pessin, J.E. (2000) Calmodulin antagonists inhibit insulin-stimulated GLUT4 (glucose transporter 4) translocation by preventing the formation of phosphatidylinositol 3,4,5-trisphosphate in 3T3L1 adipocytes. *Mol. Endocrinol.* **14**, 317–326.
8. Bogan, J.S., McKee, A.E., and Lodish, H.F. (2001) Insulin-responsive compartments containing GLUT4 in 3T3-L1 and CHO cells: regulation by amino acid concentrations. *Mol. Cell. Biol.* **21**, 4785–4806.

11

Studying Phagocytosis by Live-Cell Scintillation Proximity Assay

Walter Stockinger and Axel Nohturfft

1	Introduction.....	148
2	Materials	150
3	Methods.....	151
4	Notes	153
	References.....	154

Summary Phagocytosis of microorganisms, senescent cells, apoptotic bodies, and effete tissue material is an important process in host defense and tissue homeostasis. A method is described to measure, in living macrophages, the kinetics of particle engulfment and lysosome/phagosome targeting. Plasma membranes or lysosomes are labeled with tritiated lipids, followed by exposure of cells to scintillant microbeads. Because of the short range of tritium β -particles, geometric factors, and the confinement of lipids to membranes, scintillation can only be elicited by tracer molecules in membranes immediately vicinal to the scintillant. When the plasma membrane is labeled with [^3H]cholesterol, a signal is produced on bead–cell contact and engulfment and then reaches steady state within 45 min. When lysosomes are labeled with nonhydrolyzable [^3H]cholesterol oleyl ether, scintillation requires intracellular lysosome/phagosome attachment or fusion, and steady state is attained only after several hours. The live-cell scintillation proximity approach is useful for examining the effects of pharmacological and genetic manipulations on particle uptake and on lysosome/phagosome targeting.

Keywords Cholesterol; endocytosis; endosomes; lysosomes; phagosomes; plasma membrane.

1 Introduction

Phagocytosis involves binding of particles to cell surface receptors, formation of intracellular phagosomes by engulfment, transport of phagosomes to the perinuclear region, and fusion of phagosomes with endo-/lysosomes (1). Studies of the biochemical mechanisms and regulation of these processes often require kinetic measurements with living cells. Conventionally, live-cell experiments use light microscopy to follow the distribution of fluorescently labeled proteins. The approach is characterized by high spatial and temporal resolution, applicability to many different cell types, and the opportunity to study several markers at the same time (2,3). On the downside, analyzing the effects of multiple parameters by live-cell microscopy is time consuming, results are often difficult to quantify, and the approach can be susceptible to selection bias during both analyses and documentation (4).

Here, we describe a complementary approach that is based on scintillation proximity technology. Scintillation proximity assays generally combine scintillant particles with analytes containing weak β -emitters (5,6). Because of the short range of β -radiation emitted by isotopes such as tritium and ^{14}C , only those labeled molecules can produce scintillation that are within about $1\ \mu\text{m}$ of the scintillant (7). The approach has long been used for in vitro measurements of enzyme activity, receptor–ligand binding, and other biochemical interactions. The data are quantitative, and assays are amenable to high-throughput formats (8).

Since commercially available scintillant particles are small enough to be taken up by phagocytes ($2.5\text{--}5\ \mu\text{m}$), we recently developed scintillation proximity assays for studies with living macrophages and tritiated lipids (7,9,10). In one approach, the plasma membrane is labeled with [^3H]cholesterol to study particle envelopment and uptake (7,9). In a second protocol, lysosomes are specifically labeled with nonhydrolyzable [^3H]cholesterol oleyl ether to follow the kinetics of lysosome/phagosome targeting (10).

Cells are grown in glass scintillation vials, and scintillation is measured in standard scintillation counters. Alternatively, cells can be cultured in multiwell plates, and data are collected in a microplate scintillation reader. When a temperature-controlled counting chamber is available, data can be collected continuously with a temporal resolution of up to about 1 min. We have used the live-cell scintillation proximity approach to study (i) the kinetics of particle engulfment (7,9), (ii) lysosomal cholesterol storage (7), and (iii) lysosome/phagosome targeting (10).

To illustrate what types of data can be obtained with this method, we performed the experiment shown in Fig. 1. The solid line shows the results of an experiment designed to analyze the particle engulfment process. A line of immortalized mouse macrophages, J774 cells, was incubated overnight with liposomes containing [^3H]cholesterol oleyl ester, which is hydrolyzed to [^3H]cholesterol and oleate in lysosomes. Cholesterol partitions preferentially to the plasma membrane but distributes across all cellular organelles (11,12). The labeled cells were then placed on ice, and cultures received suspensions of scintillant yttrium silicate beads. The plate was left on ice for 15 min to allow the particles to settle on top of the cells and then moved

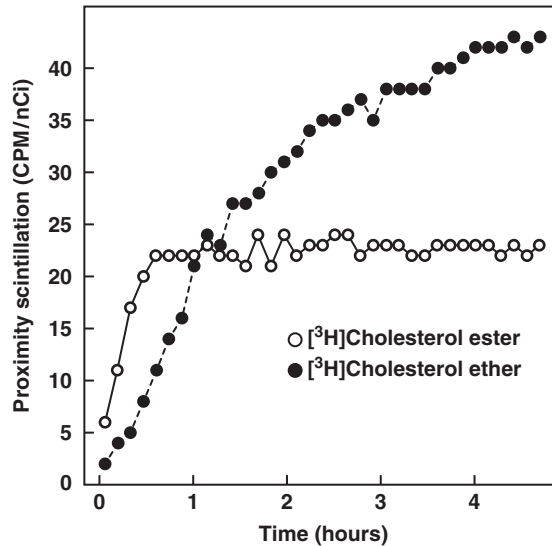


Fig. 1 Live-cell scintillation proximity assays. On d 0, mouse J774 macrophages were set up in a 24-well plate at 5×10^5 cells/well in medium A. After 30 min at 37 °C, the cells were switched to medium A plus liposomes containing [³H]cholesterol oleyl ester (solid line) or [³H]cholesterol oleyl ether (dashed line) (1 μ Ci per 0.5 mL per well final concentrations). On d 1, the medium was removed, cells were washed two times with PBS, and each well received 0.5 mL of a suspension of 100 mg/mL of scintillant yttrium silicate beads in medium B. The plate was left on ice for 15 min and then moved to a microplate scintillation counter at 33 °C. Scintillation was measured every 8 min for 5 h. The cells were then lysed to determine the total cellular radioactivity by liquid scintillation counting. Data represent proximity scintillation corrected for total cellular radioactivity. The average coefficient of variation in wells containing [³H]cholesterol oleyl ester was 5.3% with a range of 0.4% to 39.1% ($n = 3$). The average coefficient of variation in wells containing [³H]cholesterol oleyl ether was 9.1% with a range of 0.8% to 37.5% ($n = 3$).

to a microplate scintillation counter at 33 °C. Scintillation was measured every 8 min. The signal rapidly increased and reached steady state after about 45 min.

Time curves of similar shape were obtained with primary mouse peritoneal macrophages (7) and with immortalized mouse HD1A macrophages (9), although the rate of uptake in these cell types was slower. When the scintillant particles are added in the presence of phagocytosis inhibitors, scintillation remains at background levels, indicating that the signal changes can be used as a proxy for the kinetics of engulfment (7). When detergent is added to cultures at the end of experiments, the scintillation is reduced to almost zero, which demonstrates that the signal results from the presence of [³H]cholesterol in particle-proximal membranes (unpublished data).

The values represented by the dashed line in Fig. 1 were obtained with J774 cells that had been labeled overnight with liposomes containing [³H]cholesterol oleyl ether. Endocytosed cholesterol ether is stored specifically in lysosomes (10,13). The cultures were then supplemented with yttrium silicate beads, and scintillation

was measured as above. Compared to [^3H]cholesterol-labeled samples, the scintillation signal in [^3H]cholesterol ether-labeled cells at early time-points was significantly lower as little cholesterol ether is found at the cell surface (10). As would have been predicted, the rate of signal increase during the first 33 min was slower in [^3H]cholesterol ether-labeled cells (16.1 ± 1.5 cpm/nCi/h vs 32.7 ± 4.9 cpm/nCi/h), but scintillation continued to climb for much longer. As the data in Fig. 1 were corrected for total cellular radioactivity, the higher specific proximity scintillation in [^3H]cholesterol ether-labeled cells at later time-points can be partly explained by the notion that cholesterol ether accumulates predominantly in lysosomes (10), whereas cholesterol equilibrates across a much broader range of cellular pools (11).

In summary, the live-cell scintillation proximity assay provides a useful experimental tool for quantitative analyses of phagocytosis in living cells.

2 Materials

2.1 Cell Culture

1. J774A.1 macrophages (American Type Culture Collection, Manassas, VA; cat. no. TIB-67).
2. A 1:1 mixture of Dulbecco's modified Eagle's medium and Ham's F-12 medium (DMEM/F12, Mediatech, Herndon, VA, cat. no. 10-090-CV).
3. DMEM/F12 without phenol red (Mediatech, cat. no. 16-405-CV)
4. Fetal bovine serum (FBS) (Invitrogen, Carlsbad, CA).
5. A cocktail of penicillin and streptomycin sulfate (Mediatech, cat. no. 30-002-CI).
6. Medium A: DMEM/F12, 10% FBS, 100 U/mL penicillin, 100 $\mu\text{g}/\text{mL}$ streptomycin.
7. Medium B: Phenol red-free DMEM/F12, 10% FBS, 100 U/mL penicillin, 100 $\mu\text{g}/\text{mL}$ streptomycin.
8. Plastic 10-cm cell culture dishes (various manufacturers).
9. Trypsin ethylenediaminetetraacetic acid (EDTA) solution (Mediatech, cat. no. 25-052-CI).
10. Phosphate-buffered saline (PBS) (Mediatech, cat. no. 21-040-CM).
11. Tissue culture grade 1M HEPES-KOH at pH 7.4 (Mediatech, cat. no. 25-060-CI).

2.2 Liposomes

1. Egg yolk phosphatidylcholine (Sigma, St. Louis, MO; cat. no. 61751) is dissolved at 10 mM in a mixture of 95% chloroform and 5% methanol.
2. Bovine brain phosphatidylserine (Sigma, cat. no. 79406) is dissolved at 10 mM in chloroform/methanol (95:5).

3. Dicetyl phosphate (Sigma, D-2631) is dissolved at 4 mM in chloroform/methanol (95:5).
4. 1 mCi/mL (1 Ci = 37 GBq) [³H]cholesterol oleyl ester (GE Healthcare, Piscataway, NJ; cat. no. TRK886).
5. 1 mCi/ml [³H]cholesterol oleyl ether (GE Healthcare, cat. no. TRK888).
6. Water bath sonicator.

2.3 Scintillation Proximity Assay

1. Topcount NXT microplate scintillation counter equipped with two photomultipliers (Perkin Elmer, Wellesley, MA).
2. Yttrium silicate scintillating beads (GE Healthcare, cat. no. RPNQ0013).
3. Opaque white 24-well plates (Perkin Elmer, cat. no. 6005168).
4. Adhesive transparent plate covers (Perkin Elmer, cat. no. 6005198).
5. Beckman LS 6000 IC scintillation counter.
6. Liquid scintillation cocktail.
7. 20-mL scintillation vials.
8. Nonidet P-40 (Sigma, cat. no. NP40).
9. Bicinchoninic acid (BCA) protein assay reagent (Pierce Biotechnology, Rockford, IL).

3 Methods

3.1 Preparation of Liposomes

1. In a glass screw-cap tube, combine 20 μL of 10 mM phosphatidylcholine, 20 μL of 10 mM phosphatidylserine, 50 μL of 4 mM dicetyl phosphate, and 80 μL of 1 mCi/mL [³H]cholesterol oleyl ester (to label the plasma membrane) or [³H]cholesterol oleyl ether (to label lysosomes).
2. A slow current of nitrogen gas is directed into the tube through a 1-mL plastic pipet. Nitrogen-facilitated evaporation of the solvents should be performed in a fume hood. After evaporation of the solvents, the lipids will form a thin but visible film on the wall of the glass tube.
3. The lipid film is supplemented with 200 μL PBS, vigorously vortexed for 30 s, and sonicated for 2 min in a water bath sonicator. Vortexing and sonication are repeated two times. This will yield a liposome suspension containing 400 μCi/mL of tritiated lipid.
4. Suspensions can be stored at 4 °C in the dark for up to 4 wk but are sonicated again for 1 min before each additional use.

3.2 Culture of J774 Macrophages

1. J774 cells are grown in 10-cm dishes at 37 °C in an atmosphere of 8–9% CO₂ in medium A.
2. J774 cells adhere very strongly to the surface of culture dishes and are most easily trypsinated when grown to complete confluency.
3. Cultures should not be grown continuously for more than 3 mo before replacement with a fresh batch from frozen stocks.
4. J774 cultures should occasionally be tested for contamination with mycobacteria.

3.3 Proximity Scintillation Assay

1. On the evening of d 0, J774 cells are set up in 0.5 mL medium A in an opaque 24-well plate at a density of 5×10^5 cells per well (*see Note 1*).
2. Note that the white opaque microplates cited above exhibit phosphorescence after exposure to light. To reduce background during live scintillation counting, the plates should be stored in the dark and during experiments should be handled under low-light conditions (for an alternative culture vessel, *see Note 2*).
3. After 30 min at 37 °C, the cells have attached, and the medium is replaced with 0.5 mL per well of medium A containing 5 μL liposomes per milliliter medium. The resulting final concentration of tritiated lipids is 1 μCi per well per 0.5 mL medium (*see Note 3*).
4. On the morning of d 1, the medium is removed, cells are washed twice with PBS to remove the radioactive liposomes, and each well receives 0.5 mL fresh medium B.
5. The cells are incubated for another hour at 37 °C to allow for uptake of surface-bound liposomes and to chase all [³H]cholesterol ether into lysosomes or to complete hydrolysis of [³H]cholesterol ester and equilibration of [³H]cholesterol.
6. The plate is then placed on ice, the medium is removed, and each well receives 0.5 mL of an ice-cold suspension of 100 mg/mL yttrium silicate beads in medium B plus 50 mM HEPES-KOH. To ensure that each well receives the same amount of yttrium silicate, the suspension needs to be vortexed repeatedly while pipetting the 0.5-mL aliquots. At this point, the cells are kept in phenol red-free medium B to later prevent quenching of the scintillation signal. HEPES is added to help buffer the pH in the absence of CO₂ (*see Note 4*).
7. The plate is left on ice for 15 min to let the scintillant particles settle on top of the cell monolayer. This step helps synchronize the subsequent phagocytosis process. The plate should be protected from light to reduce background that might result from phosphorescence of the plate material.
8. The dish is then sealed with an adhesive plastic foil to reduce evaporation and to avoid contamination of the instrument during the subsequent counting phase.
9. After the yttrium silicate beads have settled, the plate is transferred to a Topcount NXT multiwell plate scintillation reader, and continuous scintillation

counting is started. Nuclide settings of the instrument control software are as follows: glass scintillator; low energy range; high-sensitivity efficiency mode; region A, 0–50; region B, 0–256. Wells are read for 30 s at a time. The instrument may be connected to a circulating water bath to control the temperature in the counting chamber (*see Note 5*).

10. After the final reading, the seal is removed, cells are washed three times with PBS, and the wash buffer is tested for contamination with radioactivity by liquid scintillation counting to control for washing efficiency.
11. After the final wash, the plates are sealed once more, and proximity scintillation is measured again to control for loss of cells during the washing procedure.
12. Finally, the cells are lysed by the addition of PBS containing 0.5% NP-40. To facilitate cell lysis, the plate is subjected to one freeze–thaw cycle, and lysates are transferred to microcentrifuge tubes. Particulate material containing the YSi beads and nuclei are spun down for 30 s at 16,000 *g* in a microcentrifuge. A 20- μ L aliquot of the supernatant is removed to determine total incorporated radioactivity by liquid scintillation counting, and a second 20- μ L aliquot is used to determine the protein concentration with BCA protein assay reagent.

3.4 Data Processing and Statistics

1. All conditions should be analyzed at least in triplicate wells.
2. Data generated by the Topcount NXT software can be loaded into Microsoft Excel for further analyses.
3. Scintillation counts should be corrected for total cellular radioactivity determined after proximity scintillation readings. In addition, the resulting values can be corrected for protein concentrations.
4. The data from triplicate wells can be graphed directly to illustrate the degree of scatter. Alternatively, for each round of counting, both time and scintillation counts are averaged and plotted with the standard deviation. Since the standard deviation tends to scale with the scintillation counts (7), statistical dispersion is best analyzed by calculating, for each graph point, the coefficient of variation (i.e., the quotient of the standard deviation divided by the mean); for a given trace, the overall dispersion may then be summarized by averaging all coefficients of variation and indicating their range (see legend to Fig. 1).

4 Notes

1. In addition to immortalized mouse J774 cells, we have successfully tested primary mouse peritoneal macrophages (7) and immortalized mouse HD1A macrophages (9).

2. Instead of using microplates, cells can be grown in standard glass scintillation vials that have previously been washed and autoclaved. Macrophages grow well on glass. Proximity scintillation readings are then done in a regular liquid scintillation counter using the tritium settings. This setup works well for single measurements, the vials are inexpensive, and the necessary equipment is available in most laboratory environments.
3. Scintillation readings with empty wells gave background values of about 50 cpm, whereas the protocol described above should produce readings between 500 and 2000 cpm (Fig. 1). From time to time, we found that experiments resulted in unusually low counts, making data difficult to interpret. In most cases, these problems could be solved either by preparing a new batch of liposomes or by thawing a fresh vial of cells.
4. In the experiments described above, cells were made radioactive first and then supplied with scintillant beads. The reverse approach is also possible. When studying the effects of pharmacological or genetic manipulations on phagosome maturation, it may be important to rule out effects on the uptake process. To analyze the effects of actin and calmodulin inhibitors on lysosome/phagosome targeting, we have added scintillant beads first and then supplied the cells with [³H]cholesterol ether-containing liposomes plus or minus the inhibitors (10). To verify that the inhibitors did not interfere with endocytosis of liposomes, a parallel set of wells was labeled with [³H]cholesterol ester and treated identically (10).
5. We initially did all proximity scintillation readings with the Topcount NXT microplate reader attached to a circulating water bath. However, liquid occasionally leaked into the instrument, necessitating extensive repairs. The problem was solved when it became apparent that the temperature in the counting chamber will reach 33 °C even in the absence of external control with the instrument at room temperature.

Acknowledgments This work was supported by funding from the Parseghian Medical Research Foundation and the National Institutes of Health (R01 DK59934).

References

1. Vieira, O.V., Botelho, R.J., and Grinstein, S. (2002) Phagosome maturation: aging gracefully *Biochem. J.* **366**, 689–704.
2. Ward, T.H., and Lippincott-Schwartz, J. (2006) The uses of green fluorescent protein in mammalian cells *Methods Biochem. Anal.* **47**, 305–337.
3. Giepmans, B.N., Adams, S.R., Ellisman, M.H., and Tsien, R.Y. (2006) The fluorescent toolbox for assessing protein location and function *Science* **312**, 217–224.
4. Ince, P.G. (2001) Random, chance, or hazard? *J. Clin. Pathol.* **54**, 254.
5. Udenfriend, S., Gerber, L., and Nelson, N. (1987) Scintillation proximity assay: a sensitive and continuous isotopic method for monitoring ligand/receptor and antigen/antibody interactions *Anal. Biochem.* **161**, 494–500.
6. Berry, J., and Price-Jones, M. (2005) Measurement of radioligand binding by scintillation proximity assay *Methods Mol. Biol.* **306**, 121–137.

7. Stockinger, W., Castoreno, A.B., Wang, Y., Pagnon, J.C., and Nohturfft, A. (2004) Real-time analysis of endosomal lipid transport by live cell scintillation proximity assay *J. Lipid Res.* **45**, 2151–2158.
8. Wu, S., and Liu, B. (2005) Application of scintillation proximity assay in drug discovery *BioDrugs* **19**, 383–392.
9. Castoreno, A.B., Wang, Y., Stockinger, W., et al. (2005) From the cover: Transcriptional regulation of phagocytosis-induced membrane biogenesis by sterol regulatory element binding proteins *Proc. Natl. Acad. Sci. U. S. A.* **102**, 13129–13134.
10. Stockinger, W., Zhang, S.C., Trivedi, V., et al. (2006) Differential requirements for actin polymerization, calmodulin, and Ca²⁺ define distinct stages of lysosome/phagosome targeting *Mol. Biol. Cell* **17**, 1697–1710.
11. Liscum, L., and Munn, N.J. (1999) Intracellular cholesterol transport. *Biochim. Biophys. Acta* **1438**, 19–37.
12. Voelker, D.R. (2002) In: *Biochemistry of lipids, lipoproteins and membranes*, 4th ed. (Vance, D. E., and Vance, J. E., Eds.), Elsevier, New York, pp. 449–82.
13. Stein, Y., Halperin, G., and Stein, O. (1980) Biological stability of [³H]cholesteryl oleyl ether in cultured fibroblasts and intact rat. *FEBS Lett.* **111**, 104–106.

12

Transcytosis of Polymeric Immunoglobulin A in Polarized Madin–Darby Canine Kidney Cells

Asli Oztan, Christine Rondanino, and Gerard Apodaca

1	Introduction.....	157
2	Materials	159
3	Methods.....	162
4	Notes	168
	References.....	170

Summary The transcytotic pathway allows for the bidirectional transport of endocytosed solutes, lipids, and proteins between the two membrane domains of polarized epithelial cells while maintaining the functional integrity of the epithelial tissue. A method is described to measure basolateral-to-apical transcytosis of immunoglobulin A (IgA) in polarized Madin–Darby canine kidney (MDCK) cells expressing the polymeric immunoglobulin receptor (pIgR). The cells are grown on porous Transwell filter supports, and radiolabeled ^{125}I -immunoglobulin A (IgA) is internalized from the basolateral pole of MDCK cells. During a subsequent 2-h chase, the amount of ^{125}I -IgA that is recycled, degraded, or transcytosed is quantified. This assay can be adapted to follow the postendocytic fate of other ^{125}I -labeled ligands and proteins.

Keywords Apical; basolateral; immunoglobulin A (IgA); iodination; polarized Madin–Darby canine kidney (MDCK) cells; polymeric immunoglobulin receptor (pIgR); transcytosis.

1 Introduction

Epithelial tissues are comprised of sheets of adherent cells that cover surfaces, line cavities, and form glands. They establish a selective barrier that modulates the exchange of ions, solutes, and macromolecules between a contacting

basolateral surface that is bound by cell–cell and cell–matrix interactions and a free apical surface that faces the extracellular milieu. In addition to pathways that allow for direct transport of newly synthesized cargo from the *trans*-Golgi network to either apical or basolateral plasma membrane domain, epithelial cells also have a characteristic pathway called *transcytosis*. This key process is universally found in all epithelial cells examined and allows for the transport of endocytosed proteins, lipids, and solutes from one pole of the epithelial cell to the other while maintaining the epithelial barrier (1). In some epithelial cells, such as hepatocytes, transcytosis is the predominant route for membrane proteins to reach the apical cell surface (2,3).

A well-studied example of transcytosis is the transport of immunoglobulin A (IgA) across various mucosae (4). IgA is the principal class of immunoglobulin found in the mucosal secretions of the gut, respiratory and urogenital tracts, and exocrine gland secretions (e.g., milk, saliva, and tears). Dimers of IgA are produced by submucosal plasma cells. Following secretion, IgA binds to the polymeric immunoglobulin receptor (pIgR), which is located on the basolateral surface of the epithelial cells that form the mucosa. The pIgR–IgA complex is then endocytosed, transported through a series of endosomal compartments (described below), and then on arrival at the apical membrane the extracellular domain of the pIgR is proteolytically cleaved, releasing it and bound ligand into the secretions. The cleaved extracellular domain of the pIgR is known as the secretory component. Once in secretions, IgA forms the first specific immunologic defense against infection (reviewed in *Ref. 5*).

The intracellular pathway for transcytosis of pIgR–IgA complexes has been extensively studied in polarized Madin–Darby canine kidney (MDCK) cells transfected with rabbit pIgR complementary deoxyribonucleic acid (cDNA). Our current understanding of the transcytosis pathway is shown in [Fig. 1](#). Transcytosing proteins such as IgA and its receptor pIgR are endocytosed and delivered to the basolateral early endosomes (BEEs) (step 1). The pIgR–IgA complexes are subsequently transported to common endosomes (CEs; step 2), then to Rab11-positive apical recycling endosome (ARE; step 3) (6,7), and finally to the apical surface (step 4), where proteolytic processing occurs.

We describe here a method to measure basolateral-to-apical IgA transcytosis in polarized MDCK cells expressing the rabbit pIgR. For this assay, MDCK cells are grown on porous filter supports to form well-polarized monolayers with tight junctions. IgA is radiolabeled with ^{125}I to allow for its sensitive detection and quantification. The ^{125}I -IgA is internalized from the basolateral pole of MDCK cells, and the cells are then washed with ligand-free medium to allow nonadherent ligand to dissociate from the cell surface pIgR. During a subsequent 2-h chase, the amount of ^{125}I -IgA released at the apical (transcytosed) or basolateral (recycled) pole of the cell is quantified with a gamma-counter. The amount of degraded ^{125}I -IgA is measured upon trichloroacetic acid (TCA) precipitation. This assay can be easily adapted to follow the postendocytic fate of other ^{125}I -labeled ligands, proteins, and antibodies.

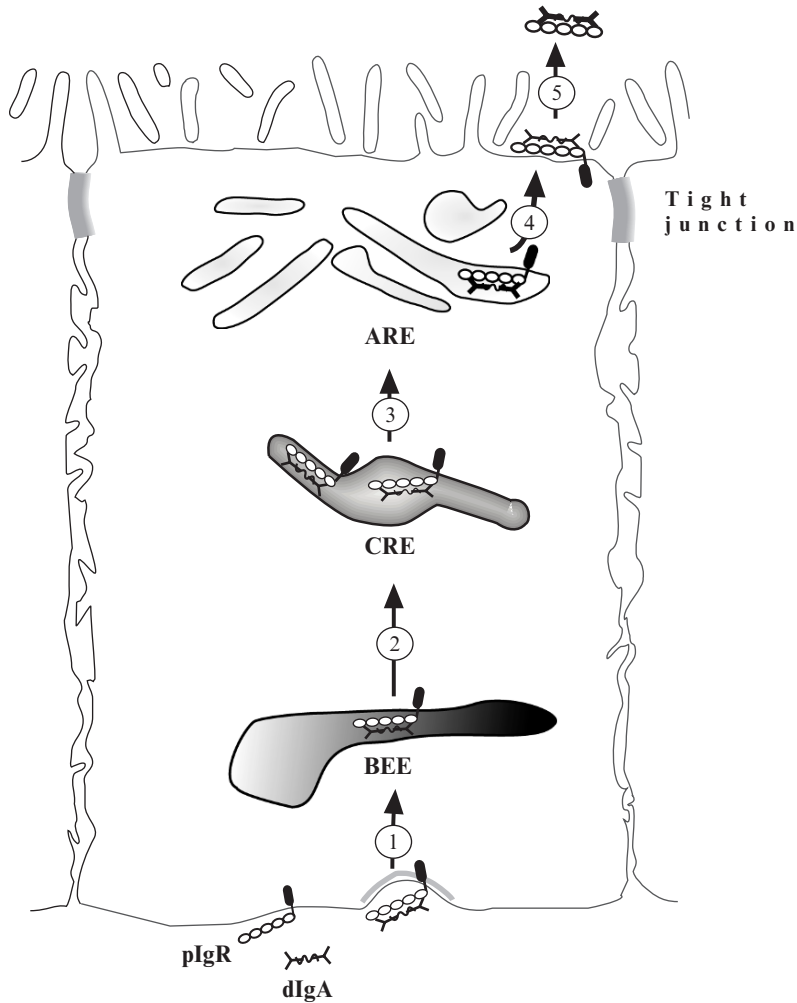


Fig. 1 Transcytosis of pIgR and its dimeric IgA (dIgA) ligand in polarized MDCK cells. The pIgR binds dIgA at the basolateral surface of the cell and is rapidly endocytosed via clathrin-coated pits (step 1). On entry in basolateral early endosomes (BEEs), pIgR–dIgA is delivered to the common recycling endosomes (CRE; step 2) and then to apical recycling endosomes (AREs; step 3). On exocytosis at the apical pole of the cell (step 4), a proteinase cleaves the extracellular domain of the receptor, releasing it and its ligand into the apical secretions (step 5).

2 Materials

2.1 Iodination

1. D-Salt cellulose plastic desalting column: column containing 2 mL of preswollen, beaded 12% cellulose; exclusion limit 5000 MW (Pierce, Rockford, IL).

- Phosphate-buffered saline (PBS, 10X): Prepare 10X stock with 1.37 M NaCl, 27 mM KCl, 80.6 mM Na_2HPO_4 , 14.7 mM KH_2PO_4 . Store at room temperature. Prepare working solution by diluting one part stock with nine parts water. The pH of 1X PBS is 7.4.
- PBS/bovine serum albumin (BSA): 1% (w/v) BSA in 1X PBS buffer. Prepare fresh.
- Human polymeric IgA (see Note 1). For long-term storage, keep at -80°C . For short-term storage (<6 mo), keep at 4°C .
- 1 M Tris-HCl, pH 8.0. Store at room temperature.
- 2 M NaCl. Prepare fresh.
- Iodine monochloride (ICl) (8,9): The preparation of ICl should be carried out in a fume hood. Because ICl is a corrosive chemical, gloves and a lab coat should be worn during preparation. Dissolve 0.15 g solid NaI in 8 mL 6N HCl. Next, forcibly inject 2 mL NaIO_3 (49.5 mg/mL in H_2O) into the NaI solution using a 5-mL syringe fitted with a 20-gage needle (see Note 2). Bring the solution up to 40 mL with water and place in a clean separatory funnel. Add 10 mL CCl_4 to the mixture and shake vigorously (see Note 3). Carbon tetrachloride is a carcinogen: Avoid breathing vapors or skin contact. Discard the lower pink organic phase and repeat the extraction with CCl_4 until the organic phase is colorless. Transfer the extracted aqueous layer to a clean Erlenmeyer flask and aerate with moist air for 8–10 h to remove any trace of CCl_4 from the aqueous phase (see Fig. 2). Prepare 0.5-mL aliquots and store away from light at -20°C . The solution is stable for several years at -20°C .
- Na^{125}I (350 mCi/mL, 17.4 Ci/mg) supplied by PerkinElmer (Boston, MA). Na^{125}I is a volatile radioactive compound that should be handled in a certified fume hood. Store megacurie quantities of ^{125}I in lead pigs either at room temperature or at 4°C . If necessary, the lead pigs can be further surrounded by 3-mm thick lead sheeting.
- NaI/PBS/BSA: Dissolve NaI (5 mg/mL) in PBS/BSA. This solution can be aliquoted and stored at -20°C .

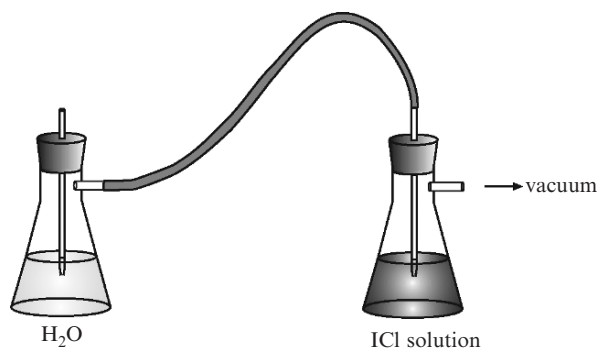


Fig. 2 Apparatus to aerate the ICl solution with moist air. The first flask contains distilled water, and the vacuum draws moist air into the second flask, which contains the ICl solution.

2.2 Cell Culture

1. MDCK type II cells expressing the pIgR (10). An MDCK tet-off cell line that expresses the pIgR is available from Clontech (cat. no. 630913, Clontech, Mountain View, CA).
2. Complete minimum essential medium (MEM): MEM with Earle's salts and L-glutamine (MEM; Cellgro[®], Mediatech, Herndon, VA) supplemented with 10% fetal bovine serum (FBS; HyClone; Logan, UT) and 1% antibiotic-antimycotic (100 U/mL penicillin G sodium, 100 μ g/mL streptomycin sulfate, and 250 ng/mL amphotericin B as Fungizone[®]; Gibco-Invitrogen; Grand Island, NY).
3. Sterile PBS (Gibco-Invitrogen).
4. Trypsin/ethylenediaminetetraacetic acid (EDTA): 0.25% (w/v) trypsin with 1 mM EDTA (Gibco-Invitrogen).
5. Freezing medium: 10% (v/v) dimethyl sulfoxide (DMSO) and 90% (v/v) FBS.
6. 70% (v/v) ethanol.
7. Transwells Costar[®], 12-mm diameter, 0.4- μ m pore size (Corning, Corning, NY).

2.3 Postendocytic Fate of Basolaterally Internalized ¹²⁵I-IgA

1. MEM/BSA (see Note 4): In a 1-L beaker, add 20 mL 1 M HEPES-NaOH, pH 7.6, 10 mL penicillin/streptomycin (10,000 U/mL penicillin G, sodium salt, and 10,000 μ g/mL streptomycin sulfate; Gibco-Invitrogen) to 900 mL of water. Add 10.7 g MEM with Hanks' salts, L-glutamine, and nonessential amino acids and without sodium bicarbonate (cat. no. M1018-10X1L, Sigma-Aldrich, St. Louis, MO); 1.4 g sodium bicarbonate; and 24 g BSA. Adjust to pH 7.4 (using either HCl or NaOH) and store at -20 °C in clean, autoclaved bottles. Thaw prior to use. It is important to swirl the bottles to disperse the components after thawing the medium. Thawed MEM/BSA is stable at 4 °C for approx 1 wk.
2. Tissue culture plates: 12-well, flat-bottom Falcon[®] (Becton Dickinson, Franklin Lakes, NJ).
3. ¹²⁵I-IgA (see Subheading 3.1.): ¹²⁵I-IgA is stored at 4 °C in a leaded pig. It is stable for approx 1 mo.
4. Collection tubes: 1.2-mL polypropylene microdilution tubes with conical bottom (USA Scientific, Ocala, FL).
5. PBS⁺: In 100 mL ice-cold 10X PBS (see Subheading 2.1.2.), add 0.1 g anhydrous CaCl₂ and 0.1 g MgCl₂•6H₂O. Bring up to 1 L with ice-cold water and stir to dissolve. Store at 4 °C.

2.4 Trichloroacetic Acid Precipitation

1. TCA: 100% (w/v) in water (Sigma). TCA is very caustic; handle with gloves in a ventilated enclosure. Store at 4 °C.

2. 12 × 75 mm polypropylene test tubes and 12-mm natural hollow top caps (Fisher Scientific, Pittsburgh, PA).
3. Fisherbrand corks (cat. no. 07782B, Fisher Scientific).

3 Methods

In this assay, iodinated polymeric IgA is internalized from the basolateral surface of polarized MDCK cells cultured on Transwell filter supports, and the percentage of internalized ligand that is recycled, degraded, or transcytosed is quantified. Efficient IgA transcytosis requires recently iodinated IgA (<4 wk old) and freshly thawed MDCK cells that are not more than 2 wk old. The same method can be modified to study the postendocytic traffic of other apically or basolaterally internalized ligands, including those that recycle at the cell surface or those that are targeted to lysosomes and degraded.

3.1 Iodination

1. Remove top and bottom caps of desalting column and then secure column in a vise clamp. Place a waste container under the column to catch the eluant. Wash the column four times by filling the column buffer reservoir with PBS/BSA and allowing the eluant to flow through the column by gravity. At the end of the final wash, allow the buffer reservoir to empty and the eluant to completely enter the column (*see Note 5*).
2. All the reagents required for the iodination reaction are prepared on ice. Three 1.5-mL Eppendorf tubes are labeled as “ligand,” “reaction,” and “waste” and then inserted into a container containing approx 4 inches of ice. One 2-mL screw-cap tube, which is used to hold the final iodinated IgA ligand product, is similarly placed on ice.
3. Place 25–50 µg polymeric IgA in the tube labeled “ligand.” The total volume of ligand should not exceed 10–20 µL for an efficient iodination reaction. Keep the ligand on ice.
4. Add 100 µL Tris-HCl (pH 8.0) to the tube labeled “reaction.” Place the ice container with labeled tubes in a fume hood. The hood is typically certified to perform iodination reactions. The investigator should wear a protective lab coat and lead apron, eyewear (e.g., goggles), and a double pair of gloves in the following steps. A Geiger counter with scintillation probe is useful for monitoring the dose of radiation and potential contamination. Lead foil or lead-impregnated Plexiglass can be used to further shield the investigator from the ¹²⁵I.
5. Prepare a 1:100 dilution of ICl reagent in 2 M NaCl and then add 20 µL of the diluted ICl/NaCl reagent to the “reaction” tube containing 100-µL Tris-HCl (pH 8.0). The contents should be mixed by titration and then placed on ice.

6. Add 4 μL Na^{125}I ($\sim 1.4 \text{ mCi}$) to the “reaction” tube, mix by titration, and incubate the reaction for 1 min (*see Note 6*). At the end of the 1-min incubation, transfer the IgA ligand to the “reaction” tube. Mix gently by titration and incubate for 10 min on ice.
7. At the end of the 10-min incubation, stop the reaction by adding 100 μL NaI /PBS/BSA to the “reaction” tube.
8. Carefully transfer the iodination mixture from the “reaction” tube and place on the surface of the washed desalting column. Once the iodination mixture has entered the column, wash the column by adding 300 μL PBS/BSA to the column bed. Collect any eluant in the tube labeled “waste.” This initial eluant usually contains little iodinated ligand (this can be confirmed with the Geiger counter) and can be discarded.
9. Replace the “waste” tube with the screw-cap tube (with cap removed) and collect the ^{125}I -IgA by eluting the column with an additional 600 μL PBS/BSA.
10. Gently mix the tube containing ^{125}I -IgA to disperse the ligand equally in the eluant and then count a 1- μL aliquot in a γ -counter. A typical reaction contains 500,000 to 1 million counts per minute ^{125}I -IgA/ μL reaction (*see Note 7*). Store iodinated ligand at 4 $^{\circ}\text{C}$ for no longer than 4 wk.

3.2 Cell Culture

1. We use MDCK type II cells expressing the wild-type rabbit pIgR (10). Cells are maintained in complete MEM in a 37 $^{\circ}\text{C}$ tissue culture incubator with 5% CO_2 /95% air. We routinely culture cells in 10-cm diameter tissue culture-treated dishes, but flasks are an acceptable alternative.
2. Cell passaging: The medium is aspirated from a confluent 10-cm dish of cells, and the cells are washed with 10 mL warm (37 $^{\circ}\text{C}$) PBS. The PBS is aspirated, 2 mL trypsin are added, and the cells are incubated at 37 $^{\circ}\text{C}$ in the tissue culture incubator until the cells detach from the plate (*see Note 8*). When the cells detach from the plate, 8 mL complete MEM is added, and the cells are resuspended by titration using a 10-mL pipet until there are no visible cell clumps remaining. For routine passaging, 1 mL of cell suspension is added to a 10-cm dish containing 9 mL complete MEM (1:10 dilution). The cells take approx 4–5 d to reach confluence (*see Note 9*).
3. Freezing and thawing cells: To freeze cells, a confluent dish of MDCK cells is trypsinized, the cells are resuspended in 8 mL complete MEM, and the cells are then recovered by centrifugation at 100 g for 5 min at room temperature. Following aspiration of the medium, the cells are carefully resuspended by titration in 1.5 mL warm (37 $^{\circ}\text{C}$) freezing medium. Aliquots (0.5 mL) of the cell suspension are placed in freezing vials, capped, and then placed in a room temperature Styrofoam container. The Styrofoam container is placed in a -70°C freezer. The cells are stable at -70°C for some time but can be transferred after 2–3 d to liquid nitrogen for extended storage. Cells are thawed by partially

immersing the cell vial containing the frozen cells in a 37 °C water bath. The cell vial is removed from the water bath, dried, rinsed with ethanol, and the cap removed in a cell culture hood. The thawed cell suspension is transferred to a 10-cm dish, and 10 mL complete MEM are slowly added to the cells. To minimize osmotic shock, the first 2 mL of MEM should be added at a rate of approx 1 mL/min. The next day, the medium is aspirated and replaced with 10 mL complete MEM. The cells typically achieve confluence by the second day of thawing. To maintain a high level of pIgR expression, new cells are thawed every 2 wk.

4. Plating cells on Transwell filters: A confluent dish of MDCK cells is trypsinized, and the cells are resuspended in 10 mL complete MEM. The cells are then recovered by centrifugation at 100 *g* for 5 min at room temperature. The trypsin-containing medium is aspirated, and the cell pellet is resuspended in 12 mL complete MEM (see **Note 10**). Place 0.5 mL cell suspension (containing $\sim 1 \times 10^6$ cells) into the apical chamber of each 12-mm Transwell. Add 2 mL complete MEM to the well that faces the basolateral surface of the Transwell unit. The cells typically form a tight, polarized monolayer by 3 d postplating (see **Note 11**). After the third day, the cells are fed daily by aspirating the basolateral, then apical medium and adding 0.5 mL complete MEM to the apical chamber and then 1.5 mL medium to the basolateral chamber. The order of medium aspiration and addition is important to prevent hydrostatic pressure-induced cell damage. Cells are typically used 3–4 d postplating on the Transwell units.

3.3 Postendocytic Fate of Basolaterally Internalized ¹²⁵I-IgA

1. Prepare a 37 °C circulating water bath (**Fig. 3**). We use a 30.5 × 50.8 × 21.6 cm (width × length × height) bath with temperature regulator/circulator (VWR, West Chester, PA). A 22.5 × 26 cm aluminum plate is placed on top of test tube racks, and the water in the bath is adjusted so that the aluminum plate is covered by approx 5 mm H₂O.
2. Place MEM/BSA in the water bath and warm to 37 °C. Label a total of eleven 1.2-mL collection tubes for each Transwell filter: tubes for apical medium collected at 7.5, 15, 30, 60, 120 min; tubes for basolateral medium collected at 7.5, 15, 30, 60, 120 min; and a tube for the filter, which is cut out at the end of the experiment.
3. Place 500 μL MEM/BSA into the wells of a 12-well plate. You will need 5 wells of MEM/BSA for each individual Transwell filter (one for each of five time-points). Perform each experimental treatment group in triplicate or quadruplicate. If performing multiple treatment groups, it is easier to use a separate 12-well plate for each time-point. Place the 12-well plates containing MEM/BSA atop the aluminum plate in the water bath to keep them warm before sample collection starts.
4. Prepare a humid labeling chamber by placing a piece of moistened filter paper in a storage container with a removable lid. A sheet of Parafilm is cut and placed

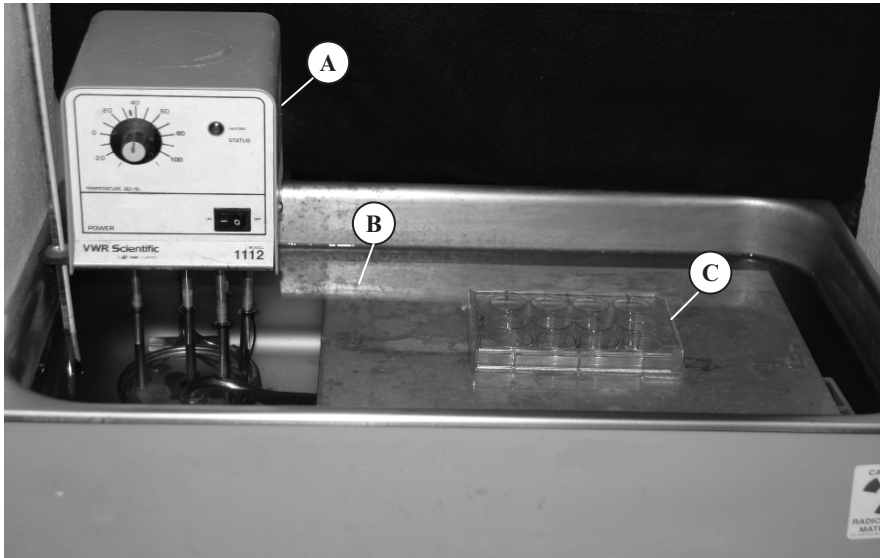


Fig. 3 Water bath used to perform the postendocytic fate assay. The water bath is equipped with a temperature regulator/circulator (A). A 22.5 × 26 cm aluminum plate (B) is placed on top of test tube racks, and the water in the bath is adjusted so that the aluminum plate is covered by approx 5 mm H₂O. A 12-well plate containing Transwell filters (C) is placed on top of the aluminum plate.

on top of the moistened filter paper. For each filter, dilute 3–4 μL ¹²⁵I-IgA in 27 μL MEM/BSA and place the drop of diluted ¹²⁵I-IgA on the sheet of Parafilm, avoiding air bubbles. Close the chamber and place it in the water bath to keep it at 37 °C.

5. Wash the Transwell-grown MDCK cells with warm MEM/BSA two times to remove the cell culture medium. Washing is accomplished by transferring Transwells to a 12-well dish, aspirating the medium (basolateral first, then apical), and then adding 1 mL MEM/BSA to the apical and then basolateral chambers of the Transwell. Following washing, the MEM/BSA is aspirated, and 300 μL MEM/BSA are added to the apical chamber of the Transwell. A Kimwipe is used to carefully remove any MEM/BSA adhering to the rim of plastic surrounding the porous filter on the basolateral side of the Transwell. The Transwell filter is placed on the 30- μL drop of ¹²⁵I-IgA in the humid labeling chamber (*see Note 12*) and pulse labeled for 10 min at 37 °C. Lead foil can be placed over the labeling chamber to shield the investigator during this incubation.
6. Next, remove unbound ligand by washing. Return the Transwell filters to a 12-well plate and add 1 mL MEM/BSA to the basolateral surface of each Transwell filter. Remove the basolateral medium by aspiration. Wash the basolateral surface an additional two times (*see Note 13*). Discard the MEM/BSA wash liquid generated in this and subsequent steps in suitable radioactive waste disposal

containers. Aspirate any remaining apical and basolateral media and then add 1 mL MEM/BSA to the apical and then basolateral chamber of each Transwell. Place the 12-well plate containing Transwells in the 37 °C water bath. Incubate the cells for 3 min to allow for nonspecifically bound ligand to dissociate from the filter and for cell surface ligand to be internalized and “chased” into the cells. The total wash and chase should take 5 min to complete. During the chase, discard the sheet of Parafilm containing residual ¹²⁵I-IgA (in step 4) in a suitable radioactive waste container.

7. At the end of the 3-min chase, aspirate the medium from both sides of the filter and add 500 μL MEM/BSA to the apical chamber. Place the filters in the 12-well plates containing MEM/BSA prepared in step 3. Start a timer as the filters are placed in the wells of MEM/BSA.
8. After 7.5 min, begin collecting samples. Lift an individual Transwell from the 12-well plate, quickly recover the apical medium using a 1-mL pipetor tip (taking care not to puncture the Transwell filter), and transfer the contents to the labeled 1.2-mL collection tubes prepared in step 2 (these are the 7.5-min apical samples). Eject the tip and use a new tip to gently transfer 500 μL MEM/BSA to the apical chamber of the Transwell. Place the same Transwell in a new well containing 500 μL MEM. Repeat the process for all Transwells in the experiment (*see Note 14*). After all of the Transwells are transferred to new wells, collect the MEM/BSA from the basal wells of the previous time-point and place in the 1.2-mL collection tubes (these are the 7.5-min basolateral samples).
9. Repeat the collection process described in step 8 at 15, 30, 60, and 120 min. At the end of 120-min chase period, you will have five apical samples (7.5, 15, 30, 60, 120 min) and five basolateral samples (7.5, 15, 30, 60, 120 min) for each Transwell filter. Finally, wash the filter and associated cells with ice-cold PBS⁺ two times to remove MEM/BSA, cut the filter from its holder using a scalpel, and place the filter into a 1.2-mL counting tube (this is the cell-associated IgA fraction for each sample).

3.4 Trichloroacetic Acid Precipitation

1. Place the collection tubes containing medium from Subheading 3.3., step 9 on ice. Add 50 μL TCA to each tube. Vortex each tube for 15 s to thoroughly mix the sample. The TCA will precipitate intact ¹²⁵I-IgA ligand but not degraded fragments of ¹²⁵I-IgA released from the cell into the culture medium (*see Note 15*).
2. Incubate samples on ice for 30–45 min and centrifuge the samples in a microfuge at 14,000 g for 10 min at 4 °C (*see Note 16*).
3. The collection tubes are placed in a rack, and the supernatant is carefully removed using a 3-mL syringe fitted with a 22-gage needle. The pellets are retained as these contain the undegraded ¹²⁵I-IgA. If quantifying the total amount of degraded ¹²⁵I-IgA, then pool all of the basolateral and apical supernatants for each Transwell in 12 × 75 mm polypropylene test tubes. If the aim is to measure

the kinetics of degradation, then place the supernatant of each apical and basolateral time-point into separate collection tubes. Cap all collection tubes (containing pellets, supernatants, or filter) with a cork stopper.

- Place the samples in a γ -counter and count the ^{125}I associated with the filter (cell-associated IgA), apical TCA pellets (transcytosed IgA), basolateral TCA pellets (recycled IgA), and the TCA supernatants of the apical and basolateral samples (degraded IgA).

3.5 Calculation of Data

- For each Transwell, sum the total counts per minute associated with the filter, apical and basolateral TCA pellets, and the apical and basolateral TCA supernatants (Table 1). This is the total ligand that was retained by the cell during the pulse-chase labeling protocol.
- For each Transwell, calculate the percentage of total ligand associated with the filter, the apical and basolateral TCA pellets for each time-point, and the pooled apical and basolateral TCA supernatants (Table 1). If examining the kinetics of degradation, then calculate the individual percentages associated with the TCA supernatant for each time-point.
- Calculate a running sum of percentages for the apical TCA pellets (transcytosis) and then for the basolateral TCA pellets (recycling) (Table 1). If examining the kinetics of degradation, then also calculate the running sum of the apical and basolateral TCA supernatants.
- Calculate the averages and standard deviation for each experimental treatment and plot the data using a graphing program such as Excel or Prism (Fig. 4).

Table 1 Representative Calculation for Quantifying the Fate of Basolaterally Internalized ^{125}I -IgA in a Single Transwell of Polarized MDCK Cells Expressing the pIgR

	Sample	Count	Percentage	Running Percentage
Apical Pellet	7.5 min	2039.0	24.6	24.6
	15 min	1525.0	18.4	43.0
	30 min	1221.0	14.7	57.7
	60 min	859.0	10.3	68.0
	120 min	341.0	4.1	72.1
Basolateral Pellet	7.5 min	363.0	4.4	4.4
	15 min	273.0	4.4	4.4
	30 min	227.0	2.7	10.4
	60 min	375.0	4.5	14.9
	120 min	93.0	1.1	16.1
Filter		249.0	3.0	(Cell Associated)
Apical Supernatant		131.0	1.6	(Degraded, Apical)
Basal Supernatant		605.0	7.6	(Degraded, Basal)
Total		8301.0		

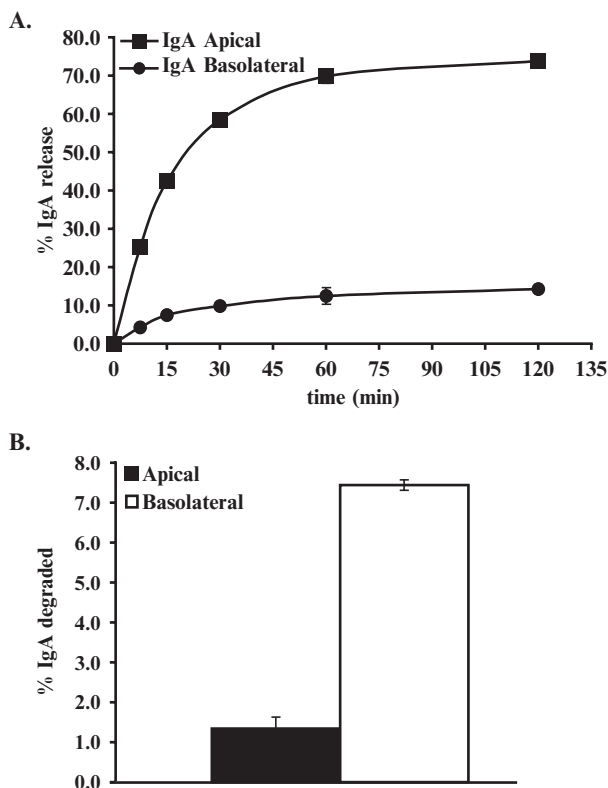


Fig. 4 Postendocytic fate of basolaterally internalized IgA in polarized MDCK cells expressing pIgR. ^{125}I -IgA was internalized from the basolateral surface of the cells for 10 min at 37°C , the cells were washed, and the cells were chased in the absence of ligand for 120 min. **(A)** The percentages of total ligand released basolaterally (recycled) and apically (transcytosed) is shown. **(B)** The percentage of degraded ligand released apically or basolaterally is shown.

4 Notes

1. The pIgR does not bind to monomeric IgA, such as that found in serum; instead, it binds to polymeric IgA complexed with J chain. Dimeric, trimeric, and tetrameric IgAs are all transcytosed with comparable efficiencies (11). We used IgA prepared by Dr. J.P. Vaerman, Catholic University of Louvain, Brussels, Belgium; however, he has since retired. An alternative source of polymeric IgA is to purify it from hybridoma supernatants (12).
2. It is very important that you rapidly and forcibly inject the NaIO_3 into the NaI solution. After mixing, there should be no precipitate, and the resulting liquid should be a clear light yellow solution. Discard any preparation that is not a clear yellow solution.
3. CCl_4 is added to extract the unreacted I_2 . After the initial extraction, a biphasic solution forms; the top layer contains ICl and has a clear yellow color, whereas

the lower CCl_4 layer is pink. Depending on the amount of I_2 , it will take at least two to four extractions to generate a clear CCl_4 layer.

4. MEM/BSA contains a tenth the amount of bicarbonate found in standard culture medium. It is buffered with HEPES to maintain a physiological pH; MEM/BSA is not intended for use inside of a cell culture incubator that is gassed with CO_2 . MEM/BSA shelf life at 4°C is largely limited by how rapidly it becomes contaminated with microbes. Contamination is apparent when the solution becomes turbid or changes to a yellow color (a result of acidification). The addition of penicillin/streptomycin is intended to suppress bacterial growth, but the antibiotics can be omitted if needed.
5. The column contains a white permeable fret above the cellulose matrix that prevents the column from running dry. It also prevents the matrix from disturbance when loading the column with sample. The void volume of the column is approx 0.7 mL.
6. In this step, the Na^{125}I is oxidized to $^{125}\text{I}_2$ (molecular iodine) in preparation for the iodination reaction. This step is time sensitive and should be accurately timed. Because reduction occurs prior to the addition of ligand, the ICI method works for a broad range of proteins (e.g., IgA, IgGs, transferrin, and recombinant proteins) and ligands, such as low-density lipoproteins that are sensitive to oxidation.
7. If the reaction is less than 100,000–200,000 cpm/ μL , it is usually considered poor and is discarded. In a typical reaction, more than 99% of the recovered iodinated products are TCA precipitable, indicating that there is little free iodine in the final eluate. This test can be performed by adding 1 μL eluate to 0.5 mL MEM/BSA, adding TCA to 10% (v/v), incubating for 30 min on ice, centrifuging for 15 min at 4°C , and counting the resulting supernatant and pellet (see Subheading 3.4. for additional details).
8. Trypsinization usually takes 10–30 min and depends on how long the cells have been cultured on the dish. An easy way to test if the trypsinization reaction is complete is to rock the dish slowly back and forth. When the cells are trypsinized, they readily come off the dish and enter the moving fluid phase. Do not overtrypsinize the cells as this can lead to cell death.
9. The cell dilution affects the time it takes for the cells to become confluent. At a dilution of 1:2, the cells will become confluent overnight. When diluted 1:5, the cells take approx 3 d to reach confluence. At 1:20, the cells take approx 7–8 d to reach confluence.
10. It is important to make sure the cell pellet is completely resuspended to ensure proper monolayer formation. Improper resuspension or plating too many cells results in cells that adhere to the apical surface of the monolayer or stratification.
11. The formation of a tight monolayer can be assessed by monitoring the transepithelial resistance across the monolayer using an Epithelial Volt Ohm Meter (EVOM) (Warner Instruments, Hamden, CT). A Transwell lacking cells but otherwise incubated in complete MEM medium is used to correct for series resistance. Although there is some variation between clones, type II MDCK cells typically achieve a transepithelial resistance of 110–150 $\text{ohm}\cdot\text{cm}^2$.
12. It is important to avoid air bubbles during the pulse-labeling step. This can be accomplished by first touching the edge of the Transwell near the edge of the drop and then slowly releasing the Transwell onto the drop of ligand.

13. The washing step is crucial to the success of the experiment. The initial three washes should take approx 2 min to complete. If these washes are performed too rapidly or with insufficient MEM/BSA, there will be a large pool of loosely adherent ligand that dissociates from the plastic associated with the Transwell cup and filter.
14. It is important to be rhythmic when collecting the samples. A useful strategy is to stagger the collection of each sample by approx 10–15 s.
15. Degraded iodinated peptides are membrane permeable and diffuse from the cell into the MEM/BSA. We have found that the majority of cell-associated ligand remaining in the filter at the end of the experiment is TCA precipitable, so we do not routinely perform TCA precipitation of the filter-associated cells.
16. We place the counting tubes in 1.5-mL Eppendorf tubes with their caps removed. The Eppendorf tube containing the counting tube is then placed in a microfuge for centrifugation.

Acknowledgments This work was supported by an American Heart Association Predoctoral Fellowship to A.O. and an American Heart Association Postdoctoral Fellowship to C.R. and by grants from the National Institutes of Health to G.A. (RO1-DK59170 and R37-DK54425).

References

1. Apodaca, G., Bomsel, M., Arden, J., Breitfeld, P.P., Tang, K., and Mostov, K.E. (1991) The polymeric immunoglobulin receptor. A model protein to study transcytosis. *J. Clin. Invest.* **87**, 1877–1882.
2. Bartles, J.R., Feracci, H.M., Stieger, B., and Hubbard, A.L. (1987) Biogenesis of the rat hepatocyte plasma membrane in vivo: comparison of the pathways taken by apical and basolateral proteins using subcellular fractionation. *J. Cell. Biol.* **105**, 1241–1251.
3. Mostov, K.E. (1994) Transepithelial transport of immunoglobulins. *Annu. Rev. Immunol.* **12**, 63–84.
4. Childers, N.K., Bruce, M.G., and McGhee, J.R. (1989) Molecular mechanisms of immunoglobulin A defense. *Annu. Rev. Microbiol.* **43**, 503–36.
5. Rojas, R., and Apodaca, G. (2002) Immunoglobulin transport across polarized epithelial cells. *Nat. Rev. Mol. Cell Biol.* **3**, 944–955.
6. Apodaca, G., Katz, L.A., and Mostov, K.E. (1994) Receptor-mediated transcytosis of IgA in MDCK cells is via apical recycling endosomes. *J. Cell. Biol.* **125**, 67–86.
7. Leung, S.M., Ruiz, W.G., and Apodaca, G. (2000) Sorting of membrane and fluid at the apical pole of polarized Madin–Darby canine kidney cells. *Mol. Biol. Cell* **11**, 2131–2150.
8. McFarlane, A.S. (1958) Efficient trace-labelling of proteins with iodine. *Nature* **182**, 53.
9. Helmkamp, R.W., Goodland, R.L., Bale, W.F., Spar, I.L., and Mutschler, L.E. (1960) High specific activity iodination of gamma-globulin with iodine-131 monochloride. *Cancer Res.* **20**, 1495–1500.
10. Breitfeld, P.P., Casanova, J.E., Harris, J.M., Simister, N.E., and Mostov, K.E. (1989) Expression and analysis of the polymeric immunoglobulin receptor in Madin–Darby canine kidney cells using retroviral vectors. *Methods Cell. Biol.* **32**, 329–337.
11. Song, W., Vaerman, J.P., and Mostov, K.E. (1995) Dimeric and tetrameric IgA are transcytosed equally by the polymeric Ig receptor. *J. Immunol.* **155**, 715–721.
12. Lullau, E., Heyse, S., Vogel, H., et al. (1996) Antigen binding properties of purified immunoglobulin A and reconstituted secretory immunoglobulin A antibodies. *J. Biol. Chem.* **271**, 16300–16309.

13

The Use of Syntaxin Chimeras to Study Polarized Protein Trafficking in Epithelial Cells

Martin B.A. ter Beest

1	Introduction.....	171
2	Materials	172
3	Methods.....	175
4	Notes	183
	References.....	186

Summary The plasma membrane of epithelial cells has two physically separated membrane domains. This membrane polarization is essential for the function of epithelial cells. It has been well established that different plasma membrane syntaxin forms are expressed in epithelial cells. In addition, these syntaxin forms can have a polarized localization, suggesting that they may play a direct role in the specificity of polarized membrane delivery. To determine the mechanism of the polarized syntaxin localization, we have made several chimeras of syntaxin 3 and 4. This allowed us to identify the protein sequences involved in this polarized localization. Using this technique, we showed that targeting information of syntaxin 3 and 4 is located in the first 30 amino acids.

Keywords Confocal microscopy; epithelial cells; immunofluorescence; polarization; protein chimera; SNARE proteins; syntaxins.

1 Introduction

Plasma membrane syntaxins are members of the SNARE (soluble *N*-ethylmaleimide-sensitive factor attachment protein receptor) protein family and are involved in exocytosis. Together with other SNARE proteins, they mediate membrane fusion at the plasma membrane (1). Mammals have five different forms of plasma membrane syntaxins, which have high protein sequence homology (2,3). It has been shown that most epithelial cells express more than one form of syntaxin. In the case of syntaxin 3 and 4, they are located respectively at the apical and basolateral

membrane domain (4–6). This would suggest that each syntaxin form is involved in a specific membrane delivery step, depending on its localization.

To identify the sequence that is important for polarized targeting of syntaxins, we have made chimeras of both syntaxin 3 and 4. We have shown that the unique localization of syntaxin 3 and 4 is dependent on the first 30 amino acids (7). In the case of syntaxin 3, changing this region with a similar region of syntaxin 4 resulted in largely basolateral localization of syntaxin 3. Using adenoviral-mediated expression, it was also shown that this chimera induces missorting of the predominantly apical secreted protein gp80/clusterin (8).

2 Materials

2.1 Cell Culture and Adenovirus Infection

1. Minimum essential medium with Earle's salts and L-glutamine (MEM; Cellgro/Mediatech, Herndon, VA), supplemented with 10% fetal bovine serum (FBS; Hyclone, Logan, UT) and 1:100 penicillin/streptomycin (10,000 IU penicillin/10,000 µg/mL streptomycin, Cellgro/Mediatech).
2. Dulbecco's modified Eagle's medium with 4.5 g/L glucose and L-glutamine without sodium pyruvate (DMEM, Cellgro/Mediatech), supplemented with 10% FBS (Hyclone) and 1:100 penicillin/streptomycin.
3. 12-mm Transwells with 0.4-µm pore polycarbonate membrane insert (cat. no. 3401, Corning, Acton, MA).
4. 20 µg/mL doxycycline (dox) (Sigma) (1000X), filter sterilized (0.2-µm filter), aliquoted, and stored at -20 °C.
5. HEPES buffer saline without calcium and magnesium (HBS⁻; Cellgro/Mediatech), supplemented with 1 mM MgCl₂.
6. Phosphate-buffered saline without calcium and magnesium (PBS⁻; from 10X stock: 27 mM KCl, 15 mM KH₂PO₄, 1.37 M NaCl, 81 mM Na₂HPO₄, Dilute 1:10 with water).

2.2 Adenovirus Preparation

1. 2.5 M CaCl₂, filter sterilized (0.2-µm filter), aliquoted, and stored at -20 °C.
2. HEPES-buffered saline (HBS; 2X): 0.283 M NaCl, 0.023 M HEPES-NaOH, 1.5 mM Na₂HPO₄, pH 7.05; filter sterilize (0.2-µm filter) and store at 4 °C.
3. 1 M HEPES-NaOH, pH 7.4; filter sterilize (0.2-µm filter) and store at 4 °C.
4. 100 mM Tris-HCl, pH 8.0.
5. Psi5 viral deoxyribonucleic acid (DNA): >0.5 µg/µL in 10 mM Tris-HCl, pH 8.0 (see [Note 1](#)).

6. The shuttle vector pADtet with construct. (Please note that for using adenovirus, BSL2 facilities are needed, and the appropriate approvals with your institute have to be in place. For additional safety information, see the National Institutes of Health Web site, <http://bmbf.od.nih.gov/contents.htm>).
7. Cre-expressing HEK293 cells (Cre8 cells).
8. HEK293 cells (American Type Culture Collection, Manassas, VA).
9. Adenovirus isolation kit (cat. no. VPK-100, Cell Biolabs, San Diego, CA).
10. Adenovirus titer kit (cat. no. VPK-109, Cell Biolabs).

2.3 Processing of Cells for Immunofluorescence

1. 4% Paraformaldehyde (*PFA is toxic, corrosive, and a suspected carcinogen.*) in PBS with CaCl_2 (1 mM) and MgCl_2 (0.5 mM). We are using PFA, 16% from EMS (Hatfield, PA) as a stock solution. Prior to use, this PFA is diluted with 10X PBS⁻ and water to 4% PFA. PFA solution that is not directly used can be frozen at -20°C . Calcium and magnesium are added from 1 M stock solutions just before use.
2. Quenching buffer: 50 mM NH_4Cl and 20 mM glycine in PBS⁻.
3. PBS⁺⁺: 2.7 mM KCl, 1.5 mM KH_2PO_4 , 137 mM NaCl, 8.1 mM Na_2HPO_4 , 1 mM CaCl_2 , 1 mM MgCl_2 . Keep at 4°C .
4. Blocking buffer (PFS): 0.025% (w/v) saponin (ICN, Aurora, OH) from a 5% stock solution (filter sterilized with a 0.45- μm filter) and 0.7% (w/v) fish skin gelatin (Sigma) in PBS⁻. Store at 4°C . Please note that this solution has only a limited shelf life.
5. 0.1% (w/v) Triton X-100 in PBS⁻.
6. Primary antibodies (in this case, anti HA-tag rabbit polyclonal, Santa Cruz Biotechnology, Santa Cruz, CA).
7. Secondary antibodies coupled to Alexa Fluor 488 (in this case, donkey anti-rabbit Alexa Fluor 488) and Phalloidin Alexa Fluor 555 (Invitrogen).
8. Clear nail polish.
9. Mounting medium (FluorSave, Calbiochem, San Diego, CA).

2.4 Apical Delivery Assay of gp80

1. Starvation medium: Dulbecco's modified Eagle's medium with 1 g/L glucose, L-glutamine, without L-cysteine, and without L-methionine (DME; Sigma, cat. no. D3916). This medium is supplemented with penicillin/streptomycin 1:100, 20 mM HEPES-NaOH, pH 7.4 (from 1 M stock), and 5% dialyzed fetal calf serum (*see Note 2*). Filter medium through 0.2- μm filter and refrigerate.
2. Chase medium: DME supplemented with penicillin/streptomycin 1:100, 20 mM HEPES-NaOH, pH 7.4 (from 1 M stock), 5% dialyzed fetal calf serum, L-cysteine, and L-methionine.

3. PBS⁺⁺.
4. 10mM L-methionine (10X). Filter sterilize (0.2- μ m filter), aliquot, and store at -20°C .
5. 10mM L-cysteine-HCl (10X). Filter sterilize (0.2- μ m filter), aliquot, and store at -20°C .
6. Redivue Pro-mix- ^{35}S in vitro cell-labeling mix > 1000 Ci/mmol (Amersham, Piscataway, NJ). (*Please note that ^{35}S compounds are volatile; see below for precautions.*)
7. Sample buffer with dithiothreitol (DTT; *see* subheading 2.5, item 9).
8. Dialyzed FBS (*see* **Note 2**).
9. Activated coal-filled autopsy bags and a plastic container containing wetted filter paper covered with Parafilm (*see* **Note 3**).
10. Tubes with threaded caps (*see* **Note 4**).
11. Pipet tips with filter.

2.5 Analysis of the Samples of the Apical Delivery Assay and Western Blotting

1. 1.5 M Tris-HCl, pH 8.8.
2. 65% (w/v) sucrose.
3. Acrylamide (30% acrylamide/0.8% bis-acrylamide, Bio-Rad, Hercules, CA). *Acrylamide is extremely toxic and carcinogenic.*
4. 0.5 M Tris-HCl, pH 6.8.
5. 10% (w/v) ammonium persulfate. Make fresh just before use.
6. 10% (w/v) sodium dodecyl sulfate (SDS).
7. TEMED (*N,N,N,N'*-tetramethyl-ethylenediamine; Bio-Rad).
8. 1 M DTT. Aliquot and keep at -20°C .
9. Sample buffer (4X): 120mM Tris-HCl, pH 6.8, 20% (v/v) glycerol, 4% (w/v) SDS, 0.01% (w/v) bromophenol blue. Aliquot and store at -20°C . Add DTT to a final concentration of 100mM from a 1 M stock.
10. Electrophoresis buffer: 384mM glycine, 80mM Tris (free base), 0.1% SDS (no need for adjusting pH).
11. Transfer buffer: 192mM glycine, 25mM Tris (free base), 20% (v/v) methanol (no need for adjusting pH).
12. Immobilon-P transfer membrane (Millipore, Billerica, MA).
13. PBS/Tween: PBS⁻ with 0.1% (w/v) Tween-20.
14. Milk powder (e.g., Carnation Instant Nonfat dry milk).
15. Secondary goat anti-rabbit conjugated with horseradish peroxidase (HRP; Jackson, Gilbertsville, PA).
16. Enhanced chemiluminescent reagents (ECL; Western Lightning Plus, PerkinElmer, Wellesley, MA) and film (Blue basic Autorad Film, ISC BioExpress, Kaysville, UT).

17. Molecular weight markers. We use the BenchMark prestained protein ladder (Invitrogen, cat no. 10748-010). The range is from approx 10kDa to approx 190kDa. The exact molecular weight of the proteins differs in each batch so please make a note for reference which batch number was used.
18. Gel fixative: 35% (v/v) methanol (*flammable and poisonous*), 55% (v/v) H₂O, and 10% (v/v) acetic acid.
19. 40% (v/v) glycerol/water.
20. Gel-drying apparatus with a cold trap to prevent vapors entering the vacuum pump (e.g., Hoefer SE450 gel dryer, Hoefer, San Francisco, CA).
21. Thick filter paper (Fisher brand chromatography paper, cat. no. 05-714-4, Fisher Scientific, Fair Lawn, NJ).

3 Methods

Polarized epithelial cells are grown on filter support to obtain optimal polarity. Access to the basolateral membrane enables the cells to efficiently take up nutrients and growth factors. Filter supports with a pore size of 0.4 μm are used; they provide sufficient access to medium but prevent cells from moving through the filter. Growing cells on filter gives some challenges with respect to immunofluorescence microscopy. It is therefore essential to use a confocal fluorescence microscope.

Epithelial cells grown on filter are not efficiently transfected with regular lipid- or polymer-based transfection agents. However, efficient gene delivery and protein expression can be obtained in a relatively short time period of 16–24 h by adenovirus. In addition, expression can be regulated by using the tetracycline inducible system developed by Gossen and Bujard (9) (see also the review in *Ref. 10*). For the following experiments, the tet-off system was used. By using MDCK cells (T23) that stably express the transactivator (11), tight regulation of protein expression can be obtained. The presence of doxycycline, a tetracycline analog, in the medium suppresses the expression of the protein. Removing doxycycline by washing and adding fresh medium without it induces protein expression.

In the following experiments, syntaxin 3 and syntaxin 3/4-(1–29) chimera (this is syntaxin 3 in which the first 29 amino acids are substituted with the first 29 amino acids of syntaxin 4) were expressed in MDCK cells using adenoviral delivery, and their localization was determined by confocal fluorescence microscopy. We also determined the effect of chimera on the apical delivery of gp80 (clusterin). Gp80 is one of the major proteins that is secreted predominantly from the apical side (8), and using a simple pulse–chase labeling, the amount of gp80 that is secreted can be determined (12).

3.1 Designing Syntaxin Chimeras

For considering which part of the sequence needs to be changed between both proteins, domains defined by exons, function, or structure can be used. In the chimera

described below, we have changed the N-terminal domain at a site defined by a very homologous sequence consisting of a conserved double phenylalanine sequence that is present in all plasma membrane syntaxins. An EcoR I site was introduced into this sequence by making a silent mutation. Chimeras of syntaxin 3 and 4 were made using this restriction site. However, it is not always possible to introduce restriction sites into the sequence. In that case, chimeras can be made by overlap-extension polymerase chain reaction (PCR). This technique has been described in much detail elsewhere (13).

3.2 Cell Culture of MDCK cells

1. MDCK cells are grown and maintained on 10-cm diameter tissue culture plates and passed every 3 d (*see Note 5*). When confluent, the plate is trypsinized by washing the plate one time with 10 mL PBS⁻.
2. Next, 1 mL trypsin is added to the plate, and excess trypsin is aspirated. The plate is incubated until the cells detach.
3. The cells are resuspended in 10 mL medium, spun down, and resuspended in 10 mL fresh medium. For passing the cells, 1 mL cells is plated in a new 10-cm cell culture dish with 9 mL fresh medium.
4. For 12-mm Transwell filters, you will need approx 0.5×10^6 cells per Transwell. This generally corresponds with approx 0.5 mL of resuspended cells. The cells are added to the top compartment of the Transwell. At the bottom compartment, 1 mL of medium is added. The medium of the Transwells is changed every 2 d, and the Transwells are used 4–6 d after plating.

3.3 Preparation of Adenovirus

3.3.1 Recombination of Adenoviral Vector

1. The first step in creating adenovirus that express the protein of interest is to cotransfect the shuttle vector with the adenoviral DNA into Cre8 cells (*see Note 6*). For this 2×10^6 cells in a 60-mm dish are plated and grown until 80% confluency. Change the medium the day before the transfection (*see Note 7*).
2. For the transfection, add 3 μ g of pADtet with syntaxin 3 or syntaxin 3/4-(1–29) and 3 μ g of psi5 adenoviral DNA to 225 μ L H₂O and mix. Next, 25 μ L of 2.5 M CaCl₂ are added dropwise and mixed carefully with a pipet. To this, 250 μ L of 2X HBS are added and mixed with a pipet. Everything is done under sterile conditions.
3. Incubate this mixture for 30 min at room temperature.
4. Add the DNA mixture dropwise to the cells and mix by gently swirling the plates.

5. Change the medium of the transfection every day. If doing multiple recombinations, use different glass pipets for aspiration and different plastic pipets for adding fresh medium. This is done to prevent cross-contamination of virus.
6. After 4–7 d, some cells should round up, and comet-shape holes should be present. These are the plaques. Keep changing medium but be careful not to dislodge the cells.
7. After 8–9 d, most cells have rounded up, and cells are harvested by resuspending the cells in their medium. Cells should easily detach. Add to 1 mL of 1 M HEPES pH 7.4 in a sterile 50-mL capped tube (*see Note 8*).
8. Freeze–thaw this cell suspension by freezing it in liquid nitrogen and thawing at 37°C. Repeat this three times. Do not let the cell suspension warm completely.
9. Spin the lysed cells for 15 min at 800 g in a cooled centrifuge and aliquot the supernatant 1 mL in 2.5-mL freezing vials. Freeze this supernatant at –80°C (this is P1).
10. Use 1 mL to infect a new 10-cm plate of cells and repeat steps 8–10 to obtain P2, P3, and P4 (*see Note 9*).

3.3.2 Large-Scale Isolation of Adenovirus

1. Infect a 10 cm plate of 293 cells (not Cre8 cells) with 1 mL P4. After 1–2 d, most of the cells are rounded up or detached. Collect and lyse the cells as described above and spin down the cell debris. The total volume of lysate will be approx 10 mL. This lysate (P5) can be kept at –80°C or can be used immediately.
2. Grow 4 × 15 cm plates with 293 cells in 15 mL medium until 80% confluency. Change the medium the day before infection.
3. Add 2.5 mL P5 lysate to the plates and swirl the plates gently. After 16–24 h, most of the cells are rounded up or detached.
4. Collect the cells in their medium by pipeting the medium directly onto the cells. This will release the cells from the plate. This suspension can be frozen at –80°C or processed immediately.
5. Freeze–thaw the cells three times and spin down cell debris at 800 g for 15 min.
6. Clear the supernatant by filtration through a 0.45- μ m filter and divide into two aliquots.
7. The virus is isolated according to the protocol supplied by the manufacturer and is described below (*see Note 10*).
8. Attach a 20-mL syringe to the purification filter and arrange in a stand above a waste-collecting container.
9. Wash the filter with 5 mL 1X wash buffer (dilute the 10X stock with water prior to use) added into the syringe. In most cases, gravity is enough to let the buffer go through. If pressure is needed, the flow rate should be such that the flowthrough proceeds dropwise.
10. Add the cleared supernatant into the syringe and let it pass the filter.

11. Wash the filter with 10 mL 1X wash buffer. Repeat this step twice with 10 mL 1X wash buffer.
12. After the wash, position a sterile 12-mL tube under the syringe and add 2.5 mL elution buffer (dilute the 2X stock with water prior to use).
13. Collect the eluate and place it on ice.
14. Wash the filter with 10 mL regeneration buffer and equilibrate with 5 mL 1X wash buffer.
15. Repeat steps 7–10 with the other aliquot and combine eluate of this step with that of step 10.
16. Add glycerol to a final concentration of 10%, aliquot the virus, and store at -80°C .
17. Discard the collected flowthrough after decontamination by adding undiluted bleach 1:5 (let it stand for at least an hour). Decontaminate filter, syringe, and other plasticware that has been in contact with virus by autoclaving before disposal.
18. The expression efficiency is determined by infecting cells with different dilutions of adenovirus as described in Subheading 3.3. and determine the percentage of protein-positive cells by immunofluorescence and the expression level by Western blotting (*see* subheading 3.6). For titering, we use the kit provided by Cell Biolabs. The procedure was done exactly according to the manufacturer's protocol (*see* Note 11).

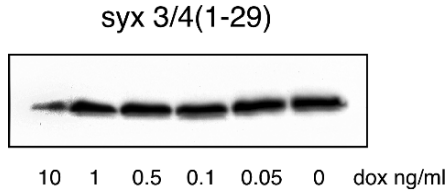
3.4 Adenoviral Infection

1. For adenoviral infection, cells grown for 4–6 d on 12-mm Transwells are used (*see* Note 12).
2. Cells are washed three times with HBS with 0.5 mM MgCl_2 and no calcium (*see* Note 13).
3. Adenovirus diluted in 200 μL buffer is added to the apical compartment. Typically, titers of $2-10 \times 10^6$ ifu (infectious units)/ cm^2 are used (*see* Note 14).
4. 0.7 mL buffer is added to the basolateral compartment, and the plate is incubated at 37°C on a nutator for 2 h. After this incubation, the buffer is removed, and fresh medium with doxycycline (20 ng/mL to complete block expression or variable concentrations) or without doxycycline is added to the cells. (Figure 1 shows the different levels of expression obtained by incubating with different concentrations of doxycycline; *see* Note 15).
5. After 16–24 h of incubation, the Transwell can be used for further experiments.

3.5 Confocal Immunofluorescence Microscopy of MDCK Cells

1. To determine protein expression levels and the effect of expression, confocal immunofluorescence is performed. After the incubation with virus, cells on Transwell filters are

Fig.1 Expression of syntaxin 3/4-(1-29) can be modulated by changing doxycycline concentrations. MDCK T23 cells were infected with adenovirus encoding of HA-tagged syntaxin 3/4-(1-29) chimera. After overnight incubation of the cells in medium with different concentrations of doxycycline, the cells were lysed, and expression levels of syntaxin 3/4-(1-29) chimera were determined by Western blotting with anti-HA antibody.



washed two times with ice-cold PBS⁺⁺, and 0.5 mL 4% PFA in PBS⁺⁺ is added to both the apical and basolateral compartments of the filters. Cells are incubated for 20 min at room temperature while gently rotating on a shaker.

2. The cells are washed three times with PBS⁻, and remaining PFA is quenched by incubating the cells for 15 min with quenching buffer.
3. After one wash with PBS⁻, the cells are blocked and permeabilized for 30 min at 37 °C in blocking buffer.
4. Next, the cells are incubated with primary antibody, in our case rabbit polyclonal anti-HA. The right dilution of the antibody needs to be empirically determined. To incubate the cells with primary antibody, an airtight container with a sheet of Parafilm on top of wetted filter paper is prepared. A drop of 35–40 μL diluted antibody in blocking buffer is placed on the Parafilm, and the Transwell is placed on this drop. Next, 100–105 μL of the remaining antibody in blocking buffer are added to the apical compartment. The cells can be incubated for 1 h at 37 °C or overnight at 4 °C while gently rotating (*see Note 16*).
5. After the primary antibody incubation, the cells are placed back in the 12-well plate and washed four times with blocking buffer.
6. Incubation with secondary antibodies is performed as described for primary antibodies (4). Fluorescent secondary antibodies are diluted 1:200 in blocking buffer. In general, we also stain for actin with Alex 555-phalloidin (1:100 dilution in blocking buffer) as the lateral and cortical actin give a good indication of the boundaries of the cells.
7. The cells are incubated for 30 min and subsequently washed four times with blocking buffer.
8. To reduce background, cells are washed twice with PBS⁻ and incubated with 0.1% Triton X-100 in PBS⁻ for 3 min. The cells are washed two times with PBS⁻ and kept for mounting. Cells can be postfixed with 4% PFA for 15 min at room temperature. Wash twice with PBS⁻ before mounting.
9. For mounting, object glasses are prepared with a rim of nail polish in the form of a square. This is necessary to prevent flattening of the cells. The square should be large enough to contain a cut-out square of filter. A drop of

mounting medium is put into this square. To mount the cells, PBS is removed by aspiration, and three cuts with a sharp, new scalpel are made in the filter in the form of a square. A fourth cut is made in such a way that a tiny piece of the filter square is still attached. With jewel forceps, the filter is gently but firmly pulled from the rest of the filter, and the side with the cells is gently drawn through the mounting medium to wet this side of the filter. Next, the filter is put into the mounting medium with cells facing up, and an object glass is added on top of this (*see Note 17*). Be careful to avoid air bubbles. Let the samples dry overnight in a dark, cool place and store the samples at 4 °C.

- For analysis of the samples, a confocal fluorescence microscope is needed. For analyzing the sample, take images at different x - y planes to determine localization of the chimera. Typically, we take two or three images, one at the middle of the cell, one image at the level of the tight junctions just below the apical membrane, and one at the level of the apical membrane. For a cross section of the cells, line scans are made from multiple x - y planes [Fig. 2 shows an example of syntaxin 3 and syntaxin 3/4-(1-29) expression in MDCK cells infected by adenovirus].

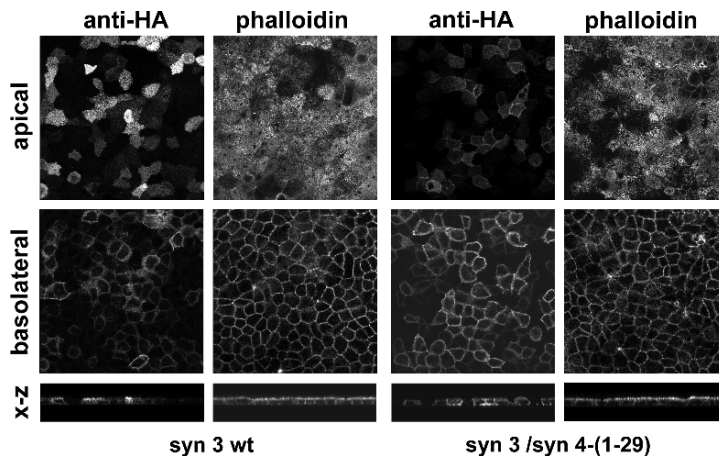


Fig. 2 Expression of syntaxin 3 wild type and syntaxin 3/4-(1-29) chimera in MDCK cells. MDCK T23 cells were infected with adenovirus encoding HA-tagged syntaxin 3 wild type and syntaxin 3/4-(1-29) chimera. After overnight incubation, the cells were fixed, and syntaxin expression was visualized with an antibody to the HA-tag followed by detection using Alexa Fluor 488 secondary antibody (anti-HA) and co-stained for F-actin using phalloidin Alexa Fluor 555 (phalloidin). The chimera shows less apical staining and a more pronounced lateral staining. The intracellular staining of syntaxin 3 is lysosomal-localized syntaxin 3. Note the relatively uniform expression of both constructs. Bar = 50 μ m.

3.6 Gel Electrophoresis and Western Blotting

1. These instructions are for SDS polyacrylamide gel electrophoresis (PAGE) using a Bio-Rad Mini-Protean 3 electrophoresis unit and blotting unit. Volumes given are for two gels when glass plates with spacers with a thickness of 1.0mm are used.
2. For a 10% gel, mix first 4 mL H₂O, 2.6 mL Tris-HCl 1.5 M at pH 8.8, and 3.3 mL acrylamide (30% acrylamide/0.8% bis-acrylamide) (*acrylamide is extremely toxic and carcinogenic*). Mix and add 50 μL ammonium persulfate and 5 μL TEMED to start the polymerization. This is enough for making two gels. After pouring this mixture between the glass plates, gently add a small volume of water on top. This will help to form a straight top surface, and it will prevent access of oxygen to the acrylamide mix, which can inhibit the polymerization reaction. The gel should polymerize between 30 and 60 min.
3. After polymerization, remove the water layer and pour the mix for the stacking gel on top of the running gel. The stacking gel mixture contains 2.7 mL H₂O, 380 μL sucrose 65%, 650 μL acrylamide (30% acrylamide/0.8% bis-acrylamide), 1.25 mL 0.5 M Tris-HCl at pH 6.8. Mix and add 50 μL ammonium persulfate and 5 μL TEMED to start the polymerization. Add the stacking gel mix and place a comb (15 wells) between the glass plates and let it polymerize. Let the gels polymerize at least for 1–2 h before use.
4. The samples are loaded (10–20 μL) on a 10% SDS-PAGE gel together with some benchmark reference marker (10 μL). It is preferred to load the samples after the gel is assembled and electrophoresis buffer is added. Use special disposable gel loading tips for the radioactive samples.
5. Run the samples at 130 V, 400 mA, until bromophenol blue reaches the bottom of the gel. This will be approx 1 h. (*Important: When running radioactive samples, the running gel buffer, glass plates, and container should be considered contaminated and disposed of or cleaned accordingly.*)
6. To transfer proteins from the gel to the filter, the Bio-Rad transfer system is used. To assemble the cassette, a glass container is filled with precooled (4 °C) transfer buffer to such a level that the cassette is sufficiently submerged. The cassette is opened, and one sponge and three pieces of filter paper are put on one side of the cassette and submerged. Next, the Immobilon prewetted in methanol is put on the filters, followed by the gel. Another three pieces of filter paper are put on the gel, followed by another sponge; everything should be sufficiently moistened with transfer buffer. This cassette is put into the blotting container together with a stirring bar and a container with ice to keep everything cool. The transfer is done at 115 V, maximum current and power for 1 h and 30 min.
7. After blotting, the membrane is taken out immediately and washed first in PBS/Tween and subsequently blocked for 1 h in 5% milk in PBS/Tween. After the block, the membrane is put in a plastic sealed pouch with the antibody diluted in milk powder/PBS/Tween (1:1000) and incubated overnight.

8. The next morning, the membrane is washed three times short (10 sec) and three times for 10 min on a rotator and further incubated with HRP-labeled goat anti-rabbit (1:10,000) for 1 h. After this incubation, the membrane is washed again as described above and washed twice quickly with PBS⁻.
9. Next, the bands are visualized by ECL. First, a 1:1 mixture of the two ECL components is made for the membrane. You will need 4–6 mL for a 10 × 10 cm membrane. A piece of plastic foil is put on a flat bottom (directly on the bench), and the membrane is placed on this piece of plastic after removing the excess PBS⁻. Next, the ECL mixture is slowly pipeted onto the membrane and incubated for 1 min. The entire membrane should be sufficiently covered with the mixture. After the 1-min incubation, excess ECL mixture is aspirated, and the membrane is wrapped in plastic and exposed to film; the film is developed (*see Note 18*).

3.7 Apical Delivery Assay of gp80

3.7.1 Pulse Chase of gp80

1. MDCK cells are grown for 4–6 d and infected with adenovirus that encodes wild-type syntaxin 3 or the chimera as described in Subheading 3.3.
2. Because ³⁵S-containing precursors are volatile, the pulse and chase are performed in a fume hood. An airtight box is made containing wetted filter paper covered with Parafilm. To further prevent contamination, the top of the container is lined with autopsy bags filled with activated coal. This is sufficient to remove most of the volatile ³⁵S. The container is prewarmed in a 37 °C water bath on an aluminum plate submerged just below the water line.
3. Thaw the ³⁵S cysteine/methionine stock solution at room temperature and pipet (with filter tip) an appropriate amount (50 μL) of this labeled material to 600 μL of pulse medium and mix with a pipet with a filter tip (*see Note 19*). For 12 Transwells, a total of 600 μCi are used (50 μCi per Transwell). To prevent contamination, the tips are collected in a blue-capped disposable plastic 50-mL tube and then disposed in the radioactive waste container. Check the tip of your pipet for contamination using a β-counter.
4. Of this mix, 50 μL are placed as drops on the Parafilm in the incubation box, and the Transwells with 300 μL nonradioactive pulse medium are placed on top of these drops. Wipe off excess medium before putting the Transwells on top of the drops but be careful not to touch the filter. Incubate for 20 min at 37 °C. This is the pulse.
5. After the pulse, the filters are placed in a new 12-well plate and washed three times with ice-cold PBS⁺⁺. After the wash, chase medium is added, and the Transwells are incubated for 2 h at 19 °C. This is to let synthesized gp80 accumulate in the Golgi (*see Note 20*).

6. After this incubation, the medium is changed with prewarmed 37°C chase medium, 0.5 mL at both the apical and basolateral side. The cells are incubated for 1 h (chase) at 37°C.
7. Next, the plate is chilled on ice, and the medium from both compartments is collected separately in centrifuge tubes. The samples are spun for 10 min in a tabletop centrifuge to remove cells and cell debris. Aliquots (300 µL) are transferred to a new tube and can be analyzed immediately or can be kept frozen at -20°C until further processing.

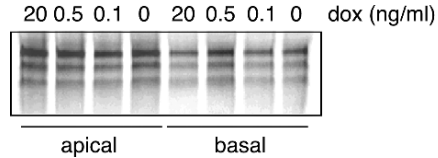
3.7.2 Analysis of the Apical Delivery Assay Samples

1. To analyze the samples, 25 µL sample is mixed with 25 µL sample buffer with DTT (fresh) and boiled for 5 min.
2. The samples (10–20 µL) are loaded on a 10% gel prepared as described in Subheading 3.3.2.
3. After running the gel, fix the gel in gel fixative for at least 4 h. After this fixation, the gel is equilibrated for an hour in 40% glycerol/H₂O. This makes the gel less prone to breakage during the drying process.
4. To dry the gel, first place three paper towels wetted with water on top of the grid. On top of this place thick filter paper wetted with gel fixative. Place the gel on top of this (*see Note 21*). Finally, cover the gel with Saran wrap. When the vacuum is applied, the gel should be tightly packed on the filter paper. Dry for at least an hour with heating and under vacuum. (Be careful to dry the gel completely. The gel will break if the vacuum is lost while it is still wet.)
5. Expose the gel to film or use a phosphorimager to analyze the gel (*Fig. 3* shows an example of gp80 samples run on a gel under reducing conditions).
6. Quantify the resulting data using an gel analyses program (e.g., IPlab for Macintosh) or the program supplied with the phosphorimager (e.g., ImageQuant, MD Dynamics for Macintosh). The percentage of apical vs basolateral delivery is calculated as the percentage of total delivery (*see Note 22*).

4 Notes

1. The Psi5 viral DNA is isolated as described by Hardy et al. (14).
2. To remove cysteine and methionine, FBS can be dialyzed in 10 mM Tris-HCl, 150 mM NaCl, pH 7.4. Dialyze in a total volume 8–10X the volume of FBS in four or five batches over 2–3 d.
3. One of the major problems with using ³⁵S-labeled methionine/cysteine is the volatility of the radioactive compound. Without certain precautions, this can result in substantial contamination. Therefore, we are using home-made

Fig. 3 The effect of syntaxin 3/4-(1–29) chimera on the polarity of gp80 secretion. MDCK T23 cells were infected with adenovirus for expression of HA-tagged syntaxin 3/4-(1–29) chimera. After overnight incubation, cells were assayed for gp80 apical and basolateral secretion by analyzing samples of medium for levels of gp80. Image as obtained by phosphorimager; note the three different bands of gp80.



- activated charcoal bags that are attached to the lid of the incubation chamber with tape. The bags are available via Fisher, can be filled with activated charcoal, and are sealed with a heat sealer. The lid is entirely covered with bags and can be removed using a disposable plastic forceps and disposed as radioactive waste. Be careful not to tear the bags and spill the radioactive coal.
4. For most incubations and sample collection, we use threaded capped tubes with a seal. This prevents the leakage and the dispersion of radioactive sample that occurs when standard tubes are snapped open. One drawback is that it is more labor intensive to open the tubes.
 5. In general, the cells do not need any change of medium, but when the plate is confluent it may be necessary to change the medium when the cells are not immediately trypsinized. When changing the medium of the cells grown on Transwells, first remove the basolateral medium and then the apical medium. When adding medium, first add medium to the apical compartment and then to the basolateral compartment. This is done to prevent detaching of the sheet of cells by upward pressure.
 6. Although several commercial systems are available, we have been using the system developed by Stephen Hardy and colleagues (14). In this system, the gene of interest is cloned in a shuttle vector (pADtet, which has a CMV/tet promoter) and is introduced in the adenoviral vector by Cre-lox recombination in cells expressing Cre (Cre8 cells). For this, Cre8 cells are transfected with shuttle vector and the adenoviral DNA (psi5).
 7. Cre8 and 293 cells are grown in DMEM with 4.5 g/L glucose and trypsinized every 3 days 1:5.
 8. We have used Falcon tubes (cat. no. 352098), which have good resistance to cracking after several freeze–thaw cycles and centrifugation.
 9. Multiple reinfections are needed to obtain complete recombination and depletion of adenoviral particles that do not contain the gene of interest. The P2, P3, and P4 should be aliquoted and kept at -80°C . These lysates can be used for future isolations. The P3 or P4 can also be used to check if the recombination was efficient by determining the expression of the protein of interest by Western blot analysis.
 10. Adenoviral isolation kits have become available. With these kits, the virus is isolated using a filter. The kits are very user friendly and time-saving. We have

compared the virus isolation kit and the standard cesium chloride gradient isolation method. No significant differences were found in the performance of the virus isolated with both methods. The composition of the buffers are not listed except for the elution buffer (25 mM Tris-HCl, 2.5 mM MgCl₂, 1 M NaCl, pH 7.5).

11. In addition, we also now use a commercially available kit to titer the virus based on detecting virus-infected cells by immunohistochemical staining.
12. The integrity of the Transwell and the epithelial monolayer is checked by adding, the day before the adenoviral infection, 1 mL medium to the apical side. If the Transwell is leaky, medium will leak to the basal compartment, and these filters are discarded.
13. The receptor for the adenovirus is not accessible from the apical compartment, and the virus cannot access the basolateral membrane via the filter. Therefore, to infect the cells, they are incubated with HBS without calcium but with 1 mM MgCl₂. The tight junctions will disassemble, but the cells remain attached to the filter.
14. Both the ifu (infectious units) and the expression level of the protein of interest need to be determined for each batch of virus as variations are possible. Also, different proteins may have variable expression levels at the same ifu.
15. We have observed two ways to regulate expression levels. First, different amounts of virus can be used, but this changes mostly the amount of cells infected. Another way is to use different concentrations of doxycycline. This determines the expression levels of protein. Note that the concentration to obtain a certain protein expression level needs to be determined empirically by both Western and immunofluorescence staining.
16. Overnight incubation at 4 °C with primary antibodies usually gives a lower background.
17. It is essential to use thin cover glasses (e.g., Corning no. 2865 18, 0.13–0.16 mm) and not to use excess nail polish as in some cases the working distance of an $\times 63$ oil lens may not be sufficient to view the entire section of the cells.
18. Note that the luminescence only lasts for a limited time (15–30 min).
19. The batch of radioactive material is usually aliquoted and kept at –80 °C.
20. We take advantage of the fact that protein transport from the Golgi is blocked at 19 °C. Therefore, accumulation and synchronization is obtained by this incubation step.
21. It is useful to include the stacking gel to check that no aggregates with labeled protein are present. However, please note that the stacking and running gel stick to the filter paper. It is therefore important to put the gel on filter paper directly at the right place as it is very difficult to reposition the gel.
22. If for some reason the total gp80 delivery is low, check total cell lysate for the presence of gp80 as delivery may in some cases be inhibited.

Acknowledgments I would like to thank Mirjam Zegers for critically reading the manuscript. This work was supported by a Ohio Division Supported Research Grant of the ACS.

References

1. Jahn, R., and Scheller, R.H. (2006) SNAREs—engines for membrane fusion. *Nat. Rev. Mol. Cell Biol.* **7**, 631–643.
2. Bennett, M.K., García-Arrara, J.E., Elferink, L.A., et al. (1993) The syntaxin family of vesicular transport receptors. *Cell* **74**, 863–873.
3. Teng, F.Y., Wang, Y., and Tang, B.L. (2001) The syntaxins. *Genome Biol.* **2**, 3012.1–3012.7.
4. Low, S., Chapin, S., Weimbs, T., Komuves, L., Bennett, M., and Mostov, K. (1996) Differential localization of syntaxin isoforms in polarized Madin–Darby canine kidney cells. *Mol. Biol. Cell* **7**, 2007–2018.
5. Gaisano, H.Y., Ghai, M., Malkus, P.N., et al. (1996) Distinct cellular locations and protein-protein interactions of the syntaxin family of proteins in rat pancreatic acinar cells. *Mol. Biol. Cell* **7**, 2019–2027.
6. Fujita, H., Tuma, P.L., Finnegan, C.M., Locco, L., and Hubbard, A.L. (1998) Endogenous syntaxins 2, 3 and 4 exhibit distinct but overlapping patterns of expression at the hepatocyte plasma membrane. *Biochem. J.* **329**, 527–538.
7. ter Beest, M.B., Chapin, S.J., Avrahami, D., and Mostov, K.E. (2005) The role of syntaxins in the specificity of vesicle targeting in polarized epithelial cells. *Mol. Biol. Cell* **16**, 5784–5792.
8. Urban, J., Parczyk, K., Leutz, A., Kayne, M., and Kondor-Koch, C. (1987) Constitutive apical secretion of an 80-kDa sulfated glycoprotein complex in the polarized epithelial Madin–Darby canine kidney cell line. *J. Cell Biol.* **105**, 2735–2743.
9. Gossen, M., and Bujard, H. (1992) Tight control of gene expression in mammalian cells by tetracycline-responsive promoters. *Proc. Natl. Acad. Sci. U. S. A.* **89**, 5547–5551.
10. Berens, C., and Hillen, W. (2003) Gene regulation by tetracyclines. Constraints of resistance regulation in bacteria shape TetR for application in eukaryotes. *Eur. J. Biochem.* **270**, 3109–3121.
11. Altschuler, Y., Barbas, S.M., Terlecky, L.J., et al. (1998) Redundant and distinct functions for dynamin-1 and dynamin-2 isoforms. *J. Cell Biol.* **143**, 1871–1881.
12. Hansen, S.H., Olsson, A., and Casanova, J.E. (1995) Wortmannin, an inhibitor of phosphoinositide 3-kinase, inhibits transcytosis in polarized epithelial cells. *J. Biol. Chem.* **270**, 28425–28432.
13. Horton, R.M., Ho, S.N., Pullen, J.K., Hunt, H.D., Cai, Z., and Pease, L.R. (1993) Gene splicing by overlap extension. *Methods Enzymol.* **217**, 270–279.
14. Hardy, S., Kitamura, M., Harris-Stansil, T., Daj, Y., and Phipps, M. (1997) Construction of adenovirus vectors through cre-*lox* recombination. *J. Virol.* **71**, 1842–1849.

14

Targeting the Epithelial SNARE Machinery by Bacterial Neurotoxins

Véronique Proux-Gillardeaux and Thierry Galli

1	Introduction.....	187
2	Materials.....	188
3	Methods.....	191
4	Notes.....	200
	References.....	200

Summary Clostridial neurotoxins are responsible for botulism and tetanus by cleaving the synaptic SNAREs (soluble *N*-ethylmaleimide-sensitive factor attachment protein receptors) synaptobrevin/VAMP2 (Vesicle-Associated Membrane Protein 2) and its partners SNAP-25 (synaptosome-associated protein of 25kDa) and syntaxin 1. SNARE proteins mediate membrane fusion, a crucial step in intracellular trafficking. There are seven isotypes of botulinic neurotoxins with different target specificities and one tetanus neurotoxin (TeNT), which targets synaptobrevin. Regarding the high sequence similarities between synaptobrevin and its nonneuronal homolog cellubrevin/VAMP3, different groups developed the use of TeNT to study cellubrevin (Cb). Here, we show how we have introduced the light chain of the TeNT into nonneuronal cells and selected clones expressing this toxin by Western blotting and by immunofluorescence. We also present how we identified which cells express TeNT by searching for a soluble green fluorescent protein (GFP) pattern of expression corresponding to cleaved GFP-tagged cellubrevin in living GFP-cellubrevin and TeNT transfected cells.

Keywords Cellubrevin; clone selection; immunofluorescence; MDCK; neurotoxin; SNARE; transfection; VAMP3; videomicroscopy; Western blot; wound healing.

1 Introduction

The neurotoxins produced by *Clostridium* bacteria are responsible for botulism and tetanus, neurological syndromes affecting the function of muscles and nerves. Clostridial neurotoxins are composed of a heavy chain responsible for their entry

into neuronal cells by endocytosis and a light chain that cleaves different proteins implicated in intracellular trafficking. The targets of the clostridial neurotoxins are the synaptic SNAREs synaptobrevin/VAMP2 and its partners SNAP-25 and syntaxin 1. SNARE proteins mediate the fusion between vesicles coming from donor compartments and the membrane of acceptor compartments through the formation of a complex between a vesicular SNARE (v-SNARE) located on vesicles and target SNAREs (t-SNAREs) on acceptor membranes. Important evidence of their requirement came from the elucidation of clostridial targets.

There is only one tetanus neurotoxin (TeNT), but seven isotypes of botulinic neurotoxins (BoNTs). BoNTs B, D, F, and G and TeNT specifically cleave synaptobrevin, whereas BoNTs A, C, and E cleave SNAP-25; BoNT C also targets syntaxin 1 (for reviews, see *Refs. 1 and 2*). When introduced into nonneuronal cells, the light chain of the tetanus neurotoxin (TeNT-LC) cleaves specifically cellubrevin/VAMP3, the nonneuronal homolog of synaptobrevin. This method has been used to show the implication of cellubrevin in transferrin (3) and in T-cell receptor (4) recycling.

We previously reported that the expression of the TeNT-LC in epithelial MDCK (Madin–Darby canine kidney) cells reduces migration, alters spreading, and enhances adhesion to different substrates, including collagen, through a negative effect on the recycling of $\beta 1$ integrin. Therefore, the use of TeNT allowed us to show that cellubrevin participates in cell migration through the regulation of cell adhesion (5).

This chapter focuses on the use of the TeNT-LC in cell biology. It points out different methods to test the activity of the TeNT in a cell line. An example with epithelial canine MDCK cells and how to select clones expressing this toxin by Western blotting and by immunofluorescence are presented here. We also present how we selected cell lines expressing exogenous TeNT by direct visualization of the cleavage of green fluorescent protein (GFP)-tagged cellubrevin so that we can determine in videomicroscopy experiments which cells lack cellubrevin. This method could also be adapted for BoNTs cleaving GFP-SNAP25 (SNAP-23) or GFP-syntaxin 1.

2 Materials

2.1 Treatment of Cell Extracts with a Purified Toxin

2.1.1 Purification of the Light Chain of the Tetanus Neurotoxin

1. 2YT medium: Add 16 g bacto-tryptone, 10 g bacto-yeast extract, and 5 g NaCl to 900 mL deionized water. Adjust to pH 7.0 with NaOH and adjust the volume to 1 L. Autoclave.
2. Sonication buffer: 300 mM NaCl, 50 mM NaH_2PO_4 , the pH is adjusted with NaOH to 8.0, 6.5, or 5.0.
3. Ni-agarose columns are prepared by adding 0.75 mL Ni-NTA agarose (Qiagen GmbH, Hilden, Germany) in Poly-Prep chromatography columns (0.8 × 4 cm) from Bio-Rad (Hercules, CA).

4. Dialysis buffer: 10 mM HEPES, 150 mM potassium glutamate/KOH, pH 7.2.
5. Coomassie brilliant blue solution: Dissolve 0.25 g Coomassie brilliant blue R250 in 90 mL ethanol:water (1:1 v/v) and 10 mL glacial acetic acid. Filter through a Whatman no. 1 filter to remove insoluble fractions. The filtered solution is used for gel staining. The same solution without Coomassie blue corresponds to the destaining solution.

2.1.2 Gel Electrophoresis

For sodium dodecyl sulfate polyacrylamide gel electrophoresis (SDS-PAGE) 1X running buffer, add 50 mL 20X NuPAGE SDS running buffer (MES or MOPS) (Invitrogen) to 950 mL deionized water.

2.1.3 Treatment of Cell Extracts with Tetanus Neurotoxin

1. Resuspension buffer: 0.32 M sucrose, 10 mM HEPES, pH 7.2, 1 mM MgCl₂.
2. Cell cracker: 8.020-mm internal diameter, 8.010-mm bead diameter (HGM, Heidelberg, Germany).

2.1.4 Western Blotting for Brevins

1. Transfer buffer: Add 14.41 g glycine (192 mM final), 3.03 g of Tris base (25 mM final), and 200 mL absolute ethanol (20% final); adjust the volume to 1 L with deionized water.
2. TBS, 10X: Add 88 g NaCl, 100 mL 1 M Tris-HCl, pH 7.4; adjust the volume to 1 L with deionized water.
3. Blocking buffer: 5% (w/v) nonfat dry milk, 0.1% Tween-20 in 1X TBS.
4. The monoclonal antibody against brevins C110.1 (Synaptic Systems, Goettingen, Germany) diluted 1000 times is used for Western blotting. This antibody recognizes synaptobrevins 1 and 2 and cellubrevin.

2.2 *Transfection and Selection of MDCK Cells Expressing GFP-Cb*

2.2.1 Transfection of MDCK Cells and Selection

1. Dulbecco's modified Eagle's medium (DMEM) (Gibco/BRL, Bethesda, MD) supplemented with 7% fetal bovine serum (FBS).
2. FBS (Gold, PAA laboratories, Les Mureaux, France).
3. Solution of trypsin (0.25%) from Gibco/BRL.
4. 1 M HEPES buffer solution, pH 7.2 to 7.5 (Invitrogen).

5. Antibiotics: G418 from Sigma is resuspended in DMEM at 40 mg/mL; aliquots are stored at -20°C and added to the medium at 200 $\mu\text{g}/\text{mL}$; puromycin dihydrochloride from Sigma is resuspended at 10 mg/mL in sterile water. Aliquots are stored at -20°C and added to the medium at 4 $\mu\text{g}/\text{mL}$.

2.2.2 Clone Selection by Limit Dilution

For clone selection by limit dilution 12-, 25-, and 30-mm coverslips (Marienfeld GmbH, Germany) are used.

2.2.3 Cell Lysis, Preparation of Samples for Western Blotting, and Choice of Expressing Clones

1. Lysis buffer (also called TSE): 50 mM Tris-HCl, pH 8.0, 150 mM NaCl, 1 mM ethylenediaminetetraacetic acid (EDTA).
2. Complete (Roche Diagnostics): Use protease inhibitor cocktail tablets to prepare a 25X stock solution by dissolving 1 tablet Complete in 2 mL H_2O ; keep at -20°C .
3. Anti-GFP monoclonal antibody: The mixture of two clones (7.1 and 13.1; Roche) at 0.4 $\mu\text{g}/\text{mL}$ gives satisfactory results for Western blotting.

2.3 Visual Test Based on Fluorescence for TeNT Activity

2.3.1 Selection of Clones by Direct Fluorescence or by Immunofluorescence

1. 10X phosphate-buffered saline (PBS): 1.37 M NaCl, 27 mM KCl, 100 mM Na_2HPO_4 , 18 mM KH_2PO_4 , pH 7.4. Autoclave.
2. 4% solution of paraformaldehyde (PFA 4%). For 1 L, heat 800 mL deionized water at 70°C . Remove from heat; add 40 g PFA (Prolabo) in a fume hood and stir. Add drops of 10 N NaOH up to 50 μL until dissolved. Filter through a Whatman no. 1 filter to remove insoluble fractions, add 100 mL 10X PBS, and complete to 1 liter with water. Cool to room temperature for use. This solution can be aliquoted and kept at -20°C .
3. Quenching solution: 1X PBS, 50 mM NH_4Cl .
4. Blocking solution: 1X PBS, 10% FBS.
5. Incubating solution: 1X PBS, 3% FBS.
6. Secondary antibody: Antimouse immunoglobulin G (IgG) conjugated to Cy3 (Jackson, West Grove, PA).

1. The evening before purification, inoculate 20 mL 2YT culture supplemented with 100 µg/mL ampicillin and 25 µg/mL kanamycin (2YT ampi kana) with these expressing bacteria and let grow at 37 °C overnight with shaking.
2. Inoculate 500 mL 2YT ampi kana with 4 mL of the overnight culture and let grow at 37 °C with shaking until the OD at 600 nm reaches 0.6 to 0.7. This step usually takes 2.5 to 3.5 h (*see Note 1*).
3. Add 100 µL 1 M IPTG to induce the expression of the 6His-TeNT. Incubate at 37 °C for 2.5 h with shaking.
4. Cells are harvested by centrifugation at 4000 g for 15 min. If necessary, the pellet can be stored at -20 °C overnight or at -80 °C for longer periods of time.
5. The pellet is resuspended in 9 mL sonication buffer pH 8.0 plus 1 mL 3 M NaCl and 100 µL 100 mM phenylmethylsulfonyl fluoride (PMSF).
6. Cells are disrupted by sonication on ice. Depending on the power output of the sonicator, 1 to 3 min at full power should be enough.
7. Cell debris is removed by centrifugation at 30,000 g for 20 min.
8. Equilibrate a Ni-agarose column with sonication buffer at pH 8.0.
9. Apply the bacterial extract supernatant onto the column.
10. Wash the column with 5 mL sonication buffer at pH 8.0 and 8 mL sonication buffer at pH 6.5.
11. TeNT-LC is eluted with 8 mL sonication buffer at pH 5.0 collected by 1-mL fractions.
12. The fractions containing TeNT-LC are determined by measurement of the OD at 280 nm.
13. Dialyze selected fractions containing TeNT-LC against dialysis buffer.
14. Purification quality and concentrations of the selected fractions are analyzed by migration of aliquots on 4–12% SDS-PAGE. Proteins are visualized by immersion of the gel in Coomassie brilliant blue solution at room temperature with gentle shaking (this takes 30 min to 2 h). The gel is destained by several baths in the destaining solution. To determine the concentration of TeNT-LC in the fractions, compare the staining intensity to BSA standards (*see Note 2*).

3.1.2 SDS-PAGE Gel Electrophoresis

These instructions assume the use of a NuPAGE system using an XCell SureLock Mini-Cell. Different types of gels are provided with different percentages of Bis-Tris gels, in the number of wells, or in their tightness.

1. Remove the top protection to expose the gel-loading wells, wash them, and fill them with 1X running buffer (avoid air bubbles that could affect sample migration). Do not forget also to remove the white stripe on the gel cassette, or there will be no migration.
2. Place the gel cassette into the lower buffer chamber in front of the core. A second cassette can be placed behind, or if only one gel has to be run replace it by the buffer dam. For each cassette, the shorter gel plate has to face the central

buffer core. Gels are blocked in the right position using the gel tension wedge and locking it by pulling its arm near the central buffer core.

3. Fill the upper buffer chamber with 200 mL running buffer until the sample wells are covered. For reduced samples, add 500 μ L NuPAGE antioxidant. Fill the lower buffer chamber with 200 mL running buffer.
4. For 10- μ L final sample preparation, add 2.5 μ L NuPAGE LDS sample buffer (4X) and for the reduced conditions 1 μ L NuPAGE reducing agent (10X). Complete to 10 μ L with deionized water. Include one well with prestained molecular weight markers. Heat samples at 95 °C for 5 min.
5. Load samples with long loading tips. To obtain a uniform run, load sample buffer in wells that do not contain samples.
6. Put on the cell safety lid and run the gel at a constant 200 V. Running times are very reproducible, approx 35 min for MES buffer and 50 min for MOPS buffer. The expected current is approx from 100 to 125 mA when starting and decreases during the run.

3.1.3 Treatment of Cell Extracts with Tetanus Neurotoxin

Treatment of cell extracts with tetanus neurotoxin is required to ascertain that the cellubrevin (Cb) expressed in the cell line used is indeed TeNT sensitive. Here, we carried out this experiment to demonstrate that canine Cb was sensitive to TeNT (5) (*see Note 3*).

1. Cells in culture are resuspended in resuspension buffer plus protease inhibitors and broken by passing through a ball bearing cell cracker.
2. Postnuclear supernatants (PNSs) are obtained by recovering the supernatant of a 5-min centrifugation at 1000 g, with the unbroken cells and nuclei retained in the pellet.
3. The recombinant TeNT-LC is produced and purified as previously described (*see Note 4*).
4. PNSs are treated with 200 nM of this toxin for 30 min at 37 °C in resuspension buffer.
5. Treated and untreated extracts are run in a 4–12% SDS-PAGE gel as previously described, and brevins (synaptobrevin or cellubrevin) are revealed by Western blotting.

3.1.4 Western Blotting for Brevins

After running of the extracts in a SDS-PAGE gel, the gel is transferred on a nitrocellulose membrane used for the revelation by Western blotting. These instructions assume the use of a Hoeffer tank transfer unit.

1. The transfer cassette in open position is put in a horizontal bath of transfer buffer with a first porous pad and two sheets of 3 MM Chr paper (Whatmann, Schleicher et Schuell) submerged.

2. Cut a sheet of nitrocellulose membrane the size of the SDS-PAGE gel. Write something on or cut it so that you can oriente your membrane and later recognize the face in contact with the gel. Put this membrane, previously wet with transfer buffer, on the 3 MM papers. It should also be submerged.
3. Break the cassette gel and cut the teeth. Carefully put the gel on the membrane. Do not forget to wet your gloves before moving the gel or it will stick to them.
4. Put two other sheets of 3 MM paper previously wet with the transfer buffer on the gel. Make sure that no bubbles are trapped in this resulting sandwich or there will be no local transfer. For that, carefully roll a 1-mL plastic pipet on this sandwich to eliminate bubbles.
5. Put a second porous pad wet with transfer buffer on this sandwich and close the transfer cassette.
6. Place the cassette into the transfer tank so that the nitrocellulose membrane is between the gel and the anode. This orientation is particularly important because proteins are moving from the gel to the anode and become attached to the membrane. If the membrane is not on the way, you will lose all your proteins in the buffer.
7. For the transfer, a 100-V electric current is applied for 2 to 3 h. To prevent overheating, transfer is carried out in a cold room. It can also be carried out overnight at 30 V.
8. Once the transfer is finished, take the cassette and open it. The prestained molecular weight markers should be visible on the membrane.
9. Incubate the membrane in blocking buffer for 30 min at room temperature with shaking.
10. The membrane is then incubated 1 h at room temperature or overnight in a cold room with shaking in blocking buffer supplemented by monoclonal antibody against brevins C110.1 diluted 1000 times. This antibody recognizes synaptobrevins 1 and 2 and cellubrevin, with the last the smallest of all three proteins.
11. When the primary antibody is removed, the solution can be kept at -20°C for several months (even years) and reused for further experiments.
12. Wash the membrane three times with TBS-Tween 0.1% for 15 min each bath.
13. Incubate the membrane at room temperature 1 h with the secondary antibody with shaking. Use a fresh 1:20,000X dilution for each experiment in TBS-Tween 0.1%.
14. Wash the membrane four times with TBS-Tween 0.1% for 15 min each bath.
15. Mix 1 mL of each solution from the ECL kit and put onto a Saran wrap spread out on the bench. Put the face of the membrane previously in contact with the gel on this drop so that all the membrane is in contact with the ECL reagent.
16. Remove the membrane from the ECL reagent and the excess of reagent on the gel by putting one corner of the membrane in contact with a Kimwipe. The blot is immediately placed in a piece of Saran wrap in an X-ray film cassette.
17. In a dark room, put a film in the cassette on the face of the blot that was previously in contact with the gel. Typically, 1 min is used for the first exposure time; afterward, modify this time according to the obtained results.

3.2 Transfection and Selection of MDCK Cells Expressing GFP-Cb

3.2.1 Transfection of MDCK Cells and Selection

MDCK cells are cultured in DMEM with 7% FBS and transfected by electroporation. This protocol uses a Bio-Rad electroporator. For each transfection, 3 million cells are necessary. This protocol has been used to select MDCK cells expressing human cellubrevin coupled to the GFP described previously (7). This allows detection of the protein in nonfixed cells and videomicroscopy experiments.

1. The day before transfection, cells are passed to reach approx 80% confluence on the day of transfection.
2. On the day of transfection, cells in culture are rinsed once with trypsin then trypsinized.
3. Cells are resuspended in DMEM plus FBS to inactivate the trypsin.
4. After centrifugation for 5 min at 900 *g*, cells are resuspended at 10×10^6 cells/mL in DMEM plus 15 mM HEPES to protect the cells.
5. Dilute 5 μ g of DNA in 50 μ L of a final 210 mM NaCl solution.
6. Place 3×10^6 cells in a 400- μ L volume into the cuvette. Electroporations are carried out at room temperature, so contrary to other protocols, cuvettes are not put on ice.
7. Add DNA to this cell mixture.
8. Select a 300-V pulse and 15 ms.
9. Immediately after the pulse, resuspend the cells in 5 mL warmed DMEM plus 15 mM HEPES.
10. Cells are then split as necessary in DMEM plus 10% FBS.
11. On the first day after transfection, change medium in the morning to remove dead cells. Depending on the results obtained, adapt, if necessary, the conditions used for electroporation (*see Note 5*).
12. If necessary, antibiotics to select transfected cells can be added in the medium at the end of the first day after transfection. For the selection of clones expressing GFP-Cb, G418 at 200 μ g/mL was added.

3.2.2 Clone Selection by Limit Dilution

Clone selection is made in 96-well tissue culture plates. The principle is to dilute cells resistant to an antibody (starting population) so that there is only one cell per three wells on average. This method can also be used for nonadhesive cells; in that case, just begin at step 2.

1. Cells from the starting population in culture are rinsed once with trypsin then trypsinized.
2. Resuspend cells in DMEM plus 10% FBS; this inactivates the trypsin. Make sure to completely dissociate cell clumps, or you could have more than one cell in a well.

3. Count cells and dilute them by a serial dilution so that 34 cells are present in 10 mL. This volume is necessary per 96-well tissue culture plate (theoretically, only 9.6 mL per plate are needed).
4. Add 100 μ L of this cell dilution in each well. Usually, prepare two tissue culture plates, depending on the proportion of cells expressing your transgene in the starting population.
5. Change the medium twice per week.
6. After 2 weeks, growing clones should be visible in the wells. If the starting dilution was appropriate, expect 17 to 30 clones on your plate. Discard the well in which you detect several proliferation starting points.
7. When 80% confluency is reached in a well, transfer the clone, half on a glass coverslip, half in a 24-well tissue culture plate. Process the coverslips for immunofluorescence. In the case of GFP-tagged protein, like GFP-Cb, directly address with a fluorescent microscope as explained for the visual test. Clones can also be selected by protein expression level in Western blotting.

3.2.3 Cell Lysis, Preparation of Samples for Western Blotting, and Choice of Expressing Clones

1. Pass MDCK cells on 5-mm tissue dishes, which are sufficient to test the presence of expressed GFP-tagged proteins in clones.
2. Rinse cells with 1X PBS and add 100 μ L cold lysis buffer plus Complete (1X) and leave them on ice 20 min or at 4 °C with shaking.
3. Scrape materials into a 1.5-mL Eppendorf tube.
4. Centrifuge at 15,000 rpm 20 min to eliminate nuclei and cell debris.
5. Keep supernatants and calculate their concentration using the Bio-Rad Protein Assay.
6. Aliquots from 20 to 50 μ g of extracts are sufficient to detect the expressed GFP-tagged protein. For 10- μ L final sample preparations, add 2.5 μ L NuPAGE LDS sample buffer (4X), and for the reduced conditions, add 1 μ L NuPAGE reducing agent (10X). Bring to 10 μ L with deionized water. Include one well with prestained molecular weight markers. Heat samples at 95 °C for 5 min before loading.
7. For the detection, use as primary antibody the anticellubrevin cl10.1 previously described or an anti-GFP monoclonal antibody.
8. After Western blotting, verify the size of the protein of interest and compare the expression level of your clones. Select clones with a reasonably good expression level and proper localization of the protein by immunofluorescence (i.e., early endosomes and plasma membrane for GFP-Cb).

3.3 Visual Test Based on Fluorescence for TeNT Activity

The visual test is based on the localization of the fluorescence in cells. In MDCK cells expressing GFP-Cb, the GFP is localized on vesicles and at the plasma membrane,

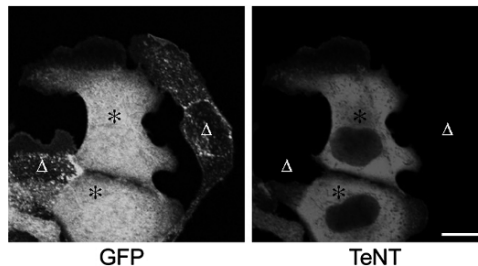
like endogenous cellubrevin. These cells are cotransfected with a pPur vector conferring puromycin resistance (Clontech, Palo Alto, CA) and a pCMV vector expressing a version of TeNT-LC modified for expression in eukaryotic cells. As a control, an inactive form of TeNT (E234Q) is also used. Wild-type and E234Q inactive TeNT in pCMV have been described previously (6). Cells are selected in medium containing 200 µg/mL G418 and 4 µg/mL puromycin. Cells expressing both wild-type TeNT and GFP-Cb show a cytosolic localization of fluorescence emitted by GFP because of the cleavage of GFP-Cb by TeNT. Thus, the localization of GFP signal is an indication of wild-type TeNT presence in living cells.

3.3.1 Selection of Clones by Direct Fluorescence or by Immunofluorescence (Fig. 2)

Process the clones for immunofluorescence as described below; for direct fluorescence, go directly from step 4 to step 12.

1. Put 12-mm coverslips in a 24-well tissue culture plate. Coverslips have to be previously sterilized by autoclave; otherwise, submerge the coverslips with a 70% ethanol preparation for 1 min, remove the coverslips, and let them completely dry in the culture hood.
2. Place the cells as previously described (cf 3.2.2) on the coverslips (25,000 to 100,000 per well) and let them grow for 24–48 h.
3. Dilute an aliquot of PFA 4% to 3% with 1X PBS. Replace cell medium into the wells with this 3% PFA for 17 min at room temperature to fix the cells.
4. Discard PFA into a hazardous waste container kept in a fume hood. Wash with 1X PBS.
5. Quench residual PFA by incubating in quenching solution for 15 min at room temperature. Wash with 1X PBS.

Fig. 2 MDCK cells expressing either GFP-Cb alone or GFP-Cb and wild-type tetanus neurotoxin. The light chain of the tetanus neurotoxin is detected by immunofluorescence (right panel) using an anti-TeNT antibody. The pattern of the direct signal of GFP-Cb (left panel) is sufficient to identify cells expressing (*) or not expressing TeNT (Δ). Cells expressing GFP-Cb alone show a vesicular pattern of fluorescence (Δ), whereas cells coexpressing wild-type TeNT (*) show diffuse labeling because of the cleavage of Cb and the liberation of soluble GFP. Bar = 13 µm. (Modified from *Ref. 5* with permission from the National Academy of Sciences.).



6. Permeabilize cells by incubation in 1X PBS plus 0.1% Triton X-100 for 10 min. Wash with 1X PBS.
7. To block nonspecific binding, incubate coverslips in blocking solution.
8. Incubate cells with primary antibodies in incubating solution for 1 h at room temperature. Antibodies can be the monoclonal antibody directed against the GFP protein previously described diluted 100 times and a monoclonal antibody against TeNT-LC (we used one generously given by H. Niemann).
9. Remove primary antibodies and wash sample three times for 5 min each with 1X PBS.
10. Dilute secondary antibodies at 1:400 in incubating solution; centrifuge 20 min at 12,000g to eliminate possible dye aggregates. Put the supernatant on cells for 1 h at room temperature.
11. Discard secondary antibodies and wash six times for 5 min each with 1X PBS.
12. Mount coverslips by carefully placing them on a drop of 1X PBS plus 50% glycerol upside down on a glass slide. Be careful when putting cells in contact with the mounting medium and avoid the formation of bubbles. Nail polish is used to seal the coverslips.
13. As soon as the polish is dry, slides can be observed on a microscope or kept at -20°C for months. Confocal laser scanning microscopy is performed with an SP2 confocal microscope (Leica, Heidelberg, Germany). Use excitation at 488 nm to stimulate GFP fluorescence in the green spectrum and excitation at 543 nm for Cy3 fluorescence with a red emission.

3.3.2 Wound-Healing Experiments (Fig. 3)

The MDCK cells can be induced to migrate by treatment with the hepatocyte growth factor (HGF) when cultured at low density or by mechanically wounding a monolayer formed when cells are cultured at high density. We selected the latter method, also called wound healing, because of its reproducibility and low cost and because a high number of cells can be observed at the same time.

1. Plate 0.5 to 1 million cells on sterile 12-mm coverslips in a 24-well tissue culture plate or, for videomicroscopy experiments, 2 million cells on sterile coverslips of the size needed for your chamber (usually 18 to 25 mm) in a six-well tissue culture plate. Allow the cells to grow for 3 to 5 days to allow monolayer formation.
2. Wound the cell monolayer by scratching with a bevel-edge needle.
3. Fix the cells at different times to perform immunofluorescence experiments as previously described (cf 3.3.1) or observe cell migration on a videomicroscope.

3.3.3 Time-Lapse Videomicroscopy and Measurement of Velocities

1. Just after wounding the monolayer, mount the coverslip in the video chamber and change the medium for DMEM⁻ supplemented with 10% FBS. This is important to remove cells detached from the support or they will readhere in the

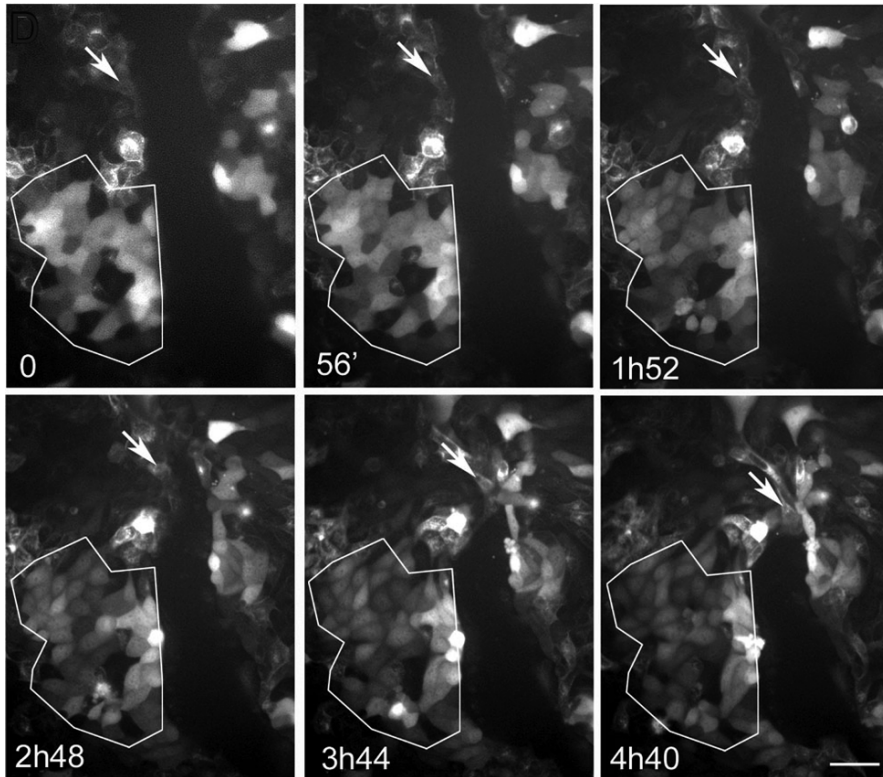


Fig. 3 Expression of tetanus neurotoxin impairs cell migration. Cell border migration of MDCK cells expressing GFP-Cb, with or without coexpression of wild-type TeNT (wt-TeNT), after monolayer injuries. Cells expressing wt-TeNT show a diffuse labeling of GFP because of the release of GFP by toxin cleavage. One area particularly rich in cells expressing wt-TeNT is outlined (bottom left sector). One cell not expressing wt-TeNT is indicated by an arrow. Note that this cell is moving faster than wt-TeNT-expressing cells. These images were extracted from a time-lapse movie, with times indicated corresponding to the time elapsed from the beginning of the film. Bar = 31 μ m. (Reproduced from *Ref. 5* with permission from the National Academy of Sciences.).

wound and disturb cell migration. Use of this medium is not essential, but it limits autofluorescence. If the microscope is not configured with a CO₂ control, supplement the medium with 10 to 15 mM HEPES.

2. Use an inverted microscope for observations. All our studies were performed with an inverted Leica DMIRE2 (Leica, Westlar, Germany) microscope placed within a temperature-controlled enclosure set at 37 °C with an $\times 20$ objective, 50-ms exposure, at a rate of 20 exposures per hour. Stream acquisitions of vesicle movement can also be performed with an $\times 63$ oil objective when studying displacement of GFP-Cb. The camera used was the Cascade, which allows an amplification of the transmitted signal up to $\times 3000$ (Roper Scientific, Photometrics).

For vesicle observations, the amplification used was $\times 2500$. Digital images are recorded and viewed using MetaMorph software (Universal Imaging, Downingtown, PA). Analyses of video sequences are done with MetaMorph and Excel (Microsoft, Redmond, WA).

After cell monolayer injuries, velocities can be measured by the displacement of individual cells over time. A minimum of three independent recordings with 60 cells have to be analyzed per condition, 20 cells per injury, 10 at each border of the wound. Statistical analyses can be performed using the Kruskal–Wallis nonparametric test with Statview software (SAS Institute, Cary, NC).

4 Notes

1. With 500 mL culture inoculated, approx 5 mg purified TeNT-LC are expected.
2. The expected molecular weight of TeNT-LC is about 50 kDa, but a dimer is often copurified.
3. Use parallel cells of already-tested species (human or rat, for example) to have a positive control of the enzymatic activity of your TeNT-LC preparation.
4. The light chain of the botulinic neurotoxin can be used as a negative control for this experiment as cellubrevin is not cleaved by this toxin.
5. This protocol gives 20–30% mortality and 30–40% of cells transfected when direct expression of a GFP protein is visualized. Nevertheless, this has to be empirically tested in each laboratory because of the heterogeneity of cell lines between different laboratories. Viability tests are recommended. The parameters selected are a compromise between the percentage of cell transfection and cell survival. In our case, the most important parameter was the voltage; if too high, almost all the cells died, but if too low, only a few cells were transfected.

Acknowledgments We are grateful to Thomas Binz and Heiner Niemann (School of Medicine of Hannover, Germany) for the generous gift of monoclonal antibody against the light chain of TeNT and the plasmids encoding TeNT. This work was supported in part by grants from INSERM (Avenir Program), the European Commission (“Signaling and Traffic” STREP 503229), the Association Française contre les Myopathies, the Association pour la Recherche sur le Cancer, the Ministère de la Recherche (ACI-BDP), the Fondation pour la Recherche Médicale, the HFSP (RGY0027/2001-B101), and the Fondation pour la Recherche sur le Cerveau to T.G. V.P.G. was supported by a postdoctoral fellowship from the Fondation pour la Recherche Médicale.

References

1. Humeau, Y., Doussau, F., Grant, N.J., and Poulain, B. (2000) How botulinum and tetanus neurotoxins block neurotransmitter release. *Biochimie* **82**, 427–446.
2. Schiavo, G., Matteoli, M., and Montecucco, C. (2000) Neurotoxins affecting neuroexocytosis. *Physiol. Rev.* **80**, 717–766.

3. Galli, T., Chilcote, T., Mundigl, O., Binz, T., Niemann, H., and De Camilli, P. (1994) Tetanus toxin-mediated cleavage of cellubrevin impairs exocytosis of transferrin receptor-containing vesicles in CHO cells *J. Cell Biol.* **125**, 1015–1024.
4. Das, V., Nal, B., Dujeancourt, A., et al. (2004) Activation-induced polarized recycling targets T cell antigen receptors to the immunological synapse; involvement of SNARE complexes. *Immunity* **20**, 577–588.
5. Proux-Gillardeaux, V., Gavard, J., Irinopoulou, T., Mege, R.M., and Galli, T. (2005) Tetanus neurotoxin-mediated cleavage of cellubrevin impairs epithelial cell migration and integrin-dependent cell adhesion. *Proc. Natl. Acad. Sci. U. S. A.* **102**, 6362–6367.
6. McMahon, H.T., Ushkaryov, Y.A., Edelman, L., et al. (1993) Cellubrevin is a ubiquitous tetanus-toxin substrate homologous to a putative synaptic vesicle fusion protein. *Nature* **364**, 346–349.
7. Martinez-Arca, S., Proux-Gillardeaux, V., Alberts, P., Louvard, D., and Galli, T. (2003) Ectopic expression of syntaxin 1 in the ER redirects TI-VAMP- and cellubrevin-containing vesicles. *J. Cell Sci.* **116**, 2805–2816.

Exocytosis of Endothelial Cells Is Regulated by *N*-Ethylmaleimide-Sensitive Factor

Munekazu Yamakuchi, Marcella Ferlito, Craig N. Morrell, Kenji Matsushita, Craig A. Fletcher, Wangsen Cao, and Charles J. Lowenstein

1 Introduction.....	203
2 Materials	204
3 Methods.....	207
4 Notes	214
References.....	215

Summary Endothelial exocytosis of granules is a rapid response to vascular injury. However, the molecular machinery that regulates exocytosis in endothelial cells is not well understood. Recently developed techniques have defined the endothelial proteins that control vesicle and granule trafficking in endothelial cells. These techniques have revealed that syntaxin 4, synaptobrevin 3, and *N*-ethylmaleimide-sensitive factor (NSF) play a critical role in endothelial granule exocytosis. Additional studies have shown that nitric oxide regulates exocytosis by chemically modifying NSF. Further characterization of the factors that regulate exocytosis will lead to novel treatments for vascular diseases such as myocardial infarction and stroke.

Keywords *N*-Ethylmaleimide-sensitive factor; granule; nitric oxide; P-selectin; vesicle; von Willebrand factor; Weibel–Palade body.

1 Introduction

The initial endothelial response to injury is exocytosis. A variety of stimuli, including hypoxia, physical trauma, or inflammatory mediators, trigger endothelial cells to release the contents of specialized granules called Weibel–Palade bodies (1). Von Willebrand factor (VWF), released by endothelial exocytosis, induces platelet rolling and thrombosis. P-Selectin externalized by exocytosis activates leukocyte rolling, the first step in leukocyte trafficking. Endothelial granules also contain additional proinflammatory and prothrombotic mediators that activate inflammation and thrombosis in response to vascular injury (2,3).

The exocytic machinery that drives vesicle trafficking and membrane fusion in endothelial cells is similar to that found in neurons and yeast (4). The adenosine 5'-triphosphate (ATP)-hydrolyzing enzyme *N*-ethylmaleimide-sensitive factor (NSF) interacts with transmembrane proteins called soluble NSF receptor attachment protein receptors (SNAREs) to regulate exocytosis. Unique SNARE molecules on the cytoplasmic surface of endothelial granules and on the cytoplasmic surface of the plasma membrane interact, specifying which particular granules fuse with a specific target membrane. Members of the superfamily of rab proteins guide the assembly of SNAREs and NSF onto the surface of granules in preparation for membrane fusion. A subset of SNAREs and rabs along with NSF regulate exocytosis in endothelial cells (5).

Exocytosis of granules from endothelial cells occurs within minutes of stimulation. Special techniques have been adapted to study the intracellular machinery that drives exocytosis and the extracellular and *in vivo* consequences of exocytosis. The discovery of the molecular machinery that regulates exocytosis from endothelial cells has led to the invention of novel peptides that inhibit exocytosis by targeting these components (6,7). Using these tools, studies have characterized novel regulators of endothelial exocytosis (5,8,9). We found that nitric oxide (NO), an endogenous messenger molecule that inhibits inflammation, chemically modifies NSF. NO S-nitrosylation of NSF may explain how NO inhibits vascular inflammation. These techniques that characterize exocytosis have led to better understanding of the importance of endothelial exocytosis in the host response to vascular injury.

2 Materials

2.1 Endothelial Cell Culture

1. Endothelial cells analyzed for exocytosis include human umbilical vein endothelial cells (HUVECs) and human aortic endothelial cells (HAECs) from Cambrex (East Rutherford, NJ).
2. Endothelial media: Endothelial growth media 2 (EGM-2). EGM-2 is supplemented with a Bullet kit supplement (Cambrex) containing growth factors and cytokines and supplemented with 2% fetal bovine serum (FBS; Cambrex).
3. Endothelial cells are grown on sterile 100-mm tissue culture dishes (Corning Life Science, Acton, MA) without matrix.
4. Solutions of trypsin (0.25%) and ethylenediaminetetraacetic acid (EDTA) (1 mM) and phosphate-buffered saline (PBS), pH 7.4, used were from Gibco/Invitrogen (Carlsbad, CA).
5. Thrombin stock: 100 U/mL containing 1% bovine serum albumin (BSA); store at -80°C . Thrombin stocks are defrosted once, and then the excess is discarded, never refrozen or rethawed.

6. Diethylenetriamine (DETA)-NONOate (Cayman Chemicals, Ann Arbor, MI): DETA-NONOate is dissolved in 10 mM NaOH solution just before adding to the media. DETA-NONOate is very sensitive to the temperature and pH of the solution. It also has a half-life of 20 h at 37 °C. DETA-NONOate powder should be dissolved in buffer on ice just before use (see [Note 1](#)).

2.2 Enzyme-Linked Immunosorbent Assay and Fluorescence Activated Cell Sorting Materials

1. Enzyme-linked immunosorbent assay (ELISA) kits to measure exocytosis of VWF from endothelial cells (American Diagnostica, Stamford, CT).
2. Antibody to P-selectin was a mouse monoclonal antibody immunoglobulin G1 (IgG1) isotype (BD Biosciences Pharmingen, San Jose, CA, 555524). Its isotype-matched control is also from BD Biosciences Pharmingen (555749).

2.3 Immunoprecipitation for S-Nitrosylated NSF

1. Cell lysis buffer: 50 mM Tris-HCl, 150 mM NaCl, 1% NP40, phenylmethylsulfonyl fluoride (PMSF), and protein inhibitor cocktail.
2. Control rabbit IgG (Santa Cruz Biotechnology, Santa Cruz, CA). Antibody to S-nitrosocysteine (Sigma, St. Louis, MO).
3. Protein A/G agarose (Santa Cruz Biotechnology).
4. Loading buffer (10X): 250 mM Tris-HCl, 1920 mM glycine, 1.0% (w/v) sodium dodecyl sulfate (SDS), pH 8.3; store at room temperature.
5. Transfer buffer (1X): 48 mM Tris-HCl, 39 mM glycine, 20% (v/v) methanol, 0.05% (w/v) SDS; store at room temperature.
6. Tris-buffered saline with Tween (TBS-T): Prepare 10X stock with 1.37 M NaCl, 27 mM KCl, 250 mM Tris-HCl, pH 7.4, 0.5% Tween-20. Dilute 100 mL with 900 mL water for use.
7. Blocking buffer: 5% (w/v) nonfat dry milk in TBS-T.
8. Primary antibody dilution buffer: TBS-T supplemented with 1% (w/v) nonfat dry milk.
9. Antibody to NSF (BD Transduction Laboratories, San Jose, CA).
10. Secondary antibody dilution buffer: TBS-T supplemented with 2.5% (w/v) nonfat dry milk.
11. Secondary antibody is anti-mouse IgG conjugated to horse radish peroxidase (HRP) (Santa Cruz Biotechnology).

2.4 S-Nitrosylation of NSF by Biotin-Switch

1. Cell lysis buffer: 250 mM HEPES-NaOH, pH 7.7, 1 mM EDTA, 0.1 mM neocuproine.

2. Control rabbit IgG (Santa Cruz Biotechnology). Antibody to S-nitrosocysteine (Sigma).
3. Protein A/G agarose (Santa Cruz Biotechnology).
4. Loading buffer (10X): 250 mM Tris-HCl, 1920 mM glycine, 1.0% (w/v) SDS, pH 8.3; the buffer is stored at room temperature.
5. Transfer buffer (1X): 48 mM Tris-HCl, 39 mM glycine, 20% (v/v) methanol, 0.05% (w/v) SDS; store at room temperature.
6. Tris-buffered saline with Tween (TBS-T, 10X): 1.37 M NaCl, 27 mM KCl, 250 mM Tris-HCl, pH 7.4, 0.5% Tween-20. Dilute 100 mL with 900 mL water for use.
7. Blocking buffer: 5% (w/v) nonfat dry milk in TBS-T.
8. Primary antibody dilution buffer: TBS-T supplemented with 1% (w/v) nonfat dry milk.
9. Antibody to NSF (BD Transduction Laboratories).
10. Secondary antibody dilution buffer: TBS-T supplemented with 2.5% (w/v) nonfat dry milk.
11. Secondary antibody is antimouse IgG conjugated to HRP (Santa Cruz Biotechnology).

2.5 Leukocyte Adhesion

1. HL-60 cells (American Type Culture Collection, Manassas, VA).
2. 3'-O-Acetyl-2',7'-bis(carboxyethyl)-4 or 5-carboxyfluorescein, diacetoxymethyl ester (BCECF-AM) (Molecular Probes/Invitrogen, Carlsbad, CA).
3. Anti-P-selectin antibodies (purchased from BD Bioscience Pharmingen).

2.6 TAT Fusion Peptides

1. TAT fusion peptides are composed of three parts (10). The N-terminal part is an 11-amino acid fragment from the human immunodeficiency virus (HIV) TAT peptide. The middle portion contains three glycine residues as a linker to decrease steric hindrances. The C-terminal portion consists of 20–30 amino acids that correspond to rationally selected domains of proteins that regulate exocytosis.

2.7 Leukocyte Rolling

1. Solutions of ketamine (100 mg/mL) and xylazine (100 mg/mL) are prepared in PBS.
2. Rhodamine 6G 0.05% is prepared in PBS.

3 Methods

3.1 Endothelial Cell Culture

1. Culture HUVECs or HAECs in EGM-2 medium supplemented with the Bullet kit growth factors and serum.
2. Change the growth medium the day after seeding and every other day thereafter (see [Note 2](#)).

3.2 ELISA for VWF Release

1. Plate HUVECs or HAECs from passages 2–4 into two 24-well plates with 250 μ L medium per well or into three 96-well plates with 100 μ L medium per well. Feed cells with endothelial medium supplemented with EGM-2 and serum and Bullet kit. Grow overnight.
2. Make sure cells are confluent the next morning. Remove the tissue culture plates from the incubator and place in a tissue culture hood on top of Styrofoam slabs to maintain the temperature at 37 °C. Do not shake cells or move plates quickly because sudden movements will cause exocytosis. Change the medium with prewarmed EGM-2 medium without serum and without Bullet kit supplements (see [Note 3](#)).
3. Add 1.0 U/mL thrombin and move plates back into the tissue culture incubator. Incubate for 30–60 min.
4. Carefully remove plates from the incubator, moving plates gently as above and placing plates on Styrofoam slabs in a tissue culture hood to maintain an even temperature.
5. Harvest supernatant. Freeze supernatant.
6. Add supernatant to VWF ELISA and add cell media standards. Watch the assay carefully; the moment the color of any sample turns blue, stop the entire assay with stop buffer.
7. Measure the OD at 450 nm in a spectrophotometer. (An example of using the ELISA to measure VWF release is shown in [Fig. 1](#).)

3.3 FACS for P-Selectin Externalization

1. Culture HUVECs or HAECs in EGM-2 medium with Bullet kit growth factors and serum. Use passages 2–5 endothelial cells. Higher-passage cells lose the ability to undergo regulated exocytosis.
2. Plate cells on a 12- or 24-well plate.
3. Culture cells for 1–2 d until confluent.

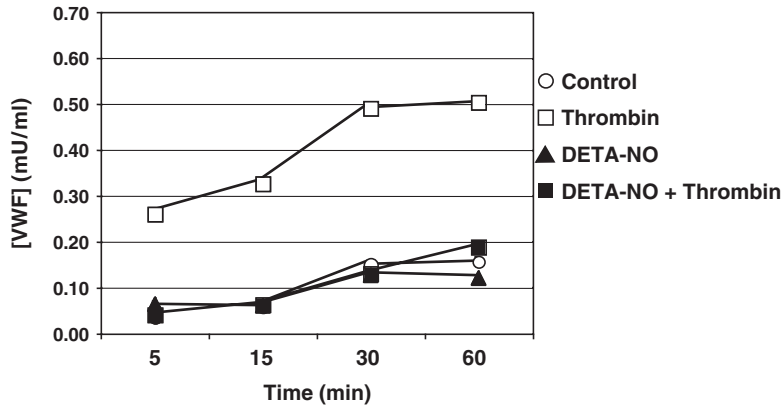


Fig. 1 Nitric oxide inhibits endothelial cell exocytosis of VWF. HAECs were pretreated with 0.5mM DETA-NONOate for 16h, washed, and then stimulated with 0.5U/mL thrombin. Media was collected at various times after thrombin stimulation and measured for VWF with an ELISA ($n = 3 \pm SD$). Some cells were pretreated with 1mM L-mono-methylarginine (L-NMMA) for 16h before thrombin stimulation.

4. Remove endothelial cells from incubator. Handle the cells carefully as above, without sudden motions, and place on Styrofoam slabs inside a tissue culture hood to maintain the temperature.
5. Refeed the cells with EGM-2 medium without growth factors or serum. Add medium gently to cells by pipeting on the side of the dish rather than the base so that the jet of medium does not stimulate the endothelial cells.
6. Add 0.5 U/mL thrombin.
7. Gently replace cells in the incubator for 30 min (*see Note 4*).
8. Gently remove cells from the incubator and place on Styrofoam slabs in a tissue culture hood.
9. Aspirate medium and wash cells with 1 mL prewarmed PBS twice.
10. Add antibody to P-selectin or an isotype-matched control antibody at 10 μ L antibody per 1 mL PBS cell medium.
11. Incubate in the dark at 22°C for 1 h.
12. Wash cells three times with 1 mL PBS. Trypsinize cells for 3 min. Add EGM-2 with fetal calf serum to inactivate trypsin. Transfer cells to Eppendorf 1.5-mL tubes.
13. Centrifuge and resuspend in PBS three times.
14. Centrifuge cells, resuspend in 500 μ L PBS, and immediately analyze by FACS.

3.4 Measurement of NSF S-Nitrosylation by Immunoprecipitation

1. Grow endothelial cells as above.
2. Treat cells with 0, 0.1, 0.5, and 1mM DETA-NONOate and culture for 16h without light (*see Note 5*).

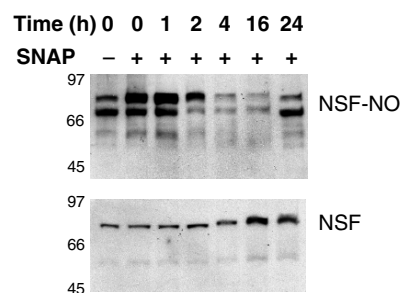
3. After 16 h, aspirate cell medium and rinse cells with cold PBS.
4. Add 0.7 mL lysis buffer to the cells in the 100-mm dish. Rock the dish gently for 15 min at 4°C. Scrape cells and transfer the resulting lysate to an Eppendorf tube.
5. Wash the dish once with 0.3 mL lysis buffer and combine with first lysate. Incubate 15 min on ice.
6. Centrifuge cell lysate at 10,000 *g* for 10 min at 4°C. Transfer the supernatant to a new Eppendorf tube and put on ice.
7. Measure the protein concentration of each sample. Prepare the diluted BSA standards in the range of 0, 0.2, 0.4, 0.6, 0.8, and 1.0 mg/mL. Pipet 10 µL of these standards and each HAEC lysate into appropriately labeled 1.5-mL Eppendorf tubes. Add 300 µL of the Coomassie reagent to each tube and vortex. Wait for a few minutes until you can see that the color developed well and read at 595 nm with the spectrophotometer. Prepare a standard curve by plotting each BSA datum. Using this curve, determine the protein concentration of each HAEC lysate. The reagents should be warmed to room temperature before use as cold temperatures may affect the assay.
8. To preclear cell lysates, add 0.25 µg of the control rabbit IgG and 20 µL of suspended protein A/G-agarose to the whole cell lysate. Incubate at 4°C for 60 min.
9. After centrifuging lysates at 1000 *g* for 30 s at 4°C, transfer supernatant (cell lysate) to a new Eppendorf tube on ice.
10. Add 10 µL anti-S-nitrosocysteine antibody and rotate the lysates slowly for 2–24 h at 4°C in the dark (*see Note 5*).
11. Add 20 µL suspended protein A/G-agarose and incubate for 1 h at 4°C on a rotator.
12. Spin 1 min at 1000 *g* at 4°C and aspirate and discard supernatant.
13. Add 500 µL lysis buffer and invert the Eppendorf tube several times.
14. Spin 1 min at 1000 *g* at 4°C, aspirate and discard supernatant, and resuspend in lysis buffer.
15. Repeat wash steps three times.
16. After final wash, resuspend beads in 50 µL Laemmli sample buffer and vortex.
17. Boil samples for 2–3 min.
18. Prepare the loading buffer by diluting 50 mL 10X running buffer with 450 mL water in a measuring cylinder. Cover with Parafilm and invert to mix.
19. Prepare a 1.5-mm thick 7.5% gel by cutting the seal of the bottom edge. Set the gel and remove the comb carefully.
20. Add the running buffer to the upper and lower chambers of the gel unit and load the 40 µL of each sample in a well. One well is used for the prestained molecular weight markers.
21. Complete the assembly of the gel unit and connect to a power supply.
22. Run at 30 mA until the blue dye fronts can be just run off the gel.
23. Transfer the samples (which have been separated by SDS polyacrylamide gel electrophoresis [PAGE]) to nitrocellulose membranes by the trans-blot machine.
24. Lay two more wetted sheets of watman chromatography grade 3 MM paper on top of the membrane, ensuring that no bubbles are trapped in the resulting sandwich. Close the transfer cassette.

25. Rinse the separating gel with PBS and place on top of the Whatman chromatography grade 3MM paper.
26. Lay a sheet of the nitrocellulose cut just larger than the size of the separating gel on the surface of the gel.
27. Lay two more wetted sheets of Whatman chromatography grade 3MM paper on top of the membrane, ensuring that no bubbles are trapped in the resulting sandwich. Close the transfer cassette.
28. Transfer proteins at 15 V for 30 min.
29. The colored molecular weight marker should be clearly visible on the membrane. The membrane can be cut to a good size using a razor blade.
30. Incubate the nitrocellulose in 40 mL blocking buffer for 1 h at room temperature on a rocking platform.
31. After the blocking buffer is discarded, add a 1:1000 dilution of the antibody to NSF in TBS-T/1% milk for 1 h at room temperature or overnight at 4 °C on a rocking platform.
32. Wash the membrane three times for 5 min each with 50 mL TBS-T.
33. Freshly prepare the HRP-conjugated secondary antibody for each experiment as a 1:2,000 dilution in TBS-T/2.5% milk and add it to the membrane for 60 min at room temperature on a rocking platform.
34. Wash the membrane three times for 15 min each with TBS-T.
35. Warm the enhanced chemiluminescence (ECL) reagent separately to room temperature. Once the final wash is removed from the blot, mix the ECL detection solutions A and B together in a ratio of 40:1 and then immediately add to the blot.
36. Wait for 1 min, wrap the membrane in the Saran wrap, and put it on an X-ray film cassette.
37. In the darkroom, place film on the membrane in an X-ray film cassette for a suitable exposure time, usually a few minutes. You can see the band around 80 kDa. (An example of immunoprecipitation to detect S-nitrosylation of NSF is shown in Fig. 2.) (See Note 6.)

3.5 Measurement of NSF S-Nitrosylation by Biotin-Switch Assay

1. Add 16 mL ice-cold assay buffer (250 mM HEPES-NaOH, pH 7.7, 1 mM EDTA, 0.1 mM neocuproine) to every gram of minced tissue (brain, heart, and spleen) and homogenize the tissue with a Polytron for about 30–45 s on ice.

Fig. 2 NO nitrosylation of NSF is reversible. HAECs were pretreated with the NO donor SNAP (100 μ M) for 4 h and washed to remove the NO donor, and cells were harvested at various times after treatment. **(Top)** Cell lysates were immunoprecipitated with antibody to nitrosocysteine and immunoblotted with antibody to NSF. **(Bottom)** Total cell lysates were immunoblotted with antibody to NSF. (Reprinted from *Ref. 8*, © 2003, with permission from Elsevier.)

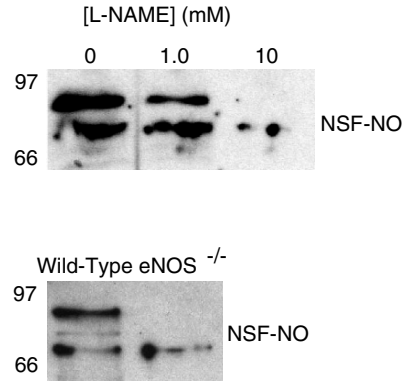


2. Centrifuge the tube at 750 *g* for 10 min at 4 °C.
3. Add 40 μ L 10% 3-([3-cholamidopropyl]dimethylamino)-1-propanesulfonate (CHAPS) per milliliter of supernatant to the mixture.
4. Dispense tissue homogenate into two 100- μ L aliquots in 1.5-mL centrifuge tubes. As a positive control, add 10 μ L of DEA-NONOate (10 mM) to the tissue homogenate. Mix the reaction mixture and incubate it in the dark for 30 min at room temperature.
5. Add the 300 μ L blocking solution (9 volumes assay buffer, 1 volume 25% SDS solution, 20 mM methylmethanethiosulfonate) to the mixture. Suspend the mixture well and incubate for 1 h at 50 °C in the dark.
6. Add cooled acetone (800 μ L at -20 °C), incubate at -20 °C for 10 min, then centrifuge at 2000 *g* for 10 min at 4 °C.
7. After removal of acetone, rinse pellet with another 800 μ L cooled acetone and centrifuge again as described above.
8. Resuspend the pellets with 60 μ L solubilization buffer (assay buffer with 1% SDS) per tube.
9. Add 2 μ L freshly prepared ascorbate solution (50 mM) to the mixture and vortex vigorously.
10. Add 20 μ L 4 mM HPDP-biotin to the mixture. Vortex and incubate at room temperature for 1 h.
11. Add cooled acetone (100 μ L at -20 °C), incubate at -20 °C for 10 min, and then centrifuge at 2000 *g* for 10 min at 4 °C.
12. Suspend pellet in 100 μ L solubilization buffer.
13. Add neutralization buffer (20 mM Tris-HCl pH 7.7, 100 mM NaCl, 1 mM EDTA, 0.5% Triton X-100) (200 μ L) and 15 μ L of streptavidin-agarose (neutravidin-agarose, Pierce). Rotate the mixture for 1 h at room temperature.
14. Centrifuge the mixture at 200 *g* at 10 s.
15. Wash the pellet with 100 μ L neutralization buffer containing 600 mM NaCl five times.
16. Add 20 μ L 4X SDS sample buffer to the pellet and load onto a 7.5% acrylamide gel for SDS-PAGE.
17. Blot the gel onto nitrocellulose membrane and perform Western blotting analysis with a monoclonal antibody to NSF. (An example of the biotin-switch assay used to detect S-nitrosylation of NSF is shown in Fig. 3.) (See Note 7.)

3.6 *Fluorescent Microscopy for Leukocyte Adhesion*

1. Grow HL-60 cells in RPMI 1640 medium with 10% FBS. Spin cells down and resuspend in HBSS solution.
2. Culture HUVECs (2×10^5) on 12-well plates at 37 °C in a humidified atmosphere of 5% CO₂ for 24 h. Cells should be 100% confluent before the experiment begins.
3. One of the endothelial cell wells should be pretreated with 1 μ g of antibody to P-selectin for 15 min in the incubator. This serves as a negative control.

Fig. 3 Nitrosylation of NSF in vivo. **(Top)** HAECs were treated with increasing concentrations of the NOS inhibitor L-NAME. Nitrosothiols were biotinylated and precipitated with avidin-agarose; precipitants were immunoblotted with antibody to NSF. NSF is S-nitrosylated in endothelial cells, and L-NAME inhibits endogenous nitrosylation of NSF. **(Bottom)** Splens from wild-type mice and mice lacking eNOS were harvested and prepared as above. NSF is S-nitrosylated only in mice expressing eNOS. (Reprinted from *Ref. 8*, © 2003, with permission from Elsevier.).

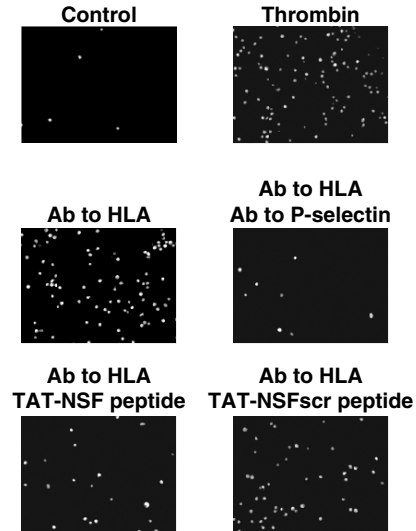


4. After 10 min, stimulate HUVECs with 0.5 U/mL thrombin for 45 min.
5. Calculate the HL-60 cell number using the hemocytometer cell count calculator. Adjust the HL-60 cell number to 1×10^7 /mL.
6. Label HL-60 cells with $10 \mu\text{M}$ BCECF-AM for 15 min at 37°C in the incubator.
7. Wash HL-60 cells with 5 mL warm HBSS solution twice.
8. Adjust the final HL-60 cell number to 1×10^8 /mL and keep them in the incubator until use.
9. Add 0.5 mL HL-60 cells to HUVECs after HUVECs have been stimulated with thrombin for 45 min as above.
10. Cover the plate with aluminum foil to prevent photobleaching and leave it at 4°C for 15 min to allow for cell adhesion.
11. Wash the HL-60/HUVEC mixture three times with fresh HBSS solution very gently to remove unbound cells.
12. Add EGM-2 medium.
13. Count the HL-60 cells adhering to endothelial cells in three to five randomly selected fields of view in each well by a fluorescent microscope.
14. Photograph the fluorescence intensity with a fluorescent microscope at $\times 10$ over an area $520 \times 700 \mu\text{m}$. (An example of fluorescent microscopy to detect leukocyte adhesion to endothelial cells is shown in [Fig. 4](#).)

3.7 TAT Fusion Peptides to Inhibit Exocytosis

1. Dissolve TAT fusion polypeptides in PBS at a solution of 1 mM.
2. Add TAT fusion polypeptides to the media of endothelial cells at a concentration of 0, 1.0, or $10 \mu\text{M}$.
3. Return cells to the incubator for 30 min.
4. Treat cells with 1.0 mU/mL thrombin for 30 min.
5. Analyze the cell medium for VWF with an ELISA (see [Note 8](#)).

Fig. 4 Antibody activates leukocyte adherence to endothelial cells. HAECs were treated with antibody to HLA (1 $\mu\text{g}/\text{mL}$) or thrombin (1 U/mL) for 45 min, and then rhodamine-6G labeled HL-60 cells were added for 15 min and then washed; adherent leukocytes were counted. Some HAECs were pretreated with antibody to P-selectin (1 $\mu\text{g}/\text{mL}$), TAT-NSF peptide (20 $\mu\text{g}/\text{mL}$), or TAT-NSFscr control peptide. (Reprinted from *Ref. 12*, © 2007, National Academy of Sciences, U. S. A.).



3.8 Intravital Microscopy for Leukocyte Rolling

1. Anesthetize 5- to 6-week-old mice with an intramuscular injection of ketamine (80 mg/kg) and xylazine (13 mg/kg). This dose produces 30–45 min of anesthesia.
2. Inject mice intravenously with 50 μL 0.05% rhodamine 6G to label leukocytes in vivo.
3. Expose the abdominal organs with a midline incision. Exteriorize the intestines on a culture dish such that the mesentery and mesenteric vessels are lying flat.
4. Place the mouse on an inverted fluorescent microscope stage with the stage warmer set at 37 $^{\circ}\text{C}$. Select a vessel of appropriate size (~120–180 μm), artery or vein. The velocity of leukocytes is slower in venules and easier to measure. Using a red fluorescent filter, fluorescent rhodamine 6G leukocytes can now be seen flowing in the vessel.
5. Collect baseline nonstimulated images prior to induction of endothelial cell exocytosis.
6. Induce endothelial exocytosis by either superfusion of a degranulating agent such as histamine (1 μM) or intravenous injection of a degranulating agent such as angiotensin.
7. Collect images over time. Determine endothelial cell exocytosis indirectly by measuring change in leukocyte velocity from baseline or counting the number of leukocytes/frame at a given time-point normalized to the area of the imaged vessel.
8. As an alternative means to determine endothelial cell exocytosis, fluorescent 1- μm carbamide beads can be conjugated either covalently or noncovalently to an anti-P-selectin antibody and injected into the mouse prior to stimulation. Change in microsphere velocity vs baseline can be determined as a measure of endothelial exocytosis (*see Note 9*).

4 Notes

1. All NO donors are unstable. DETA-NONOate is very sensitive to the temperature and pH of the solution. DETA-NONOate has a half-life of 20 h at 37 °C. DETA-NONOate powder should be dissolved on ice just before use. NO donors like DETA-NONOate should never be heated since they might explode.
2. HAECs and HUVECs grow slowly, and HAECs will not proliferate past passage numbers 7–8. We usually use endothelial cells at less than passage 5.
3. Endothelial cells should be handled very carefully since we have found that a variety of physical stimuli can activate exocytosis. For example, the metal base of tissue culture hoods is cooler than 37 °C and conducts heat away from endothelial cells and their media; this cooling activates exocytosis. Therefore, we place our cell cultures on top of Styrofoam slabs in the tissue culture hood and leave the cells exposed to room temperature for as short a time as possible. Shear stress can activate exocytosis, so we add media to the side of the endothelial tissue culture dish instead of pipeting media directly on top of endothelial cells. Abrupt motion (such as rapping the side of the tissue culture dish or dropping the dish onto the tissue culture incubator base) can also activate exocytosis. Thus, endothelial cells need to be treated gently during studies of exocytosis.
4. P-Selectin is a challenging marker to study for exocytosis since after externalization it is rapidly internalized. We treat endothelial cells with thrombin for 10–30 min but no longer than 30 min when analyzing P-selectin externalization.
5. S-Nitrosocysteine bonds are unstable; light cleaves the cysteine–NO bond, so the immunoprecipitation should be performed in the dark.
6. Several techniques have been used to study NO modification of target proteins. This method uses immunoprecipitation of nitrosothiol groups followed by immunoblotting of the specific protein (in this case, NSF) (8). This technique is more rapid than other techniques but depends on the quality of the antibody to nitrosothiol.
7. This method of studying NO modification of target proteins relies on blocking all free-thiol groups, followed by removal of NO from nitrosothiols; the free thiols are then reacted with a compound containing biotin so that the target proteins can be precipitated. This technique, often called the Jaffrey technique or the biotin-switch assay, is more lengthy than other techniques but is more specific (11).
8. These fusion polypeptides enter cells and inhibit NSF, thus blocking exocytosis (6,7). The polypeptides contain a TAT domain and an NSF domain (10). The TAT domain is a fragment of the TAT protein from HIV that can cross cell membranes. The NSF domain is a peptide containing a sequence from NSF that inhibits NSF activity.
9. Intravital microscopy is a technique used to study exocytosis in vivo. The vessels are stimulated with a compound such as histamine or FeCl₃, which triggers endothelial cell exocytosis. Exocytosis leads to the externalization of P-selectin, which mediates platelet rolling and leukocyte rolling along the vessel. Platelets or leukocytes are labeled with a fluorescent dye to visualize rolling along the vessel.

Acknowledgments We would like to thank Ms. Jacqueline Hewitt for assistance preparing the manuscript. Supported was received by grants from the National Institutes of Health (P01 HL56091, R01 HL074061, R01 HL78635, P01 HL65608), AHA (EIG 0140210N), the Ciccarone Center, the John and Cora H. Davis Foundation, and the Clarence Doodeman Professorship to C.J.L. and by grants RR07002 and HL074945 from the National Institutes of Health to C.M.

References

1. Weibel, E.R., and Palade, J.E. (1964) New cytoplasmic components in arterial endothelium. *J. Cell Biol.* **23**, 101–106.
2. Lowenstein, C.J., Morrell, C.N., and Yamakuchi, M. (2005) Regulation of Weibel–Palade body exocytosis. *Trends Cardiovasc. Med.* **15**, 302–308.
3. Wagner, D.D. (1993) The Weibel–Palade body: the storage granule for von Willebrand factor and P-selectin. *Thromb. Haemost.* **70**, 105–110.
4. Jahn, R., and Sudhof, T.C. (1999) Membrane fusion and exocytosis. *Annu. Rev. Biochem.* **68**, 863–911.
5. Lowenstein, C.J., and Tsuda, H. (2006) *N*-Ethylmaleimide-sensitive factor: a redox sensor in exocytosis. *Biol. Chem.* **387**, 1377–1383.
6. Matsushita, K., Morrell, C.N., and Lowenstein, C.J. (2005) A novel class of fusion polypeptides inhibits exocytosis. *Mol. Pharmacol.* **67**, 1137–1144.
7. Morrell, C.N., Matsushita, K., and Lowenstein, C.J. (2005) A novel inhibitor of *N*-ethylmaleimide-sensitive factor decreases leukocyte trafficking and peritonitis. *J. Pharmacol. Exp. Ther.* **314**, 155–161.
8. Matsushita, K., Morrell, C.N., Cambien, B., et al. (2003) Nitric oxide regulates exocytosis by S-nitrosylation of *N*-ethylmaleimide-sensitive factor. *Cell* **115**, 139–150.
9. Matsushita, K., Morrell, C.N., and Lowenstein, C.J. (2004) Sphingosine 1-phosphate activates Weibel–Palade body exocytosis. *Proc. Natl. Acad. Sci. U. S. A.* **101**, 11483–11487.
10. Becker-Hapak, M., McAllister, S.S., and Dowdy, S.F. (2001) TAT-mediated protein transduction into mammalian cells. *Methods* **24**, 247–256.
11. Jaffrey, S.R., and Snyder, S.H. (2001) The biotin switch method for the detection of S-nitrosylated proteins. *Sci STKE* (86), PL1.
12. Yamakuchi, M., Kirkiles-Smith, N.C., Ferlito, M., et al. (2007) Antibody to human leukocyte antigen triggers endothelial exocytosis. *Proc. Natl. Acad. Sci. U. S. A.* **104**, 1301–1306.

16

Molecular Dissection of HCl Secretion in Gastric Parietal Cells Using Streptolysin O Permeabilization

Xia Ding, Fang Wu, Zhen Guo, and Xuebiao Yao

1 Introduction.....	218
2 Materials	219
3 Methods.....	220
4 Notes	225
References.....	226

Summary Histamine-stimulated gastric acid secretion involves a transient elevation of intracellular Ca^{2+} and the cyclic adenosine monophosphate (cAMP)-dependent protein kinase A (PKA) cascade through phosphorylation, the actions of which ultimately result in the fusion of vesicles containing H,K-ATPase (adenosine triphosphatase) to the apical plasma membrane of parietal cells. To dissect the signaling events underlying gastric acid secretion, we have developed a permeabilized gastric gland model using streptolysin O (SLO). The advantage of this model is its ability to retain cytosolic components that are required for the secretory machinery while granting accessibility for the introduction of macromolecules into the cytoplasm. Our studies showed that acid secretion in SLO-permeabilized glands is a cAMP-dependent process and involves the recruitment of H,K-ATPase-rich tubulovesicles into the apical plasma membrane as judged by biochemical assays. These studies established a functional permeabilized gland model in which the resting-to-secreting transition can be triggered by second messengers, while the manipulation of the cytoplasmic environment can be achieved with ease.

Keywords Acid secretion; H,K-ATPase; parietal cells; permeabilization; streptolysin O.

1 Introduction

Stimulation of gastric acid secretion in parietal cells by histamine involves a transit rise in intracellular Ca^{2+} (e.g., 1,2) and activation of the cyclic adenosine monophosphate (cAMP)-dependent protein kinase A (PKA) cascade that leads to final proton pumping (e.g., 3,4). In resting parietal cells, the enzyme responsible for gastric acid secretion, H,K-ATPase (H,K-adenosine triphosphatase) is sequestered in cytoplasmic membrane compartments of low K permeability, the tubulovesicles. Stimulation of parietal cells causes cytoskeletal remodeling and a fusion of the tubulovesicles with the apical membrane (e.g., 5,6). It was proposed that ezrin couples the activation of PKA to the apical membrane remodeling associated with parietal cell secretion (7). We have mapped the PKA-mediated phosphorylation site on serine 66 of ezrin and illustrated the PKA-mediated phosphoregulation of ezrin in gastric acid secretion (8). However, it is still not clear whether other phosphorylation sites, such as threonine 235, are involved in parietal cell secretion.

The development of permeabilized cell preparations has provided a valuable experimental system for dissection of the intracellular signaling cascade by direct manipulation of the cytoplasmic environment. We previously reported a novel permeabilized gland model using α -toxin isolated from *Staphylococcus aureus* and presented evidence that functional and morphological transformation can be triggered by addition of cAMP (9,10). Using this permeable model, [^{32}P]-ATP was used to direct phosphorylated target proteins. A number of proteins with phosphorylation–dephosphorylation that is specifically modulated by cAMP were found. Because of the small pore size produced (~2-nm diameter; 9), α -toxin permeabilization allows the entry of only small molecules, such as nucleotides and phalloidin. It was useful in determining the metabolic properties (11) and phosphoproteins associated with cell activation in isolated gastric glands (11). Thus, the development of a permeabilized system that allows the addition of larger molecules such as proteins would be extremely useful for the dissection of the intracellular activation cascade.

We have examined the use of another bacterial pore-forming toxin isolated from β -hemolytic group A streptococci, streptolysin O (SLO). While pores formed by α -toxin only allow passage of molecules with a molecular weight less than 1 kDa, the pores formed by SLO are large enough to allow passage of proteins up to 200 kDa (12). These SLO-treated glands retain the ability to transform from a resting to a stimulated state, and like other permeabilized models of rabbit glands, stimulation occurs with the addition of cAMP (13). Thus, we established a SLO-permeabilized gastric gland system in which functional transformation of parietal cells can be triggered by addition of cAMP/ATP. The ability to introduce macromolecules into this permeable model with ease will facilitate the dissection of molecular interactions underlying parietal cell acid secretion.

2 Materials

2.1 Isolation of Gastric Glands and SLO Permeabilization

1. Phosphate-buffered saline (PBS): 2.25 mM K_2HPO_4 , 6 mM Na_2HPO_4 , 1.75 mM NaH_2PO_4 , 136 mM NaCl, 1 mM $CaCl_2$, and 1 mM $MgSO_4$, pH 7.4.
2. Minimal essential medium (MEM; Invitrogen, San Diego, CA): 1 mM NaH_2PO_4 , 117 mM NaCl, 1.8 mM $CaCl_2$, 0.8 mM $MgSO_4$, 5.33 mM KCl, 20 mM D-glucose, and 20.4 mM $NaHCO_3$, pH 7.4, supplemented with 10 μ M cimetidine (Sigma, St. Louis, MO).
3. Collagenase (Sigma) is dissolved in MEM at the concentration of 1 mg/mL and prepared prior to use.
4. SLO was obtained from S. Bhakdi (University of Mainz, Germany). Stock solutions of SLO were prepared at 1 mg/mL (750,000 lytic units per mg) in 0.1% bovine serum albumin, and 10 mM HEPES (pH 7.2) and stored at $-80^\circ C$.
5. High-potassium (HK) buffer: 10 mM Tris base, 20 mM HEPES acid, 100 mM KCl, 20 mM NaCl, 1.2 mM $MgSO_2$, 1 mM NaH_2PO_2 , and 40 mM mannitol, pH 7.4.
6. ^{14}C -aminopyrine (Amersham Bioscience, Piscataway, NJ, USA).
7. 10 mM pyruvate and 1 mM succinate (Sigma).
8. H,K-ATPase-specific proton pump inhibitor omeprazole (Sigma) is dissolved in methanol to make 1 mM stock (use at 1:1000).

2.2 Preparation of Gastric Subcellular Fractions

1. Homogenization buffer: 125 mM mannitol, 40 mM sucrose, 1 mM ethylenediaminetetraacetic acid (EDTA), and 5 mM ethylene glycol-bis(2-amino-ethyl-ether)-*N,N,N',N'*-tetraacetic acid (EGTA), Tris-HCl, pH 6.7. Store at $4^\circ C$.
2. Sucrose medium: 300 mM sucrose, 0.2 mM EDTA, and 5 mM Tris-HCl, pH 7.4. Store at $4^\circ C$.
3. Tight-fitting Teflon pestle (Fisher Scientific). Store at $4^\circ C$.
4. Centrifuge rotors, JA-20 and Ti-35 (Beckman). Store at $4^\circ C$.
5. Centrifuge tubes for JA-20 and Ti-35 (Beckman, USA). Store at $4^\circ C$.

2.3 Sodium Dodecyl Sulfate Polyacrylamide Gel Electrophoresis (SDS-PAGE)

1. Separating buffer (4X): 1.5 M Tris-HCl, pH 8.7, 0.4% SDS.
2. Stacking buffer (4X): 0.5 M Tris-HCl, pH 6.8, 0.4% SDS.
3. Thirty percent acrylamide/bis solution (37.5:1 with 2.6% bis-acrylamide) (this is a neurotoxin when unpolymerized and so care should be taken not to receive exposure) and *N,N,N,N'*-tetramethylethylenediamine (TEMED; Bio-Rad, Hercules, CA).

4. Ammonium persulfate: Prepare 10% solution in water and immediately freeze in single-use (200- μ L) aliquots at -20°C .
5. Water-saturated isobutanol: Shake equal volumes of water and isobutanol in a glass bottle and allow to separate. Use the top layer.
6. Running buffer (5X): 125 mM Tris-HCl, 960 mM glycine, 0.5% (w/v) SDS.
7. Broad-range molecular weight markers (Bio-Rad).

2.4 Enzymatic Assay

1. *p*-Nitrophenylphosphatase (*p*NPPase) assay solution: 7.5 mM Tris-HCl, pH 7.5, 3.5 mM MgSO_4 , 0.1 mM ouabain, 30 mM sucrose, and 20 μ M EDTA in both the presence and absence of 20 mM KCl. Store at -20°C .
2. 5 mM *p*-nitrophenyl phosphate (EMD Bioscience, San Diego, CA). Store at -20°C .
3. Spectrophotometer (Fisher Scientific).
4. Clinic centrifuge (Fisher Scientific).
5. Glass centrifuge tubes (Fisher Scientific).
6. Quench solution: 0.5 N NaOH.

3 Methods

3.1 Isolation of Gastric Glands

1. Sedate a New Zealand White rabbit with 0.5 mL nembutal intravenously. Perfuse the stomach with PBS under high pressure.
2. Remove the stomach, scrape the gastric mucosa from the smooth muscle layer, and finely mince the mucosa.
3. Wash the minced mucosa with PBS three times and with the HEPES-MEM buffer: 20 mM HEPES, pH 7.4, in MEM.
4. Digest the minced mucosa for approx 30 min in about 20 mL HEPES-MEM containing 20 mg collagenase at 37°C .
5. Terminate the collagenase digestion by diluting the solution into 200 mL HEPES-MEM followed by filtration through a nylon mesh to remove large pieces of undigested mucosa.
6. Isolate intact gastric glands by allowing the digestion mixture to settle for 10–15 min and then wash by settling three times in HEPES-MEM.

3.2 SLO Permeabilization of Gastric Glands

1. Wash intact glands in HEPES-MEM two times by settling at 4°C in ice-cold K buffer.

2. Add SLO to a final concentration of 1 $\mu\text{g}/\text{mL}$ and mix the glands (at 5% cytocrit) by inversion; then, incubate on ice until the glands have completely settled (10 to 15 min) (see **Note 1**).
3. Remove the K-buffer supernatant containing excess SLO and wash the glands two more times by settling at 4 °C in ice-cold K buffer (see **Note 2**).
4. Finally, resuspend glands in K-buffer solution containing 1 mM pyruvate and 10 mM succinate, then incubate glandular suspension at 37 °C for 3 min to allow the SLO pores to form.
5. Use SLO-treated glands immediately or maintain on ice until use.

3.3 ¹⁴C-Aminopyrine Uptake Assays of SLO-Permeabilized Gastric Glands

1. For both intact and permeabilized preparations, keep glands in the resting state with cimetidine (100 μM) and initiate stimulation for the intact preparations by adding 1 mM dibutyryl cAMP. For permeabilized preparations, stimulate SLO-permeabilized glandular cells with cAMP (100 μM) plus ATP (1 mM).
2. Incubate gland preparations for 20 min at 37 °C with shaking (~160 oscillation/min) in the presence of various reagents, including recombinant full-length ezrin and ezrin mutants. An example of assessing the function of ezrin proteins on the aminopyrine (AP) uptake is shown in **Fig. 1**.
3. Spin glandular cells in an Eppendorf centrifuge for 5 s at 200 g to pellet the cells.
4. Remove an aliquot of supernatant for counting in a liquid scintillation counter (Beckman).
5. Dry the pellets; weigh and reconstitute the pellets in 1 mM potassium hydroxide. Subject aliquots of samples to scintillation counting as mentioned above.
6. Calculate AP accumulation based on the ratio of $[\text{AP}]_{\text{intracellular}}/[\text{AP}]_{\text{extracellular}}$. In some cases, the data are expressed as a fraction of the stimulated control to normalize AP uptake values among the various preparations. Examples of AP uptake assays are shown in **Figs. 1 and 2**.

3.4 Preparation of Subcellular Fractionations of Gastric Glands

Perform all fractionation procedures under ice-cold conditions.

1. Rinse the treated intact and SLO-permeabilized glands with homogenizing buffer and homogenize them with a tight-fitting Teflon pestle.
2. Centrifuge the homogenate at 40 g for 5 min using a JA-20 rotor to produce the pellet P_0 (whole cells and debris).
3. Spin the resulting supernatant at 4000 g for 10 min using a JA-20 rotor to produce a plasma membrane-rich fraction P_1 .

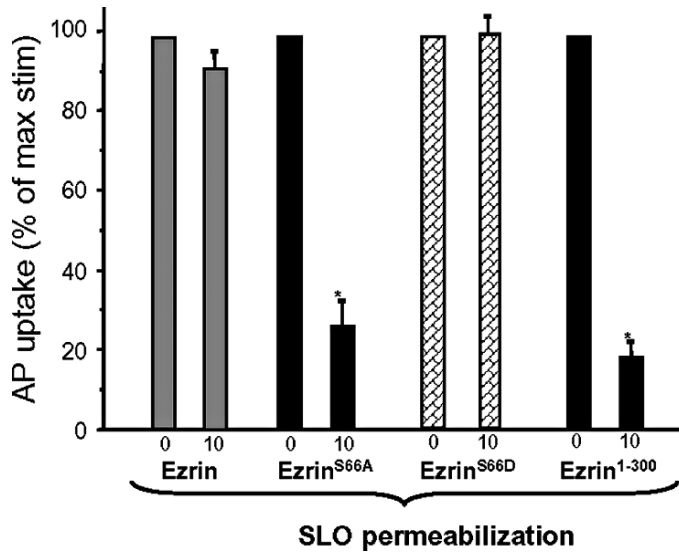


Fig. 1 Regulation of acid secretion in SLO-permeabilized gastric glands by addition of recombinant ezrin proteins. Various recombinant GST-tagged ezrin protein samples were purified using glutathione affinity beads, and the protein samples were desalted for the secretory activity (AP) assay. Recombinant glutathione transferase (GST) ezrin (wild type, S66A, S66D) and its deletion mutants (ezrin1–300) were purified as GST fusion proteins from bacteria and added to the SLO-permeabilized gland suspensions in the indicated amounts (in μg protein). Glands were then stimulated with cAMP plus ATP, and AP uptakes were measured. AP uptakes are shown for resting and stimulated controls and for stimulated glands treated with either wild-type ezrin or its mutants. AP data are plotted as percentage of the stimulated control for each experiment. Error bars represent SE; $n = 4$ for all experiments. *Significant difference from stimulated controls ($p < 0.01$).

- Centrifuge the resulting supernatant at 14,500 g for 10 min using a JA-20 rotor to produce an organelle-rich fraction P_2 .
- Transfer to a Ti35 rotor and centrifuge at 48,200 g for 90 min to produce a microsome-rich fraction P_3 and a supernatant fraction S_3 (cytosol).
- Suspend the pellets in sucrose medium and assess the protein concentration using bovine serum albumin as a standard. An example of subcellular fractionation experiments is shown in Fig. 3.

3.5 Enzymatic Assay of *p*NPPase Activity in the Subcellular Fractionations of Gastric Glands

The potassium-dependent phosphatase activity is measured in *p*NPPase assay solution in both the presence and absence of 20 mM KCl.

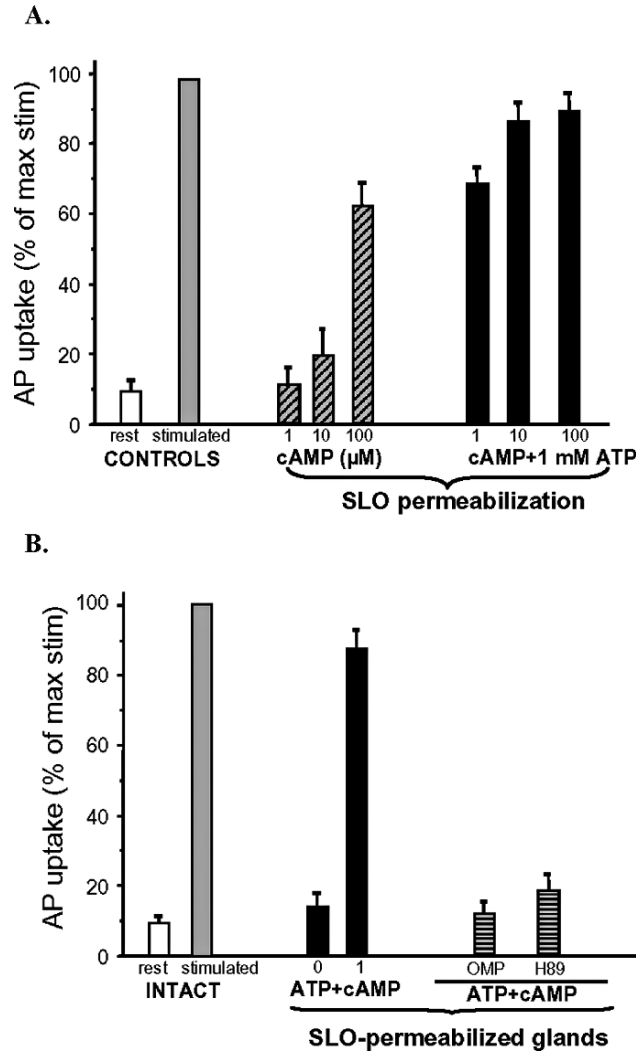


Fig. 2 Acid secretion in SLO-permeabilized gastric glands is regulated by cAMP-dependent protein kinase activation. **(A)** cAMP increases accumulation of AP on SLO-permeabilized gastric glands. Glands were permeabilized with SLO and incubated with increasing amounts of cAMP in the presence and absence of 1 mM ATP with mitochondria substrates (succinate and pyruvate). Average AP ratios for intact glands were 157 ± 4.1 , while AP ratios of SLO-permeabilized glands were 127 ± 3.9 . AP data are plotted as percentage of the stimulated control for each experiment. Error bars represent SE; $n = 4$ for all experiments. *Significant difference from stimulated controls ($p < 0.01$). **(B)** cAMP-stimulated acid secretion in SLO-permeabilized gastric glands is mediated by PKA. Glands were permeabilized with SLO and stimulated with cAMP plus ATP. Both H89, a PKA inhibitor ($10 \mu\text{M}$) and omeprazole, a proton pump inhibitor ($5 \mu\text{M}$) minimized the AP uptake in SLO-permeabilized glands. AP data are plotted as percentage of the stimulated control for each experiment. Error bars represent SE; $n = 4$ for all experiments. *Significant difference from stimulated controls ($p < 0.01$).

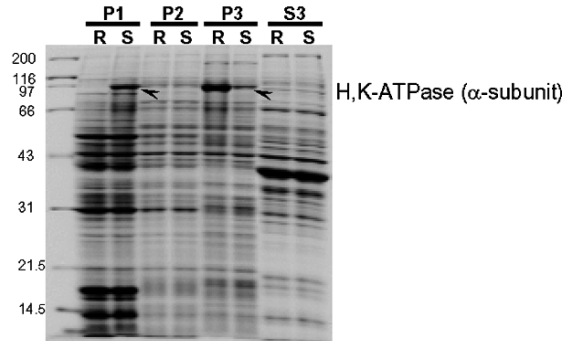
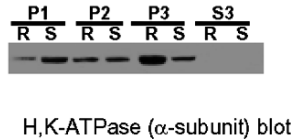
A.**B.**

Fig. 3 Stimulation of acid secretion in SLO-permeabilized gastric glands involves translocation of H,K-ATPase. (A) SLO-permeabilized glands were treated with cimetidine or stimulated with dbcAMP (S) for 20 min before homogenization. Subcellular fractions from resting and stimulated glands were separated by SDS-PAGE. Various subcellular fractions are indicated by P₁, P₂, P₃, and S₃, as described in text. Coomassie blue-stained gel shows no gross change of protein bands within any given subcellular fraction in response to treatment except for a band with an apparent molecular mass of 96 kDa, which is more intense in the P₁ fraction and slightly less intense in the P₃ fraction of stimulated glands (marked by black arrows). (B) Western blot from an equivalent gel was probed with an antibody against the μ -subunit of H,K-ATPase to confirm the translocation of H,K-ATPase of SLO-permeabilized gland in response to cAMP stimulation.

1. Make aliquots of the subcellular fractions (20 μ g total proteins) from treated and permeabilized gland preparations.
2. Mix the protein samples from the aforementioned fractions with 5 mM sodium *p*-nitrophenyl phosphate and run the assay in duplicates.
3. Incubate the mixture at 25 °C for 20 min.
4. Terminate the reaction by addition of 1.5 mL 0.5 N NaOH.
5. Collect liberated *p*-nitrophenol (in supernatant) by a brief spin at 500 g for 5 min.
6. Determine *p*-nitrophenol using a spectrophotometer at a 410-nm wavelength.
7. Potassium-dependent *p*NPPase is defined as the activity of phosphatase in the presence of 20 mM potassium after subtraction of the rate in the absence of potassium. Examples of subcellular fractionation experiments are shown in Table 1.

Table 1 Redistribution of H,K-ATPase of SLO-Permeabilized Glands in Response to CAMP Stimulation

Index of Act.	Intact glands		SLO glands	
	Rest	Stimulated	Rest	Stimulated
AP uptake ratio	12.1 ± 2.7	157 ± 4.1	18.3 ± 3.7	127 ± 3.9
P ₁ /P ₃ , pNPPase	0.23 ± 0.05	0.59 ± 0.12	0.24 ± 0.04	0.45 ± 0.11
P ₁ /P ₃ , α-subunit	0.18 ± 0.03	1.19 ± 0.13	0.23 ± 0.06	1.01 ± 0.29

All data are given as means ± SE of 4 gland preparations. Intact glands were treated with 100 μM cimetidine (rest), and with 1mM dbcAMP (stimulated) for 20 min before fractionation. SLO-permeabilized glands were treated (cimetidine (rest) or with 100 μM cAMP plus 1 mM ATP (stimulated) for 20 min. An aliquot of each gland preparation was taken for measurement of AP uptake ratio before homogenization and separating cell fractions. For each cell fraction, activity of K-stimulated pNPPase was measured enzymatically, and the amount of α-subunit protein was quantitated by densitometry of western blots. Measurements of pNPPase and α-subunit protein are expressed as the P₁/P₃ ratio, i.e., activity in P₁ fraction (plasma membrane enriched) divided by activity in P₃ fraction (tubulovesicle enriched).

4 Notes

1. Our trial experiment determined that a concentration of SLO in the range of 0.05–5 μg/mL was optimal for permeabilization of gastric glands. Glands treated with much lower SLO concentration (e.g., 0.05 and 0.5 μg/mL) gave reduced values in our assay of AP uptake. These SLO-treated glands were poorly permeabilized judging by the entry of small molecular chemicals such as rhodamine-labeled phalloidin, a filamentous actin-binding compound, into parietal cells. When glands were treated with much higher concentrations of SLO (e.g., 5 μg/mL), the permeability of glandular cells was improved judging by a higher percentage of glandular cells marked by rhodamine-phalloidin, but the ability of these glands to uptake AP was greatly reduced compared to that of glands treated with 1 μg/mL SLO. Therefore, 1 μg/mL SLO was chosen as a standard condition for permeabilizing the glands. For application of SLO in different cell types, the optimal concentration should be determined in trial experiments.
2. Since SLO permeabilizes the plasma membrane of mammalian cells in a temperature-dependent manner, it is essential to incubate SLO with target cells on ice to allow the maximal level of SLO binding while minimizing the possibility of SLO internalization. The permeabilization will be initiated after removing the excess SLO.

Acknowledgments We would like to thank Professor John G. Forte for insightful discussion and support. This work was supported by grants from the Chinese Natural Science Foundation, Chinese 973 project (2002CB713700), Chinese 863 project (2001AA215331), and the National Institutes of Health (DK-56292) to X.Y. X.Y. is a GCC Distinguished Cancer Research Scholar.

References

1. Chew, C.S. (1986) Cholecystokinin, carbachol, gastrin, histamine, and forskolin increase $[Ca^{2+}]_i$ in gastric glands. *Am. J. Physiol.* **250**, G814–G823.
2. Negulescu, P.A., and Machen, T.E. (1988) Intracellular Ca^{2+} regulation during secretagogue stimulation of the parietal cell. *Am. J. Physiol.* **254**, C130–C140.
3. Forte, J.G., and Yao, X. (1996) The membrane recruitment and recycling hypothesis of gastric HCl secretion. *Trends Cell Biol.* **6**, 45–48.
4. Yao, X., and Forte, J.G. (2003) Cell biology of acid secretion by the parietal cell. *Annu. Rev. Physiol.* **65**, 103–131.
5. Wolosin, J.M., and Forte, J.G. (1984) Stimulation of oxyntic cell triggers K and Cl conductances in apical H,K-ATPase membrane. *Am. J. Physiol.* **246**, C537–C545.
6. Forte, J.G., and Soll, A. (1989) Cell biology of hydrochloric acid secretion. In: *Handbook of Physiology*, (J.G. Forte, Ed.) Vol. 3. American Physiology Society, Bethesda pp. 207–228.
7. Urushidani, T., Hanzel, D.K., and Forte, J.G. (1989) Characterization of an 80-kDa phosphoprotein involved in parietal cell stimulation. *Am. J. Physiol.* **256**, G1070–G1081.
8. Zhou, R., Cao, X., Watson, C., et al. (2003) Characterization of protein kinase A-mediated phosphorylation of ezrin in gastric parietal cell activation. *J. Biol. Chem.* **278**, 35651–35659.
9. Yao, X., Karam, S.M., Ramilo, M., Rong, Q., Thibodeau, A., and Forte, J.G. (1996) Stimulation of gastric acid secretion by cAMP in a novel α -toxin-permeabilized gland model. *Am. J. Physiol.* **271**, C61–C73.
10. Thibodeau, A., Yao, X., and Forte, J.G. (1994) Acid secretion in α -toxin-permeabilized gastric glands. *Biochem. Cell Biol.* **72**, 26–35.
11. Rong, Q., Utevskaia, O., Ramilo, M., Chow, D., and Forte, J.G. (1998) Nucleotide metabolism by gastric glands and H,K-ATPase-enriched membranes. *Am. J. Physiol.* **274**, G103–G110.
12. Buckingham, L., and Duncan, J.L. (1983) Approximate dimensions of membrane lesions produced by streptolysin S and streptolysin O. *Biochim. Biophys. Acta* **729**, 115–122.
13. Ammar, D.A., Zhou, R., Forte, J.G., and Yao, X. (2002) Syntaxin 3 is required for cAMP-induced acid secretion: streptolysin O-permeabilized gastric gland model. *Am. J. Physiol.* **282**, G23–G33.

17

Addressing Membrane Protein Topology Using the Fluorescence Protease Protection (FPP) Assay

Holger Lorenz, Dale W. Hailey, and Jennifer Lippincott-Schwartz

1	Introduction.....	227
2	Materials.....	228
3	Methods.....	229
4	Notes.....	231
	References.....	233

Summary Determining a protein's correct topological distribution within the cell is essential for understanding the proper functioning of many proteins. Here, we describe a fluorescence-based technique, termed FPP for fluorescence protease protection, to determine protein topology in living cells. The FPP assay uses the restricted proteolytic digestibility of green fluorescent protein-tagged membrane proteins to reveal their intramembrane orientation. Membrane protein topology can be assessed using this technique for proteins residing in organelles as diverse as the Golgi apparatus, the endoplasmic reticulum (ER), peroxisomes, mitochondria, and autophagosomes. To illustrate the technique, we describe its use for deciphering the topology of a membrane protein in the ER.

Keywords Digitonin permeabilization; fluorescence assay; membrane protein; topology.

1 Introduction

Cellular membranes act as barriers and scaffolds, separating different cellular environments. Within such membranes, proteins adopt specific topologies to achieve their proper cellular function. Because the way a transmembrane protein distributes across a membrane bilayer dictates which of its domains (i.e., cytoplasmic, transmembrane, extracellular, or intraluminal) is accessible to modifying enzymes and interacting partners, understanding a protein's topological distribution is essential for understanding its function.

Both experimental and theoretical approaches have been employed to determine the topology of membrane proteins. Many of these approaches, including biochemical modification and antibody labeling, are demanding with respect to time, effort, and expense of materials and do not always provide congruent data (1,2). Here, we describe an alternative method to obtain information regarding membrane protein topology using GFP (green fluorescent protein)-tagged fusion proteins.

The approach, referred to as the fluorescence protease protection (FPP) assay, provides basic information about the position of the GFP tag relative to the membrane (3). It requires no additional design beyond the construction of a GFP fusion protein expressed in either tissue culture or primary cells. The assay is principally based on the inaccessibility of proteases to protected intracellular regions of permeabilized cells (4). The protease-induced destruction of GFP attached to a protein of interest after plasma membrane permeabilization reveals whether the GFP tag is oriented facing the cytosol or facing a protected intracellular environment.

The cholesterol-binding drug digitonin is used to selectively permeabilize the plasma membrane in the FPP assay. Digitonin permeabilization has been successfully used in yeast and numerous mammalian cells (5–8). The extent of permeabilization is sufficient to allow cytosolic contents to diffuse across the plasma membrane, while intracellular organelles and the cytoskeletal system are retained (7,8). After digitonin permeabilization, the protease trypsin or proteinase K is added to the medium. These proteases readily enter the cytoplasm from the extracellular environment but cannot cross the intact membranes of intracellular organelles. Any GFP molecule attached to a protein of interest facing the cytosol, therefore, will be destroyed and lose its fluorescence. It thus becomes possible to determine whether an organellar protein is membrane associated or luminal, which portion of a membrane protein faces the lumen (or cell exterior) and cytoplasm, and whether a protein associated with nonmembranous structures is protected from molecules in the surrounding nucleoplasm or cytoplasm.

2 Materials

1. GFP expression vector (Clontech, Mountain View, CA) containing DNA encoding the protein of interest.
2. Mammalian cells to be transfected with GFP fusion protein.
3. Transfection reagents for mammalian cells (e.g., FuGENE 6 transfection reagent, Roche, Indianapolis, IN; or Lipofectamine, Invitrogen, Carlsbad, CA).
4. Standard cell culture medium for cells of interest.
5. KHM buffer: 110 mM potassium acetate, 20 mM HEPES, 2 mM MgCl₂.
6. Digitonin.
7. Trypsin or an alternative protease, such as proteinase K, reconstituted in KHM buffer.
8. Lab-Tek chambered cover glass (Nalge Nunc International, Rochester, NY).
9. Fluorescence microscope with image acquisition-and-capture system.

3 Methods

The FPP assay described outlines (Subheading 3.1.) the principle construction of the expression plasmid, (Subheading 3.2.) the expression of a GFP-tagged fusion protein in mammalian cells, (Subheading 3.3.) the selective permeabilization of the plasma membrane, (Subheading 3.4.) the degradation of exposed peptides on protease application, and (Subheading 3.5.) the determination of membrane protein topology by fluorescence microscopy.

3.1 *Expression Plasmid Construction*

GFP or any other fluorescent protein variant such as cyan fluorescent protein (CFP) or yellow fluorescent protein (YFP) can be fused to the deoxyribonucleic acid (DNA) coding for the membrane protein of interest. For single-spanning membrane proteins, two versions of the protein should be created: an amino- and a carboxy-terminal fusion protein with GFP. For multispanning membrane proteins, either a fusion protein with GFP inserted within the protein of interest or a truncated fusion protein should be made. It is important to note the exact position of GFP within the fusion protein's amino acid sequence (*see Note 1*). As a control, transfect cells with DNA encoding GFP alone. DNA cloning and modification can be performed by standard recombinant DNA methods (9).

3.2 *Preparation and Transfection of Sample Cells*

1. Passage the cells of interest into cell chambers (e.g., Lab-Tek chambered cover glass). Because the cells in the chamber will be both transfected with DNA and monitored under the microscope, plate enough cells so that at the time of the FPP assay the cells are about 60–90% confluent.
2. At 16 to 24 h postpassage, transfect cells with the expression plasmid encoding the GFP-tagged fusion protein using a standard transfection protocol. Culture cells at the appropriate conditions until fluorescent signals are detectable (6–20 h posttransfection).

3.3 *Selective Permeabilization of the Plasma Membrane*

1. Remove cell culture medium and wash cells three times for 1 min each in KHM buffer at a temperature that is appropriate for the experiment. Temperatures ranging from 20 °C to 37 °C are suitable for the FPP protocol.

2. Place chamber containing cells on the fluorescence microscope stage. Set up microscope for fluorescence imaging and record first images, which represent the prepermeabilization situation.
3. To permeabilize the plasma membrane, add digitonin-containing KHM buffer to the cells. Determine the effective digitonin concentration by applying increasing concentrations of digitonin to cells that express only GFP. GFP diffuses freely in the cytosol and nucleoplasm. Effective permeabilization of the plasma membrane by digitonin results in the disappearance of the GFP signal within 10–60 s. A good starting concentration for most cell lines tested (COS-7, NRK, HeLa, BHK, N2a) is 20 μM digitonin. If 20 μM digitonin is insufficient to permeabilize the cells, increase the digitonin concentration in 20- μM increments. Use the lowest possible digitonin concentration that provides efficient plasma membrane permeabilization (see **Note 2**).
4. Incubate cells that express the protein of interest tagged with GFP in KHM buffer containing the (previously determined) effective digitonin concentration. Efficient permeabilization of most cell lines occurs within 1 min after digitonin application.
5. Take images of the cells after digitonin application to capture the postpermeabilization situation (see **Notes 3 and 4**).

3.4 Degradation of Exposed Amino Acids on Protease Application

1. Wash permeabilized cells quickly but thoroughly in KHM buffer.
2. Add 4–8 mM of the protease trypsin (in KHM buffer) directly onto the cells. Immediately begin taking images on the fluorescence microscope to record whether fluorescent signals persist or disappear. Alternatively, 50 $\mu\text{g mL}^{-1}$ proteinase K can be used for the FPP assay (see **Note 3**).

3.5 Determination of Protein Topology by Fluorescence Microscopy

Assess recorded images and quantify signal intensities to determine the subcellular localization and topology of the protein. Freely available image analysis software (i.e., NIH Image, Image J) or software on existing microscope platforms (e.g., Zeiss LSM Image Examiner, Zeiss Microimaging, Thornwood, NY) can be used to measure fluorescence intensities.

4 Notes

1. Incubation of permeabilized cells with proteases (*see* Subheading 3.4.) provides more detailed information about the protein's subcellular localization and topology. At this point, knowing the exact position of the GFP tag within the fusion protein sequence becomes important for topology determinations (*see* Subheading 3.1.). If a protein is contained within a protected subcellular environment, such as the lumen of intracellular organelles, the GFP signal will be unaffected by the addition of protease regardless of the specific placement of the GFP tag within the fusion protein (i.e., N- or C-terminal or central). In contrast, if the protein of interest spans the membrane of an intracellular organelle such that some domains are facing the organelle's lumen and other domains are exposed to the cytosol, the placement of the GFP tag will dictate whether its fluorescence is resistant to protease addition (Figs. 1 and 2, middle and bottom panels).
2. Regarding potential pitfalls, the most crucial step in the FPP protocol is the selective permeabilization of the plasma membrane by digitonin (*see* Subheading 3.3.). For each particular experiment, it is highly recommended to adjust this step depending on the cells and particular conditions used. The best way to establish appropriate conditions is to express GFP alone in the cells of interest.

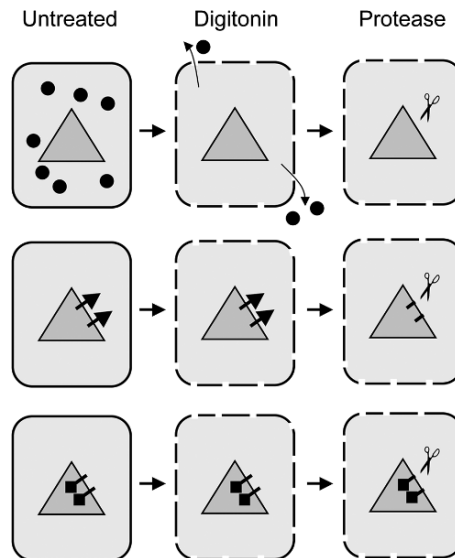


Fig. 1 Schematic presentation of the FPP assay illustrating cells before (left column) and after digitonin (middle column) and trypsin (right column) application. The filled circle symbols (top panel) represent unbound cytosolic molecules. The arrow symbols with the pointed (middle panel) and square ends (bottom panel) represent transmembrane proteins bound to a membrane (big triangles) with the fluorescent tag facing the cytoplasm or the organelle's lumen, respectively. The pre- (left column) and postpermeabilization (middle column, digitonin) conditions and the resulting phenotypes after protease (scissor symbol, right column) treatment are shown.

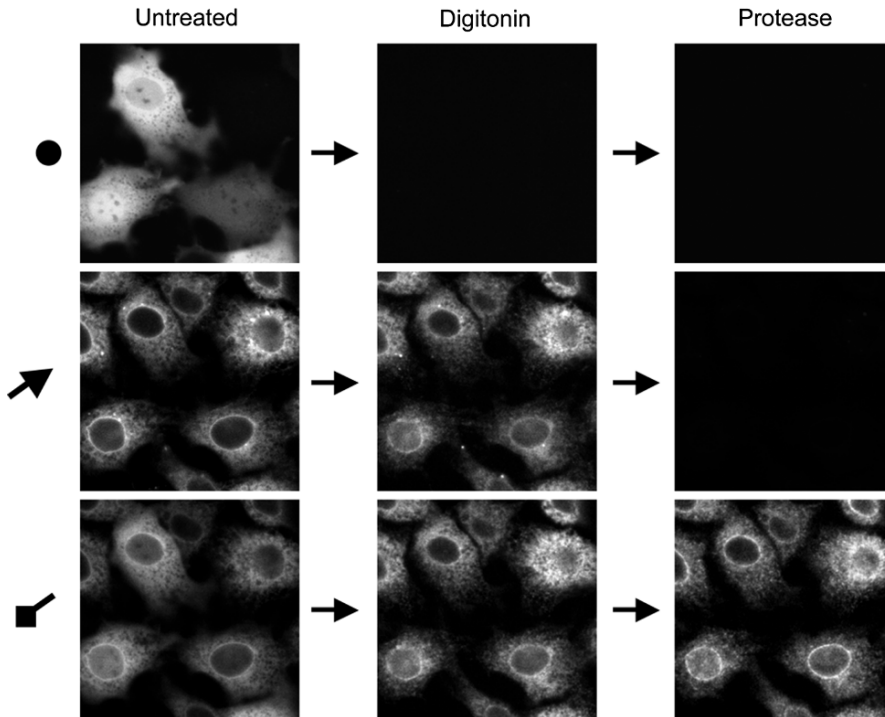


Fig. 2 Protein topology determination by FPP. Micrographs show NRK cells expressing GFP alone (top panel) and either the type I membrane protein CD3 δ (**10**) tagged C-terminally to YFP (middle panel) or CD3 δ tagged N-terminally to CFP (bottom panel). Performing the FPP assay with these cells reveals that CD3 δ is membrane bound, unlike GFP alone (compare postdigitonin treatment), and that only the N-terminal portion of CD3 δ is protected from protease (compare postprotease treatment). Therefore, the type I membrane orientation of CD3 δ could be derived from the FPP assay. Individual images were taken before (left panel, untreated) and after treatment with 20 μ M digitonin (middle panel) and 4 mM trypsin (right panel). The filled circle and arrow symbols on the left of each panel correspond to the schematic presentation of the FPP assay in Fig. 1.

GFP easily diffuses out of the cytoplasm and across the plasma membrane on efficient digitonin permeabilization. Therefore, by using GFP, the lowest efficient digitonin concentration can be determined. This will significantly reduce any risks of affecting intracellular membranes. After successful permeabilization, it is recommended that the digitonin-containing KHM buffer be washed off the cells prior to protease application.

3. On permeabilization of the plasma membrane by digitonin (see Subheading 3.3.), the FPP assay will immediately provide data regarding a protein's localization. The disappearance of intracellular fluorescent signals indicates that the protein of interest is freely diffusing in the cytosol or nucleoplasm and is neither membrane associated nor localized in the lumen of an intracellular organelle (Figs. 1 and 2, top panels).
4. Fluorescent signals that are retained on cell permeabilization indicate that the protein of interest is not freely diffusing in the cytosol and nucleoplasm.

References

1. Traxler, B., Boyd, D., and Beckwith, J. (1993) The topological analysis of integral cytoplasmic membrane proteins. *J. Membr. Biol.* **132**, 1–11.
2. Ott, C.M., and Lingappa, V.R. (2002) Integral membrane protein biosynthesis: why topology is hard to predict. *J. Cell Sci.* **115**, 2003–2009.
3. Lorenz, H., Hailey, D.W., and Lippincott-Schwartz, J. (2006) Fluorescence protease protection of GFP chimeras to reveal protein topology and subcellular localization. *Nature Methods* **3**, 205–210.
4. Lorenz, H., Hailey, D.W., Wunder, C., and Lippincott-Schwartz, J. (2006) The fluorescence protease protection (FPP) assay to determine protein localization and membrane topology. *Nature Prot.* **1**, 276–279.
5. Cordeiro, C., and Freire, A.P. (1995) Digitonin permeabilization of *Saccharomyces cerevisiae* cells for in situ enzyme assay. *Anal. Biochem.* **229**, 145–148.
6. Gowda, L.R., Joshi, M.S., and Bhat, S.G. (1988) In situ assay of intracellular enzymes of yeast (*Kluyveromyces fragilis*) by digitonin permeabilization of cell membrane. *Anal. Biochem.* **175**, 531–536.
7. Plutner, H., Davidson, H.W., Saraste, J., and Balch, W.E. (1992) Morphological analysis of protein transport from the ER to Golgi membranes in digitonin-permeabilized cells: role of the P58 containing compartment. *J. Cell Biol.* **119**, 1097–1116.
8. Wilson, R., Allen, A.J., Oliver, J., Brookman, J.L., High, S., and Bulleid, N.J. (1995) The translocation, folding, assembly and redox-dependent degradation of secretory and membrane proteins in semi-permeabilized mammalian cells. *Biochem. J.* **307**, 679–687.
9. Sambrook, J., Fritsch, E.F., and Maniatis, T. (1989) *Molecular Cloning, a Laboratory Manual*, 2nd ed., Cold Spring Harbor Laboratory Press, Cold Spring Harbor, NY.
10. Yang, M., Omura, S., Bonifacino, J.S., and Weissman, A. M. (1998) Novel aspects of degradation of T cell receptor subunits from the endoplasmic reticulum (ER) in T cells: importance of oligosaccharide processing, ubiquitination, and proteasome-dependent removal from ER membranes. *J. Exp. Med.* **187**, 835–846.

18

Visualizing Clathrin-Mediated IgE Receptor Internalization by Electron and Atomic Force Microscopy

Alan R. Burns, Janet M. Oliver, Janet R. Pfeiffer, and Bridget S. Wilson

1 Introduction.....	235
2 Materials.....	239
3 Methods.....	241
4 Notes.....	244
References.....	244

Summary A significant step in the immunoglobulin E (IgE) receptor signaling pathway in mast cell membranes is receptor internalization by clathrin-coated vesicles. Visualization in native membrane sheets of the emerging clathrin lattice structures containing the IgE receptor and associated signaling partners has been accomplished with high-resolution transmission electron microscopy (TEM). More recently, membrane sheets with labeled clathrin have also been characterized with atomic force microscopy (AFM) in combination with fluorescence imaging. We discuss here the procedure for creating fixed, native cell membrane sheets, labeling with immunogold or fluorescent labels, and utilization for TEM or AFM/fluorescence imaging of clathrin-mediated IgE internalization.

Keywords Atomic force microscopy; clathrin; electron microscopy; IgE receptor; membrane sheets.

1 Introduction

1.1 Immunoglobulin E Receptor Signaling, Membrane Organization, and Clathrin-Coated Pits

Receptor-induced endocytosis via clathrin-coated pits is a critical pathway for internalization of external ligands (1). Using high-resolution transmission electron microscopy (TEM) and immunogold labeling of intact membrane sheets, we have shown that the crosslinked immunoglobulin E (IgE) receptor

FcεRI is internalized through pits (2,3). Following activation of IgE-primed receptors by multivalent antigen, FcεRI crosslinking results in clustering and redistribution to “dark” membrane regions that are characteristically more electron dense than bulk membrane and are often bordered by clathrin-coated pits. The tyrosine kinase Syk is also recruited to the dark patches and mixes extensively with the receptors (2). The dark regions are caused in part by osmium staining but also are thought to harbor numerous proteins (3). For example, TEM has identified in the receptor-rich dark patches in activated cells the lipid remodeling enzyme PLCγ2, phosphatidylinositol 3-kinase, the scaffolding adaptor Gab2, the guanosine 5'-triphosphate (GTP) exchange factor Vav, the adaptor protein Grb2, the adaptor/ubiquitin ligase Cbl, and others, leading to the hypothesis that these areas represent primary sites of active signaling (4).

Clathrin-coated vesicles are striking features of membrane sheets. In actively endocytosing cells, clathrin vesicles are often grouped closely together in various stages of vesicle formation prior to the fission process (Fig. 1A). These sites often border dark patches of membrane (arrow, Fig. 1A) or are closely associated with cable-like structures (Fig. 1B) previously shown to contain filamentous actin (4). They can be readily identified by the characteristic honeycomb lattice appearance of the budding vesicle (5). We also identify them through immunogold and immunofluorescence labeling with anticlathrin antibodies (Figs. 1A, 2B), as well as through immunogold labeling of adaptor proteins such as AP2 (5) (labeled with anti-AP2 antibodies; see arrows, Fig. 1B). Other features, such as the specific targeting of the Eps15 endocytic factor (5) to the neck of pre-fission vesicles, can be demonstrated using this technology (arrows, Fig. 1D). Importantly, immunogold-labeled IgE receptors can be visualized as they enter clathrin-coated vesicles (arrow, Fig. 1C). The presence of clathrin-coated pits identifies dark patches not only as primary signaling domains but also as the principal location for receptor internalization. Although Syk is present in the dark patches, it does not accompany the receptor into coated pits (2) thus, internalization very likely represents an important step in signal termination.

1.2 Atomic Force Microscopy of Membrane Sheets

In the preceding subheading, we briefly summarized the significant insights regarding lateral distributions of signaling proteins following FcεRI activation that can be obtained with high-resolution TEM and nanoscale immunogold labeling of membrane sheets. This work is complemented by the use of atomic force microscopy (AFM) to examine the topography of the cytoplasmic face of plasma membrane sheets. AFM has been used extensively to characterize biological samples because it provides true height topography and can be routinely performed in natural fluid environments, a clear advantage over vacuum conditions imposed by TEM. It has also been well established that AFM can provide undistorted images of soft,

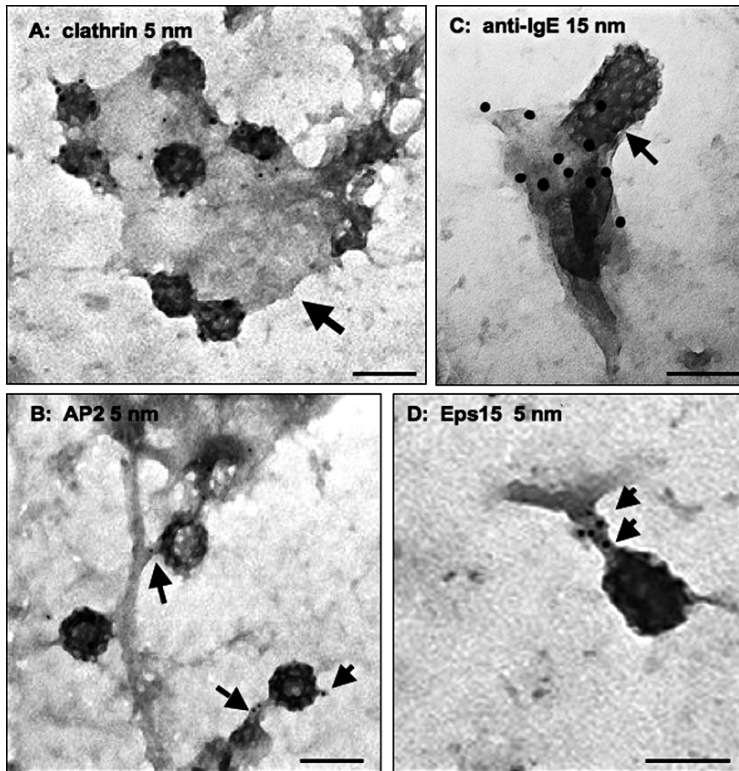


Fig. 1 TEM images of clathrin-coated vesicles on membrane sheets. All scale bars = 0.1 μm . (A) A cluster of budding vesicles labeled with anticlathrin antibodies and 5-nm gold secondary antibodies. The arrow points to the dark patch in the membrane sheet, which is caused in part by osmium staining. (B) Vesicles labeled with antibodies to the clathrin adaptor AP-2. Several 5-nm gold particles are marked with arrows. (C) Vesicle containing gold-labeled IgE receptor (arrow). Cells were primed with IgE and stimulated with 15-nm colloidal gold conjugated to rabbit anti-IgE for 2 min. The dark “signaling” patch immediately surrounding the vesicle contains numerous gold particles marking receptors. (D) The neck of this vesicle is labeled with antibodies to the endocytic protein Eps15 (arrows point to 5-nm gold particles).

compliant membrane structures (6), including membrane sheets (7,8). A key feature of our AFM is the ability to correlate membrane topographic features with the locations of fluorescently tagged proteins and lipids through simultaneous acquisition of AFM and confocal fluorescence images (9,10) (see Fig. 2 A,B).

Examples of AFM imaging of the inner (cytoplasmic) side of plasma membrane sheets are shown in Fig. 2. Simultaneous AFM (Fig. 2A) and fluorescence (Fig. 2B) imaging of mast cell sheets has revealed numerous irregular-shape raised domains that label with both resting and activated Fc ϵ RI and clathrin. They are most likely clusters of proteins that show up as the dark patches in TEM discussed above (Fig. 1A) (7). Higher-resolution AFM images indicate that these particular domains of

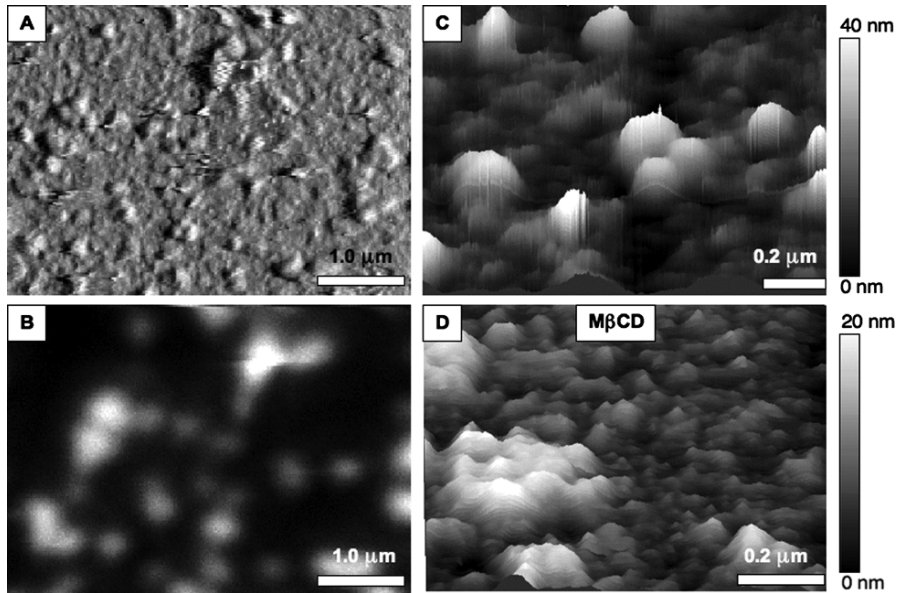


Fig. 2 AFM images of membrane sheets labeled with mouse monoclonal anticlathrin heavy chain and Alexa 488 F(ab')₂ goat antimouse IgG. **(A)** AFM deflection image revealing raised domains that label with clathrin. **(B)** Fluorescence image acquired simultaneously with AFM image in **(A)**. Note the strong correlation of fluorescence spots with raised domains. **(C)** AFM topography of clathrin-labeled raised domains in control cells. Note the round appearance and average height of approx 40 nm. **(D)** AFM topography of clathrin-labeled raised domains in membranes harvested from cells that have been subjected to cholesterol depletion with methyl-β-cyclodextrin (MβCD). Note that the domains are now flatter and half the height of the control cells in **(C)**.

clustered proteins are rounded and have a height relative to the surrounding membrane of approx 40 nm. Treatment of cells with methyl-β-cyclodextrin (MβCD), which extracts cholesterol from the membrane, reduces the height and flattens the clathrin-labeled domains. This is consistent with TEM data and reveals that cholesterol is an important component of the clathrin–signaling protein complexes.

1.3 Membrane Sheets for TEM and AFM

TEM analysis procedures are described elsewhere (11), as are the methods of AFM of membranes (12). The focus of this chapter is thus preparation of membrane sheets for TEM and AFM by which components of the IgE signaling network, including clathrin, are labeled. Successful membrane sheets will contain obvious features in TEM such as clathrin-coated pits and, for nonhematopoietic cells, caveolae. The appearance of these endocytic structures varies somewhat among cell types

and preparative techniques, and it is advisable to use specific antibodies (anticlathrin, anticaveolin) to positively identify these features early in a membrane sheet project. This is particularly important for AFM, for which height and width of domains extending into the cytoplasm may be insufficient for full identification. It is important to recognize that membrane sheets seen by TEM often contain a mix of coated pits, as well as flat clathrin arrays with diameters from 80 to 100 nm. As mentioned, the flat arrays are abundant in cells treated with M β CD (11). Flat array “remnants” are also abundant on mast cell membrane sheets within 10 min of antigen stimulation and internalization of over 100,000 IgE receptors.

The overall strategy for sheet preparation is based on the “rip-and-flip” procedure originated by Sanan and Anderson (13) for harvesting and fixing apical membrane surfaces. Similar “unroofing” procedures for ventral surfaces were discussed thoroughly by Heuser (14) and Drees et al. (15).

2 Materials

2.1 Laboratory Supplies

1. 15- and 25-mm round glass coverslips (Electron Microscopy Sciences, Hatfield, PA).
2. TEM grids: Hexagonal, nickel (no. 26431, 200 mesh; Ernest Fullam, Latham, NY), Formvar[®] and carbon coated.
3. Filter paper (Whatman’s ashless, no. 42, 11.0-cm circles).
4. Cellulose acetate disks (Osmonics, Minnetonka, MN, cat. no. A02SP02500).
5. No. 1 black rubber stopper (TEM only).
6. A 37°C slide warmer with lid (Cole-Parmer, Vernon Hills, IL); line sides with damp paper towels to establish moist chamber.
7. Fume hood.
8. Curved forceps (2 pair; Electron Microscopy Sciences, cat. no. 72801-D).
9. Aspirating apparatus.
10. Divided Petri dishes.
11. Parafilm[®].
12. Glow discharge apparatus.
13. Moist chamber for sheet incubation during labeling.
14. Coverslip holder (Warner Instruments) for 25-mm coverslips used in AFM.

2.2 Working Solutions

Prepare on day of use. Sterile, doubly distilled water is used unless otherwise indicated.

1. HEPES buffer: 25 mM HEPES, 25 mM KCl, 2.5 mM Mg (CH₃COO)₂, pH 7.2.

2. Phosphate-buffered saline (PBS) buffer: 0.137 M NaCl, 0.003 M KCl, 0.007 M Na₂HPO₄, pH 7.4.
3. Bovine serum albumin (BSA): 0.1% in PBS buffer.
4. Poly-L-lysine: Prepare 8 mg/mL poly-L-lysine hydrobromide stock and store at -20°C. Thaw and dilute in water on day of use. For TEM, use 0.48 mg/mL. For AFM, use 0.2 mg/mL.
5. 2% paraformaldehyde (from 16% EM grade stock solution, Electron Microscopy Sciences) in HEPES buffer.
6. 2% glutaraldehyde (from 8% EM grade stock solution, Electron Microscopy Sciences) in PBS.
7. Sodium cacodylate buffer: Prepare stock solution of 0.2 M sodium cacodylate, pH 7.2, and store at 4°C. Use at 0.1 M (TEM only).
8. 1% osmium solution (from 4% stock solution of osmium tetroxide OsO₄, Electron Microscopy Sciences). Dilute on day of use in 0.1 M sodium cacodylate buffer (TEM only).
9. 1% tannic acid in sodium cacodylate buffer. Filter with a 0.2-μm Millipore filter disk (TEM only).
10. 1% uranyl acetate, prepared in water from 2% stock solution (uranyl acetate powder, a Electron Microscopy Sciences) (*see Note 1*). Once made, keep in 60-mL syringe wrapped with foil. Use new 0.2-μm Millipore filter and filter small amount for staining; add to equal volume of water (TEM only).

2.3 Immunogold Labels for TEM

Best results are obtained with monoclonal antibodies or affinity-purified polyclonal antibodies. Labeling specificity should be confirmed by Western blotting or other immunochemical techniques. It is often desirable to label two membrane proteins on the same sheet using primary antibodies raised in different species, followed by gold-conjugated secondary reagents of two distinct sizes (e.g., 5-nm antimouse secondary antibodies and 10-nm antirabbit secondary antibodies). In our experience, gold reagents from Amersham (GE Healthcare) are reliable in size and quality. Because primary antibodies are raised in only a limited number of species, it is rarely possible to label more than two different proteins in one experiment.

2.4 Fluorescence Labels for AFM/Fluorescence Imaging

Various fluorophores conjugated to secondary antibodies are used in combination with the primary antibodies noted above. Alexa 488-conjugated secondary reagents from Molecular Probes or Jackson Laboratories are brightly fluorescent and more photostable than fluorescein-conjugated antibodies. For IgE receptor studies, care must be taken to control for crossreactivity with mouse IgE used to prime receptors. Various protein-

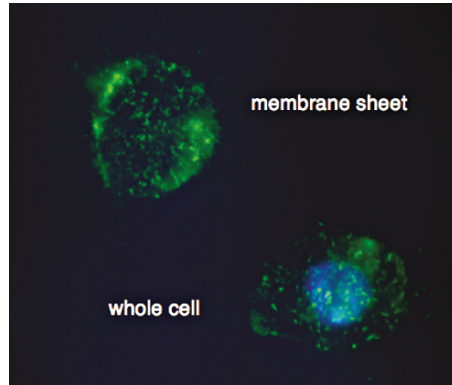


Fig. 3 Demonstration of the combination of fluorescent membrane label (in this case, fluorescein-phalloidin as a marker for the cortical actin cytoskeleton) and Hoechst nuclear stain to identify membrane sheets suitable for AFM imaging. A “good” membrane sheet candidate for AFM imaging is seen in the upper left-hand corner, whereas the cell in the lower right-hand corner is a whole cell, or is incompletely “ripped,” since it contains an intact Hoechst-stained nucleus.

labeling kits are also available from commercial sources (Molecular Probes, Sigma). Finally, it is important to note that Hoechst 33342 nuclear stain (e.g., Molecular Probes) is required to distinguish whole cells from sheets (Subheading 3.3.; Fig. 3).

3 Methods

3.1. *Whole Cell Activation, Labeling, and Fixation Prior to Sheet Preparation for Both TEM and AFM*

1. Prepare cells by plating onto sterile, 15-mm clean glass coverslips. Culture 1–4 d, to 70–80% confluent.
2. Decide if you will “activate” the cells (stimulate immune response) or subject the cells to other pretreatments (cholesterol depletion, pharmacological inhibitors, etc.). Specific procedures will differ with cell lines and signaling systems of interest.
3. Step 3 is specific to activation of the mast cell IgE receptor system. Prime cells with dinitrophenyl (DNP)-specific IgE for 2–24 h, followed by rinsing with PBS or fresh medium. IgE may be labeled with a fluorophore (e.g., Alexa 488 IgE). Remove coverslips with cells from culture dish and wick off excess medium. Gently wipe bottom of coverslip and place on surface of slide warmer set at 37 °C. Quickly (to keep cells from drying out) add 100 μ L of DNP-BSA medium (0.1 μ g/mL) and incubate the coverslips for a defined incubation period (1–10 min). Close the lid to keep chamber moist.

4. One can stop the reaction at the end of incubation by transferring to cold buffer. However, we recommend a light pre-fix at this stage by adding 100 μ L 0.5% paraformaldehyde to the coverslip (see **Note 2**). The coverslip is then held in the moist chamber for 7 min at room temperature, followed by a rinse in HEPES buffer.

3.2 Preparation of Sheets for TEM

1. Line 2-mL Petri dish with Parafilm and apply large drops of thawed, diluted poly-L-lysine solution.
2. Glow discharge EM grids (previously Formvar and carbon coated) for 30 s.
3. Float grids on poly-L-lysine drops for 30 min at room temperature with cell contact side *down*; cover Petri dish.
4. Transfer the grids facedown to distilled water for 10 s.
5. Using a sheet of filter paper, wick off excess water and place onto filter paper, treated side *up*.
6. Prepare cellulose acetate disks on glass or plastic surface. First, place a drop of HEPES buffer on the surface, apply the disk, then aspirate off excess medium so that the disk does not move when tapped with the aspirator. Place two or three grids with the poly-L-lysine side up on the acetate disk.
7. Remove excess buffer from cell coverslip by wicking. Turn the coverslip so that cells face the grids and put the coverslip over grids. Place a cork or other stopper on top and press for 1–20 s depending on cell type and confluence. The time/firmness of this step is established by trial and error.
8. Gently remove the stopper. Turn the coverslip over and remove grids by sliding to the edge of the coverslip. Transfer grids *facedown* onto droplets of 2% paraformaldehyde (grids will float on top of droplet). Hold for 10–30 min at room temperature.
9. Transfer grids to PBS in quadrant Petri dishes. Since cells are now fixed, all further steps are performed at room temperature.
10. To label the cytoplasmic face of the sheet with gold-conjugated probes and the traditional two-step protocol, prepare 100 μ L droplets of primary antibody solutions. Keep things organized by using divided Petri dishes or labeled sheets of Parafilm. Aim for saturating concentrations of the primary antibody (2–10 μ g/mL in 0.1% BSA solution). If feasible, identical grids should be incubated with isotype-matched, irrelevant IgG as a negative control. Multiple grids (two or three) can be placed facedown on each droplet of antibody solution for labeling. Incubate 30–60 min in moist chamber.
11. Rinse three times with PBS buffer for 5 min.
12. Set up 100- μ L droplets of secondary antibody conjugated to 3- to 10-nm colloidal gold particles in 0.1% BSA solution. Use the recommended dilution from manufacturer (usually 1:20). Place grids facedown on droplets and incubate for 30 min in the moist chamber.

13. Rinse three times for 5 min in PBS buffer, then postfix by incubating grids face-down on droplets of 2% glutaraldehyde for 10 min, again in the moist chamber.
14. Transfer to PBS buffer. Grids may be stored overnight at this step.
15. Proceed with osmium staining using the droplet method (*see Note 3*). Working in the hood, place small squares of Parafilm on the glass plate and secure to the plate by rubbing gently. Add 100- μ L droplets of 1% osmium to squares, transfer the grids facedown, and incubate for 10 min in the hood.
16. Transfer the grids facedown to Petri dishes containing 0.1 M sodium cacodylate buffer. Rinse once for 5 min.
17. Transfer grids to a Petri dish containing water. Rinse twice for 5 min.
18. Make new Parafilm squares on glass and add droplets of freshly filtered tannic acid to each square. Transfer the grids facedown to these droplets and incubate 10 min.
19. Transfer grids to a Petri dish containing water. Rinse three times for 5 min each.
20. Make new Parafilm squares for filtered uranyl acetate. Add 100- μ L droplets to each square. Transfer the grids facedown to the droplets and incubate 10 min.
21. Transfer the grids to water, rinsing twice for 1 min each. Wick off excess water from the back of the grid (do not touch face) and air dry. Store faceup in a labeled container lined with Whatman paper until ready for TEM.

3.3 Preparation of Sheets for AFM/Fluorescence

Instead of grids, we use 25-mm diameter glass coverslips that are eventually mounted in a Warner coverslip holder. Instead of gold nanoparticles, fluorescent labels are used.

1. Clean 25-mm coverslips in ethanol and glow discharge for 30 s.
2. Immerse in thawed, diluted poly-L-lysine for 30 min.
3. Rinse in water for 10 s and air dry.
4. Fix cells (grown on 15-mm coverslips \pm stimulation at 37 °C) in 0.5% paraformaldehyde in PBS buffer containing Hoechst 33342 nuclear stain for 7 min at room temperature.
5. Rinse 15-mm coverslip containing fixed cells in PBS buffer.
6. Dip these 15-mm coverslips in HEPES buffer, wick off most of the moisture with a Kimwipe[®], and place cell side down onto center of the 25-mm poly-L-lysine-coated coverslip, resting on moist filter paper. Do not apply pressure.
7. Leave glass “sandwich” for 10 min at room temperature, making sure filter paper on the bottom stays moist.
8. Transfer the two coverslips, still sandwiched together, into a Petri dish filled with HEPES buffer. Position the sandwich with the 25-mm coverslip on top; while floating, coverslips will separate, and the 25-mm coverslip may be removed with forceps.

9. Fix 25-mm coverslip with 2% paraformaldehyde for 30 min.
10. Rinse coverslips and label sequentially with primary and fluorophore-conjugated secondary antibodies (or other fluorescent probes).
11. Rinse in PBS buffer three times.
12. Mount in coverslip holder and quickly add PBS buffer before sheets dry out.
13. Can be stored covered with Parafilm at 4°C overnight before AFM/fluorescence imaging.
14. Once at the AFM microscope, it is critical to use both the fluorescent membrane label (to locate sheets on the coverslips) and the Hoechst label (to avoid whole cells and partially fragmented cells that still contain a nucleus). An example is shown in Fig. 3, in which the presence of a Hoechst-stained nucleus rules out the cell in the lower right corner for AFM imaging.

4 Notes

1. The 2% uranyl acetate is a saturated solution and has a tendency to fall out of solution. Gentle heating is needed when making stock solution.
2. This light pre-fix has the distinct advantage that it helps to preserve the cortical cytoskeleton attached to the inner membrane without rendering the cells too “stiff.” If you intend to label the outside of the whole cell with antibody and gold reagents, it is advisable to substitute a stronger pre-fix (such as 2% paraformaldehyde) and to extend the incubation time (up to 30 min) to prevent antibody-induced cluster artifacts (11,16). However, it tends to lower the yield and quality of sheets recovered. Prepare 2% paraformaldehyde solution in the slightly hypotonic HEPES buffer to facilitate a small amount of cell swelling and improved recovery of sheets (14).
3. Osmium staining can obscure gold labels in clathrin-coated pits and can be omitted if desired.

Acknowledgments A.R. Burns was supported in part by the Division of Materials Science, Office of Basic Energy Sciences, U.S. Department of Energy. Sandia is a multiprogram laboratory operated by Sandia Corporation, a Lockheed Martin Company, for the United States Department of Energy under contract DE-AC04-94AL85000. B.S. Wilson was supported in part by National Institutes of Health grants A1051575 and CA119232, and J.M. Oliver was supported through National Institutes of Health grants GM49814 and P20 GM067594 that established the New Mexico Center for the Spatiotemporal Modeling of Cell Signaling. Use of the electron microscopy facility at the University of New Mexico School of Medicine is gratefully acknowledged.

References

1. Maxfield, F., and McGraw, T. (2004) Endocytic recycling. *Nat. Rev. Mol. Cell Biol.* **5**, 121–132.
2. Wilson, B., Pfeiffer, J., and Oliver, J. (2000) Observing FcεRI signaling from the inside of the mast cell membrane. *J. Cell Biol.* **149**, 1131–1142.

3. Wilson, B., Steinberg, S., Liederman, K., et al. (2004) Markers for detergent-resistant lipid rafts occupy distinct and dynamic domains in native membranes. *Mol. Biol. Cell* **15**, 2580–2592.
4. Wilson, B., Pfeiffer, J., Surviladze, Z., Gaudet, E., and Oliver, J. (2001) High resolution mapping reveals distinct FcεRI and LAT domains in activated mast cells. *J. Cell Biol.* **154**, 645–658.
5. Brodsky, F., Chen, C.-Y., Knuehl, C., Towler, M., and Wakeman, D. (2001) Biological basket weaving: formation and function of clathrin-coated vesicles. *Annu. Rev. Cell Dev. Biol.* **17**, 517–568.
6. Müller, D., Heymann, J., Oesterhelt, F., et al. (2000) Atomic force microscopy of native purple membrane. *Biochim. Biophys. Acta* **1460**, 27–38.
7. Frankel, D., Pfeiffer, J., Surviladze, Z., et al. (2006) Revealing the topography of cellular membrane domains by combined AFM/fluorescence imaging. *Biophys. J.* **90**, 2404–2413.
8. Franz, C., and Müller, D. (2005) Analyzing focal adhesion structure by atomic force microscopy. *J. Cell Sci.* **118**, 5315–5323.
9. Burns, A. (2003) Domain structure in model membrane bilayers investigated by simultaneous atomic force microscopy and fluorescence imaging. *Langmuir* **19**, 8358–8363.
10. Burns, A., Frankel, D., and Buranda, T. (2005) Local mobility in lipid domains of supported bilayers characterized by atomic force microscopy and fluorescence correlation spectroscopy. *Biophys. J.* **89**, 1081–1093.
11. Wilson, B., Pfeifer, J., Raymond-Stinz, M., et al. (2007) Exploring membrane domains using native membrane sheets and transmission electron microscopy. In *Lipid Rafts, Methods in Molecular Biology* (T. McIntosh, ed.), Humana Press, Totowa, NJ, v. 398, pp. 245–261.
12. Burns, A. (2007) Atomic force microscopy of lipid domains in supported model systems. In *Lipid Rafts, Methods in Molecular Biology* (T. McIntosh, ed.), Humana Press, Totowa, NJ, v. 398, pp. 263–282.
13. Sanan, D., and Anderson, R. (1991) Simultaneous visualization of LDL receptor distribution and clathrin lattices on membranes torn from the upper surface of cultured cells. *J. Histochem. Cytochem.* **39**, 1017–1024.
14. Heuser, J. (2000) The production of cell cortices for light and electron microscopy. *Traffic* **1**, 545–552.
15. Drees, F., Reilein, A., and Nelson, W. (2005) Cell adhesion assays: fabrication of an ε-cadherin substratum and isolation of lateral and basal membrane patches. In: *Cell Migration: Developmental Methods and Protocols, Methods in Molecular Biology*, Vol. 294 (J.-L. Guan, ed.), Humana Press, Totowa, NJ, pp. 303–320.
16. Kusumi, A., and Suzuki, K. (2005) Toward understanding the dynamics of membrane-raft-based molecular interactions. *Biochim. Biophys. Acta* **1746**, 234–251.

19

Analyzing Endosomes in Nonsectioned Cells by Transmission Electron Microscopy

Willem Stoorvogel

1 Introduction.....	247
2 Materials	249
3 Methods.....	252
4 Notes	256
References.....	257

Summary Cells take up plasma membrane proteins and lipids, together with plasma membrane-associated and fluid phase-endocytosed constituents, via distinct endocytic mechanisms. After having pinched off from the plasma membrane, endocytic vesicles fuse with endosomes; from there endocytosed molecules are sorted and transported by means of vesicular transport intermediates to distinct destinations, including lysosomes, the *trans*-Golgi network, and the plasma membrane. To study endosomal sorting processes, both light microscopic and electron microscopic techniques have been employed. A novel technique, involving 3,3'-diaminobenzidine (DAB) cytochemistry-based whole-mount immunoelectron microscopy, can be used to study the structure of endocytic compartments as well as the subendosomal/lysosomal distribution of relevant proteins in nonsectioned cells at high resolution.

Keywords 3,3'-Diaminobenzidine (DAB) cytochemistry; endosomes; immunoelectron microscopy; lysosomes; protein sorting; whole mount.

1 Introduction

Morphologic analysis of protein transport through endosomes and lysosomes is often hampered by the small size and heterogeneous characteristics as well as by the highly dynamic nature of these compartments and by low labeling densities of suitable marker proteins. Endosome-/lysosome-associated tubules and associated buds commonly have diameters in the range of 80–150 nm. To visualize sorting into or the association of marker proteins with endosomal subdomains, immunoelectron

microscopic techniques are required. Cryosections of aldehyde-fixed material are good substrates for immunocytochemistry, and immunolabeled cryosections have been extremely useful for the study of protein trafficking within the endocytic tract. However, limited epitope accessibility on cryosections of fixed material and its inherent two-dimensional (2D) presentation may limit the applicability of this approach.

An alternative approach that for certain applications may circumvent such difficulties is whole-mount immunoelectron microscopy. This technique is based on 3'-diaminobenzidine (DAB) cytochemistry (1) and was originally developed as a key tool for the identification of a novel class of clathrin-coated vesicles that bud from endosomes (2). Subsequently, this approach has been used in a series of other studies (3–7). It involves labeling of the endocytic tract of live cells, which are cultured directly on top of an electron microscopic grid, with horseradish peroxidase (HRP) either by fluid phase or, when conjugated to ligands, by receptor-mediated endocytosis. The secretory pathway can also be labeled by transfecting cells with complementary deoxyribonucleic acid (cDNA) encoding chimeras of secretory proteins and HRP.

After loading with HRP, the peroxidase activity is used to selectively polymerize DAB in the lumen of HRP-containing compartments of live intact cells in which membrane transport has been halted by reducing the temperature to 0–4 °C. Monomeric DAB diffuses through the plasma membrane and into the lumen of HRP-containing compartments where, in the concomitant presence of H₂O₂, DAB is polymerized and locally crosslinked to luminal and integral membrane proteins. DAB polymerization occurs within seconds, as demonstrated by video reflection microscopy (J. Heuser, Washington University, St. Louis MO, personal communication). DAB polymerization at the extracellular face of the plasma membrane can be prevented by adding ascorbic acid, a membrane-impermeable radical scavenger, concomitantly with the DAB and H₂O₂.

The electron-dense DAB polymer in intracellular compartments serves as a marker that can easily be detected by electron microscopy. Importantly, crosslinking of the DAB polymer to the endosomal/lysosomal protein contents results in selective fixation of such HRP-containing compartments. In this way, tubular aspects of endosomes are extremely well preserved compared to aldehyde fixation protocols. Soluble cytosolic proteins, which are not fixed by DAB cytochemistry, are then removed in the next step on permeabilization of the plasma membrane with saponin. The resulting electron-lucent cells can be studied as whole-mount preparations using transmission electron microscopy (Fig. 1).

The full accessibility of the cytoplasmic surfaces of endosomes/lysosomes results in relative high labeling efficiencies for antibodies that are directed against cytoplasmic domains of integral membrane proteins or cytosolic proteins associated with DAB-filled compartments. Subsequent labeling of the associated antibodies with colloidal gold particles then allows the localization of proteins (Fig. 2), even of low abundant proteins that may remain undetected using conventional immunoelectron microscopy on sectioned cells (see [Notes 1 and 2](#)). Especially, studies on regulatory factors in membrane traffic, such as Rabs, ARFs, and coat components, may benefit from whole-mount immunoelectron microscopy. This procedure may also be helpful in studies of lateral segregation of integral membrane proteins or of the

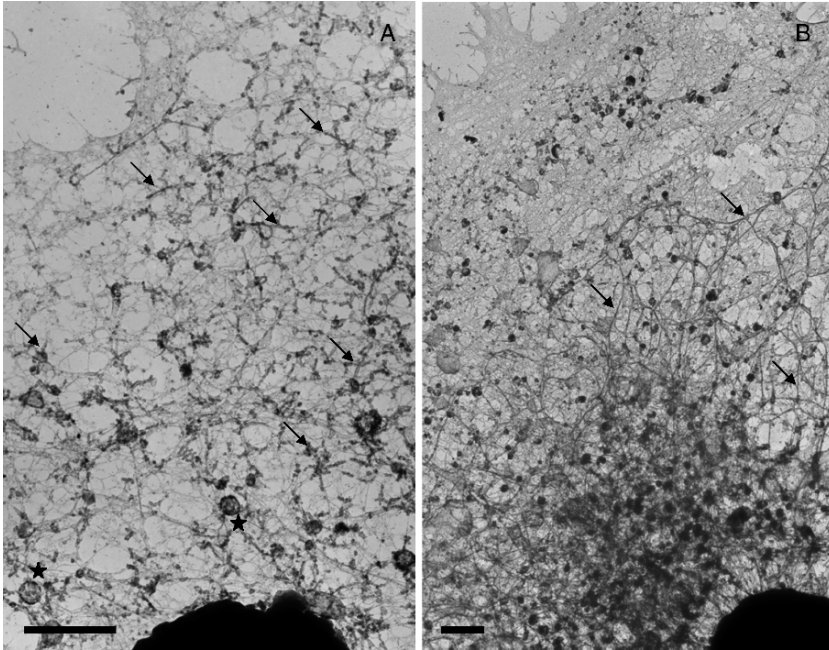


Fig. 1 (A) A431 cells were incubated for 1 h at 37 °C in the presence of Tf–HRP and processed for whole-mount immunocytochemistry. Numerous individual endosomes consisting of vacuoles (exemplified by stars) and tubules (exemplified by arrows) are identified by the electron-dense DAB precipitate. Part of the nucleus is at the bottom, part of the edge of the cell at the left upper corner. (B) Cells were prepared as in A except that Brefeldin A was present during the last 5 min of Tf–HRP uptake. Note the large tubular endosomal network (as exemplified by the arrows), indicating that this technique preserves the integrity of endosomal tubules when present. Bar = 2 μm.

vacuolar association of molecules in signal transduction pathways. As the cells are not sectioned, this method can also help to determine 3D structures and membrane continuities in the vacuolar system (*see Note 3*). Finally, associations of vesicles with the cytoskeleton can be studied using this approach.

2 Materials

2.1 Cell Culture on Grids

1. Golden grids (100–200 mesh, Electron Microscopy Sciences, Hatfield, PA). The grids are rinsed in 85% H_3PO_4 for 1 h, water four times, acetone four times, chloroform four times (in ultrasonic water bath) sequentially and dried in air.
2. Formvar (Merck, Darmstadt, Germany) is dissolved at 1.1 g in 100 mL chloroform (analytical grade) by continuous stirring for 1 h.

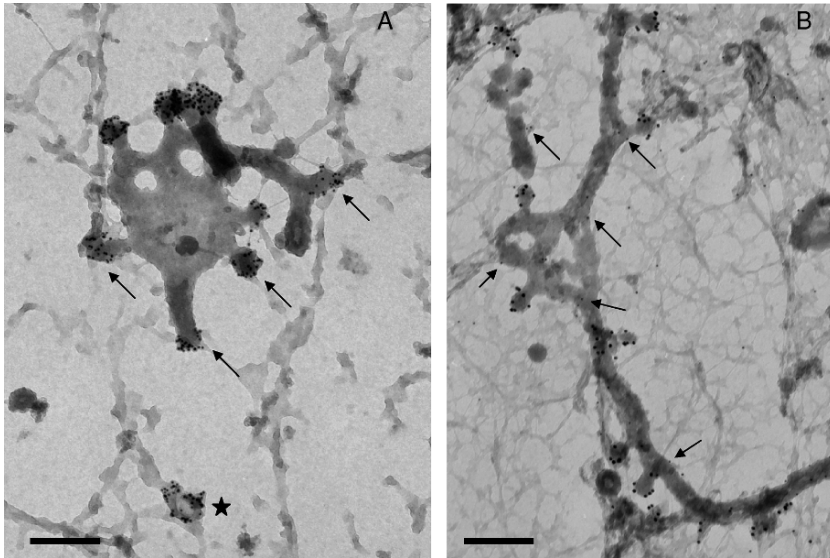


Fig. 2 A431 cells were processed as indicated in Fig. 1A. **(A)** Cells were single immunolabeled for clathrin (10-nm gold). Note the clathrin-coated buds (arrows) on DAB-filled endosomes. A clathrin coated vesicle is indicated by the asterisk. **(B)** Cells were double immunolabeled for clathrin (10nm gold) and the cytoplasmic domain of the transferrin receptor (5-nm gold; exemplified by the arrows). Bar = 200nm.

3. Gelatin (tissue culture grade; Sigma, St. Louis, MO) is dissolved at 0.5% in water, sterilized in an autoclave, and stored at 4°C. Before coating, the gelatin solution is warmed to 37°C.
4. Glutaraldehyde is provided as an 8% EM-grade stock solution (Polyscience, Niles, IL) and stored at 4°C. The 0.5% glutaraldehyde is prepared by mixing 1 part glutaraldehyde with 15 parts Dulbecco's phosphate-buffered saline (PBS).
5. 0.2M phosphate buffer is freshly prepared by mixing 19 mL of a 0.2M stock solution NaH_2PO_4 with 81 mL of a 0.2M stock solution Na_2HPO_4 . The pH should be 7.4.

2.2 Horseradish Peroxidase and Transferrin–Horseradish Peroxidase

1. The fluid-phase endocytosis marker HRP (Sigma, type II) is dissolved at 40 mg/mL in sterile PBS and dialyzed first 4 h against 500 mL sterile PBS, then overnight against 500 mL culture medium. The HRP solution is then centrifuged in an Eppendorf centrifuge at maximal speed for 5 min to remove insoluble debris. Finally, the HRP is diluted to 5 mg/mL in culture medium as required.
2. Human apo-transferrin (Tf) (Sigma).
3. HRP type VI (Sigma) for conjugation to Tf.

4. *N*-Succinimidyl 3-[2-pyridyldithio]-propionate (SPDP) (Sigma) is freshly dissolved at 40 mM in absolute ethanol. Remaining SPDP is discarded.
5. Sephadex G25 resin (Sigma-Aldrich) is hydrated in water and stored overnight at 4 °C.
6. Proteins are concentrated using Centricon filters with a 30-kDa cutoff (Millipore) by centrifugation in 15-min runs at 5000×g in a Sorvall centrifuge using a SS-34 fixed-angle rotor containing rubber inserts.
7. PBS: Dulbecco's PBS lacking Mg²⁺ and Ca²⁺.
8. 0.1 M sodium acetate/HCl, 0.1 M NaCl, pH 4.5.
9. Dithiothreitol (Sigma) in water: 0.5 M stock freshly prepared.
10. Superdex 200 26/60 (Amersham, Piscataway, NJ).
11. 0.15 M NaCl, 20 mM Tris-HCl, pH 7.2.
12. Fe³⁺ saturation buffer: Add 1 mM NaHCO₃, 2 mM sodium nitrilotriacetate, and 0.25 mM FeCl₃ to 0.25 M Tris-HCl, pH 8.2.
13. 0.15 M NaCl, 20 mM HEPES/NaOH, pH 7.4.

2.3 DAB Polymerization

1. 15 mg/mL DAB (BDH Limited, Poole, England) 10X stock solution: Filter using 0.2-µm filters (Millipore, Billerica, MA) and store in 1-mL aliquots at -20 °C.
2. 0.5 M ascorbic acid (Merck) 10X stock solution; store in 1-mL aliquots at -20 °C.
3. Freshly prepare DAB buffer: 1.5 mg/mL DAB, 70 mM NaCl, 50 mM ascorbic acid, 20 mM HEPES (Gibco BRL, UK), 2 mM CaCl₂. Adjust to pH 7.0 with 1 N NaOH just prior to use (during incubation of cells with HRP or Tf/HRP). Monitor the pH using pH paper. Do not use an electronic pH meter since this solution is detrimental to the pH electrode. After setting the pH, the solution is adjusted to 280–300 mosM using 5 M NaCl. When plasma membrane-associated clathrin-coated pits are examined, ascorbic acid should be omitted from the DAB buffer to allow extracellular HRP-catalyzed DAB polymerization. In this case, additional NaCl should be added to the DAB buffer to compensate osmolarity to 280–300 mosM. After setting the pH, the DAB buffer should be used within 30–60 min. Make sure the temperature of the buffer is at 0 °C when added to the cells. Add 0.005% H₂O₂ from a 30% stock solution 1 min before use.
4. PBS complete: Dulbecco's PBS containing CaCl₂ and MgCl₂.
5. Permeabilization buffer: Dulbecco's PBS containing 10 mM ethylene glycol-bis(2-amino-ethylether)-*N,N,N',N'*-tetraacetic acid (EGTA), 0.5 mM MgCl₂, 8.3 mM CaCl₂, 1 mg/mL saponin (Merck), 5 mM ascorbic acid, NaOH at pH 7.4. The pH has to be readjusted to 7.4 using 1 N NaOH because of formation of EGTA-Ca²⁺ complexes and the presence of ascorbic acid. Using a pH meter Saponin is added after pH adjustment for protection of the pH electrode.

6. Stripping buffer (when desired): 0.5 M Tris-HCl, pH 7.4, containing 1 mg/mL saponin.
7. Washing buffer: Dulbecco's PBS containing 10 mM EGTA, 0.5 mM MgCl₂, 8.3 mM CaCl₂. Readjust to pH 7.4 using 1 N NaOH.
8. Glutaraldehyde is provided as an 8% EM-grade stock solution (Polyscience) and stored at 4 °C. Paraformaldehyde (Electron Microscopy Sciences) is dissolved in a fume hood at 8 g in 75 mL water under constant stirring at 60 °C by adding 0.1 N NaOH until the solution is cleared and has reached pH 7.0. Water is added to an end volume of 100 mL (8% final solution). The paraformaldehyde solution is stored in sealed aliquots at -20 °C. When required, thaw at 40–50 °C and mix until the solution becomes clear. Prepare 4% paraformaldehyde by mixing equal volumes of 8% paraformaldehyde with 0.2 M phosphate buffer, pH 7.4. A mixture of 0.2% glutaraldehyde and 2% paraformaldehyde is prepared by mixing 5 parts 0.1 M phosphate buffer, pH 7.4, with 2.5 parts paraformaldehyde, 0.5 parts glutaraldehyde, and 2 parts water.
9. Quench buffer: Dulbecco's PBS containing 50 mM NH₄Cl.

2.4 Immunolabeling

1. Blocking buffer: Dulbecco's PBS, 1 mg/mL saponin, 20 mM glycine, 0.1% cold water fish gelatin (Sigma; G-7765), 0.02% NaN₂.
2. For low nonspecific binding, it is important to use protein A coupled to H₂O₂-treated gold. This can be ordered at Cell Microscopy Center, UMC Utrecht G.02.525, Heidelberglaan 100, 3584 CX Utrecht, The Netherlands (g.posthuma@umcutrecht.nl).
3. 1% glutaraldehyde in 0.1 M phosphate buffer, pH 7.4.
4. PBS, 20 mM glycine.

3 Methods

3.1 Preparation Grids

For whole mount immunocytochemistry, cells are grown on 100- to 200-mesh golden grids carrying a carbon-coated Formvar film. The coatings are home-made as any contamination may affect cell attachment and quality.

1. The Formvar film is made on a glass object slide that is first cleaned by extensive wiping with a chamois and lens paper sequentially. The Formvar solution is poured in a funnel that can hold the glass slide in an upright position and has two stopcock valves in its outlet. The upper valve is used to regulate the flow; the second is an on/off switch. The glass slide is inserted into the Formvar solution,

which should cover about two-thirds of its length. The Formvar solution is drained from the funnel in about 10 s.

2. The slide is removed from the funnel; the film is cut 0.5 mm from the edges with a razor blade. The film is floated on top of water by slowly inserting the slide in a vertical position into a beaker filled with water. The thickness of the film should be about 70 nm, which will give it a silver-white appearance on the water surface when illuminated with a lamp. The cleaned grids are placed with their shiny side up on top of the floating film. To collect the grids, a second glass object slide, covered with stretched Parafilm, is pressed vertically onto the floating Formvar film at a 90° angle into the water such that the grids are submerged and pressed between the Parafilm and Formvar film.
3. After drying, samples of the grids are checked in the electron microscope at $\times 20,000$ for strength and quality of the film.
4. A layer of carbon is evaporated onto the Formvar-coated grids using standard techniques.
5. Grids are stored until use.

3.2 *Cell Culture on Grids*

1. The coated grids are removed from the Parafilm after carving through the Formvar film around the edge of the grid using EM tweezers and placed with the Formvar film up in a 6-cm tissue culture dish. Some cell types can be cultured straight onto the carbon-coated film. In this case, grids should be sterilized by microwaving for 10 s. When microwaved dry, microorganisms dye almost instantly. Alternatively, grids may first be coated with gelatin for good cell adhesion. Toward this end, the grids are covered with 0.5% gelatin in water for 10 min, washed with water, fixed for 30 min with 0.5% glutaraldehyde in PBS, and washed four times with tissue culture medium. The amino acids in this medium quench remaining free aldehydes. When the grids tend to float, it is best to let drops of fluid fall directly on top of the grids to make them sink. You may also gently push them down with the blunt tip of a 10-mL plastic pipet. Small air bubbles may remain trapped under the grid; they can be removed during washing by sucking away the medium from under the grid at their edge using an Eppendorf pipet with modest suction. Be careful not to suck the grids onto your pipet as this removes the Formvar film. Grids are both coated with gelatin and sterilized by this procedure.
2. Leave the grids for at least 1 d in culture medium in the incubator before cell seeding. Detach cells using trypsin/EDTA until they can be removed from their support by shaking and seed 4 mL of an appropriate dilution into the dish onto the grids. After seeding, immediately place the dish into the incubator, allow the cells to settle by sedimentation, and do not touch until the next day or the cells may roll off the grids. Cells are ready for use after 2 d of culture; earlier experiments may result in cell loss.

3.3 Preparation Tf–HRP

1. Tf–HRP is prepared as described in *Ref. 8*. Dissolve Tf in 5 mL PBS. Add 35 μ L 40 mM SPDP, mix on a vortex, and incubate 30 min at room temperature. Separate on 30-mL Sephadex G25 column in PBS. Collect 1-mL fractions, measure A280, and pool the main protein-containing fractions. Concentrate protein to 5 mL using a Centricon microconcentrator.
2. Dissolve 100 mg HRP in 5 mL PBS. Slowly add 930 μ L 40 mM SPDP while vortexing and incubate 30 min at room temperature. Separate on 30-mL Sephadex G25 column in 0.1 M acetate, 0.1 M NaCl, pH 4.5. Collect and pool brown fractions. Concentrate pooled fractions to less than 5 mL using a Centricon microconcentrator. Add 50 mM dithiothreitol from a freshly prepared 0.5 M stock and incubate for 20 min at room temperature. Separate on a 30-mL Sephadex G25 column in PBS. Collect and pool brown fractions; discard the tail of the peak. Concentrate pooled fractions to less than 5 mL using a Centricon microconcentrator.
3. Mix the SPDP-conjugated HRP and Tf preparations; couple overnight at 4 °C while rotating end over end. Concentrate pooled fractions to approx 2 mL using a Centricon microconcentrator. Centrifuge 5 min in Eppendorf centrifuge at maximal speed to remove aggregates. Separate on a 120-mL Superdex 200 26/60 column (Amersham) in 20 mM Tris-HCl, pH 7.2, 0.15 M NaCl.
4. Collect 1.5-mL fractions; measure A280 and A403 to determine total protein- and HRP-containing fractions, respectively. Separate relevant fractions for analysis by sodium dodecyl sulfate polyacrylamide gel electrophoresis (SDS-PAGE) (10%) at nonreducing conditions. Note that reducing conditions dissociate the conjugate. Pool the fractions containing low molecular weight Tf–HRP conjugates and no large conjugates or free Tf.
5. To saturate Tf–HRP with Fe³⁺, an equal volume of Fe³⁺ saturation buffer is added to the pooled Tf–HRP fractions and incubated for 1 h at room temperature. The sample is then dialyzed extensively (four 1-L changes, minimal 4 h each) against 150 mM NaCl, 20 mM HEPES/NaOH, pH 7.4.
6. The final concentration of Tf–HRP is determined by adsorption at A280 using Tf as a reference. The A280 of 1 mg/mL Tf is 1.43. Samples are stored in aliquots at –80 °C.

3.4 Endocytosis of Tf–HRP or HRP and DAB Polymerization

1. Cells on grids are washed three times with culture medium (e.g., DMEM) lacking serum at 37 °C. Tf in serum would compete for Tf–HRP binding to the transferring receptor. Cells are then incubated with prewarmed and CO₂-equilibrated culture medium lacking serum but containing 25 μ g/mL Tf–HRP, 5 mg/mL HRP, or both for 1–2 h in a CO₂ incubator. Depending on the goal of the experiment, HRP can

be endocytosed either in pulse or pulse–chase fashion. For labeling of lysosomes, it is advised to allow uptake for at least 2 h. In our experience, fluid-phase endocytosed HRP efficiently labels sorting endosomes and lysosomes but not recycling endosomes. In most cell types, uptake and recycling of the Tf occurs with $t_{1/2}$ of 2 and 20 min, respectively. Therefore, continuous uptake of Tf–HRP for 30–60 min suffices to label the entire uptake and recycling pathway. To label the entire endocytic tract, including the lysosomal degradation and recycling pathways, HRP and Tf–HRP can be endocytosed simultaneously.

2. During HRP uptake, prepare the DAB buffer and keep at 0 °C.
3. After uptake of HRP, Tf–HRP, or both, the medium is removed and replaced immediately by PBS complete at 0 °C. The cells are washed rapidly (<5 s per wash), either once (for Tf–HRP) or three times (for HRP) with PBS complete at 0 °C. Abundant presence of extracellular HRP should be prevented as this results in DAB deposits at the plasma membrane, even in the presence of ascorbic acid.
4. Add the DAB buffer to the cells for 30 min at 0 °C. The DAB buffer is refreshed after 5 min.
5. Wash the cells four times with PBS complete at 0 °C to remove all free DAB and transfer the grids to a clean tissue culture dish. The cells are then permeabilized gently for 30 min at 0 °C on a slow rocking platform at 0–4 °C using permeabilization buffer. Saponin binds cholesterol in membranes, forming pores through which soluble cytosolic proteins leak out. Membrane-bound proteins, the nucleus, cytoskeleton, and proteins crosslinked to the DAB polymer remain cell associated.
6. If desired, coat proteins, such as clathrin and adaptor complexes, can be removed from membranes to expose underlying epitopes by incubating permeabilized cells for 15 min at 0 °C in stripping buffer prior to fixation. Remove Tris-HCL by extensive washing with permeabilization buffer.
7. Wash the cells once with washing buffer at 0–4 °C.
8. Fix the cells for 1 h at 4 °C with either 4% paraformaldehyde or a mixture of 0.2% glutaraldehyde and 2% paraformaldehyde.
9. Wash the grids three times with PBS and block remaining aldehydes in quench buffer at room temperature.

3.5 Immunolabeling

All the following treatments can be performed at room temperature.

1. Transfer grids to 96-well round-bottom plates containing blocking buffer for easy and individual manipulation.
2. Block for a minimum of 2 h prior to labeling. Cells can be stored as such for several days at 4 °C.

3. The cells are (double or triple) immunolabeled according to the method of Slot et al. (9) using 5-, 10-, and 15-nm protein A–colloidal gold particles. The cells are fixed with glutaraldehyde after each of the sequential labeling steps to permanently immobilize the colloidal gold label and exclude cross-labeling. Cross-labeling can be checked in control experiments in which the primary antibody of the second label is omitted. Nonspecific labeling should be checked using nonrelevant antibodies. Add a minimum of 30 μ L antibody in blocking buffer and incubate for 30 min at room temperature.
4. Wash three times with 200 μ L blocking buffer by sucking away the buffer using a yellow pipet tip mounted on a glass Pasteur pipet and a vacuum line. This allows easy switching between grids with clean yellow tips. Refill the wells immediately to prevent drying of the cells. Use a repeating pipet set at 200 μ L and mounted with a yellow pipet tip for refilling the wells. During refilling, the grids may swirl around in the well, which improves the washing procedure.
5. Primary antibodies may be labeled with secondary antibodies (optional) (e.g., rabbit antimouse immunoglobulin G [IgG]) using the same procedure as above.
6. IgG is labeled with protein A–coupled colloidal gold in blocking buffer using the same procedure as above.
7. Labeled cells are fixed with 1% glutaraldehyde in 0.1 M phosphate buffer pH 7.4 for 1 h, washed three times with PBS, and incubated for 10 min in PBS, glycine.
8. Subsequently, other epitopes can be labeled using another size gold probe. Note that protein A binding sites on IgG, but not all Ig epitopes are blocked by glutaraldehyde. This is important for setting out double-labeling strategies.
9. After labeling second or third epitopes, cells are fixed again with 1% glutaraldehyde as indicated above.
10. After labeling, the cells are extensively washed with water and dehydrated by sequential passage through 50%, 70%, 90%, 96%, and absolute ethanol. Ethanol is substituted by liquid CO₂, and the cells are dried in a critical point drying apparatus.
11. A film of carbon is evaporated onto the samples while rotating the grids under varying angles.
12. The grids are stored dry in a box containing P₂O₅.
13. The grids are examined using a transmission electron microscope at 60–80 kV.

4 Notes

1. Although whole-mount immunoelectron microscopy allows for efficient 3D localization of proteins at the cytoplasmic surface of vacuoles, a limiting aspect is that it can be used only to study the distribution of antigens associated with

HRP-loaded vesicles. To determine the extent to which proteins are associated with HRP-loaded vesicles, other morphological techniques, such as immunoelectron microscopy on cryosections, are required.

2. Whole-mount immunoelectron microscopy can be combined with fluorescence microscopy on the same preparation.
3. In whole-mount preparations, especially in the perinuclear area, crowding by DAB-labeled organelles may blur the view. Although this imposes limits to the 3D impression, the advantage of high labeling efficiencies remains.

References

1. Stoorvogel, W. (1998) Analysis of the endocytic system by using horseradish peroxidase. *Trends Cell Biol.* **8**, 503–505.
2. Stoorvogel, W., Oorschot, V., and Geuze, H.J. (1996) A novel class of clathrin-coated vesicles budding from endosomes. *J. Cell Biol.* **132**, 21–33.
3. Dell'Angelica, E.C., Klumperman, J., Stoorvogel, W., and Bonifacino, J.S. (1998) Association of the AP-3 adaptor complex with clathrin. *Science* **280**, 431–434.
4. Kleijmeer, M., Ramm, G., Schuurhuis, D., et al. (2001) Reorganization of multivesicular bodies regulates MHC class II antigen presentation by dendritic cells. *J. Cell Biol.* **155**, 53–63.
5. Ramm, G., Pond, L., Watts, C., and Stoorvogel, W. (2000) Clathrin-coated lattices and buds on MHC class II compartments do not selectively recruit mature MHC-II. *J. Cell Sci.* **113**(Pt. 2), 303–313.
6. van Dam, E.M., Ten, B.T., Jansen, K., Spijkers, P., and Stoorvogel, W. (2002) Endocytosed transferrin receptors recycle via distinct dynamin and phosphatidylinositol 3-kinase-dependent pathways. *J. Biol. Chem.* **277**, 48876–48883.
7. van Dam, E.M., and Stoorvogel, W. (2002) Dynamin-dependent transferrin receptor recycling by endosome-derived clathrin-coated vesicles. *Mol. Biol. Cell* **13**, 169–182.
8. Stoorvogel, W., Geuze, H.J., Griffith, J.M., and Strous, G.J. (1988) The pathways of endocytosed transferrin and secretory protein are connected in the *trans*-Golgi reticulum. *J. Cell Biol.* **106**, 1821–1829.
9. Slot, J.W., Geuze, H.J., Gigengack, S., Lienhard, G.E., and James, D.E. (1991) Immunolocalization of the insulin regulatable glucose transporter in brown adipose tissue of the rat. *J. Cell Biol.* **113**, 123–135.

20

Imaging Exocytosis of Single Insulin Secretory Granules With TIRF Microscopy

Shinya Nagamatsu and Mica Ohara-Imaizumi

1 Introduction.....	259
2 Materials	261
3 Methods.....	264
4 Notes	266
References.....	267

Summary The total internal reflection fluorescence (TIRF) technique is a powerful tool for visualizing the process of insulin exocytosis. This technique allows us to observe the events just beneath the plasma membrane, allowing us to explore the molecular mechanism of insulin exocytotic processes such as docking and fusion. In this review, we describe the method of TIRF for visualizing insulin exocytosis in pancreatic β -cells.

Keywords Exocytosis; insulin; pancreatic β -cells; TIRFM.

1 Introduction

Total internal reflection fluorescence (TIRF) microscopy is a technique that specifically illuminates fluorophores in a thin optical section above the interface between two media with different refractive indices (1,2). This technique is a powerful tool for exploring the mechanism of insulin exocytosis. In the process of insulin exocytosis, β -granules approach the plasma membrane from intracellular space and dock to the plasma membrane with subsequent fusion; therefore, if the events just beneath the plasma membrane are able to be imaged by TIRF, valuable information must be obtained.

In TIRF microscopy, laser light is directed obliquely at the interface between two media from a high to a low refractive index with an incident angle greater than the critical angle of total internal reflection. Under these conditions, laser light is

totally internally reflected at the interface. Even so, some of the light penetrates the medium of lower refractive index as an electromagnetic field called the *evanescent wave*. The evanescent wave vanishes exponentially with distances (Fig. 1). Evanescent field penetration depths (the distance from the interface) are usually less than 100 nm, resulting in images with very low background fluorescence, virtually no out-of-focus fluorescence, and minimal exposure of cells to light at any other planes in the sample. This offers a great advantage over the optical resolution achievable with confocal microscopy (~500 nm). The cells are grown on the glass coverslip; imaging of fluorophores immediately below the plasma membrane can be achieved in live cells.

In pioneering work by Daniel Axelrod, this technique was first applied to the study of live cells, primarily to investigate cell surface adhesions (3), then several studies of protein dynamics, topography of cell–substrate contacts, endocytosis, or exocytosis using this technique were reported (4–9). We applied this system to pancreatic β -cells to visualize insulin exocytosis. To specifically label insulin secretory granules, we generated a construct of expression vector in which green fluorescent protein (GFP) is located at the C-terminus of preproinsulin (insulin–GFP) as mentioned below (Section 2.3). We describe the methodology of TIRF microscopy in pancreatic β -cells.

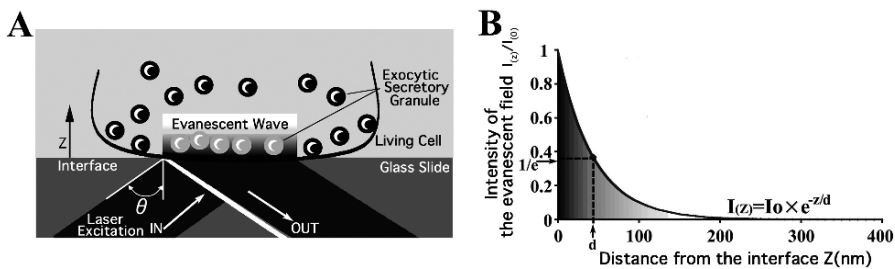


Fig. 1 TIRF excitation using an evanescent field. **(A)** Schematic drawing of the evanescent wave excitation. When a light beam propagating through a transparent medium of high refractive index n_1 (e.g., coverslip) encounters an interface with a medium of lower refractive index n_2 (e.g., adhering cells), total internal reflection occurs at incidence angles (θ), which are greater than the critical angle. Although being totally reflected, some of the incident light beam evokes an evanescent field that penetrates into the medium of lower refractive index. **(B)** The intensity of the evanescent field exponentially decays with increasing distance from the interface: $I_{(z)} = I_{(0)} e^{-z/d}$, where $I_{(z)}$ represents the intensity at a perpendicular distance z from the interface, and $I_{(0)}$ is the intensity at the interface. The theoretical penetration depth (d , the distance where the intensity has decreased to $I_{(0)}/e$) depends on the incidence angle θ , wavelength λ , as well as the refractive index of the glass (n_1) and medium (n_2): $d = (\lambda/4\pi)(n_1^2 \sin^2 \theta - n_2^2)^{-1/2}$. The penetration depth, which usually ranges between 30 and 100 nm, decreases with increasing θ (see Note 1 and Refs. 3 and 10).

2 Materials

2.1 Setup of TIRF Microscopy System

An overview of the TIRF microscopy system is shown in Fig. 2. The Olympus objective-type TIRF system was used with minor modifications (*see Note 2*).

1. Light from an Ar laser (488nm; Melles Griot, Carlsbad, CA) or a He/Ne laser (543 nm; Melles Griot) was introduced to an inverted microscope (IX70, Olympus, Tokyo, Japan) through a single-mode fiber and two illumination lenses; the light was focused at the back focal plane of a high-aperture objective lens (Apo $\times 100$ OHR; numerical aperture [NA] 1.65, Olympus; *see Note 3*). The focal point was moved off axis to the most peripheral position in the objective lens by simply shifting the position of the fiber using micrometer laser adjustment.
2. To observe GFP alone, we used a 488-nm laser line for excitation and a 515-nm long-pass filter for the barrier. To observe the fluorescent image of Red Fluorescent Protein (RFP) or Cyanine dye, Cy3, we used a 543-nm laser line and a long-pass 590-nm filter. Two lasers can be introduced simultaneously with the laser combiner unit (Olympus). A filter wheel system (LUDL Electronic Products, Hawthorne, NY) is used with several interchangeable filters that can be rotated to bring the appropriate filter into the light path in a synchronized fashion. A computer-controlled shutter (Uniblitz, Vincent Associates) is used with several interchangeable filters that can be rotated to bring the appropriate filter into the light path in a synchronized fashion. A computer-controlled shutter

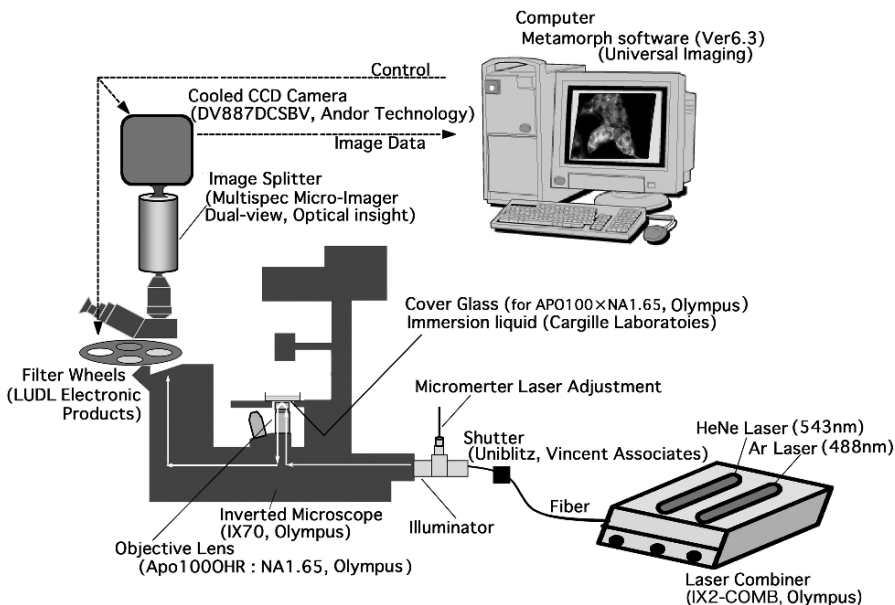


Fig. 2 Schematic representation of the TIRF setup described in the text.

(Uniblitz, Vincent Associates, Rochester, NY) is placed between the laser combiner unit and illuminator to prevent photobleaching of cells between exposures. Images were collected by a cooled charge-coupled device (CCD) camera (DV887DCSBV, Andor Technology, Belfast, Northern Ireland; operated with Metamorph version 6.2, Universal Imaging, Downingtown, PA) (*see Note 4*). Images were acquired at 50- to 300-ms intervals.

3. To observe the fluorescence image of GFP and Cy3 simultaneously under TIRF illumination, we used the 488-nm laser line for excitation and an image splitter (MultiSpec Micro-Imager, Optical Insight, Santa Fe, NM) that divided the green and red components of the images with a 565-nm dichroic mirror (Q565, Chroma, Brattleboro, VT) and passed the green component through a 530- \pm 15-nm bandpass filter (HQ530/30m; Chroma) and the red component through a 630- \pm 25-nm bandpass filter (HQ630/50m; Chroma) (*see Note 5*). The images were then projected side by side onto the CCD camera. The two images were brought into focus in the same plane by adding weak lenses to one channel, and they were brought into register by careful adjustment of the mirrors in the image splitter (11,12) (*see Note 6*).
4. Most analyses, including tracking (single projection of difference images) and area calculations were performed using Metamorph software.

2.2 Cell Culture

2.2.1 Culture of MIN6 Cells

1. MIN6 cells were a kind gift from Dr. J.-I. Miyazaki (Osaka University, Osaka, Japan).
2. DMEM (Dulbecco's modified Eagle's medium, high glucose) supplemented with 10% fetal bovine serum (FBS), 50 unit/mL penicillin, 50 μ g/mL streptomycin, 28.4 μ M 2-mercaptoethanol (Gibco/Invitrogen, Carlsbad, CA).
3. Trypsin-EDTA (ethylenediaminetetraacetic acid) solution: 0.25% trypsin, 1 mM EDTA (Gibco/Invitrogen).
4. Phosphate-buffered saline (PBS; pH 7.4, without CaCl₂ and MgCl₂) (Gibco/Invitrogen).
5. Fibronectin (1 mg/mL) (Koken, Tokyo).
6. Coverslips: High refractive index ($n = 1.8$) (Olympus, Tokyo) (*see Note 7*). Coverslips were treated with fibronectin in PBS for 15 min.

2.2.2 Primary Culture of Pancreatic β -Cells

1. Animals: Male Wistar rats (weight 200 g).
2. RPMI1640 (11 mM glucose; GIBCO/Invitrogen) supplemented with 10% FBS, 200 U/mL penicillin, 200 μ g/mL streptomycin.
3. Hanks' balanced salt solution (HBSS; Gibco/Invitrogen).

4. Ca^{2+} -free Krebs-Ringer buffer (KRB) containing 1 mM EDTA (Gibco/Invitrogen).
5. Type IV collagenase (Gibco/Invitrogen).
6. High refractive index ($n = 1.8$) coverslips (Olympus) treated with (40 $\mu\text{g}/\text{mL}$) fibronectin in PBS for 15 min.

2.3 Probes for Labeling of Secretory Granules

2.3.1 MIN6 Cells

Plasmid: Human preproinsulin complementary deoxyribonucleic acid (cDNA) pchi 1–19 (provided by Professor G. I. Bell, University of Chicago, Chicago, IL) lacking a TGA stop codon was amplified by polymerase chain reaction (PCR) using forward primer 5'-*GAATTCCGGGGGTCCTTCTGCCATG*-3' (EcoR1 site is italicized) and reverse primer 5'-*GGATCCCAGTTGCAGTAGTTCTCCAGC*-3', where TGA was replaced by TGG. The product was subcloned into a pGEMTeasy vector (Promega, Madison, WI). The approx 0.3-kb insulin cDNA fragment lacking a stop codon was cleaved by EcoR1 and BamH1 double digestion, which was subcloned into the EcoR1 and BamH1 site of multiple cloning sites of pEGFP-N1 (insulin-GFP) (Clontech/Takara Bio, Otsu, Japan) (13). Recombinant adenovirus-encoding insulin-GFP was produced using above insulin-GFP by manufacturer's protocol (adenovirus expression system, Takara Bio).

2.3.2 Primary Cultured β -Cells

Adenovirus: For the recombinant adenovirus production of insulin-GFP, a cDNA fragment containing preproinsulin and GFP was cut by EcoR1 and NotI restriction enzymes; this was ligated into the pAdex1CA cosmid vector, and Adex1CA insulin-GFP was prepared and amplified by the standard protocol (Takara Bio) as described previously (14). The reverse primer used here encodes the C-terminus of preproinsulin, encoding LENYCNWD. The fusion with the N-terminus of enhanced GFP includes a short linker (provided by the pEGFP-N1 plasmid) such that the sequence reads LENYCNWDPPVATM (14).

2.4 TIRF Imaging

1. Low-glucose KRB: 110 mM NaCl, 4.4 mM KCl, 1.45 mM KH_2PO_4 , 1.2 mM MgSO_4 , 2.3 mM calcium gluconate, 4.8 mM NaHCO_3 , 2.2 mM glucose, 10 mM HEPES, 0.3% bovine serum albumin (BSA); pH 7.4.
2. High-glucose KRB: Use the same composition as a low-glucose KRB except increase glucose concentration to 22 mM.

3. High-KCl KRB: Reduce NaCl to maintain the isotonicity of the solution.
4. Immersion oil: Diiodomethane sulfur immersion oil ($n = 1.78$, Cargille Laboratories, NJ) was used to make contact between the objective lens and the coverslip (*see Note 7*).

3 Methods

3.1 Culture and Transfection of MIN6 Cells

1. Cells were seeded in a T-75 plastic flask, incubated in an atmosphere of 5% CO₂ at 37°C, and subcultured by regular trypsinization (wash with PBS and treat with trypsin-EDTA) and reseeded. For TIRF observation, cells were seeded on fibronectin-coated high refractive index cover glass.
2. MIN6 cells were transfected with the expression vector using Effectene transfection reagent (Qiagen, Hilden, Germany), according to the manufacturer's protocol. All TIRF experiments were performed between 2 and 3 d after transfection.

3.2 Primary Culture and Infection of Pancreatic β -Cells

1. Preparation of β -cells: For preparation of islets of Langerhans from rat, a detailed isolation procedure by collagenase digestion was described by Lacy and Kostianovsky (15). A rat was anesthetized, and the bile duct was cannulated. HBSS was injected into the duct, and then the pancreas was removed. The pancreas was sequentially immersed into 5, 2.5, 1.25 mg/mL collagenase in HBSS and agitated by hand, followed by two buffer washes after each digestion. Islets were then collected by centrifugation. Isolated islets were dissociated into single cells by incubation in Ca²⁺-free KRB and cultured on fibronectin-coated high refractive index glass coverslips in RPMI1640 at 37°C in an atmosphere of 95% air/5% CO₂.
2. Infection: For the infection of the pancreatic β -cells with the recombinant adenovirus, cultured single cells were incubated with RPMI 1640 medium (5% FBS) and the required adenovirus (Adex1CA insulin-GFP: 30 multiplicity of infection per cell) for 1 h at 37°C, after which RPMI 1640 medium with 10% FBS was added. All experiments were performed between 2 and 3 d after infection.

3.3 Observation of Exocytotic Images of Secretory Granules

1. Turn TIRF system on 30 min before use.
2. Mount the insulin-GFP-transfected MIN6 cells or infected β -cells on the high refractive index coverslips in an open chamber and incubate them in low-glucose KRB for 30 min at 37°C.

3. Transfer coverslips to the thermostat-controlled stage (37°C) of the TIRF microscope.
4. Find insulin–GFP-expressing cells in epifluorescence first.
5. Incline the optic fiber of TIRF microscopy from epifluorescent illumination mode to evanescent wave illumination mode using the micrometer laser adjustment.
6. Precisely focus the image with the z-focus drive.
7. Lower the laser intensity and use ND (neutral density) filters to minimize photodamage and increase CCD sensitivity/gain and image contrast.
8. Use Metamorph software to acquire images at 50- to 300-ms intervals. Stimulate cells by switching buffers in a mounted chamber from low-glucose KRB to high-glucose KRB or high-KCl KRB. For bath application, stimulation with glucose and KCl is achieved by addition of 52 mM glucose-KRB or 100 mM KCl-KRB into the chamber (final concentration 50 mM KCl or 22 mM glucose).
9. Continue acquiring the images 20 min after high-glucose stimulation.
10. Save the acquired images to a hard disk drive on a computer or to other physical media.

3.4 Analysis of Images

Most analyses, including tracking and area calculations, are performed using Metamorph software. To analyze the data, fusion events are manually selected, and the average fluorescence intensity of individual granules in a $1 \times 1 \mu\text{m}$ square placed over the granule center is calculated. The number of fusion events is manually counted while looping 6000 frame time lapses. Sequences are exported as single TIFF files and further processed using Adobe Photoshop 7.0, or they are converted into QuickTime movies.

3.5 Example of Insulin Exocytosis by TIRF Images

Pancreatic β -cells release insulin by glucose stimulation with a biphasic pattern, which consists of a rapidly initiated and transient first phase followed by a sustained second phase. The precise molecular mechanism of phasic insulin exocytosis is unknown. We tried to obtain direct imaging of insulin exocytosis during first- and second-phase insulin exocytosis (14).

We infected rat primary pancreatic β -cells with recombinant adenovirus encoding insulin–GFP to label the insulin secretory granules and then examined the dynamic motion of granules near the plasma membrane. TIRF images of single β -cells in which fluorescence spots represent the insulin granules docked to the plasma membrane. The cells were stimulated by 22 mM glucose, then the sequential images of single granules were acquired every 50 ms (Fig. 3A). The data revealed the marked difference in exocytotic pathways between first and second phase. As shown in Fig. 3B,

during the first phase, within the first 4 min after the addition of 22 mM glucose, the fusing granules originated mostly from morphologically previously docked granules that were visible before glucose stimulation. The fluorescent spot suddenly brightened and vanished within 300ms. On the other hand, during the second phase, the fusing granules arose from “newcomers,” which had been absent or only dimly visible before stimulation.

4 Notes

1. For example, when a laser light ($\lambda = 488 \text{ nm}$) propagates through the high refractive index glass ($n_1 = 1.8$) at the incidence angle ($\theta = 65^\circ$) onto the cells ($n_2 = 1.37$), d equals 44 nm calculated from the formula (Fig. 1B).
2. Two types of TIRF microscopy have been developed: prism type and objective type (through-the-lens type). The prism-type TIRF microscopy is mostly home-made. This setup is easily accomplished since it requires only the microscope, prism, and laser, all components that are readily available. The drawback for this setup is

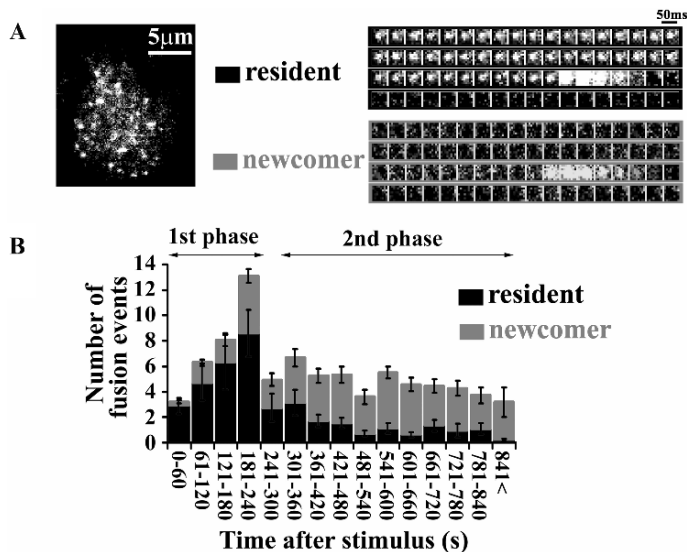


Fig. 3 TIRF images and analysis of single GFP-labeled insulin granule motion in rat primary β -cells during glucose stimulation. (A) Left panel: The real-time motion of GFP-labeled insulin granules was imaged to the plasma membrane. This is the TIRF image of a single cell harboring insulin-GFP, showing that many insulin granules docked to the plasma membrane. Right panel: Sequential images ($1 \mu\text{m} \times 1 \mu\text{m}$ per 50-ms interval) of a granule docking and fusing with the plasma membrane were presented during 22 mM glucose stimulation. (B) Histogram showing the number of fusion events at 60-s intervals after stimulation. The black columns show the fusion from residents (previously docked granules), and the gray columns show that from newcomers.

the requirement that the specimen be positioned between the prism and the microscope objective, making it difficult to perform manipulations, to inject media into the specimen space, and to carry out physiological measurements. Objective-type TIRF microscopy generates the evanescent field with the objective lens that is used for viewing the cell. The objective-type microscopes are commercially available from Olympus, Nikon, and Zeiss. This setup requires that the laser be introduced through the microscope and greatly benefits from an objective lens with a numerical aperture (NA) larger than 1.4. The specimen must be located on the top surface of the cover glass. The preparation, facing away from the objective, is accessible and permits the use of other instrumentation, such as micromanipulators.

3. We use a high aperture objective lens (Olympus APO $\times 100$ /NA 1.65 apochromatic objective lens). Living cells typically have a refractive index of about 1.37. To achieve TIRF, such a specimen must be illuminated with NA greater than 1.37. Recently, 1.4- to 1.45-NA objectives using normal cover glass and immersion oil have been available from Olympus, Nikon, and Zeiss.
4. Underlying all direct imaging of living cells is the desire to preserve the living subject for as long as possible through minimization of both phototoxic cell damage and photobleaching of the incorporated fluorophores. More sensitive CCD (electron multiplying CCD) is suitable for a TIRF microscopy system, which not only exhibits the sensitivity and speed to capture dynamic membrane events from within very thin ($<100\text{nm}$) small excitation volume but also enables the laser excitation power to be attenuated.
5. The penetration depth is dependent on the wavelength (λ). To analyze the colocalization of GFP and RFP/Cy3, we only use the 488-nm laser line for excitation. However, the fluorescence intensity of the red component by 488-nm excitation is relatively low compared to that by 543-nm excitation.
6. Before each experimental session, we took an alignment image that showed density by means of scattered 90-nm TetraSpeck fluorescent beads (Molecular Probes, Eugene, OR). They were visible in both the green and red channels and thus provided markers in the x - y plane. Beads in the two images were brought into superposition by shifting one image using Metamorph software.
7. To maintain the NA (1.65) and to achieve a high-quality image, a special immersion medium with a high refractive index (immersion liquid: $n_d = 1.78$, Cargille Laboratories) and special cover glass of high refractive index glass ($n_d = 1.788$, Olympus) must be used.

References

1. Axelrod, D. (2001) Total internal reflection fluorescent microscopy in cell biology. *Traffic* **2**, 764–774.
2. Schneckenburger, H. (2005) Total internal reflection fluorescence microscopy: technical innovations and novel applications. *Curr. Opin. Biotechnol.* **16**, 13–18.
3. Axelrod, D. (1981) Cell surface contacts illuminated by total internal reflection fluorescence. *J. Cell. Biol.* **89**, 141–145.

4. Truskey, G.A., Burmeister, J.S., Grapa, E., and Reichert, W.M. (1992) Total internal reflection fluorescence microscopy (TIRFM). II. Topographical mapping of relative cell/substratum separation distances. *J. Cell. Sci.* **103**, 491–499.
5. Vale, R.D., Funatsu, T., Pierce, D.W., Romberg, L., Harada, Y., and Yanagida, T. (1996) Direct observation of single kinesin molecules moving along microtubules. *Nature* **380**, 451–453.
6. Sund, S.E., and Axelrod, D. (2000) Actin dynamics at the living cell submembrane imaged by total internal reflection fluorescence photobleaching. *Biophys. J.* **79**, 1655–1669.
7. Dickson, R.M., Norris, D.J., Tzeng, Y.L., and Moerner, W.E. (1996) Three-dimensional imaging of single molecules solvated in pores of poly(acrylamide) gels. *Science* **274**, 966–969.
8. Oheim, M., Loerke, D., Stuhmer, W., and Chow, R.H. (1998) The last few milliseconds in the life of a secretory granule. Docking, dynamics and fusion visualized by total internal reflection fluorescence microscopy (TIRFM). *Eur. J. Biophys.* **27**, 83–98.
9. Sako, Y., Minoghchi, S., and Yanagida, T. (2000) Single-molecule imaging of EGFR signaling on the surface of living cells. *Nat. Cell. Biol.* **2**, 168–172.
10. Steyer, J.A., and Almers, W. (2001) A real-time view of life within 100nm of the plasma membrane. *Nat. Rev. Mol. Cell Biol.* **2**, 268–275.
11. Ohara-Imaizumi, M., Nishiwaki, C., Kikuta, T., Kumakura, K., Nakamichi, Y., and Nagamatsu, S. (2004) Site of docking and fusion of insulin secretory granules in live MIN6 beta cells analyzed by TAT-conjugated anti-syntaxin 1 antibody and total internal reflection fluorescence microscopy. *J. Biol. Chem.* **279**, 8403–8408.
12. Ohara-Imaizumi, M., Ohtsuka T., Matsushima, S., et al. (2005) ELKS, a protein structurally related to the active zone-associated protein CAST, is expressed in pancreatic β cells and functions in insulin exocytosis: Interaction of ELKS with exocytotic microscopy. *Mol. Biol. Cell.* **16**, 3289–3300.
13. Ohara-Imaizumi, M., Nakamichi, Y., Tanaka, T., Ishida, H., and Nagamatsu, S. (2002) Imaging exocytosis of single insulin secretory granules with evanescent wave microscopy: distinct behavior of granule motion in biphasic insulin release. *J. Biol. Chem.* **277**, 3805–3808.
14. Ohara-Imaizumi, M., Nishiwaki, C., Kikuta, T., Nagai, S., Nakamichi, Y., and Nagamatsu, S. (2004) TIRF imaging of docking and fusion of single insulin granule motion in primary rat pancreatic β -cells: different behavior of granule motion between normal and Goto-Kakizaki diabetic rat beta-cells. *Biochem. J.* **381**, 13–18.
15. Lacy, P.E., and Kostianovsky, M. (1967) Method for the isolation of intact islet of Langerhans from the rat pancreas. *Diabetes* **16**, 35–39.

21

Reconstitution of Depolarization and Ca²⁺-Evoked Secretion in *Xenopus* Oocytes Monitored by Membrane Capacitance

Roy Cohen, Bernhard M. Schmitt, and Daphne Atlas

1	Introduction.....	270
2	Materials.....	271
3	Methods.....	273
4	Notes.....	280
	References.....	281

Summary The identity of the proteins that constitute the “minimal molecular machinery” required for depolarization-evoked neurotransmitter release at synapses is still not fully disclosed. Using capacitance monitoring combined with heterologous protein expression in *Xenopus* oocytes, we were able to reconstitute a fast (<.5 s) secretion that was triggered directly by membrane depolarization. The functional assembly of voltage-gated Ca²⁺ channel (Cav1.2 or Cav2.2) coexpressed with syntaxin 1A, synaptosome-associated protein of 25kDa (SNAP-25), and synaptotagmin led to the reconstitution of depolarization-evoked secretion. Botulinum C1, botulinum A, and tetanus toxin were used to establish that this minimal set of proteins, named the excitosome complex, was necessary and sufficient for reconstituting depolarization-induced exocytosis. Similar to synaptic transmission, the capacitance changes were sensitive to neurotoxins, modulated by divalent cations (Ca²⁺, Ba²⁺, and Sr²⁺) or channels (Lc or N type; ionotropic glutamate GLUR3), and depended nonlinearly on extracellular divalent cation concentration. Expression of a recombinant intracellular domain of the calcium channel (Lc_{753–893}) abolished evoked release in the reconstituted assay. Also, mutations at the synaptotagmin C2A polylysine motif, a channel interaction site, abolished depolarization-evoked capacitance transients, consistent with release studies in PC12 cells. Because of its improved speed, native trigger, and great experimental versatility, this reconstitution assay provides a novel, promising tool to study synaptic and nonsynaptic exocytosis and examine the role of other proteins implicated in these processes.

Keywords: Ca²⁺ channels; capacitance; Cav1.2; evoked release; excitosome; exocytosis; reconstitution; synaptic transmission; synaptotagmin; syntaxin.

1 Introduction

Neuronal cells communicate by secreting neurotransmitters in a process triggered by the entry of Ca^{2+} ions voltage-gated Ca^{2+} channels (VGCCs) (1). Regulated exocytosis is the Ca^{2+} -dependent fusion of cytoplasmic vesicles with the plasma membrane. When coupled to membrane depolarization, this process can achieve extreme speed and efficiency (2) that is difficult to follow when using conventional reconstitution assays.

Understanding neuronal exocytosis requires both the identification of the presumably common “minimal machinery of membrane fusion” (3,4) and the specific molecular additions that knead generic membrane fusion into the rapid, voltage-operated process that eventually affords synaptic transmission (5). Although various reconstitution assays of regulated secretion have been reported, the exocytosis process lost the characteristic physiological traits of neuronal exocytosis, namely, the onset of the signal and its speed. Previously, all reconstituted assays of vesicle fusion occurred over minutes or hours instead of a few milliseconds, and the fusion was not triggered by membrane depolarization (6).

Thus, direct evidence from reconstituted systems regarding the molecular machinery of neuronal exocytosis is missing. The simple extrapolation from slow, Ca^{2+} -regulated membrane fusion is discredited by the known complexity and diversity of exocytotic mechanisms as well as by persisting conflicts regarding the interpretation of the available data (4, 7–12).

Several reports have shown reconstitution of regulated secretion using oocytes of the South African clawed frog *Xenopus laevis* in their attempts to reconstitute exocytosis. For instance, Ca^{2+} -dependent release of adenosine 5'-triphosphate (ATP) could be reconstituted in *Xenopus* oocytes by injection of total messenger ribonucleic acid (mRNA) isolated from rat cerebellum (13) or from the electric lobe of *Torpedo marmorata* (14) and by injection of chromaffin granules (15) or of membrane vesicles (16, 17). Although these experiments provide a proof that exocytosis can be reconstituted in *Xenopus* oocytes, these assays do not provide an experimental platform that would allow study of the molecular requirements of synaptic exocytosis.

The coexpression of various voltage-gated Ca^{2+} channels in *Xenopus* oocytes (Cav1.2, Cav2.1, Cav2.2, Cav2.3) along with synaptic proteins showed functional interaction between the channel and the exocytotic proteins (18–23). A functional heterocomplex composed of the Ca^{2+} channel, syntaxin 1A, synaptotagmin, and synaptosome-associated protein of 25kDa (SNAP-25) was kinetically defined and named the *excitosome* (20,21,24,25). This complex associates the vesicle with the Ca^{2+} channel via syntaxin 1A, SNAP-25, and synaptotagmin, postulated to act at the final stage of the release process.

Our new approach is to use the *Xenopus* oocytes expressing exocytotic proteins and voltage-gated calcium channels as a versatile assessment for the reconstitution and functional characterization of fast, depolarization-induced exocytosis. The technical

details for eliciting depolarization-evoked release, the molecular requirements of this reconstituted process, as well as the identification of the supporting proteins are described. We showed that the excitosome complex is responsible for triggering secretion during membrane depolarization (26).

Our findings constitute the first data on regulated exocytosis that were obtained in a reconstituted system in which exocytosis was directly triggered by depolarization in a rather short time resolution. The ease of operating the assay will facilitate further exploration and identification of various molecular entities that participate in the regulation of evoked neurotransmission.

2 Materials

2.1 Isolation of *Xenopus* Oocytes

1. Female frogs, *Xenopus laevis* (>1 yr old).
2. Collagenase I 154 U/mL; Worthington, Lakewood, NJ, USA.
3. ND96 solution for collagenase digestion (no CaCl_2): 96 mM NaCl, 2 mM KCl, 1 mM MgCl_2 , 5 mM HEPES, pH 7.4, 2 mg/mL collagenase.
4. Incubation buffer: ND96 solution supplemented with 1.8 M CaCl_2 , 2.5 M sodium pyruvate, 100 U/mL penicillin, and 100 $\mu\text{g/mL}$ streptomycin at 20°C for 12–20 h before complementary ribonucleic acid (cRNA) injection (19,20).

2.2 In Vitro Transcription and Complementary Deoxyribonucleic Acid Constructs

1. T7/T3 polymerase (Stratagene, La Jolla, CA, USA)
2. In vitro transcription (Fermentas, Glen Burnie, MD, USA) in the presence of the cap analog m7G(5')ppp(5') G cap analog (NEB, Ipswich, MA, USA).
3. Deoxyribonucleic acid (DNA) plasmids for the channel subunits α_1 1.2 (Lc type; rabbit; 5 ng/oocyte; L. Birenbaumer), α_2/δ (rabbit; A. Schwartz), β_2A (rat; 10 ng/oocyte; L. Birenbaumer). DNA plasmids for SNAP-25 (0.5 ng/oocyte), syntaxin 1A (0.5 ng/oocyte), and synaptotagmin I (1.0 ng/oocyte).
4. Drummond nanoinjector (Drummond Scientific, Broomall, PA, USA).

2.3 Capacitance Monitoring

1. Capacitance monitoring requires standard hardware for performing two-electrode voltage-clamp in *Xenopus* oocytes and software suitable for (a) repeated

application of fast stimuli and recording of the corresponding current response with a high sampling rate, (b) real-time computation of the average currents \hat{I}_m^{up} , \hat{I}_m^{down} and membrane capacitance C_m , and (3) real-time display and storage of C_m .

2. **Hardware:** Standard hardware for performing two-electrode voltage-clamp in *Xenopus* oocytes. The current electrode should have relatively low resistance (0.4–1.0 M Ω) to ensure good clamp performance. The intrinsic capacitance of the microelectrodes is lower than the oocyte's membrane capacitance by several orders of magnitude and thus negligible (no compensation necessary). Agar bridges may affect clamp speed, but this effect is usually small unless their resistance is exceptionally high. The particular type of amplifier may affect clamp fidelity: So-called proportional-integral (PI) controllers can offer advantages over proportional controllers when membrane currents are high or clamp gain cannot be maximized. Although most voltage-clamp amplifiers operate as proportional feedback controllers, a few support PI control (e.g., TEC amplifiers from NPI Electronic, Tamm, Germany). Even in the absence of oscillations, proportional feedback alone is associated with a clamp error of relative magnitude $1/(1 + A)$, where A is the clamp gain. The integral feedback component of PI controllers can achieve perfect voltage control even with relatively low proportional gain (e.g., when higher gains would cause oscillations).
3. **Software:** The combination of PULSE and X-CHART (both from HEKA Elektronik, Lambrecht, Germany) was used extensively and found to perform well (26–28). PULSE is used to apply the fast voltage ramp stimuli, to record the current response, and to compute \hat{I}_m^{up} and \hat{I}_m^{down} . X-CHART, which runs simultaneously, is used to acquire the \hat{I}_m^{up} and \hat{I}_m^{down} values from PULSE in real time, to compute C_m from these values, and to display and store the results. The final C_m values can be stored separately by X-CHART, making storage of the high-frequency current trace acquired by PULSE dispensable.
4. **Alternative software:** Recently, PULSE was succeeded by PATCHMASTER. This program incorporates some of the capabilities of X-CHART, albeit only partially and without the ability to exchange data with X-CHART. PATCHMASTER does allow capacitance monitoring according to the paired-ramps principle, including real-time analysis and display. However, PATCHMASTER computes the capacitance data from the original current responses. As a consequence, the high-frequency current traces need to be stored (claiming significant memory), and it takes considerable time to open stored capacitance recordings. Moreover, data display via the "online analysis" in PATCHMASTER is cumbersome and less flexible than with X-CHART. Finally, capacitance monitoring via paired ramps can be carried out by jointly using CLAMPEX and CLAMPFIT (from Axon Instruments, now Molecular Devices, Sunnyvale, CA). CLAMPEX allows for fast stimulation and acquisition of the current response, while CLAMPFIT is capable to compute, display, and store capacitance in real-time.

3 Methods

3.1 Isolation of *Xenopus* Oocytes

1. Stage V–VI oocytes were removed surgically from the ovaries of anesthetized animals and transferred into ND96 solution (nominally Ca^{2+} free) containing 2 mg/mL collagenase.
2. After 2 h shaking at 22 °C, the oocytes are washed extensively and placed into a ND96 solution containing 1.8 M CaCl_2 , 2.5 mM sodium pyruvate, 100 U/mL penicillin, and 100 $\mu\text{g}/\text{mL}$ streptomycin at 20 °C for 12–20 h before cRNA injection.
3. The incubation buffer is replaced every 12 h, and only healthy-looking oocytes are kept.

3.2 In Vitro Transcription and cRNA Injection

1. Plasmids were linearized and transcribed with T7/T3 polymerase and in vitro transcription in the presence of the cap analog G (5') ppp(5')G.
2. The in vitro-transcribed capped cRNAs were injected in a final volume of 40 nL.
3. Plasmid DNA for the channel subunits, α_1 1.2 (5 ng/oocyte), α_2/δ (5 ng/oocyte), and β_2A (10 ng/oocyte) were injected 12 h after oocyte isolation.
4. One day later, the oocytes were injected either with water (for controls) or with a mixture of cRNAs encoding SNAP-25 (0.5 ng/oocyte), syntaxin 1A (0.5 ng/oocyte), and synaptotagmin I (1.0 ng/oocyte).

3.3 Capacitance Monitoring in *Xenopus* Oocytes

1. At 5 to 6 d after cRNA injection, membrane capacitance C_m was monitored in the two-electrode voltage-clamp configuration.
2. Triggering exocytosis: Capacitance is monitored continuously together with membrane potential V_m and current I_m , then reconstituted “synaptic” exocytosis is triggered by membrane depolarization (its native stimulus), after which capacitance is monitored again immediately. Start from a holding potential of -80 mV, then clamp the oocyte to 0 mV twice for 500 ms, separated by 100 ms at -80 mV.
3. It is important to note that calibration of cRNA injection is required. In most experiments, this was achieved by a ratio of 1:1:2 in syntaxin/SNAP-25/syt I cRNA injected. Depolarization-induced capacitance changes can be studied 5 to 6 d after cRNA injection. A small background of depolarization-induced C_m

changes is observed even in the absence of synaptic proteins. Oocytes injected with the Ca^{2+} channel subunits only serve to measure the magnitude of this background (“basal secretion”). The nature of this background secretion is not clear but may be caused by Ca^{2+} accumulation or the participation of endogenous proteins. Expressing the complete set of synaptic proteins (“excitosome”) should result in depolarization-induced capacitance changes that are five- to eightfold higher than basal secretion (26).

4. The C_m obtained in the presence of the channel subunits serve as the basal secretion, which could result from Ca^{2+} accumulation or the involvement of endogenous synaptic proteins.
5. The contribution of basal C_m is five- to eightfold lower than observed by the excitosome (26).
6. Monitoring C_m changes: Capacitance monitoring employs up- and down-ramps ($\pm 20\text{mV}$ in 20ms each) to elicit membrane currents. These currents represent the sum of resistive and a capacitive current component. Because switching from up- to down-ramp reverses the sign of the capacitive component but not that of the resistive component (Fig. 1), subtraction of the down-ramp current integral from the up ramp current integral eliminates the resistive component. The resulting pure capacitive charge allows one to compute, together with the known amplitude of the voltage stimulus, membrane capacitance. Continuous monitoring is achieved by applying this stimulus repetitively at a high rate (up to $10/\text{s}$). A detailed description of the underlying principles as well as results of performance testing can be found in Ref. 27.
7. Voltage stimulus: For paired ramps, in a typical voltage stimulus, command voltage V_{com} increases by 40mV within 20ms , equivalent to a ramp slope of $2\text{V}/\text{s}$ (Fig. 1C). With this slope, capacitance is obtained from the difference ($\hat{I}_m^{\text{up}} - \hat{I}_m^{\text{down}}$) via simple division by 4:

$$C = \left(\hat{I}_m^{\text{up}} - \hat{I}_m^{\text{down}} \right) \times \left(\frac{\Delta t}{2\Delta V} \right) \Rightarrow C_m = \frac{\left(\hat{I}_m^{\text{up}} - \hat{I}_m^{\text{down}} \right)}{4} \quad (1)$$

Stage V–VI oocytes of *Xenopus laevis* typically have a membrane capacitance of $150\text{--}300\text{nF}$. This voltage stimulus thus elicits capacitive currents of $300\text{--}600\text{nA}$. The actual ramps may be preceded and followed by a short period of constant voltage. These constant segments help to ensure good clamp quality and to minimize the confounding effects of any putative time-dependent processes stemming from recording arrangement or oocyte. When PULSE is used to control the amplifier, the voltage stimulus is programmed as a “Sequence” in the “Pulse Generator” window (F9, or select from “Pulse” menu of the main menu in PULSE). Choose a high sampling frequency (e.g., 20kHz) to fully exploit the averaging principle inherent in the paired-ramps approach. Link the ramps stimulus to itself (“chain-linked sequence”) to repeat the stimulus infinitely. Define “relevant segments” for subsequent online computation of

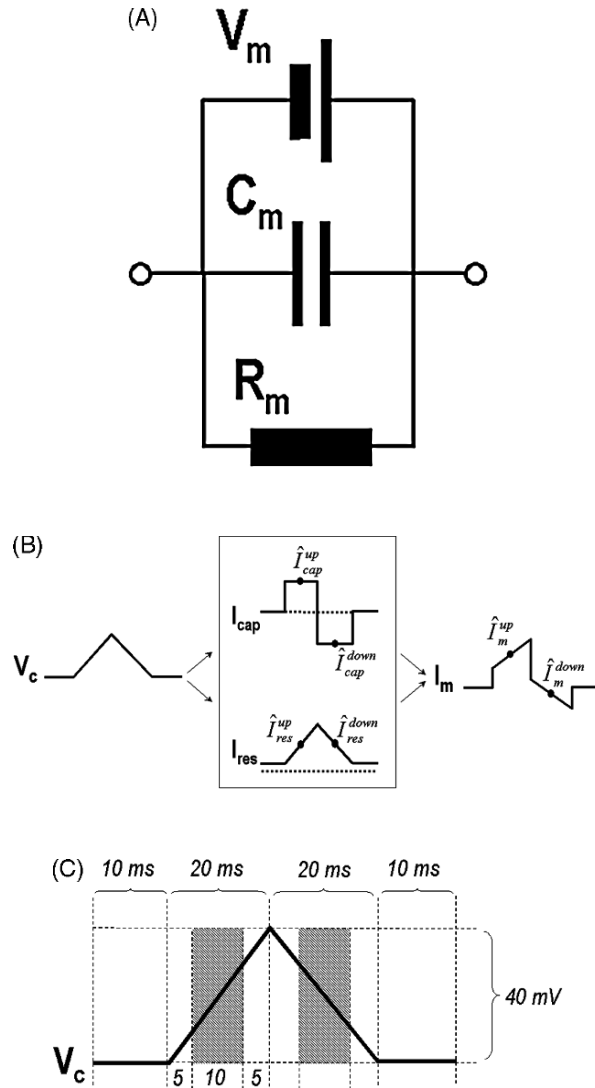


Fig. 1 (A) Equivalent circuit of a cell to which the paired-ramps approach can be applied successfully. The circuit consists of three elements with unknown parameters: a voltage source V_m , a capacitance C_m , and a resistance R_m . Capacitance monitoring via the paired-ramps approach allows for theoretically exact C_m measurements, provided all parameters are time invariant. (B) Principle of capacitance monitoring via paired ramps. The voltage stimulus (*left*) elicits both capacitive and resistive currents (*center*), which superimpose and constitute the total membrane current (*right*). With Paired ramps with slopes that are of identical magnitude but opposite sign, the resistive current component can be eliminated, and the remaining capacitive current can be used to calculate membrane capacitance (see text for detailed explanation). (C) Typical ramp stimulus. Shaded areas indicate the time windows from which membrane current is averaged (see text for detailed explanation).

- capacitance (e.g., segment 2, corresponding to the up-ramp. Use “relative stimuli” to allow random shifting of the entire stimulus together with the holding potential as set in the “amplifier” window of PULSE. The up- and down-ramps (± 20 mV in 20 ms each) elicit membrane currents that are the sum of resistive and a capacitive current component. Switching from up- to down-ramp reverses the sign of the capacitive component but not that of the resistive component (see above). Subtraction of the down-ramp current integral from the up-ramp current integral eliminates the resistive component; the resulting pure capacitive charge allows one to compute, together with the known amplitude of the voltage stimulus, membrane capacitance (see **Notes 1 and 2**).
8. Online computation of \hat{I}_{m}^{up} and \hat{I}_{m}^{down} in X-CHART: When one is using PULSE together with X-CHART, computation of C_m comprises determination of \hat{I}_{m}^{up} and \hat{I}_{m}^{down} in PULSE and subsequent computation of C_m in X-CHART from these two figures. Determination of \hat{I}_{m}^{up} and \hat{I}_{m}^{down} is programmed via the “online analysis” of PULSE (F7 or “online analysis” from the “Pulse” menu from the main menu). For “Range 1” and “Range 2”, select “time” and “mean,” respectively. Next, define the time windows over which current is averaged (Fig. 1C). It is not necessary to work with the mean current determined from the entire up- and down-ramps, respectively, as long as the two time windows are symmetrically placed around the “tip” of the angle formed by the two ramps. The advantage of this approach is increased robustness: The initial portions of the current trace are particularly susceptible to distortion by slow clamp or oscillations, and limiting the analysis to the center portions simply avoids these potential problem zones. A good starting point is to use a time window comprising the center half of the ramp by setting the boundaries of “Range 1” to 25% and 75% and the boundaries of “Range 2” to 125% and 175% (percentages defined with respect to the “relevant segment” as defined in the “Pulse Generator”; here, the up-ramp or segment 2). The parameters of this online analysis should be stored as a “macro” (consult PULSE manual for details).
 9. Computation of C_m from \hat{I}_{m}^{up} and \hat{I}_{m}^{down} in X-CHART: This is programmed within the “Edit traces and parameters” window of X-CHART. Under category “type,” select the two results of the online analysis in PULSE (\hat{I}_{m}^{up} and \hat{I}_{m}^{down}) to load them into X-CHART. Set trace 3 to “difference” with arguments 1 and 2 to obtain the difference $\hat{I}_{m}^{up} - \hat{I}_{m}^{down}$. Finally, set trace 4 to “trace*[P7]” to multiply this difference by the appropriate proportionality factor to yield capacitance (in nF). With a ramp of 2 V/s, this factor is 0.25; enter this figure in the field “P7.”
 10. Real-time display in X-CHART: It is convenient to display voltage, current, and capacitance simultaneously in the “Graph” window of X-CHART. This is achieved by using two additional traces in the “Edit traces and parameters” window to load “V-mon” and “I-mon” from PULSE into X-CHART.
 11. Averaging of multiple current responses: When high precision is more important to the experimenter than maximal time resolution, several current

responses can be averaged before computing capacitance from them. The number of traces to be averaged is set in the “oscilloscope” window of PULSE (see [Note 3](#)).

3.4 Implementation

In a typical experiment, an oocyte is placed in the chamber; the electrodes are positioned for impalement and zeroed. Then, a new PULSE file is opened, the appropriate online analysis is selected, the timer in the “oscilloscope” window is reset to zero, and the continuous paired-ramps stimulus is started. Then, the oocyte can be impaled, superfused, and clamped. Capacitance recording can be interrupted and restarted (e.g., to record current–voltage curves). At the end of the experiment, the clamp is switched off, and the microelectrodes are removed, with the tips remaining in the bath. The resulting X-CHART recording will thus document the spontaneous membrane potential, the C_m time course, and potential electrode drift. Diameter and membrane capacitance of oocyte cell and granule membranes are shown in [Fig. 2A](#). Schematic presentation of the proteins involved in the configuration of the excito-some complex is shown in [Fig. 2B](#). Continuous monitoring of membrane capacitance demonstrated by representative original traces of voltage, current, and capacitance is indicated in [Fig. 2C](#).

3.5 Advantages of the Novel Method over Other Reconstituted Assays of Exocytosis

1. Reconstitution of depolarization-induced exocytosis in *Xenopus* oocytes offers significant advantages over other forms of reconstituted exocytosis. First, it provides a more realistic reconstitution assay of synaptic exocytosis. Our reconstitution assay uses the native trigger of synaptic exocytosis (membrane depolarization) under voltage-clamped conditions (as opposed to elevation of Ca^{2+} concentration, probably an event downstream of depolarization (29)). The speed of the reconstituted form of exocytosis is also closer to the original synaptic process and occurs within milliseconds (as opposed to minutes or hours in other reconstitution assays). Proteins expressed in *Xenopus* oocytes are full-length proteins and properly processed, targeted, and anchored (as opposed to reconstitution assays, which employ truncated recombinant proteins and artificial membranes). Second, reconstitution in *Xenopus* oocytes offers unprecedented control over expression and expression levels of putative synaptic proteins. This experimental flexibility is instrumental in testing rigorously the role of individual proteins in synaptic exocytosis. Moreover, capacitance as a measure of exocytosis is simple, robust, accurate ($\pm 1\%$), precise ($\pm 0.05\%$), and time resolved (16 Hz) (see *Ref.*

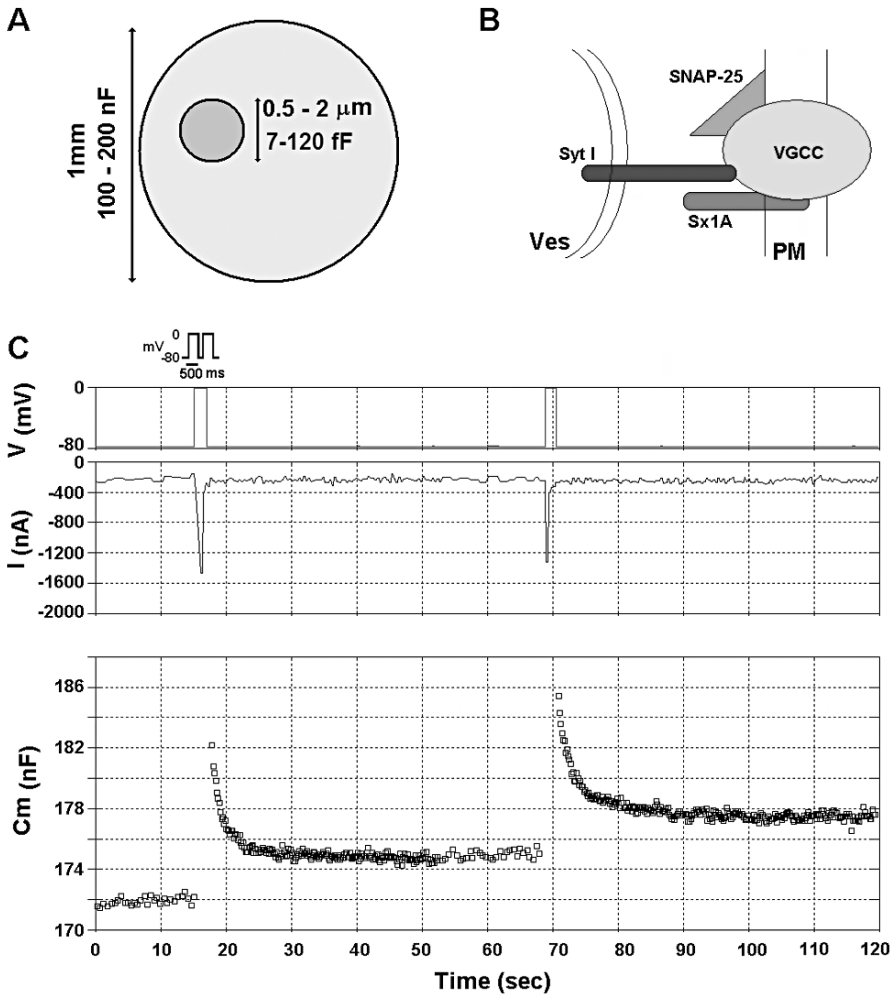


Fig. 2 Reconstitution of depolarization evoked secretion in *Xenopus* oocytes. **(A)** Diameter and capacitance of *Xenopus laevis* oocyte cell membrane and granules. Granule capacitance, 7–120 fF. **(B)** Schematic presentation of the minimal set of proteins generating the excitosome complex: VGCC, the Lc-type channel (Ca_v 1.2) subunits (α_1 1.2, $\beta_2\text{A}$ $\alpha_2\delta$) at the plasma membrane (PM); synaptotagmin (Syt 1) at the vesicle membrane (ves); syntaxin 1A (Sx), and SNAP 25. **(C)** Continuous monitoring of membrane capacitance showing the effect of depolarization on membrane capacitance C_m in the oocytes expressing the excitosome proteins Cav1.2, syntaxin 1A, synaptotagmin, and SNAP-25. Representative original traces of voltage (*upper*), current (*middle*), and C_m (*lower*) detected during oocyte stimulation by a double pulse of 500 ms given 100 ms apart (as indicated in small inset) applied to oocytes injected with the cRNA encoding the excitosome proteins. ΔC_m was calculated as the difference between the basal C_m and the C_m at the end of the depolarizing pulse just after membrane current I_m returned to its level before the voltage pulse. The fast-decaying transient at the beginning of the trace was not taken into the calculated ΔC_m .

27 for detailed performance testing). The effect of synaptotagmin mutated at a selective polylysine motif (30) and the effect of a recombinant cytosolic domain of the Cav1.2 (20) on secretion were determined as shown in Fig. 3A, B and Fig. 3C, D, respectively.

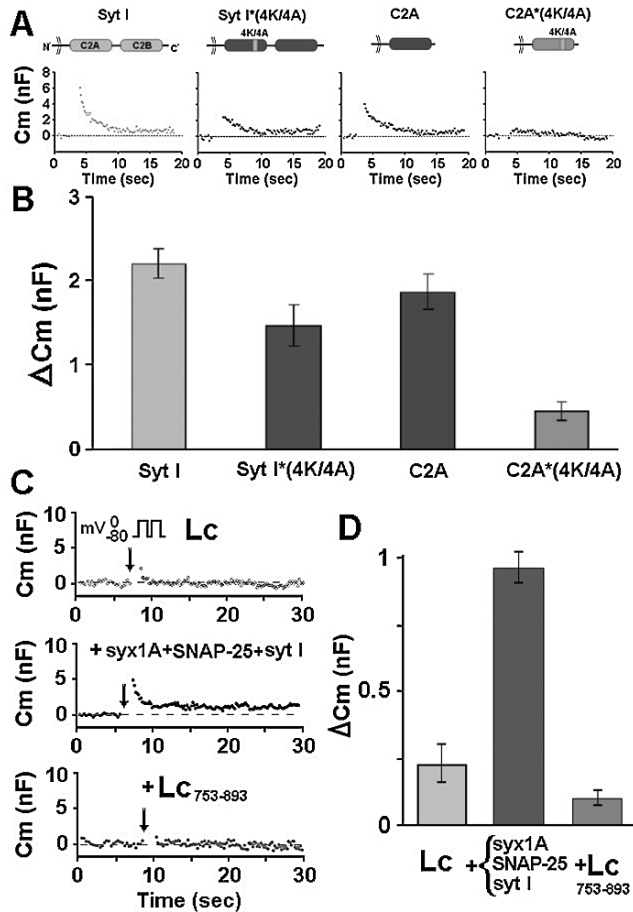


Fig. 3 Employing the reconstituted assay to study modulation of depolarization-evoked secretion. **(A)** and **(B)** The effects of synaptotagmin mutated at the polylysine motif of the C2A domain. **(A)** Monitoring C_m in *Xenopus* oocytes expressing the excitosome complex (Cav1.2, α_1 1.2, β 2A, α 2 δ) with syntaxin 1A, SNAP-25 and wild-type synaptotagmin 1 or with the Syt 1 mutants Syt 1*(4K/4A), truncated Syt 1 (C2A), or truncated mutant C2A*(4K/4A) (29) triggered by a double 500-ms voltage step from the holding potential (-80 mV) to 0-mV pulse separated by a 100-ms hyperpolarization. **(B)** Summary of the effect of depolarization on membrane C_m in groups of oocytes as in **(A)** ($n = 12-15$). **(C)** and **(D)** The effect of intracellular L-channel II-III linker on secretion. **(C)** Monitoring C_m in *Xenopus* oocytes coexpressing the channel (Ca_v 1.2, α_1 1.2, β 2A, α 2 δ) with the intracellular recombinant Cav1.2 loop (Lc₇₅₃₋₈₉₃) (Upper); the excitosome complex (middle) and the excitosome complex co-expressed with the Lc₇₅₃₋₈₉₃ (lower). **(D)** Summary effect of depolarization as in **(A)** on membrane C_m groups as in **(C)** ($n = 12-15$).

2. The *Xenopus* oocyte is not an excitable cell: Native oocytes do not respond to membrane depolarization, but as any other type of cell, they do respond to calcium elevations. Our new assay takes advantage of the fact that although the oocyte has practically no voltage-gated calcium channels, it contains vesicles/cortical granules that, on maturation when the oocyte becomes an egg, are exocytosed in response to the fertilization potential to secrete lectin (31,32), previously determined by capacitance changes (33,34).

4 Notes

1. Limited clamp speed and fidelity are problems in any two-electrode voltage-clamp experiment, including capacitance monitoring. Steady-state clamp errors and slow clamp typically result from insufficient proportional gain in the feedback loop of the voltage-clamp amplifier. On the other hand, proportional gain that is too high causes oscillations. To detect nonideal voltage-clamp regularly verify good clamp quality by inspecting the paired-ramps pulses or square-wave test pulses during an experiment (e.g., in the “oscilloscope” window of PULSE) in addition to the “slow” capacitance trace in X-CHART. The fast traces reveal discrepancies between command potential and measured membrane potential (make sure to display both; with some amplifiers, e.g., from Dagan, this may require specific electrode arrangements). To prevent nonideal voltage-clamp, tune the amplifier carefully to optimize clamp gain before starting capacitance monitoring. Check microelectrode resistance: High resistance of the current electrode may result in slow clamp; high resistance of the voltage electrode may cause excessive noise or oscillations. Clamp performance can be achieved for a wider range of recording conditions with a PI controller-type feedback amplifier.
2. Series resistance R_s acts as a voltage divider and thus decreases the actual voltage drop across the plasma membrane. The relative error is $R_s/(R_s + R_m)$; this means that this error is particularly big when membrane resistance is low (or membrane current is high). Series resistance errors are hard to detect with the standard recording arrangement. Continuous detection of R_s in two-electrode voltage-clamp experiments is possible using a novel hardware device (Rs box, NPI Electronic, Tamm, Germany). Because relatively simple laws govern the effect of series resistance on the capacitance measurements via paired ramps, direct determination of R_s computation of the true capacitance from the apparent capacitance. If desired, this correction can be automated and carried out in real time during experimentation (this requires PULSE, X-CHART, and a telegraphing amplifier capable of computer-controlled switching between voltage clamp and current clamp mode; contact us for details).
3. The paired-ramps stimulus sweeps across a considerable voltage range and may thus induce voltage-dependent gating of ion channels. For instance, reconstitution of depolarization-induced exocytosis usually involves overexpression of voltage-gated calcium channels, and even untreated oocytes of *Xenopus laevis*

may express voltage-dependent conductances (6). Two problems arise: First, the time dependence of channel gating (frequently with different time constants for opening and closing), the nonlinear leak currents during up- and down-ramp are not symmetrical any longer (*hysteresis*), which invalidates the calculation of membrane capacitance. Secondly, voltage gating is associated with intramembrane charge movements that contribute to overall membrane capacitance in a nonlinear voltage-dependent way (*nonlinear capacitance*). Effects on voltage gating may be misinterpreted as changes of membrane surface area. Voltage gating becomes apparent (a) from the current–voltage (I–V) relationship; (b) from a nonlinear capacitance–voltage (C–V) relationship (a C–V curve can be determined by monitoring capacitance and then stepping the holding potential to various values); and (c) as a distortion of the current response to the paired ramps voltage stimulus. Avoid very negative membrane potentials (e.g., more negative than –100 millivolts). To avoid distortion by voltage gating, choose holding potential and magnitude or direction of the ramp stimulus in a way that avoids the voltage range at which the particular ion channel is activated or inactivated. Voltage-gated calcium channels typically activate at positive membrane potential and do not pose particular problems at the usual holding potentials (e.g., –60).

References

1. Katz, B., and Miledi, R. (1969) Spontaneous and evoked activity of motor nerve endings in calcium Ringer. *J. Physiol.* **203**, 689–706.
2. Augustine, G.J., and Kasai, H. (2007) Bernard Katz, quantal transmitter release, and the foundations of presynaptic physiology. *J. Physiol* **578**, 623–625.
3. Mayer, A. (2002) Membrane fusion in eukaryotic cells. *Annu. Rev. Cell. Dev. Biol.* **18**, 289–314.
4. Jahn, R., Lang, T., and Sudhof, T.C. (2003) Membrane fusion. *Cell* **112**, 519–533.
5. Martin, T.F. (2003) Tuning exocytosis for speed: fast and slow modes. *Biochim. Biophys. Acta* **1641**, 157–165.
6. Weber, T., Zemelman, B.V., McNew, J.A., et al. (1998) SNAREpins: minimal machinery for membrane fusion. *Cell* **92**, 759–772.
7. Avery, J., Jahn, R., and Edwardson, J.M. (1999) Reconstitution of regulated exocytosis in cell-free systems: a critical appraisal. *Annu. Rev. Physiol.* **61**, 777–807.
8. Cook, N.R., and Davidson, H.W. (2001) In vitro assays of vesicular transport. *Traffic* **2**, 19–25.
9. Weimer, R.M., and Jorgensen, E.M. (2003) Controversies in synaptic vesicle exocytosis. *J. Cell Sci.* **116**, 3661–3666.
10. Duman, J.G., and Forte, J.G. (2003) What is the role of SNARE proteins in membrane fusion? *Am. J. Physiol. Cell Physiol.* **285**, C237–C249.
11. Szule, J.A., and Coorsen, J.R. (2003) Revisiting the role of SNAREs in exocytosis and membrane fusion. *Biochim. Biophys. Acta* **1641**, 121–135.
12. Edwardson, J.M. (1998) A cell-free system for Ca²⁺-regulated exocytosis. *Methods* **16**, 209–214.
13. Alder, J., Lu, B., Valtorta, F., Greengard, P., and Poo, M.M. (1992) Calcium-dependent transmitter secretion reconstituted in *Xenopus* oocytes: requirement for synaptophysin. *Science* **257**, 657–661.

14. Cavalli, A., Eder-Colli, L., Dunant, Y., Loctin, F., and Morel, N. (1991) Release of acetylcholine by *Xenopus* oocytes injected with mRNAs from cholinergic neurons. *EMBO J.* **10**, 1671–1675.
15. Scheuner, D., Logsdon, C.D., and Holz, R.W. (1992) Bovine chromaffin granule membranes undergo Ca(2+)-regulated exocytosis in frog oocytes. *J. Cell Biol.* **116**, 359–365.
16. Marsal, J., Tigyi, G., and Miledi, R. (1995) Incorporation of acetylcholine receptors and Cl⁻ channels in *Xenopus* oocytes injected with *Torpedo* electroplaque membranes. *Proc. Natl. Acad. Sci. U. S. A.* **92**, 5224–5228.
17. Aleu, J., Martin-Satue, M., Navarro, P., et al. (2003) Release of ATP induced by hypertonic solutions in *Xenopus* oocytes. *J. Physiol.* **547**, 209–219.
18. Trus, M., Wisner, O., Goodnough, M.C., and Atlas, D. (2001) The transmembrane domain of syntaxin 1A negatively regulates voltage-sensitive Ca(2+) channels. *Neuroscience* **104**, 599–607.
19. Wisner, O., Bennett, M.K., and Atlas, D. (1996) Functional interaction of syntaxin and SNAP-25 with voltage-sensitive L- and N-type Ca²⁺ channels. *EMBO J.* **15**, 4100–4110.
20. Wisner, O., Trus, M., Hernandez, A., et al. (1999) The voltage sensitive Lc-type Ca²⁺ channel is functionally coupled to the exocytotic machinery. *Proc. Natl. Acad. Sci. U. S. A.* **96**, 248–253.
21. Tobi, D., Wisner, O., Trus, M., and Atlas, D. (1998) N-type voltage-sensitive calcium channel interacts with syntaxin, synaptotagmin and SNAP-25 in a multiprotein complex. *Recept. Channels* **6**, 89–98.
22. Cohen, R., and Atlas, D. (2004) R-type voltage-gated Ca(2+) channel interacts with synaptic proteins and recruits synaptotagmin to the plasma membrane of *Xenopus* oocytes. *Neuroscience* **128**, 831–841.
23. Bezprozvanny, I., Zhong, P., Scheller, R.H., and Tsien, R.W. (2000) Molecular determinants of the functional interaction between syntaxin and N-type Ca²⁺ channel gating. *Proc. Natl. Acad. Sci. U. S. A.* **97**, 13943–13948.
24. Atlas, D. (2001) Functional and physical coupling of voltage-sensitive calcium channels with exocytotic proteins: ramifications for the secretion mechanism. *J. Neurochem.* **77**, 972–985.
25. Atlas, D., Wisner, O., and Trus, M. (2001) The voltage-gated Ca²⁺ channel is the Ca²⁺ sensor of fast neurotransmitter release. *Cell Mol. Neurobiol.* **21**, 717–731.
26. Cohen, R., Schmitt, B. M., and Atlas, D. (2005) Molecular identification and reconstitution of depolarization-induced exocytosis monitored by membrane capacitance. *Biophys. J.* **89**, 4364–4373.
27. Schmitt, B.M., and Koepsell, H. (2002) An improved method for real-time monitoring of membrane capacitance in *Xenopus laevis* oocytes. *Biophys. J.* **82**, 1345–1357.
28. Schmitt, B.M., and Koepsell, H. (2005) Alkali cation binding and permeation in the rat organic cation transporter rOCT2. *J. Biol. Chem.* **280**, 24481–24490.
29. Lerner, I., Trus, M., Cohen, R., Yizhar, O., Nussinovitch, I. and Atlas, D. (2006) Ion interaction at the pore of Lc-type Ca²⁺ channel is sufficient to mediate depolarization-induced exocytosis. *J. Neurochem* **97**, 116–127.
30. Cohen, R., Elferink, L.A., and Atlas, D. (2003) The C2A domain of synaptotagmin alters the kinetics of voltage-gated Ca²⁺ channels Ca(v)1.2 (Lc-type) and Ca(v)2.3 (R-type). *J. Biol. Chem.* **278**, 9258–9266.
31. Scheuner, D., and Holz, R.W. (1994) Evidence that the ability to respond to a calcium stimulus in exocytosis is determined by the secretory granule membrane: comparison of exocytosis of injected bovine chromaffin granule membranes and endogenous cortical granules in *Xenopus laevis* oocytes. *Cell Mol. Neurobiol.* **14**, 245–257.
32. Kohan, S.A., and Gundersen, C.B. (2003) Protein synthesis is required for the transition to Ca(2+)-dependent regulated secretion in progesterone-matured *Xenopus* oocytes. *J. Exp. Zool. A Comp. Exp. Biol.* **300**, 113–125.
33. Jaffe, L.A., and Schlichter, L.C. (1985) Fertilization-induced ionic conductances in eggs of the frog, *Rana pipiens*. *J. Physiol.* **358**, 299–319.
34. Jaffe, L.A., Hagiwara, S., and Kado, R.T. (1978) The time course of cortical vesicle fusion in sea urchin eggs observed as membrane capacitance changes. *Dev. Biol.* **67**, 243–248.

22

Low-Noise Recording of Single-Vesicle Capacitance Steps in Cell-Attached Patches

Vitaly Klyachko, Zhenjie Zhang, and Meyer Jackson

1 Introduction.....	283
2 Materials	285
3 Methods.....	287
4 Notes	292
References.....	294

Summary Capacitance recording provides a readout of membrane area that can be used to monitor exo- and endocytosis in neurons and secretory cells in real time. By interfacing a lock-in amplifier to a patch-clamp amplifier, the capacitance of cell-attached membrane patches can be measured with sufficient sensitivity to reveal the fusion and retrieval of single vesicles as unitary stepwise changes in capacitance. The small size of many secretory vesicles, especially of synaptic vesicles, places a premium on the reduction of noise in a capacitance recording. With care, the capacitance noise in cell-attached patches can be reduced to below 10 aF root-mean-square (rms), thus bringing into view steps resulting from the fusion of vesicles as small as about 18 nm in diameter. Thus, the lowest achievable noise level enables the resolution of changes in capacitance associated with the smallest secretory vesicles. This chapter presents the method of capacitance recording from cell-attached patches with an emphasis on noise reduction. It also addresses the closely related issue of extracting fusion pore properties from these recordings.

Keywords Neuropeptides; patch clamp; quantal release; secretion.

1 Introduction

Fusion and retrieval of secretory vesicles can be monitored as changes in membrane capacitance by virtue of the linear relationship between capacitance and membrane surface area (1–3). Individual exo- and endocytotic events produce stepwise or quantal increases and decreases, respectively, in membrane capacitance (1,4,5). In the whole-cell configuration, the resolution of capacitance measure-

ments is limited by intrinsic thermal noise arising from the entire plasma membrane. Thus, only very large granules with diameters close to approx $1\ \mu\text{m}$ produce unitary signals that can be clearly detected. This limitation can be overcome by measuring from cell-attached patches, and in this configuration the noise can be reduced to approx $10\ \text{aF}$ ($1\ \text{aF} = 10^{-18}\text{F}$), so that capacitance steps associated with the smallest known vesicles can be seen. The cell-attached patch configuration was first used to record single-vesicle capacitance steps by Neher and Marty (*1*), and subsequent improvements in noise level have permitted the resolution of smaller and smaller unitary events (*5–14*). Applications of these improved methods to a variety of experimental preparations have led to important advances in our understanding of the mechanisms of exocytosis.

In addition to detecting single-vesicle fusion events, capacitance measurements provide a tool for the study of fusion pores that form during the initial contact of a vesicle with the plasma membrane (*15,16*). Again, the noise in a recording is critical, and without special measures to reduce noise, fusion pores can only be characterized for large dense-core vesicles (LDCVs) (*5,7,9,13,17*). The low-noise single-vesicle capacitance recording technique presented here is sufficiently sensitive to study fusion pores in both small synaptic vesicle (SSV) fusion and LDCV fusion (*11*). Low-noise capacitance measurements in synaptic preparations such as the calyx of Held (*14*) and hippocampal mossy fibers could thus provide a wealth of information on the basic mechanisms of neurotransmitter release in synapses.

Membrane capacitance is measured in the frequency domain, in which a sinusoidal voltage command charges and discharges the membrane capacitance. This method has been described in great detail (*2,18*). The present discussion addresses aspects specific for noise reduction to record single-vesicle steps in the cell-attached patch mode (*10,11*). The amplitude of the resulting sinusoidal current and its phase shift relative to the sinusoidal voltage input are then determined with a phase-sensitive detector (PSD) to yield changes in membrane capacitance. Although a computer can perform the PSD operations, in high-resolution measurements the PSD is implemented in hardware with a lock-in amplifier (*1,2*). The lock-in amplifier generates the sinusoidal voltage used to stimulate the membrane and detects the response at the same reference frequency. The lock-in amplifier then resolves this response into two components based on a phase relationship with the stimulus voltage. An analysis of the equivalent circuit of a cell-attached membrane patch has shown that when the patch-clamp amplifier compensation circuitry cancels the capacitance of the membrane, the phase of the PSD can be adjusted so that the two outputs reflect the membrane conductance and capacitance (*1,3*). Convention dictates that the conductance is taken as the real (Re) component, corresponding to a 0° phase shift, and the capacitance is taken as the imaginary (Im) component, corresponding to a 90° phase shift.

The method described here is a variation of the patch-clamp technique, about which much has been written (*19–21*). This well-established technology is revisited here, but more thorough discussions can be consulted. The method of single-vesicle capacitance recording follows our own work in pituitary nerve terminals (*11*), and

a brief protocol for posterior pituitary slices is included. But, the method is general and can be applied to any cell type for the study of membrane trafficking at the plasma membrane.

2 Materials

2.1 Posterior Pituitary Slices

1. Recording/dissecting solution (referred to as artificial cerebrospinal fluid, aCSF): 125 mM NaCl, 4 mM KCl, 26 mM NaHCO₃, 1.25 mM NaH₂PO₄, 2 mM CaCl₂, 1 mM MgCl₂, and 10 mM glucose. The pH is 7.3 when bubbled with 95% O₂/5% CO₂.
2. A set of dissecting tools.
3. Slice storage vials connected to a 95% O₂/5% CO₂ tank.

2.2 Pipet Preparation and Coating

1. Thick-wall (0.85-mm id, 1.5-mm od) borosilicate glass capillaries (Garner Glass, Claremont, CA) for patch pipet fabrication (*see Note 1*).
2. A patch pipet puller.
3. Sylgard 184 kit (Dow Corning, Midland, MI) (*see Note 2*). Sylgard coating is prepared by mixing the silicone elastomer base with the curing agent in a 7:1 ratio (*see Note 3*). Premixed Sylgard can be stored at -20°C in small (~1-mL) aliquots for several months. Depending on the desired number of pipets to be coated (10–15 pipets/aliquot), two or three aliquots are placed at room temperature 30 min before coating.
4. Adjustable heat gun to cure the Sylgard.
5. Glass heat polishing device with ×400 magnification (*see Note 4*).

2.3 Electrophysiological Recordings

1. Patch-clamp amplifier (Instrutech, ALA, HEKA, Molecular Devices). Amplifiers with lower noise perform better. The amplifier is modified by the installation of 100-Ω resistor in series with the capacitance compensation potentiometer of the amplifier. This resistance may vary depending on the resistance of the potentiometer in the patch clamp and the range of the capacitance compensation circuitry. In the EPC-7 (Instrutech, ALA, HEKA), the potentiometer is 10 kΩ and the range of the circuit is 10 pF, so dithering a 100-Ω resistor in and out of a position in series with the potentiometer gives a

100-fF change in recorded capacitance. This resistor is installed with both a manual switch that can be toggled to generate a capacitance step and a transistor-transistor logic (TTL)-gated reed switch that can be driven by the computer interface. This switch is used for both phase adjustment and calibration. Figure 1 presents a diagram to show how the electrical instruments are connected.

2. A two-phase lock-in amplifier (SR830, Stanford Research Systems, Sunnyvale, CA).
3. A switchable electronic summation circuit for adding two analog signals. This can be built with an operational amplifier. Some electronic instruments can be used for this function, such as the model 902 low-pass filter from Frequency Devices (Haverhill, MA).
4. Other standard components of a patch-clamp recording setup, including vibration isolation table, microscope, micromanipulator, computer, and interface (19–21).
5. Two dual-channel oscilloscopes.
6. A TTL-gated device for pressure application of solutions through a micropipet (Picospritzer, General Valve Corporation, Fairfield, NJ).
7. aCSF (Subheading 2.1., item 1) is prepared from stock solutions the day of an experiment.

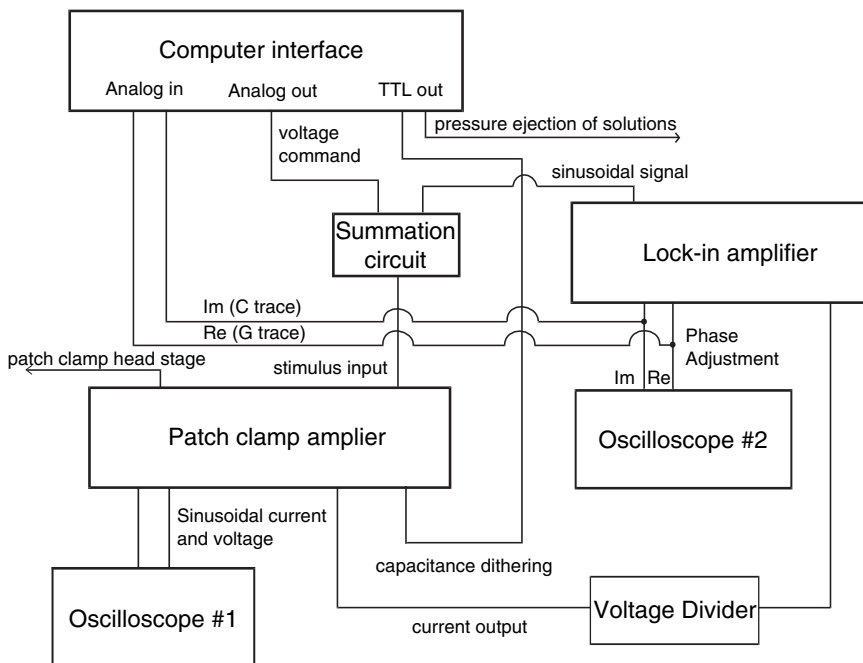


Fig. 1 A diagram illustrates the various instruments used in low-noise capacitance recording and how they are interconnected.

8. Pipet solution: 125 mM NaCl, 4 mM KCl, 10 mM CaCl₂, 1 mM MgCl₂, 13 mM TEA, and 10 mM HEPES, pH 7.2 (*see Note 5*).
9. Dimethylpolysiloxane silicone oil, viscosity 100–200 cSt (Sigma, St. Louis, MO) (22). Store at room temperature.
10. Depolarizing solution: 115 or 130 mM KCl, 10 mM NaCl, 2 mM CaCl₂, 1 mM MgCl₂, 10 mM HEPES, pH 7.2; store at 4 °C.
11. Ionomycin (EMD, San Diego, CA) is prepared as a 50 mM stock solution in dimethyl sulfoxide (DMSO) and stored at –20 °C in small aliquots.
12. Polyethylene transfer pipets or Pasteur pipets.
13. 5:1 voltage divider (easily made in-house; also commercially available from many electronics suppliers).
14. Fine-mesh slice-retaining grid or “harp” (23) to hold slices down in a recording chamber (fabricated in-house; commercially available from Warner Instruments, Hamden, CT).

3 Methods

3.1 Technique Overview

High-resolution single-vesicle capacitance measurements are performed with a patch-clamp amplifier in the cell-attached patch-clamp configuration. The patch clamp is interfaced to a lock-in amplifier, as well as a computer interface, according to the diagram in Fig. 1. In the typical patch-clamp experiment, the current output of the patch clamp amplifier is read into an analog input of the computer interface. In capacitance recording, this sinusoidal current has little value as a raw signal and need not be read into the computer. Instead, the current output of the patch clamp is read into the lock-in amplifier, and the outputs of the lock-in amplifier are read into the computer.

An approximate mathematical treatment of the relevant equivalent circuit shows that the Re and Im outputs from the lock-in amplifier are proportional to membrane conductance and capacitance, respectively (1,3). Because of the requirements for small changes in circuit parameters and other approximations used in the equivalent circuit analysis, a special technique is required to determine the phase setting for the correct separation of capacitance and conductance changes.

Several phase-adjustment methods have been developed for whole-cell capacitance measurements (1,2,18,24,25); in cell-attached recordings, only the method originally developed by Neher and Marty, also known as the piecewise linear technique, is commonly used (1). In this technique, the capacitance compensation of the patch-clamp amplifier is adjusted in the beginning of each recording to completely cancel the patch capacitance currents. Then, the correct phase setting is determined with “capacitance dithering”: the value of the slow capacitance compensation element of the amplifier is changed by a small fixed value (*see* Subheading 2.3., item 1), and the phase of the

sinusoidal voltage stimulus is adjusted until dithering produces no deflection in the conductance trace. This dithering also provides a defined capacitance value for calibration. With the correct phase setting, capacitance and conductance changes are independent (orthogonal).

3.2 *Experimental Setup*

The instrumentation is illustrated in Fig. 1. This diagram shows each of the electrical components outlined here and how they are connected.

1. The sinusoidal output of the lock-in amplifier is connected to the switchable electronic summation input.
2. The output of the computer interface is connected to the second switchable summation input for summation with the lock-in signal. This signal provides the membrane command potential and is typically set in the computer software. The data switch is used to select or combine the sine wave signal from the lock-in amplifier and the command potential from the computer.
3. The output of the summation circuit is connected to the stimulus input of a patch-clamp amplifier.
4. The current output and command voltage monitor signal from the patch-clamp amplifier are connected to the two channels of the oscilloscope (oscilloscope 1).
5. An unfiltered current output signal from the patch-clamp amplifier is connected to the 5:1 voltage divider, and the output of the voltage divider is connected to the input of the lock-in amplifier.
6. X and Y output channels of the lock-in amplifier (accessible from the front or back panels of the SR830) are connected to the second oscilloscope (oscilloscope 2) and to the analog inputs of the computer interface.
7. A TTL output from the computer interface is connected to the TTL-gated switch for the dithering resistor installed in the patch-clamp amplifier. A separate TTL output of the computer interface is used to drive the pressure application of solutions for evoking secretion.

3.3 *Slice Preparation*

1. Prepare slices from the posterior pituitary gland of a Sprague–Dawley rat (11,26). Decapitate rat after CO₂-induced narcosis. Remove the pituitary rapidly and place in ice-cold 95% O₂/5% CO₂-saturated aCSF.
2. After approx 5 minutes, mount the whole pituitary in a slicing chamber and slice using a vibratome (HR2 Slicer; Sigmann Elektronik, Germany) at a thickness setting of approx 75 μm.

3. Transfer slices to individual storage vials and maintain for up to 4h in 95% O₂/5% CO₂-bubbled aCSF until recording.

3.4 Patch Pipet Fabrication

1. Pull 3- to 5-M Ω patch electrodes with a pipet puller.
2. Under the dissecting scope, coat pipets with Sylgard. Apply the coating as close to the tip as possible (*see Note 6*). Apply multiple coating/drying cycles to each pipet (typically three) until a thick, approx 1-mm coating has been applied nearly all the way to the tip.
3. Just before recording, heat polish the pipet tip to remove excess Sylgard coating and to smooth the rough glass edges (*see Note 7*).

3.5 Cell-Attached Capacitance Measurements

1. Place a slice under the harp in a recording chamber on the microscope stage with continuous perfusion of bubbled aCSF.
2. View individual nerve terminals in an upright DIC microscope (26) and obtain a cell-attached patch recording with a seal of several gigaohm (*see Note 8*).
3. Set the holding potential to 0mV. The slow component of the capacitance compensation control of the patch-clamp amplifier (C_{slow} of the EPC-7) is set to the smallest value, and the conductance of the capacitance compensation circuitry (G_{slow} of the EPC-7) is set to 0.2 μ S. Adjust the gain to 50 mV/pA (*see Note 9*).
4. Stop perfusion and reduce the level of the bathing solution by lowering the suction pipet of the perfusion system.
5. Apply dimethylpolysiloxane silicone oil slowly and gently from a Pasteur or plastic transfer pipet to cover the surface of the recording solution until a layer of about 1 mm has formed. It is necessary to apply the oil after the patch pipet has been immersed in recording solutions because exposure of the pipet tip to oil increases the difficulty of obtaining gigaohm seals (*see Note 10*). An alternative method avoids use of silicone oil. The pipet solution is filled to the minimum level that barely allows contact with the Ag-AgCl wire in the electrode. This reduces the noise to 10 aF rms. Combined with the reduction in bathing fluid level (step 4), the noise level can fall as low as 3–5 aF rms with a 3-ms filter setting on the lock-in amplifier (step 9).
6. Set the lock-in amplifier Reference section to Internal Mode and adjust the sine wave to 10–50 kHz and 100–200 mV rms (*see Note 11*). Sum the lock-in

amplifier output signal with the command potential of 0 mV by switching the electronic summation circuit.

7. The sinusoidal current and voltage outputs from the patch-clamp amplifier are viewed simultaneously on oscilloscope 1; the sinusoidal component in the current is nulled using the fast capacitance compensation controls of the patch-clamp amplifier (C_{fast} and τ_{fast} of the EPC-7). Adjust these controls until the sine wave disappears from the current output viewed on the oscilloscope (*see Note 12*).
8. The phase setting of the lock-in amplifier is adjusted to obtain complete separation of the capacitance and conductance signals in two independent channels: two outputs of the lock-in amplifier are simultaneously viewed on oscilloscope 2, and the phase is adjusted to eliminate or minimize changes in the conductance (X or Re) trace induced by dithering the resistor installed in the capacitance compensation circuit of the patch-clamp amplifier. To prevent saturation of the patch-clamp amplifier by capacitance dithering, the stimulus input of the patch-clamp amplifier is reduced to the lowest range (1:1000 for the EPC-7) during phase adjustment. During data analysis, one can often see that the phase setting made during an experiment is imperfect because large nonreversing capacitance steps have small projections in the Re trace. Correcting these small phase errors and other detailed data analysis procedures are described in the next subheading.
9. The high-frequency sinusoidal component produced by the lock-in is removed from the output capacitance and conductance signals by adjusting the time constant of a low-pass filter in the lock-in amplifier to 3 or 10 ms, 24 dB. This step also reduces the noise in these outputs (*see Note 13*).
10. Now, actual recording can be performed: The in-phase (Re, conductance) and 90°-out-of-phase (Im, capacitance) outputs of the lock-in amplifier are digitized (typically at 16-bit resolution) and read into the computer. Sample single-vesicle signals are shown in Fig. 2. Both the Im and Re traces show stepwise changes that signal the opening and closing of a fusion pore. Both large (LDCV) and small (microvesicle) events are presented. The Re and Im traces are viewed simultaneously on the computer monitor, and spontaneous exocytosis and endocytosis are recorded for intervals of a few minutes. Because the phase has a tendency to drift with time (*see Note 12*), we found it best to keep recordings short and readjust the phase at the beginning of each recording.
11. Evoke activity by positioning a micropipet close to the nerve terminal and ejecting depolarization solution with pressure (*see Note 14*). This pipet should be positioned before establishing the patch recording.
12. Alternatively, activity can be evoked by applying a solution of ionomycin (5–10 μM) from the micropipet or by backfilling the patch pipet with a second solution containing 20–100 μM ionomycin (after tip-filling the patch pipet with standard recording solution) (*see Note 15*).

3.6 Off-Line Phase Correction and Data Analysis

1. The phase adjustment detailed in Subheading 3.5., step 8 usually is imperfect. Because of these imperfections, exocytotic capacitance steps produce small projections in the G trace. These projections remain even after fusion has gone to completion, so they cannot reflect the presence of a finite fusion pore conductance. To correct these small phase errors off-line, the C and G traces are recomputed from the recorded Re and Im traces with an additional phase shift ϕ according to the following formulas (3):

$$G_{\text{corr}} = \text{Re} \cdot \cos(\phi) + \text{Im} \cdot \sin(\phi)$$

$$C_{\text{corr}} = -\text{Re} \cdot \sin(\phi) + \text{Im} \cdot \cos(\phi)$$

The additional phase shift ϕ is changed in 2° steps until the projection on the G trace disappears. This correction usually changes the phase setting by $2\text{--}30^\circ$ from the value set during an experiment.

2. Fusion pore analysis: Fusion pores with nonzero conductance reduce the apparent vesicle capacitance (Im) signal and produce a correlated increase in the conductance (Re) signal (3,5). The fusion pore conductance and true vesicle capacitance are calculated from these traces according to the following formulas:

$$C_v = \frac{1}{\omega} \frac{\text{Re}^2 + \text{Im}^2}{\text{Im}}, G_p = \frac{\text{Re}^2 + \text{Im}^2}{\text{Re}}$$

where $\omega = 2\pi\phi$, and ϕ is the frequency setting of the lock-in amplifier in hertz (10). This calculation is illustrated for large- and small-vesicle events in the lower two traces of Fig. 2.

3. The detection limits in pore conductance measurement are determined by the noise level, sine wave frequency, and vesicle size and can be estimated according to the following formulas (10):

$$G_p^{\text{lower}} = A\omega\Delta C$$

$$G_p^{\text{upper}} = \frac{1}{A} \frac{\omega C_v^2}{\Delta C},$$

where C_v is the vesicle capacitance, A is the signal-to-noise ratio, ΔC is the capacitance noise (rms), and ω is as defined above. From the noise levels in our recordings from pituitary nerve terminals, the detection range for SSV fusion pores can

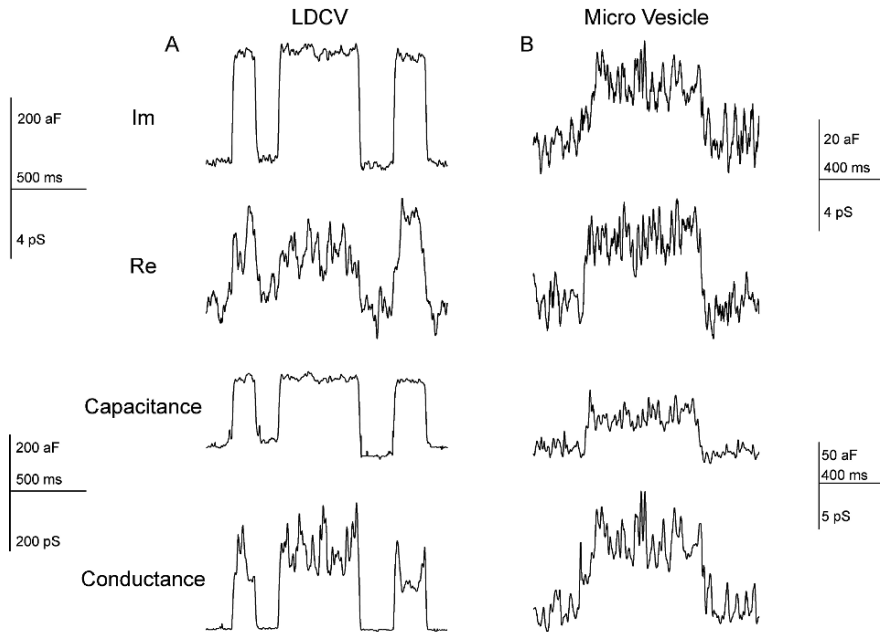


Fig. 2

Fig. 2 Real and imaginary components of a lock-in amplifier recording from a cell-attached membrane patch in a mouse pituitary nerve terminal. A large dense-core vesicle (LDCV) and a microvesicle produce large and small steps, respectively, in the Im traces. Both events are kiss-and-run type with the signal returning to baseline as the fusion pore closes. Vesicle capacitance and fusion pore conductance can be reconstructed from the Re and Im traces using the formulas in **Subheading 3.6.2**. Re and Im traces were recorded with 30-kHz, 150-mV sinusoidal waves.

be estimated as 1.5–40 pS at 10 kHz and 8–200 pS at 50 kHz with a signal-to-noise ratio of at least 3. For LDCVs, the lower range is the same as that for SSVs, and the upper range is a few nanosiemens.

4 Notes

1. Quartz pipets can be used to reduce the noise of capacitance measurements (27). However, because quartz melts at a much higher temperature than other types of pipet glass, pulling and heat polishing quartz pipets require special equipment (such as a P-2000 laser-based micropipet puller, Sutter Instruments, Novato, CA).
2. Similar semiconductor protective coatings, R6101 (Dow Corning, Midland, MI) or RTV615 (GE, Waterford, NY), can be used instead of Sylgard. In some experiments, we added Q-dope (GC Electronics, Rockford, IL) to the tip-coating

- step. Because of a higher viscosity of Q-dope, it might be easier than Sylgard to apply close to the pipet tip.
3. Sylgard silicone elastomer base is mixed with a curing agent at a 7:1 ratio rather than the 10:1 ratio recommended by the manufacturer. This increases the Sylgard viscosity, allows coating of the pipet closer to the tip, and produces thicker coats.
 4. A heat-polishing setup can be constructed by connecting a piece of thin platinum wire to an electrical current source and mounting this heater on a microscope stage. Installing a foot switch makes this operation much easier.
 5. TEA was added to block K^+ channels, but since channel openings were infrequent, it was often omitted. In preparations in which significant single-channel activity is observed at the selected holding potential, appropriate channel antagonists should be added to the pipet solution.
 6. Pipets should be held upright during coating and Sylgard curing since Sylgard has a tendency to creep along the glass surface and block the pipet tip.
 7. Pipets in which visible amounts of Sylgard accumulate inside the tip are discarded; these pipettes have a much lower success rate of forming gigaohm seals, although the Sylgard can be removed from outside the tip by heat polishing.
 8. A minimal amount of suction should be applied during sealing to minimize the membrane distortion at the pipet tip.
 9. The gain can be set higher than 50 mV/pA, but this does not improve signal quality much, and because of unavoidable drift, the output signals of the lock-in amplifier frequently saturate. Lower gain settings cannot be used; the feedback resistor in the head stage of most patch-clamp amplifiers switches to a lower value with gain settings of 20 mV/pA or lower, and this increases the noise severalfold.
 10. A practical consequence of the adverse effects of the oil on the ease of seal formation is that the oil must be removed for a subsequent recording attempt, or a new slice must be taken. In practice, oil removal is difficult, and we take a new recording chamber and new slice for each new recording. The chambers are then thoroughly cleaned for the next experiment.
 11. The largest sine wave amplitude that does not saturate the patch-clamp amplifier should be used to increase the resolution of capacitance measurements. In addition, the lock-in frequency is selected in the range of 10–50 kHz, at which resolution is optimal. Resolution decreases at frequencies below and above this range (10). Because phase adjustments become trickier at higher frequencies, we generally use the range 10–30 kHz. The amplitude of the sine wave is typically set to 100–200 mV rms.
 12. Because of slow drift in electrical parameters, particularly stray capacitance, this adjustment should be checked and repeated as necessary, usually at the beginning of each 2- or 3-min recording episode. This also applies to the phase adjustment in Subheading 3.5., step 8.
 13. The output filter settings of the lock-in amplifier are selected as a compromise between better time resolution (shorter time constant) and lower noise (stronger filtering with longer time constants). We found that 3 or 10 ms are usually the minimal time constant setting that allows resolution of small vesicles with at

least a 3:1 signal-to-noise ratio. In some cases, however, time constants as short as 500 μ s have been used.

14. We found that depolarization with KCl did not have an effect in 55% of the patches tested, and these fell into two groups. Some patches had high activity prior to depolarization, suggesting that the initial intracellular Ca^{2+} may have been elevated. In other recordings, the depth of the nerve terminal within the tissue appeared to prevent access of the KCl solution (11).
15. Of the two methods of ionomycin application—pressure ejection from a micropipet and backfilling the recording pipet—the latter method was more effective. Pressure application of ionomycin from a micropipet damaged the nerve terminal, often before the effect of ionomycin on exocytosis became evident. When loaded into the back of the patch pipet, the ionomycin effect was evident in 30% of the patches tested. This likely reflects the slow rate of diffusion of ionomycin from the back of the patch pipet into the tip and a localized action of ionomycin, limited to the patch of membrane under recording. Finally, we also found that application of hypertonic solutions failed to induce vesicle fusion. In these experiments, hypertonic solutions were applied from a micropipet positioned on the opposite side of the terminal from the patch pipet. Thus, the absence of an effect may have been caused by the cell-attached configuration; solutions applied outside the patch electrode fail to reach the membrane isolated by the recording pipet.

References

1. Neher, E., and Marty, A. (1982) Discrete changes of cell membrane capacitance observed under conditions of enhanced secretion in bovine adrenal chromaffin cells. *Proc. Natl. Acad. Sci. U. S. A.* **79**, 6712–6716.
2. Lindau, M., and Neher, E. (1988) Patch-clamp techniques for time-resolved capacitance measurements in single cells. *Pflugers Arch.* **411**, 137–146.
3. Lindau, M. (1991) Time-resolved capacitance measurements: monitoring exocytosis in single cells. *Q. Rev. Biophys.* **24**, 75–101.
4. Fernandez, J.M., Neher, E., and Gomperts, B.D. (1984) Capacitance measurements reveal stepwise fusion events in degranulating mast cells. *Nature* **312**, 453–455.
5. Lollike, K., Borregaard, N., and Lindau, M. (1995) The exocytotic fusion pore of small granules has a conductance similar to an ion channel. *J. Cell. Biol.* **129**, 99–104.
6. Kreft, M., and Zorec, R. (1997) Cell-attached measurements of attofarad capacitance steps in rat melanotrophs. *Pflugers Arch.* **434**, 212–214.
7. Albillos, A., Dernick, G., Horstmann, H., Almers, W., Alvarez de Toledo, G., and Lindau, M. (1997) The exocytotic event in chromaffin cells revealed by patch amperometry. *Nature* **389**, 509–512.
8. Lollike, K., Borregaard, N., and Lindau, M. (1998) Capacitance flickers and pseudoflickers of small granules, measured in the cell-attached configuration. *Biophys. J.* **75**, 53–59.
9. Henkel, A.W., Meiri, H., Horstmann, H., Lindau, M., and Almers, W. (2000) Rhythmic opening and closing of vesicles during constitutive exo- and endocytosis in chromaffin cells. *EMBO J.* **19**, 84–93.
10. Debus, K., and Lindau, M. (2000) Resolution of patch capacitance recordings and of fusion pore conductances in small vesicles. *Biophys. J.* **78**, 2983–97.

11. Klyachko, V.A., and Jackson, M.B. (2002) Capacitance steps and fusion pores of small and large-dense-core vesicles in nerve terminals. *Nature* **418**, 89–92.
12. Chowdhury, H.H., Kreft, M., and Zorec, R. (2002) Distinct effect of actin cytoskeleton disassembly on exo- and endocytic events in a membrane patch of rat melanotrophs. *J. Physiol.* **545**, 879–886.
13. Dernick, G., Alvarez de Toledo, G., and Lindau, M. (2003) Exocytosis of single chromaffin granules in cell-free inside-out membrane patches. *Nat. Cell Biol.* **5**, 358–362.
14. He, L., Wu, X.-S., Mohan, R., and Wu, L.-G. (2006) Two modes of fusion pore opening revealed by cell-attached recordings at a synapse. *Nature* **444**, 102–105.
15. Lindau, M., and Almers, W. (1995) Structure and function of fusion pores in exocytosis and ectoplasmic membrane fusion. *Curr. Opin. Cell Biol.* **7**, 509–517.
16. Jackson, M.B., and Chapman, E.R. (2006) Fusion pores and fusion machines in Ca²⁺-triggered exocytosis. *Annu. Rev. Biophys. Biomol. Struct.* **35**, 135–60.
17. Ales, E., Tabares, L., Poyato, J., Valero, V., Lindau, M., and Alvarez de Toledo, G., (1999) High calcium concentrations shift the mode of exocytosis to the kiss-and-run mechanism. *Nature Cell Biol.* **1**, 40–44.
18. Gillis, K.D. (1995) Techniques for membrane capacitance measurement. In *Single-Channel Recording* (Sakmann, B., and Neher, E., eds.), Plenum Press, New York, pp. 155–198.
19. Rudy, B., and Iversen, L., eds. (1992) *Ion Channels*. Methods in Enzymology **207**, Academic Press, San Diego, CA.
20. Sakmann, B., and Neher, E. (1995) *Single-Channel Recording*, 2nd ed., Plenum Press, New York, NY.
21. Gerfen, C., Holmes, A., Rogawski, M., Sibley, D.R., Skolnick, P., and Wray, S., eds. (1997) *Current Protocols in Neuroscience*. John Wiley & Sons, Hoboken, NJ.
22. Rae, J., Cooper, K., Gates, P., and Watsky, M. (1991) Low access resistance perforated patch recordings using amphotericin B. *J. Neurosci. Meth.* **37**, 15–26.
23. Edwards, F.A., Konnerth, A., Sakmann, B., and Takahashi, T., (1989) A thin slice preparation for patch recordings from neurones of mammalian central nervous system. *Pflugers Arch.* **414**, 600–612.
24. Joshi, C., and Fernandez, J.M. (1988) Capacitance measurements. An analysis of the phase detector technique used to study exocytosis and endocytosis. *Biophys. J.* **53**, 885–892.
25. Fidler, N., and Fernandez, J.M. (1989) Phase tracking: an improved phase detection technique for cell membrane capacitance measurements *Biophys. J.* **56**, 1153–1162.
26. Jackson, M.B. (1993) Passive current flow and morphology in the terminal arborizations of the posterior pituitary *J. Neurophysiol.* **69**, 692–702.
27. Benndorf, K. (1995) Low noise recording, In *Single-Channel Recording*, 2nd ed. (Sakmann, B., and Neher, E., eds.), Plenum Press, New York, pp. 129–145.

23

Good Practices in Single-Cell Amperometry

David J. Machado, Mónica S. Montesinos, and Ricardo Borges

1 Introduction.....	297
2 Materials	298
3 Methods.....	300
4 Notes	308
References.....	313

Summary Single-cell amperometry is a powerful tool for the study of the mechanisms underlying secretion from cells that release electrochemically active substances like catecholamines, histamine, or serotonin. Amperometry has changed our view of the secretory process and the quantal release phenomenon. Today, it is a relatively easy technique to set up and affordable for most laboratories. Amperometry can help solve many interesting problems in cell physiology or pharmacology. However, there are a number of issues about the experimental design, data analysis, and result interpretation that need to be considered. Here, we compile some recommendations and advice on how to conduct experiments with amperometry, covering tissue culture, electrode types and their construction, calibration, equipment, data acquisition, and strategies for electrical noise reduction. We concentrate on cultured chromaffin cells, although most of the information is equally applicable to other cell types.

Keywords Adrenal; chromaffin cell; electrodes; exocytosis; secretion; voltammetry.

1 Introduction

Carbon fiber electrodes were first used by Françoise Gonon in the 1980s to measure free substances in the central nervous system (1). In the early 1990s, Wightman and his colleagues (2) combined amperometry with carbon fiber microelectrodes to quantify the secretory responses from single chromaffin cells. Moreover, these authors initiated a new era in the study not only of the secretion from individual

chromaffin cells but of the kinetics of single-event exocytosis. Amperometric techniques have provided a powerful tool to clarify several mechanisms involved in the stimulus–secretion coupling processes and in exocytosis.

Amperometry and fast cyclic voltammetry are now widely used techniques to study secretory responses from single cells (i.e., measurement of the total amount of an oxidizing substance released) or the kinetics of exocytosis (i.e., kinetics of the discharge of transmitter from individual vesicles).

Amperometry is a noninvasive technique with high sensitivity and a unique time-course resolution. In addition, its use is nondeleterious to the cell, and apparently it does not affect the normal function of the secretory responses. However, it has two major limitations: First, it only detects substances after vesicle fusion has occurred and its content has diffused to the electrode tip; in other words, it is blind to what happens before vesicle fusion and pore formation. Second, it only detects those substances that can be oxidized at the holding potential applied to the electrode. Nevertheless, from the observation of amperometric traces, it is possible to infer some of the events occurring within the secretory vesicle before fusion (synthesis and storage of neurotransmitters). In addition, cell incubation with electroactive substances, which can be taken up by the cell and subsequently by the storage vesicles, acting as a false neurotransmitter, can sometimes overcome the problem of the detection of electrochemically inactive secretory products.

2 Materials

2.1 Chromaffin Cell Preparation

Standard culture room facilities with an inverted stereomicroscope ($\times 200$ magnification).

1. Petri dishes, 35-mm \varnothing , and 24-well culture plates.
2. Glass coverslips (12 mm \varnothing ; Marienfeld, Lauda-Königshofen, Germany).
3. Papain Worthington Biochemical Corp, Lakewood, NY.
4. Collagenase 1A (Sigma cat. no. C2674).
5. Bovine serum albumin fraction V (St. Louis, MO).
6. Poly-D-lysine.

Other chemicals are purchased from Sigma.

7. Sterile Locke's buffer: 154 mM NaCl, 5.6 mM KCl, 3.6 mM NaHCO₃, 5.0 mM HEPES, and 5.6 mM glucose, adjusted to pH 7.3. We also add gentamicin (40 μ g/mL) and penicillin G (50 IU/mL).
8. Standard Dulbecco's modified Eagle's medium (DMEM) supplemented with 10% fetal calf serum, 50 IU/mL penicillin, and 40 μ g/mL gentamicin (*see Note 1*).

2.2 Carbon Fiber Electrodes (see Note 2)

2.2.1 Glass-Encased Electrodes

1. Glass capillaries: Although it is not critical, the use of soft-glass capillaries is recommended. Electrical insulation will be improved with thick glass walls. We use type 8250 borosilicate glass from World Precision Instruments (Stevenage, UK) with 1.65/1.0 mm \varnothing .
2. Carbon fiber: The usual source of fibers was Amoco, but now they no longer produce these carbon fibers. Current sources are Alfa Aesar (www.alfa.com) and Cytec Engineered Materials (www.cytec.com). Diameters range from 4 to 30 μm . For single-cell recordings, it is better to use 5- to 11- μm diameter fibers. For the puller, any commercially available puller can be used.
3. Epoxy resin: A number of resins are currently available. We have used Epon 828, and as a curing agent we employ 15% (by weight) m-phenylenediamine (Epoxi Technology, www.epotek.com; Miller-Stephenson Chem. Co., www.miller-stephenson.com), with high fluidity to enter into the capillaries.
4. Beveler: It is critical that the tip of the electrodes have an even polished surface (Fig. 1d). We do not recommend the use of diamond pastes or alumina as grinder abrasives because they leave dirty electrode surfaces. There are some commercially available grinders, such as the EG-40 (Narishige, Tokyo, Japan) or the BV-10 (Sutter Instruments, Novato, CA); however, we have built, and use, a very good simple grinder following the procedure described elsewhere (3).

2.2.2 Plastic-Encased Carbon Fiber Electrodes (Chow's Method)

The following are needed for Chow's method for plastic-encased carbon fiber electrodes in addition to glass capillaries, carbon fibers, and an electrode puller: polyethylene tubing (PE10, Portex 800-100-100, Técnicas Médicas Mab, Barcelona, Spain); forceps with their fine tips covered with rubber or plastic tubing; standard soldering iron with a new tip; epoxy glue.

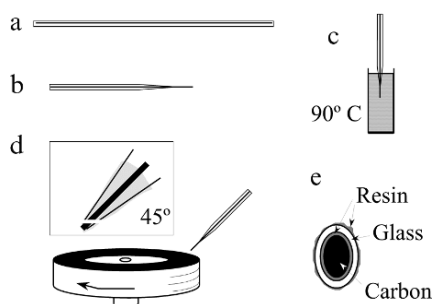


Fig. 1 Carbon fiber microelectrode construction following Wightman's method (see text).

2.2.3 Plastic-Encased Carbon Fiber Electrodes (Hille's Method)

For plastic-encased carbon fiber electrodes according to Hille's method, the following are necessary: carbon fibers as described above; standard 0.1- to 10- μ L pipet tips of clear plastic; electrophoresis power supply and cables; stainless steel wire with 0.3- to 0.4-mm \varnothing .

2.2.4 Commercially Available Electrodes

For most applications, commercially available carbon fibers are a good and time-saving alternative. Several companies produce electrodes suitable for single-cell amperometry. [Table 1](#) shows some of these manufacturers and their Internet addresses.

Table 1 Commercially Available Carbon Fiber Microelectrodes

ALA Scientific Instruments Inc.	www.alascience.com
Dagan Corporation	www.dagan.com
NPI Electronic Instruments for Life Science	www.npielectronic.com
Scientifica	www.scientifica.com
World Precision Instruments Inc.	www.wpiinc.com

2.3 Other Equipment

1. Antivibration table and Faraday's cage are mandatory (*see Note 3*).
2. Reference electrode: We use an Ag/AgCl pellet (EP2, World Precision Instruments, Sarasota, FL) placed by the side wall of the perfusion chamber. The liquid height level should be reduced to less than 2 mm to reduce noise.
3. Potentiostat: In the work discussed in this chapter, we use the terms *potentiostat* and *amplifier* interchangeably because patch-clamp amplifiers can behave as a potentiostat for most applications. Others also use the term *picoammeter* (4). There are many instruments currently available for amperometry. The limited amount of current necessary to maintain the oxidative potential at the electrode tip allows the use of a two-electrode configuration, which is the usual configuration of most patch-clamp amplifiers (*see Note 4*).
4. Acquisition systems: *See Note 5*.

3 Methods

3.1 Mice Chromaffin Cell Isolation

Any method described for chromaffin cell isolation and culture seems to be appropriate for amperometric studies. The following is a rule of thumb for amperometric studies from chromaffin cells of any species:

1. The isolation procedure should try to obtain healthy cells rather than a high yield. We recommend reducing the concentration of digesting enzymes (by 15% of the described concentrations given in the studies cited below) and minimizing the mechanical maneuvers during tissue digestion. For bovine chromaffin cells, we followed a modification of the original recipe using a bolus, rather than perfusion, of collagenase injected through the adrenal vein (5,6). For rat cells, we follow the conditions described by Gilibert (7), and for the mouse we follow a modification of the procedure described by Sørensen et al. (8).
2. Cells must be plated at low density (~20,000 to 50,000 per cm²).
3. Replace the culture medium every 2 d using serum-free medium.
4. Cells usually secrete best within 24 h from isolation; even better, they can be used advantageously a few hours after culture.

The following is the procedure for mice chromaffin cell isolation:

1. Sterilize the glass coverslips by brief flaming of both sides inside a laminar flow air hood and place them on the wells.
2. Put a drop of 0.01% solution of poly-D-lysine sine (in sterile pure water) ov in water over each coverslip and after 1 min wash three times with sterile pure water.
3. Sterilize the plate by ultraviolet (UV) light exposure in the hood for 30 min. The treated glass can be used within 1 wk.
4. Euthanize the animals by cervical dislocation. Open the abdomen and remove both adrenals by pulling the glands with an angled forceps.
5. Under a stereomicroscope (×20 magnification), carefully remove the adrenal capsule and as much as possible of the cortical tissue. Work on a piece of clean filter paper wetted with Locke's buffer. It helps to avoid drying and overheating of the tissue by the lamp. Transfer the medullary tissue to a sterile (35-mm Ø) Petri dish containing 1 mL sterile Locke's buffer. All procedures are carried out at room temperature.
6. Remove the buffer and replace in a 15-mL Falcon tube with 0.2 mL papain solution in Locke's buffer (8IU for two glands) at 37°C for 15 min without shaking.
7. Wash the tissue twice with 800 µL fresh Locke's solution.
8. Remove the liquid completely and add 0.2 mL DMEM supplemented with 10% fetal calf serum, 50 IU/mL penicillin, and 40 µg/mL gentamicin.
9. Disaggregate the pellet by several successive passes, first through a 1000-µL and then through a 100-µL pipet, until the suspension has a turbid aspect.
10. Take 20 µL of this cell suspension to count the number of cells in a Neubauer hemocytometer. Dilute, if necessary, the cell suspension to get the proper cell density.
11. Put a drop of the cell suspension on each of the 12-mm Ø poly-D-lysine-coated coverslips. Allow cells to settle for 20 min at 37°C and add 1 mL DMEM.
12. The cells are then placed in a cell culture incubator at 37°C on a 5% CO₂ in air atmosphere.
13. The cells are used at room temperature 0–3 d thereafter.

3.2 *Glass-Encased Electrodes*

For glass-encased electrodes, we use a modification of the technique described by Wightman and his colleagues from the University of North Carolina (4,9).

1. Introduce a single carbon fiber into a glass capillary by gentle aspiration from the opposite end of the capillary (Fig. 1a). Work on a white and clean surface like a sheet of paper. For aspiration, a water vacuum pump or a moderate-potency vacuum pump can be used. Hold one end of the carbon fiber on the table with the fourth finger. Connect the capillary to the vacuum and aspirate the fiber. When the fiber is completely inserted, hold the capillary with the thumb and the index finger and remove it from the vacuum source.
2. The glass capillary is pulled until it breaks, and the exposed carbon fiber is cut at the middle with small scissors, thus producing two electrodes (Fig. 1b).
3. The tip surface of the carbon fiber should be perfectly insulated at the tip of the glass pipet. To allow entry of resin into the pipet, leave a small space surrounding the carbon fiber. The usual way to cut the glass tip is to use a scalpel or small scissors under microscopic observation. Alternatively, it can be done by putting the electrode onto a slide slightly fixed with a piece of plasticine. Under microscope guidance, push the electrode carefully with one finger against a hard object such as a piece of a broken slide glued to the first slide. Gently push the electrode tip toward the piece of broken slide such that the protruding carbon fiber first touches the glass, then bends, and finally breaks at the glass tip.
4. To ensure good penetration, it is important to maintain it at 90° C (Fig. 1c). Place the resin plus the curing agent in a 3-mL plastic tube and heat it by introducing the tube into a 40-mL beaker with water placed on a heated stirring plate. Take four or five electrodes with their tips aligned and dip them 2–3 mm into the heated resin for 30–40 s to allow the epoxy resin to enter and seal the tip (Fig. 1c). It is important to remove the electrodes slowly from the resin to avoid the formation of bubbles.
5. Leave the electrodes overnight at room temperature. The next day, cure the resin by placing the electrodes in an oven, first at 100°C for 2 h and then at 150°C for an additional 2 h. Electrode tips are fragile and are difficult to transport with security. We have an easy and inexpensive procedure to make a multiple electrode carrier for curing and for later electrode storage: Take an A4 or similar sheet of paper and fold it three times along its long side and attach it to a cardboard. Tightly place over the folded paper, upside down, a piece of heat-resistant office tape (Scotch 3M, Cergy Pontoise, France) 5 cm longer than the cardboard and attach the ends to the opposite side of the cardboard. Now, the adherent surface of the tape faces up, forming a 20–30° angle with the cardboard; the electrodes can be fixed, leaving their tips up, thus protecting them from accidental breakage.
6. Electrode tips are polished at 45° on a black diamond grinder using 2-propanol as a lubricant (Fig. 1d). Electrode tips resulting from the polishing (inset) will have an even elliptical surface with a known active area (Fig. 1e). Identify the position of the polished tip by marking the back of the electrode with typewriter corrector (Tippex®) before polishing.

7. This method allows the constructions of tens of electrodes. The cured electrodes last almost indefinitely. We usually make 100 or 200 electrodes at a time except for step 6. We polish four or five electrodes the day of the experiment. Electrodes can be reused after brief repolishing.

3.3 Plastic-Encased Carbon Fiber Electrodes

The plastic-encased carbon fiber electrode procedure was first developed in the laboratory of Erwin Neher (10). Different laboratories have since made several modifications. It consists of a plastic-encapsulated carbon fiber that is glued to the lumen of a glass capillary that provides the connection to the head stage of the potentiostat. Figure 2 shows the method as originally described.

1. Put a 3-mL plastic test tube at approx 45° inclination and fill it with 2-propanol. Place inside a polyethylene tubing long enough to overhang approx 1 cm (similar to Fig. 3a).
2. With the help of fine-tip forceps, pick a carbon fiber of approx the same size as the plastic tubing and introduce it into the polyethylene tubing (see Fig. 3b). The 2-propanol reduces the static attraction, thus facilitating the entry of the carbon

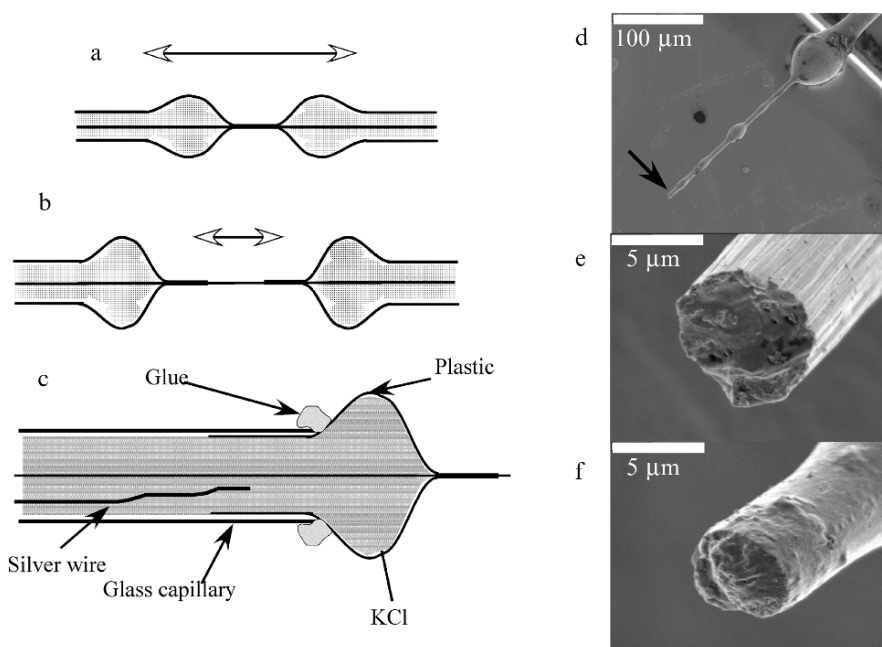


Fig. 2 The construction of plastic-encased electrodes following Chow's method (explanation in the text).

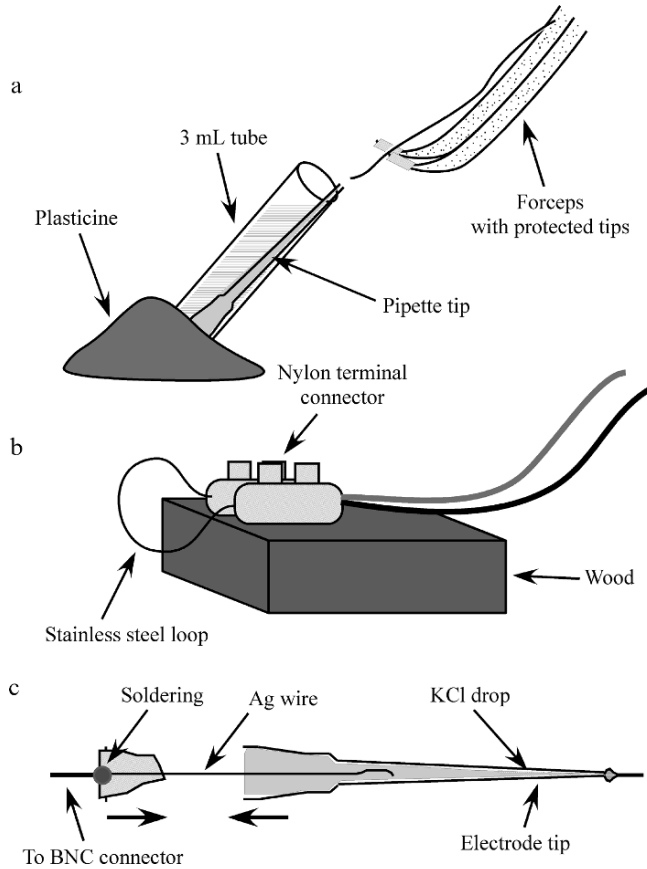


Fig. 3 Electrode construction using pipet tips (explanation in the text).

fiber. Cut the tubing in approx 3-cm pieces with a scalpel, place it on a filter paper, and allow the 2-propanol to evaporate.

3. Melting can be done either by using a soldering iron with a new tip or by applying an electric current to a stainless steel cable loop (Fig. 3b; see below). Take the tubing piece with both hands (or two forceps) and slowly let it approach to within about 2 mm of the heat source until it becomes clear. Note that two beads will appear at both sides of the heat source as the plastic retracts (Fig. 2a).
4. Pull the plastic tubing carefully until it stretches about 2 mm (Fig. 2b). Rapidly remove it from the heat source and allow it to cool for 10 s or more.
5. Bring the stretched portion of the tubing again near to the heat source until it melts. Then, cut at the center by touching the heat source briefly (~1 s) to cut the fiber. This last step produces extra melting of the plastic, which now finely covers the sides of the carbon fiber tips.

6. Cut a 10-cm glass capillary in two pieces of similar size and introduce the broad end of each of the plastic pieces resulting from step 5 into the glass capillary. Push the glass capillary until it touches the upper portion of the plastic bead (Fig. 2c).
7. Seal the plastic tubing to the glass capillary using epoxy glue and allow it to harden (Fig. 2c).
8. Just before the experiment, cut the protruding carbon fiber electrode as close as possible to the plastic tip using a new scalpel blade (arrow in Fig. 2d).
9. The glass capillaries are backfilled with 3M KCl solution in an amount just enough to allow the electrical connection to the Ag filament of the amplifier. Do not overfill the capillary; it will notably increase the noise (see Note 6).

3.4 Other Plastic Electrodes

An alternative method was proposed by Bertil Hille's laboratory using plastic pipet tips (11). They have the same disadvantages described in the 3.3 section these electrodes can be made in less than 1 min, they are cheap, and they only require minimal modifications in the connector to the preamplifier. The method is a good alternative for laboratories that lack pullers or grinders.

1. Put a 3-mL transparent tube into a piece of plasticine so it forms a 45° angle over the table.
2. Fill the tube with 2-propanol and place in it a 10- μ L pipet tip upside-down.
3. With the help of tip-protected forceps, introduce a carbon fiber inside the pipet tip (Fig. 3a).
4. Screw two terminal nylon connectors to a piece of wood. Attach to the terminals a stainless steel wire 3 cm long, forming a 1-cm loop. Connect the steel wire to an electrophoresis power supply and apply a voltage (1–4 V) with enough current to heat the filament to near red (Fig. 3b).
5. Pull and cut the tip as explained in the text for plastic electrodes.
6. Connect the electrode to the head stage of the potentiostat by soldering an 0.25 Ag mm \emptyset wire to a 0.5-mm \emptyset cooper terminal. A cone to hold the tip connection can be made with a ring of silicone tubing (Fig. 3c).

3.5 Calibration and Selection Criteria

The use of an electrode for amperometry without proper calibration is like measuring the pH of a solution without a properly calibrated pH meter. However, most of the published articles lack mention of this basic precaution.

To perform the calibration of electrodes, we use two different systems developed in Mark Wightman's laboratory (12), which are described in Fig. 4. The system

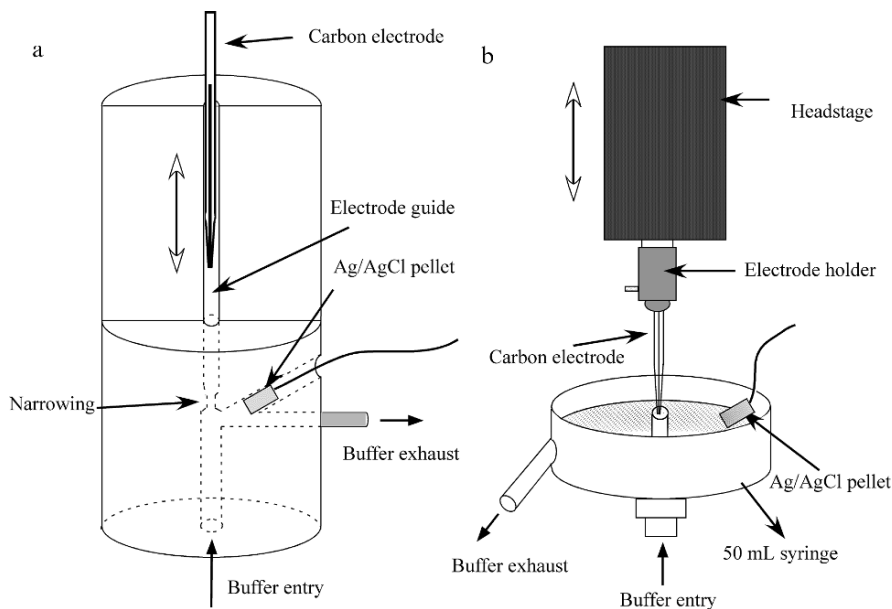


Fig. 4 Two flow injection systems suitable for electrode calibration. **(a)** A 3-cm \varnothing methacrylate rod is drilled in the center with a 2-mm \varnothing drill except at the narrowing segment, where it progressively narrows to a 1-mm \varnothing to trap the electrode. The rod is cut as shown to use the resulting slot as the electrode guide. An Ag/AgCl pellet is used as the reference electrode. The buffer enters the flow cell through the lower side, bathes the electrode tip, and makes an electrical connection with the reference electrode. The carbon fiber electrode is connected to the head stage (not shown). **(b)** The plunger of a 50-mL plastic syringe is removed, and the body of the syringe is cut at approx 2 cm from the lower end. A plastic tube is inserted into the syringe orifice to create a liquid connection between the reference and carbon fiber electrode. The buffer that enters from the bottom escapes through a piece of tubing glued to the syringe side. The electrode attached to the head stage of the amplifier is inserted into the buffer using a micromanipulator (not shown).

described in Fig. 4a can only be used to calibrate glass-encased electrodes. Its main advantage is that the electrodes can be introduced/removed by hand without using micromanipulators. The system described in Fig. 4b can be used to calibrate any kind of electrode. Either system requires that the control buffer (usually Krebs-HEPES solution) can be changed to a freshly prepared buffer containing 20–50 μM norepinephrine, other catecholamines, or another substance to test. Although buffers can be pumped into the flow cells using a syringe, use of a buffer reservoir placed approx 40 cm over the system is even easier. The exchange of buffers can be performed using a couple of electrovalves (Lee Company, Westbrook, CT; Fig. 5a). Because the magnitude of the electrochemical signal is highly dependent on the flow, all measurements are done under stop-flow conditions. Figure 5b shows a typical trace obtained from a calibration run (see Note 7).

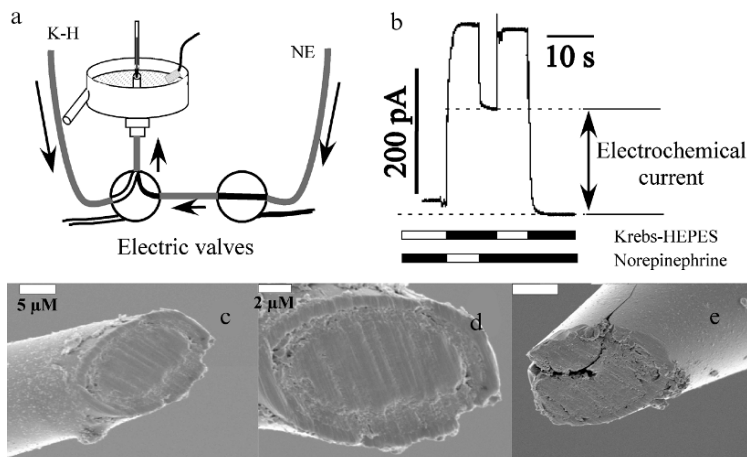


Fig. 5 Calibration of carbon fiber electrodes using norepinephrine. **(a)** Solutions are changed by means of a pair of electronic valves. **(b)** Krebs-HEPES (K-H) solution passing at a moderate rate of approx 2 mL/min should produce a brief initial jump when the electrical connection is made (not shown). The open-valve periods are represented as open segments below the current record. Switching the solution to 50 μM norepinephrine (NE) results in a rapid positive deflection that reaches 280 ± 25 pA for a disk electrode with a 6- μm radius (open norepinephrine bar). When the norepinephrine solution is not flowing, the oxidation current drops to a steady state of 185 ± 15 pA (solid bar). Switching to the Krebs reservoir (open bar) produces an initial uprising as the remnant norepinephrine in the inflow tubing flows toward the electrode before dropping to the basal level as the norepinephrine is washed away. Measurements should be done under conditions of stop-flow (solid bars). **(c)** Scanning microscopy image showing a typical carbon fiber electrode tip. **(d)** Higher magnification of the same electrode; note the different layers around the carbon fiber as in Fig. 1e. **(e)** Electrode with a fissure; its active surface is large, and the current will be larger than expected. However, the current will drop in conditions of stop-flow.

3.6 Strategies for Noise Reduction

Usually, the source of noise is the line noise (50 or 60 Hz, and their harmonics) and a high-frequency noise (i.e., radio). Try to evaluate the effects of switching on and off all the surrounding equipment and lights plus the effect of you approaching or moving away from the system.

The use of a good ground with a single end point where all the pieces of equipment are connected is strongly recommended. If an independent ground is installed, be sure that no part of the equipment is connected to another ground. Place the microscope as far as possible from the front of the Faraday's cage and ground it; place the microscope condenser as close to the specimen as possible. Also ground the cage, the table, and the equipment rack. Connect to the ground the amplifiers and the motorized manipulators. Avoid introducing inside the cage any kind of unnecessary apparatus and cables. The connection cable from the head stage to the computer should be as short as possible and should not pass near a noise source

such as a cathode tube computer monitor. Sometimes a grounded cable attached along this cable reduces the noise notably (*see Note 8*).

3.7 Performing Experiments

The distance of carbon fiber to the cell membrane affects the quality of recordings. We usually carry out the amperometric recordings with the disk electrode placed in full contact with the cell membrane. It leaves a layer of saline (~10–20 nm) between both even surfaces. This is approx the dimension of a synaptic cleft. The electrical insulation of the carbon fiber (glass plus resin; *Figs. 1e* and *5c–e*) reduces the amount of catecholamines diffusing from outside and means that most of the spikes have originated under the electrode with little distortion from outside. It is important that the angle of the electrode with the underlying cell membrane is the same as that formed during polishing. The use of piezoelectric manipulators and contrast optics (phase contrast or Nomarski) helps greatly (*see Note 9*).

4 Notes

1. The use of mouse chromaffin cells has several advantages over bovine or pig: Their isolation is fast, and the cell culture procedure consumes only small amounts of enzymes, serum, and media. The digestion of the adrenal tissue from animals younger than 1 mo can be achieved with excellent results using papain instead of collagenase (8). The availability of genetically modified animals and the possibility of using animals chronically maintained under drug treatments or stressed conditions result in great advantage over other animal species. We use round glass coverslips with 12-mm Ø; these can be easily placed on 24-well culture plates. Cell adhesion improves notably with pretreatment of the glass with poly-D-lysine. With practice, both adrenals from a mouse produce enough cells to fill half of one plate.
2. Carbon fiber microelectrodes offer many advantages over the first electrodes made with carbon paste. Although noble metals such as platinum could be theoretically used, they are unstable for use in single-cell measurements.

The small surface of carbon fiber microelectrodes provides an excellent relationship between faradic and capacitive currents. Capacitive current occurs between the two surfaces of conductive materials when they are exposed to an electrical potential. Their magnitude is directly proportional to the second power of the radius of the exposed disk surface of the electrically insulated carbon fiber. A standard fiber of 5- μm radius will render an active surface for a 45° polished tip of about 113 μm^2 . This electrode will reach full electrical equilibrium at normally used potentials in amperometry (+0.6 to +0.8 V) within a second. However, this delay is a limitation on fast voltammetric

studies, in which the large voltage ramps used require baseline subtraction. For a detailed description of the use of microelectrodes in voltammetry, please refer to *Refs. 4 and 9*.

There are several procedures for carbon fiber electrode construction suitable for amperometric recordings. In addition, the electrodes can be purchased directly from commercial sources. Two major categories of electrodes are currently used for electrochemistry: cylindrical electrodes, in which the carbon fiber protrudes, without isolation, a few hundreds of micrometers from the glass tip, and disk electrodes, in which an electrically insulated fiber is carefully cut to expose exclusively a circle at the end of the fiber. Because the desired active area is the surface of the electrode tip touching/near the cell surface, it is important to completely insulate the rest of the carbon fiber. Disk electrodes are preferable to cylindrical electrodes; the disk design favorably increases the relation between faradic and capacitive currents. A small active surface also means lower current circulating through the electrode, thus reducing the electronic noise.

It is important to consider that the major part of the noise will be generated between the electrode tip and the head stage preamplifier. It is always easier to eliminate the sources of noise rather than attempt to reduce it after data acquisition. The quality of the electrical insulation of the fiber is one of the crucial parts in the removal of electric noise. Two main strategies have been used in electrode construction for this purpose: glass- and plastic-encased electrodes.

Smaller sizes are more difficult to use because even minimal amounts of dust cause a drop in electrode sensitivity, although these small-diameter electrodes are convenient for mapping the active secretory zones on the surface of cells (*13*).

3. At least two micromanipulators are necessary. One with good precision and stability is required to move the head stage of the amplifier. The other micromanipulator is used to position a drug delivery system close to the cell. We use a self-made pneumatic system to inject drugs in the vicinity of the cell. Because some of the solution in the puffer will leak out of the pipet, its tip should be placed at more than 40 μm from the cell membrane. Because of the effects of flow on electrochemical detection, the use of continuous perfusion systems should be avoided during the recordings. However, it is recommended to renew the solution in the chamber after a few minutes of recording.
4. In our hands, the amplifier with the best signal-to-noise relation is the Axopatch 200B (Molecular Devices, Sunnyvale, CA, USA). However, for most types of studies many other potentiostats/amplifiers on the market are appropriate. Custom-made potentiostats can be built in a local electronic workshop. Below are few recommendations to follow for any potentiostat to be used for amperometric measurement of electroactive substances:
 - Holding potential: Almost all current amplifiers can supply a working potential up to +800 mV. However, with older amplifiers like the EPC-7 (HEKA Electronics, Lambrecht, Germany), this voltage can be applied by either a power supply or by an external 9-V battery using a proper serial resistor to drive 6–7 V (the equipment divides by 10 the external applied voltage).

- Bandwidth: At least 4kHz are needed for amperometry experiments on bovine chromaffin cells. It will become necessary to use up to 10kHz on PC12 or up to 100kHz in some neurons.
 - Noise: The noise of the whole system should not exceed 3 pA using a 2-kHz low-pass filter. There are several strategies for noise reduction (see below), but you should avoid the use of analog low-pass filters below 2kHz.
5. Modern computers are rapid enough to eliminate the use of the analogical recording systems used in the past. In addition, there are many analogic/digital boards (ADDA) suitable for acquiring amperometric data. We use a 16-byte board (PCI-6052E, National Instruments, Austin, TX) on bipolar mode. It is important to accommodate the output signal from the amplifier to the input characteristics of the board to avoid redundant data. For instance, if the amplifier gives a ± 1 V output voltage and the board is set to ± 10 V, 90% of its acquisition capability is not used.

Another important point is to accommodate the precision of the data acquisition system to the board's characteristics. Many programs acquire data with double (64-byte) or single (32-byte) precision. However, few boards can supply (and it is not necessary) data with this precision, thus resulting in a useless amount of information that takes a lot of disk space and slows the data processing.

To acquire data, we use a locally written program in LabView for Macintosh. This program is freely available on request. The acquisition frequencies range from 4kHz for bovine cells to 10kHz for superior cervical ganglia cells. A single file usually lasts for 2 min of recording, but several files can be concatenated for longer records.

6. An advantage of these electrodes is that they do not require a grinder for polishing the tips. However, the size of their active surface is more variable than with Wightman's method because the tip of the electrode is made by cutting/breaking the carbon fiber. Frequently, the plastic coat retracts from the tip, thus creating a cylindrical electrode (see above) as shown in Fig. 2e. The glassy nature of carbon fibers makes them extremely hard and brittle, thus producing uneven surfaces (Fig. 2f) with different sizes of exposed areas. Furthermore, these surfaces cannot be placed in full contact with the chromaffin cell membrane, while full contact is obtained with the polished electrodes.

Several strategies have been used to improve the sensitivity and selectivity of carbon fiber electrodes. However, the treatment of electrodes with perfluorosulfonated polymers like Nafion® drastically reduces their time resolution and makes them useless for fast amperometric recordings. There are several treatments to increase their responsiveness. For instance, the real active surface can be increased by cleaning the tips by soaking them in nonpolar solvents like acetone or 2-propanol for 10–20 min. This treatment also improves the electrode sensitivity by adding functional groups to the carbon molecular net (9). We use 2-propanol as a lubricant during the grinding procedure (Fig. 1).

7. A flow-injection calibration system is easy to build. This system allows obtaining concentration-response curves for one or multiple electrochemically active substances.

The calibration of the electrodes produces important information. High basal levels (>15 pA) indicate a larger electrode surface, usually resulting from a bad seal, electrode protrusion, or fissures (Fig. 5e). These electrodes usually record large oxidation current, but they are not useful for amperometric recordings because part of the exposed surface will be away from the cell. The electric noise is also increased. We discard these electrodes.

If the oxidation current is small, it means that the active surface is smaller than expected; sometimes this is caused by debris at the tip of the electrode. If after microscopic inspection the tip is narrow enough to perform an extra polish or cut, do that and repeat the calibration.

A very slow ascending slope indicates a dirty surface. The electrode tip needs to be cleaned by repolishing, cutting, or immersion in 2-propanol. A useful trick consists of placing the tip of the electrode at approx 0.5 mm over the surface of the spinning grinder wheel and then applying a few drops of 2-propanol over the surface of the grinder. The flow of the 2-propanol is usually enough to remove the debris deposited on the electrode surface.

An excessive drop in current after stopping the flow of norepinephrine in the calibration cell indicates the presence of dead volume between the carbon fiber and the insulation. These electrodes can be used to quantify secretion but not for kinetic analyses of spikes.

The main concern comes from an electrode that rapidly loses its sensibility. The causes are difficult to establish. Sometimes dirty solutions, grinder, or scalpel blades originate the problem, as does incompletely cured sealing epoxy. Also, it may be caused by the use of poor-quality carbon fibers. To test how good a given protocol for electrode making is, leave the electrode in the calibration system and give repeated norepinephrine pulses for an hour. For good electrodes, the oxidation current should not decay more than 15%.

It is desirable to recalibrate the electrodes at the end of the experiment. It will help elucidate whether apparent changes in the secretory response are caused by a decrease in the sensibility of the electrode used.

The flow system also provides valuable information about the substances (drugs) used in the experiments. Some might be electroactive and produce changes in the oxidation current by themselves. Caution should also be taken when a new substance, mainly negatively charged or highly lipophilic, is used. These substances can attach to the electrode surface, thus reducing its sensitivity, as occurs with tyramine or estrogens at high concentrations.

Finally, two electrodes with a very similar calibration profile can be interchangeable. A good practice to become familiarized with carbon electrode characteristics and limitations is to spend time at the flow cell calibration system. One of the main lessons from these observations is that attempting to compare cell recordings obtained with two different uncalibrated electrodes or before and after the same electrode has been recut or repolished will always produce erroneous results.

8. It is always preferably to acquire low-noise signals rather than trying to remove noise once the record has been acquired (see also Chapter 24, this volume). Noise reduction strategy is a combination of logical thinking and luck. Because the high amplification applied to the amperometric current, most of the noise originates at the environment of the carbon fiber electrode. To reduce noise, it will become necessary to do several trial-and-error runs and to check which maneuvers effectively reduce it. Use of an on-line Fourier analysis available with most acquisition software is helpful.

The distance of the head stage connector (British Navy connector, BNC) to the tip of the electrode should be reduced to the absolute minimum. Avoid filling the electrode with more KCl solution than strictly necessary to ensure the electrical connection. If the carbon fiber inside the electrode is long enough, avoid filling the narrow part of the electrode tip with saline. Silver wires and pellets from both the bath and the electrode should be perfectly chlorinated; we use immersion in a bleach solution for 20 min. To avoid scratching the silver wire, briefly pass the back of the glass capillaries through a Bunsen flame before using them.

Reduce as much as possible the volume and the surface of the liquid in the perfusion chamber.

9. A secretory cell is not a machine; if you are going to apply successive stimuli, leave enough recovery time between them. It is almost impossible to evaluate the kinetic features of individual spikes under conditions of strong stimulation like high K^+ . However, these stimuli can be used when kinetic analysis is not important for our studies.

As stated, sensitivity of electrodes may change during the course of an experiment. For this reason, it is recommended to perform recordings by alternating control and problem cells. To obtain enough data for statistical analysis, it is crucial to have enough cells with enough “good” secretory spikes for each experimental condition. Remember that one cell with 200 spikes statistically is $n = 1$, and it should not be compared with another cells with only 10 spikes.

Another precaution is about the stimulation system. There is no perfect one. The easiest system is the pressure-driven drug delivery micropipet. However, a glass pipet dipped in saline always leaks its contents, and the drug concentration becomes diluted at the tip. This is easy to observe by loading a puffer pipet with ink. To minimize the problem of constant exposure of the cell membrane to significant concentrations of the drug, place the pipet tip at least $40\ \mu\text{m}$ or more away from the cell. Also, every 20–30 min remove the pipet from the cell chamber and apply pressure to wash out the solution from its tip.

If you are going to record from several cells of the same coverslip, it is a good practice to start from cells situated away from the puffer side to reduce the effects of secretagogues and secretory products on the adjacent cells.

Acknowledgments We are in debt to R. Mark Wightman and Tim J. Schroeder for teaching us the technique of amperometry. We would like to thank also Juan Luis González Álvarez from the Electron Microscopy Service of the University of La Laguna for his help with EM images and O. Humberto Viveros (Yoly Scientific Consulting, Encinitas, CA) for his helpful comments on the

manuscript. This work was supported by the Spanish Ministry of Education (MEC, grant BFU2004-08038). M.S.M. is recipient of an FPI scholarship from MEC, and J.D.M. has a “Juan de la Cierva” contract from MEC.

References

1. Ponchon, J.L., Cespuglio, R., Gonon, F., Jouvét, M., and Pujol, J.F. (1979) Normal pulse polarography with carbon fiber electrodes for in vitro and in vivo determination of catecholamines. *Anal. Chem.* **51**, 1483–1486.
2. Wightman, R.M., Jankowski, J.A., Kennedy, R.T., et al. (1991) Temporally resolved catecholamine spikes correspond to single vesicle release from individual chromaffin cells. *Proc. Natl. Acad. Sci. U. S. A.* **88**, 10754–10758.
3. Borges, R., Diaz, J., Camacho, M., and Machado, J.D. (2005) A simple way to build a grinder for carbon-fibre electrodes for amperometry or voltammetry. *Pflugers Arch.* **450**, 280–282.
4. Cahill, P.S., Walker, Q.D., Finnegan, J.M., Mickelson, G.E., Travis, E.R., and Wightman, R.M. (1996) Microelectrodes for the measurement of catecholamines in biological systems. *Anal. Chem.* **68**, 3180–3186.
5. Livett, B.G. (1984) Adrenal medullary chromaffin cells in vitro. *Physiol. Rev.* **64**, 1103–1161.
6. Moro, M.A., Lopez, M.G., Gandía, L., Michelena, P., and García, A.G. (1990) Separation and culture of living adrenaline- and noradrenaline-containing cells from bovine adrenal medullae. *Anal. Biochem.* **185**, 243–248.
7. Gilabert, J.A. (2004) Necessary conditions to maintain rat adrenal chromaffin cells in primary culture. In *Cell Biology of the Chromaffin Cell* (Gandía, L., and Borges, R., eds.), Instituto Teófilo Hernando, La Laguna, Spain, pp. 269–274. Available at: <http://webpages.ull.es/users/isccb12/TheBook.htm>.
8. Sørensen, J.B., Nagy, G., Varoqueaux, F., et al. (2003) Differential control of the releasable vesicle pools by SNAP-25 splice variants and SNAP-23. *Cell* **114**, 75–86.
9. Kawagoe, K.T., Zimmerman, J.B., and Wightman, R.M. (1993) Principles of voltammetry and microelectrode surface states. *J. Neurosci. Meth.* **48**, 225–240.
10. Chow, R., and von Ruden, L. (1995) Electrochemical detection of secretion from single cells. In *Single-Channel Recording* (Sackman, B., and Neher, E., eds.), Plenum Press, New York, pp. 245–275.
11. Koh, D.S., Moody, M.W., Nguyen, T.D., and Hille, B. (2000) Regulation of exocytosis by protein kinases and Ca²⁺ in pancreatic duct epithelial cells. *J. Gen. Physiol.* **116**, 507–520.
12. Schroeder, T.J. (1994) Temporally and spatially resolved measurements of exocytosis. Doctoral thesis, Department of Chemistry, University of North Carolina, Chapel Hill.
13. Schroeder, T.J., Jankowski, J.A., Senyshyn, J., Holz, R.W., and Wightman, R.M. (1994) Zones of exocytotic release on bovine adrenal medullary cells in culture. *J. Biol. Chem.* **269**, 17215–17220.

24

Analysis of Single-Vesicle Exocytotic Events Recorded by Amperometry

Eugene V. Mosharov

1 Introduction.....	315
2 Materials.....	316
3 Methods.....	317
4 Notes.....	323
References.....	327

Summary Analysis of the shape of the amperometric spikes that originate from the oxidation of monoamine molecules released during the fusion of individual secretory vesicles provides valuable data about molecular steps involved in stimulation-dependent transmitter release. The sensitivity of amperometry permits the detection of the monoamines released from individual vesicles, giving information about intracellular transmitter homeostasis (synthesis, degradation, reuptake, etc.) and about the release probability (vesicle availability and sensitivity of fusion machinery to Ca^{+2}). Furthermore, temporal resolution of amperometry allows for the observation of the real-time kinetics of monoamine release during exocytosis. Here, we provide algorithms for computerized analysis of the amperometric signal with emphasis on routines that confer consistent determination of spike parameters on recordings with different sampling rates, signal-to-noise levels, spike durations, and surrounding signal.

Keywords Amperometry; catecholamine; exocytosis; LDCV; monoamine; quanta analysis.

1 Introduction

Carbon fiber amperometry, originally developed by Wightman and colleagues (1), has vastly influenced the contemporary view of secretory neurotransmission by providing valuable information about the fine kinetics of transmitter release during vesicular exocytosis. During amperometric recordings, a carbon fiber microelectrode

held at a positive potential sufficient to oxidize the molecules of interest is placed against the surface of a secretory cell. Exocytotic activity is observed as amperometric “spikes”—electrochemical current caused by the transfer of electrons following transmitter oxidation. The sensitivity of amperometry permits the detection of the molecules released from individual vesicles, which can be correlated with the status of the intracellular transmitter homeostasis and an overall ability of the vesicles to participate in exocytosis. Furthermore, excellent temporal resolution of amperometry allows for the observation of the real-time kinetics of monoamine release from the vesicles. In particular, the properties of the initial “fusion pores,” narrow channels connecting vesicle lumen with the external medium, can be studied in detail.

Following amperometric data acquisition discussed in the Chapter 23, the recordings are analyzed on a computer with an aim to display the data as representative single-spike shape characteristics (Fig. 1). Changes in these parameters are then correlated with known molecular steps associated with transmitter release during vesicular fusion (reviewed in *Ref. 2*). Below is a step-by-step methodology of amperometric trace processing, including signal filtering, detection of exocytotic events, determination of spike shape characteristics, and data manipulation and statistical analysis.

2 Materials

All analytical steps can be performed by software capable of working with large waveforms generated during amperometric data acquisition. For this purpose, we use Igor Pro (WaveMetrics, Lake Oswego, OR) as this program can also be employed to acquire the data and because it has many built-in math functions and interface

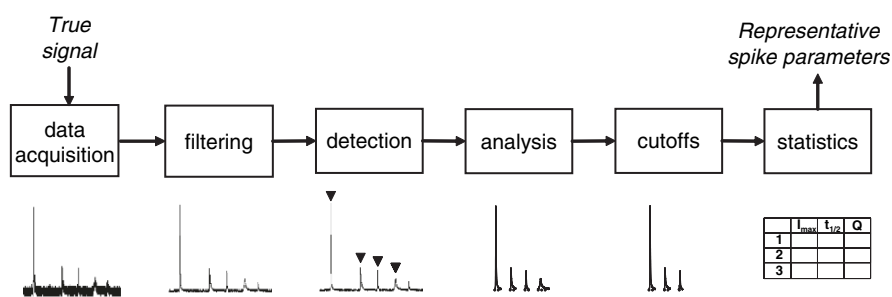


Fig. 1 An overview of amperometric data acquisition and analysis. The original “true” amperometric signal is ultimately represented by spike characteristics analyzed and pooled from multiple recordings. Each analytical step may introduce some degree of signal distortion, depending on the internal characteristics of the recording (signal frequencies, noise level, etc.) and on user-defined parameters of data acquisition and analysis (filtering, detection thresholds, cutoffs, etc.).

features that simplify the programming. Two Igor-based macros for analysis of amperometric events are freely available from Dr. Borges's laboratory (<http://webpages.ull.es/users/rborges/> [written by Miguel A. Brioso]) and Dr. Sulzer's laboratory (<http://www.sulzerlab.org/download.html> [which I wrote]).

3 Methods

3.1 Digital Filters

Before the analysis, amperometric traces are commonly digitally filtered with low-pass filters that attenuate high-frequency “white” noise or notch filters that eliminate line frequency noise at 50/60 Hz. Preference should be given to filters that are better suited for time domain analysis, have constant group delay, and do not produce rippling of the current (Gibbs phenomenon). Gaussian finite or infinite response filters qualify and can be easily programmed (*see Note 1*).

While data filtering enhances the sensitivity of spike detection, overfiltering should be avoided as it distorts spike shapes by reducing amplitude and increasing duration. The choice of an optimal filter corner frequency (-3 -dB cutoff frequency, F_c) for a particular type of recording can be simplified by using a two-step filtering protocol that allows choosing one filter (F_{c1} cutoff higher than the signal frequency) that does not distort spike shapes and another (lower F_{c2}) that increases the signal-to-noise ratio sufficiently for event detection (*see Note 2*). Because all traces in an experimental series have to be filtered using the same set of filters, the cutoffs should be chosen prior to analysis using representative recordings from all experimental groups, and the filters with the highest corner frequencies should be used for all traces.

3.2 Spike Detection

An amperometric event is identified as a spike when the time derivative of the current (dI/dt) exceeds a user-defined threshold (*see Note 3*).

1. Standard deviation of the noise of the current (SD_I) and its time derivative ($SD_{dI/dt}$) are calculated on a few-seconds long spike-free segment of a trace.
2. Spike detection threshold is set to three to five times the $SD_{dI/dt}$.
3. A search for the local maximum on the dI/dt that exceeds the threshold is performed. The location of this maximum $T(dI/dt)_{max}$ is the starting point in the analysis of each spike on the trace.

3.3 Major Spike Shape Characteristics

Consecutive steps during the analysis of individual amperometric events are shown in Fig. 2.

1. Time at spike maximum T_{max} is found between $T(dI/dt)_{max}$ and the time-point having the same current value on the descending segment of the spike (3) (solid circles on Fig. 3A).
2. To locate the spike beginning T_{bkg1} , the program searches for a steady-state current that precedes the spike and persists for a certain duration ΔT_{min} . The search is performed from $T(dI/dt)_{max}$ and toward the beginning of the trace.
 - a. The trace is divided into equal ΔT_{min} segments and the average current values are compared between the adjacent segments (Fig. 3B).
 - b. The steady state (I_{SS}) is found if two segments have currents within one SD_I of each other.
 - c. T_{bkg1} is set to the first time-point at the I_{SS} current value.

Spike width at $T(dI/dt)_{max}$ is used as the initial ΔT_{min} value (Fig. 3A), and it is essential to repeat the procedure with $2 \times \Delta T_{min}$ or longer increments to account for the presence of prespike feet with steady states (Fig. 3B). If longer increments result in lower steady-state values, the latter is used as T_{bkg1} (see Note 4).

3. When determining spike end T_{bkg2} , an increasing contribution of high-frequency noise complicates the assessment of the time-point when the transmitter concentration reaches background levels (Fig. 3C). Therefore, the search for T_{bkg2} is performed on the trace over-filtered with the F_{c2} filter (see Note 2), which usually does not affect low frequencies present in the decaying phase of the spike. To avoid artifacts associated with background drifts and spike overlaps, T_{bkg2} is determined as follows:

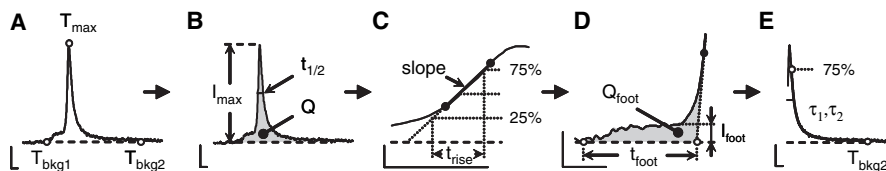


Fig. 2 Calculation of spike parameters. (A) Establishing baseline (dashed line); T_{max} , T_{bkg1} and T_{bkg2} are spike maximum, beginning, and end, respectively. (B) Calculation of amplitude, duration, and charge of a spike. (C) Rising phase parameters slope and t_{rise} from 25% to 75% of I_{max} are derived using linear fit of the current between two points on the ascending segment of the spike (thick line). (D) Prespike foot amplitude, duration, and charge are determined on a spike segment that precedes the extrapolated linear fit of the rising phase. (E) Spike falling phase is characterized by the time constants of double-exponential fit of the current between 75% of I_{max} and T_{bkg2} . Bars = 20 pA and 2.5 ms.

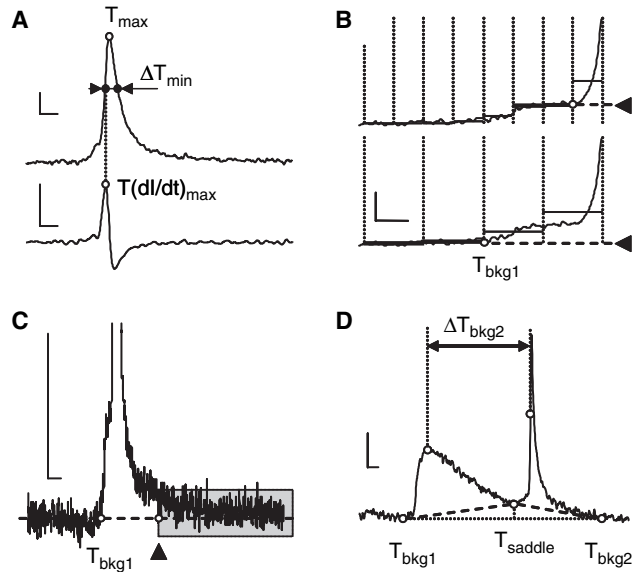


Fig. 3 (A) Algorithm for finding T_{max} . Upper panel shows amperometric current and lower panel its time derivative. (B) Search for the steady-state current that precedes a spike. Vertical lines denote trace segments with duration ΔT_{min} (upper) and $2 \times \Delta T_{min}$ (lower); horizontal solid lines represent average current within each segment; I_{ss} found by the routine are indicated by arrowheads. (C) Example of the effect of high-frequency noise on the accuracy of T_{bkg2} determination. Arrowhead indicates the first time-point at the same current as T_{bkg1} . Depending on the algorithms used to find T_{bkg2} and the degree of trace filtering, spike end might be found anywhere within the highlighted region. (D) Finding baselines of two overlapping spikes. As no current below $2 \times SD_I$ of T_{bkg1} is found within ΔT_{bkg2} , the end of the first spike is set temporary to the minimum of current between the two spikes (T_{saddle}). Dashed lines represent temporary baselines of the spikes, which are corrected later during the analysis of overlapping events (dotted line). Bars = 20 pA, 20 pA/ms, and 5 ms.

- a. The search is made for the next amperometric event; Subheading 3.2., step 3 is repeated starting from T_{max} of the current spike and forward. Time interval (ΔT_{bkg2}) between T_{max} of the current spike and $T(dI/dt)_{max}$ of the next spike or, if not found, the end of the trace is where the program will look for T_{bkg2} (Fig. 3D).
- b. Next, the routine tries to find the current that is equal to or within two SD_I of the T_{bkg1} .
- c. If unsuccessful, T_{bkg2} is set at the minimum of the current within ΔT_{bkg2} (see Subheading 3.5.).
4. Spike amplitude I_{max} (pA) is measured between the current at T_{max} and the baseline current under the spike maximum (Fig. 2B).
5. Spike half-width $t_{1/2}$ (ms) is evaluated at 50% of I_{max} .
6. The amount of transmitter released during an exocytotic event Q (A/s, Coulombs, C) is estimated from spike area above the baseline (Fig. 2B, gray). For catecholamine

release, the number of transmitter molecules is calculated as $N = Q/(n \times F)$, where F is Faraday's constant, and n is the number of electrons donated by each catechol moiety (4):

$$N[\text{molecules}] = Q[\text{pC}] \times 10^{-12} \left[\frac{\text{C}}{\text{pC}} \right] \times \frac{6.023 \times 10^{23} \left[\frac{\text{electrons}}{\text{mole}} \right]}{2 \left[\frac{\text{electrons}}{\text{molecule}} \right] \times 96,485 \left[\frac{\text{C}}{\text{mole}} \right]}$$

$$= Q[\text{pC}] \times 3.121 \times 10^6 \left[\frac{\text{molecule}}{\text{pC}} \right]$$

3.4 Fine Spike Shape Characteristics

1. Spike rising phase and prespike foot (PSF) parameters (Fig. 2C,D) are derived using the linear fit of the current between two points on the ascending segment of the spike. The middle of the linear segment is at $T(dI/dt)_{max}$ (see Note 5), while the two time-points are found at [current at $T(dI/dt)_{max}$] \pm (1/2 of ΔI between currents at T_{max} and $T(dI/dt)_{max}$] (filled circles in Fig. 4A). For a spike without PSF, these points are approx at 25% and 75% of I_{max} .
2. The tangent of the linear regression (B coefficient) is the *slope* of the spike's rising phase (pA/ms).
3. The spike beginning excluding the foot, the time-point that is also used as PSF end (point T_x in Fig. 4A,B), is found by extrapolating the linear fit onto the spike's baseline (see Note 6).
4. Spike rise time t_{rise} (ms) is measured on the extrapolated rising phase of a spike (three open circles in Fig. 4A). It therefore represents time required for a spike to reach a certain percentage of its I_{max} if PSF were not present. For example, to obtain t_{rise} from 25% to 75% of I_{max} :
 - a. The lower point ($T_{25\%}$) is calculated as $T_x + (I_{max} \times 0.25)/slope$.
 - b. The upper point ($T_{75\%}$) is found at $(I_{max} \times 0.75)$ current within the trace segment between T_{max} and T_x .
5. Time to peak tP (ms), which equals t_{rise} from zero to 100% of I_{max} , is the delta time between T_{max} and T_x .
6. The PSF end is at T_x , while its beginning is at T_{bkgI} . Foot duration t_{foot} is the delta between the two points (Fig. 4B).
7. PSF charge Q_{foot} is the area of the region that precedes the linear rising phase of the spike (Fig. 4B, grayed area).
8. Depending on PSF shape and on the aims of a study, two different methods exist to determine the amplitude of PSF, I_{foot} :
 - a. For the whole-population analysis of quantal events, I_{foot} is calculated as average current within the t_{foot} (Fig. 4C).

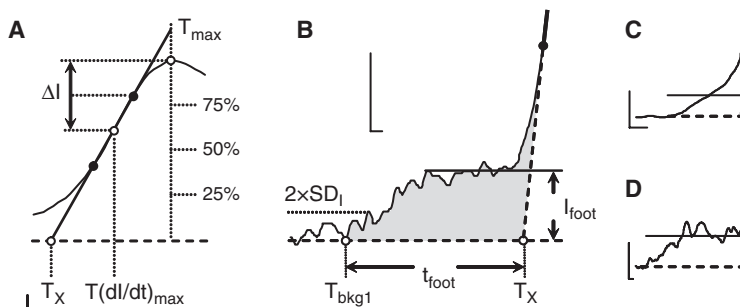


Fig. 4 Determination of spike (A) rising phase parameters and (B) PSF characteristics. Examples of PSF without (C) and with (D) detectable steady states. Horizontal lines indicate I_{foot} , which equals average (C) or steady-state (D) currents within t_{foot} . Dashed lines represent spike baselines. Bars = 10 pA and 1 ms.

- b. If analysis only considers individual spikes that display PSF with steady states, the steady state is searched for within t_{foot} employing the same algorithms that were used to define T_{bkg1} (see Subheading 3.3., step 2) (Fig. 4D); half of a user-defined minimal PSF duration is employed as ΔT_{min} .
9. The falling phases in amperometric events from large dense-core vesicle (LDCV) recordings are characterized by two time constants, τ_1 and τ_2 , of the double-exponential fit of the current between 75% of I_{max} on the falling spike phase and T_{bkg2} (Fig. 2E; see Note 7).

For each detected amperometric event, a program determines all shape characteristics as described above and then loops back to Subheading 3.2., step 3 to search for the next spike. The cycle is repeated until the end of a trace is reached.

3.5 Analysis of Overlapping Spikes

The program first finds all amperometric spikes and then checks for the overlaps. Any two spikes are considered overlapping if the current at T_{bkg2} of the first spike is higher than at its T_{bkg1} (tilted baseline), and the T_{bkg2} of the first spike coincides with the T_{bkg1} of the next spike (see Note 8). It follows that all events with T_{bkg2} defined by Subheading 3.3., step 3c overlap with other spikes and have to be separated or deleted (see Note 9). When the overlaps are separated:

1. The beginning and the end of an overlap-containing event are first refined using the same algorithms as for a singlet spike (Fig. 3D): T_{bkg1} is at the steady-state current to the left of the first spike (Subheading 3.3., step 2), and T_{bkg2} is at the same as T_{bkg1} current to the right of the last spike (Subheading 3.3., step 3b).
2. The current at the baseline of the second overlapping spike is approximated as: $I = A_0 + A_1 \times \exp((t - T_{saddle})/\tau)$, where A_0 is the current at T_{bkg2} of this spike,

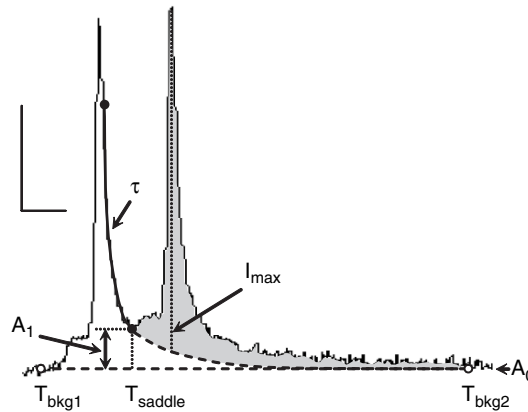


Fig. 5 Analysis of overlapping spikes. The baseline of the second spike is approximated using exponential fit constants of the falling phase of the first spike. The trace was generated by summing two identical recordings, one of which was offset by 15 ms; the first and second spikes are therefore identical. Dashed lines represent spike baselines; shaded area is an amperometric charge of the second spike. Bars = 50 pA and 10 ms.

A_1 is the delta between currents at T_{bkg2} and T_{saddle} , and τ is the slower time constant from the double-exponential fit of the falling phase of the first spike (Fig. 5).

3. I_{max} , $t_{1/2}$, and Q values are recalculated for both overlapping spikes in accordance with the new baselines.

3.6 Excluding Spikes from Analysis

The threshold for any cutoff criterion should be carefully evaluated, particularly if the cutoff parameter itself is influenced by treatments used in a study. The distribution of spike characteristics before and after a cutoff is introduced should be examined to check for possible population distortions. One obvious cutoff, which is executed by the program automatically, is to dispose of events that display unreasonable (e.g., negative) values for any of the spike characteristics. Besides that, several other cutoffs can be employed.

1. Minimal I_{max} is used as a criterion to eliminate very small spikes that are buried in the noise. In addition, spike detection becomes less dependent on the level of noise present in individual recordings—small spikes that will be detected on recordings with lower noise will be rejected anyway. Clearly, using I_{max} as a cutoff requires some preliminary analysis of the noise present in all experimental traces. Typically, on recordings from LDCV-containing cells, amperometric events with $I_{max} < 3\text{--}5$ pA are deleted.
2. Similarly, PSF that are smaller than $2 \times SD_I$ of the amperometric signal at T_{bkg1} (dotted line in Fig. 4B) are deleted (5).

3. Another cutoff sometimes used during PSF analysis is intended to only consider the feet originating from transmitter release via a restricting fusion pore (5). The duration of “native” PSFs that are present even during an instantaneous transmitter release are estimated as $0.33 \times t_{rise}$ (50–90%).
4. As spike parameters can be distorted by “diffusional filtering,” maximal $t_{1/2}$ or t_{rise} are sometimes used as cutoffs to eliminate “slow” spikes (5).
5. Because recordings having a different number of spikes have the same statistical “weight” (see Subheading 3.8.), only cells that produce a substantial number of release events, usually more than 10–20, are included in the analysis.

3.7 Whole-Trace Parameters

The *total number* of amperometric events and an *interspike interval* reflect the probability of release following stimulated secretion. Interspike intervals are calculated as durations between T_{max} values of neighboring spikes. The time constant τ of the exponential fit of their distribution can be employed to estimate the probability of random spike overlap as $P = 1 - \exp(-t/\tau)$, where t is the average $t_{1/2}$ of amperometric spikes.

3.8 Data Pooling and Statistical Analysis

Because the distributions of spike characteristics are often skewed and may contain multiple subpopulations, statistical tests that assume normal distribution of data samples (analysis of variance [ANOVA], *t*-test, etc.) usually cannot be employed. Therefore (6):

1. For every recording from a cell or release site, the median is calculated for each spike parameter (see Note 10).
2. The populations of the medians from multiple cells are analyzed using parametric or nonparametric tests.

As an additional means of analysis, the populations of spike characteristics pooled from all cells within each experimental group can be compared using nonparametric tests and normal probability plots (see Note 11). The latter are especially helpful for the analysis of subpopulations of values that might be affected by treatments exclusively.

4 Notes

1. For a Gaussian infinite impulse response (IIR) filter, the fast Fourier transform of an amperometric trace is multiplied by a Gaussian of selected width to

achieve -3 dB attenuation of frequency at a desired cutoff (F_c Hz). The Gaussian is computed as:

$$G(x) = \exp\left(-\frac{x^2}{\sigma^2}\right); \quad \text{where} \quad \sigma = \frac{F_c}{\sqrt{-\ln(1/\sqrt{2})}} \approx 1.7 \times F_c$$

A binomial finite impulse response (FIR) filter convolves the data with normalized coefficients derived from Pascal's triangle at a level equal to the smoothing parameter. The following empirical formula can be used to express the level of binomial smoothing from Igor Pro (*Coeff*, the half-width of the base of Pascal's triangle) in the units of cutoff frequency (Hz):

$$F_c = A \times \frac{SR}{\sqrt{Coeff}}, \quad \text{where } A = 0.183 \text{ and } SR \text{ is the sampling rate in hertz.}$$

- The multistep filtering protocol is shown in Fig. 6. One filter (F_{c1}) with a corner frequency twice as high as the frequency of the signal is used to reduce the noise for spike analysis; a separate, coarser filter (F_{c2}) with a corner frequency twice as low as the frequency of the signal enhances the signal-to-noise ratio on the dI/dt trace where the spikes are detected (#). The advantage of this design is that it improves the sensitivity of spike detection, whereas the trace that is used to calculate spike parameters (*) is filtered only once, making it easier to account

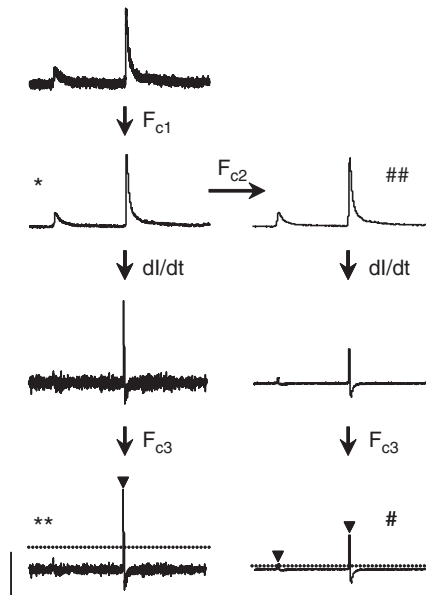


Fig. 6 The cutoffs of the low-pass Gaussian filters are F_{c1} , 600 Hz; F_{c2} , 150 Hz; F_{c3} , 300 Hz. $F_{sp}(max)$ is approx 300 Hz. Arrowheads on the bottom panels denote spikes that exceeded $5 \times SD_{dI/dt}$ (dotted lines). Bars = 20 pA, 10 pA/ms, and 100 ms.

for possible signal distortion. The third filter (F_{c3}) is employed to counter the decrease of signal-to-noise ratio during differentiation, and a lightly filtered copy of the differential is generated (***) to be used when analyzing the spike-rising phase (Subheading 3.4., step 1). Finally, a heavier filtered trace copy (##) is used during the search for T_{bkg2} (Subheading 3.3., step 3).

The ratio of the amplitude of the tallest dI/dt spike to the amplitude of the corresponding spike on the nondifferentiated trace (the latter is roughly estimated as delta current between two time-points at the intercepts of dI/dt with zero to the left and to the right of dI/dt maximum) represents twice the frequency of this “fastest” spike, $F_{sp}(\max)$. The initial F_{c1} and F_{c2} values can be set to $2 \times F_{sp}(\max)$ and $0.5 \times F_{sp}(\max)$, correspondingly; dI/dt is filtered with $F_{c3} = F_{sp}(\max)$. In practice, because of the presence of very high frequency noise, $F_{sp}(\max)$ values found on an unfiltered amperometric trace are overestimated for relatively slow spikes found on LDCV recordings. To counter this, the routine filters the trace with a $3 \times F_{sp}(\max)$ filter and then repeats the procedure for finding the $F_{sp}(\max)$ described above.

For amperometric recordings from rat chromaffin cell (sampling frequency 10–40 kHz): $F_{sp}(\max) = 200\text{--}1000$ Hz, $F_{c1} = 500\text{--}1000$ Hz, $F_{c2} = 100\text{--}400$ Hz, $F_{c3} = 200\text{--}1000$ Hz. For recordings from dopamine midbrain neurons (sampling frequency 100–200 kHz): $F_{sp}(\max) = 5\text{--}10$ kHz, $F_{c1} = 10\text{--}20$ kHz, $F_{c2} =$ not used, $F_{c3} = 5\text{--}10$ kHz.

3. On a typical amperometric trace, differentiation decreases the signal-to-noise ratio, thereby demanding additional filtering of the dI/dt (F_{c3} in Fig. 6). In addition, spikes that have slow rise times, even if they are tall, might be missed by the program. A similar problem may arise during the analysis of PSFs, which typically have rise times slower than those of the main spikes. Often, the problems with detection efficiency can be solved by optimizing the filters (e.g., decreasing F_{c2}) so that the signal-to-noise ratio on the dI/dt becomes sufficient to detect all spikes of interest and all of their features.
4. Some feet with very long steady states may still be missed by this routine, and their baseline should be readjusted manually. Also note, that because the method employs SD_i to find the steady state, it is dependent on the degree of filtering applied to the trace.
5. Because amperometric spikes are asymmetrical, filtering may shift the position of I and dI/dt maxima. Therefore, a lightly filtered copy of dI/dt is generated (indicated with ** in Fig. 6) to be used during rising phase and PSF analysis.
6. T_x is calculated as $T(dI/dt)_{\max} - slope^{-1} \times (I(dI/dt)_{\max} - I_{bkg1})$, where the last two parameters are amperometric currents at $T(dI/dt)_{\max}$ and T_{bkg1} , respectively.
7. In our previous study (2), we fit the falling phase of each spike with single- and double-exponential functions, and the latter was employed if $\chi^2(\text{single})/\chi^2(\text{double})$ was more than two. Using this ratio as a cutoff, we estimated that approx 45% of the spikes from chromaffin cell recordings have falling phases that are better fit with a double-exponential function, similar to results for PC12 cells (7). For a thorough analysis of spike falling phases, a separate analysis of the two spike subpopulations may be required.

8. To account for the presence of overlaps composed of more than two spikes, the algorithm is extended as follows:
 - a. For every spike on the trace, the measure of its proximity from the next one is calculated as T_{bkg1} of the second spike minus T_{bkg2} of the first spike minus twice the average between all spikes $t_{1/2}$. This variable, ΔT_{prox} , is negative if two spikes are closer than $2 \times t_{1/2}$.
 - b. The first spike within an overlap S_1 will have tilted baseline and $\Delta T_{prox} < 0$.
 - c. The last spike in the overlapping group S_n will be the first one after S_1 to have $\Delta T_{prox} > 0$.
 - d. To confirm that trace baseline did not return to its initial level between the two spikes, the search for the current within $2 \times SD_I$ of T_{bkg1} of S_1 is performed within the interval between the maxima of S_1 and S_n . If none is found, all spikes between S_1 and S_n are considered overlapping.
9. There have been no established guidelines regarding the exclusion of overlaps from the analysis. While it seems reasonable to eliminate overlaps when studying the fine kinetics of amperometric events (PSF, falling phase), other spike parameters ($t_{1/2}$, I_{max} , Q , t_{rise}) can often be approximated within 15% accuracy even in extreme cases when spikes overlap by 50–60% (2). The extent of spike overlap is calculated as $I_{saddle}/I_{max} \times 100$, where I_{saddle} is the current at the minimum between the spikes, and I_{max} is the amplitude of the first spike (10% overlap in Fig. 5). See Ref. 2 for more discussion.
10. The mode, the most frequently occurring value, of a data sample may work better than the median as a representative of a distribution's maximum. However, as the mode is found at the largest bin of the histogram of the sample, it can be sensitive to the choice of the bin width, especially for small populations. The mean of the values can also be used if a sample of spike characteristics is normally distributed. However, the presence of occasional outliers may significantly bias the mean. The outliers can be detected using normal probability plots (see Note 11). These values are usually 2.5 to 3 standard deviations from the sample's mean and represent less than 1% of the population (8). The presence of extreme values is less of a concern if the medians or modes of the populations are used.
11. Normal probability plotting is a graphical method for determining whether sample data conform to a hypothesized normal distribution based on visual examination of the plot (9). The data are plotted against a theoretical normal distribution in such a way that the points should form an approximate straight line. Departures from this line indicate departures from normality, and if the plot is fit with more than one line, multiple subpopulations are present (8). To make a normal probability plot:
 - a. All data points are ranked from smallest to largest.
 - b. For each observation x_i , the cumulative frequency p_i is calculated as i/n , where n is the total number of points.

- c. For each p_i , the inverse of the cumulative standard normal distribution that has a mean of zero and a standard deviation of one is calculated using $y_i = \text{NORMSINV}(p_i)$ function in Excel (Microsoft).
- d. The dependence of x_i on y_i produces a normal probability plot, which presents each data point in terms of its deviation from the predicted mean of the population.

Acknowledgments I thank Drs. David Sulzer and Ricardo Borges for critique of the manuscript. This work was supported by grants from the Parkinson's Disease Foundation and Picower Foundation awarded to D. Sulzer.

References

1. Wightman, R.M., Jankowski, J.A., Kennedy, R.T., et al. (1991) Temporally resolved catecholamine spikes correspond to single vesicle release from individual chromaffin cells. *Proc. Natl. Acad. Sci. U. S. A.* **88**, 10754–10758.
2. Mosharov, E.V., and Sulzer, D. (2005) Analysis of exocytotic events recorded by amperometry. *Nat. Methods* **2**, 651–658.
3. Segura, F., Brioso, M.A., Gómez, J.F., Machado, J.D., and Borges, R. (2000) Automatic analysis for amperometrical recordings of exocytosis. *J. Neurosci. Methods* **103**, 151–156.
4. Kissinger, P.T., Hart, J.B., and Adams, R.N. (1973) Voltammetry in brain tissue—a new neurophysiological measurement. *Brain Res.* **55**, 209–213.
5. Chow, R.H., and von Ruden, L. (1995) In *Single-Channel Recording* (Sakmann, B., and Neher, E., eds.), Plenum Press, New York, pp. 245–276.
6. Colliver, T., Hess, E.J., Pothos, E.N., Sulzer, D., and Ewing, A.G. (2000) Quantitative and statistical analysis of the shape of amperometric spikes recorded from two populations of cells. *J. Neurochem.* **74**, 1086–1097.
7. Wang, C.T., Grishanin, R., Earles, C.A., Chang, P.Y., Martin, T.F., Chapman, E.R., and Jackson, M.B. (2001) Synaptotagmin modulation of fusion pore kinetics in regulated exocytosis of dense-core vesicles. *Science* **294**, 1111–1115.
8. Sulzer, D., and Pothos, E.N. (2000) Regulation of quantal size by presynaptic mechanisms. *Rev. Neurosci.* **11**, 159–212.
9. Ott, R.L., and Longnecker, M. (2001) *An Introduction to Statistical Methods and Data Analysis*, Duxbury Press, Belmont, CA.

Part IV
Analysis of Exocytosis and Endocytosis
in Model Organisms

Application of RNAi Technology and Fluorescent Protein Markers to Study Membrane Traffic in *Caenorhabditis elegans*

Dmitry Poteryaev and Anne Spang

1 Introduction.....	331
2 Materials	333
3 Methods.....	337
4 Notes	344
References.....	346

Summary Ribonucleic acid interference (RNAi) is a powerful tool for study of the intracellular membrane transport and membrane organelle behavior in the nematode *Caenorhabditis elegans*. This model organism has gained popularity in the trafficking field because of its relative simplicity, yet multicellularity. *Caenorhabditis elegans* is fully sequenced and has an annotated genome, it is easy to maintain, and a growing number of transgenic strains bearing markers for different membrane compartments are available. *Caenorhabditis elegans* is particularly well suited for protein downregulation by RNAi because of the simple but efficient methods of double-stranded RNA (dsRNA) delivery. The phenomenon of systemic RNAi in the worm further facilitates this approach. In this chapter, we describe methods and applications of RNAi in the field of membrane traffic. We summarize the fluorescent markers used as a readout for the effects of gene knockdown in different cells and tissues and give details for data acquisition and analysis.

Keywords *C. elegans*; confocal microscopy; embryo; endocytosis; endoplasmic reticulum; GFP; membrane dynamics; membrane trafficking; protein transport; RNAi.

1 Introduction

Only recently, the potential of *Caenorhabditis elegans* as a model for membrane traffic and membrane dynamics was recognized. Comparing *C. elegans* to yeast, flies, mice, and cultured mammalian cell lines, the worm has great advantages as well as some weaknesses. It cannot beat the yeast yet when it comes to ease and speed of creating transgenic lines and knockouts. However, *C. elegans* is a multicellular

organism with differentiated tissues, which is closer to humans in terms of orthologous genes, cell organization, and intracellular interactions. The functions of genes should ideally be studied in the context of a whole organism. These studies are very difficult or sometimes impossible in vertebrates and of course not possible by definition in isolated cells in culture. *Caenorhabditis elegans*, in contrast, offers such an opportunity.

The phenomenon of ribonucleic acid interference (RNAi) was initially discovered in plants but was developed as a powerful tool for gene silencing in *C. elegans*. The biological role of RNAi seems to be to confer resistance to viruses, since the enzymatic machinery of RNAi is triggered by viral double-stranded (ds) RNA. RNAi may also protect against the self-propagation of transposons. RNAi in worms is still a much less complicated technique than in higher organisms.

Different delivery methods of dsRNA in *C. elegans* have been described in detail (1). In addition, we advise the reader to consult the Web resource devoted to

Table 1 Telltale signs of RNAi phenotypes having a trafficking defect

Phenotype	Visualization method	Possible defect	Examples
The animals are dumpy, that is, short and fat.	Dissecting binocular (Bino)	Endocytic pathway (End)	5
Molting defects. The larvae are unable to shed the old cuticle during molting.	Bino, Nomarskii optics (DIC)	End, Secretion (Sec)	16
Cuticle defects	Bino, DIC	Sec	7
Vacuolated intestine.	Bino, DIC	End, Sec	6
Swiss cheese phenotype. Embryonic blastomeres display "holes" in the cytoplasm.	DIC	End	17
Glo. Gut birefringent granules are absent or severely reduced in number.	Polarization optics or fluorescent binocular/microscope (Fl)	End	14
Coelomocytes with too big or too small endocytic vacuoles.	DIC	End	18
Weak eggshell, osmotically sensitive embryos, permeable eggshell.	DIC, Fl using FM4-64	Sec, End	19
Increased or decreased yolk granule size in oocytes/embryos.	DIC or Fl (for VIT-2::GFP strain)	End	2,5
Rme receptor-mediated endocytosis defective. Body cavity filled with GFP, while oocytes/embryos are devoid of GFP.	Fl, in VIT-2::GFP strain	End (direct evidence)	5
Cup coelomocyte uptake defective. Body cavity is filled with GFP.	Fl, in ssGFP-expressing strains	End (direct evidence)	18

C. elegans maintenance, biology, and methods, including RNAi: www.wormbook.org. We concentrate here on RNAi in the context of membrane traffic and the analysis of phenotypes related to membrane transport and dynamics. We would like to emphasize that, when it comes to choosing a specific technique, RNAi by feeding or soaking, although simple, are inferior in penetrance to RNAi by injection of dsRNA in a few ways. Generally, RNAi by injection causes stronger gene downregulation, often persisting more than one generation (if not lethal). The strength of RNAi can be more readily adjusted by injecting more or less-concentrated dsRNA. This is particularly useful in case of sterility caused by dsRNA, and when observation of embryonic or postembryonic phenotypes is desirable (2). On the other hand, in so-called genomewide (*see Note 1*) screens, there is no easy alternative to RNAi by feeding a bacterial library. The growing number of null alleles (gene knockouts) produced by two consortia will allow faster progress in understanding the regulation of membrane traffic in *C. elegans*. There are, however, several caveats in their use (*see Note 2*), making RNAi still indispensable, even in the foreseeable future, when the worm could make it to the “yeast” stage, at which for virtually all predicted open reading frames, a strain with a null allele will exist.

Studying membrane traffic and organelle behavior by RNAi requires appropriate and solid readouts. Initial characterization may be fairly simple (*Table 1*). The fine dissection of a trafficking pathway is achieved by using transgenic strains bearing fluorescent proteins marking specific membrane organelles and/or cargo. The most popular markers are listed in *Table 2* and are discussed in this chapter. Synthetic fluorescent compounds marking organelles and traffic pathways also are useful, although their application is limited in *C. elegans* (*see Note 3*). They are listed in *Table 3*.

Currently, virtually all aspects of membrane transport, such as exo- and endocytosis (3–5), intracellular (6) and intercellular (7) transport, and mitosis and cytokinesis (2,8), have sparked considerable interest in *C. elegans*.

2 Materials

2.1 dsRNA Production

1. Polymerase chain reaction (PCR): Thermal cycler; reagents for performing PCR; normal Taq polymerase, without proofreading activity, is acceptable.
2. Oligonucleotides targeting a coding segment within a gene of interest. Both forward and reverse primers must have a T7 RNA polymerase promoter sequence at 5' ends.
3. In vitro transcription kit (T7 RiboMAX Express, Promega, Madison, W.).

Table 2 List of fluorescent protein fusions marking specific membrane compartments in different *C. elegans* tissues

Fusion protein	Compartment marked	Reference
<i>Oocytes and early embryos</i>		
GFP::SPI2 (signal peptidase complex subunit)	ER	2
GFP:PH ^{PLC181} (PH domain of phospholipase C δ)	Plasma membrane	20
C:AV-1::GFP (caveolin)	Caveolin-containing granules (localization depends on the cell cycle)	21
VIT-2::GFP (yolk protein 170)	Yolk granules/endocytic compartments	5
GFP::MAN1	Inner nuclear membrane	22
<i>Coelomocytes</i>		
pmyo-3::ssGFP (secreted soluble GFP expressed in muscles)	Endocytic pathway (excluding lysosomes)	18
phsp::ssGFP (heat shock-inducible ssGFP)	Endocytic pathway (excluding lysosomes); used in pulse-chase experiments (see Note 7)	15
pmyo-3::dsRed2	Accumulates in lysosomes	23
GFP:PH ^{PLC181}	Plasma membrane	23
GFP::RAB-5	Early endosomes	23
GFP::RME-1 (EPS15 homology domain protein)	Plasma membrane/endocytic recycling compartment	9
RME-8::GFP, RME-8::RFP (DnaJ domain protein)	Endosomes (presumably both early and late)	24, 25
RAB-7::GFP	Late endosomes	17
CUP-5::GFP (putative Ca ²⁺ channel)	Late endosomes/lysosomes	25
2xFYVE::GFP	Phosphoinositide-3 phosphates (endosomes)	26
CHC::GFP (clathrin heavy chain)	Clathrin at the plasma membrane and vesicles	
Mannosidase II::GFP	Golgi	25
Cytochrome b5::GFP	Smooth ER	23
ARF-6::RFP (Arf family small GTPase)	ARF-6-dependent ERC	26
MTM-6, MTM-9::GFP (myotubularins)	ARF-6/RME-1 endocytic recycling pathway <i>Intestine</i>	26
GFP/RFP::RAB-10	Endosomes, Golgi	6
GFP/RFP::RAB-5	Early endosomes	6
hTfR::GFP (transferring receptor)	Clathrin-dependent uptake and recycling	6
hTAC::GFP (IL-2 receptor α -chain)	Clathrin-independent endocytic pathway	6

GFP::GLO-1 (gut granule-specific Rab GTPase)	Lysosomal-related gut granules	14
GFP/RFP::RAB-7	Late endosomes	6
GFP/RFP::RAB-11	Basolateral recycling endosomes	6
MANS::GFP (mannosyl transferase)	Golgi	6
GFP/RFP::RME-1	Basolateral and apical recycling endosomes	6
	<i>Hypodermal epithelium</i>	
VHA-5::RFP, VHA-8::YFP (V0 and V1 subunits of vacuolar H ⁺ -ATPase)	Apical membrane stacks, multivesicular bodies	7
WRT-2::GFP (Hedgehog-related protein)	Apical secretion pathway	7
	<i>Muscles</i>	
COGC-3, COGC-1::GFP (conserved oligomeric Golgi complex)	Golgi	27
RFP::SP12	ER	27
YFP::TRAM (translocon-associated membrane protein)	ER	27
Signal peptide::GFP::KDEL	ER	28
TOM-70::YFP/CFP	Mitochondrial outer membrane	28
GFP::DRP-1 (dynammin-related protein)	Mitochondrial scission sites	28
	<i>Markers with ubiquitous expression</i>	
VPS-27::GFP (Hrs ortholog)	Multivesicular bodies	29
LMP-1::GFP (LAMP-1)	Lysosomes	25
LGG-1::GFP (microtubule-associated anchor protein)	Autophagosomes	30
MAA-1::GFP (membrane-associated acyl-CoA binding protein)	Endosomes, Golgi	31

Table 3 Small Fluorescent Dyes for Membrane Traffic Research in *C. elegans*

Dye	Reported application	Method of delivery	Example
FM4-64 (Invitrogen)	Plasma membrane, endocytic pathway in embryos, endocytosis in the gut	Laser puncture of the eggshell and bathing (at 32 μ M), injection into body cavity, or feeding (40 μ M)	19
BSA-Texas Red (Invitrogen)	Endocytic pathway in coelomocytes	Injection into body cavity (0.1–1 mg/mL)	15
LysoTracker (Invitrogen)	Lysosomes in many tissues	Feeding (2 μ M, calculated for NGM plate volume)	17, 14
LysoSensor-dextran (Invitrogen)	Lysosomes in the gut and coelomocytes	Injection into body cavity (at 5 mg/mL)	Poteryaev, unpublished
Dehydroergosterol (Sigma-Aldrich)	Cholesterol transport, many tissues	Feeding; see Ref. 32 for details	32

2.2 Worm Maintenance and Handling

1. Dissecting binocular.
2. Worm picks made from iridium-platinum wire flattened at the picking end.
3. Mouth pipets, made from 100 \times 1.5 mm glass capillaries. One end is pulled and broken in a Pasteur pipet fashion.
4. Nematode growth medium (NGM) agar plates seeded with *Escherichia coli* strain OP50 (available from CGC, <http://biosci.umn.edu/CGC/CGChomepage.htm>).
5. M9 buffer: 2.2 mM KH_2PO_4 , 4.2 mM Na_2HPO_4 , 85.6 mM NaCl, 1 mM MgSO_4 , pH 6.5 (does not need to be adjusted).

2.3 Worm Microinjection

1. Inverted DIC microscope (such as Axiovert from Zeiss, with a free-sliding stage with centered rotation) equipped with \times 10 and \times 40 objectives, micromanipulator (Luigs and Neumann/Narashige/Zeiss), and microinjecting device with needle holder (Eppendorf Femtojet/Narashige).
2. Needle puller (Sutter Instrument).
3. Microcapillary loading tips (Microloaders, Eppendorf).
4. Needle-breaking device: A microcapillary glued onto 24 \times 60 mm glass coverslip and covered with mineral oil.
5. Heavy mineral oil (Sigma-Aldrich).
6. Injection pads: 24 \times 60 mm glass coverslips with dried drops of 0.8% agarose in water.
7. Pulled borosilicate glass capillaries with filaments (injection needles). We use capillaries from World Precision Instruments (1B120F-4, outer/inner diameter 1.2/0.68 mm, length 100 mm).

2.4 Microscopy

1. Microscope slides, coverslips.
2. Agarose pads for microscopy of worms or embryos (prepared fresh). Put a microscope slide between two other slides that have a thin stripe of laboratory adhesive tape on their flat sides. Melt 2% agarose in water and put a drop of this on the middle slide. Flatten the agarose immediately with a another slide. Remove the cover slide just before use.
3. Levamisole (tetramisole hydrochloride, Sigma): 10 mM solution in M9.
4. Confocal laser scanning microscope/multiphoton/spinning disk confocal microscope/epifluorescent microscope equipped with deconvolution software.
5. Image analysis and procession software (either the software packages at the confocal microscope workstation or freeware such as NIH ImageJ program).

2.5 *Caenorhabditis elegans* Strains

Many strains are available from *C. elegans* Genetics Center. Check <http://biosci.umn.edu/CGC/Strains/strains.htm> for availability. Otherwise, contact the researchers who produced the strain you need. The *C. elegans* research community has traditionally maintained high ethical standards in dissemination of materials.

3 Methods

3.1 Candidate Gene Approach

RNAi is a method of reverse genetics. That is, you move from a gene toward its function. Consider the following points when using the so-called candidate gene approach. The candidate gene approach, in a context of RNAi in *C. elegans*, can be defined as the study of the influence of gene downregulation on a certain biological process, such as membrane traffic in our case.

1. The trafficking defects that you aim to observe should be relatively easy and unambiguously scored. For example, if you can score a phenotype using just a fluorescent binocular, viewing worms on a plate and spending only seconds or minutes for each RNAi experiment, you can easily perform a high-throughput screen (and forget about the candidate approach). If, however, you are only able to detect a desired phenotype (i.e., cytokinesis failure or change in the behavior of a membrane organelle) by spending hours cutting worms and making movies at the microscope, then the number of your candidates is quite limited.
2. Each tissue in *C. elegans* has certain advantages and disadvantages with respect to RNAi (see Subheading 3.2.). When picking a candidate gene, try to determine its expression pattern. This can be found in the following databases:

<http://www.wormbase.org>, <http://nematode.lab.nig.ac.jp>, and <http://elegans.bcgsc.bc.ca/home/>. Naturally, the function of a gene in membrane traffic should be studied only in the tissues where it is expressed.

3. A candidate gene may have homologs (paralogs) in the *C. elegans* genome. It is helpful if it also has homologs in other model organisms and something is known about their functions. A *C. elegans* protein does not always function in the same pathway as its closest yeast or mammalian counterpart (2). Therefore, all *C. elegans* paralogs should be tested.

3.2 *Choosing the Tissue in Which to Study the Phenotype of a Gene Knockdown*

3.2.1 Germline

RNAi has the fastest and generally strongest effect in oocytes and early embryos by injection of dsRNA into hermaphrodites or by feeding *E. coli* expressing dsRNA. The oocytes and early blastomeres are ideally suited for imaging many trafficking events since they are the biggest cells in the worm. The fast embryonic divisions facilitate monitoring membrane-bound organelle behavior linked to the cell cycle. A downside of this system is the phenomenon of germline silencing of extrachromosomal reporter arrays. The integrated arrays, which are not silenced, are more difficult to produce. Thus, there are only a few markers available so far. However, this will change in the near future.

Grant and Hirsh (5) established the oocyte as a model to study receptor-mediated endocytosis in *C. elegans* and screened for novel genes involved in this process. They used the green fluorescent protein (GFP) fused to yolk protein, which is synthesized in the gut of adult hermaphrodites and taken up by maturing oocytes, to dissect the endocytic pathway. We studied cell cycle-linked dynamics of the endoplasmic reticulum (ER) in the early embryo using the ER marker SP12::GFP (2). RNAi was the main method for showing the involvement of several proteins in the rapid change of ER morphology. Oocytes and early embryos are the only cells in which one can study the effects of RNAi if it leads to embryonic lethality.

3.2.2 Coelomocytes

Coelomocytes are six specialized scavenger cells residing in the body cavity (pseudocoelom) that are highly active in fluid-phase endocytosis. Coelomocytes have become a focus of endocytic transport research because of several advantages: Their endocytic compartments are unusually big, making them easy to image (Fig. 1); transgenic animals with reporters under coelomocyte-specific promoters are easy to make; endocytic tracers are readily taken up from the body cavity. Delivery methods of the endocytic tracers to the body cavity include direct microinjection or secretion of a fluorescent reporter protein (such as soluble GFP) by muscle cells (3).

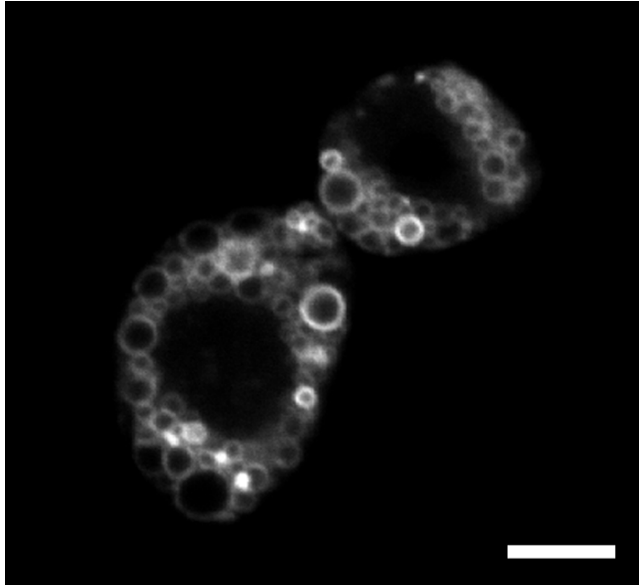


Fig. 1 A pair of coelomocytes in which GFP::RAB-7 is visualized on the membranes of late endosomes. Live imaging in the anaesthetized worm. Bar = 10 μ m.

There is no need to dissect the worm for imaging of coelomocytes. In most cases, the animals are just immobilized by levamisole and put on a slide with an agarose pad.

The effects of RNAi in coelomocytes are seen in the F_1 progeny of the animals exposed to dsRNA (regardless of delivery method). Several endocytosis-related genes have proven to be difficult to use RNAi in coelomocytes compared to germline. We recommend microinjection of dsRNA since, especially for coelomocytes, this method is most effective. The biggest collection of endocytic effectors and pathway markers is available for the coelomocytes. Coelomocytes are suited for knockdown of the genes, which are not essential for viability.

3.2.3 Hypodermal Epithelium

The epithelium is a favored model for study of the intracellular membrane transport in polarized cells. *Caenorhabditis elegans* provides an in vivo model to elucidate the mechanisms involved in apical exocytosis. For instance, Liegeois and coworkers chose to analyze apical secretion of cuticle proteins by the epidermis (7). The cuticle includes glycosylated collagens, glycosyl phosphatidylinositol-linked cuticlins, and lipid-modified Hedgehog-related peptides. The abnormal cuticle therefore may result from defects of secretion from the epithelium. This phenotype can be used as a readout in RNAi screens and would be suitable for a high-throughput approach.

3.2.4 Intestine

The worm intestine consists of large epithelial cells that, in addition to the digestive function, serve as a storage depot for the worm. Furthermore, the intestine regulates the fluid balance in the body and synthesizes and secretes the yolk for the oocytes. Naturally, secretion, endocytosis, and transcytosis are very important for the function of the intestine. Several laboratories successfully used RNAi to target the traffic-related genes in the intestine (*see Note 4*), some on a genomewide scale.

Targeting the traffic-related genes by RNAi results in several easily distinguishable phenotypes in the gut, such as failure of yolk secretion from the gut, which will appear as Rme (receptor-mediated endocytosis defective) phenotype; defects in transport of apical or basolateral fluid-phase markers (5,9); and vacuolization of the gut.

Intestinal cells also provide an easy target for RNAi. In the intestine, RNAi by feeding is as efficient as RNAi by microinjection. The effects frequently can be seen in the P₀ generation. A number of fluorescent protein reporters are available, and the intestine is easily accessible to small fluorescent dyes, which can be delivered by feeding.

3.2.5 Muscles

Several aspects of membrane organelle behavior and transport have been studied in *C. elegans* muscles, employing a number of markers under muscle-specific promoters (Table 2). Muscle cells are easy to target for RNAi by any method. However, RNAi as a method to interfere with the membrane transport in this tissue has not been used yet.

3.2.6 Neurons

Neurons respond poorly to RNAi. In the generic wild-type strain (Bristol N2), the majority of neuronal genes known to have uncoordinated phenotypes when mutated are impossible to knock down by RNAi. This can be overcome by using a mutant hypersensitive to RNAi, such as *rrf-3*. However, most of these strains have other defects and should be used with caution. Usually, *C. elegans* researchers refrain from using RNAi in neurons to study intracellular transport and rely on genetic mutants.

3.3 *Telltale Signs of RNAi Phenotypes Having a Trafficking Defect*

There are several classes of phenotypes frequently associated with defects in secretory or endocytic pathways (besides sterility and embryonic/larval lethality, which are not specific). They are easy to spot, often with the dissecting binocular. These phenotypes may help in the initial extensive analysis of the RNAi experiments (Table 1).

3.4 RNAi by Injection and Observation of Phenotype in Early Embryos Using Confocal Microscopy

3.4.1 dsRNA Preparation

The most straightforward way to obtain dsRNA for injection is to use a PCR fragment of the gene of interest as a template for RNA synthesis. The fragment must correspond to a coding segment of a gene. The length can be from 200 to 1000 bp. Within this range, longer fragments may target mRNA more efficiently. The source of deoxyribonucleic acid (DNA) for PCR amplification may be either the total genomic DNA, complementary DNA (cDNA), or individual cosmid or plasmid clones. Both forward and reverse primers must contain the T7 RNA polymerase promoters at their 5' end. Thus, both sense and antisense strands are transcribed and anneal to each other, yielding a dsRNA. The transcription reaction product is treated with phenol-chloroform and precipitated with isopropanol. The DNA template may be removed by deoxyribonuclease (DNase) digestion (*see Note 5*). The dsRNA is dissolved in TE buffer. The typical concentration range is 1–5 $\mu\text{g}/\mu\text{L}$. RNAi of essential genes involved in the secretion pathway often leads to sterility. Therefore, the dsRNA concentration must be gradually reduced to 0.2 $\mu\text{g}/\mu\text{L}$ to observe phenotypes in early embryos (2). To target two or more genes simultaneously, mix the dsRNAs in equal proportions. Beware that the efficiency of knockdown may be reduced compared to the efficiency of targeting each gene individually (10).

3.4.2 Preparing Needles for Injection

Load the injection needle with 2 μL dsRNA solution using microloader tips. Insert the needle into the holder and supply pressure to the injection system. Position the needle in the center of view ($\times 10$ objective). Withdraw the needle and put the needle-breaking device and focus at the lateral side of the microcapillary. Bring the injection needle in focus again; move close to the breaking capillary at a sharp angle. Use the sliding stage or the micromanipulator to touch the capillary slightly with the tip of the needle. Push the “inject” button immediately. The flow of liquid should be visible. If not, repeat breaking. If the opening is too small, the needle will not work and will clog immediately in the worm. If the opening is too big, your worms will die because of the big holes in their bodies.

3.4.3 Worm Mounting

Scoop one to five worms from the feeding plate with a worm pick and transfer them to the injection pad in a drop of injection oil. The worms should stick to the dry agarose. The number of animals to inject depends on your experience. To prevent fatal dehydration of the worms, the time between sticking them on the pad and rehydrating after injection should be 2–3 min.

3.4.4 Injection

Focus on the worms with the $\times 10$ objective. Switch to the $\times 40$ objective and bring the needle near the worm. With a swift movement (best achieved by manually sliding the stage), insert the needle into the worm. For RNAi, the exact location of the needle is not critical. Try to hit the distal gonadal arm, gut, or body cavity. Avoid hitting the head. Push the “inject” button. The injected part of the worm should visibly inflate. Take the needle out, push the “clean/flush” button to partially rehydrate the injected worm and to clean the needle. Proceed to the next worm on the same pad or move back to the dissecting binocular for worm recovery.

3.4.5 Recovery

Allow animals to rehydrate for 10 min after injection by adding a drop of M9 buffer on the pad.

Transfer animals with a mouth pipet to NGM agar plates with an OP50 lawn.

For RNAi in, for example, the SP12::GFP strain, inject a suitable number of L4 larvae or young hermaphrodites with dsRNAi at 1 mg/mL in injection buffer. For a single experiment, the number of animals surviving the injection should be at least 10–20.

Allow the effect of RNAi to develop over night. The earliest time-point at which the animals can be analyzed is 14–16 h postinjection. Sometimes, 24 h are needed for the full effect of RNAi to take place.

3.4.6 Preparing Specimens for Microscopy

Inspect the animals: The hermaphrodites should be alive, respond to touch, and should not spill guts. For imaging oocytes and embryos in utero, transfer worms to the object slide with an agarose pad in a drop (10 μ L) of 10 mM levamisole. Levamisole is used to immobilize and anesthetize the worms without killing them. Cover the specimen with a coverslip that has a thin layer of Vaseline spread on the edges. This provides a seal and shields the worms from excessive pressure.

To image single embryos, transfer the hermaphrodites to a drop of M9 with levamisole in an glass dish. Using fine hypodermic needles (26 gauge) as scissors, cut the worms open. The levamisole causes muscle contraction, thus helping to expel eggs from the uterus. Transfer the eggs to the agarose pads with a mouth pipet. You can also take the cut worms along; the last embryos will be released on the slide from the uterus. Seal the slide as above.

The confocal microscope should be on and running before you prepare your specimen. Some gene knockdowns lead to a permeable eggshell and osmotic sensitivity. This greatly reduces the time window for your experiment. Use your wild-type worms expressing the same fluorescent marker to figure out the best settings and parameters for imaging.

3.4.7 Imaging

1. Locate the worms or embryos with a low-magnification objective ($\times 10$ or $\times 20$) using transmitted light. For imaging with a laser, use the oil immersion $\times 63$ (numerical aperture [NA] 1.32) objective (or similar). Adjust the imaging parameters so that they do not interfere with embryonic viability within the time frame of the experiment (*see Note 6*). When imaging the dynamics of an organelle, such as ER in oocytes/early embryos, the optimal imaging parameters are critical for the interpretation of a phenotype.
2. Time between frames in time-lapse recording: With a conventional confocal microscope, the time required to scan a single frame can be quite long. Therefore, too short intervals between scans (too frequent sampling) can lead to excessive photobleaching of a fluorophore and photodamage of the cell. If the scan lasts 10 s, then the interval between scans should be at least 15 s. Ideally, the scan should last about 1 s, but this is only possible with multiphoton custom-built microscopes or with spinning disk confocal microscopes. Multiphoton microscopes allow filming the cells at a rate as fast as 1 frame per second.
3. Scan average: The imaging of fine membrane structures like the ER in the early embryo (*Fig. 2*) requires substantial averaging of the scans to improve the signal-to-noise ratio. Because of the rapid dynamics of the ER, certain restrictions apply. Use the line average instead of the frame average in the scan mode. The number of the average should not increase above eight per line.
4. Use the highest frame resolution (normally, 1024×1024 or 1024×512 pixels).
5. Photomultiplier (PMT) gain and offset: Increasing the PMT gain can improve specimen viability and reduce photobleaching since less laser power is required. Offset increase helps to reduce background and unfocused fluorescence. For representative SP12::GFP imaging, the gain and offset are set almost to the maximum.

3.4.8 Postfilming Image Processing

As a rule, try to optimize the imaging parameters, such as PMT gain and offset, scan average, and the like during imaging rather than trying to improve poor-quality images using graphic software. Linear and especially nonlinear filters should be applied with caution so original information is not obscured or misrepresented. Confocal images often benefit from the use of a sharpening filter. Gaussian blur eliminates the random pixel noise and sometimes is helpful for better representing continuous structures, such as ER sheets. All manipulations of the original image should be clearly indicated when reporting the experimental conditions. The details of confocal image postproduction can be found in *Ref. 11*.

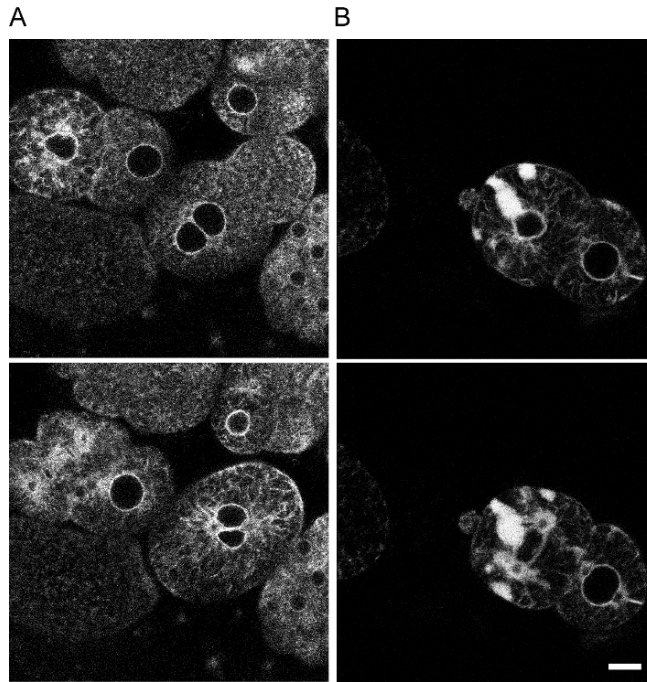


Fig. 2 The dynamics of ER during embryonic cell divisions in *C. elegans*. Time-lapse confocal microscopy of RNAi-treated GFP::SP12-expressing embryos. During the prophase and metaphase of mitosis, ER forms “sheets” that disappear during late anaphase/telophase. Each division of this cycle is repeated. A Cdc48/p97 homolog is required for ER transitions. **(A)** Control RNAi. The simultaneous RNAi of two Cdc48 homologs C41C4.8 and C06A1.1 resulted in the wild-type ER behavior during early cell division and did not interfere with ER cycling. **(B)** Knockdown by RNAi of the third Cdc48 homolog (K04G2.3) causes the ER to collapse. Bar = 10 μ m. (Modified with permission from *Ref. 2*).

4 Notes

1. One caveat of using a bacterial feeding library for RNAi on a genome-wide scale is that a significant number of clones are missing, contain no insert, or cannot be regrown on delivery of the library. Thus, the total loss can be up to 24% (12). If you plan to use individual clones from the library, always confirm the presence of an insert with a correct size by PCR or restriction digest of a plasmid. We routinely do bacterial colony PCRs with T7 primers for controls.
2. The knockout technology in *C. elegans* is based on isolation of random deletions. Often, the produced alleles eliminate only a portion of the gene target or are in-frame with the coding sequence. Without further evidence, such alleles must be presumed to retain some function. If a knockout allele is maternal

embryonic lethal, it precludes the study of the corresponding gene function at later developmental stages. By varying the strength of RNAi, it is possible to circumvent this problem. If a gene of interest has a paralog with a function that is redundant, RNAi may frequently target both genes simultaneously (providing that there is a stretch of about 100 nucleotides with 80% identity). In the knockout strain, in which only one of the paralogs is deleted, the other may compensate for the biological function.

3. The main problem with the delivery of a fluorescent dye to the embryos is the impermeable eggshell. Therefore, it must be punctured with a laser pulse, making the embryo accessible to dye in the bathing solution. Somatic tissues can be accessed if a dye is fed to the animal or injected into the body cavity (13).
4. Hermann and coworkers (14) have proposed the gut granules as a model system for understanding the formation of specialized, lysosome-related organelles, such as melanosomes and platelet granules in mammals. The gut granules could provide a simple model for several congenital lysosome-related organelle disorders in humans.
5. DNase treatment is not absolutely necessary but facilitates analysis of the transcription products by gel electrophoresis.
6. A sudden embryonic arrest during image acquisition always raises a red flag. Check if this happens as well in RNAi-treated embryos using the same dsRNA during the transmitted light imaging. If this is not the case, you have induced an arrest caused by photodamage. Lower the laser strength, acquisition time, and frequency. Normally, it should be possible to image the embryos with the confocal microscope for more than 1 h without apparent damage. The following parameters work well for us: argon laser (488 nm) at 25% power, time-lapse recording with 20-s intervals, 10-s scan duration. It is a good idea to image the wild-type or control RNAi-treated embryos with the same parameters and leave them on the slide overnight. If you see that embryos progressed in development or even hatched the next day, your experimental conditions are optimal.
7. The strain expressing secreted soluble GFP under a heat shock-inducible promoter is used as a tool to probe the lysosomal degradation pathway in coelomocytes. During an *in vivo* pulse–chase experiment, the worms are shifted to 33 °C for 30 min and then returned to ambient temperature (20–25 °C). The heat shock at 33 °C results in the secretion of a finite pulse of GFP into the pseudocoelom. The fate of the GFP can then be followed as a function of time. If the pathway to the lysosome or lysosomal function is compromised, the GFP fails to be degraded (or is degraded much slower) in the coelomocytes. In the wild type, no GFP is detected 24 h after heat shock (15).

Acknowledgments Protocols were based on many works published by members of the worm research community. We apologize for any omissions in reference. We would like to acknowledge funding by the Biozentrum of the University of Basel.

References

1. Timmons, L. (2006) Delivery methods for RNA interference in *C. elegans*. *Methods Mol. Biol.* **351**, 119–125.
2. Poteryaev, D., and Spang, A. (2005) A role of SAND-family proteins in endocytosis. *Biochem. Soc. Trans.* **33**, 606–608.
3. Fares, H., and Grant, B. (2002) Deciphering endocytosis in *Caenorhabditis elegans*. *Traffic* **3**, 11–19.
4. Koushika, S.P., and Nonet, M.L. (2000) Sorting and transport in *C. elegans*: a model system with a sequenced genome. *Curr. Opin. Cell Biol.* **12**, 517–523.
5. Grant, B., and Hirsh, D. (1999) Receptor-mediated endocytosis in the *Caenorhabditis elegans* oocyte. *Mol. Biol. Cell* **10**, 4311–4326.
6. Chen, C.C., Schweinsberg, P.J., Vashist, S., Mareiniss, D.P., Lambie, E.J., and Grant, B.D. (2006) RAB-10 is required for endocytic recycling in the *Caenorhabditis elegans* intestine. *Mol. Biol. Cell* **17**, 1286–1297.
7. Liegeois, S., Benedetto, A., Garnier, J.M., Schwab, Y., and Labouesse, M. (2006) The V0-ATPase mediates apical secretion of exosomes containing Hedgehog-related proteins in *Caenorhabditis elegans*. *J. Cell Biol.* **173**, 949–961.
8. Skop, A.R., Bergmann, D., Mohler, W.A., and White, J.G. (2001) Completion of cytokinesis in *C. elegans* requires a brefeldin A-sensitive membrane accumulation at the cleavage furrow apex. *Curr. Biol.* **11**, 735–746.
9. Grant, B., Zhang, Y., Paupard, M.C., Lin, S.X., Hall, D.H., and Hirsh, D. (2001) Evidence that RME-1, a conserved *C. elegans* EH-domain protein, functions in endocytic recycling. *Nat. Cell Biol.* **3**, 573–579.
10. Ahringer, J. (2006) Reverse genetics. In *WormBook C. elegans research Community*, (ed.), WormBook, doi/10.1895/wormbook.47.1, <http://www.wormbook.org>
11. Halder, G., and Paddock, S.W. (1999) Presentation of confocal images. *Methods Mol. Biol.* **122**, 373–384.
12. Lamitina, T. (2006) Functional genomic approaches in *C. elegans*. *Methods Mol. Biol.* **351**, 127–138.
13. Hutter, H. (2006) Fluorescent reporter methods. *Methods Mol. Biol.* **351**, 155–173.
14. Hermann, G.J., Schroeder, L.K., Hieb, C.A., et al. (2005) Genetic analysis of lysosomal trafficking in *Caenorhabditis elegans*. *Mol. Biol. Cell* **16**, 3273–3288.
15. Fares, H., and Greenwald, I. (2001) Regulation of endocytosis by CUP-5, the *Caenorhabditis elegans* mucopolipin-1 homolog. *Nat. Genet.* **28**, 64–68.
16. Frand, A.R., Russel, S., and Ruvkun, G. (2005) Functional genomic analysis of *C. elegans* molting. *PLoS Biol.* **3**, e312.
17. Nicot, A.S., Fares, H., Payraastre, B., Chisholm, A.D., Labouesse, M., and Laporte, J. (2006) The phosphoinositide kinase PIKfyve/Fab1p regulates terminal lysosome maturation in *Caenorhabditis elegans*. *Mol. Biol. Cell.* **17**, 3062–3074.
18. Fares, H., and Greenwald, I. (2001) Genetic analysis of endocytosis in *Caenorhabditis elegans*: coelomocyte uptake defective mutants. *Genetics*, **159**, 133–145.
19. Rappleye, C.A., Paredes, A.R., Smith, C.W., McDonald, K.L., and Aroian, R.V. (1999) The coronin-like protein POD-1 is required for anterior-posterior axis formation and cellular architecture in the nematode *Caenorhabditis elegans*. *Genes Dev.* **13**, 2838–2851.
20. Audhya, A., Hyndman, F., McLeod, I.X., et al. (2005) A complex containing the Sm protein CAR-1 and the RNA helicase CGH-1 is required for embryonic cytokinesis in *Caenorhabditis elegans*. *J. Cell Biol.* **171**, 267–279.
21. Sato, K., Sato, M., Audhya, A., Oegema, K., Schweinsberg, P., and Grant, B.D. (2006) Dynamic regulation of caveolin-1 trafficking in the germ line and embryo of *Caenorhabditis elegans*. *Mol. Biol. Cell* **17**, 3085–3094.
22. Franz, C., Askjaer, P., Antonin, W., et al. (2005) Nup155 regulates nuclear envelope and nuclear pore complex formation in nematodes and vertebrates. *EMBO J.* **24**, 3519–3531.

23. Patton, A., Knuth, S., Schaheen, B., Dang, H., Greenwald, I., and Fares, H. (2005) Endocytosis function of a ligand-gated ion channel homolog in *Caenorhabditis elegans*. *Curr. Biol.* **15**, 1045–1050.
24. Zhang, Y., Grant, B., and Hirsh, D. (2001) RME-8, a conserved J-domain protein, is required for endocytosis in *Caenorhabditis elegans*. *Mol. Biol. Cell.* **12**, 2011–2021.
25. Treusch, S., Knuth, S., Slaugenhaupt, S.A., Goldin, E., Grant, B.D., and Fares, H. (2004) *Caenorhabditis elegans* functional orthologue of human protein h-mucolipin-1 is required for lysosome biogenesis. *Proc. Natl. Acad. Sci. U. S. A.* **101**, 4483–4488.
26. Dang, H., Li, Z., Skolnik, E.Y., and Fares, H. (2004) Disease-related myotubularins function in endocytic traffic in *Caenorhabditis elegans*. *Mol Biol. Cell* **15**, 189–196.
27. Kubota, Y., Sano, M., Goda, S., Suzuki, N., and Nishiwaki, K. (2006) The conserved oligomeric Golgi complex acts in organ morphogenesis via glycosylation of an ADAM protease in *C. elegans*. *Development* **133**, 263–273.
28. Labrousse, A.M., Zappaterra, M.D., Rube, D.A., and van der Blik, A.M. (1999) *C. elegans* dynamin-related protein DRP-1 controls severing of the mitochondrial outer membrane. *Mol. Cell* **4**, 815–826.
29. Roudier, N., Lefebvre, C., and Legouis, R. (2005) CeVPS-27 is an endosomal protein required for the molting and the endocytic trafficking of the low-density lipoprotein receptor-related protein 1 in *Caenorhabditis elegans*. *Traffic* **6**, 695–705.
30. Melendez, A., Talloczy, Z., Seaman, M., Eskelinen, E.L., Hall, D.H., and Levine, B. (2003) Autophagy genes are essential for dauer development and life-span extension in *C. elegans*. *Science* **301**, 1387–1391.
31. Larsen, M.K., Tuck, S., Faergeman, N.J., and Knudsen, J. (2006) MAA-1, a novel acyl-CoA-binding protein involved in endosomal vesicle transport in *Caenorhabditis elegans*. *Mol. Biol. Cell* **17**, 4318–4329.
32. Matyash, V., Geier, C., Henske, A., et al. (2001) Distribution and transport of cholesterol in *Caenorhabditis elegans*. *Mol. Biol. Cell.* **12**, 1725–1736.

26

FM 1-43 Labeling of Synaptic Vesicle Pools at the *Drosophila* Neuromuscular Junction

Patrik Verstreken, Tomoko Ohyama, and Hugo J. Bellen

1 Introduction.....	350
2 Materials	354
3 Methods.....	357
4 Notes	366
References.....	368

Summary To maintain transmitter release during intense stimulation, neurons need to efficiently recycle vesicles at the synapse. Following membrane fusion, vesicles are reshaped and formed from the plasma membrane by bulk or clathrin-mediated endocytosis. Most synapses, including the *Drosophila* neuromuscular junction (NMJ), can also recycle synaptic vesicles directly by closing the fusion pore, a process referred to as “kiss and run.” While the process of clathrin-mediated vesicle retrieval is under intense investigation, the kiss-and-run phenomenon remains much less accepted. To gain better insight into the mechanisms of synaptic vesicle recycling, it is therefore critical not only to identify and characterize novel players involved in the process, but also to develop novel methods to study vesicle recycling. Although in recent years numerous techniques to study vesicle traffic have been developed (see also this volume), in this chapter we outline established procedures that use the fluorescent dye FM 1-43 or related compounds to study vesicle cycling. We describe how FM 1-43 can be used to study and visualize clathrin-mediated or bulk endocytosis from the presynaptic membrane as well as exocytosis of labeled vesicles at the *Drosophila* NMJ, one of the best-characterized model synapses to study synaptic function in a genetic model system.

Keywords Bouton; clathrin-mediated endocytosis; exocytosis; exo–endo cycling pool; kiss and run; live imaging; readily releasable pool; reserve pool; vesicle cycling.

1 Introduction

In *Drosophila*, genes that affect the synaptic vesicle cycle are often essential for life, and mutant animals often die during development (e.g., *Ref. 1*). Several mutations in genes critical for neurotransmitter release lead to embryonic or early larval lethality, and their small size hampers functional analyses of motor neuron function. However, most mutants affecting the vesicle cycle, without abolishing it, survive to the third-instar larval stage, allowing the study of loss of gene function at mutant third-instar neuromuscular junctions (NMJs). While the molecular mechanisms of vesicle recycling have been studied at several types of synapses, the NMJ of third-instar *Drosophila* larvae is unique in that it allows testing synaptic structure and function by combining elaborate fly genetics with the ability to conduct numerous *in vivo* functional assays, including electrophysiology, live imaging, immunohistochemistry, electron microscopy, and more. In this chapter, we focus on the use of FM 1-43 (N-(3-triethylammoniumpropyl)-4-(4-(dibutylamino)styryl)pyridinium dibromide) to follow vesicle trafficking; excellent chapters on methods for some of these other techniques appear in *Ref. 2*.

FM dyes are fluorescent molecules widely used to follow endocytosis, vesicle trafficking, and vesicle fusion/exocytosis in various systems. FM 1-43 and its derivatives (*see Fig. 1* and <http://probes.invitrogen.com/handbook/sections/1601.html>) are styryl dyes that harbor a water-soluble polar head group and a lipid-soluble hydrophobic tail, separated by a central region that determines their fluorescent properties (reviewed in *Ref. 3*). FM 1-43 is virtually nonfluorescent in aqueous solution but increases its quantum yield more than 40-fold when bound to liposomes, which have an environment very similar to synaptic vesicle membranes (4). FM dyes bind the outer membrane leaflet (or on endocytosis, the inside of a synaptic vesicle), and this membrane association is reversible, allowing the dye to be used to study vesicle fusion and exocytosis.

The affinity of an FM dye for membranes is determined by its tail region. FM variants with a long tail, such as FM 1-84, bind membranes more tightly than those with short tails, such as FM 2-10 (5). In contrast, dyes commonly used to follow vesicle endo- and exocytosis, including FM 1-43, FM 5-95, and FM 4-64 (*Fig. 1A*), show very similar membrane-binding properties, although FM 4-64 is somewhat more hydrophobic, slightly increasing its affinity for membranes. Finally, different types of FM molecules harbor different spectral properties depending on the linker between the head and the tail region (*Fig. 1A*). For example when excited with 488-nm blue light, FM 1-43 emits maximally at 598 nm, while FM 4-64 emits maximally at 750 nm, enabling double-labeling experiments with other dyes and probes (*Fig. 1B,C*).

We and others have used FM 1-43 and FM 4-64 in *Drosophila* to study not only the molecular mechanisms of endocytosis but also vesicle trafficking and exocytosis (6–13). FM 1-43 binds membranes and on endocytosis is internalized and trapped in synaptic vesicles, providing a measure of endocytic efficiency. Noteworthy, during kiss-and-run recycling, the vesicle lumen is only accessible to the extracellular

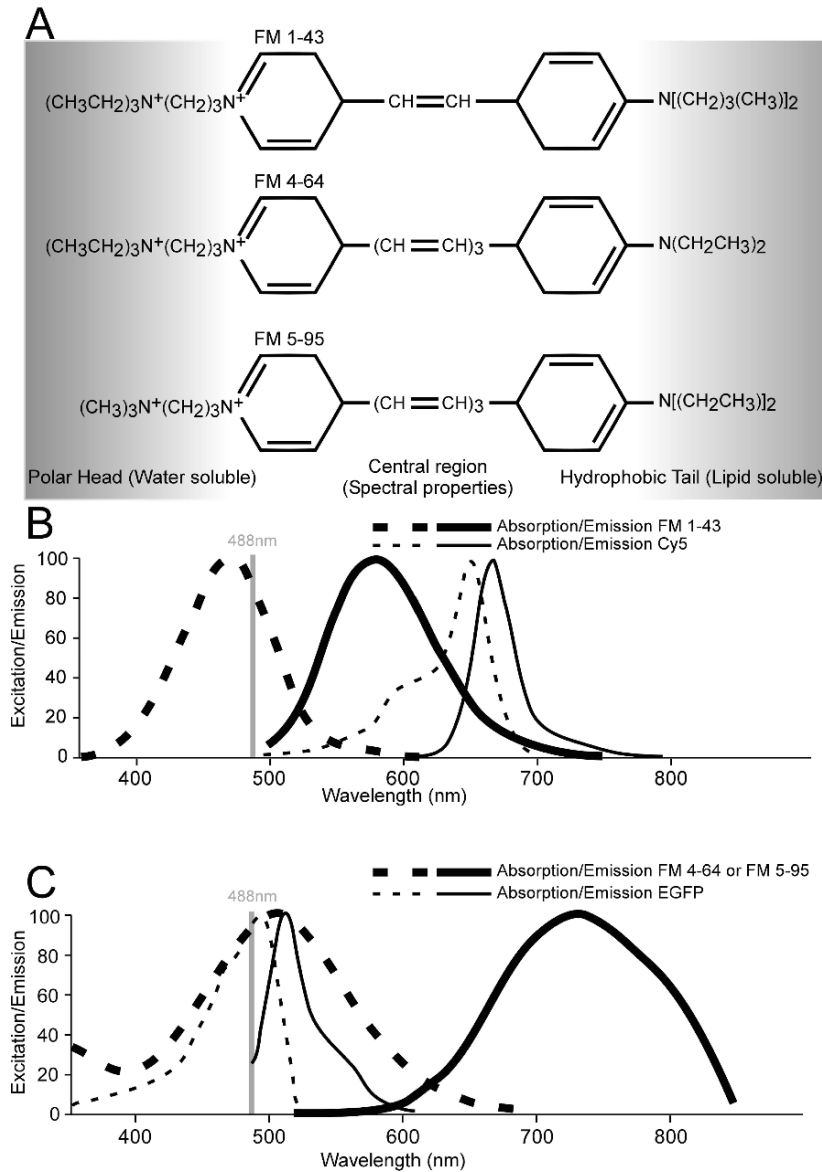


Fig. 1 Properties of FM 1-43 and other styryl dyes. **(A)** Chemical structure of FM 1-43, FM 4-64, and FM 5-95. The “head” region of these dyes is charged and therefore water soluble, while the length of their tail determines their membrane affinity. These dyes each differ in specific spectral properties as described in the text. **(B)** and **(C)** Spectral properties of FM 1-43 and FM 4-64 when bound to lipids. The spectral properties of Cy5 or eGFP (enhanced green fluorescent protein) are sufficiently different from FM 1-43 or FM 4-64, respectively, to allow for double-labeling experiments. The 488-nm laser line excites both FM dyes.

space by a fusion pore too small to allow entry of FM 1-43 (4, 14). Hence, whereas vesicles internalized by bulk endocytosis or clathrin-mediated endocytosis are readily tagged in the presence of FM 1-43, kiss-and-run vesicles seem to escape labeling by the dye (4,5,7,14–17) (but see *Refs. 18 and 19*).

Most synapses contain functionally different types of synaptic vesicles, and depending on stimulation conditions, these vesicles participate in release (Fig. 2). *Drosophila* NMJs, like several other types of synapses, harbor an exo–endo cycling pool of vesicles (ECP; also referred to as “cycling pool” in *Ref. 20*), participating in release during mild as well as intense stimulation, and a reserve pool (RP) of vesicles that only participates in release during intense stimulation (21,22). While ECP vesicles endocytose during stimulation, work from several laboratories has shown that RP vesicles are mostly derived from internalized membrane following stimulation (reviewed in *Refs. 20 and 23*). Hence, by using specific stimulation paradigms, it is possible to specifically mobilize ECP or RP vesicles and test their function in vivo at the *Drosophila* NMJ (9,22,24) (Fig. 2A,B). In Table 1, we outline some stimulation conditions that allow for mobilization of specific vesicle pools. Depending on your experimental need, these stimulation protocols can be combined or adapted using the protocols described below (for an example, see *Ref. 9*).

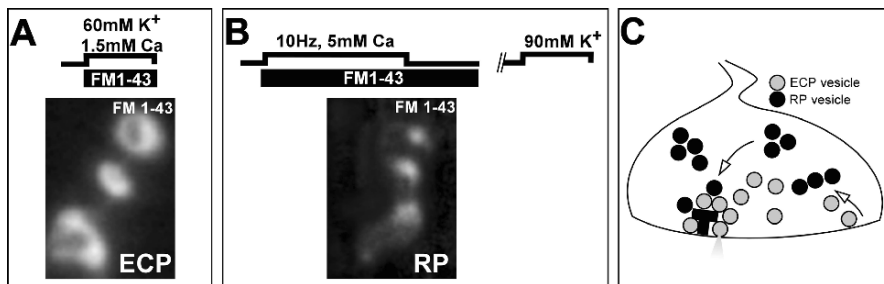


Fig. 2 Different vesicle pools at the *Drosophila* NMJ. (A) Larval fillet incubated for 5 min in HL-3 with $4\mu\text{M}$ FM 1-43, 60mM KCl, and 1.5mM calcium, washed, and imaged (see text and Table 1 for details). Note the doughnut-like bouton labeling representing FM 1-43-labeled exo–endo cycling vesicles (ECP). (B) Preparation first incubated in HL-3 with $4\mu\text{M}$ FM 1-43 and 5mM calcium and the motor nerve stimulated for 10 min at 10 Hz. The FM 1-43 was left in the bath an additional 5 min and then washed. This protocol labels both the ECP and the reserve pool (RP) (not shown). The preparation was then incubated in HL-3 with 60mM KCl and 1.5mM calcium without FM 1-43 for 5 min, washed, and imaged. This unloading protocol mobilizes (and unloads) the ECP. FM 1-43-labeled vesicles that are retained following KCl unloading are located in the reserve pool (RP). (C) Schematic representation of the different vesicle pools in a bouton of the *Drosophila* NMJ. Dark vesicles are RP vesicles; they only participate in release during intense stimulation, and newly endocytosed vesicles following stimulation will preferentially refill this vesicle pool. In contrast, ECP vesicles participate in exocytosis during both mild and intense stimulation and are refilled preferentially during stimulation (9,22,23).

Table 1 ECP and RP Loading and Unloading Protocols at the *Drosophila* Neuromuscular Junction

SV pool	No.	Stimulation protocol	Ca concentration (mM)	FM 1-43 loading period	Reference
ECP	1	60–90mM K ⁺ , 1–10 min	1.5–2	Add FM 1-43 during stimulation	9, 21, 24
	2	3Hz, 5–50 min	1.5–2	Add FM 1-43 during stimulation	9, 22
ECP + RP	1	30 Hz, 5–15 min	0.2–2	Add FM 1-43 during stimulation	21, 29
	2	10Hz, 10 min	2–5	Add FM 1-43 during stimulation and then incubate in FM 1-43 for 5 min with or without Ca ²⁺ right after stimulation	9, 21
RP	3	(1) Pretreatment with cyclosporin A ^a (2) 60mM K ⁺ , 5 min	2	Add FM 1-43 during stimulation	21, 30
	4	(1) 60mM K ⁺ stimulation, 5 min (2) Wash with HL-3 without Ca ²⁺ (3) 10Hz, 5 min	2	Add FM 1-43 during K ⁺ and nerve stimulation	24
	5	Veratridine (100μM), 5 min ^b	2	Add FM 1-43 during stimulation	22, 29
	1	30Hz, 5 min	2	Add FM 1-43 in HL-3 without Ca ²⁺ only right after stimulation, for 5 min	22
RP	2	(1) ECP + RP 1, 2, or 4 (2) Wash with HL-3 without Ca ²⁺ (3) 60–90mM K ⁺ (unload), 3–10 min	2	Add FM 1-43 during loading of ECP + RP; do not add FM 1-43 during unloading of the ECP with K ⁺ stimulation	22–24
	3	Veratridine (100μM), 5 min ^b	0	Add FM 1-43 during stimulation	22, 29

^aCyclosporin A: Inhibitor of calcineurin, Ca²⁺/calmodulin-dependent protein phosphatase 2B, which enhances endocytosis. The pretreatment consists of an incubation in 10μM cyclosporin A for 20 min in the absence of FM 1-43. Subsequent stimulation with K⁺ will label the ECP as well as the RP (21,30).

^bVeratridine: Opens voltage-gated Na⁺ channels and increases Ca²⁺ release from internal stores. Ca²⁺ release from internal stores has been linked to loading of vesicles in the RP (22,29).

2 Materials

2.1 Larval Dissection

1. Preparation of Sylgard dissection plates (Dow Corning, Midland, MI, USA, 184 Silicone Elastomer kit, Fisher cat. no. NC9644388): Mix 1 volume of silicone elastomer curing agent in 10 volumes silicone elastomer in a plastic disposable cup and place under vacuum to remove air bubbles (takes about 30 min). Pour the solution into small Petri dishes that will fit your imaging station (confocal microscope or charge-coupled device [CCD] camera); we use 35 × 10 mm plates (Corning New York, NY, USA cat. no. 430165). Place the plates horizontally in a 60 °C oven overnight for the Sylgard to polymerize.
2. Insect dissection pins (Fine Science Tools, Foster City, CA, USA Vancouver, cat. no. 260002-10): Cut the top two-thirds of the pins with scissors and use the bottom (pointy) part. You need six pins per larva.
3. Fine dissection forceps (World Precision Instruments [WPI] Sarasota, FL, USA Dumont no. 55, cat. no. 14099) and dissection scissors (Vannas fine scissors, WPI cat. no. 500086).
4. Dissection microscope (Olympus Tokyo, Japan SZ40). Muscles and motor neurons will be easier to discern with a dissection microscope with diascopic (bottom) lighting.
5. HL-3 solution without calcium: 110 mM NaCl, 5 mM KCl, 10 mM NaHCO₃, 5 mM HEPES, 30 mM sucrose, 5 mM threalose, 10 mM MgCl₂, pH 7.2. Prepare fresh; do not use this solution for longer than 2 d, and store at 4 °C.

2.2 FM 1-43 Labeling and Unloading

1. FM 1-43 stock solution (1000X): Dissolve FM 1-43 powder (Invitrogen, Carlsbad, CA, USA T-35356 or T-3163) in water to a final concentration of 4 mM. Store the FM 1-43 stock solution in 20-μL aliquots at -20 °C. FM 1-43 is light sensitive; keep in the dark. In case you wish to fix the samples after labeling, substitute FM 1-43FX (Invitrogen, F-35355; see Subheading 3.6.).
2. HL-3 + 90 mM KCl solution: 25 mM NaCl, 90 mM KCl, 10 mM NaHCO₃, 5 mM HEPES, 30 mM sucrose, 5 mM threalose, 10 mM MgCl₂, pH to 7.2. Prepare fresh; do not use this solution for longer than 2 d, and store at 4 °C. Add CaCl₂ (1 M standard solution) to obtain a final concentration of 1.5 mM CaCl₂ (or another concentration you wish to use in your experiment).

2.3 Electrical Nerve Stimulation

1. HL-3 solution with calcium: 110 mM NaCl, 5 mM KCl, 10 mM NaHCO₃, 5 mM HEPES, 30 mM sucrose, 5 mM threalose, 10 mM MgCl₂, pH to 7.2. Prepare fresh; do not use this solution for longer than 2 d, and store at 4 °C. Add CaCl₂

- (1 M standard solution) to obtain a final concentration of 1.5 mM CaCl₂ (or another concentration you wish to use in your experiment).
2. Personal computer (PC) with Clampex 8.2 software (Axon Laboratories Union City, CA, USA). Create a stimulation protocol in Clampex to control the Digidata and stimulus isolation unit. For an example of how to create a 10-Hz, 10-min stimulation program, see [Note 1](#).
 3. Digidata (Axon Instruments Union City, CA, USA 1322A) connected to the PC.
 4. Stimulus isolation unit (WPI stimulus isolator A365); connect the “Digital out” port you configured in the stimulation protocol of the Digidata to the input slot on the stimulus isolation unit (“input”). If you configured the 10-Hz, 10-min protocol as described in [Note 1](#), this will be port 0.
 5. Stimulation electrode: Pull a sharp, long, tapered glass electrode (we use 10-cm borosilicate electrodes with filament and outer diameter 1.5 mm, inner diameter 1.1 mm, Sutter Instrument, Novato, CA, USA cat. no. BF150-110-10; and a Sutter Instrument Flaming Brown micropipet puller, model P97). Carefully break the very tip of the electrode ([Fig. 3A](#)) and fire polish it using a heated filament (we use a Narishige East Meadow, NY, USA Microforge MF830) such that the edge becomes smooth ([Fig. 3B](#)) and the opening of the electrode will fit the motor neuron snugly ([Fig. 3D](#); see also *Ref. 2*).
 6. Stimulation electrode holder (A-M Systems Sequim, WA, USA suction electrode, cat. no. 573000) mounted on a Narishige micromanipulator (cat. no. M152) with magnetic stand (cat. no. GJ-8) with a fire-polished stimulation electrode (see [Fig. 3C](#)) backfilled with HL-3 solution with calcium. We use a WPI Microfil tip attached to a syringe for backfilling of electrodes (WPI cat. no. MF28G-5). Connect one of the two poles of the stimulus isolation unit output to the stimulation electrode, wrap a silver wire connected to the other pole of the stimulus isolation unit around the stimulation electrode such that the wire is positioned close to the tip of the electrode (see [Fig. 3C](#)).

2.4 Image Acquisition and Analysis

1. Water immersion lens (Zeiss Thornwood, NY, USA 40X, NA 0.75).
2. We use a Zeiss 510 confocal microscope or a Zeiss digital camera (Axiocam MRm) mounted on a Zeiss Axioskop microscope for image acquisition. Here, we describe image acquisition with a confocal microscope, but the procedure can very easily be adapted to other image acquisition systems.
3. Amira 2.2. software package (Konrad-Zuse-Zentrum Berlin [ZIB], Indeed Visual Concepts GmbH, Template Graphics Software Inc. Berlin, Germany) for data quantification and image processing.

2.5 Weakly Labeled Samples

1. Solutions and tools described in **Subheading 2.2.** with FM 1-43FX replacing FM 1-43.

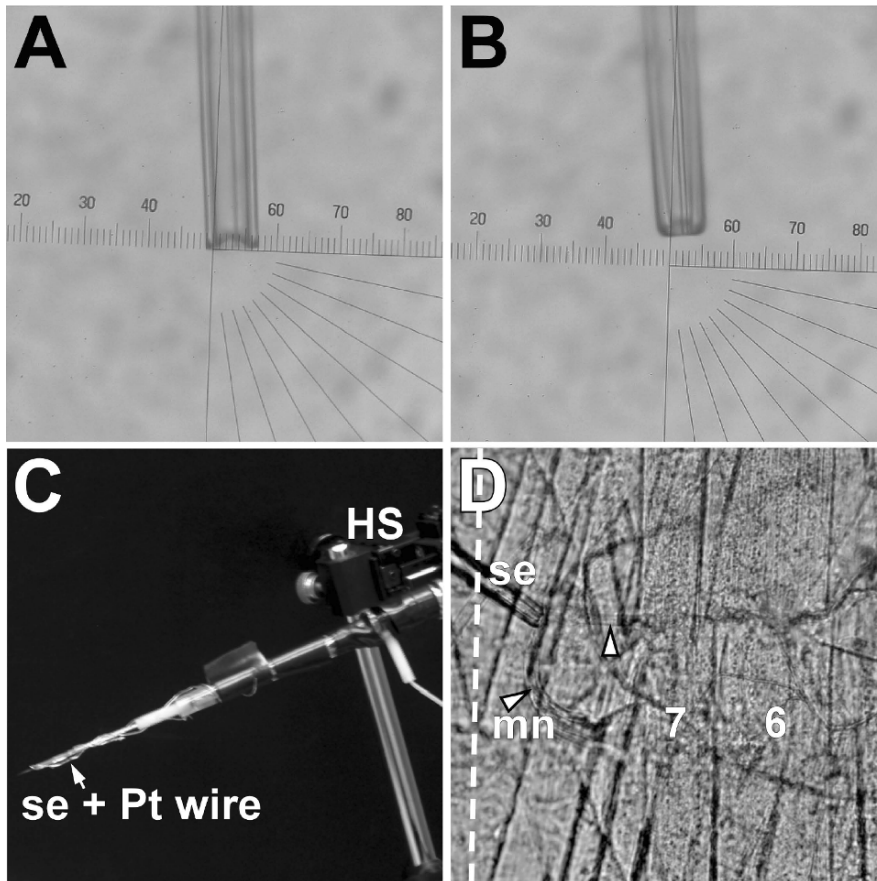


Fig. 3 Preparation of a suction electrode for nerve stimulation. **(A)** A fine, long, tapered glass electrode with a broken end. **(B)** The same electrode as in **(A)** with fire-polished edges. The opening will snugly fit the motor nerve of a wild-type larva. **(C)** A head stage (HS) with an attached suction stimulation electrode holder. The fire-polished suction electrode (se) was backfilled with bath buffer inserted in the holder and the silver (Ag) ground wire wrapped around it. **(D)** Nomarski image of the ventral musculature of an L3 larva in which one motor nerve loop (mn; marked by arrowheads) is sucked into the suction electrode (se). The brain is located on top. Motor neurons always enter the anterior portion of each hemisegment they innervate. The motor neuron innervates marked muscle fibers 6 and 7. See [Figs. 4](#) and [5](#) for additional details. The ventral midline is marked by a dashed line.

2. Formaldehyde fix solution: Prepare a fresh 3.7% (v/v) solution by diluting a 37% stock (Sigma St. Louis, MO, USA cat. no. 2106-01) ten times in HL-3 without calcium.
3. Block solution: 5% (v/v) normal goat serum (Invitrogen cat. no. PCN5000) in HL-3 without calcium, prepared fresh.
4. Rabbit anti-horseradish peroxidase (HRP) antibody (Jackson ImmunoResearch West Grove, PA, USA cat. no. 323-005-021).

5. Goat antirabbit Cy 5-conjugated immunoglobulin G (IgG) secondary antibody (Jackson ImmunoResearch cat. no. 112-175-003) or antirabbit Alexa > 647-nm conjugated antibodies (Invitrogen).
6. Mounting medium: Vectashield (Vector Burlingame, CA, USA cat. no. PK-6102), microscope slides, and coverslips.

3 Methods

We describe a set of protocols to load *Drosophila* NMJ synapses with FM 1-43 by stimulating synapses either using potassium stimulation or using electrical nerve stimulation (*see Table 1*). We subsequently describe a protocol for unloading FM 1-43, allowing not only testing for mobilization of synaptic vesicle pools but also testing the efficiency of vesicle exocytosis. We also outline a procedure to capture FM 1-43 images using a confocal microscope and a method to quantify labeling intensity following loading or unloading. Finally, we deal with weakly labeled synapses such as those in severe endocytic mutants or embryonic NMJs (*7,13*).

In general, when studying a mutant in *Drosophila*, animals with the same genetic background not harboring the mutation serve as wild-type positive controls. We believe that when performing FM 1-43 dye uptake/release experiments such as those described in Subheadings 3.2.–3.4., it is wise also to perform a negative control in which dye uptake is inhibited. One possibility is to perform a mock uptake experiment by incubating the wild-type control preparation in 4 μ M FM 1-43 in HL-3 without calcium for the same duration as the positive control. However, in such a situation, larvae are not stimulated, muscle membranes are not depolarized, and hence these negative controls are not treated exactly as the experimental samples. A better negative control is to repeat the FM 1-43 labeling protocol on *shibire^{ts1}* animals at high temperature and compare these results to controls and experimental samples that were also tested at high (and low) temperature (*see Subheading 3.6*). Hence, negative controls, positive controls, and mutant animals are treated identically, and background labeling caused by muscle contractions or stimulation protocols are similar and can be directly compared (*7,8,10*).

3.1 Dissection of L3 *Drosophila* Larvae

1. Grow wild-type, mutant larvae, or both under similar conditions and pick L3 larvae of identical size for the experiments.
2. Transfer one larva to a Sylgard plate containing dissection pins and HL-3 solution without calcium. Turn the larva dorsal side up and gently push an insect dissection pin through the anterior portion of the larva, directly posterior to the mouth hooks.
3. Gently push another pin through the posterior end of the larva, in between the two trachea that line the dorsal side, and stretch the larva longitudinally (*Fig. 4A*).

4. Very gently poke a *small* hole in the dorsal center of the larva by rubbing the sharp end of an insect pin over the cuticle (Fig. 4B).
5. Carefully, and without touching the ventral musculature, insert dissection scissors in the hole and cut the larva longitudinally open in between the two dorsally located trachea (Fig. 4C).
6. Slowly tease out the intestine and fat bodies without disrupting the musculature, central brain, and motor nerves (Fig. 4D).
7. Spread the larva open by placing an additional dissection pin in each corner of the larva, exposing the ventral body musculature. Carefully clean out any remaining intestine, trachea, and fat bodies and inspect the integrity of the muscles and motor neurons (Fig. 4E,F).
8. Wash the preparation with fresh HL-3 solution without calcium. Do not add the solution on top of the larva as this may damage the muscles; instead, gently pipet the solution on the side of the Sylgard plate.
9. Finally, remove the anterior dissection pin to relax the motor neurons that emerge from the ventral nerve cord (Fig. 3G) and cut the motor nerves by inserting the dissection scissors underneath the nerves and cutting them without touching the underlying musculature (Fig. 4H). If the motor nerves are not cut, the central nervous system (CNS) may continue innervating the NMJ, and you do not control the amount of stimulation the NMJ receives during your experiment, confounding comparison between wild-type and mutant samples.

3.2 Labeling of Synaptic Vesicles with FM 1-43 Using KCl Stimulation

1. FM 1-43 labeling solution: Add 1 μ L FM 1-43 stock solution to 1 mL HL-3 plus 90 mM KCl solution with calcium (final concentration of FM 1-43 is 4 μ M).
2. Incubate the dissected larva in FM 1-43 labeling solution by replacing the HL-3 solution without calcium. Do not add the solution on top of the larva but gently pipet the solution on the side of the larva. Start a timer; once you add the labeling solution, exocytosis and endocytosis are induced, and FM 1-43 labeling ensues. The incubation time will depend on your experiment (Table 1) but a 1-min incubation leads to robust labeling in wild-type animals (e.g., Fig. 5D). Since some mutants are temperature sensitive, it may be necessary to perform experiments at high temperature (see Note 2 if this is the case).
3. Following stimulation, remove FM 1-43 labeling solution and wash five times over a total of 5–10 min with a generous amount of HL-3 solution without calcium to stop stimulating and to remove dye not internalized. Do not add the solution on top of the larva but gently pipet the solution on the side of the larva to avoid muscle damage. Gently perfuse the wash solution by pipeting up and down.
4. Image labeled vesicles on a confocal microscope with an $\times 40$ water immersion lens and quantify intensity of labeling as described in Subheading 3.5.

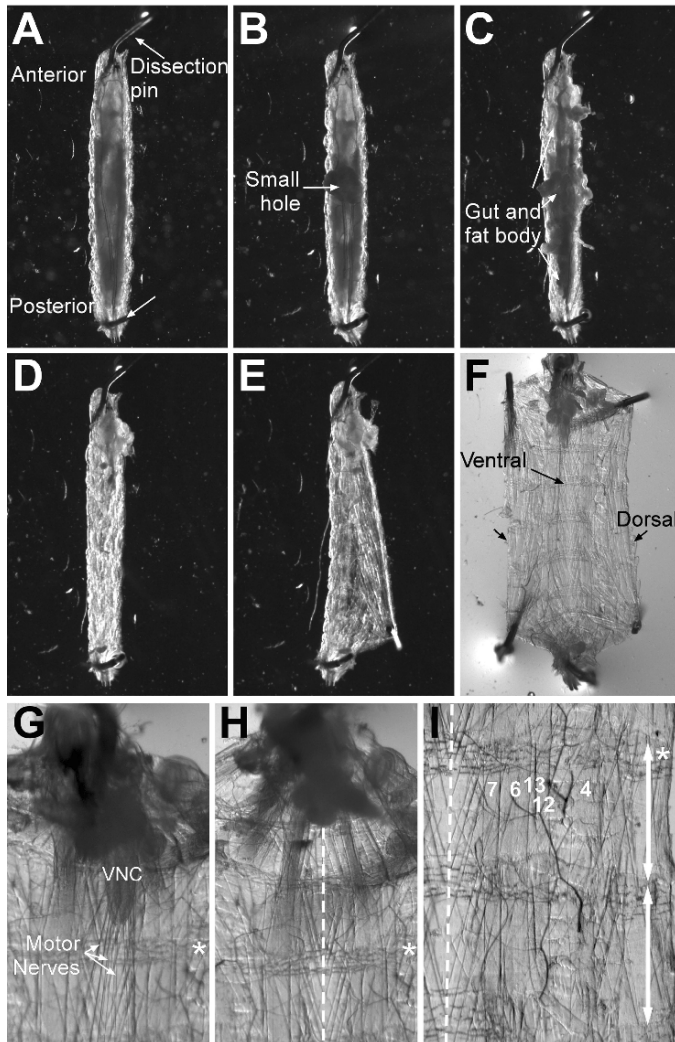


Fig. 4 Overview of a third-instar larval fillet preparation. **(A)–(F)** Different steps involved in filleting a third-instar larva. **(A)** Pinned-down L3 larva; ventral is down, dorsal is up, anterior is to the top, and posterior is to the bottom. **(B)** The same larva with a small hole poked in its dorsal side. **(C)** Dorsally cut open larva **(D)** cleaned of gut, fat bodies, and large trachea. **(E)** and **(F)** Pinned-open larva, exposing the ventral musculature (ventral is medial, and dorsal is lateral). **(G)** Higher magnification image showing the ventral nerve cord (VNC) and motor nerves that emerge from it. The asterisk marks the same location in the fillet in panels **(G)–(I)**. **(H)** The same larva with severed motor nerves, preventing direct CNS-mediated stimulation of the NMJs. The dashed line marks the ventral midline in **(H)** and **(I)**. **(I)** High-magnification image of two hemisegments (each marked by an arrow) showing the repeated pattern of muscle fibers. Fibers commonly used for analyses are marked (4, 7, 6, 13, and 12).

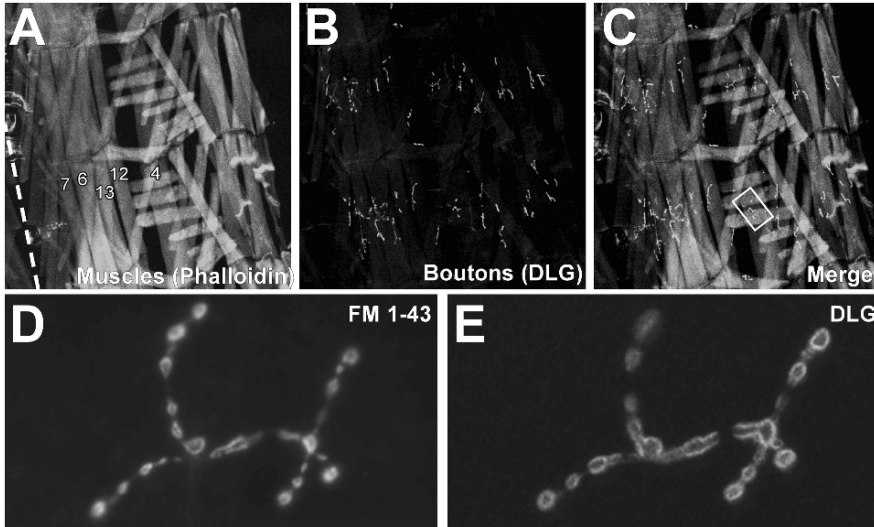


Fig. 5 FM 1-43 labeling of a third-instar larval fillet. **(A)–(E)** Third instar larval fillet incubated for 1 min in HL-3 with $4\ \mu\text{M}$ FM 1-43, $90\ \text{mM}$ KCl, and $1.5\ \text{mM}$ calcium, washed, and the FM 1-43 imaged **(D)**. The same preparation was then briefly fixed with 3.7% formaldehyde and labeled with mouse anti-DLG antibodies (28; 4F3 monoclonal antibody; Developmental Studies Hybridoma bank) used at 1:50 **(B)**, **(C)**, and **(E)** to reveal synaptic boutons at the NMJs and Alexa 635-conjugated phalloidin (Invitrogen cat. no. A34054) used at $0.001\ \text{unit}/\mu\text{L}$ **(A)** and **(C)** to reveal muscles. **(A)–(C)** two hemisegments labeled with phalloidin **(A)** and DLG **(B)**, merged in **(C)**. The dashed line in **(A)** shows the ventral midline, and muscles commonly used in the genetic analysis of synaptic function are marked. **(D)** FM 1-43 labeling (before fixation of the preparation) of the NMJ in the boxed area on muscle 4 shown in **(C)**. **(E)** The same synapse as shown in **(D)**, labeled with DLG (see **B**) following fixation of the preparation.

3.3 Labeling of Synaptic Vesicles with FM 1-43 Using Electrical Nerve Stimulation

The procedure described here is best performed on an electrophysiology rig equipped with a compound or stereomicroscope, a stimulus isolation unit, and a head stage that allows you to attach the suction electrode as described in Materials.

1. FM 1-43 solution: Add $1\ \mu\text{L}$ FM 1-43 stock solution to 1 mL HL-3 solution with calcium (final concentration of FM 1-43 is $4\ \mu\text{M}$).
2. Incubate the dissected larva in FM 1-43 solution by replacing the HL-3 solution without calcium. Do not add the solution on top of the larva but gently pipet the solution on the side of the larva.
3. Turn the stimulus isolation unit on. Then, use the head-stage controllers to bring the suction electrode to a position close to one of the cut nerves innervating the segment you wish to stimulate and suck either the end of the nerve or a loop of the

nerve into the polished end of the electrode (Fig. 3D). Make sure the stretching of the nerve does not strain the NMJs excessively. You can relax the strain by repositioning the suction electrode using the head-stage controllers.

4. Set the stimulation strength on the stimulus isolator to two times threshold. Please refer to [Note 3](#) if you need to determine the threshold for stimulation.
5. Open the 10-min, 10-Hz stimulation protocol in Clampex and click the start button. Since some mutants are temperature sensitive, it may be necessary to perform experiments at high temperature. Please refer to [Note 2](#) if this is the case.
6. When stimulation stops, quickly remove FM 1-43 labeling solution with a pipet and wash five times over 5–10 min with a generous amount of HL-3 solution without calcium to remove dye not internalized. Do not add the solution on top of the larva but gently pipet the solution on the side of the larva to avoid muscle damage. Gently perfuse the wash solution by pipeting up and down. While washing, blow the nerve out of the suction electrode and remove electrode.
7. Image labeled vesicles on a confocal microscope with an $\times 40$ water immersion lens and quantify intensity of labeling as described in Subheading 3.5.

3.4 Unloading of FM 1-43-Labeled Vesicles

We describe a protocol to unload synapses that were previously loaded with FM 1-43. The most straightforward approach is using KCl stimulation, the method described here. However, it is also possible to use nerve stimulation to unload vesicles, as is briefly described in [Note 4](#).

1. Label vesicles with FM 1-43 using KCl stimulation or nerve stimulation by following a protocol outlined in Subheading 3.2. or 3.3.
2. Remove the HL-3 solution without calcium wash solution and incubate the labeled larva in HL-3 plus 90 mM KCl solution with calcium (*without* FM 1-43). Do not add the solution on top of the larva but gently pipet the solution on the side of the larva. Start a timer; once you add the HL-3 plus 90 mM KCl solution, exocytosis and endocytosis are induced, and FM 1-43-labeled vesicles will fuse with the membrane and release their FM 1-43 in the bath solution. The incubation time depends on your experiment ([Table 1](#)), but 10-min incubation leads to unloading of most of the dye in wild-type animals. Since some mutants are temperature sensitive, it may be necessary to perform experiments at high temperature. Please refer to [Note 2](#) if this is the case.
3. Following unloading, remove the HL-3 plus 90 mM KCl solution and wash five times over 5–10 min with a generous amount of HL-3 solution without calcium to stop stimulation. Do not add the solution on top of the larva but gently pipet the solution on the side of the larva. Perfuse the wash solution by pipeting up and down.
4. Image remaining labeling on a confocal microscope with an $\times 40$ water immersion lens and quantify intensity of labeling as described in Subheading 3.5. Take extra care to image the same boutons that were imaged after loading with FM 1-43 (Subheading 3.2. or 3.3.).

3.5 *Imaging and Quantification of FM 1-43 Labeling*

3.5.1 FM 1-43 Imaging

We describe a procedure to image FM 1-43-labeled boutons using a confocal microscope, but this strategy can easily be adapted if you wish to use a CCD camera as outlined in [Note 5](#). Historically, most analyses of *Drosophila* NMJs are performed on synapses located on muscles 4, 6, 7, 12, or 13, likely because they are large and easily accessible. We therefore suggest imaging boutons on these muscles. [Figures 4H,I](#) and [5A](#) show the L3 larval musculature and the NMJs that innervate them ([Fig. 5B–E](#)). NMJs on specific muscles in each segment show a stereotypic innervation pattern (e.g., muscle 4 in [Fig. 5D,E](#)), and before imaging boutons, it is useful to familiarize yourself with the muscle and NMJ layout ([25,26](#)).

1. Place the Sylgard plate with the labeled preparation bathed in HL-3 without calcium on the stage of the confocal microscope and view FM 1-43-labeled NMJs using a mercury lamp and FITC optics under the $\times 40$ water immersion lens. (While FITC optics allow you to capture some of the FM 1-43 emission, an FITC excitation filter and TRITC emission filter configuration will allow you to capture significantly more fluorescence). Although background labeling in muscles and trachea is typically observed, clear, bright bouton labeling should be obvious in wild-type animals. You should observe labeling in individual boutons ([Figs. 2A,5D](#)). You may observe hazy rings around the boutons because of insufficient washing (*see* [Note 6](#)). If you are testing uptake in mutants, synaptic vesicle labeling may be reduced, and it may be hard (if not impossible) to identify boutons. If this is the case, please refer to Subheading 3.6.
2. When you find a string of boutons on an identified muscle you wish to image, open the program that controls the confocal microscope and excite the sample using a 488-nm laser line (at 20% laser power) and acquire fluorescence of more than 505 nm using a 505-nm long-pass filter ([Fig. 1B](#)). Please refer to Subheading 3.6. if you are using fixed samples labeled with Cy 5-conjugated antibodies as you will need to use a bandpass filter to exclude Cy 5 fluorescence in the FM 1-43 channel ([Fig. 1B](#)).
3. Use standard confocal settings and scan the boutons from top to bottom at 0.5- μm intervals. In 8-bit mode, individual pixels can acquire an intensity between 0 and 255. However, pixel values of 0 or 255 are undefined; they could just as well be less than 0 or more than 255. Hence, to avoid erroneous quantification results, it is therefore important that all bouton pixels have an intensity value of less than 255, and all muscle pixels have a value of more than 0. Finally, scanning your samples with laser light will bleach the FM 1-43; adjust the scan speed accordingly to minimize bleaching.
4. Save the image stack either as a Zeiss database file or a series of TIFF files if you plan to use Amira 2.2 for quantification of labeling intensity.

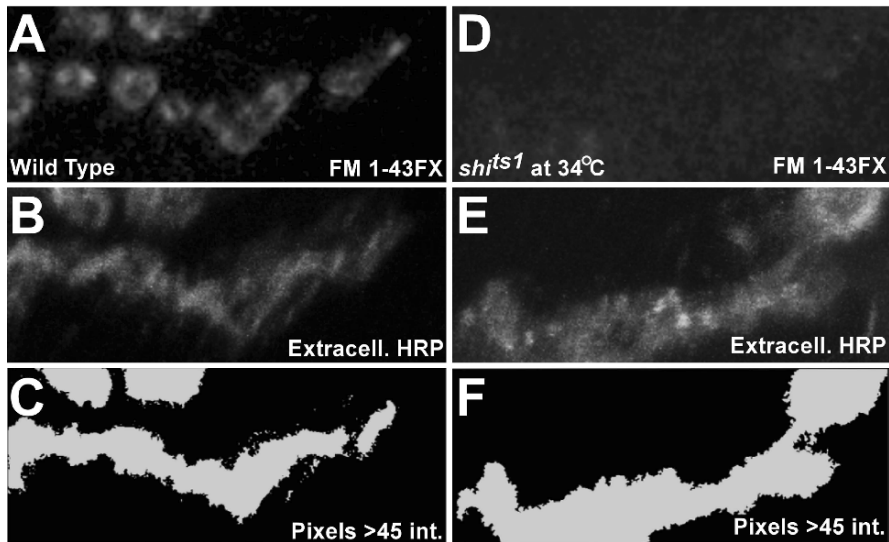


Fig. 6 Weakly labeled FM 1-43FX preparations. (A)–(C) A wild-type fillet incubated for 1 min in HL-3 with $4\mu\text{M}$ FM 1-43FX, 90mM KCl, and 1.5mM calcium, washed, fixed in formaldehyde, and labeled with anti-HRP antibodies without permeabilization (13). HRP antibodies (B) label boutons that endocytosed FM 1-43FX (A). Using Amira, the HRP channel (B) was segmented; all pixels with intensity 45 or higher are white in (C) and mark the area that is used to quantify the average pixel intensity of the FM 1-43 channel (A). (D)–(F) A *shibire^{ts1}* mutant fillet incubated at 34°C for 1 min in HL-3 with $4\mu\text{M}$ FM 1-43FX, 90mM KCl, and 1.5mM calcium, washed, fixed in formaldehyde, and labeled with anti-HRP antibodies without permeabilization (13). (D) *shibire^{ts1}* shows minimal FM 1-43FX uptake at high temperature, and boutons are not discernible; however, boutons can be revealed using extracellular anti-HRP labeling (E). Using Amira, the HRP channel was then segmented; all pixels with intensity 45 or higher are white in (F) and mark the area that is used to quantify the average pixel intensity of the FM 1-43 channel shown in (D).

3.5.2 Quantification of FM 1-43 Labeling Intensity

The basic procedure to quantify labeling intensity includes segmenting your data into a volume that comprises the pixels with intensity that you wish to quantify and then calculating the average pixel intensity within this volume. You will need to select a volume encompassing FM 1-43-labeled pixels (i.e., the boutons) and a volume that contains background pixels. In general, you can manually outline which volume is boutonnic using the FM 1-43 fluorescence as a guide. However, if you are working with weakly labeled samples, you may choose to fix the preparation and label it with antibodies that mark the boutons independent of FM 1-43 labeling, allowing you to use the independent marker as an outline of the bouton volume (Fig. 6). While we describe the basic protocol to quantify FM 1-43 labeling intensity here, a strategy using an independent marker of boutons to quantify FM 1-43 labeling intensity is explained in Subheading 3.6.

1. To quantify FM 1-43 labeling intensity: Open Amira 2.2, load the series of TIFF files.

2. Right click the data field that contains your imaging data and select “compute,” then “label voxel.”
3. Click the label voxel compute module, drag the “exterior-interior” slide bar to its maximum value of 255, and click “Do it.” This will exclude all pixels at this point from the analysis, allowing you now to manually add the pixels you wish to include.
4. To add pixels: Click the green “labels” data field and then the pencil tool to open the image segmentation editor of Amira. The image segmentation editor is a tool that will allow you to add pixels to the volume you wish to quantify. The editor shows the scanned confocal slices to guide you in adding or removing pixels to this volume. You can scan through the different confocal slices using the left and right arrows or using the slide bar in the segmentation editor.
5. Click on “interior” and, using the tools provided in the editor, highlight the boutonnic areas in each section that should be included in the analysis. When done, click 3D and “+” to add the highlighted area to the “interior” field. The selected areas in each slice should be surrounded by a brown line.
6. Select background area for quantification by right clicking below the “interior” field and select “new material.” Again, using the editor tools, select the muscle area you wish to use for background quantification in each section of the confocal stack. Click “+” to add the selected area to “material 1.”
7. To measure average pixel intensities in the selected volumes, right click the green “labels” field, select “measure” and then “tissue statistics.” Next, right click on the very left side of the tissue statistics measure module and connect “field” in the drop-down menu to the original FM 1-43 data field. Click on tissue statistics and click “do it”; a statistics data field will appear. Finally, click this data field and click “show.” The values you read in the “mean” column for “interior” and “material 1” are the mean boutonnic and background intensities, respectively. The average absolute pixel intensity is the difference between these two values.

3.6 Adapted Protocol for Weakly Labeled Samples

If you are testing FM 1-43 dye uptake in mutants that severely affects membrane uptake or if you are using embryo fillets (e.g., 1,7,8,13), it is difficult to image the boutons and to outline the boutonnic areas for quantification. In such cases, one might be tempted to image those boutons that did take up some dye, ignoring those that did not, erroneously overestimating the average FM 1-43 labeling intensity (e.g., 18). Here, we describe a protocol to label neuronal membranes independently of FM 1-43 dye uptake, allowing one to use the label as an outline of boutons for quantifying FM 1-43 intensity (Fig. 6). However, we would like to note that although this procedure may circumvent problems with weakly labeled samples, fixing of FM 1-43FX slightly reduces its fluorescence, decreasing the signal-to-noise ratio. In addition, since fixing your preparation precludes additional loading

or unloading steps, you will not be able to image the same boutons in loading/unloading experiments.

1. Follow loading/unloading protocols described in Subheadings 3.2.–3.4., replacing FM 1-43 with FM 1-43FX.
2. Remove the HL-3 without calcium and gently add formaldehyde fix solution.
3. Fix the sample for 5 min and quickly wash several times with HL-3 without calcium. Carefully remove the insect dissection pins and transfer the fixed sample to a 1.5-mL microfuge tube filled with HL-3 without calcium. Rock the tube gently and replace the HL-3 without calcium several times (> ten times) over a 10-min period.
4. Add 200 μ L block solution and 4 μ L anti-HRP antibody. Gently rock the preparation at room temperature for 30 min. Note that permeabilization with Tween-20 or Triton X-100 is not recommended as this will partly wash out the FM 1-43. However, since the anti-HRP antibody recognizes an extracellular glycoprotein (β -subunit of neuronal Na⁺K⁺ATPase); adding detergent is not necessary.
5. With a 1-mL pipet, remove the antibody (store for later reuse) and wash the preparation several times (> ten times) in HL-3 without calcium over a period of 10 min.
6. Add 200 μ L block solution and 2 μ L Cy 5-conjugated antirabbit antibody. Gently rock the preparation at room temperature for 30 min.
7. With a 1-mL pipet, remove the antibody (and store for later reuse) and wash the preparation several times (> ten times) in HL-3 without calcium over a period of 10 min.
8. Remove the preparation from the microfuge tube and place brain side up on a microscope slide in a drop of Vectashield. Cover with a coverslip and seal with transparent nail polish.
9. Use a confocal microscope to image FM 1-43 (488-nm excitation; emission: bandpass filter 505–600 nm) and Cy 5 (633-nm excitation; emission: long-pass filter > 650 nm). See also Subheading 3.5.1., steps 3 and 4 for additional instructions on how to capture and save images. You should save the FM 1-43 channel and Cy 5 channel as two separate series of TIFF files if you plan to use Amira 2.2 for quantification.
10. To quantify FM 1-43 labeling intensity in Cy 5-labeled samples, open the FM 1-43 channel series of TIFF files and the Cy 5 channel series of TIFF files in Amira 2.2. Rather than using the FM 1-43 scans to segment the data, you should use the Cy 5 channel by right clicking on the data field and choosing “compute” and then “label voxel.” Now, follow the instructions in Subheading 3.5.2., steps 3–6 to outline the bouton volumes for quantification. Alternatively, you may choose to automatically outline boutons using intensity thresholding, as is briefly discussed in [Note 7 \(Fig. 6C,F\)](#). Finally, right click the Cy 5 “.labels” field, choose “measure,” then “tissue statistics.” Next, right click on the very left side of the tissue statistics measure module and connect “field” in the drop-down menu to the FM 1-43 data field. Click on tissue statistics and click “do it”; a statistics data field will

appear. Finally, click this data field and click “show.” The values you read in the “mean” column for “interior” and “material 1” are the mean bouton and background FM 1-43 labeling intensities, respectively, as defined in the Cy5 channel. The average absolute FM 1-43 pixel intensity is the difference between these two values.

4 Notes

1. To create a 10-Hz, 10-min stimulation protocol program in Clampex, open the program and select acquire, new protocol. In the mode/rate tab, change runs/trial to 1, sweeps/run to 6000, and samples/sweep/signal to 1000 (one sweep should now be 100 ms). Change the sampling interval per signal to 100 (the sampling rate should read 10 kHz). In the trigger tab make sure “start trial with” shows “immediate” and “trigger source” shows “internal timer.” In the wave 0 tab, uncheck “analog waveform,” check “digital outputs,” and make sure “waveform 0” shows “use holding.” Then, in columns A, B, and C change “type” to “step” and “first duration (samples)” to 100, 3, and 0, respectively. Finally, the “digital bit pattern” for column A should read “0000,” for column B “0001,” and for column C “0000.” These settings run a program that will open Digital Port 0 (the fourth position in the Digital bit pattern) on the Digidata for 0.3 ms every 100 ms (i.e., 10 Hz) for 10 min. When the program runs, the stimulus isolator will stimulate the motor neuron each 100 ms for a duration of 0.3 ms over a total period of 10 min. Save the protocol for future use. Stimulation frequency and duration can be adjusted as required for your experiment.
2. It is sometimes necessary to perform FM 1-43 labeling experiments (such as those in Subheadings 3.2.–3.4.) at high temperature since some mutants show normal or marginally compromised FM 1-43 dye uptake at low temperature that is dramatically exacerbated at high temperature (Fig. 6D–F) (e.g., 10). To heat your samples, you may use a commercially available heating element (Harvard Apparatus Temperature Controller TC-202A), or you can improvise a heated chamber using a water bath. Regardless of the method used, it is absolutely critical that you monitor the temperature of the labeling solution with a thermometer during the entire experiment. If you are, for example, using *shibire^{ts1}*, a temperature-sensitive mutant that blocks all vesicle recycling at high temperature (6,7,27), the temperature should never drop below 30 °C, or some endocytosis will ensue, and synapses will be partly labeled.
3. To determine stimulation threshold of a preparation incubating in HL-3 with calcium (1.5 mM) (see Subheading 3.3.), you can stimulate the motor neuron at 1 Hz (using a 1-Hz stimulation protocol in Clampex) and then slowly increase the stimulation strength on the stimulus isolator until you observe muscle twitching in the segment stimulated (Fig. 3D). Note, however, that if your preparation at this point is incubating in FM 1-43 solution, you are inducing some FM

1-43 dye uptake. To keep dye uptake to a minimum, try to keep the number of stimuli presented during this test period limited or add the FM 1-43 only after determining the stimulation threshold.

4. In Subheading 3.4., we described a protocol for dye unloading using KCl stimulation. However, unloading using nerve stimulation is also possible. Simply incubate the labeled preparation in HL-3 with calcium (1.5 mM) but no FM 1-43 dye and stimulate the motor neuron as described in Subheading 3.3. Please refer to [Table 1](#) for paradigms that lead to loading or unloading of vesicle pools at the *Drosophila* NMJ.
5. Although image acquisition with a confocal microscope has the advantage of capturing fluorescence throughout the 3D volume of the bouton, it is also possible to image FM 1-43-labeled boutons using a CCD camera (*see* Subheadings 2.4. and 3.5.1.). A CCD camera has the advantage that it is faster and quantification of labeling intensity is a bit easier as you do not need to highlight bouton areas in each section, but only in one image (*see* Subheading 3.5.2.). Regardless of the method of imaging, comparative studies on wild-type animals show very similar absolute fluorescence intensities for both acquisition methods (around 100 arbitrary units on a scale of 0 to 255 for CS larvae labeled for 1 min with KCl stimulation; P.V., unpublished results). In summary, imaging with a confocal microscope may yield more “in-focus” images with less background, whereas a CCD camera has the advantage of speed and easier quantification.
6. If you observe hazy rings around the boutons, you may not have washed enough. This is usually membrane labeling in the subsynaptic reticulum of the muscle and does not represent labeled synaptic vesicles; extra washes should clear this labeling.
7. As an alternative to manual thresholding of bouton areas for quantification (as outlined in Subheadings 3.5.2. and 3.6.), it is also possible to semiautomatically determine bouton areas. To do this, you should follow the procedure outlined in Subheading 3.6. and stain FM 1-43-labeled preparations with a neuronal membrane marker such as anti-HRP antibodies. Scan the data and open the data files in Amira 2.2. Right click the Cy 5 channel data field and choose “compute” and then “label voxel.” Rather than excluding all pixels by dragging the “exterior-interior” slide bar to its maximum value of 255, you should place the slide bar at a lower intensity threshold value. All pixels with an intensity above this set value will be automatically included for analysis: When you click “do it” and open the segmentation editor of the .labels field, you will notice that some pixels are now included in the “interior” ([Fig. 6](#)). These are the pixels with an intensity value equal to or higher than the threshold you set. If needed, in the segmentation editor you may now manually add/remove areas you do not wish to use for quantification, and you can also add another material that contains an area for background quantification as is described in Subheading 3.5.2., step 6. Then, right click the .labels data field, choose measure and then tissue statistics. Finally, right click on the very left side of the tissue statistics measure module and connect “field” in the drop-

down menu to the FM 1-43 data field. Use the tissue statistics module in “measure” to display the boutonnic and background FM 1-43 intensities as outlined in Subheading 3.6., step 10.

Acknowledgments We would like to thank Nikolaos Giagtzoglou, Hiroshi Tsuda, and Koen J.T. Venken for helpful comments. This work was supported by HHMI, and HJB is an HHMI investigator. P.V. was supported by an R.L. Kirchstein NRS award and a Marie Curie Excellence grant.

References

1. Rohrbough, J., Rushton, E., Palanker, L., et al. (2004) Ceramidase regulates synaptic vesicle exocytosis and trafficking. *J. Neurosci.* **24**, 7789–7803.
2. Sullivan, W., Ashburner, M., and Hawley, R.S. (2000) *Drosophila Protocols*, Cold Spring Harbor Laboratory Press, Cold Spring Harbor, NY.
3. Cochilla, A.J., Angleson, J.K., and Betz, W.J. (1999) Monitoring secretory membrane with FM1-43 fluorescence. *Annu. Rev. Neurosci.* **22**, 1–10.
4. Richards, D.A., Bai, J., and Chapman, E.R. (2005) Two modes of exocytosis at hippocampal synapses revealed by rate of FM1-43 efflux from individual vesicles. *J. Cell Biol.* **168**, 929–939.
5. Klingauf, J., Kavalali, E.T., and Tsien, R.W. (1998) Kinetics and regulation of fast endocytosis at hippocampal synapses. *Nature* **394**, 581–585.
6. Ramaswami, M., Krishnan, K.S., and Kelly, R.B. (1994) Intermediates in synaptic vesicle recycling revealed by optical imaging of *Drosophila neuromuscular junctions*. *Neuron* **13**, 363–375.
7. Verstreken, P., Kjaerulff, O., Lloyd, T.E., et al. (2002) Endophilin mutations block clathrin-mediated endocytosis but not neurotransmitter release. *Cell* **109**, 101–112.
8. Verstreken, P., Koh, T.W., Schulze, K.L., et al. (2003) Synaptojanin is recruited by endophilin to promote synaptic vesicle uncoating. *Neuron* **40**, 733–48.
9. Verstreken, P., Ly, C.V., Venken, K.J., Koh, T.W., Zhou, Y., and Bellen, H.J. (2005) Synaptic mitochondria are critical for mobilization of reserve pool vesicles at *Drosophila neuromuscular junctions*. *Neuron* **47**, 365–378.
10. Koh, T.W., Verstreken, P., and Bellen, H.J. (2004) Dap160/intersectin acts as a stabilizing scaffold required for synaptic development and vesicle endocytosis. *Neuron* **43**, 193–205.
11. Marie, B., Sweeney, S.T., Poskanzer, K.E., Roos, J., Kelly, R.B., and Davis, G.W. (2004) Dap160/intersectin scaffolds the periaxial zone to achieve high-fidelity endocytosis and normal synaptic growth. *Neuron* **43**, 207–219.
12. Trotta, N., Rodesch, C.K., Fergestad, T., and Broadie, K. (2004) Cellular bases of activity-dependent paralysis in *Drosophila* stress-sensitive mutants. *J. Neurobiol.* **60**, 328–347.
13. Hiesinger, P.R., Fayyazuddin, A., Mehta, S.Q., et al. (2005) The v-ATPase V0 subunit a1 is required for a late step in synaptic vesicle exocytosis in *Drosophila*. *Cell* **121**, 607–620.
14. Sun, J.Y., Wu, X.S., and Wu, L.G. (2002) Single and multiple vesicle fusion induce different rates of endocytosis at a central synapse. *Nature* **417**, 555–559.
15. Pawlu, C., DiAntonio, A., and Heckmann, M. (2004) Postfusional control of quantal current shape. *Neuron* **42**, 607–618.
16. Klyachko, V.A., and Jackson, M.B. (2002) Capacitance steps and fusion pores of small and large-dense-core vesicles in nerve terminals. *Nature* **418**, 89–92.
17. Harata, N.C., Choi, S., Pyle, J.L., Aravanis, A.M., and Tsien, R.W. (2006) Frequency-dependent kinetics and prevalence of kiss-and-run and reuse at hippocampal synapses studied with novel quenching methods. *Neuron* **49**, 243–256.

18. Dickman, D.K., Horne, J.A., Meinertzhagen, I.A., and Schwarz, T.L. (2005) A slowed classical pathway rather than kiss-and-run mediates endocytosis at synapses lacking synaptotagmin and endophilin. *Cell* **123**, 521–533.
19. Granseth, B., Odermatt, B., Royle, S.J., and Lagnado, L. (2006) Clathrin-mediated endocytosis is the dominant mechanism of vesicle retrieval at hippocampal synapses. *Neuron* **51**, 773–786.
20. Rizzoli, S.O., and Betz, W.J. (2005) Synaptic vesicle pools. *Nat. Rev. Neurosci.* **6**, 57–69.
21. Kuromi, H., and Kidokoro, Y. (2000) Tetanic stimulation recruits vesicles from reserve pool via a cAMP-mediated process in *Drosophila* synapses. *Neuron* **27**, 133–143.
22. Kuromi, H., and Kidokoro, Y. (2002) Selective replenishment of two vesicle pools depends on the source of Ca²⁺ at the *Drosophila* synapse. *Neuron* **35**, 333–343.
23. Ly, C.V., and Verstreken, P. (2006) Mitochondria at the synapse. *Neuroscientist* **12**, 291–299.
24. Acharya, U., Edwards, M.B., Jorquera, R.A., et al. (2006) *Drosophila melanogaster* Scramblases modulate synaptic transmission. *J. Cell Biol.* **173**, 69–82.
25. Keshishian, H., Broadie, K., Chiba, A., and Bate, M. (1996) The *Drosophila* neuromuscular junction: a model system for studying synaptic development and function. *Annu. Rev. Neurosci.* **19**, 545–575.
26. Johansen, J., Halpern, M.E., Johansen, K.M., and Keshishian, H. (1989) Stereotypic morphology of glutamatergic synapses on identified muscle cells of *Drosophila* larvae. *J. Neurosci.* **9**, 710–725.
27. Delgado, R., Maureira, C., Oliva, C., Kidokoro, Y., and Labarca, P. (2000) Size of vesicle pools, rates of mobilization, and recycling at neuromuscular synapses of a *Drosophila* mutant, shibire. *Neuron* **28**, 941–953.
28. Parnas, D., Haghighi, A.P., Fetter, R.D., Kim, S.W., and Goodman, C.S. (2001) Regulation of postsynaptic structure and protein localization by the Rho-type guanine nucleotide exchange factor dPix. *Neuron* **32**, 415–424.
29. Kuromi, H., Honda, A., and Kidokoro, Y. (2004) Ca²⁺ influx through distinct routes controls exocytosis and endocytosis at *Drosophila* presynaptic terminals. *Neuron* **41**, 101–111.
30. Kuromi, H., and Kidokoro, Y. (1999) The optically determined size of exo/endo cycling vesicle pool correlates with the quantal content at the neuromuscular junction of *Drosophila* larvae. *J. Neurosci.* **19**, 1557–1565.

Probing E-Cadherin Endocytosis by Morpholino-Mediated Rab5 Knockdown in Zebrafish

Florian Ulrich and Carl-Philipp Heisenberg

1	Introduction.....	372
2	Materials.....	372
3	Methods.....	377
4	Notes.....	382
	References.....	386

Summary The controlled internalization of membrane receptors and lipids is crucial for cells to control signaling pathways and interact with their environment. During clathrin-mediated endocytosis, membrane constituents are transported via endocytic vesicles into early endosomes, from which they are further distributed within the cell. The small guanosine triphosphatase (GTPase) Rab5 is both required and sufficient for the formation of these early endosomes and can be used to experimentally address endocytic processes. Recent evidence shows that endocytic turnover of E-cadherin regulates the migration of mesendodermal cells during zebrafish gastrulation by modulating their adhesive interactions with neighboring cells. This in turn leads to effective and synchronized movement within the embryo. In this review, we discuss techniques to manipulate E-cadherin endocytosis by morpholino-mediated knockdown of *rab5* during zebrafish gastrulation. We describe the use of antibodies specifically directed against zebrafish E-cadherin to detect its intracellular localization and of in situ hybridization and primary cell culture to reveal patterns of cell migration and adhesion, respectively.

Keywords Cell migration; endocytosis; endosomes; gastrulation; mesendoderm; morpholino; small GTPase *rab5*; zebrafish.

1 Introduction

The controlled internalization of adhesion molecules such as integrins and cadherins is one mechanism by which cells modulate their adhesive interaction with other cells or substrates. Such regulation of adhesion is paramount to the control of tissue morphogenesis during development (1–3).

The guanosine triphosphatase (GTPase) dynamin mediates the internalization of plasma membrane constituents into endocytic vesicles that will undergo Rab5-mediated fusion with early endosomes. Inhibiting Rab5 activity leads to the accumulation of very small endocytic vesicles because of the failure of fusing with early endosomes and consequently inhibits endocytic transport into these intracellular compartments (4–6).

Studies showed that Wnt11-dependent mesendodermal cell migration in zebrafish embryos is regulated by dynamin- and Rab5-dependent endocytosis of E-cadherin. This control of cadherin-based, adhesive cell–cell contacts is required for effective and synchronized movement of mesendodermal progenitors to the anterior pole (7).

In this review, we present protocols that effectively probe E-cadherin endocytosis downstream of Wnt11 by interfering with Rab5 function. Rab5-mediated effects on cell migration were analyzed by in situ hybridization (ISH) of whole-mount embryos, while adhesive interactions between mesendodermal cells were tested by an in vitro cell reaggregation assay (7–11). Rab5-dependent changes in the intracellular distribution of endogenous E-cadherin were detected by immunofluorescence using a zebrafish specific E-cadherin antibody (12).

2 Materials

2.1 General Remarks

Buffers are autoclaved at 103 kPa and 121 °C. Alternatively, they can be sterile filtered through 0.22 µm pore filters (Millipore, Billerica, MA).

2.2 Zebrafish Lines

1. Zebrafish are maintained under standard laboratory conditions at 28 °C (13). For ISH analysis or cell culture analysis, any strain (AB, Gol^{*}, TL, Tü, Wik) can be used. The *slb/wnt11* embryos are homozygous carriers of the *tx226* allele (14).
2. For immunostaining and heat-shock treatment, *slb/wnt11*^{tx226} embryos transgenic for *hs-wnt11*-HA are used. These express Wnt11-HA under the control of a heat-shock promoter. Control embryos do not have the transgene and are from the same founder line (7).

3. E2 embryo medium (10X): 5 mM KCl, 15 mM NaCl, 27 mM CaCl₂, 10 mM MgSO₄, 7 mM NaHCO₃, 100 mM HEPES. Adjust to pH 6.5. Dilute 1:10 with micropore water prior to use and store at room temperature (RT).

2.3 Morpholino and Messenger Ribonucleic Acid Injections

1. For information about messenger ribonucleic acid (mRNA) and morpholino (MO) sequences, see Tables 1 and 2, respectively.
2. Danieau's buffer: 58 mM NaCl, 0.7 mM KCl, 0.4 mM MgSO₄, 0.6 mM Ca(NO₃)₂, 5.0 mM HEPES; adjust to pH 7.6.
3. Diethylpyrocarbonate (DEPC)-treated water: Dissolve DEPC in millipore water (0.1% v/v), incubate overnight at RT, and autoclave. DEPC will bind to primary and secondary amino groups and therefore inactivate enzymes such as ribonucleases (RNases). Excess DEPC degrades to ethanol and CO₂ during the procedure.
4. MO (GeneTools, Philomath, OR) are dissolved in Danieau's buffer or millipore water at a concentration of 8 mg/mL (corresponding to 1 mM) and stored as 10- μ L aliquots at -20°C. Refreezing of MO is not recommended since repeated freeze-thaw cycles reduces efficiency.
5. mRNAs are in vitro transcribed from complementary deoxyribonucleic acids (cDNAs) in pCS2 vector (15) using the mMessage mMachine kit from Ambion (Austin, TX). The mRNAs are dissolved in DEPC-treated millipore water. The mRNA solution is stable for several days/weeks at -20°C. However, for long-term storage, -80°C is recommended. See Table 1 for references.

Table 1 Plasmids for mRNA for Injections and Antisense Probes

Name	Gene	Vector	Application	Amount Injected	Reference
GAP43-GFP	Enhanced GFP, membrane bound	pCS2	mRNA injection	50–100 pg	23
Cyclops	<i>D. rerio cyclops</i>	pCS2	mRNA injection	100 pg	24
yfp-rab5c	<i>D. rerio rab5c</i>	pCS2	mRNA injection	100 pg	5
hgg1	<i>D. rerio hatching gland gene 1</i>	pBluescript	Antisense riboprobe	n/a	19
dlx3	<i>D. rerio distal-less box 3</i>	pBluescript	Antisense riboprobe	n/a	18
ntl	<i>D. rerio no tail</i>	pBluescript	Antisense riboprobe	n/a	19

Table 2 Antisense Morpholino Oligonucleotides Described in This Review

Name	Target	Sequence	Amount injected	Remarks	Reference
E-cadherin	5'-UTR	5'-TAA ATC GCA GCT CTT CCT TCC AAC G-3'	4–8 ng	n/a	10
Rab5c	Start-ATG	5'-CGCTGGTCCACCTCGC CCCGCCATG-3'	4–8 ng	Coupled to fluorescein	7

6. For mRNA injections, needles are pulled from thin-wall glass capillaries with filament (World Precision Instruments, Sarasota, FL) with a Flaming Brown P-97 needle puller (Sutter Instruments, Novato, CA) and loaded with mRNA solution using Eppendorf Microloader tips (Eppendorf, Hamburg, Germany).
7. To align embryos, use a standard glass slide (2.5 × 7.6 cm) in the lid of an empty 9-cm Petri dish (Fig. 1).

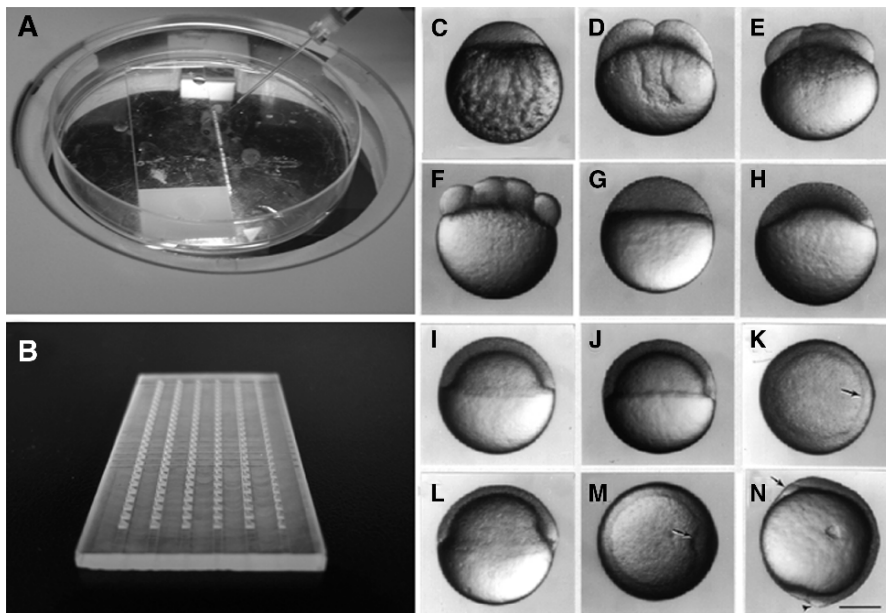


Fig. 1 Injection setup, mounting, and stages of development. (A) Injection setup. A glass needle filled with solution is angled to inject embryos that are aligned along a glass slide that sits in the Petri dish. (B) Plastic mold used for preparing agarose mounting forms. When placed onto liquid agarose solution within a 9-cm Petri dish, the knobs on this mold leave small chambers in the agarose after gelling. Each of these small chambers can harbor one embryo. (C)–(N) Embryonic stages in early zebrafish development. (C)–(F) One-, two-, four-, and eight-cell stage. Microinjections of mRNA and MO are best performed during these stages. (G) and (H) Sphere and dome stage, respectively. These are the right stages to dissociate the cells for primary cell culture. (I)–(M) Onset of gastrulation. To analyze effects on E-cadherin localization in *slb hs-wnt11-HA* embryos, perform heat shocks when cells start to internalize. This is recognizable as a slight indentation on the dorsal side (J); see also arrow in (K). When the shield has formed and the prechordal plate has been internalized (L), (M), the effects on E-cadherin localization in activated *slb hs-wnt11-HA* embryos are most easily recognizable. (N) Bud stage. The prechordal plate (arrow) has migrated anterior to the ectoderm. This is a good stage to analyze movement phenotypes by in situ hybridization. (Parts C–N reprinted from Ref. 13 with permission from Wiley-Liss, a subsidiary of John Wiley and Sons, Inc.).

2.4 *In Situ Hybridization of Embryos*

1. Tweezers used for manual dechoriation: Watchmaker forceps no. 3 or 5 (Dumont, Sarasota, FL).
2. Paraformaldehyde (PFA) solution: 4% PFA (v/v) in 81 mM Na₂HPO₄ and 19 mM NaH₂PO₄, pH 7.4. The solution is divided into 2- to 5-mL aliquots and stored at -20°C.
3. Proteinase K from Fermentas (Burlington, ON, Canada).
4. Phosphate-buffered saline (PBS): To prepare 1 L of 10X PBS solution, dissolve 80 g NaCl, 2 g KCl, 14.4 g Na₂HPO₄, and 2.4 g KH₂PO₄ in 800 mL millipore water while mixing. Fill to 1 L with water. The pH is 6.8 and will change to 7.4 on dilution to 1X PBS. Final concentrations are 137 mM NaCl, 10 mM phosphate, 2.7 mM KCl at pH 7.4.
5. PBST: 0.1% (v/v) Tween-20 in PBS.
6. SSC (saline sodium citrate) solutions: For 20X SSC, use 300 mM NaCl and 300 mM sodium citrate; adjust pH to 7.0 and store at RT. Dilute 10X or 100X and add 0.1% Tween-20 for 2X SSCT or 0.2X SSCT, respectively.
7. Maleic acid buffer (MABT) solutions: 150 mM NaCl, 100 mM maleic acid, 0.1% Tween-20. Adjust to pH 7.5 and store at RT.
8. Hybridization (Hyb⁺) solution: Dissolve Torula RNA (Sigma-Aldrich, St. Louis, MO) to 5 mg/mL in 50% (v/v) formamide, 5X SSC medium, 0.01% (v/v) Tween-20. Add 50 µg/mL heparin (Sigma-Aldrich). Adjust to pH 6.0 by adding 92 µL 1 M citric acid per 10 mL Hyb⁺. Store solution at -20°C.
9. Digoxigenin (DIG)-labeled antisense RNA: Synthesized from cDNA in pBluescript (Stratagene, La Jolla, CA) using a DIG labeling kit (Roche Diagnostics, Basel, Switzerland) and dissolved in 200 µL Hyb⁺. See [Table 1](#) for more information about antisense riboprobes.
10. As strength of the riboprobes varies, probe concentration should be tested using 1:100, 1:300, and 1:500 dilutions.
11. Blocking buffer: 2% blocking reagent (Sigma-Aldrich) in MABT.
12. Antibody solution: α-DIG antibody, alkaline phosphatase-coupled Fab fragments (Roche Diagnostics, Basel, Switzerland) 1:5000 in blocking buffer.
13. Tris base solution: 0.1 M Tris, adjusted to pH 9.5.
14. BM purple solution (Roche Diagnostics).
15. Glycerol solutions: 100% and dilutions of 30%, 50% and 70% in PBST.
16. Depression slides (Aquatic Eco-Systems, Apopka, FL).

2.5 *Cell Culture*

1. Prepare reagents and buffers under sterile conditions.
2. 96-well plates (Nunc, Wiesbaden, Germany).
3. Neubauer chamber for cell counting.

4. E2 embryo medium (10X): 5 mM KCl, 15 mM NaCl, 27 mM CaCl₂, 10 mM MgSO₄, 7 mM NaHCO₃, 100 mM HEPES. Adjust to pH 6.5. Dilute 1:10 with micropore water prior to use and store at RT.
5. Pronase solution: 2 mg/mL pronase (Roche Diagnostics) in E2 medium.
6. Fibronectin: 0.5 mg/mL bovine fibronectin (Invitrogen, Paisley, UK) in PBS; store as 10- μ L aliquots at -20 °C.
7. Agarose dishes: 2% low-melting-point agarose (Roche Diagnostics) in E2 medium. Heat to 50 °C, pour into 6.5-cm Petri dishes, and let gel. Dishes that are not immediately used should be sealed with Parafilm to prevent drying and stored at 4 °C for several days.
8. Trypsin/EDTA (ethylenediaminetetraacetic acid) solution from Invitrogen.
9. Cell culture medium: 62.5 mL Dulbecco's modified Eagle's medium (DMEM); 1.0 mL penicillin/streptomycin; 1.0 mL transferrin-selenium-X; 1.0 mL 200 mM L-glutamate (all from Invitrogen); add millipore water to 100 mL, sterile filter, and store at 4 °C.

2.6 Immunofluorescence

1. PFA solution: 2% PFA (v/v) in 81 mM Na₂HPO₄ and 19 mM NaH₂PO₄, pH 7.4. The solution is divided into 2- to 5-mL aliquots and stored at -20 °C.
2. PBS: To prepare 1 L of 10X PBS solution, dissolve 80 g NaCl, 2 g KCl, 14.4 g Na₂HPO₄, and 2.4 g KH₂PO₄ in 800 mL millipore water under mixing. Fill to 1 L with water. The pH is 6.8 and will change to 7.4 on dilution to 1X PBS. Final concentrations are 137 mM NaCl, 10 mM phosphate, 2.7 mM KCl, pH 7.4.
3. PBT: 0.05% (v/v) Triton X-100 in PBS.
4. PBSTT: 0.05% (v/v) Triton X-100 and 0.1% (v/v) Tween-20 in PBS.
5. Blocking buffer: 10% (v/v) goat serum (Roche Diagnostics, Basel, Switzerland), 1% dimethyl sulfoxide (DMSO) (v/v), and 0.05% NaN₃ (w/v) in PBSTT. Store at RT. Goat serum should be inactivated for 20 min at 56 °C prior to use and can be stored as aliquots at -20 °C.
6. Agarose dishes: 2% agarose (Invitrogen) in E3 medium. Dishes that are not immediately used should be sealed with Parafilm to prevent drying and stored at 4 °C for several days.
7. Molded agarose dishes: 2% agarose (Invitrogen) in PBS. Heat to 50 °C, pour into 9-cm Petri dishes, and deposit a Plexiglass form (shown in Fig. 1) into the agarose. Allow 30 min to gel, seal with Parafilm, and store at 4 °C until further use.
8. Primary antibody: α -E-cadherin, polyclonal rabbit antibody, raised against a synthetic peptide (N-DKDLPPFAGPFKVEPQGDTSKN-C) derived from the extracellular domain of zebrafish E-cadherin (12), at a dilution of 1:500 to 1:750 in blocking buffer. Add 0.05% NaN₃ to prevent bacterial growth and store for several weeks at 4 °C. The solution can be reused several times.
9. Secondary antibody: Cy2/3/5 (Jackson Immunolabs) or Alexa 488/568/647 (Molecular Probes)-coupled antirabbit immunoglobulin G (IgG), used at a concentration of 1:500 to 1:1000 in 5% goat serum in PBSTT.

3 Methods

To analyze mesendodermal cell migration, the position of the prechordal plate relative to other tissues within the embryo can be visualized by ISH. Useful antisense probes that mark mesendodermal and ectodermal tissues are *no tail*, *hgg1*, and *dlx3*; see also [Table 1 \(7,16\)](#).

Cell adhesion can be analyzed in an in vitro primary cell culture assay. Injection of *cyclops* mRNA ectopically induces mesendodermal cell fates throughout most of the embryo. Dissociated cells from these embryos reaggregate on a fibronectin substrate in the presence of Ca²⁺ ions and form distinct aggregates (10). The reduction in size and coherence of these clusters in response to loss of function of Slb/Wnt11, E-cadherin, or Rab5 indicates a defect in adhesive interactions (7,10,11).

At the onset of mesendodermal cell movements, E-cadherin, which is usually localized at the plasma membrane and in some intracellular structures, increases its intracellular localization when Slb/Wnt11 is ectopically expressed. This can be detected by comparing E-cadherin antibody staining in *slb* control embryos with activated transgenic *slb hs-wnt11-HA* embryos ectopically expressing Slb/Wnt11 (7). To test if the changes in intracellular cadherin distribution are mediated by endocytosis, MO-based knockdown of Rab5 activity can be performed. Inhibiting Rab5 activity leads to suppression of Wnt11-mediated increase in intracellular E-cadherin localization. Furthermore, activating endocytosis by expressing an activated form of Rab5c (*da-rab5c*-amino acid exchange Q79L) leads to an increase in intracellular E-cadherin, which colocalizes with the early endosomal marker YFP-Rab5c (7).

3.1 Morpholino and mRNA Injections

1. For injected amounts of mRNA and MO, see [Tables 1 and 2](#).
2. [Figure 1](#) gives an overview of zebrafish developmental stages that are most relevant for the protocols described in this subheading.
3. To obtain optimally staged specimens, zebrafish embryos are harvested within 10 min of adult pairing and transferred into E2 medium. Alternatively, embryos can be collected over a longer time and hand sorted at the two- or four-cell stage, when single blastomeres are readily visible (see [Note 1](#)).
4. Keep the embryos between 20 °C and 25 °C during the injections but afterward between 25 °C and 31 °C (see [Note 2](#)).
5. Thaw mRNA or MO aliquots on ice. Prior to use, centrifuge MO aliquots 15 min at full speed using a tabletop centrifuge (if possible, cooled to 4 °C; see [Note 3](#)).
6. An injection needle is backfilled with 1–2 μL injection solution, and the desired drop size is adjusted using a scale bar slide.
7. Nondechorionated zebrafish embryos are removed from the E2 medium with a plastic Pasteur pipet and aligned alongside a glass slide inside the lid of a 9-cm Petri dish (see [Note 4](#)).

8. Inject 500–1000 pL of the solution into either single blastomeres or the yolk directly underneath the blastomeres (Fig. 1; see Note 5).
9. After injection, the embryos are transferred back into E2 medium and incubated at 25–31 °C until the desired stage.

3.2 Heat-Shock Treatment of *slb hs-wnt11*-HA Embryos

1. Timing is extremely important to effectively heat shock embryos. Therefore, it is essential that embryos are collected within 5–10 min immediately after egg laying. In addition, they should be hand sorted at the two- to four-cell stage (see Fig. 1) to ensure that all embryos are developmentally synchronized.
2. Shortly before the heat-shock treatment, preheat Eppendorf tubes containing E2 medium in a 39 °C water bath.
3. Keep embryos at 28 °C in E2 medium until a small indentation can be seen on the dorsal side (Fig. 1J,K). Transfer the embryos into the Eppendorf tube with prewarmed E2 medium. Place them in the water bath for 20 min at 39 °C.
4. Transfer the embryos back into a Petri dish and keep them at 28 °C until the desired stage (see Note 6).

3.3 In Situ Hybridization of Embryos

1. Embryos are fixed at the desired stage in 4% PFA overnight at 4 °C or for 4 h at RT. After fixation, embryos are washed two or three times for 5 min at RT in PBST, then manually dechorionated in a Petri dish of PBST using tweezers (see Note 7).
2. For long-term storage, wash embryos four or five times in 100% methanol and keep them in 100% methanol. They can be stored at –20 °C for several months. Prior to use, rehydrate by washing 5 min each in 75%, 50%, and 25% methanol in PBST, followed by four 5-min washes in PBST.
3. If the fixed embryos are older than tailbud, they have to be incubated between 5 and 15 min, depending on the developmental stage, with proteinase K at RT, followed by 30-min fixation in 4% PFA and four 5-min washes in PBST (see Note 8).
4. Transfer embryos into Eppendorf tubes and prehybridize for 2–3 h at 65 °C in Hyb⁺ solution. This can best be achieved using a heat block that holds the tubes horizontal such that the contact between the embryos and the Hyb⁺ solution is maximized. As long as the embryos are in Hyb⁺, take thorough care never to expose them to air (see Note 9).
5. Replace the Hyb⁺ solution with a Hyb⁺ solution containing DIG-labeled anti-sense probe in the appropriate concentration. Keep overnight in a 65 °C heat block (see Note 10).
6. After incubation, store the probe solution at –20 °C. It can be reused several times depending on its strength and concentration.

7. Wash embryos thoroughly at 65 °C for 10 min each with Hyb⁺/2X SSCT 2:1, Hyb⁺/2X SSCT 1:2, 2X SSCT, followed by 30 min twice, each at 65 °C with 0.2X SSCT (see **Note 11**).
8. Switch to RT for the next washes: 10 min each with SSCT/MABT 2:1, SSCT/MABT 1:2, then twice for 30 min with MABT alone.
9. Replace the MABT with 2% block/MABT and incubate 5 h at RT.
10. Incubate the embryos with anti-DIG antibody in 2% block/MABT for 4 h at RT or overnight at 4 °C.
11. Wash the embryos four times for 15 min in MABT, then exchange the MABT solution for 0.1 M Tris base, pH 9.5. Incubate 5 min at RT.
12. Exchange the Tris base for BM purple solution and let stain for 2–3 h, depending on the riboprobe, at RT in darkness. A specific signal should be observed by watching the embryos under a normal dissecting microscope with an upright light source (see **Notes 12 and 13**).
13. Stop the reaction by washing the embryos four times for 5 min at RT with PBST. To remove trace alkaline phosphatase activity, reflux the stained embryos 30 min at RT with 4% PFA. Wash three times with PBST and take embryos through a concentration series of 30%, 50%, 70% glycerol/PBST over a 3- to 4-h incubation at RT (see **Note 14**).
14. Store embryos in 70% glycerol at 4 °C in darkness (see **Note 15**).
15. Mount embryos in 100% glycerol using a depression slide. Take photos with a digital camera (Spot Diagnostics, Sterling Heights, MI) mounted on a dissecting microscope.
16. **Figure 2** shows an example of ISH staining at the end of gastrulation.

3.4 Cell Culture

1. All steps following dechoriation of the embryos should be done under sterile conditions (see **Note 16**).

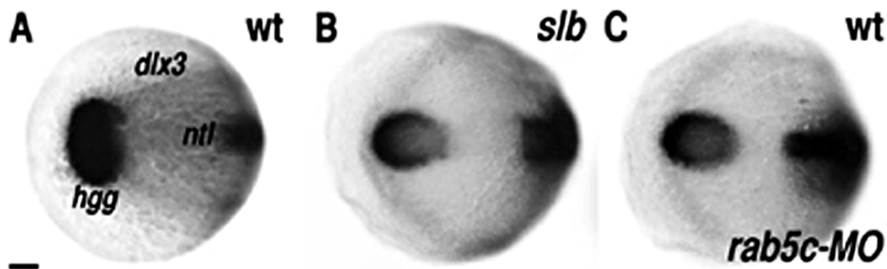


Fig. 2 In situ hybridization of tailbud stage embryos. Position of the prechordal plate marked by *hgg1* relative to the anterior edge of the neural plate as marked with *dlx3* and the notochord anlage marked by *ntl* at bud stage in a wild-type control embryo (**A**), a *slb/wnt11* mutant embryo (**B**), and a wild-type embryo injected with 4 ng *rab5c*-MO (**C**). Dorsal views with anterior to the left. Bar = 50 μ m. (Reprinted from *Ref. 7* with permission from Elsevier.).

2. Dechorionated embryos must never contact plastic as the yolk sticks to it, tearing the embryo apart.
3. At least 3 h before embryo dissociation, coat the wells of a multiwell plate with 35.4 ng fibronectin/mm². For a 96-well plate, add 500 μ L cell culture medium to an aliquot of 10 μ L frozen fibronectin solution in PBS (500 ng/mL) and distribute 100 μ L of this solution into each well.
4. To induce mesendodermal cell fates, inject 100 pg *cyclops* mRNA at the one- to two-cell stage. Additional Gap43-GFP mRNA can also be injected to later visualize cell membrane by confocal imaging. See [Table 1](#) for information about mRNA.
5. Transfer sphere-dome stage embryos (see [Fig. 1G,H](#)) in E2 medium to small agarose-coated dishes. Dechorionate embryos for 5–10 min at RT by replacing E2 medium with pronase solution prewarmed to 37 °C. Observe the embryos under a dissecting scope. The chorion should get slight ruffles and bubbles and occasionally tear open without destroying the embryos.
6. Once the chorions open, transfer embryos with a glass Pasteur pipet into a new agarose dish containing E2 medium. Repeat this washing step four or five times, always using a new Pasteur pipet. The chorions will eventually detach from the embryos by the shear forces inside the Pasteur pipets and float to the top of the medium.
7. Transfer the embryos with a glass Pasteur pipet into an empty 15-mL Falcon tube. Suck away excess buffer. Take care not to expose the embryos to air as this causes them to burst.
8. Add prewarmed trypsin/EDTA solution and shake the cell suspension until no clumps are visible. Incubate for 3 min at 37 °C.
9. During the trypsin incubation, remove the buffer from the multiwell plate. The fibronectin coat should start to dry by the time the cells are plated.
10. Stop the trypsin/EDTA reaction by adding 10% (v/v) chicken serum and gently spin the cells down for 3 min at 1000 rpm. Resuspend in fresh cell culture medium at RT.
11. Adjust the cell concentration to $2 \cdot 10^5$ cells/mL, using a Neubauer chamber.
12. Plate 50–100 μ L of the cell suspension per well of a 96-well chamber (see [Notes 17 and 18](#)).
13. Incubate cells for 4–8 h at 25 °C and 2% CO₂. Clusters should start to form between 1 and 2 h ([7,11](#); see [Note 19](#)).
14. [Figure 3](#) shows examples of cell clustering under wild-type and different mutant conditions, both acquired through DIC or confocal optics.

3.5 Immunofluorescence

1. For an overview about useful antibodies, see [Table 3](#).
2. Transgenic *slb hs-wnt11* embryos, together with siblings from the same founder line that do not carry transgenic *hs-wnt11-HA*, are used.

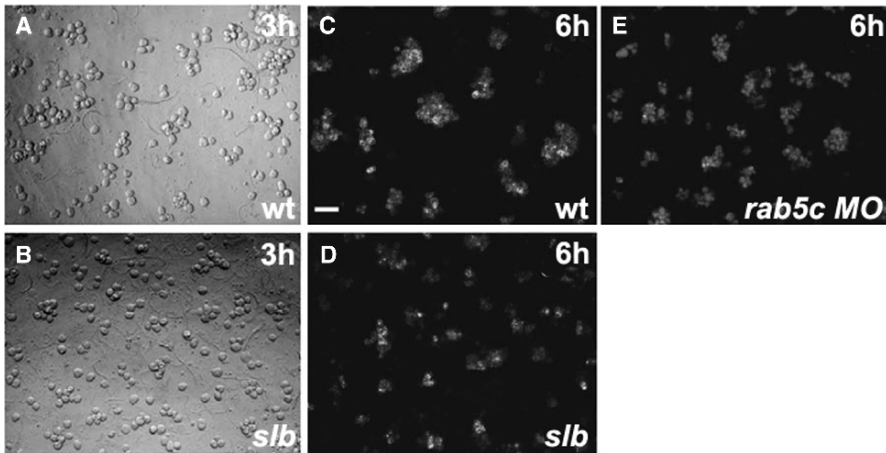


Fig. 3 Cell culture of zebrafish mesendodermal cells. Reaggregation of mesendodermal progenitors cultured on fibronectin. (A), (B) DIC images after 3h; (C)–(E) confocal images after 6h of culture. (A), (C) Wild type; (B), (D) *slb/wnt11* mutant; and (E) wild-type mesendodermal cells, injected with 4ng *rab5c*-MO (coupled to fluorescein). Cells in (C)–(E) are labeled with GAP43-GFP. The scale bar in (C) represents 100 μm . (Reprinted from Ref. 7, and with permission from Elsevier and Company of Biologists, respectively.).

3. To functionally address Rab5-dependent E-cadherin endocytosis or to correlate intracellular E-cadherin staining with rab5-dependent early endosomes, *rab5c* MO or YFP-*rab5c* mRNA, respectively, is injected. See Table 1 for injected amounts. These injections are performed using methods outlined in Subheading 3.1. (see Note 20).
4. Heat shock embryos at the beginning of gastrulation as described in Subheading 3.2., then fix them in 2% PFA for 4h at RT (see Note 21). Gently rock them while fixing.
5. Wash embryos for times for 10 min at RT and then manually dechorionate them in PBT using tweezers (see Notes 7 and 22).
6. Fixed and dechorionated embryos can be used immediately or stored in PBST for several weeks. In the latter case, add a drop of 4% PFA to stabilize the embryos and 0.05% sodium azide to prevent mold growth.
7. Wash embryos four times for 10 min at RT in PBSTT and incubate overnight at 4°C in blocking buffer. Afterward, incubate embryos for 4h at RT with E-cadherin antibody, wash four times for 30 min with PBSTT, and incubate for 4h at RT with a secondary antibody. Alternatively, incubate embryos in secondary antibody overnight at 4°C (see Note 23).
8. Wash antibody out by four 30-min rinses at RT in PBSTT. Embryos can be stored in darkness for several days at 4°C in PBSTT. Add 0.05% (w/v) NaN_3 to prevent bacterial growth.
9. To see if the heat shock was successful, HA antibodies can be used. For more information on this antibody, see Table 3.

Table 3 Antibodies Described in This Review

Name	Antigen	Antibody	Species	Source	Reference
E-cadherin	Peptide, extra-cellular domain of zebrafish E-cadherin	Polyclonal serum	Rabbit	Marrs Lab	12
HA	HA peptide	Monoclonal IgG1	Rat	Roche Diagnostics, clone 3F10	22
Cy 5-coupled GαR	Heavy and light chains of rabbit IgG	Polyclonal serum affinity purified and coupled to Cy5 dye	Goat	Jackson Immunoresearch, 111-175-003	–
Alexa Fluor 546-coupled GαR	Heavy and light chains of rat IgG	Polyclonal serum affinity purified and coupled to Alexa Fluor 543 dye	Goat	Molecular Probes, A-11081	–

10. Mount embryos in PBSTT on an agarose dish with holes that fit the embryos, similar to dishes used for transplantations (*see* Subheading 2.). Orient embryos with the dorsal region of the germ ring (embryonic shield) facing the objective (*see* [Note 24](#)).
11. The antibody stainings can be observed using epifluorescence or confocal optics. In our case, a Leica TCS-SP2 confocal laser scanning microscope with an $\times 63$ objective and a low numerical aperture (NA) (0.9) gave the best results.
12. Useful laser lines are 647 nm for detection of the E-cadherin antibody and 488 nm for detection of YFP-Rab5c. A third antibody can be detected at 568 nm.
13. [Figure 4](#) shows confocal sections of E-cadherin and YFP-Rab5c costainings under different functional conditions (*see* [Notes 23, 25, and 26](#)).

4 Notes

1. MO and control embryos should always be siblings from an egg-lay that does not vary more than 10–15 min in age. Accurate staging of the embryos is important because the observed effects on E-cadherin endocytosis and cell movements are transient. For example, the effects on E-cadherin endocytosis are most obvious at early but not late stages of gastrulation, and the prechordal plate movement, which is most strongly affected at late gastrulation, partially recovers later during somitogenesis. Classification of MO-based effects can therefore be difficult, if not impossible, if embryos are not synchronized in developmental stage and

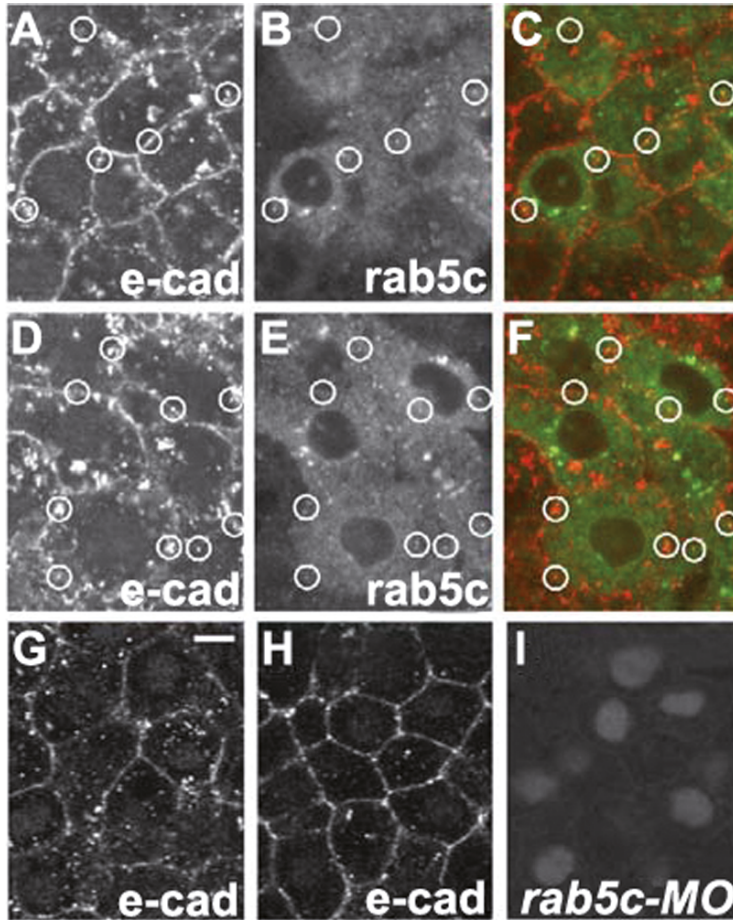


Fig. 4 Subcellular localization of E-cadherin. Confocal sections of dorsal ectodermal cells at the onset of gastrulation are shown. (A)–(F) Ectodermal cells in *slb/wnt11* mutant embryos (A)–(C) and *slb hs-wnt11-HA* transgenic embryos (D)–(F) 30 min after heat-shock treatment (see **Subheading 3**). E-cadherin detected by zebrafish E-cadherin antibody (A) and (D); Rab5-positive endosomes marked by YFP-Rab5c (B) and (E). Merged images in (C) and (F). Circles mark several E-cadherin-positive vesicles close to the plasma membrane that colocalize with YFP-Rab5c. (G)–(I) E-cadherin staining in *slb hs-wnt11-HA* transgenic embryos 30 min after the heat shock either uninjected (G) or injected with 4 ng *rab5c*-MO (H). Bar = 10 μ m. (I) Localization of fluorescein-labeled *rab5c*-MO in (H). (Reprinted from *Ref. 7* with permission from Elsevier.).

analyzed at the correct time. In general, wild-type zebrafish that are “trained” to lay eggs on specific days of the week will give rise to several hundred embryos within 10 min, making it easy to obtain embryos without the need for extensive staging. Alternatively, staging is most convenient when the embryos are still between the two- and eight-cell stage as the number of blastomeres is easily identifiable (see [Fig. 1](#)).

2. Exposure to low temperature (18–25 °C) before midblastula transition (3–4 h after fertilization) tends to affect dorsoventral patterning (17).
3. MO solutions tend to form small crystals that can clog the injection needle. Therefore, after thawing, it is advisable to centrifuge them for several minutes to remove any crystals.
4. Embryos can be pipeted and aligned along a glass slide as shown in Fig. 1A. Excess liquid will be drawn underneath the glass slide and can be collected as it pools at the opposite side of the Petri dish lid. Capillary force will hold the embryos in place. Up to 75 embryos can be placed in a row along one glass slide.
5. Up to 1 nL can be injected without harming the embryo. Until the 32-cell stage, the blastomeres are still connected via cytoplasmic bridges to the yolk. For this reason, MO injected before the 8-cell stage (Fig. 1F) distributes evenly within the embryo. mRNA tends to diffuse slower and is therefore best injected before the two- to four-cell stage (Fig. 1D,E).
6. To analyze cell movement by ISH, embryos at any stage during gastrulation can be used. However, alterations in movement behaviors in different experimental backgrounds are most distinct at bud stage (Fig. 1N). Differences in the distribution of intracellular E-cadherin in response to the expression of the *hs-wnt11-HA* transgene are most prominent at shield stage. Fix the embryo 30 min after the heat-shock treatment to allow the transgene enough time to act (see Fig. 1L,M).
7. Be careful with embryos that are fixed at early gastrulation stages; they are fragile and can easily lose their blastoderm cap after removing the chorion.
8. The older the embryos are, the longer they should be incubated with proteinase K. Embryos that are at one- to five-somite stages only need to be treated a few seconds, while older embryos need several minutes to digest the epidermis.
9. If the embryos are exposed to air, formamide will precipitate on the embryos and cause a strong background to appear during the staining reaction.
10. A useful combination of ISH riboprobes for visualizing cell/tissue localizations during gastrulation is *hatching gland gene 1* (*hgg1*), *no tail* (*ntl*), and *distal-less box 3* (*dlx3*) (18–20); see also Table 1. If possible, prewarm all solutions to 65 °C prior to use. To avoid evaporation of buffer and concentration of the probe, place aluminum foil such that it contacts the heat block and covers the Eppendorf tubes. This keeps equal temperatures at the top and bottom of the Eppendorf tubes. If the ISH protocol gives too much or too little signal, the hybridization steps should be carried out using higher or lower temperatures, respectively.
11. Using longer times for the washing steps can sometimes significantly reduce the background.
12. The probes *hgg1* and *ntl* (staining the shield and the notochord, respectively) are readily visible directly after shield stage, whereas *dlx3*, which stains the anterior border of the neural plate only, is only found at bud stage.
13. If the signal is too weak after this time, the staining reaction can be prolonged by incubating overnight or longer at 4 °C. Be careful not to overstain as unspecific

background will eventually appear. Adding new BM purple after several hours of incubation can also increase the staining efficiency. To keep background as low as possible, it is crucial to thoroughly wash the embryos.

14. If no refixation step is performed, trace alkaline phosphatase activity will slowly lead to an accumulation of unspecific signal after several weeks. Therefore, this step is advisable when the stainings are stored for a longer time period.
15. If the signal strength is good and the plates are protected from drying out, nice staining can still be detectable after several months or even years.
16. This is merely to keep the cell culture media sterile. Under the conditions listed here, the primary mesendodermal cell culture will not survive for more than 1 or 2d.
17. For larger wells (e.g., 24-well chamber), the volume and thus the amount of cells can be scaled up without any problem.
18. When plating cells from the suspension onto the fibronectin, great care should be taken to thoroughly mix the cells as they sediment fast, easily leading to unequal distribution of the cells among different wells.
19. Primary mesendodermal cells are sensitive to the pH of the medium. If this value continually increases, the cells eventually die. The buffer used here contains carbonate salts; therefore, CO₂ must be supplied during the incubation. An alternative is to use carbonate free buffer that keeps its pH value stable without external CO₂.
20. There are five different *rab5* isoforms in zebrafish: *rab5a*, *rab5a2*, *rab5b*, *rab5c*, and *rab5c-like*. These are expressed in variable abundance and timing. The methods introduced here focus on *rab5c*, which is both expressed during gastrulation and shows a clearly recognizable gastrulation phenotype when “knocked down.” However, similar results have also been obtained using *rab5a2*.
21. PFA forms covalent bonds with basic amino acid residues, such as arginine and lysine, which can effectively mask the antigenicity. This is a special problem in the case of proteins with many of these basic residues. We observed that fixation with 4% PFA overnight, even at 4 °C, strongly impairs the binding of the E-cadherin antibody. In general, lower percentages of PFA and shorter fixation times improve the E-cadherin staining, while the fixation temperature appears to have a less-severe effect.
22. After fixing in 2% PFA, embryos tend to be more fragile than with 4% PFA. Therefore, more care has to be applied during dechoriation.
23. Some of the secondary antibodies produce “spotty” background in our hands. Therefore, for us, the Cy2/3/5-coupled secondary antibodies from Jackson Immunolabs (Suffolk, UK) work best. To further prevent background staining, the antibody can be preincubated overnight at 4 °C at a concentration of 1:10 with gastrulation-stage embryos. To further reduce background staining, it is possible to centrifuge the primary and secondary antibodies prior to use for 30 min at 100,000 g in a preparative ultracentrifuge. This will remove sticky aggregates of antibody that sometimes produce a “dotty” background (21).
24. In our initial study (7), we imaged the ectodermal cells over the prechordal mesoderm as the intracellular E-cadherin localization was similar in both tissues, but

- the closeness of the ectoderm to the objective enabled a more reliable analysis under different functional conditions. In principle, paraffin sections of fixed embryos can also be stained with the E-cadherin antibody. However, they are difficult to analyze as paraffin embedding seems to produce unspecific background.
25. The E-cadherin staining pattern is very sensitive to the experimental conditions applied. It is crucial that the embryos are synchronized “down to the minute” and are at the correct stage. Only a small subset of E-cadherin is localized in endocytic vesicles. To see a difference under distinct functional conditions, the embryos have to be analyzed at the onset of gastrulation, when the effect of *slb/wnt11* on E-cadherin endocytosis is most pronounced. Even more, the heat shock induces a mosaic expression of *slb/wnt11*-HA such that not all cells show an equal degree of internalization. Similarly, the injected YFP-Rab5c distributes in a mosaic pattern. Therefore, it is advisable only to analyze colocalization in those cells that display a comparable YFP-Rab5c signal and to do this in a large subset of embryos and experiments.
 26. The effect of *slb/wnt11* on E-cadherin endocytosis can be best seen in immediate proximity to the plasma membrane (Fig. 4A–F), indicating a spatially restricted pattern of internalized E-cadherin vesicles (7).

References

1. Miller, J.R., and McClay, D.R. (1997) Characterization of the role of cadherin in regulating cell adhesion during sea urchin development. *Dev. Biol.* **192**, 323–339.
2. Jarrett, O., Stow, J.L., Yap, A.S., and Key, B. (2002) Dynamin-dependent endocytosis is necessary for convergent-extension movements in *Xenopus* animal cap explants. *Int. J. Dev. Biol.* **46**, 467–473.
3. Claassen, A.K., Anderson, K.I., Marois, E., and Eaton, S. (2005) Hexagonal packing of *Drosophila* wing epithelial cells by the planar cell polarity pathway. *Dev. Cell* **9**, 805–817.
4. Zerial, M., and McBride, H. (2001) Rab proteins as membrane organizers. *Nat. Rev. Mol. Cell Biol.* **2**, 107–117.
5. Scholpp, S., and Brand, M. (2004) Endocytosis controls spreading and effective signaling range of Fgf8 protein. *Curr. Biol.* **14**, 1834–1841.
6. Pelkmans, L., Burli, T., Zerial, M., and Helenius, A. (2004) Caveolin-stabilized membrane domains as multifunctional transport and sorting devices in endocytic membrane traffic. *Cell* **118**, 767–780.
7. Ulrich, F., Krieg, M., Schoetz, E.-M., et al. (2005) Wnt11 functions in gastrulation by controlling cell cohesion through Rab5c and E-cadherin. *Dev. Cell* **9**, 555–564.
8. Ulrich, F., Concha, M.L., Heid, P.J., et al. (2003) Slb/Wnt11 controls hypoblast cell migration and morphogenesis at the onset of zebrafish gastrulation. *Development* **130**, 5375–5384.
9. Kilian, B., Mansukoski, H., Barbosa, F.C., Ulrich, F., Tada, M., and Heisenberg, C.-P. (2003) The role of Ppt/Wnt5 in regulating cell shape and movement during zebrafish gastrulation. *Mech. Dev.* **120**, 467–476.
10. Montero, J.A., Carvalho, L., Wilsch-Bräuninger, M., Kilian, B., Mustafa, C., and Heisenberg, C.-P. (2005) Shield formation at the onset of zebrafish gastrulation. *Development* **132**, 1187–1198.
11. Puech, P.H., Taubenberger, A., Ulrich, F., Krieg, M., Müller, D.J., and Heisenberg, C.-P. (2005) Measuring cell adhesion forces of primary gastrulating cells from zebrafish using atomic force microscopy. *J. Cell Sci.* **118**, 4199–4206.

12. Babb, S.G., Barnett, J., Doedens, A.L., et al. (2001) Zebrafish E-cadherin: expression during early embryogenesis and regulation during brain development. *Dev. Dyn.* **221**, 231–237.
13. Westerfield, M. (2000) *The Zebrafish Book. A Guide for the Laboratory Use of Zebrafish (Danio rerio)*, 4th ed., University of Oregon Press, Eugene.
14. Heisenberg, C.-P., Brand, M., Jiang, Y.J., et al. (1996) Genes involved in forebrain development in the zebrafish, *Danio rerio*. *Development* **123**, 191–203.
15. Ro, H., Soun, K., Kim, E.J., and Rhee, M. (2004) Novel vector systems optimized for injecting in vitro-synthesized mRNA into zebrafish embryos. *Mol. Cells* **17**, 373–376.
16. Heisenberg, C.-P., Tada, M., Rauch, G.J., et al. (2000) Silberblick/Wnt11 mediates convergent extension movements during zebrafish gastrulation. *Nature* **405**, 76–81.
17. Kimmel, C.B., Ballard, W.W., Kimmel, S.R., Ullmann, B., and Schilling, T.F. (1995) Stages of embryonic development of the zebrafish. *Dev. Dyn.* **203**, 253–310.
18. Akimenko, M.A., Ekker, M., Wegner, J., Lin, W., and Westerfield, M. (1994) Combinatorial expression of three zebrafish genes related to distal-less: part of a homeobox gene code for the head. *J. Neurosci.* **14**, 3475–3486.
19. Schulte-Merker, S., Hammerschmidt, M., Beuchle, D., Cho, K.W., De Robertis, E.M., and Nüsslein-Volhard, C. (1994) Expression of zebrafish goosecoid and no tail gene products in wild-type and mutant no tail embryos. *Development* **120**, 843–852.
20. Thisse, C., Thisse, B., Halpern, M.E., and Postlethwait, J.H. (1994) Goosecoid expression in neurectoderm and mesendoderm is disrupted in zebrafish *cyclops* gastrulas. *Dev. Biol.* **164**, 420–429.
21. Harlow, E., and Lane, D. (1999) *Using Antibodies: A Laboratory Manual*. Cold Spring Harbor Laboratory Press, Cold Spring Harbor, NY.
22. Wilson, I.A., Niman, H.L., Houghten, R.A., Cherenon, A.R., Connolly, M.L., and Lerner, R.A. (1984) The structure of an antigenic determinant in a protein. *Cell* **37**, 767–778.
23. Okada, A., Lansford, R., Weimann, J.M., Fraser, S.E., and McConnell, S.K. (1999) Imaging cells in the developing nervous system with retrovirus expressing modified green fluorescent protein. *Exp. Neurol.* **156**, 394–406.
24. Rebagliati, M.R., Toyama, R., Haffter, P., and Dawid, I. B. (1998) Cyclops encodes a nodal-related factor involved in midline signaling. *Proc. Natl. Acad. Sci. U. S. A.* **95**, 9932–9937.

Quantifying Endocytosis In Vivo Using Intravital Two-Photon Microscopy

Ruben M. Sandoval and Bruce A. Molitoris

1 Introduction.....	390
2 Materials.....	391
3 Methods.....	392
4 Notes.....	401
References.....	402

Summary The recent introduction of multiphoton microscopy coupled with advances in optics, computer sciences, designer fluorophores, molecular labeling, and previously developed physiologic approaches have empowered investigators to quantitatively study the cell-specific dynamic events, such as endocytosis, within a functioning organ with subcellular resolution. This rapidly emerging field of investigation, with superior spatial and temporal resolution and high sensitivity, enables investigators to track molecules and determine their mode of cellular uptake, intracellular trafficking, and metabolism in a cell-specific fashion in complex heterogeneous organs such as the kidney with repeated determinations possible over a prolonged period of time. This approach is enhanced by the ability to obtain and quantify volumetric data with using up to three different fluorophores simultaneously. We have utilized this intravital approach to understand and quantify kidney proximal tubule cell uptake and intracellular distribution and metabolism of fluorescently labeled molecules, including folic acid, gentamicin, and small interfering ribonucleic acid (siRNA). Limitations of this technique include tissue penetration, which is the major barrier to successful clinical utilization of this technology. However, its use in preclinical animal models offers new insight into physiologic processes and the pathophysiology and treatment of disease processes.

Keywords Aminoglycosides; dextrans; gentamicin; kidney imaging; proximal tubule cells; siRNA.

1 Introduction

Following glomerular filtration, the filtered low molecular weight proteins and low molecular weight solutes are reabsorbed by kidney epithelial cells. The proximal tubule plays a major role in protein reclamation, utilizing both fluid-phase and receptor-mediated endocytosis. Once internalized via the endocytic process, low molecular weight proteins can either undergo transcytosis or be degraded.

The proximal tubular cell is one of the most active, efficient, and effective mammalian cells involved in endocytosis (1). This high level of endocytosis, however, exposes the proximal tubular cell to increased amounts of potentially nephrotoxic agents when these agents are administered for therapy of a disease process. For example, aminoglycoside antibiotics are low molecular weight polycationic compounds that are rapidly filtered and actively taken up by proximal tubular cells (2–4). Accumulation of these compounds within proximal tubular cells leads to acute kidney injury requiring the discontinuation of the antibiotic. Therefore, understanding and quantifying the process of endocytosis within the proximal tubular cell, especially the ability to potentially alter this process, is of major interest to physicians and biologists (1,3,5). Our laboratory has been working on techniques utilizing two-photon microscopy both to observe proximal tubular endocytosis and to quantify it within the living rat. Our findings have both mechanistic and therapeutic implications for a number of compounds and disease processes.

Advances in optical imaging are fueling a rapid evolution in how complex biological processes are studied *in vivo*. Illumination of fluorophores utilizing two-photon microscopy generates fluorescence only at the objective focal plane, unlike standard confocal microscopy, in which the entire depth of the specimen is illuminated. Images generated in this manner are inherently confocal and do not require the use of pinholes (as is done for single-photon confocal imaging). In addition, illumination does not occur continuously; it is delivered in discrete temporal pulses of “photon packets” hundreds of femtoseconds apart.

Coupling these advances in imaging with novel physiologic and surgical approaches has allowed the study of many processes within a working, fully functioning, systemically attached organ such as the kidney. A key characteristic of the kidney is the scavenging of essential metabolites to prevent loss via urinary excretion. Endocytosis occurs primarily in specialized, polarized cells called proximal tubule cells that are part of the early nephron segment. Here, we describe the means to study and quantify this important renal function by intravital two-photon microscopy. Having been described in detail, the surgical preparation required for renal imaging could serve as a basis for the study of additional renal functions when coupled with the use of appropriate fluorescent markers.

2 Materials

2.1 Solutions and Fluorescent Markers

1. Solution: 0.9% sodium chloride (Sigma, St. Louis, MO) in double-distilled water (ddH₂O) (here noted as 1X NaCl).
2. Nuclear dye: Hoechst 33342, stock 10 mg/mL in double-distilled water (Invitrogen/Molecular Probes, Eugene, OR).
3. Endocytosis markers (freely filtered): 3000 MW dextran conjugated to cascade blue, rhodamine, or Texas red (Invitrogen/Molecular Probes); 10,000 MW dextran conjugated to cascade blue, rhodamine, or Texas red (Invitrogen/Molecular Probes).
4. Vasculature marker (nonfiltered): 500,000 MW fluorescein dextran (Invitrogen/Molecular Probes).
5. Slide-a-Lyzer dialysis cassettes: 10,000 MW cutoff, 3- to 15-mL capacity (Pierce Biotechnology, Rockford, IL).

2.2 Microscopy

1. Inverted two-photon microscope with appropriate filters to detect Hoechst/DAPI (4',6-diamidino-2-phenylindole) fluorescein, and rhodamine/Texas red. Dual-pass fluorescein/rhodamine filter cube for epifluorescence illumination with Hg arc light source to survey kidney cortex prior to imaging or infusion of dyes. A DAPI/fluorescein/rhodamine triple-pass filter is not recommended because of ultraviolet (UV) illumination of tissue and possible phototoxicity.
2. Water immersion objectives that allow for deeper imaging with longer working distances, for example, our Nikon ×60 WI objective, numerical aperture (NA) 1.2.
3. Plastic dish: 50 mm with 40-mm coverslip bottom (WillCo-dish, Amsterdam, Netherlands, 170-μm thick glass)
4. Objective heater.

2.3 Surgical Tools/Specimen

1. Blunt-tipped straight forceps (2 pairs).
2. Long-nosed hemostat (1 pair).
3. Surgical scissors (1 pair).
4. Blood pressure monitoring apparatus, either cuff or via direct access to arterial line.

5. Infusion pump to deliver 1X NaCl at approx 1.5 mL/h for prolonged experiments (optional).
6. Venous access lines, both femoral and jugular for infusion of dyes or a slow continuous infusion of 1X NaCl at 1.5 mL/h for longer experiments.
7. PE-50 tubing for intravenous/arterial lines.
8. Water-circulating blanket warmer.
9. Repti Therm undertank heater 4 × 5 inch pad, placed under the head.
10. Anesthesia: Inactin (55 mg/kg body weight, Sigma); sodium pentobarbital (55 mg/kg body weight, Besse Scientific, Louisville, KY); or an inhalation anesthetic such as halothane (5% induction, 1–2% maintenance).
11. Fine-tipped Sharpie.
12. Male or female rat, approx 200–450 g desired weight.

2.4 Quantitative Analysis

1. Personal computer (PC) with minimum requirements for supporting Metamorph software, at least 1–2 GB RAM recommended.
2. Metamorph image-processing software version 6.3r1 (Molecular Devices, Sunnyvale, CA).
3. Microsoft Excel spreadsheet; Metamorph can export numerical data to MS Excel for analysis.

3 Methods

3.1 Dye Preparation

1. Nuclear dye Hoechst 33342- from the 10 mg/mL stock solution add 50–65 μ L (500–650 μ g) to 350 μ L 1X NaCl (*see Note 1*).
2. Endocytic markers: 3,000 or 10,000 MW dextrans. Reconstitute the lyophilized dextrans to a stock concentration of 20 mg/mL in 1X NaCl (do not refreeze after reconstitution; stable for at least 6–12 mo at 4 °C after reconstitution).
3. Dilute approx 80 μ L of the stock endocytic marker solution in 400 μ L 1X NaCl for a working solution. Alternatively, this can be mixed with 300–400 μ L 500,000 MW fluorescein dextran (vascular marker).
4. Vascular marker: 500,000 MW fluorescein dextran. Reconstitute in 1X NaCl at a concentration of 6.667 mg/mL (10 mg in 1.5 mL). Follow directions for dialysis in 5 L 1X NaCl overnight at room temperature (RT) using Slide-a-Lyzer cassette. Reconstitute a minimum of four vials (do not refreeze after reconstitution; stable for at least 6–12 mo at 4 °C after dialysis).
5. Use approx 300–400 μ L of the vascular marker either alone or mixed with an endocytic marker.

3.2 *Microscope Preparation*

1. Turn on the heating blanket and place it on the stage to warm it. Connect and place the Repti Therm pad on the stage where the rat's head will rest and secure to the stage with tape along the edge of the pad. At this time, the objective heater should be placed around the objective and turned on.
2. Tape the 50-mm coverslip bottom dish to a removable dish holder that couples to the microscope stage. Put a strip of tape on the bottom of the dish holder with a portion of the tape covering the opening where the dish will sit. Place the dish on the holder and adhere the bottom of the cover glass to the tape. Make sure no more than 50% of the coverslip dish is adhered to leave the rest available for imaging (*see Note 2*).
3. Turn on the microscope and two-photon system. Make sure the laser is on for at least 20–30 min to allow the optics to warm up.
4. Warm up and prepare instruments that will be utilized to monitor blood pressure and core body temperature.

3.3 *Surgical Preparation*

1. After anesthesia, insert a femoral arterial line to monitor blood pressure (if your system utilizes a cuff monitor, omit this) and venous lines for infusion of dyes and 1X NaCl. Use short access lines where fluorescent dyes will be infused to minimize the amount left after delivery.
2. Shave the rat from the center of the stomach along the midline and along the left side to the back (*see Fig. 1A*). The area below the ribs to the upper portion of the hip along the left side should be well shaved; wipe area down with warm water to remove excess clippings.
3. Lay the rat flat on its right side so the left side is facing up. Make sure the rat is perfectly flat, stretched out lengthwise. The forefeet should be touching each other as should the rear feet (*see Fig. 1B*).
4. Gently palpate to feel the kidney. It should be located below the rib cage (*see Fig. 1A*). Once you feel the kidney, keep hold of it and draw a line with the Sharpie down the center. The line should run in a lengthwise plane from the lower rib cage to the upper hip, not from the stomach to the back.
5. Using the forceps, pull the skin up and with the hemostats pinch the skin below the rib cage along the drawn line to crush the skin; hold for 5 s. Cut along the crushed tissue with the surgical scissors; there should be no bleeding. Widen the incision with the two forceps.
6. Next crush the outer muscle layer as before and cut the tissue along the same plane; widen the incision with the two forceps.
7. Using the same techniques, grip the inner muscle layer just above the kidney (*see Note 3*). The area you crush with the hemostats should be smaller than the

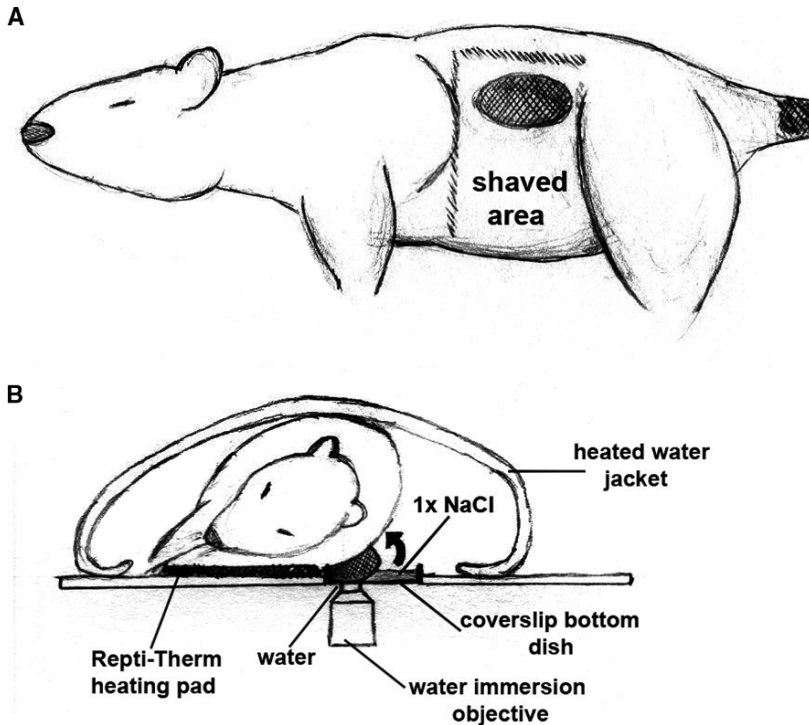


Fig. 1 Surgical preparation of rat to expose a kidney for intravital imaging. **(A)** After shaving the midsection and locating the kidney by palpation, sequential incisions through the skin and first and second muscle layers are made to expose the kidney. **(B)** The rat is carefully placed on the microscope stage with the kidney in a coverslip bottom dish filled with 1X NaCl. The kidney is rolled/flipped back slightly (see drawn curved arrow) so the ventral side is touching the coverslip and dorsal side is touching the outer skin. The kidney is positioned as close to the edge of the coverslip dish (front edge, closest to the microscopist) as possible to minimize motion caused by breathing.

previous two areas and harder to secure because of the muscle thickness (the rat will reflexively twitch when you grip this last layer; the anesthesia is not wearing off). It is important to start small on this incision as a large incision will prevent the kidney from remaining exteriorized, and a suture will have to be placed to decrease the incision size.

8. Once the final incision is made, you will see some white fat unlike that associated with other organs. Gently pull on this fat, and you will see the kidney move closer to the incision.
9. Using both pairs of forceps, work your way down to the lower pole of the kidney in a "hand-over-hand" fashion. Upon reaching the lower pole, gently pull the kidney out through the incision. This may be facilitated by pushing the kidney with the other hand as you are pulling.
10. Once the kidney is exteriorized, administer the nuclear dye via one of the intravenous lines to allow localization to the nuclei. Flush the line with 1X NaCl to

ensure no residual Hoechst remains. Further information to supplement Subheadings 3.1.–3.3. can be found in *Ref. 6*.

3.4 Placement of Rat on the Stage

1. Fill the coverslip bottom dish with enough prewarmed 1X NaCl to cover the bottom of the dish; do not overfill. Ensure water immersion objectives have a bead of water prior to placing the rat on the stage (*see Note 4*).
2. Place the rat on the stage with the head toward the right, legs to the left facing you. Once on the stage, move the rat closer to you and make sure the ventral side of the kidney is touching the coverslip bottom and the dorsal side is facing up (toward the skin/fur). Moving the kidney forward as close as possible to the dish edge (closest to you) will ensure that most of the torso is outside the dish and limits the effects of breathing on movement during image acquisition (*Fig. 1B*).
3. Set up to measure all relevant physiologic parameters. In our system, the femoral access lines are purposely put in with longer tubing because the pressure monitor and pump to infuse 1X NaCl are some distance away from the microscope stage.
4. Insert a rectal temperature probe to monitor core body temperature and to measure that parameter as well.

3.5 A Survey of Native Kidney Morphology via Fluorescence

1. After placing the rat on the stage, note the different structures visible through the eyepiece under epifluorescence illumination (*Fig. 2A*). Briefly, proximal tubule cells will have an inherent autofluorescence associated within the lysosomes. These structures appear yellow-orange through a dual-pass fluorescein/rhodamine filter cube.
2. Although proximal tubules will make up the majority of the tubules in a field, occasionally you will see a tubule devoid of any orange autofluorescence; these are distal tubules or collecting ducts (*Fig. 2A, DT/CD*). Their lack of autofluorescence will be more evident under two-photon observation.
3. In Sprague–Dawley rats, superficial glomeruli are not visible; to visualize these structures, use the Munich–Wistar strain, which have an abundant amount of superficial glomeruli. As with the distal tubules and collecting ducts, the glomeruli will have no associated autofluorescence. Their structure is a circular void of fluorescence surrounded by orange tubules.
4. Typically, a portion of the leading S1 segment can be seen immediately adjacent to the circular void. On careful examination you may see the connection to the Bowman's capsule as you go in and out of focus around the glomeruli.

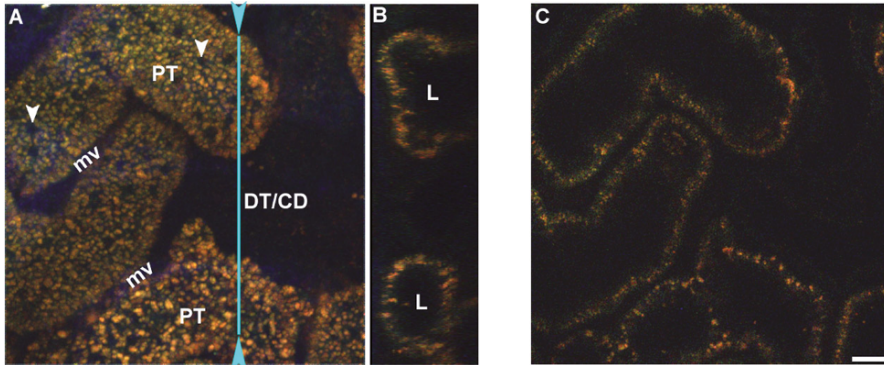


Fig. 2 A survey of renal landmarks. **(A)** This two-photon, intravital 3D reconstruction of the kidney taken before infusion of any fluorescent dyes shows several features. Most prominent are the proximal tubules (PTs) with their inherent reddish-orange autofluorescence emanating from mature lysosomes. Within this 3D reconstruction, the uniform-size “holes” lacking any fluorescence are the nuclei (white arrowheads). Distal tubules or collecting ducts (DT/CD) display no autofluorescence. The microvasculature (mv) is found running between the tubular structures. When viewing the kidney under wide-field epifluorescence illumination, the morphology will be similar to this intravital 3D reconstruction. **(B)** An orthogonal view of the area below the cyan line in **(A)** shows the tubular lumen of the proximal tubules at the top and bottom in cross-section with a distal tubule or collecting duct in between. The proximal tubule lumens are labeled with L's. **(C)** A single plane from the through-focus volume showing the lumens of the proximal tubules, similar to that seen in **(B)**. Bar = 20 μ m.

3.6 Visualizing Endocytosis

1. Our system utilizes a 5-W pump laser to excite the Ti:sapphire laser system, with output from the Ti:sapphire approx 650–750 mW prior to entry into the light path, which will reduce output even further.
2. Typically, the transmitted laser power is set for excitation from 25% to 40%.
3. Set the sensitivity on the detectors to mimic what is seen through the eyepiece. In our studies, the images acquired prior to infusion of dyes will show lysosomes as orange. If there is shift to either red or yellowish-green fluorescence, the sensitivity is adjusted to bring the image back to the standard reference image (reducing the sensitivity on the red or green detectors, respectively).
4. The Bio-Rad MRC-1024 system is routinely set up to collect a 512 \times 512 pixel image in approx 1 s; this is a good intermediate between an adequate-size viewing field (under an \times 60 water immersion objective, NA 1.2) and collection time. Sacrificing size will increase the rate of image acquisition and vice-versa.
5. The images generated contain eight-bit data, meaning the visible intensity range of acquired fluorescent structure ranging from black to white spans numerical values between 0 and 255. Here, background fluorescence, for example, will have values ranging between 5 and 20, where no morphologic structures are

present, and circular endosomes and lysosomes will have pixels with numerical values much higher, ranging on average between 30 and 255 depending on the amount of fluorescent dextran internalized.

6. Prior to infusion of either a 3,000 or 10,000 MW dextran (cascade blue, Texas red, or rhodamine; see **Note 5**), we typically set up to collect 200 sequential frames (a time series) and start the acquisition as the plunger on the syringe is pushed to deliver the dextrans (see **Note 6**).
7. Within four to five frames, you will see the appearance of the dextran dyes in the vasculature followed by (if you are imaging a glomerulus, you will see it in the capillary loops simultaneously) filtration into the proximal tubular lumens (or Bowman's space and S1 segment if you are imaging a glomerulus).
8. The 3,000 MW dextran should filter approx halfway through the time series, while the 10,000 MW dextran should filter through just as the series collection is completed. Regardless, within approx 6 min you should see a small fluorescent band at the subapical region, with small endosomes forming directly underneath this zone (**Fig. 3A**).
9. If motion is at a minimum, additional data can be obtained by acquiring a through-focus three-dimensional (3D) image stack (Z-series). To expedite the Z-series acquisition, we collect images at every micrometer in the Z-axis plane.

3.7 Quantifying Endocytosis

1. Because of the dynamic nature of endocytosis, it is important to determine what the end point of the experiment is going to be. The first hour can produce a wide variation in intensity within the endosomal pool. During the first 15 min, the majority of the internalized dextran is localized in small, fluorescently dim vesicles at or below the subapical region. As trafficking and endocytic vesicle fusion progress, the size and intensity of the vesicles increase, reaching peak intensity within the lysosomes. Because of nonspecific binding of dextrans at the apical membrane, fluorescent dextrans containing early endosomes are continually generated for at least 1 h; certain compounds, such as fluorescent folate, prolong this phenomenon even longer (1). This can be problematic because the dynamic range of many imaging systems cannot efficiently capture all the different endosome populations with their varying degrees of fluorescence without saturating the lysosomal pool (**Fig. 5**).
2. For the quantitative aspect of this experiment (**Fig. 4**), a 1.6-mg bolus (80 μ L of the stock solution) of 10,000 MW cascade blue dextran is administered intravenously in 400 μ L of 1X NaCl 24 h prior to imaging to generate more uniform intensity within the endosomal pool. Three-dimensional through-focus volumes are collected ranging from 50 to 70 μ m in depth. For analysis, a 10- μ m thickness is used.

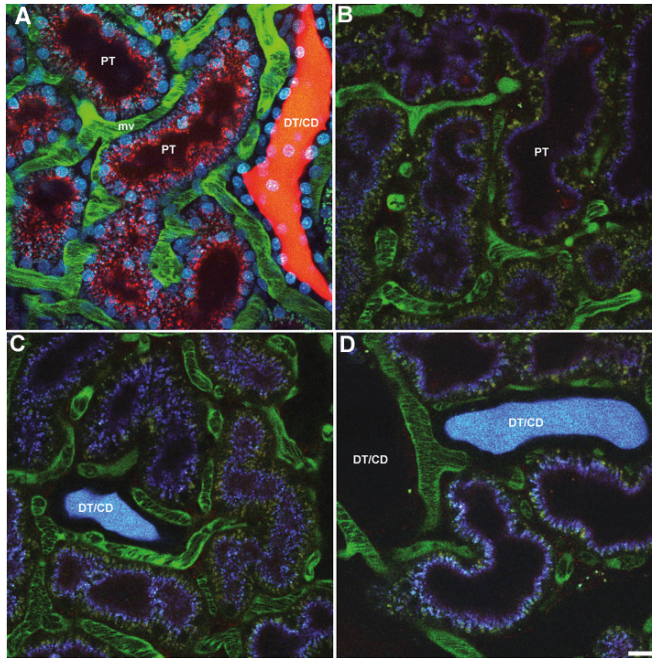


Fig. 3 Delineation of renal landmarks by infusion of fluorescent dyes. (A) A Sprague–Dawley rat was given a 3,000 MW anionic cascade blue dextran (CBdx, blue) 60 min prior to imaging, followed by infusion of the nuclear dye Hoechst 33342 (cyan blue). During the imaging session, a 3,000 MW neutral Texas red dextran (TRdx, red), and a 500,000 MW anionic Fluorescein dextran (500 K FLdx, green) were infused together. The image is a 3D reconstruction of a 6- μ m thick volume that shows progression of endocytosis. The CBdx given approx 60 min prior is localized almost exclusively to the lysosomal compartment at the basal side of the proximal tubules (PT). The TRdx, given approx 10–15 min prior to acquisition is localized almost exclusively at the apical surface of the PT, bound to the brush border, and internalized via small early endosomes. Also visible is the microvasculature (mv) in which the 500,000 FLdx fills the plasma but is excluded from the circulating red blood cells (seen as oblong shadows). A distal tubule/collecting duct (DT/CD) is seen in the right-hand side, with TRdx in the lumen of the tubule, but not internalized via endocytosis. The nuclei are also seen in cyan blue. (B)–(D) A 10,000 MW anionic cascade blue dextran (10 K CBdx, blue), along with a 500,000 MW FLdx (green) was administered intravenously and images acquired at 6 min (B), 30 min (C), and 60 min (D) postinfusion. At 6 min, the 10,000 MW CBdex is localized entirely at the subapical region in a continuous blue line around the lumen of the proximal tubules; small endosomes are seen below the subapical region. After 30 min of internalization, late endosomes have formed, and a small portion of this pool has fused with the lysosomes, as is evident by the change in lysosomal auto-fluorescence from a green-yellow color to white. By 60 min, the majority of the internalized 10,000 MW CBdex is localized within the lysosomes, as determined by more of the color shift from greenish-yellow to white. Note the 10,000 MW CBdex that fills the lumen of the DT/CD in (C) and (D) without internalization. Bar = 20 μ m.

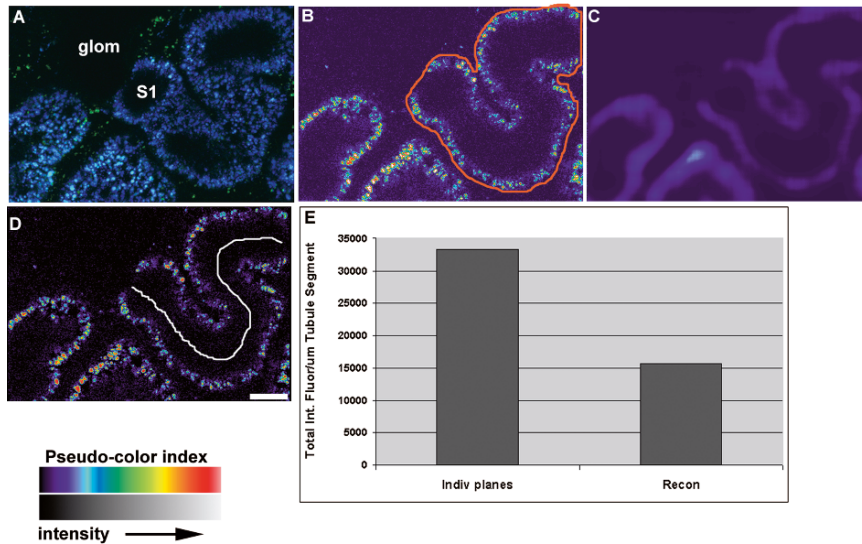


Fig. 4 Quantitative analysis of a 10,000MW anionic dextran 24 h after infusion. **(A)** Through-focus optical planes 62 μm deep were acquired on a Munich–Wistar rat; 10 μm were selected for analysis and are seen here in this color reconstruction. **(B)** An individual raw image plane from the data set is shown with the area of interest (outlined) to be analyzed and displayed in pseudocolor to facilitate observation of low-intensity fluorescence. **(C)** A background image from the individual planes is generated by applying a 32×32 pixel median filter. **(D)** The background is then subtracted from the raw data to generate the background-subtracted image shown. **(E)** After thresholding the individual background-subtracted planes to highlight only the endosomes, the total integrated fluorescence (TIF) for the selected region is obtained. In this graph, a line was drawn along the inner tubule of the S1 segment (seen in D; 160 μm long; see Note 8) and the values expressed as TIF per micrometer of tubule segment (see Note 8). A pseudocolor index scale is provided in the lower left to show the color associated with the corresponding black-and-white intensity in the micrographs. Bar = 20 μm .

3.7.1 Background Subtraction

1. Generate a background image from the 10- μm volumes; a 32×32 pixel median filter is applied to the entire 10-image volume (see Fig. 4A, color image of raw projected volume), and a blurred version of the image volume is generated (see Fig. 4C, single image from blurred volume). (see Note 6).
2. This blurred volume was then subtracted from the original raw volume (see Fig. 4B, single image from raw volume) to generate a background-subtracted volume (see Fig. 4D, single image from background-subtracted volume) (see Note 7).

3.7.2 Thresholding the Endosomal Pool

1. Once the background-subtracted volume is generated, the individual images are thresholded to highlight only the areas containing fluorescent signals

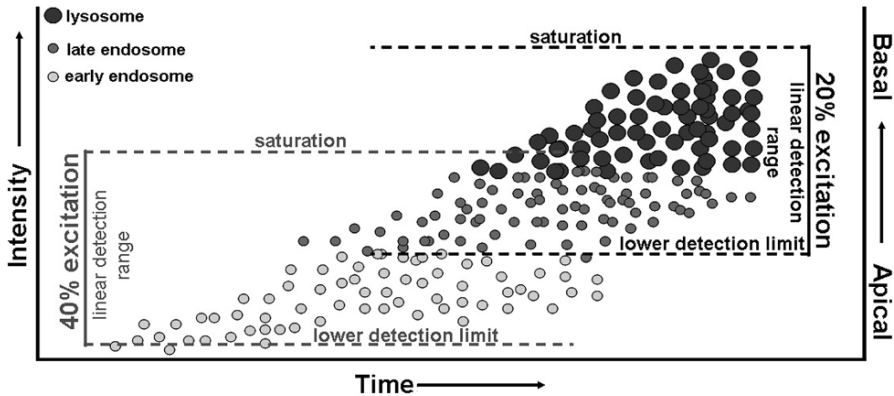


Fig. 5 Dynamic range of the endosomal pool increases as intracellular trafficking from early endosomes to lysosomes progresses. During the first few minutes after infusion of low molecular weight dextrans, small subapical vesicles will form. These structures will have low fluorescence intensity, and detection will require using a higher laser power for visualization. As time progresses, vesicles will fuse and become “brighter” as they form late endosomes and fuse with lysosomes. During this time, dextrans bound to the surface will continue to be internalized, and a broader range of fluorescence intensities will be seen within these vesicles. Generally, the less-intense structures will be found at the subapical/apical region, while the brighter structures localize closer to the basal surface near the lysosomes. The intensity of the lysosomes will be many times brighter than that of the early endosomes; continued use of the same excitation/emission settings will result in saturation of the lysosomal signal. It may therefore be necessary to decrease the laser power used to excite and visualize the lysosomes to keep them in the linear operating range of the detectors.

within the endosomes. A numerical threshold range between 30 and 255 for this experiment highlighted all the endosomes while excluding background (see [Note 8](#)).

2. Next, a region is drawn around the S1 segment adjacent to a glomerulus ([Fig. 4B](#)) to limit the area of analysis.

3.7.3 Quantifying the Data

1. Total integrated fluorescence (TIF), the product of the average pixel intensity and the number of pixels ($TIF = \text{Average intensity} \times \text{Number of pixels thresholded}$), is determined for each individual image plane from the 10- μm volume. Metamorph will give this value, which is exported to MS Excel (2).
2. The TIF values are then added to give the cumulative TIF for the highlighted segment.
3. Next, a line is drawn down the center of the tubule to determine the length of the tubule (in this case, 160 μm ; see [Note 9](#)).

4. The cumulative TIF is divided by 160 to present the data as TIF per micrometer of tubule segment. An alternative method for quantifying a 10- μm volume is to generate a 3D projection from the background-subtracted images and follow the same guidelines above for the single image. This method may be acceptable in flat, subconfluent cultured cells but will lead to an underestimation of the cumulative TIF within proximal tubule cells in vivo (*see Note 10*).

4 Notes

1. Do not mix the dextrans with the nuclear dye as a precipitant may form.
2. It is essential the dish holder forms a good seal with the coverslip dish as inevitably fluids will spill out of the dish. Having an open dish holder will cause biological fluids to run down onto the objective turret and corrode the thread screws as well as mar optical coatings in the light path below the objective.
3. You may want to palpate again for the kidney to make sure you are crushing/cutting into the right area. When you pull up with the forceps, the outer layer should be thin. If you are having difficulty securing the tissue with the forceps, you are likely gripping part of the inner layer as well. After the incision is made, widen the area cut with the forceps to expose the inner and final muscle layer.
4. During prolonged imaging sessions, the water between the objective and coverslip may evaporate. Take a 1-mL syringe, place a long piece of PE-200 tubing at the tip, and fill with prewarmed double-distilled water. Drop the objective and rotate the objective turret so that a bead of water can be placed on the immersion objective without having to displace the rat.
5. Dextrans conjugated to Texas red will generally carry a net neutral charge, while those conjugated to either rhodamine or cascade blue will carry an anionic charge. Fluorescein does not make a good dextran conjugate for following endocytosis as it is pH sensitive, and intensity will drop sharply in acidic endosomal compartments. Alternatively, one could use fluorescein-like fluorophores such as Alexa 488 or Oregon green with greatly decreased pH sensitivity, although bleed-through emissions overlapping into the Texas red/rhodamine channel are another reason these are undesired in dual-labeled experiments.
6. General note: When calculating doses of any dye, it is important to start with an approximate concentration used in cell culture. This concentration is then extrapolated to the plasma volume of a rat. Usually, 7% of the animal's body weight (g = mL) is assumed to be blood, of which approx half is plasma. For a 200g rat, 14mL of blood volume is assumed, of which 7mL is plasma. If a dye is used at 100 $\mu\text{g}/\text{mL}$ in culture medium, then approx 0.7mg should be administered. This is only a starting point, and one should remember small compounds are generally cleared rapidly by filtration with a half-life nowhere near what is found in cell culture.
7. In micrographs seen in Fig. 4, only Fig. 4A is a standard RGB color image. Figure 4B–D are single-channel images from the 10,000MW cascade blue

dextran seen in pseudocolor to better distinguish the varying intensities seen in the lysosomal pool. An index matching the pseudocolor scale to the black/white intensity is seen in the lower left-hand side of this figure.

8. Thresholding values in Metamorph select pixels having a range between the determined numerical values (i.e., 30–255, above background to the top of the eight-bit scale). In doing so, only those values are used in determining TIF. If no threshold is used, the background pixels will also be used in determining the TIF for the selected region, generating lower-than-actual values.
9. To determine the segment length, the number of pixels that make up the line generated in Fig. 4D are multiplied by the pixel size of the microscope system, in this case 0.333 $\mu\text{m}/\text{pixel}$.
10. When quantifying endocytosis in cell culture, it is sometimes common practice to take a 3D through-focus series of cells, process the individual planes for background subtraction, generate a 3D projection of the image volume, and then quantify the endosomes. This technique is not desired for intravital imaging. Because of the increased cell diameter and more densely packed nature of proximal tubule cells in vivo, many of the endosomes/lysosomes overlap in z-axis, and an underestimation of the fluorescence will occur. In the graph generated for this figure, the value on the left (“Indiv planes”) is derived from generating the TIF/ μm segment for each plane and adding the resulting values. The value on the right (“Recon”) is derived from generating a projection and then calculating the TIF/micrometer segment. This shortcut captures approx half the data present in the volume.

Acknowledgments We are indebted to Kenneth W. Dunn for invaluable input regarding ongoing studies. This work was supported by National Institutes of Health grants P50-DK-61594 and PO1-DK-53465, a Veterans Affairs Merit Review (to B.A. Molitoris), and an Indiana Genomics Initiative grant from the Lilly Foundation to the Indiana University School of Medicine.

References

1. Sandoval, R.M., Kennedy, M.D., Low, P.S., and Molitoris, B.A. (2004). Uptake and trafficking of fluorescent conjugates of folic acid in intact kidney determined using intravital two-photon microscopy. *Am. J. Physiol. Cell Physiol.* **287**, C517–C526.
2. Molitoris, B.A., and Sandoval, R.M. (2005). Intravital multiphoton microscopy of dynamic renal processes. *Am. J. Physiol. Renal Physiol.* **288**, F1084–F1089.
3. Molitoris, B.A., and Sandoval, R.M. (2006). Pharmacophotonics: utilizing multi-photon microscopy to quantify drug delivery and intracellular trafficking in the kidney. *Adv. Drug Deliv. Rev.* **58**, 809–823.
4. Sandoval, R.M., Reilly, J.P., Running, W., et al. (2006). A non-nephrotoxic gentamicin congener that retains antimicrobial efficacy. *J. Am. Soc. Nephrol.* **17**, 2697–2705.
5. Yu, W., Sandoval, R.M., and Molitoris, B.A. (2005). Quantitative intravital microscopy using a generalized polarity concept for kidney studies. *Am. J. Physiol. Cell Physiol.* **289**, C1197–C1208.
6. Dunn, K.W., Sandoval, R.M., Kelly, K.J., et al. (2002). Functional studies of the kidney of living animals using multicolor two-photon microscopy. *Am. J. Physiol. Cell Physiol.* **283**, C905–C916.

Index

A

- Acidic seawater, 63
- F-Actin
 - coated vacuoles, 16
 - depolymerizing drugs, 26
 - motor, 20
- Activating domain (AD), GAL4 transcription activator, 114
- Adaptor protein (AP)2 complex, 8, 16
- Adenoviral infection, 178
- Adenovirus preparation
 - adenoviral vector recombination, 176–177
 - isolation of, 177–178
- Adherens junctions (AJs)
 - cadherins, 88–89
 - cell-cell adhesion, 77
- 3T3-L1 Adipocytes, HA-GLUT4, ectopic expression, 132
- AJ-enriched fraction isolation
 - materials for, 78–79
 - methods for, 80–81
- Alexa 488-conjugated, fluorophores, 241
- Alzheimer precursor protein (APP), 122
- Amiloride, for inhibition of macropinocytosis, 25
- Amperometric events, analytical steps of, 316–317
- Amperometric spikes
 - analysis of, 315
 - analytical spikes exclusion, 322–323
 - detection of, 317
 - digital filters, 317
 - overlapping analysis, 321–322
 - shape characteristics, 318–321
 - statistical analysis and data pooling, 323
 - Whole-Trace parameters, 323

Amperometry, 298

- data acquisition and analysis of, 316
 - resolution and sensitivity of, 315–316
 - traces, 317, 323, 325
- Anticlatrin antibodies, 236
 - AP180/clathrin, 5
 - Apical delivery assay, gp80, 173–174
 - Arf1-GTPase, 8
 - β -Arrestins, 5
 - Artificial seawater (ASW), 63
 - Atomic force microscopy (AFM) of membrane sheets, 237–239
 - fluorescence labels for, 241

B

- Baby hamster kidney cells (BHKcells), 89
- Background subtraction, endocytosis quantification, 399
- Basolateral early endosomes (BEE), 158–159
- Bicaudal 1 and 2 (BICD1, BICD2)
 - interaction with GTPases Rab6 and Rab1, 121
 - p150^{Glued} binding, 122
- Biotinylated proteins, cell lysis and isolation of, 94
- BOSC23 cells, 131, 134
- Botulinic neurotoxins (BoNTs), 38, 188
 - neuronal SNAREs, 38
 - VAMP2 cleavage, 39
- Botulism, 187
- Bovine aortic endothelial (BAEK), 6
- Buffers
 - for ileal mucosal total membranes and brush border preparation, 99–100
 - lysis buffer and wash buffer, 92
 - phosphate-buffered saline (PBS), 91

C

- Ca²⁺ channels, 269
- Caco-2 cell (human colon cancer cell)
 - cell culture media and conditions, 99
 - Ileal BBM and total membrane incubation, 106–107
 - total cellular membrane preparation from for lipid rafts isolation, 101
- Ca²⁺-dependent release of adenosine 5'-triphosphate (ATP), 270
- E-Cadherin. *See also* E-Cadherin endocytosis in zebrafish
 - adherens junctions (AJs), 77
 - cell–cell contact-dependent inhibition of, 78
 - endocytic recycling of, 90
 - endocytosis modes of, 78
 - staining pattern, 386
- E-Cadherin endocytosis in zebrafish
 - cell culture, technique of, 375–376, 379–380
 - detection of, 372
 - embryonic injection, mounting and stages, 374
 - embryonic In Situ Hybridization (ISH), 375, 378–379
 - embryonic somitogenesis of, 382
 - gastrulation in, 371, 374, 382–386
 - Heat-Shock treatment, 372–373, 378
 - ISH analysis, 372–373, 378–379
 - messenger ribonucleic acid (mRNA) and morpholino injection, 373–374, 377–378
 - regulation of, 371
 - slb/wnt1* effects, 386
 - subcellular localization, 383
- Caenorhabditis elegans*
 - cuticle proteins secretion, 339
 - embryos
 - cell divisions, 338, 344
 - imaging and postfilming, 343
 - needles preparation and worm mounting, 341
 - intestine regulation and muscles membrane organelle, 340
 - oocyte, receptor-mediated endocytosis, 338
 - rrf-3 strain in, 340
 - small fluorescent dyes for research, 336
- Ca²⁺-evoked secretion in *Xenopus* oocytes, 269
- capacitance monitoring, 271–273
 - online computation, 276
 - paired-ramps approach, 275
 - voltage stimulus and monitoring Cm changes, 274
 - reconstitution of depolarization evoked secretion, 278–280
 - transcription and CRNA injection, 273
- Calcium-free seawater, 64
- Candidate gene approach, *C. elegans*, 337–338
- Capacitance, 269
- Capacitance recording from cell-attached patches, 283
 - low-noise single-vesicle capacitance recording, SSV and LDCV fusion, 284
- Carbon fiber electrodes, 297, 299. *See also* Single-cell amperometry 297–298
 - companies producing electrodes, 300
 - glass-encased electrodes, 299
 - plastic-encased carbon fiber electrodes, 299, 300
 - Chow's method, 299
 - Hille's method, 300
- Ca²⁺-regulated membrane fusion, 270
- Cargo proteins
 - endocytosis and recycling by sulfo-NHS-SS-biotin- labeled, 94
 - regulator proteins effect, 95
- Catecholamine release in spike analysis, 319–320
- Ca²⁺-triggered exocytosis of single secretory granules, imaging, 51
 - cell culture and transfection, 52–53, 55, 56
 - fluorescence microscopy, 54, 56
 - membrane sheets generation, 53, 56
- Caveolae, 6
- Caveolar-mediated endocytosis, 6
- Caveolin isoforms, 10
- Cbl, adaptor/ubiquitin ligase, 236
- cDNA library amplification, 118–119
- Cef* (Cadherin extracellular fragment)
 - preparation
 - materials for, 79
 - methods for, 82
- Cell-cell adhesion molecules, 77
- Cell culture
 - BOSC23 cells, 131
 - MDCK type II cells, 161
 - 3T3-L1 cells and viral infection, 131–132
- Cell-free assay
 - E-cadherin endocytosis
 - materials for, 79–80
 - methods for, 82–84
 - secretory granules
 - cell culture and transfection, materials for, 52–53
 - exocytotic sites, 52

- fluorescence microscopy, 54, 56–57
 - PC12 cells, culturing and transfection
 - of, 55–56
 - plasma membrane sheet generation, 53, 56
 - secretory organelles, fluorescent labeling of, 51, 55
 - Cell lysis buffers, 99
 - Cell-surface biotinylation
 - occludin intracellular transport, 90
 - sulfo-NHSSS-biotin and, 93
 - Cell surface proteins, dynamics of recycling analysis
 - anti-HA antibody and
 - determination, 135
 - BOSC23 and 3T3-L1 cells, 131–132
 - BOSC23 cells, propagation, 134
 - detergents, effect of, 133
 - fluorescence assays, 132
 - steady-state kinetics, 142–143
 - 3T3-L1 Preadipocytes, propagation, 136–137
 - transition kinetics, 141–142
 - transition-state and steady-state experiments, 133, 136, 138, 139
 - Cellubrevin in transferrin, implication, 188
 - CFSW. *See* Calcium-free seawater
 - Chinese hamster ovary (CHO), 8
 - Cholesterol-binding drug digitonin, FPP assay, 228
 - Clampex software in electrical nerve stimulation, 355
 - Clathrin adaptor complex disruption, 10
 - Clathrin assembly lymphoid myeloid leukemia protein (CALM), 5
 - Clathrin associated sorting proteins (CLASPs), 5
 - Clathrin-coated vesicles (CCVs), 5, 26, 236–237
 - Clathrin-dependent endocytosis, 4–6
 - Clathrin-independent endocytosis, 6–7
 - Clathrin-mediated endocytosis, inhibitors, 17
 - chlorpromazine, 19–20
 - cytosolic acidification, 19
 - hypertonic sucrose, 17–18
 - monodansylcadaverine, 20
 - phenylarsine oxide, 21
 - potassium depletion, 18–19
 - Clostridial neurotoxins, 187, 188
 - Coat protein complexes I and II, 7–8
 - Coelomocytes in endocytic research, 338–339
 - Colony-lift filter assay, 120
 - Confocal immunofluorescence microscopy, MDCK cells
 - adenovirus infection of, 178–179
 - syntaxin expression in, 180
 - Confocal microscopy observation, *C. elegans* embryos, 341–344
 - Content-mixing assay
 - HPTS fluorescence, 37, 46
 - VAMP2 reconstitution efficiency estimation, 49
 - v- and t-SNARE liposomes fusion, 39, 46
 - COPI coatomer, 8. *See also* Coat protein complexes I and II
 - Culture materials, *Caenorhabditis elegans*
 - dsRNA production, 333
 - maintenance, handling and microinjection, 336
 - strains and microscopy, 337
 - Culture methods, *Caenorhabditis elegans*
 - germline and coelomocytes selection, 338
 - hypodermal epithelium selection, 339
 - intestine, muscles and neurons selection, 340
 - phenotypic gene knockdown, tissues in, 338–340
 - phenotypic RNAi
 - injection and observation, 341–344
 - telltale signs, 340
 - Cutoff criteria threshold, spikes exclusion, 322–323
 - Cytochalasin D blocks actin polymerization, 26
- D**
- Data filtering in amperometric spike detection, 317
 - Density gradient preparation material, OptiPrep, 98
 - Density gradient ultracentrifugation (DGUC)
 - Brush border (BB) isolation buffers, 99–100
 - principle of, 97–98
 - sucrose, 98
 - 3,3'-Diaminobenzidine (DAB), 247, 248
 - polymerization, 250–251
 - Digitonin permeabilization, 228
 - Dimethyl amiloride (DMA), 25
 - Disabled-2 (Dab2), 5
 - DNA-binding domain (BD), GAL4
 - transcription activator, 114
 - Double-stranded RNA (dsRNA)
 - microinjection, coelomocytes, 339

- Drosophila melanogaster*, 4
- Bicaudal-D protein, 122
 - neuromuscular junctions (NMJs), synaptic vesicle pools labeling
 - confocal microscope imaging, 355
 - exo/endo cycling (ECP) and reserve pool (RP), function, 352
 - function of, 349
 - image analysis and acquisition, 355
 - larval dissection, method and materials, 354, 357–358
 - loading and unloading protocols, 353
 - neuronal membranes label, 364
 - third-instar larval fillet FM 1-43 labeling, 359–360
 - vesicle pools of, 352
 - weakly labeled protocol, 355–357, 364–366
 - Dynamamin- and Rab5-dependent endocytosis regulation (DLC2A), 372
- E**
- Embryonic heat-shock treatment, 372, 378
 - Embryonic ISH tailbud stage, 379
 - EMTs. *See* Epithelial-mesenchymal transitions
 - Endocytosis, 5, 16
 - dynamamin-dependent endocytosis, 7
 - E-cadherin of, 78
 - occludin of, 94
 - pathways, categorization, 4
 - quantification
 - anionic dextran analysis, 399
 - background subtraction and threshold endosomal pool, 399–400
 - delineation of renal landmarks, 398
 - dye preparation, 392
 - fluorescent dextrans role in, 397
 - fluorescent markers, solutions and microscopy, 391
 - limitations of, 389
 - microscope and surgical preparation, 393–395
 - physiologic approaches, 389, 390
 - renal landmarks, 396
 - visualization of, 396–397
 - research, phenotypic and developmental effects, 10–11
 - Endosomal protein, EEA1, 27
 - Endosome-/lysosome-associated tubules, 247
 - Endosomes in nonsectioned cells, TEM analysis, 247
 - cell culture on grids, 253
 - DAB polymerization, 254–255
 - endocytosis of Tf-HRP/HRP, 254–255
 - grids preparation, 252
 - immunolabeling, 255–256
 - Tf-HRP preparation, 254
 - Epidermal growth factor (EGFR), 5
 - Epithelial cells
 - adenoviral infection, 178
 - adenoviral-mediated expression, 175
 - cell culture and adenovirus infection, 172
 - membrane polarization, 171
 - selective barrier, 157
 - syntaxin, expression and localization, 171–172
 - Epithelial- mesenchymal transitions, 90
 - Epithelial MTD-1A cells
 - occludin endocytosis and recycling, 94
 - regulator proteins expression in, 93
 - Epithelial snare machinery, targeting by bacterial neurotoxins
 - purification of light chain of tetanus neurotoxin, 191
 - SDS-PAGE gel electrophoresis, 192–193
 - selection of clones, 197–198
 - test based on fluorescence for TeNT activity, 190–191, 196–197
 - time-lapse videomicroscopy, 198–200
 - transfection and selection of MDCK cells, 189–190, 195–196
 - treatment, cell extracts with purified toxin, 188–189
 - Western Blotting for Brevins, 193–194
 - Eps15, endocytic factor, 5, 236
 - N*-Ethylmaleimide-sensitive factor, exocytosis regulation
 - ELISA for VWF release, 207
 - endothelial cell culture, 204–205, 207
 - FACS for P-selectin externalization, 207–208
 - immunoprecipitation for S-Nitrosylated NSF, 205, 208–210
 - leukocyte adhesion and fluorescent microscopy, 206, 211–212
 - leukocyte rolling and intravital microscopy, 206, 213
 - S-Nitrosylation of NSF by Biotin-Switch, 205–206, 210–211
 - TAT fusion peptides, 206, 212
 - N*-Ethylmaleimide-sensitive factor (NSF), 204
 - 5-(*N*-Ethyl- *N*-isopropyl) amiloride (EIPA), 25
 - Excitosome, 270, 271
 - Exocytotic activity and event, 316, 319

F

- Falling phases, amperometric events, 321, 325
- Fast cyclic voltammetry, 298
- Fibroblastic BHK cells
 - cargo and regulator proteins expression in, 92–93
 - occludin endocytosis and recycling, 94
- Finite impulse response (FIR) filter, 324
- Fluorescence dequenching
 - content-mixing assay, 39
 - lipid-mixing assay, 38
- Fluorescence intensity, endosomal pool, 400
- Fluorescence microscopy
 - exocytosis monitoring, 56–57
 - GFP and TMA-DPH, 54
- Fluorescence protease protection (FPP) assay, protein topology
 - digitonin and trypsin, application, 231
 - expression plasmid construction, 229
 - fluorescence microscopy, 230, 232
 - selective permeabilization, 229–230
 - transfection, 229
- Fluorescence redistribution after photobleaching
 - cortical granules imaging parameters, 71–72
 - secretory vesicle membrane, 63
- Fluorescent dye FM 1-43
 - intensity quantification procedure, 363
 - properties of, 350, 351
 - role of, 350
- Fluorescent dye use
 - kidney survey, 395–396
 - renal landmarks delineation, 398
- Fluorescent proteins marking application in *C. elegans*, 333
- Fluorophore-conjugated Fabs generation
 - Fabs separation and testing, 70
 - IgGs elution, 68
 - immobilized protein and sealing process, 67
- Fluorophore HPTS (pyranine), 39
- FM 1-43 synaptic vesicles labeling, in *Drosophila*, 354–364
- FRAP. *See* Fluorescence redistribution after photobleaching

G

- Gab2, scaffolding adaptor, 236
- β -Galactosidase reporter assay, 120

- GAL4, transcription activator
 - functional domains of, 114
- Gastric acid secretion in parietal cells, stimulation, 218
- Gaussian infinite impulse response (IIR) filter, 323–324
- GDP-dissociation inhibitor (GDI) and factors (GDFs), 9
- Gene knockdown phenotypes, *C. elegans* embryos, 338–340
- Genomewide screening in *C. elegans*, 333
- Germline silencing phenomenon, *C. elegans*, 338
- GFP expression vector, 228
- Glass scintillation vials, 148, 154
- Glucose transporter number 4 (GLUT4), 129
- GLUT4, protein trafficking, 129. *See also* Cell surface proteins, dynamics of recycling analysis
- GM130, Rab1 effector protein, 123
- gp80, protein, 182
- G protein-coupled receptors, 5
- Grb2, adaptor protein, 236
- Green fluorescent protein (GFP), 52, 188, 228, 260, 338
- Growth hormone receptor, 7
- GTPase-activating proteins (GAPs), 8, 9
- GTPase cycle, Ypt/Rab proteins, 111
- GTPases Rab1 and Rab6 identification
 - alzheimer precursor protein (APP) and, 122
 - Bicaudal 1 and 2 (BICD1, BICD2), interaction of, 121–122
 - buffers and solutions, 112–113
 - culture media for, 112
 - p150^{Glued} binding, 122–123
 - yeast transformation, 117–118
- Guanosine triphosphatase (GTPase), 7, 9–10

H

- HA antibodies in heat shock treatment, 382
- Hatching gland gene 1 (hgg1) in gastrula visualization, 384
- HEK293 and HeLa S-3 cells, 10
- β -Hemolytic group A streptococci, 218
- Hermansky-Pudlak syndrome, 10
- Histamine, 218
- H,K-ATPase, 218
- Horseradish peroxidase (HRP), 248, 250
- HPTS fluorescence, 38, 39
- Human PRA1 protein, 9

I

- Immunofluorescence labeling, zebrafish
 - antibody, 376, 380–382
 - epifluorescence or confocal optics in, 382
 - transgenic slb hs-wnt11 embryos in, 380
- Immunoglobulin A, 236
 - internalization of, 158, 162
 - iodination of, 162–163
 - postendocytic fate of, 161, 164, 168
 - transcytosis of, 157–158
 - trichloroacetic acid precipitation, 166–167
- ImmunoPure digest buffer, 69
- Integral TJ proteins, 90
- Integrin, cell-matrix adhesion molecule, 78
- Intracellular membrane fusion, 38
 - cognate v- and t-SNAREs pairing, 38
 - HPTS fluorescence, 39
 - secretory and endocytic pathway, 37
- Intracellular trafficking, endosomal
 - pool, 400
- Intravital imaging, rat kidney, 394
- Intravital two-photon microscopy
 - fluorophores illumination and techniques of, 390
 - quantifying endocytosis, 389
 - renal function quantification and study, 390
- Intrinsic cellular variables, 140, 142
- Iodination materials, 159–160

J

- J774 cells, mouse macrophages
 - incubation and hydrolysis, 148
 - scintillation estimation, 149
- Junctional Rab13-binding protein (JRAB), 89

K

- K44A dynamin mutant, 10
- Kiss-and-run recycling, *Drosophila* NMJs, 350–352

L

- Large dense-core vesicle (LDCV), characteristic, 321
- Latrunculins, nonselective inhibitors, 26
- Lipid-mixing assay
 - based on fluorescence resonance energy transfer, 37, 45, 46
 - fluorescence dequenching, 38

- Lipid raft/caveolae-mediated endocytosis, inhibitors, 21
 - cholesterol oxidase, 24
 - methyl- β -cyclodextrin (M β CD), 22–23
 - polyene antibiotics, 23–24
 - statins, 22
- Lipid rafts (LRs)
 - function of, 106
 - isolation by density gradient floatation, 104–107
- Liposomes, 7, 150
- Live-cell experiments, phagocytosis, 148
- Live-cell scintillation proximity assay
 - cell culture media, 150
 - J774 macrophages culture, 152
 - mouse macrophages, 148–149
 - scintillant particles and analytes, 148
- Low-density lipoproteins (LDLR), 5
- Low-noise capacitance recording
 - cell-attached capacitance measurements, 289–290
 - instruments, 286
 - off-line phase correction and data analysis, 291–292
 - technique, 287–288
- Lysosomes, 149

M

- Macropinocytosis and phagocytosis, inhibitors
 - F-actin-depolymerizing drugs, 26
 - phosphoinositide metabolism inhibitors, 26–27
 - sodium-proton exchange inhibitors, 25–26
- Madin-Darby canine kidney cells (MDCK cells), 7, 188
 - cell culture, 161
 - confocal immunofluorescence microscopy of, 178–180
 - IgA transcytosis in, 157
 - syntaxin expression in, 175
 - trypsinization of, 176
- Matchmaker GAL4-based two-hybrid system, 114. *See also* Yeast two-hybrid system
- Membrane pellet, 83, 85, 101–102
- Membrane proteins, 130, 227
- Mesenchymal-epithelial transitions (METs), 90
- Mesendodermal cell culture, zebrafish, 381
- Microplate scintillation counter, 149, 151
- M1 muscarinic acetylcholine receptor, 7
- Mock uptake experiment, *Drosophila* NMJ, 357

- Molecular biology/genetic tools, exo- and endocytosis of proteins, 4
- Molecule interacting with CasL-like 2 (MICAL-L2), 89
- Morpholino-mediated Rab5. *See also*
 E-cadherin endocytosis
 in zebrafish
 activity inhibition, 372, 377
 manipulation techniques, 371
 in situ hybridization (ISH) analysis, 372
- Morphological structure, rat kidney, 395
- Multistep filtering spike analysis, advantages, 324
- Mutant third-instar neuromuscular junctions (NMJs), 350
- N**
- NBD fluorescence and membrane fusion, 38, 39
- Nephrotoxic agents accumulation, 390
- Nerve stimulation suction electrode preparation, 356
- Neuronal cells, 270
- Neuropeptide Y-green fluorescent protein, 51
 plasmid encoding, 53
 plasmid transfection for expression, 55
 turnover rate of, 58
- Neuropeptide Y-green fluorescent protein (NPY-GFP), 51
- Neurotoxins and neuronal SNAREs, 38–39
- Neurotransmitter
 membrane protein complexes, 51
- NMJ stereotypic innervation pattern, 362
- NO S-nitrosylation, NSF, 204
- NPY-GFP. *See* Neuropeptide Y-green fluorescent protein
- NSF, chemically modifies, 204
- O**
- Occludin
 endocytosis and recycling of, 94
 polymerization of, 90
 transmembrane proteins, 89
- OptiPrep density gradients ultracentrifugation
 membrane vesicles fractionation, 97, 103, 105
 organelles from PS120 cells separated by, 106
 rabbit ileal BBM and Caco-2 cells, 107
- Overlapping spikes analysis, 321–322
- P**
- Phagocytosis, 27, 147–148
- Phagosomes, 16
- Phase-sensitive detector (PSD), 284
- Phosphoinositide 3-kinase (PI3K), 26
- Phosphoinositide-specific PLC, 26
- Phosphoproteins, 218
- pIgR. *See* Polymeric immunoglobulin receptor
- pIgR-IgA complexes transcytosis, 158
- PI3K- and PLC-generated lipid mediators, 27
- Plasma membrane proteins, 51, 130
 exocytosis, 56–57
 fluorescent docked secretory granules, 53
 ultrasound pulse and, 55
- Plasma membrane syntaxins
 adenovirus-mediated expression, 175
 localization of, 172
 SNARE protein family, 171
- Plasmids bait and prey, 113
- Polarized protein trafficking in epithelial cells, analysis
 chimeras of syntaxin 3 and 4, use of, 171–172
- Poly-l-lysine, 64
- Polymerase chain reaction (PCR), 113, 333
- Polymeric immunoglobulin receptor, 157
 t ranscytosis in polarized MDCK cells, 158–159
- 3T3-L1Preadipocytes
 differentiation of, 137–138
 propagation of, 136–137
 retroviral infection of, 137
- Proteases, 228, 230
- Protein expression and purification methods
 t-SNARE, 41–42
 VAMP2 (v-SNARE protein), 42–43
- Proteing labeling reagents, 64
- Protein kinase A (PKA), 218
- Proximal tubule, role of, 390
- PS120 cells
 cell culture media and conditions, 99
 intracellular organelles seperation, 106
 total cellular membrane preparation from, 102
- P-Selectin, 203
- R**
- Rab6A GTPase and Alzheimer precursor protein (APP), 122
- Rab5 and 9, 9, 10
- Rabbit ileal brush border membranes
 preparation, 102–103
- Rab9-GDI complexes, 10
- Rab GTPase function, 9, 111
- Rab5-GTP mutant overexpression, 9

- Rab1-Iporin2 interaction, 123
Rac and *Cdc42* activation, E-Cadherin
 materials for, 80
 methods for, 85
 Rap1 activation and nectin, 86
 Rat brain cytosol preparation
 materials for, 79
 methods for, 82
 Rat chromaffin cell, amperometric
 recordings, 325
 Rat kidney
 endocytosis images generation, 396
 morphological survey and structure of, 395
 Receptor-induced endocytosis, 236
 Recombinant adenovirus infection, epithelial
 MTD-1A cells, 93
 Recombinant T7 vaccinia virus system, 92–93
 Renal survey landmarks, rat, 396
 Reporter genes
 autoactivation, 118–119
 expression of, 115
lacZ and *HIS3*, 114
 Retroviral particles
 culture media, 131
 production of, 134
 refreezing of, 144
 RhoGDI. *See* Rho-GDP dissociation inhibitor
 Rho-GDP dissociation inhibitor, 86
 Ribonucleic acid interference (RNAi) in
C. elegans
 biological role, 332
 early embryos, injection and observation
 of, 341–344
 membrane traffic and phenotypic
 analysis, 333
 membrane transport, 331
 Rip-and-flip procedure, sheet preparation
 TEM and AFM, 239
 RNAi-mediated knockdown of
 caveolin-1, 4, 6
- S**
Saccaromyces cerevisiae sec mutants, 4
 Scintillant particles, 148
 Scintillation mouse J774 macrophages,
 149–150
 SDS-PAGE, Sodium dodecyl sulfate
 polyacrylamide gel electrophoresis
 Sea urchin egg, secretory granule lipids and
 proteins, FRAP analysis
 cortical granule lawns, preparation, 67
 egg cell surface transformation, 61
 egg cortex preparations, 66
 fluorescence bleaching experiments, 71
 generating fluorophore-conjugated Fabs,
 64–65, 68
 handling of, 66
 protein dependent signaling pathways, 62
 SNARE protein and, 62–63
sec mutants in yeast, 4
 Secretory organelles fusion
 cell-free assay for, 52
 green fluorescent protein (GFP), labeled
 with, 52
 Sheets preparation
 AFM/Fluorescence, 243–244
 TEM and, 242–243
shibrie mutants in *Drosophila*, 4
 Single-cell amperometry, 297–298
 calibration and selection, 305–307
 two flow injection systems, 306
 using norepinephrine, 307
 glass-encased electrodes, use, 302–303
 mice chromaffin cell isolation, 300–301
 noise reduction process, 307–308
 plastic-encased carbon fiber electrode
 procedure, 303–305
 Single insulin secretory, exocytosis imaging
 MIN6 cells and pancreatic β -cells culture,
 262–263
 primary β -cells glucose stimulation, TIRF
 images and analysis, 266
 recombinant adenovirus cultured single
 cells for infection, 264
 TIRF setup and excitation using
 evanescent field, 260–262
 transfection, 264
 Small GTPases, 9
 Small interfering RNA (siRNA), 5
 SNAP-25, 188
 SNARE. *See* Soluble N-ethylmaleimide-sensitive
 factor attachment protein receptor
 t-SNARE liposomes
 expression and purification of, 41–42
 reconstitution of, 40–41
 in vitro fusion of, 37–38
 v-SNARE liposomes
 fusion of labeled, 37
 reconstitution of, 44–45
 VAMP2 purification, 42–43
 SNARE-mediated vesicle fusion,
 measurement
 content-mixing assay with DPX,
 45–48
 fluorescence signal of NBD in
 lipid-mixing assay, equation, 49
 lipid-mixing assay, 45

- protein expression and purification, 39–40, 41
- t-SNARE
 - expression and purification of, 41–42
 - liposomes, reconstitution, 43–44
- VAMP2, expression and purification of, 42–43
- v- and t-SNARE liposomes, reconstitution, 40–41, 43–44
- v-SNARE liposomes, reconstitution, 43–45
- Sodium dodecyl sulfate polyacrylamide gel electrophoresis, materials, 100
- Soluble N-ethylmaleimide-sensitive factor attachment protein receptor
 - classification of, 38
 - α -helical regions of, 37
 - intracellular fusion by, 37
- Soluble N-ethylmaleimide-sensitive factor attachment protein receptors (SNAREs), 8–9
 - v- and t-SNAREs, 38–39, 188
- Spikes
 - characteristics, distribution, 322
 - determination, 321
 - exclusion analysis, 322–323
 - parameters, calculation, 318
 - rising phase and prespike foot (PSF) in shape characteristics, 320–321
 - shape characteristics
 - fine, 320–321
 - large dense-core vesicle (LDCV) in, 321
 - major, 318–320
- Staphylococcus aureus*, 218
- Statistical analysis and data pooling, amperometric spikes, 323
- Steady-state assay
 - advantage of, 143
 - steady-state kinetics, 142–143
 - 3T3-L1 preadipocytes, 139
- Stimulation electrode in *Drosophila* NMJs
 - experiment, 355
- Stimulus-dependent secretion, cortical granules, 62
- Streptolysin O permeabilization, HCl
 - secretion in gastric parietal cells
 - 14C-aminopyrine uptake assays, 221
 - cAMP-dependent protein kinase activation, 223
 - isolation of gastric glands, 220
 - pNPPase activity, 222, 224
 - recombinant ezrin proteins use of, 222
 - redistribution of H,K-ATPase, in response to CAMP stimulation, 225
 - SLO permeabilization of gastric glands, 220–221
 - translocation of H,K-ATPase, 224
 - Strongylocentrotus purpuratus*, 62
 - Subcellular membrane vesicles, separation technique for, 97
 - SV40 virus, 6
 - Synaptic SNAREs synaptobrevin/VAMP2, 188
 - Synaptic vesicle recycling, mechanisms, 349, 350
 - Synaptosome-associated protein, 270
 - Synaptotagmin, 270
 - Syntaxin, 188, 269, 270
 - Syntaxin chimeras, designing, 175–176

T

 - T-cell receptor, 188
 - Tetanus neurotoxin (TeNT), 188
 - Threshold endosomal pool, endocytosis quantification, 399–400
 - Threshold spike detection, 317, 322
 - Thrombosis, 203
 - Tight junctions (TJs), cellular structures, 89
 - Topcount NXT microplate scintillation counter, 151
 - Torpedo marmorata*, 270
 - Total cellular membranes preparation
 - Caco-2 cells for isolation of lipid rafts, 101
 - PS120 cells for subcellular organelle fractionation, 102
 - rabbit ileal mucosa, 102
 - Total integrated fluorescence (TIF), 399, 400
 - Total internal reflection fluorescence (TIRF), 259, 260
 - α -Toxin, 218
 - Transcytosis
 - basolaterally internalized 125I-IgA, 164–166, 168
 - iodination, 159, 162
 - of pIgR and dimeric IgA (dIgA) ligand in polarized MDCK cells, 158–159
 - Transferrin, 6, 9, 250
 - trans-Golgi network (TGN), 5
 - Transition state assay, GLUT4
 - advantage of, 143
 - anti-HA antibody, 138
 - cell surface recycling measurement, 130
 - HA epitope tag, 133–134
 - 3T3-L1 preadipocytes
 - differentiation of, 137–138

Transition state assay, GLUT4 (*cont.*)
 propagation of, 136–137
 retroviral infection of, 137
 transition kinetics
 exocytosis and endocytosis, 141
 HA-GLUT4 transport, 142
 Transmembrane proteins, 129, 130
 Transmission electron microscopy
 (TEM), 236
 immunogold labels for, 240–241
 Trichloroacetic acid precipitation, ¹²⁵I-IgA
 ligand, 167–168
 T7/T3 polymerase, 273
 Tyrosine kinase, 16, 236

V

VAMP2 (v-SNARE protein)
 purification of, 42–43
 Vav, guanosine 5'-triphosphate (GTP)
 exchange factor, 236
 Vesicular trafficking, 3
 in exocytosis, manipulation
 clathrin adaptors in the trans-golgi
 network, 8
 coat protein complexes I and II, role,
 7–8
 vesicle recognition and fusion
 machinery, 8–9
 GTPases, role and effectors, 9–10
 Voltage-gated Ca²⁺ channels
 (VGCCs), 270
 Von Willebrand factor (VWF), 203

W

Weibel-Palade bodies, 203
 Western blotting

biotinylated occludin and claudin-1, 95
 materials for, 101
 of membrane vesicles, 104–105
 Whole-Trace parameters, amperometric
 spikes, 323

X

Xenopus laevis, 270, 274
Xenopus oocytes, 269, 271

Y

Yeast plasmids
 isolation of, 121
 plasmid inserts analysis, 120–121
 Yeast two-hybrid system
 approaches for, 123
 cotransformation assay, 122–123
 principle of, 114
 protein–protein interactions, 111
 Rab6A and Mint3, interaction of, 122
 Rab1–Iporin2 interaction, 123
 yeast transformation, 120
 Y190 yeast cells, transformation of,
 115
 Ypt/Rab proteins, 111
 Yttrium silicate beads, 148–149, 152
 Y190, yeast strain, 111
 reporter gene expression, 114

Z

Zebrafish
 embryonic cell culture, 375, 379–380
rab5 isoforms of, 385
 Wnt11-dependent mesendodermal cell
 migration, 372